Computational Methods Applied to the Study of the Structure, Spectra, and Reactivity of Small Organic Molecules

By

Andrew N. Owen

A dissertation submitted in partial fulfillment of

the requirements for the degree of

Doctor of Philosophy

(Chemistry)

at the

UNIVERSITY OF WISCONSIN-MADISON

2022

Date of final oral examination: 08/12/2022

The dissertation is approved by the following members of the Final Oral Committee:

Robert J. McMahon, Professor, Chemistry (Organic)

R. Claude Woods, Professor, Chemistry (Physical)

Edwin L. Sibert, III, Professor, Chemistry (Physical)

Etienne Garand, Professor, Chemistry (Analytical)

To Sara, for her patient support.

Computational Methods Applied to the Study of the Structure, Spectra, and Reactivity of Small Organic Molecules

Andrew Nickolas Owen

Under the supervision of Professors Robert J. McMahon and R. Claude Woods at the

University of Wisconsin – Madison

ABSTRACT

Quantum chemical *ab initio* methods are applied to a variety of systems to support experimental efforts and to model reactions in harsh environments. High level geometry optimizations and vibrational frequency calculations are combined with experimental fits of rotational spectra to obtain highly precise semi-experimental equilibrium structures (r_e^{SE}) of hydrazoic acid (HN_3) and pyridazine (*ortho* $C_4H_4N_2$ analog of benzene). Purely theoretical equilibrium structures (r_e) are obtained for both HN_3 and pyridazine and require corrections to account for the size of the basis set, for electron correlation, for relativity, and for the Born-Oppenheimer approximation. These corrections bring the theoretical r_e structures into agreement with the experimentally obtained r_e^{SE} structures. Further, application of a novel analysis of the r_e^{SE} structure determination (*xrefiteration*) provides confidence that these r_e^{SE} structures are highly accurate, in addition to being highly precise.

A combination of density function theory (DFT) and *ab initio* methods are used to model reactions in several systems. The diastereoselectivity observed in the synthesis of 1-cyano-1,3-butadienes is satisfactorily explained by the computational investigation of the conformational interconversion of the proposed intermediates. A purely theoretical investigation of the reactions of highly unsaturated carbon chains (C_nH_2) utilizes spin-flip methods to describe the resulting radical species and intervening reactions and finds that the products of [4+2] cycloadditions are more likely to retain the initially formed six-membered ring than are the products of [2+2] cycloadditions to retain the initially formed four-membered ring.

Finally, we describe our application of established theory to derive formulas that can be used for the prediction of the vibration-rotation coupling constants that are used to fit the rotational spectra of coupled vibrational states. Our initial results predict the experimentally determined values of F_{bc} for the coupled-state fits of benzonitrile to within 15%, and the formulas can be used to explain the origin of the proportional relationship of the coupling constants that was observed. The derivation also gives rise to the α corrections to the rotational constants in agreement with previous derivations. Furthermore, the preliminary results of a computer algebra program we are developing are presented and discussed.

ACKNOWLEDGEMENTS

I'm deeply grateful for the financial support I've received from the University and the Chemistry Department, and I greatly appreciate Bob McMahon's support over the uncertain times of the last few years. I thank Claude Woods for his insights into quantum mechanics and ancient Greek, for his uncanny ability to ask just the right question, and for recounting his numerous adventures. I'd like to give special thanks to Brian Esselman for his mentorship over the years in regard to both teaching and research. While the former may have been part of his job, the latter certainly wasn't, and I appreciate the time and energy he's put towards my growth as a teacher and a researcher.

A big thanks to the wonderful group members that I've had the pleasure to work with, to teach with, to celebrate with, to commiserate with, and to grow with. I'd like to thank Vanessa and Maria in particular for their collaboration, their advice, and their friendship from the moment I joined the group, and for the myriad conversations we've had over lunch or while I was waiting for a calculation to finish.

Thanks to my family for their love and support, for listening to explanations about things they likely didn't care about, and for having a higher opinion of my academic prowess than is probably warranted.

There have been many teachers over the years who have, in some form or another, helped me realize my potential as a scientist. Thanks to the chemistry professors at my undergraduate for engaging with the guy who just hung out and studied in the chemistry building, and for encouraging him to continue on to graduate school. I'd especially like to thank a certain middle school science teacher who, when I asked what light was made of, blew my mind with the concept of photons. That moment sparked my fascination and desire to learn how nature works, from subatomic particles to galaxies and everything in between.

Finally, I give my love and gratitude to my wife Sara. You've listened to my presentations, checked my grammar, and have been a sounding board on many an occasion. I'm incredibly grateful for your patience as my postgraduate studies have drawn out longer than intended. You've always believed in me and encouraged me, and your love has been a balm when nothing seems to be working as it should. I could not have done this without you.

Je vous souhaite d'être follement aimée.

OVERVIEW

Theoretical calculations on molecular structures and reactions are applied to a variety of experimental efforts within the McMahon | Woods research group. The chapters herein can be sorted into two groups: one group focuses on computational modeling of the mechanisms of reactions of small molecules in (harsh) environments (Chapters 4, 5, and 6) while the second group focuses on the accurate determination of the structure of small molecules and the prediction of properties relevant to rotational spectroscopy (Chapters 1, 2, and 7).

Chapter 1 describes the development and application of a novel algorithm (called *xrefiteration*) for the assessment of the accuracy of semi-experimental equilibrium structure (r_e^{SE}) determinations. An r_e^{SE} structure determination uses high-quality experimental fits of rotational spectra of a molecule and its related isotopologues and combines the data with results of theoretical structure calculations to determine the molecule's bonding parameters to a high precision. The *xrefiteration* algorithm is applied to these structure determinations to better understand the effect of individual isotopologues on the resulting r_e^{SE} structural parameters and allows for more meaningful comparison of the r_e^{SE} structure to purely theoretical predictions. Example analyses on a variety of r_e^{SE} structure determinations are provided.

Chapters 2 and 3 detail the r_e^{SE} structure determinations of hydrazoic acid (HN_3) and pyridazine, respectively. The r_e^{SE} structure of HN_3 was previously obtained by our group but has now been improved through the use of higher-level theoretical predictions. The high precision of the resulting r_e^{SE} structure is such that even a CCSD(T)/cc-pCV6Z geometry optimization is not within the uncertainties of the r_e^{SE} structural parameters. Further calculations are conducted to correct for extrapolation to the complete basis set limit, for improved treatment of electron correlation, for effects due to relativity, and for the Born-Oppenheimer approximation.

Application of these corrections results in a "best theoretical estimate" (BTE) that agrees with the highly precise r_e^{SE} structure. Application of the *xrefiteration* analysis provides further confidence that both the r_e^{SE} and the BTE structures are quite accurate. The r_e^{SE} structure of pyridazine was also previously obtained by our group but we have since extended the spectroscopic data set, including the measurement of previously undetected isotopologues. While the resulting r_e^{SE} structure is not as precise as that of HN_3, the determination of the BTE structure and the application of the *xrefiteration* analysis gives us high confidence that the structure is also accurate.

Chapter 4 models the reaction mechanism believed to occur in the synthesis of 1-cyano-1,3-butadiene from an aqueous solution of 1,4-dibromo-2-butene and cyanide. Under cool conditions, the synthetic procedure applied to *Z*-1,4-dibromo-2-butene obtained 1-cyano-1,3-butadiene in good yield with a diastereomeric ratio of 10:1 favoring the *E* diastereomer over the *Z* diastereomer. Under warm conditions, the synthetic procedure applied to *E*-1,4-dibromo-2-butene resulted in a much lower yield of 1-cyano-1,3-butadiene with a diastereomeric ration of 2:3, now favoring the *Z* diastereomer. The proposed rate-determining step – the 1,4-elimination of HBr from the 1-bromo-4-cyano-2-butene intermediate – was modeled computationally. We determined the intermediate species was rapidly interconverting between a variety of conformational isomers. By application of the Curtin-Hammett principle, we found the relative energy of the transitions states for the proposed rate-determining step adequately predicted the diastereomeric ratios of the two different procedures.

Chapters 5 and 6 are theoretical investigations of reaction mechanisms under harsh conditions. Chapter 5 considers the transformation of cyanobutadienes to form the aromatic pyridine under astrochemical conditions. The activation barriers for the transformation under neutral conditions were found to be too high to be likely to occur in the interstellar medium. The

transformation catalyzed by atomic hydrogen – while possessing activation barriers considerably lower than the neutral pathway – is also unlikely to occur. The transformation catalyzed by the trihydrogen cation H_3^+, however, does not contain high energy activation barriers and is likely to occur. The transfer of a proton from H_3^+ to cyanobutadiene at the beginning of the transformation is considerably exothermic, presumably due to the ability of the larger $C_5H_6N^+$ molecule to distribute the positive charge than H_3^+. The attachment of H^+ provides the intermediate with more than enough internal energy to overcome the activation barriers for the transformation to pyridine. The high stability of the final intermediate pyridinium (protonated pyridine) suggests that it could be a notable sink of pyridine in the interstellar medium, where pyridine has yet to be detected.

Chapter 6 considers the combination of polyynes (C_nH_2) that are believed to occur within the *ring coalescence and annealing* model of the formation of fullerene. Prior work by our group revealed that the initial [2+2] cycloaddition initially proposed within the *ring coalescence and annealing* model lead to an intermediate that had little to no barrier to undergoing a *retro*-Bergman cyclization and forming an eight-membered ring. We compared this reaction mechanism to an alternative [4+2] cycloaddition. Application of sophisticated theoretical treatments to increasingly more substituted versions of the two reaction pathways revealed that beginning with a [4+2] cycloaddition resulted in intermediates with significant activation barriers for undergoing the *retro*-Bergman cyclization in question, while beginning with the [2+2] cycloaddition consistently had no activation barrier for the same.

Chapter 7 again considers application of theoretical methods for rotational spectroscopy. In particular, we develop and implement a methodology for the prediction of vibration-rotation coupling constants used for the fitting of rotational spectra. Having theoretical predictions for the vibration-rotation coupling constants is likely to aid spectroscopists in the fitting of the complex

rotational spectra arising from vibration-rotation coupling. Furthermore, the lack of theoretical predictions for the vibration-rotation coupling constants (excepting the trivial first-order Coriolis coupling constant) prevents spectroscopists from assessing the quality of the coupled-state fit, and the lowers the confidence that such fits can be extended beyond the original frequency window that the spectra were observed in. Building on the theoretical foundation already within the literature, we derive the formulas necessary for prediction of the second-order Coriolis coupling constants. Furthermore, we developed a program to conduct such derivations for the higher-order coupling constants, and to process computational output files to obtain numeric predictions. The results of our derivation and that of the program are compared to experimental coupled-state fits, and we discuss next steps towards obtaining predictions of the higher-order coupling constants.

TABLE OF CONTENTS

LIST OF SCHEMES

Chapter 4: Understanding the Diastereotopic Outcomes of Cyanobutadiene Syntheses *via* Conformational Analysis of Reactions' Potential Energy Surfaces

LIST OF TABLES

LIST OF FIGURES

Chapter 1: xrefiteration – Analyzing the Effect of Isotopologues on Semi-Experimental Equilibrium Structure Determinations

Chapter 1: *xrefiteration* – Analyzing the Effect of Isotopologues on Semi-Experimental Equilibrium Structure Determinations

Previously published, in part, within:

Orr, V. L.; Ichikawa, Y.; Patel, A. R.; Kougias, S. M.; Kobayashi, K.; Stanton, J. F.; Esselman, B. J.; Woods, R. C.; McMahon, R. J., Precise Equilibrium Structure Determination of Thiophene (C_4H_4S) by Rotational Spectroscopy – Structure of a Five-Membered Heterocycle Containing a Third-Row Atom. *Journal of Chemical Physics* **2021**, *154*, 244310.

https://doi.org/10.1063/5.0055267

Esselman, B. J.; Zdanovskaia, M. A.; Owen, A. N.; Stanton, J. F.; Woods, R. C.; McMahon, R. J., Precise Equilibrium Structure Determination of Thiazole (C_3H_3NS) from Twenty-Four Isotopologues. *Journal of Chemical Physics.* **2021**, *155*, 054302.

https://doi.org/10.1063/5.0057221

Owen, A. N.; Zdanovskaia, M. A.; Esselman, B. J.; Stanton, J. F.; Woods, R. C.; McMahon, R. J. Semi-Experimental Equilibrium (r_e^{SE}) and Theoretical Structures of Pyridazine (o-$C_4H_4N_2$). *Journal of Physical Chemistry A.* **2021**, *125* (36), 7976-7987.

https://doi.org/10.1021/acs.jpca.1c06187

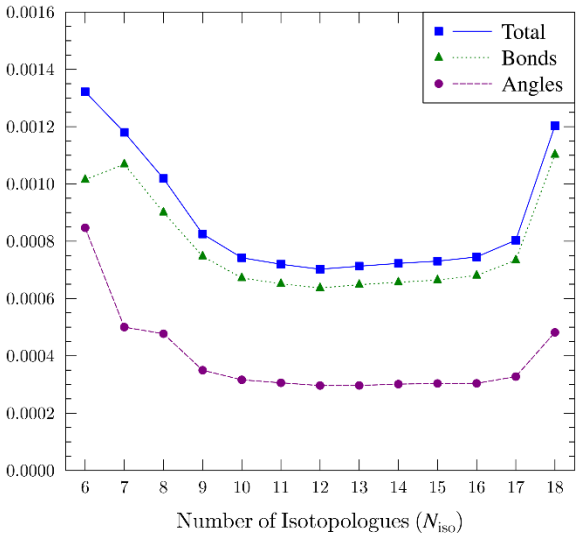

ABSTRACT

The effect of including additional isotopologues in the data set for r_e^{SE} structure determinations was examined using the novel *xrefiteration* routine for the r_e^{SE} structure determinations of hydrazoic acid, pyridazine, pyrimidine, thiophene, and thiazole. In all molecules considered, incorporation of additional isotopologues beyond the minimal set resulted in an immediate and significant improvement in the total relative uncertainty (δr_e^{SE}) of the structural parameters. The incorporation of further isotopologues continues to reduce the δr_e^{SE} for most molecules, until a typical rise at the end of the analyses due to incorporation of the last of the isotopologues. The δr_e^{SE} values, however, remain well below their initial values, leading to the conclusion that more isotopologue data leads to a more precise r_e^{SE} structure. Examination of the structural parameters throughout the analysis provides insight into how well each structural parameter is determined, and further comparison to theoretical structure predictions provides insight into the accuracy of the structures.

INTRODUCTION

Molecular structure can be determined using rotational spectroscopy, *via* the substitution structure (r_s) method or semi-experimental equilibrium structure (r_e^{SE}) method, which rely on the changes to the moments of inertia (and thus the change in the rotational constants and resulting rotational spectra) that occur upon isotopic substitution of the atoms' positions.[1] Rotational spectroscopy allows for highly precise determination of the molecular structure due to the precise and numerous measurements of rotational transitions as compared to other spectroscopy methods.[2] In our group in particular, the union of synthesis and rotational spectroscopy have allowed for a considerable number of isotopologues to be included in the data set used for the structure determination of a molecule.[3-9] Traditionally, studies using the r_e^{SE} structure methodology have often been limited to using only the isotopologues minimally necessary to obtain an r_s structure, specifically the normal isotopologue and all singly substituted isotopologues.[10-11] Although spectroscopic data from additional, multiply substituted isotopologues provides further constraints on atom positions and thereby improves the precision and accuracy of the r_e^{SE} structure, such an approach is not universally employed. The trade-off for this improvement is the increased experimental effort needed to acquire spectroscopic data for additional isotopologues, particularly if they are not observable at natural abundance and require chemical synthesis/isotopic enrichment. Therefore, to inform our choice of the number of additional isotopologues to include in structure determinations, we systematically examine the effect of including isotopologues beyond the minimal set on the r_e^{SE} structure.

COMPUTATIONAL METHODS

The high accuracy and precision of our recent semi-experimental structure determinations derive, in part, from the inclusion of a large number of multiply substituted isotopologues in the data sets.[3-7] This approach contrasts with the Kraitchman analysis for structure determination (r_s substitution structure)[10-13] and other implementations of the semi-experimental structure determination (r_e^{SE})[14-15] that commonly rely on single-atom isotopic substitution is sufficient for determining a molecular structure, the data set of singly substituted isotopologues represents the smallest set that is sufficient to do so.[1] Herein, we refer to a data set consisting of the normal isotopologue and singly substituted isotopologues as the "minimal data set" or the "minimal set". Since the data sets for our structural determinations substantially exceed the "minimal data set", there are opportunities to develop new methods for analyzing and interpreting data.

To assess the impact of the number of isotopologues (N_{iso}) included in a data set used for an r_e^{SE} structure determination, one could simply compare the r_e^{SE} structure obtained using a minimal set of isotopologues to the r_e^{SE} structure obtained using all of the available isotopologues. This comparison, however, does not provide information about how the r_e^{SE} structure changes as a function of N_{iso} or how the incorporation of additional isotopologues impacts the structure. A more informative approach to assess the impact of the number of isotopologues is to determine the r_e^{SE} structural parameters using the minimal set, then sequentially add each isotopologue to the data set, and observe how the r_e^{SE} structural parameters and their statistical uncertainties change. Because the r_e^{SE} structure is a state function of the moments of inertia with respect to the isotopologues in the data set, the order in which the isotopologues are added has no effect on the final r_e^{SE} structure but does determine which intermediate r_e^{SE} structures that are generated. Determining each intermediate r_e^{SE} structure for every permutation of the addition of all

isotopologues would be a rigorous approach, but it is not practical. Not only would it be cumbersome to obtain such an r_e^{SE} analysis,* it is not clear how one would interpret the results. Thus, the analysis method requires a different procedure for selecting which isotopologue should be added to the working set of isotopologues.

We employed an approach where the isotopologue data set is sequentially expanded to include the isotopologue whose inclusion results in the greatest reduction of the statistical uncertainties of the r_e^{SE} parameters. This criterion enables the analysis to probe the change in the r_e^{SE} structure *via* the addition of a single isotopologue. If an isotopologue provides structural information consistent with that already in the data set, adding that isotopologue should have the impact of reducing the overall statistical uncertainty by providing redundant information. If an isotopologue provides structural information that is not consistent with the rest of the data set (due to poor determination of its spectroscopic constants, providing structural information counter to that provided in the current data set, high error in the atomic position due to the location of principal axes, *etc*.), adding that isotopologue may result in the r_e^{SE} structural parameters with larger statistical uncertainty. Because all isotopologues will eventually be added to the r_e^{SE}, the isotopologues that are not consistent with the rest of the data set will be represented by a characteristic increase in the statistical uncertainty at the end of the routine (*vide infra*).

This approach has been implemented as a bash shell script – dubbed *xrefiteration* (because it iteratively utilizes the *xrefit* module of CFOUR) – and has been briefly described in two previous works.[6-7] It is implemented as a bash shell script, which performs the following algorithm (depicted in Figure 1.1):

* Using our recent work on pyridazine (see Chapter 3) as an example, there are 12 additional isotopologues beyond the core set which corresponds to 12! ≈ 479,000,000 permutations and, assuming 0.1 s per *xrefit* execution, ~13,000 processor hours.

1) For the "accepted" set of isotopologues, execute *xrefit* to obtain an initial r_e^{SE} structure. The initial accepted set can be user-defined, but defaults to the "minimal set" as identified by assuming that the first isotopologue in the input file is the normal isotopologue and identifying all isotopologues that differ by single isotopic substitution.
2) For each isotopologue that is not part of the accepted set, execute *xrefit* to obtain an r_e^{SE} structure using the accepted set of isotopologues plus that additional isotopologue.
3) Of the resulting r_e^{SE} structures obtained in step 2, the additional isotopologue that resulted in the lowest statistical uncertainties of the structural parameters is added to the accepted set of isotopologues. To obtain a single metric by which to evaluate the total statistical uncertainty, we calculated the relative (and thus dimensionless) uncertainties of the bond distances [Eq. (1.1)], angles [Eq. (1.2)], and dihedral angles [Eq. (1.3)], and combined the results to give the total relative statistical uncertainty of the r_e^{SE} structure (δr_e^{SE}) in Eq (1.4)

.

$$\delta r_e^{\mathrm{SE}}\left(\mathrm{bonds}\right)=\sqrt{\sum_i\left(\frac{2\sigma_{\mathrm{fit}}\left(R_i\right)}{R_i}\right)^2} \tag{1.1}$$

$$\delta r_e^{\mathrm{SE}}\left(\mathrm{angles}\right)=\sqrt{\sum_i\left(\frac{2\sigma_{\mathrm{fit}}\left(\theta_i\right)}{\theta_i}\right)^2} \tag{1.2}$$

$$\delta r_e^{\mathrm{SE}}\left(\mathrm{dihedrals}\right)=\sqrt{\sum_i\left(\frac{2\sigma_{\mathrm{fit}}\left(\phi_i\right)}{\phi_i}\right)^2} \tag{1.3}$$

$$\delta r_e^{\mathrm{SE}}=\sqrt{\left[\delta r_e^{\mathrm{SE}}\left(\mathrm{bonds}\right)\right]^2+\left[\delta r_e^{\mathrm{SE}}\left(\mathrm{angles}\right)\right]^2+\left[\delta r_e^{\mathrm{SE}}\left(\mathrm{dihedrals}\right)\right]^2} \tag{1.4}$$

4) Repeat steps 2 and 3 until all isotopologues have been incorporated into the accepted set, at which point a final r_e^{SE} structure is calculated by executing *xrefit*.

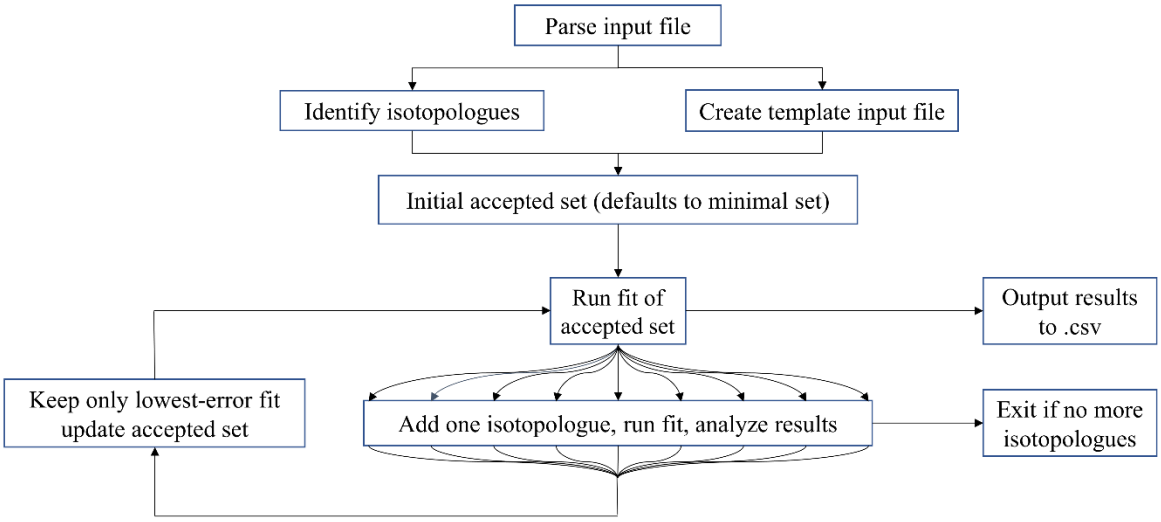

Figure 1.1. Flow chart depicting the *xrefiteration* algorithm.

The routine collects various components of the r_e^{SE} calculations it has performed and provides a summary output file (.csv) for analysis. A detailed explanation of the routine and its options are included in the Supporting Information. The script, example input and output files, a .html report, and the script used to generate the report are included in the supporting information of Ref. 9.

The *xrefiteration* routine has been applied to several r_e^{SE} structure determinations in our group: hydrazoic acid,[8] pyrimidine,[5] pyridazine,[9] thiophene,[7] and thiazole[6] (Figure 1.2). The results of these analyses are summarized here; further details are included in the cited references (excepting that of pyrimidine) and in Chapters 2 and 3 of this thesis.

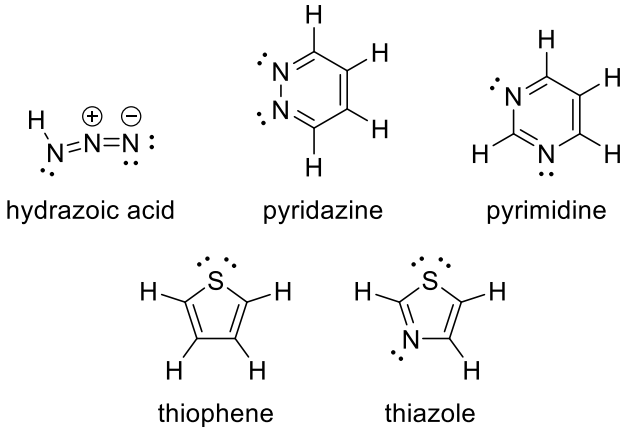

Figure 1.2. Molecules with r_e^{SE} structure determinations analyzed with the *xrefiteration* routine.

RESULTS AND DISCUSSION

To illustrate the nature of the *xrefiteration* algorithm, consider the first iteration of the *xrefiteration* analysis of the pyridazine data set, using the minimal set of isotopologues as the initial accepted set: pyridazine and [3-^{13}C]-, [4-^{13}C]-, [^{15}N]-, [3-^{2}H]-, and [4-^{2}H]-pyridazine. First, the routine executes an initial run using the data from these six isotopologues and analyzes the results, which gives the total δr_e^{SE} of 0.001322 for the minimal set (recall that δr_e^{SE} is a combination of relative – and thus unitless – values).

Second, the algorithm introduces one additional isotopologue to the previous accepted data set and runs *xrefit*; this is repeated for each of the remaining isotopologues. There is a total of eighteen isotopologues of pyridazine for which experimental data was obtained, and since six of these isotopologues were used in the previous (in this case, initial) iteration, a total of twelve isotopologues remain to be tested for acceptance. The data for each of these twelve isotopologues is combined with the previous six isotopologues to create twelve input files, each consisting of a total of seven isotopologues: the accepted set from the previous (initial) iteration and one of the

remaining isotopologues. Then *xrefit* is executed for each of these input files, and the resulting output files are analyzed.

As summarized in Table 1.1, we see that the δr_e^{SE} of the twelve test cases vary up to ~10% with respect to the previous accepted set. Of the twelve r_e^{SE} structures thus generated, we see that the r_e^{SE} structure resulting from the addition of the [3,5-^{2}H] isotopologue to the previous six isotopologues has the lowest total δr_e^{SE} of 0.001180. Therefore, the third step of the algorithm is to select the [3,5-^{2}H] isotopologue for incorporation into the accepted set of isotopologues for the next iteration, which will contain a total of seven isotopologues with eleven remaining. The routine then repeats the above steps until all isotopologues are included in the data set for the r_e^{SE} structure determination.

Table 1.1. The δr_e^{SE} of Test r_e^{SE} Structures in the First Iteration of the *xrefiteration* Analysis of Pyridazine

Isotopologues used to obtain r_e^{SE}	δr_e^{SE} (Total)
normal, [3-^{13}C], [4-^{13}C], [^{15}N], [3-^{2}H], [4-^{2}H][a]	0.001322
normal, [3-^{13}C], [4-^{13}C], [^{15}N], [3-^{2}H], [4-^{2}H], and **[3,4-^{2}H]**	0.001260
normal, [3-^{13}C], [4-^{13}C], [^{15}N], [3-^{2}H], [4-^{2}H], and **[3,5-^{2}H]**[b]	0.001180
normal, [3-^{13}C], [4-^{13}C], [^{15}N], [3-^{2}H], [4-^{2}H], and **[3,6-^{2}H]**	0.001277
normal, [3-^{13}C], [4-^{13}C], [^{15}N], [3-^{2}H], [4-^{2}H], and **[4,5-^{2}H]**	0.001304
normal, [3-^{13}C], [4-^{13}C], [^{15}N], [3-^{2}H], [4-^{2}H], and **[4-^{2}H, 3-^{13}C]**	0.001227
normal, [3-^{13}C], [4-^{13}C], [^{15}N], [3-^{2}H], [4-^{2}H], and **[4-^{2}H, 4-^{13}C]**	0.001303
normal, [3-^{13}C], [4-^{13}C], [^{15}N], [3-^{2}H], [4-^{2}H], and **[4-^{2}H, 5-^{13}C]**	0.001222
normal, [3-^{13}C], [4-^{13}C], [^{15}N], [3-^{2}H], [4-^{2}H], and **[4-^{2}H, 6-^{13}C]**	0.001310
normal, [3-^{13}C], [4-^{13}C], [^{15}N], [3-^{2}H], [4-^{2}H], and **[3,4,5-^{2}H]**	0.001294
normal, [3-^{13}C], [4-^{13}C], [^{15}N], [3-^{2}H], [4-^{2}H], and **[3,4,6-^{2}H]**	0.001412
normal, [3-^{13}C], [4-^{13}C], [^{15}N], [3-^{2}H], [4-^{2}H], and **[3,4,5,6-^{2}H]**	0.001307
normal, [3-^{13}C], [4-^{13}C], [^{15}N], [3-^{2}H], [4-^{2}H], and **[4,5-^{2}H, 4-^{13}C]**	0.001342

[a] The isotopologue data set from the previous iteration is provided for reference.

[b] This isotopologue data set is highlighted to indicate it has the lowest δr_e^{SE} of the structures in the current iteration.

While additional tables like that of Table 1.1 could be created for the remaining iterations, it is easier to visualize the process by plotting the δr_e^{SE} of the test cases against the total number of isotopologues. Such is done for pyrimidine in Figure 1.3. For a particular N_{iso}, the test case with the lowest δr_e^{SE} is also the one that becomes the accepted set for that iteration. Individual isotopologues can also be tracked across test cases, as represented by the lines drawn in the figure. Note that once an isotopologue has been added to the accepted set, there are no further test cases where that isotopologue is being added; this is visualized in the figure as the trace for that isotopologue terminating in the dotted line representing the accepted sets.

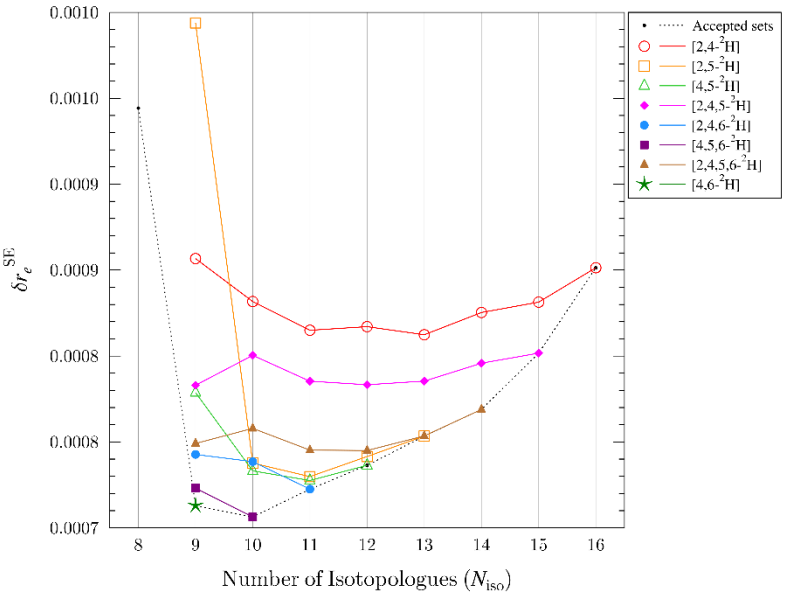

Figure 1.3. Total relative error of all r_e^{SE} structures generated during the *xrefiteration* routine for sixteen isotopologues of pyrimidine, beginning from the minimal set. The dotted line connects the accepted sets of each iteration.

There are some common observations in examining plots like that of Figure 1.3. First, the δr_e^{SE} of the test cases involving a particular isotopologue tend to decrease as N_{iso} increases.

Another tendency is for there to be a clustering of the isotopologue traces, such as those of [2,5-^{2}H]-, [4,5-^{2}H]-, and [2,4,5-^{2}H]-pyrimidine above $N_{iso} = 10$. In that grouping, the δr_e^{SE} of the test cases generated are very similar, suggesting those isotopologues have similar impacts on the precision of the r_e^{SE} structure determination. One feature is represented by the trace of [2,5-^{2}H]-pyrimidine in Figure 1.3, where the inclusion of that isotopologue in the first test case at $N_{iso} = 9$ results in a δr_e^{SE} larger than the initial set, but upon addition of another isotopologue the addition of the [2,5-^{2}H] isotopologue results in a much smaller δr_e^{SE} that is comparable to other test cases. Such behavior is likely due to a poor determination of some structural parameter(s) by the initial set, parameter(s) for which the [2,5-^{2}H] isotopologue data contains the necessary information but disagrees with the value poorly determined by the minimal set. Inclusion of an additional isotopologue serves to bridge that disagreement. Another feature – which is lacking in Figure 1.3 but is common in preliminary analyses – is the presence of an isotopologue trace at significantly higher δr_e^{SE} than the rest, which *might*[*] indicate an issue with the underlying data for that isotopologue: an error in the corrections to the rotational constants, a poor fit of the spectral data, *etc*. Therefore, this graph can be particularly useful for identifying problems in the preliminary analysis of the data set. Finally, there are instances where inclusion of an isotopologue into the accepted set raises the δr_e^{SE} for subsequent test cases of certain other isotopologues. For example, in Figure 1.3, the δr_e^{SE} for the [2,4,5-^{2}H] and [2,4,5,6-^{2}H] isotopologues is larger at $N_{iso} = 10$ than at $N_{iso} = 9$. This suggests that the isotopologue being added in that iteration ([4,6-^{2}H]) contains structural information differing from that provided by those two isotopologues. In principle, there may be a way to extract insights about the relationship of the isotopologues to each other with

[*] See the discussion of the *xrefiteration* analysis of pyridazine in Chapter 3.

respect to the structural information they are providing, but in practice we have not yet developed a rigorous method for extracting such insights.

Throughout the course of the analysis, the *xrefiteration* routine keeps track of the δr_e^{SE}, the contributing components [δr_e^{SE}(bonds), δr_e^{SE}(angles), and δr_e^{SE}(dihedrals)], the values of the structural parameters, and the statistical uncertainties of the fit to the structure parameters. The δr_e^{SE} and its components can be plotted on the same graph, while the parameter values and their uncertainties are best plotted on individual graphs for each parameter. Figure 1.4 displays the δr_e^{SE} and its components across the *xrefiteration* analysis for thiophene and shows a sharp decrease in the δr_e^{SE} as the first few isotopologues beyond the minimal set are added. As more isotopologues are added, δr_e^{SE} continues to decrease and eventually plateaus, until only a couple of isotopologues remain to be included in the accepted set. The addition of these last two isotopologues ([2,3-^{2}H] and [2,4-^{2}H]) increases the δr_e^{SE} but overall, the δr_e^{SE} for the full set of isotopologues is nearly half that of the δr_e^{SE} for the minimal set of isotopologues. The rise in δr_e^{SE} at the end of the *xrefiteration* analysis is typical and can be understood by the nature of the algorithm: in each iteration, the isotopologue that resulted in the lowest δr_e^{SE} was added to the accepted set while isotopologues that resulted in higher δr_e^{SE} were carried over to the next iteration. By the end of the analysis, the isotopologue(s) that remain consistently had higher δr_e^{SE} when included in the data set, so when they are finally included, the δr_e^{SE} increases.

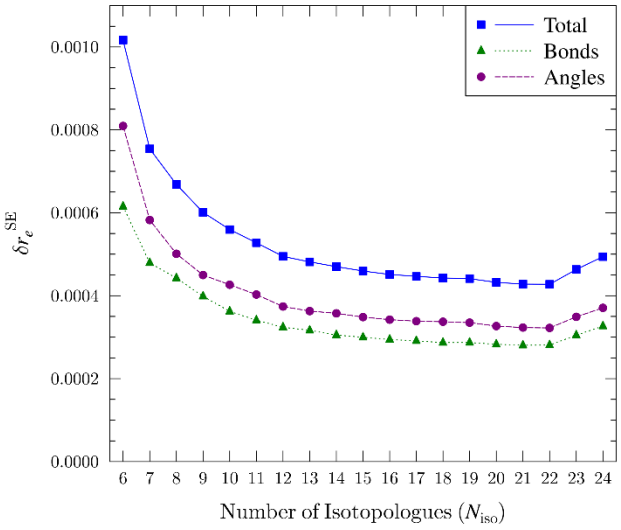

N_{iso}	Isotopologue Added
6	Minimal Set
7	[2,3,5-^{2}H, ^{34}S]
8	[2,5-^{2}H, 2-^{13}C]
9	[2,5-^{2}H, ^{34}S]
10	[2,5-^{2}H, 3-^{13}C]
11	[2,3,4,5-^{2}H]
12	[3-^{2}H, 4-^{13}C]
13	[2,3,5-^{2}H]
14	[3-^{2}H, ^{34}S]
15	[2,5-^{2}H]
16	[2,3,4-^{2}H]
17	[2-^{2}H, ^{34}S]
18	[^{33}S]
19	[3-^{2}H, 5-^{13}C]
20	[3-^{2}H, 3-^{13}C]
21	[3-^{2}H, 2-^{13}C]
22	[3,4-^{2}H]
23	[2,3-^{2}H]
24	[2,4-^{2}H]

Figure 1.4. Plot of δr_e^{SE} as a function of the number of isotopologues (N_{iso}) incorporated into the structure determination data set for thiophene. The total relative statistical uncertainty (δr_e^{SE}, blue squares), the relative statistical uncertainty in the bond distances (green triangles), and the relative statistical uncertainty in the angles (purple circles) are presented. The "Minimal Set" is composed of the normal and [2-^{13}C], [3-^{13}C], [^{34}S], [2-^{2}H], [3-^{2}H] isotopologues of thiophene.

As shown in Figure 1.5, the *xrefiteration* analyses for pyridazine, pyrimidine, and thiazole share similar characteristics with that of thiophene. The δr_e^{SE} for all molecules generally decreases as N_{iso} increases and is especially pronounced for the first isotopologue addition beyond the minimal set of single isotopic substitutions. As additional isotopologues are incorporated into the data set, δr_e^{SE} continues to decrease for hydrazoic acid, thiophene, and thiazole, until a slight uptick at the end for thiophene and thiazole. Pyridazine and pyrimidine, however, plateau shortly after the initial sharp decrease, then continue to rise slightly through the rest of the *xrefiteration* analysis. In this progression, pyrimidine increases more than pyridazine, until the addition of the final isotopologue to the pyridazine data set. (The origin of this increase in δr_e^{SE} of pyridazine is discussed in detail in Chapter 3 of this thesis.) Overall, the *xrefiteration* analysis of these

molecules demonstrates that inclusion of a few isotopologues beyond the minimal set has an immediate and significant effect, and addition of further isotopologues generally continues to reduce the δr_e^{SE}.

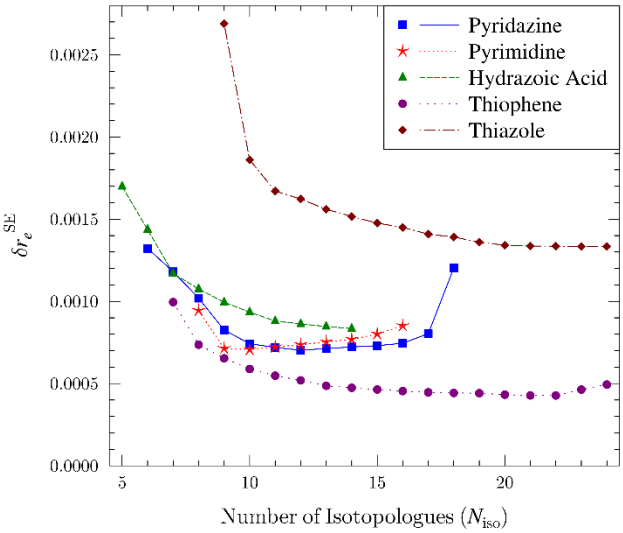

Figure 1.5. Comparison of total relative statistical uncertainty (δr_e^{SE}) as additional isotopologues are included in the data set for the r_e^{SE} structure determinations of hydrazoic acid, pyrimidine, pyridazine, thiophene, and thiazole, beginning from each of their respective minimal set of isotopologues.

Additional insights into the r_e^{SE} structure determination and the isotopologue data set can be found by examining the structural parameters of the r_e^{SE} structures obtained in the *xrefiteration* analysis. Figure 1.6 presents the values and statistical uncertainties of the parameters of thiazole throughout the *xrefiteration* analysis in comparison to the best theoretical estimate (BTE)[5-7] values and demonstrates a variety of behaviors across the many structural parameters. Some parameters show little change in their values or uncertainties across the *xrefiteration* analysis ($R_{C4\text{-}H}$, $\theta_{C4\text{-}C5\text{-}S}$, $\theta_{C5\text{-}C4\text{-}N}$ and $\theta_{C2\text{-}S\text{-}C5}$), strongly suggesting that these parameters are well-determined even while

using the initial set of isotopologues. The uncertainties of these parameters contribute little to the change in δr_e^{SE} for thiazole shown in Figure 1.6. Most parameters display moderate changes but appear to converge *i.e.*, remain consistent in value and uncertainty, by the end of the analysis ($R_{C5\text{-}H}$, $R_{C4\text{-}C5}$, $R_{C4\text{-}N}$, $R_{C5\text{-}S}$, $R_{C2\text{-}S}$, $\theta_{C4\text{-}C5\text{-}H}$, and $\theta_{C5\text{-}C4\text{-}H}$), demonstrating the importance of including many isotopologues in the r_e^{SE} structure determination. The uncertainties of these parameters are largely responsible for the steady decrease in the δr_e^{SE} in the later parts of the *xrefiteration* analysis. Several parameters have immediate and significant changes to their values and uncertainties that brings them into better agreement with the BTE values ($R_{C2\text{-}H}$ and $\theta_{S\text{-}C2\text{-}H}$), demonstrating how impactful just a few additional isotopologues beyond the minimal set can be for the r_e^{SE} structure determination. The uncertainties of these parameters are largely responsible for the sharp decrease in δr_e^{SE} that occurs at the beginning of the *xrefiteration* analysis.

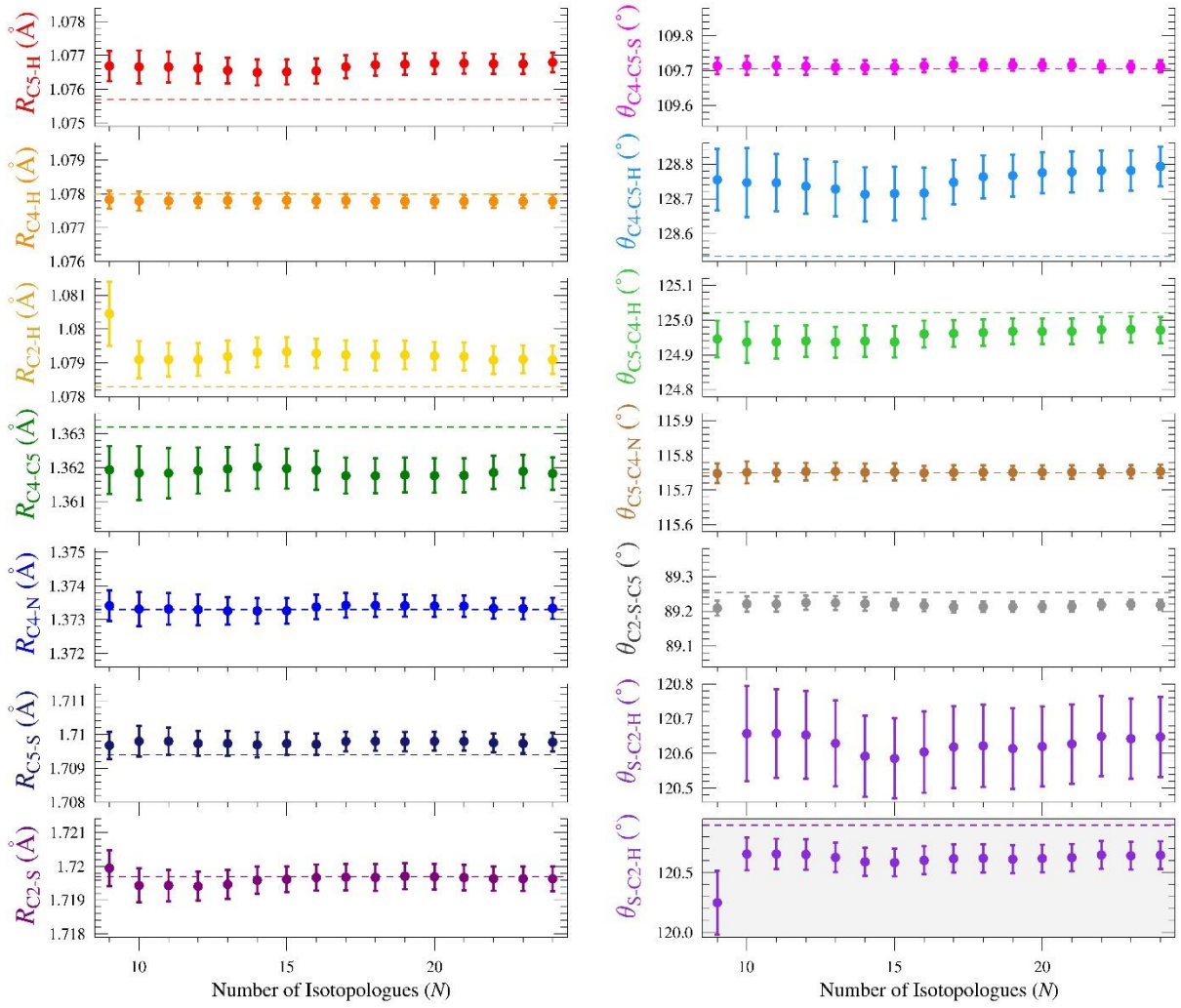

Figure 1.6. Plots of structural parameters of thiazole as a function of the number of isotopologues (N_{iso}) and their 2σ uncertainties, with consistent scales for each distance (0.0035 Å) and each angle (0.34°). The dashed line in each plot is the best theoretical estimate (BTE) value calculated for that parameter. A plot of $\theta_{S\text{-}C2\text{-}H}$ is additionally provided on a separate *y*-axis scale (gray background) that enables visualization of all data points and corresponding error bars. The isotopologue ordering is given in Table 1.2 in the Supporting Information.

The power in examining the structural parameters throughout the *xrefiteration* analysis lies in the comparison to the BTE values predicted for the structure. As shown in Figure 1.6, at the beginning of the *xrefiteration* analysis $R_{C2\text{-}H}$ and $\theta_{S\text{-}C2\text{-}H}$ have the largest statistical uncertainties and disagreement with the BTE values. The inclusion of an additional isotopologue reduces the uncertainties in these parameters by a factor of two and reduces the disagreement with the BTE values by more than a factor of two. Considering the set of parameters that are not in agreement with the BTE values ($R_{C5\text{-}H}$, $R_{C2\text{-}H}$, $\theta_{C4\text{-}C5\text{-}H}$, $\theta_{C5\text{-}C4\text{-}H}$, $\theta_{C2\text{-}S\text{-}C5}$, and $\theta_{S\text{-}C2\text{-}H}$) reveals atoms C2 and C5 as common factors, which is notable since these atoms lie very close to the *b* inertial axis of thiazole and historically their positions are the most difficult to determine.[16]

CONCLUSIONS

A novel routine, *xrefiteration*, was developed to examine the impact of additional isotopologues on r_e^{SE} structure determinations. The routine begins with the r_e^{SE} structure determination of an initial set of isotopologues (often the minimal set necessary for an r_s structure determination) and iteratively adds the remaining isotopologues to the data set until the full r_e^{SE} structure is obtained. The order in which the isotopologues are added is determined by selecting the isotopologue whose inclusion results in the lowest total relative uncertainty (δr_e^{SE}). Typically, the inclusion of additional isotopologues is found to immediately and significantly decrease δr_e^{SE} and continue to decrease – though with diminishing returns – as more isotopologues are added, until a slight increase at the end of the analysis. A large increase in the δr_e^{SE} due to the inclusion of an isotopologue may indicate the underlying experimental or computational data is of poor quality, but this is merely a measure of the precision – not the accuracy – of the r_e^{SE} structure.

We found that tracking the values of the structural parameters throughout the *xrefiteration* analysis provided more insight into the structure determination of the molecule. A structural parameter can be said to be well-determined when the inclusion of additional isotopologues has little effect on the values of the parameter with respect to the magnitude of the uncertainties. Furthermore, good agreement between the structural parameter of the r_e^{SE} structure and that of a high-level theoretical calculation strongly suggests such a parameter is also accurate. Of the molecules we've examined thus far, application of this analysis reveals that some molecules *e.g.*, pyridazine, are well-determined starting from the minimal set of isotopologues while other molecules *e.g.*, thiophene and thiazole, are still not well-determined even after including all available isotopologues. Being able to determine how many isotopologues (and which) are needed on an *a priori* basis thus remains an open challenge and the *xrefiteration* routine provides the foundation for addressing it.

ACKNOWLEDGEMENTS

We gratefully acknowledge the National Science Foundation for support of this project (CHE-1664912, CHE-1954270).

REFERENCES

1. Puzzarini, C.; Barone, V., Diving for Accurate Structures in the Ocean of Molecular Systems with the Help of Spectroscopy and Quantum Chemistry. *Acc. Chem. Res.* **2018,** *51* (2), 548-556.

2. Gordy, W.; Cook, R., *Microwave Molecular Spectra*. 3rd. ed.; Wiley Interscience: New York, 1984; Vol. XVIII.

3. Esselman, B. J.; Amberger, B. K.; Shutter, J. D.; Daane, M. A.; Stanton, J. F.; Woods, R. C.; McMahon, R. J., Rotational Spectroscopy of Pyridazine and its Isotopologs from 235-360 GHz: Equilibrium Structure and Vibrational Satellites. *J. Chem. Phys.* **2013,** *139*, 224304.

4. Amberger, B. K.; Esselman, B. J.; Stanton, J. F.; Woods, R. C.; McMahon, R. J., Precise Equilibrium Structure Determination of Hydrazoic Acid (HN_3) by Millimeter-wave Spectroscopy. *J. Chem. Phys.* **2015,** *143* (10), 104310.

5. Heim, Z. N.; Amberger, B. K.; Esselman, B. J.; Stanton, J. F.; Woods, R. C.; McMahon, R. J., Molecular structure determination: Equilibrium structure of pyrimidine (*m*-$C_4H_4N_2$) from rotational spectroscopy (r_e^{SE}) and high-level ab initio calculation (r_e) agree within the uncertainty of experimental measurement. *J. Chem. Phys.* **2020,** *152* (10), 104303.

6. Esselman, B. J.; Zdanovskaia, M. A.; Owen, A. N.; Stanton, J. F.; Woods, R. C.; McMahon, R. J., Precise Equilibrium Structure Determination of Thiazole (C_3H_3NS) from Twenty-Four Isotopologues. *J. Chem. Phys.* **2021,** *155*, 054302.

7. Orr, V. L.; Ichikawa, Y.; Patel, A. R.; Kougias, S. M.; Kobayashi, K.; Stanton, J. F.; Esselman, B. J.; Woods, R. C.; McMahon, R. J., Precise Equilibrium Structure Determination of Thiophene (C_4H_4S) by Rotational Spectroscopy – Structure of a Five-Membered Heterocycle Containing a Third-Row Atom. *J. Chem. Phys.* **2021,** *154*, 244310.

8. Owen, A. N.; Sahool, N. P.; Esselman, B. J.; Stanton, J. F.; Woods, R. C.; McMahon, R. J., Improved Structure Determination of Hydrazoic Acid (HN_3). *Manuscript in Preparation* **2021**.

9. Owen, A. N.; Zdanovskaia, M. A.; Esselman, B. J.; Stanton, J. F.; Woods, R. C.; McMahon, R. J., Semi-Experimental Equilibrium (r_e^{SE}) and Theoretical Structures of Pyridazine (*o*-$C_4H_4N_2$). *J. Phys. Chem. A* **2021,** *125* (36), 7976-7987.

10. Costain, C. C., Determination of Molecular Structures from Ground State Rotational Constants. *J. Chem. Phys.* **1958,** *29* (4), 864-874.

11. Kraitchman, J., Determination of Molecular Structure from Microwave Spectroscopic Data. *Am. J. Phys.* **1953,** *21* (1), 17-24.

12. Rudolph, H. D., Extending Kraitchman's equations. *J. Mol. Spectrosc.* **1981,** *89* (2), 430-439.

13. Pierce, L., Note on the use of ground-state rotational constants in the determination of molecular structures. *J. Mol. Spectrosc.* **1959,** *3* (1), 575-580.

14. Demaison, J.; Vogt, N.; Ksenafontov, D. N., Accuracy of semiexperimental equilibrium structures: Sulfine as an example. *J. Mol. Struct.* **2020,** *1206*, 127676.

15. Puzzarini, C.; Bloino, J.; Tasinato, N.; Barone, V., Accuracy and Interpretability: The Devil and the Holy Grail. New Routes across Old Boundaries in Computational Spectroscopy. *Chem. Rev.* **2019,** *119* (13), 8131-8191.

16. Nygaard, L.; Asmussen, E.; Høg, J. H.; Maheshwari, R. C.; Nielsen, C. H.; Petersen, I. B.; Rastrup-Andersen, J.; Sørensen, G. O., Microwave spectra of isotopic thiazoles. Molecular structure and 14N quadrupole coupling constants of thiazole. *J. Mol. Struct.* **1971,** *8* (1), 225-233.

SUPPORTING INFORMATION

Table of Contents

Table 1.2. Order of Addition for Isotopologues of Thiophene in the *xrefiteration* Analysis of Thiazole

N_{iso}	Isotopologue Added
9	Initial set normal, [^{34}S], [2-^{13}C], [3-^{15}N], [4-^{13}C], [5-^{13}C], [2-^{2}H], [4-^{2}H], [5-^{2}H]
10	[2,4,5-^{2}H]
11	[2,5-^{2}H, 4-^{13}C]
12	[2-^{2}H, ^{15}N]
13	[2-^{2}H, 5-^{13}C]
14	[2-^{2}H, 2-^{13}C]
15	[2-^{2}H, ^{34}S]
16	[2-^{2}H, 4-^{13}C]
17	[2,5-^{2}H, ^{34}S]
18	[2,5-^{2}H, 5-^{13}C]
19	[2,5-^{2}H, 2-^{13}C]
20	[2,5-^{2}H]
21	[2-^{2}H, ^{33}S]
22	[2,5-^{2}H, ^{15}N]
23	[^{33}S]
24	[2,5-^{2}H, ^{33}S]

xrefiteration Usage Guide

Requirements

- bash

  The *xrefiteration* script was written for use on the Phoenix Cluster at the UW-Madison Department of Chemistry HPC Center (https://hpc.chem.wisc.edu), operating GNU bash, version 4.2.46(2)-release (x86_64-redhat-linux-gnu). The script has not been tested on any other system.

- CFOUR (http://www.cfour.de)

- Location of CFOUR *xrefit* added to PATH

  Execute the following command before use,

  ```
  export PATH=/full/path/to/your/CFOUR/bin:$PATH
  ```

  or add that line to the `.bash_profile` file in your home directory. You can check this was done correctly by executing `which xrefit` and the correct path should appear.

- Script saved as `xrefiteration` with execute permissions.

  While the script doesn't have to be saved as *xrefiteration*, it is recommended since this guide and the script's help text refers to the script by that name.

  The command `chmod +x xrefiteration` should allow the script to run.

xrefiteration input file

The *xrefiteration* input file is the same as the standard *xrefit* INPUT file, with two exceptions: (a) specific parameter labels, and (b) additional isotopologue labels.

a) When defining the ZMAT, the parameter labels must begin with 'R' if it is a bond, 'A' if it is an angle, and 'D' if it is a dihedral angle. The script uses the parameter labels to identify which of the parameters being optimized by xrefit are bonds, angles, and dihedral angles, in order to correctly calculate the δr_e^{SE} for each type of parameter.

b) When providing the atomic numbers for the isotopologues, an additional label (`iso###`) is added after the last atomic number to specify which isotopologue that is. This is necessary for the script to keep track of the individual isotopologues and report the results properly, as well as for utilizing options involving specific isotopologues (*vide infra*).

To understand the changes, compare the pyridazine *xrefiteration* input file provided (pyridazine_xrefiteration_input.txt) against that of the example *xrefit* INPUT file (pyridazine_example_xrefit_input.txt), which is what would normally have been used for obtaining the full r_e^{SE} structure determination of pyridazine.

Running xrefiteration

Once the above requirements have been satisfied and the input file has been prepared, xrefiteration can be run using `xrefiteration inputfilename`. Status text will be printed to the screen as the script runs to monitor the progress. The script can be aborted at any time using the Ctrl+C command in bash.

For an example, here is the output for running the provided pyridazine_xrefiteration_input.txt.

```
$ xrefiteration pyridazine_xrefiteration_input.txt
Fitting A B & C axes.
There will be 12 runs.
RUN000 uses isotopologues 001 002 003 004 005 006
RUN001 uses isotopologues 001 002 003 004 005 006 008
RUN002 uses isotopologues 001 002 003 004 005 006 008 019
RUN003 uses isotopologues 001 002 003 004 005 006 008 019 010
RUN004 uses isotopologues 001 002 003 004 005 006 008 019 010 017
RUN005 uses isotopologues 001 002 003 004 005 006 008 019 010 017 027
RUN006 uses isotopologues 001 002 003 004 005 006 008 019 010 017 027 023
RUN007 uses isotopologues 001 002 003 004 005 006 008 019 010 017 027 023
018
RUN008 uses isotopologues 001 002 003 004 005 006 008 019 010 017 027 023
018 009
RUN009 uses isotopologues 001 002 003 004 005 006 008 019 010 017 027 023
018 009 025
RUN010 uses isotopologues 001 002 003 004 005 006 008 019 010 017 027 023
018 009 025 020
RUN011 uses isotopologues 001 002 003 004 005 006 008 019 010 017 027 023
018 009 025 020 024
RUN012 uses isotopologues 001 002 003 004 005 006 008 019 010 017 027 023
018 009 025 020 024 007
$
```

The isotopologues listed represent the accepted set being used in the current iteration (RUN). The isotopologues used in RUN000 are the initial set, which in this case defaulted to the minimal set, while the last RUN uses all provided isotopologues, representing the full data set.

A variety of files are generated by the execution of the script:

```
$ ls
fort.16
INPUT
pyridazine_xrefiteration_input-allruns.csv
pyridazine_xrefiteration_input_isotopologuesmasseslist.txt
pyridazine_xrefiteration_input-results.csv
pyridazine_xrefiteration_input_RUN000.out
pyridazine_xrefiteration_input_RUN001.out
pyridazine_xrefiteration_input_RUN002.out
pyridazine_xrefiteration_input_RUN003.out
pyridazine_xrefiteration_input_RUN004.out
pyridazine_xrefiteration_input_RUN005.out
pyridazine_xrefiteration_input_RUN006.out
pyridazine_xrefiteration_input_RUN007.out
pyridazine_xrefiteration_input_RUN008.out
pyridazine_xrefiteration_input_RUN009.out
pyridazine_xrefiteration_input_RUN010.out
pyridazine_xrefiteration_input_RUN011.out
pyridazine_xrefiteration_input_RUN012.out
pyridazine_xrefiteration_input.template
pyridazine_xrefiteration_input.txt
VMLSYM
$
```

As *xrefiteration* progresses through each iteration, it collects the parameter values and fit errors in the "-allruns.csv" file, along with the calculated δr_e^{SE} of each type, noting which isotopologues were included in the data set and which was most recently incorporated. The results of the r_e^{SE} calculated after inclusion of the next isotopologue are collected in the "-results.csv" file and the corresponding *xrefit* output is kept, suffixed with "_RUN###.out". Therefore, the last "_RUN###.out" is the *xrefit* output for using all provided isotopologues, while the first ("_RUN000.out") is the *xrefit* output for the initial set of isotopologues.

NOTE: the script appends the results to the .csv files, so rerunning the same input filename will place the results at the end of the .csv files, not the top, and will not replace the files. The script will, however, replace any "_RUN###.out" files of the same name.

The ".template" and "_isotopologuesmasseslist.txt" files are generated by *xrefiteration* based on the input you provided and is used to generate all *xrefit* INPUT files that are executed throughout the routine. The "fort.16", "INPUT", and "VMLSYM" files are left over from executing *xrefit*. These files can be discarded once the routine has finished.

Help text

Help text for the xrefiteration script is built in and is printed upon entering the command `xrefiteration` or `xrefiteration --help` and will also display if the script doesn't understand the options (*vide infra*) being provided.

```
$ xrefiteration
```

OR

```
$ xrefiteration --help
```

prints

```
Usage: xrefiteration arguments filename

Optional arguments:
-a    Runs full analysis on initial set of isotopologues that the user is
      prompted to provide as a space-delimited list of the iso numbers,
      e.g. "1 2 5 9".
-b    Runs xrefit for a custom combination of isotopologues, without
      running the full analysis, using list provided by the user, e.g. "1
      2 5 9".
-c    Keeps the outputs of all xrefit runs for further analysis by the
      user.
-d    Runs full analysis allowing only the specified axes to be fit. User
      will be prompted to enter the axes, e.g. "a C" fits A & C axes only
```

```
      (order & case insensitive). Default is to fit all three A, B, & C
      axes.
-e    Runs xrefit for all single "knockouts" of the full data set. That
      is, the data for one isotopologue is excluded from the full data
      set and xrefit executed. This is repeated for all isotopologues in
      the data set, with results written to "-knockouts.csv"
-f    Runs an additional "correlation" analysis of the isotopologues not
      part of the initial accepted set by running all pair-wise additions
      to the accepted set. Saved to "-pairs.csv"   !!!Experimental!!!
-g    Prompts the user to select an alternate metric to use as the metric
      for xrefiteration analysis.  A numbered list will be printed and
      the user needs to enter the number corresponding to the desired
      metric.
-h    Isotopologues are weighted by the values provided in the input file.
      This option is incompatible with option (-d).
--help      Prints this help text.

This script automatically runs and analyzes CFOUR xrefit program for the
user-provided file such that beginning from the initial set of
isotopologues, the isotopologue that lowers the error of the least-squares
fit the most is added to the next run of xrefit, until all isotopologues
have been added. The outputs of every xrefit calculation are collected in
the "-allruns.csv" file, while the final summary of the xrefiteration
analysis is in the "-results.csv" file for convenient analysis in Excel.
The xrefit output file form each iteration of the analysis is kept as
"_RUN###.out"

Note: the default initial set is given by whichever isotopologue is listed
first, plus any isotopologues that differ by only 1 substitution from the
first.

Note: the errors (uncertainties) provided by xrefit are 1 sigma.
```

Optional arguments

The following provides additional information regarding the optional arguments. If an unrecognized option is specified by the user, the script will first print `!!! Unrecognized Option _ !!!` followed by the help text, where the underscore will be the option the user provided.

`-a  Runs full analysis on initial set of isotopologues that the user is prompted to provide as a space-delimited list of the iso numbers, e.g. "1 2 5 9".`

This argument allows the user to specify which isotopologues they would like to use for the initial set. The default is to use whichever isotopologue is listed first in the input file, plus any additional isotopologues that differ by a single isotopic substitution. In some cases, however, this may not be ideal. For example, if the molecule contains a sulfur atom and the ^{33}S and ^{34}S singly substituted isotopologues are included in the data set, the routine will include both isotopologues by default in the initial set, even though only one of them is required to obtain a substitution structure. If the user provides five or fewer isotopologues, they will be asked to confirm if this was desired.

`-b  Runs xrefit for a custom combination of isotopologues, without running the full analysis, using list provided by the user.`

This argument allows the user to run *xrefit* for a specific combination of isotopologues using the *xrefiteration* input file, instead of manually editing the *xrefit* INPUT. The results will also be appended to the .csv files, allowing the user to run multiple custom combinations while keeping the results centralized. The *xrefit* output files are also saved as ".custom######" files and will not be replaced by subsequent executions of *xrefiteration*.

`-c  Keeps the outputs of all xrefit runs for further analysis by the user.`

The default is for *xrefiteration* to remove the extra *xrefit* outputs that were generated during each iterations' test of which isotopologue addition lowers the δr_e^{SE} the most. The user can use this option to prevent that.

```
-d    Runs full analysis allowing only the specified axes to be fit. User will
      be prompted to enter the axes, e.g. "a C" fits A & C axes only (order &
      case insensitive). Default is to fit all three A, B, & C axes.
```

This argument will change the weighting of the axes in the *xrefit* inputs generated. If the axis is being fit, its weight is set to one and if not, its weight is set to zero, for all isotopologues in the input file.

```
-e    Runs xrefit for all single "knockouts" of the full data set. That is, the
      data for one isotopologue is excluded from the full data set and xrefit
      executed. This is repeated for all isotopologues in the data set, with
      results written to "-knockouts.csv"
```

This option executes an additional analysis, where all but one isotopologue is included in the data set for r_e^{SE} structure determination in *xrefit*. The results of this should allow the user to identify which isotopologues have the largest impact on individual structural parameters or on the structure as a whole.

```
-f    Runs an additional "correlation" analysis of the isotopologues not part
      of the initial accepted set by running all pair-wise additions to the
      accepted set. Saved to "-pairs.csv"   !!!Experimental!!!
```

This is an experimental analysis that can be executed during the *xrefiteration* routine. If selected, this will run all combinations of the initial accepted set with one and with two additional isotopologues included and output the results to the specified .csv file.

`-g  Prompts the user to select an alternate metric to use as the metric for xrefiteration analysis. A numbered list will be printed and the user needs to enter the number corresponding to the desired metric.`

This option allows the user to change the metric that drives the *xrefiteration* algorithm. By default, the algorithm uses the Total Relative Error (δr_e^{SE}) to select which isotopologue should be used next to expand the data set. Using this option, the user can select the Bonds' Relative Error, Angles' Relative Error, or Dihedrals' Relative Error, as well the error corresponding to any of the Z-matrix parameters being fit by *xrefit*. A numbered list of the available metrics will be printed to the screen, and the user needs to enter the number corresponding to the desired metric. The *xrefiteration* analysis, and any other options specified, will then run using this desired metric.

`-h  Isotopologues are weighted by the values provided in the input file. This option is incompatible with option (-d).`

By default, *xrefiteration* fits all axes [or those selected using option (-d)] equally at a value of 1, ignoring any weights provided by the user in the original input file. Using this option tells the script to use the weights provided in the original input file, allowing the user to provide alternative weights. The *xrefiteration* analysis, and any other options specified, will then run using the provided weights of each isotopologue. This option is particularly useful for handling a molecule with high symmetry and redundant rotational constants, but which may change upon isotopic substitution. As noted, this option is incompatible with option (-d) and will result in an error message, asking the user to select either (-d) or (-h).

Chapter 2: The Semi-Experimental and Theoretical Structures of Hydrazoic Acid

Previously published within:

Andrew N. Owen, Nitai P. Sahoo, Brian J. Esselman, John F. Stanton, R. Claude Woods, Robert J. McMahon, Semi-experimental equilibrium (r_e^{SE}) and theoretical structures of hydrazoic acid (HN_3). *Journal of Chemical Physics.* **2022**, *157* (3), 034303. https://doi.org/10.1063/5.0101064

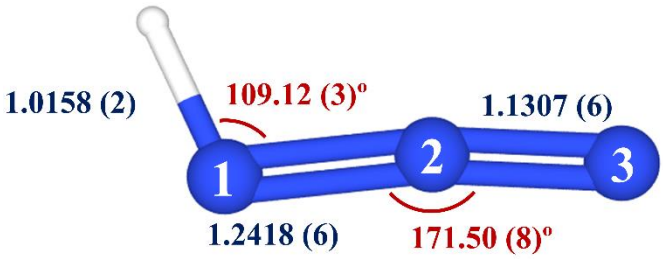

ABSTRACT

Hydrazoic acid (HN_3) is used as a case study for investigating the accuracy and precision by which a molecular structure – specifically, a semi-experimental equilibrium structure (r_e^{SE}) – may be determined using current state-of-the-art methodology. The influence of the theoretical corrections for effects of vibration-rotation coupling and electron-mass distribution that are employed in the analysis is explored in detail. The small size of HN_3 allowed us to deploy considerable computational resources to probe the basis-set dependence of these corrections using a series of CCSD(T) calculations with cc-pCV*X*Z (*X* = D, T, Q, 5) basis sets. We extrapolated the resulting corrections to the complete basis set (CBS) limit to obtain CCSD(T)/CBS corrections, which were used in a subsequent r_e^{SE} structure determination. The r_e^{SE} parameters obtained using the CCSD(T)/cc-pCV5Z corrections are nearly identical to those obtained using the CCSD(T)/CBS corrections, with uncertainties in the bond distances and angles of less than 0.0006 Å and 0.08°, respectively. The previously obtained r_e^{SE} structure using CCSD(T)/ANO2 agrees with that using CCSD(T)/cc-pCV5Z to within 0.00008 Å and 0.016° for bond distances and angles, respectively, and with only 25% larger uncertainties, validating the idea that r_e^{SE} structure determinations can be carried out with significantly smaller basis sets than those needed for similarly accurate, strictly *ab initio* determinations. Although the purely computational r_e structural parameters (CCSD(T)/cc-pCV6Z) fall outside of the statistical uncertainties (2σ) of the corresponding r_e^{SE} structural parameters, the discrepancy is rectified by applying corrections to address the theoretical limitations of the CCSD(T)/cc-pCV6Z geometry with respect to basis set, electron correlation, relativity, and the Born-Oppenheimer approximation, thereby supporting the contention that the semi-experimental approach is both an accurate and vastly more efficient method for structure determinations than is brute-force computation.

INTRODUCTION

The recent theoretical and semi-experimental equilibrium structure determinations of pyrimidine,[1] thiophene,[2] thiazole,[3] and pyridazine[4] set an impressive standard for the agreement that is possible between semi-experimental (r_e^{SE}) and theoretical (r_e) equilibrium structures. Following the work on these larger aromatic systems,[1] we were interested in revisiting our previous work[5] on hydrazoic acid (HN_3) to determine how accurately the r_e^{SE} and r_e parameters could be determined for a small molecule by pushing the limits of computation. From both the experimental and theoretical points of view, HN_3 (Figure 2.1) is nearly an ideal candidate for this type of investigation. On the experimental side, HN_3 is a small molecule that possesses a moderate dipole with both *a*- and *b*-axis components, producing intense rotational transitions across the microwave and millimeter-wave frequency range. It is easily synthesized from sodium azide and aqueous acidic solution, allowing for convenient isotopologue generation.[5] With only four atoms, rotational constants of 14 isotopologues (of 16 possible stable isotopologues) have been observed, providing 28 independent moments of inertia to determine its five independent structural parameters. One potential complication in the structure determination, however, is the presence of coupling between the ground vibrational state and low-lying, vibrationally excited states.[5-6] On the theoretical side, the electronic structure calculations involve only 22 electrons (including core electrons), allowing for fast computations of the geometry optimization and anharmonic vibrational frequencies, even when utilizing sophisticated treatments for electron correlation and larger basis sets. For these reasons, HN_3 can be used as a case study to probe the limits of structure determination for asymmetric top molecules.

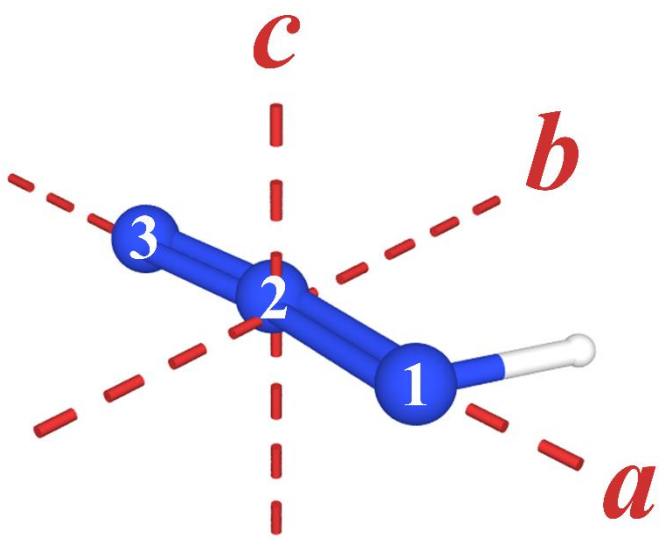

Figure 2.1. Hydrazoic acid (HN_3, C_s, μ_a = 0.837 D, μ_b = 1.48 D, and κ = −0.999) with principal axes and atom numbering.

The nearly linear arrangement of the nitrogen atoms in hydrazoic acid was established in the early 20th century, as well as the substantial deviation of the hydrogen atom from the axis of the nitrogen atoms.[7-9] Substitution structures refined the bond distances and the terminal N–N–H angle, but the position of the central nitrogen atom remained poorly determined,[10-14] and thus the angle could only be estimated.[15] The crystal structure of hydrazoic acid, first reported by Evers *et al.*,[16] revealed the bent nitrogen chain (N–N–N angle 172.8°) in the solid state.[17] The first complete gas phase structure determination of hydrazoic acid was the recent semi-experimental substitution structure (r_e^{SE}) obtained using the rotational spectra of 14 isotopologues.[5] That work included isotopic substitutions of the central nitrogen atom for the first time and confirmed the N–N–N angle.

Computational investigations of HN_3 have consistently supported the slight bend of the nitrogen-atom chain.[5, 16, 18-20] Amberger *et al.* reported a high-level computational study involving coupled-cluster theory with single, double, and perturbative triple excitations [CCSD(T)] and the

cc-pCV5Z basis,* which predicted bond distances and angles to within 0.0012 Å and 0.25°, respectively, of the r_e^{SE} structure determined therein.[5] While the agreement between the theoretical and r_e^{SE} structures published in that work was indeed quite good, improvements in our implementation of the r_e^{SE} structure analysis and those possible in the theoretical treatments of the equilibrium structure suggest even better agreement could be achieved.

METHODS

Rotational Spectroscopy

The average "determinable rotational constants" (A_0'', B_0'', and C_0'')[21] for 14 isotopologues of HN_3 (determined from the spectroscopic constants in both A- and S-reduced Hamiltonians, I^r representation), were taken directly from the supplemental material of our previous work.[5] These determinable constants are free of the effects of centrifugal distortion and are independent of the choice of A or S reduction used in the least-squares fitting. Details of the synthesis of the isotopologues, the instrumentation, the spectra, and further analyses are reported in the earlier study. Due to complications arising from the coupling between the ground state and low-lying bending fundamentals ν_5 and ν_6, care must be taken to ensure that the rotational constants used in the structure determination are unperturbed. The rotational constants determined in our previous work[5] (which did not address the *c*-type Coriolis and *a*-type Coriolis couplings between the ground state and fundamentals ν_5 and ν_6, respectively) and determined in a more recent work[6] (which contains additional ground-state transitions and addresses the coupling of ν_5 and ν_6) are provided

* The CCSD(T)/cc-pCV5Z optimized parameters of hydrazoic acid reported in Table VI and Figure 3 of Amberger *et al.*, 2015, are incorrect; specifically, the parameters are inconsistent with the CCSD(T)/cc-pCV5Z optimization output file in the supplementary material of that same work. The values that are present in the output file of the supplementary material were replicated in this work, and all references and comparisons herein involving the previous CCSD(T)/cc-pCV5Z structure refer to these correct CCSD(T)/cc-pCV5Z values.

in Table 2.1. Neither of these least-squares fits adequately addresses the coupling present in the system, as evidenced by the relatively poor agreement between the computed centrifugal distortion constants and their corresponding experimentally determined values. In particular, the *K*-dependent computed and experimental centrifugal distortion constants (Δ_K, δ_K, Φ_K, and ϕ_K) do not have the expected level of agreement, making it likely that both fits have allowed Coriolis coupling to be absorbed into those constants. A collaborative effort is underway to address the unresolved coupling issues of the ground and vibrationally excited states of HN_3 and DN3. Fortunately, the close agreement of the rotational constants between the two previous published least-squares fits[5-6] provides confidence that the ground state rotational constants can be used in a structure determination without addressing the coupling. While addressing the Coriolis-coupling in different ways, the two least-squares fits obtained rotational constants that differ only in the sixth significant figure. Furthermore, the determinable constants from the A- or an S-reduction least-squares fit agree to within a few kHz. Confidence in the rotational constants derived from this agreement is critically important because the interactions between the ground state and vibrationally excited states for many isotopologues observed at natural abundance cannot be addressed in a practical manner due to the low intensity of the rotational transitions for these species.

Table 2.1. Spectroscopic Constants of HN_3 (A-Reduced Hamiltonian, I^r Representation)

	CCSD(T)/cc-pCV5Z	Amberger *et al.*[5]	Vávra *et al.*[6, a]
A_0 (MHz)	611182	611034.132 (29)	611036.218 (13)
B_0 (MHz)	12053	12034.983 (62)	12035.03574 (95)
C_0 (MHz)	11801	11780.6713 (66)	11780.62295 (77)
Δ_J (kHz)	4.75	4.9174 (10)	4.91845 (24)
Δ_{JK} (kHz)	774	797.98 (15)	771.43 (61)
Δ_K (kHz)	226000	267559 (27)	146050 (620)
δ_J (kHz)	0.0778	0.09118 (22)	0.091726 (28)
δ_K (kHz)	318	403.9 (31)	428.96 (41)
Φ_J (Hz)	−0.000966	[0][b]	[0][b]
Φ_{JK} (Hz)	1.95	1.19 (10)	[0][b]
Φ_{KJ} (Hz)	−983	255 (14)	16.89 (42)
Φ_K (Hz)	282000	[0][b]	661.1 (20)
ϕ_J (Hz)	0.0000784	[0][b]	[0][b]
ϕ_{JK} (Hz)	1.46	[0][b]	[0][b]
ϕ_K (Hz)	3960	[0][b]	[0][b]
L_{KKJ} (mHz)		−40010 (400)	[0][b]
$\Delta_{i\,0}$ (uÅ^2)	0.0685	0.0794	0.0798
N_{lines}		78 mmw	273 mmw / 859 ir
σ_{fit} (MHz)		0.032	0.042 / 72.5

[a] *a*-type and *c*-type Coriolis couplings addressed with the ground state, *v*5 and *v*6, see previous work[6] for details.

[b] Computed sextic centrifugal distortion constants not available during previous work and values fixed to zero.

Computations

A developmental version of CFOUR was used to conduct all *ab initio* calculations.[22] These consisted of geometry optimizations, anharmonic VPT2, and magnetic properties calculations at CCSD(T) using frozen-core approximated (cc-pV*X*Z) or all-electron (cc-pCV*X*Z) Dunning-style basis sets (for X = D, T, Q, and 5). Isotopologue-dependent corrections to the rotational constants were calculated to account for vibration-rotation interactions using the results of the VPT2 calculations and for electron-mass distributions using the results of magnetic property calculations. These corrections were then combined with the average determinable A_0'', B_0'', and C_0'' constants to obtain semi-experimental equilibrium constants (B_e^x) for each isotopologue, using Eq. (2.S1).

The r_e^{SE} structure of HN_3 was then determined by a nonlinear least-squares fit of the corresponding moments of inertia, using the *xrefit* module included within CFOUR, with all values weighted equally.

Further analysis of the r_e^{SE} structure determination was conducted using the *xrefiteration* routine, which is described in detail in Chapter 1 of this thesis and elsewhere.[4] Concisely, an initial r_e^{SE} structure determination is obtained for the "minimal set" of isotopologues, which consist of the normal isotopologue and any isotopologue differing by a single isotopic substitution. The *xrefiteration* routine then obtains a set of r_e^{SE} structures where only one previously unincorporated isotopologue of those remaining is added into the dataset. The routine then estimates the overall "apparent precision" by calculating the total relative uncertainty (δr_e^{SE}) of the resulting structures using Eq. (2.1), where R_i, θ_i, and ϕ_i represent bond distances, angles, and dihedrals, respectively, and σ_{fit} is the statistical uncertainty from the least-squares fit of the r_e^{SE}.

$$\delta r_e^{SE} = \sqrt{\sum_i \left(\frac{2\sigma_{fit}(R_i)}{R_i} \right)^2 + \sum_i \left(\frac{2\sigma_{fit}(\theta_i)}{\theta_i} \right)^2 + \sum_i \left(\frac{2\sigma_{fit}(\phi_i)}{\phi_i} \right)^2} \qquad (2.1)$$

The r_e^{SE} structure with the smallest apparent precision is kept and the process is repeated until all isotopologues are included. As we demonstrated for thiophene,[2] thiazole,[3] and pyridazine,[4] the utility of this analysis lies in tracking the progression of the structural parameters in comparison to the theoretical values to assess the accuracy of the final structure.

Finally, we calculated a "best theoretical estimate" (BTE) equilibrium structure for HN_3, using the previously described methodology,[1-4] which takes into account the following contributions to the geometry beyond a normal coupled cluster geometry optimization:

1. Residual basis set effects, Eq. (2.2), by means of extrapolation to the complete basis set (CBS) limit using CCSD(T)/cc-pCV*X*Z (*X* = Q, 5, and 6).

$$\Delta R(\text{basis}) = R(\infty) - R(\text{CCSD(T)/cc-pCV6Z}) \tag{2.2}$$

2. Residual electron correlation effects, Eq. (2.3), by use of CCSDT(Q).[23]

$$\Delta R(\text{corr}) = R(\text{CCSDT(Q)/cc-pCVTZ}) - R(\text{CCSD(T)/cc-pCVTZ}) \tag{2.3}$$

3. Scalar relativistic effects, Eq. (2.4), by use of the X2C-1e variant of coupled-cluster theory.[24-26]

$$\Delta R(\text{rel}) = R(\text{CCSD(T)/cc-pCV5Z})_{\text{SFX2C-1e}} - R(\text{CCSD(T)/cc-pCV5Z}) \tag{2.4}$$

4. Effect of the Born-Oppenheimer approximation, Eq. (2.5), by use of the diagonal Born-Oppenheimer correction (DBOC).[27-28]

$$\Delta R(\text{DBOC}) = R(\text{SCF/cc-pCVTZ})_{\text{DBOC}} - R(\text{SCF/cc-pCVTZ}) \tag{2.5}$$

The correction to the CCSD(T)/cc-pCV56Z optimization necessary to obtain the BTE is then given by the sum of the above corrections for each parameter, as in Eq. (2.6).

$$\Delta R(\text{best}) = \Delta R(\text{basis}) + \Delta R(\text{corr}) + \Delta R(\text{rel}) + \Delta R(\text{DBOC}) \tag{2.6}$$

RESULTS AND DISCUSSION

Structure Determinations

The planar structure of HN_3 allows an assessment of the quality of the computed corrections to the rotational corrections, specifically by examining inertial defects associated with the experimental and semi-experimental rotational constants. The inertial defect is precisely zero for a rigid planar structure, but the uncorrected experimental rotational constants (B_0^x) will have a non-zero inertial defect ($\Delta_{i\,0}$) due to vibration-rotation interactions and the electron-mass

distribution. These deviations are addressed by the computational corrections used to obtain the semi-experimental B_e^x rotational constants and should bring the approximate $\Delta_{i\,e}$ closer to zero. Previously for HN_3,[5] the inertial defect was reduced to about 3% of its original value after inclusion of the vibration-rotation corrections (Table 2.2). Subsequent addition of an isotopologue-independent electron-mass correction to the rotational constants did not further reduce the magnitude of the inertial defect but slightly increased its value. In cases where the electron-mass distribution in the molecule is not well-described by subsuming the electron masses into the nearby nuclei,[1-4, 29] use of isotopologue-dependent electron-mass corrections has been shown to reduce the $\Delta_{i\,e}$ by about one order of magnitude. In the current study, CCSD(T)/cc-pCV5Z corrections have been applied to the rotational constants resulting in inertial defects roughly two-thirds the magnitude of the ANO2-corrected inertial defects. The inertial defects with both vibration-rotation and electron-mass corrections, however, are still slightly larger than those using just the vibration-rotation corrections at the cc-pCV5Z level, similar to the relationship previously observed at the ANO2 level. The extensive computational analysis in the current study allows us to extrapolate the vibration-rotation and electron-mass corrections to the rotational constants to the CBS limit (Supporting Information, Table 2.6). Application of these CBS corrections to the B_0^x constants to obtain the semi-experimental B_e^x constants results in inertial defects that are nearly identical to those obtained at the cc-pCV5Z level, with identical standard deviations (Table 2.2). The close agreement of the inertial defects obtained using either cc-pCV5Z or CBS corrections suggest that the cc-pCV5Z basis is sufficient for obtaining accurate corrections to the rotational constants. The lack of improvement to the inertial defect with inclusion of the electron-mass correction is consistent with the earlier study[5] and this lack of improvement is broadly consistent with the near-

cylindrical nature of HN_3 where electron mass is radially distributed around the H–N–N–N backbone in the in-plane and out-of-plane π orbitals.[20]

Table 2.2. Inertia Defects (Δ_i) of Hydrazoic Acid Isotopologues

	Exp.[5]	ANO2[5]		cc-pCV5Z		CBS	
Isotopologue	$\Delta_{i\,0}$ (uÅ^2)	$\Delta_{i\,e}$ (uÅ^2)[a]	$\Delta_{i\,e}$ (uÅ^2)[b]	$\Delta_{i\,e}$ (uÅ^2)[a]	$\Delta_{i\,e}$ (uÅ^2)[b]	$\Delta_{i\,e}$ (uÅ^2)[a]	$\Delta_{i\,e}$ (uÅ^2)[b]
normal	0.0735	0.00353	0.00360	0.00273	0.00280	0.00274	0.00289
[^{2}H]	0.0963	0.00342	0.00343	0.00236	0.00243	0.00276	0.00291
[1-^{15}N]	0.0738	0.00355	0.00363	0.00274	0.00281	0.00271	0.00286
[2-^{15}N]	0.0736	0.00350	0.00357	0.00270	0.00277	0.00275	0.00290
[3-^{15}N]	0.0736	0.00353	0.00362	0.00273	0.00280	0.00238	0.00253
[^{2}H, 1-^{15}N]	0.0967	0.00345	0.00345	0.00237	0.00245	0.00240	0.00255
[^{2}H, 2-^{15}N]	0.0962	0.00345	0.00346	0.00239	0.00246	0.00241	0.00256
[^{2}H, 3-^{15}N]	0.0964	0.00343	0.00344	0.00236	0.00244	0.00239	0.00254
[1,2-^{15}N]	0.0739	0.00354	0.00362	0.00273	0.00280	0.00275	0.00290
[1,3-^{15}N]	0.0739	0.00354	0.00363	0.00273	0.00280	0.00275	0.00290
[2,3-^{15}N]	0.0737	0.00348	0.00356	0.00267	0.00274	0.00269	0.00284
[^{2}H, 1,2-^{15}N]	0.0966	0.00346	0.00347	0.00239	0.00246	0.00241	0.00256
[^{2}H, 1,3-^{15}N]	0.0969	0.00346	0.00347	0.00238	0.00246	0.00241	0.00256
[^{2}H, 2,3-^{15}N]	0.0963	0.00343	0.00345	0.00237	0.00244	0.00239	0.00254
Average ($\bar{x}$)	0.0851	0.00348	0.00353	0.00255	0.00262	0.00257	0.00272
Std. Dev. (s)	0.0118	0.00005	0.00008	0.00018	0.00018	0.00018	0.00018

[a] Vibration-rotation interaction corrections only.

[b] Vibration-rotation interaction and electron-mass corrections.

The r_e^{SE} structure determinations in Table 2.3 (and visualized in Figure 2.6 in the Supporting Information) using previously obtained data and increasingly larger correlation-consistent basis sets clearly demonstrate the improvement in the fitting of the structural parameters as the basis set grows larger. The structure obtained using corrections with the largest basis set (cc-pCV5Z, Figure 2.2) has the smallest statistical uncertainties and agrees well with the r_e^{SE} structure obtained using the CBS corrections described above. Unsurprisingly, the parameters of the r_e^{SE} cc-pCVDZ structure are the most poorly determined of all the r_e^{SE} structures, with

uncertainties in the parameters nearly twice as large as those obtained using the triple-zeta basis. Notably, the r_e^{SE} structure previously obtained using the ANO2 corrections is similar to that using the cc-pCVTZ corrections, with nearly identical 2σ uncertainties in the parameters, and with values of the parameters in better agreement with the r_e^{SE} cc-pCV5Z values.

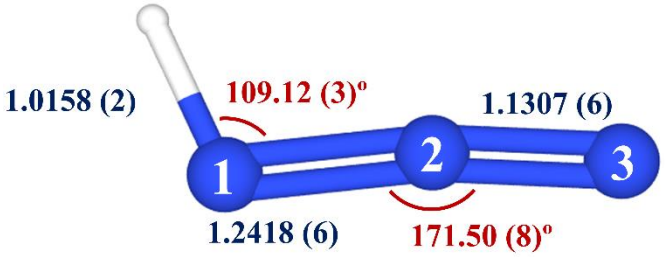

Figure 2.2. Semi-experimental equilibrium structure (r_e^{SE}) of hydrazoic acid with 2σ statistical uncertainties from least-squares fitting the isotopologue moments of inertia, after applying computed corrections (CCSD(T)/cc-pCV5Z) for the effects of vibration-rotation coupling and electron-mass distribution.

To examine the effects of the different isotopologues on the r_e^{SE} structure, we conducted an *xrefiteration* analysis on the r_e^{SE} CCSD(T)/cc-pCV5Z structure. For hydrazoic acid, the minimal set necessary to obtain a substitution structure is comprised of the normal isotopologue and the singly substituted isotopologues ([^{2}H]-, [1-^{15}N]-, [2-^{15}N]-, and [3-^{15}N]-hydrazoic acid). Using the *xrefiteration* routine, we obtained the r_e^{SE} structure using this minimal set as the initial set and then iteratively expanded the set of isotopologues until all were included. The isotopologue added to expand the set was that with the lowest "apparent precision", calculated using Eq. 2.1, in which δr_e^{SE} is the total relative *i.e.*, dimensionless, uncertainty of the structural parameters explicitly determined in the fit. As shown in Figure 2.3 (and enumerated in Table 2.7 of the Supporting Information), the effect of adding isotopologues beyond the minimal set required for a

substitution structure is immediately noticeable, with the inclusion of the first additional isotopologue ([^{2}H, 3-^{15}N]) reducing δr_e^{SE} by 15%. Addition of the next isotopologue ([^{2}H, 1,2-^{15}N]) reduces δr_e^{SE} by 30% relative to the minimal set. With each iteration of the algorithm, δr_e^{SE} of the resulting r_e^{SE} structure continues to decrease, eventually to 50% smaller than the initial value. Notably, a rise in the δr_e^{SE} at the end of the *xrefiteration* analysis, observed in previous works,[2-4] did not occur here. In those previous works, we observed that the last few isotopologues tend to increase the δr_e^{SE} due to the nature of the algorithm: the isotopologues that raise the δr_e^{SE} are only added at the end of the analysis, after all isotopologues that lower the δr_e^{SE} have been added. The absence of such behavior for the HN_3 r_e^{SE} structure suggests that even the "worst"* of the isotopologues in the data set still lower the δr_e^{SE}, giving us confidence that the underlying spectroscopic data and theoretical corrections for the r_e^{SE} structure determination are consistent. Therefore, given that the data set contains 14 of the 16 possible stable isotopologues of HN_3, we suspect that such consistency corresponds to accuracy.

* The use of the word "worst" here refers to the degree to which information provided by the isotopologue in question is consistent with the information provided by the other isotopologues in the data set and does not necessarily reflect the quality of the spectroscopic data or computed corrections for that isotopologue. As seen in pyridazine,[4] the inclusion of the final isotopologue resulted in a dramatic increase in the δr_e^{SE} but was required for accurate determination of several parameters.

Table 2.3. Summary of r_e^{SE} Structural Parameters of Hydrazoic Acid[a]

Parameter	ANO2[5]	cc-pCVDZ	cc-pCVTZ	cc-pCVQZ	cc-pCV5Z	CBS
$R_{H–N1}$ (Å)	1.01577 (32)	1.01572 (59)	1.01571 (33)	1.01583 (26)	1.01584 (24)	1.01584 (25)
$R_{N1–N2}$ (Å)	1.24174 (74)	1.24166 (133)	1.24166 (74)	1.24176 (58)	1.24178 (55)	1.24178 (57)
$R_{N2–N3}$ (Å)	1.13066 (76)	1.13080 (136)	1.13066 (75)	1.13068 (59)	1.13068 (56)	1.13068 (58)
$\theta_{H–N1–N2}$ (°)	109.133 (34)	109.192 (62)	109.148 (35)	109.116 (27)	109.118 (26)	109.117 (27)
$\theta_{N1–N2–N3}$ (°)	171.50 (10)	171.47 (18)	171.53 (10)	171.499 (80)	171.497 (76)	171.495 (79)

[a] Evaluated from the average determinable rotational constants of 14 isotopologues, with corrections for vibration-rotation coupling and electron-mass distribution computed at CCSD(T) using the specified basis set.

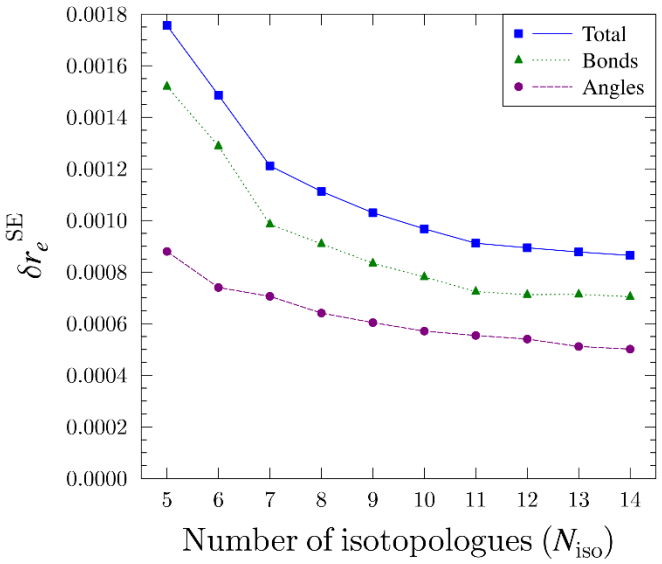

N_{iso}	Isotopologue Added
5	Minimal Set
6	[^{2}H, 3-^{15}N]
7	[^{2}H, 1,2-^{15}N]
8	[1,2-^{15}N]
9	[2,3-^{15}N]
10	[^{2}H, 2,3-^{15}N]
11	[^{2}H, 1-^{15}N]
12	[^{2}H, 2-^{15}N]
13	[1,3-^{15}N]
14	[^{2}H, 1,3-^{15}N]

Figure 2.3. Plot of the δr_e^{SE} value as a function of the number of isotopologues (N_{iso}) incorporated into the r_e^{SE} CCSD(T)/cc-pCV5Z structure determination data set. The total relative statistical uncertainty (δr_e^{SE}, blue squares), the relative statistical uncertainty in the bond distances (green triangles), and the relative statistical uncertainty in the bond angles (purple circles) are presented.

To assess the quality of the r_e^{SE} structure of HN_3, we examined how the parameters of the structure change throughout the *xrefiteration* analysis. As demonstrated by Figure 2.4 and Table 2.4, there is remarkably little change in the parameter values throughout the *xrefiteration* analysis. The variation in the values of the bond distances and angles is <0.00005 Å and <0.001°, respectively, which is well within the 2σ uncertainties of the respective parameters. Such variation in the parameters throughout the *xrefiteration* analysis contrasts with that observed in our previous works: ~0.0004 Å and ~0.05° for the bond distances and angles of pyridazine and thiophene, and ~0.0014 Å and ~0.4° for the bond distances and angles of thiazole. It appears that the HN_3 structure converges very rapidly, and, after nine isotopologues, the only change in the structural parameter

values is 0.00001 Å for $R_{N1–N2}$. The convergence of the structural parameters and their close agreement with their BTE values (dotted lines in Figure 2.4) provides confidence that the resulting r_e^{SE} structure is both accurate and precise, despite the unaddressed coupling in the least-squares fits used to determine the experimental rotational constants.

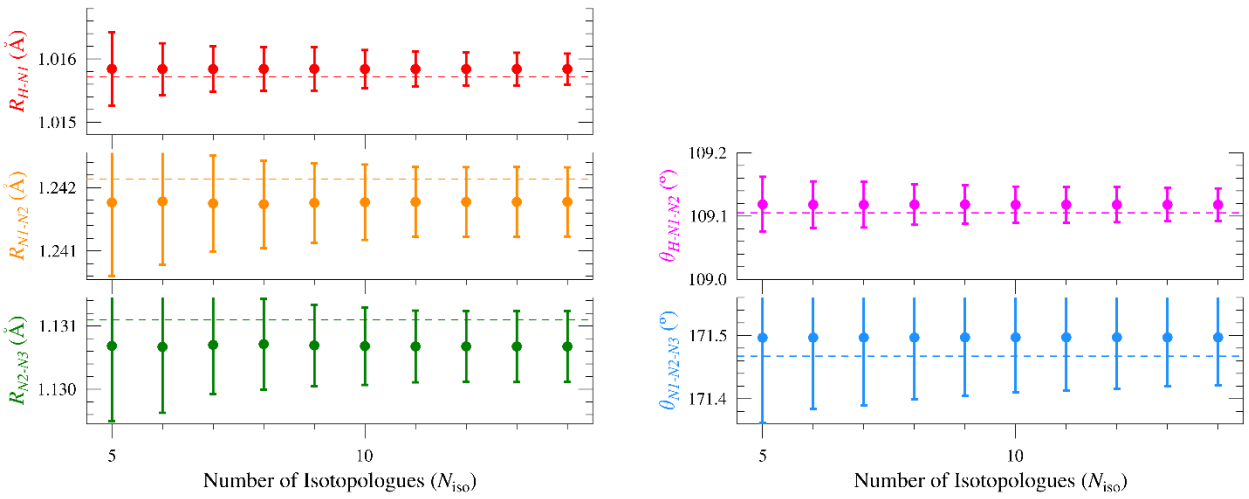

Figure 2.4. Plots of the r_e^{SE} CCSD(T)/cc-pCV5Z structural parameters of hydrazoic acid as a function of the number of isotopologues (N_{iso}) and their 2σ uncertainties with consistent scales for each distance (0.002 Å) and each angle (0.2°). The dashed line in each plot is the BTE value calculated for that parameter. The isotopologue ordering along the *x*-axis is the same as that in Figure 2.3.

Table 2.4. Values of the Structural Parameters of Hydrazoic Acid During the Iterative Analysis of the r_e^{SE} CCSD(T)/cc-pCV5Z (*xrefiteration*)

	Isotopologue	Parameters				
N_{iso} [a]	Added	$R_{H–N1}$ (Å)	$R_{N1–N2}$ (Å)	$R_{N2–N3}$ (Å)	$\theta_{H–N1–N2}$ (°)	$\theta_{N1–N2–N3}$ (°)
5	Minimal Set [b]	1.01584 (58)	1.24177 (116)	1.13069 (119)	109.119 (43)	171.496 (135)
6	[^{2}H, 3-^{15}N]	1.01584 (41)	1.24178 (100)	1.13067 (104)	109.118 (37)	171.497 (113)
7	[^{2}H, 1,2-^{15}N]	1.01584 (36)	1.24175 (76)	1.13070 (78)	109.118 (36)	171.497 (107)
8	[1,2-^{15}N]	1.01584 (35)	1.24174 (69)	1.13071 (72)	109.118 (32)	171.497 (98)
9	[2,3-^{15}N]	1.01584 (34)	1.24176 (63)	1.13069 (64)	109.118 (30)	171.497 (92)
10	[^{2}H, 2,3-^{15}N]	1.01584 (30)	1.24177 (59)	1.13068 (61)	109.118 (29)	171.497 (87)
11	[^{2}H, 1-^{15}N]	1.01584 (28)	1.24177 (55)	1.13068 (57)	109.118 (28)	171.497 (84)
12	[^{2}H, 2-^{15}N]	1.01584 (26)	1.24177 (55)	1.13068 (56)	109.118 (28)	171.497 (82)
13	[1,3-^{15}N]	1.01584 (26)	1.24178 (55)	1.13068 (56)	109.118 (26)	171.497 (77)
14	[^{2}H, 1,3-^{15}N]	1.01584 (24)	1.24178 (55)	1.13068 (56)	109.118 (26)	171.497 (76)

[a] Number of isotopologues in the iteration

[b] The initial iteration consists of the normal isotopologue and [^{2}H]-, [1-^{15}N]-, [2-^{15}N]-, and [3-^{15}N]-hydrazoic acid

Theoretical Predictions

As with the aromatic heterocycles that we have recently studied,[1-4] we obtained CCSD(T) geometry optimizations using up to and including the all-electron quintuple-zeta basis set. The small size of HN_3 allowed us to expand the basis set even further to the all-electron sextuple-zeta basis set. Interestingly, we see that the purely theoretical r_e structural parameters computed using CCSD(T)/cc-pCV6Z do not fall within the statistical uncertainties of the r_e^{SE} parameters. As we noted in related works,[1-4] molecular structures predicted using CCSD(T) computations with a large basis set – while an adequate approach in a wide variety of computational contexts[30-31] – are insufficiently accurate for comparison to the high precision of r_e^{SE} structure determinations. Furthermore, extrapolating the parameters to the CBS limit (Supporting Information, Table 2.9, "r_e+ΔR(basis)") is not sufficient to bring the theoretical parameters into agreement with the r_e^{SE} parameters.

Similar to that observed with the r_e^{SE} structures when the basis set increases in size, the r_e parameters also converge at an exponential rate (Table 2.8 and Figure 2.7 in the Supporting Information) with the exception of $\theta_{N1–N2–N3}$. The non-exponential behavior of this angle leads to a spurious $R(\infty)$ value that is closer to the triple-zeta value than it is to the sextuple-zeta value. As such, we set the $R(\infty)$ value for $\theta_{N1–N2–N3}$ to the sextuple-zeta value, which is equivalent to setting the ΔR(basis) correction for $\theta_{N1–N2–N3}$ to zero, as given in Table 2.5. Ultimately, this change has practically no effect on the outcome of the BTE structure and the following discussion: the angle is now slightly smaller but still well within the statistical uncertainty of the r_e^{SE} CCSD(T)/cc-pCV5Z value.

The precision of the r_e^{SE} structure is such that correcting for the size of the basis set is insufficient to bring the r_e structure into agreement. To do so, the r_e structure must also be treated for electron correlation and for effects due to relativity and the (diagonal) Born-Oppenheimer correction. As demonstrated in Table 2.5 and Figure 2.5, the inclusion of such effects results in a best theoretical estimate (BTE) structure that is in complete agreement with the r_e^{SE} structure. All parameters from the BTE structure fall within the statistical uncertainties of the r_e^{SE} structure. As is typically the case, the CBS correction [Eq. (2.2)] contracts the bond lengths while the correlation correction [Eq. (2.3)] lengthens the bonds (Table 2.5). Unlike pyrimidine, where the DBOC correction lengthened the bonds and the relativistic correction contracted the bonds, we observe mixed effects of the DBOC and relativistic corrections on the HN_3 bond lengths (Table 2.5); such was also the case for pyridazine. The largest magnitude correction is the correlation correction for all parameters except $\theta_{H–N1–N2}$.

Table 2.5. Corrections Used in Determining the Best Theoretical Estimate (BTE) of the Equilibrium Structural Parameters of Hydrazoic Acid, with Comparison to the r_e^{SE} Determined Values.

Parameter	ΔR(basis) eqn (2)	ΔR(corr) eqn (3)	ΔR(rel) eqn (4)	ΔR(DBOC) eqn (5)	ΔR(best) eqn (6)	CCSD(T)/ cc-pCV6Z	BTE [a]	r_e^{SE} CCSD(T)/ cc-pCV5Z
$R_{H–N1}$ (Å)	−0.000010	0.00014	0.000027	0.000078	0.00024	1.01548	1.01572	1.01584 (24)
$R_{N1–N2}$ (Å)	−0.00011	0.00133	0.00019	−0.000065	0.00135	1.24078	1.24213	1.24178 (55)
$R_{N2–N3}$ (Å)	−0.000078	0.00213	−0.00019	−0.000015	0.00185	1.12925	1.13109	1.13068 (56)
$\theta_{H–N1–N2}$ (°)	0.015	0.062	−0.087	0.012	0.0018	109.103	109.105	109.118 (26)
$\theta_{N1–N2–N3}$ (°)	0 [b]	−0.208	−0.026	0.0041	−0.166	171.697	171.467	171.497 (76)

[a] Obtained by adding the ΔR(best) correction to the CCSD(T)/cc-pCV6Z optimized values.

[b] This angle does not converge at an exponential rate with respect to the size of the basis set, leading to a spurious $R(\infty)$ value upon extrapolation. As such, the $R(\infty)$ value for this angle has been set to that of the CCSD(T)/cc-pCV6Z structure, which results in a ΔR(basis) of this angle of zero per Eq. (2.2).

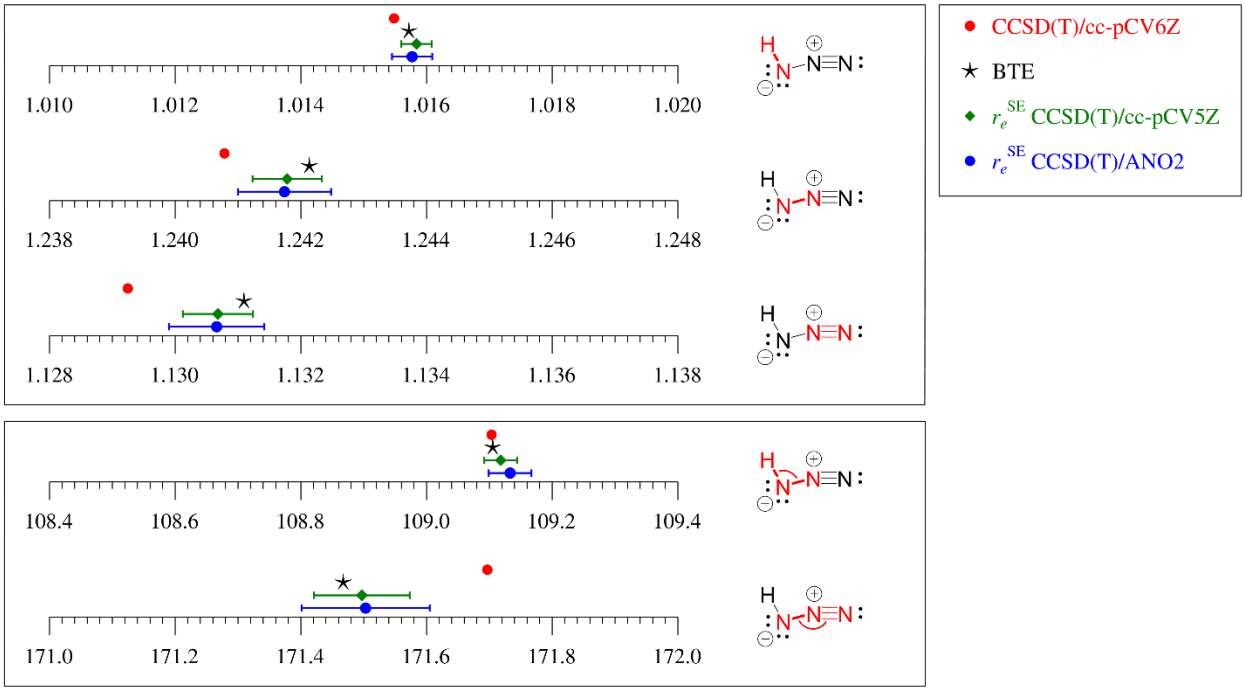

Figure 2.5. Graphical comparison of the hydrazoic acid structural parameters with bond distances in angstroms (Å) and angles in degrees (°). Uncertainties shown are 2σ. Data for r_e^{SE} CCSD(T)/ANO2 are taken from Ref. 5.

CONCLUSIONS

The r_e^{SE} structure determinations of HN_3 using CCSD(T)/cc-pCV5Z corrections for the effects of vibration-rotation coupling and electron-mass distribution resulted in a modest reduction of the statistical uncertainties (2σ) of the structural parameters over those previously obtained with CCSD(T)/ANO2 corrections. Given that these two r_e^{SE} structures determined the bond distances and bond angles to within 0.0001 Å and 0.02° of each other, the smaller ANO2 basis is recommended for r_e^{SE} structure determinations of larger molecules, where a quintuple-zeta basis set is impractical. In our previous work on pyridazine, application of isotopologue-dependent electron-mass corrections resulted in a dramatic improvement in the semi-experimental inertial

defects ($\Delta_{i\ e}$), but similar treatment for HN_3 in this work did not. The lack of a reduction in $\Delta_{i\ e}$ for HN_3 upon inclusion of the isotopologue-dependent electron-mass corrections is puzzling. While HN_3 is highly prolate and pyridazine is highly oblate, why (or even if) the near-cylindrical shape and radial distribution of the electrons of HN_3 would affect the electron-mass corrections is not clear. The more likely explanation is that the VPT2 corrections for treating the vibration-rotation interactions – while reducing the inertial defect – are not accurately adjusting the rotational constants and the subsequent electron-mass corrections (being smaller in magnitude) are unable to affect a change, in which case higher-order perturbation theory may be required.

Given the high level of theory used to obtain the corrections and the inclusion of rotational constants from 14 of the 16 possible isotopologues, further improvement to the r_e^{SE} structure determination will be difficult to achieve. Analysis of the present r_e^{SE} structure determination using the *xrefiteration* routine revealed continuous improvement in the r_e^{SE} structure as additional isotopologues were included in the data set, with very little variation in the values of the structural parameters, suggesting the underlying data is remarkably self-consistent. While the purely theoretical r_e structural parameters computed using CCSD(T)/cc-pCV6Z do not fall within the statistical uncertainties (2σ) of the r_e^{SE} structure, structural parameters obtained from the "best theoretical estimate" are in excellent agreement with the semi-experimental values. The molecular structure of hydrazoic acid, already known to high precision through previous work, has been further refined by improvements in computational methods and theoretical analyses, illustrating the state-of-the-art for contemporary gas-phase structure determination.

ACKNOWLEDGEMENTS

We gratefully acknowledge the National Science Foundation for support of this project (CHE-1664912 and CHE-1954270).

REFERENCES

1. Heim, Z. N.; Amberger, B. K.; Esselman, B. J.; Stanton, J. F.; Woods, R. C.; McMahon, R. J., Molecular structure determination: Equilibrium structure of pyrimidine (*m*-$C_4H_4N_2$) from rotational spectroscopy (r_e^{SE}) and high-level ab initio calculation (r_e) agree within the uncertainty of experimental measurement. *J. Chem. Phys.* **2020,** *152* (10), 104303.

2. Orr, V. L.; Ichikawa, Y.; Patel, A. R.; Kougias, S. M.; Kobayashi, K.; Stanton, J. F.; Esselman, B. J.; Woods, R. C.; McMahon, R. J., Precise Equilibrium Structure Determination of Thiophene (C_4H_4S) by Rotational Spectroscopy – Structure of a Five-Membered Heterocycle Containing a Third-Row Atom. *J. Chem. Phys.* **2021,** *154*, 244310.

3. Esselman, B. J.; Zdanovskaia, M. A.; Owen, A. N.; Stanton, J. F.; Woods, R. C.; McMahon, R. J., Precise Equilibrium Structure Determination of Thiazole (C_3H_3NS) from Twenty-Four Isotopologues. *J. Chem. Phys.* **2021,** *155*, 054302.

4. Owen, A. N.; Zdanovskaia, M. A.; Esselman, B. J.; Stanton, J. F.; Woods, R. C.; McMahon, R. J., Semi-Experimental Equilibrium (r_e^{SE}) and Theoretical Structures of Pyridazine (*o*-$C_4H_4N_2$). *J. Phys. Chem. A* **2021,** *125* (36), 7976-7987.

5. Amberger, B. K.; Esselman, B. J.; Stanton, J. F.; Woods, R. C.; McMahon, R. J., Precise Equilibrium Structure Determination of Hydrazoic Acid (HN_3) by Millimeter-wave Spectroscopy. *J. Chem. Phys.* **2015,** *143* (10), 104310.

6. Vávra, K.; Kania, P.; Koucký, J.; Kisiel, Z.; Urban, Š., Rotational spectra of hydrazoic acid. *J. Mol. Spectrosc.* **2017,** *337*, 27-31.

7. Herzberg, G.; Patat, F.; Verleger, H., Über die geometrische Struktur des N_3H-Moleküls. *Zeitschrift für Elektrochemie und Angewandte Physikalische Chemie* **1935,** *41*, 522-524.

8. Eyster, E. H., The Rotational Structure of the Hydrazoic Acid Bands in the Photographic Infra-Red. *J. Chem. Phys.* **1940,** *8*, 135-142.

9. Schomaker, V.; Spurr, R., The Structures of Nitrous Oxide and of Hydrogen Azide. *J. Am. Chem. Soc.* **1942,** *64* (5), 1184-1187.

10. Amble, E.; Dailey, B. P., The Structure and Dipole Moment of Hydrazoic Acid. *J. Chem. Phys.* **1950,** *18* (10), 1422-1422.

11. Winnewisser, M.; Cook, R. L., Centrifugal Distortion Effects and Structure of Hydrazoic Acid from the Millimeter Wave Rotational Spectra. *J. Chem. Phys.* **1964,** *41* (4), 999-1004.

12. Bendtsen, J.; Winnewisser, M., Ground state spectroscopic constants and dipole moment of hydrazoic acid, $H^{14}N_3$. *Chem. Phys. Lett.* **1975,** *33* (1), 141-145.

13. Bendtsen, J.; Winnewisser, M., Absorption spectrum of deuterated hydrazoic acid, $D^{14}N_3$ in the microwave and millimeterwave region. *Chem. Phys.* **1979,** *40* (3), 359-365.

14. Bendtsen, J., Raman spectrum of the ν_2 band of $H^{14}N_3$. *J. Raman Spectrosc.* **1980,** *9* (3), 162-165.

15. Winnewisser, B. P., The substitution structure of hydrazoic acid, HNNN. *J. Mol. Spectrosc.* **1980,** *82* (1), 220-223.

16. Evers, J.; Göbel, M.; Krumm, B.; Martin, F.; Medvedyev, S.; Oehlinger, G.; Steemann, F. X.; Troyan, I.; Klapötke, T. M.; Eremets, M. I., Molecular Structure of Hydrazoic Acid

with Hydrogen-Bonded Tetramers in Nearly Planar Layers. *J. Am. Chem. Soc.* **2011,** *133* (31), 12100-12105.

17. Evers, J.; Oehlinger, G.; Steemann, F. X.; Klapötke, T. M., Molecular Structure of Hydrazoic Acid from 55 K to Close to the Melting Point Determined with Synchrotron Radiation. *Inorg. Chem.* **2020,** *59* (23), 17671-17677.

18. Harrison, S. W.; Fischer, C. R.; Kemmey, P. J., Calculation of the equilibrium conformation of HN_3. *Chem. Phys. Lett.* **1975,** *36* (2), 229-231.

19. Lievin, J.; Breulet, J.; Verhaegen, G., *Ab initio* study of hydrazoic acid. *Theor. Chim. Acta* **1979,** *52* (1), 75-88.

20. Sevin, A.; Le Roux, J. P.; Bigot, B.; Devaquet, A., Theoretical *ab initio* SCF-CI study of the photochemical behavior of HN_3 and related species. *Chem. Phys.* **1980,** *45* (2), 305-314.

21. Gordy, W.; Cook, R., *Microwave Molecular Spectra*. 3rd. ed.; Wiley Interscience: New York, 1984; Vol. XVIII.

22. Stanton, J. F.; Gauss, J.; Harding, M. E.; Szalay, P. G. *CFOUR*, 2.0; 2014.

23. Bomble, Y. J.; Stanton, J. F.; Kallay, M.; Gauss, J., Coupled-cluster methods including noniterative corrections for quadruple excitations. *J. Chem. Phys.* **2005,** *123* (5), 054101, 054101.

24. Dyall, K. G., Interfacing relativistic and nonrelativistic methods. IV. One- and two-electron scalar approximations. *J. Chem. Phys.* **2001,** *115* (20), 9136-9143.

25. Liu, W.; Peng, D., Exact two-component Hamiltonians revisited. *J. Chem. Phys.* **2009,** *131* (3), 031104, 031104.

26. Cheng, L.; Gauss, J., Analytic energy gradients for the spin-free exact two-component theory using an exact block diagonalization for the one-electron Dirac Hamiltonian. *J. Chem. Phys.* **2011,** *135* (8), 084114, 084114.

27. Born, M.; Huang, K., *Dynamical Theory of Crystal Lattices*. Oxford University Press: New York, 1956.

28. Handy, N. C.; Yamaguchi, Y.; Schaefer, H. F., The Diagonal Correction to the Born-Oppenheimer Approximation - Its Effect on the Singlet-Triplet Splitting of CH_2 and Other Molecular Effects. *J. Chem. Phys.* **1986,** *84* (8), 4481-4484.

29. Stanton, J. F.; Gauss, J.; Christiansen, O., Equilibrium geometries of cyclic SiC_3 isomers. *J. Chem. Phys.* **2001,** *114* (7), 2993-2995.

30. Stanton, J. F., Why CCSD(T) works: a different perspective. *Chem. Phys. Lett.* **1997,** *281* (1), 130-134.

31. Bartlett, R. J.; Musiał, M., Coupled-cluster theory in quantum chemistry. *Rev. Mod. Phys.* **2007,** *79* (1), 291-352.

SUPPORTING INFORMATION

Table of Contents

Evaluation of Semi-Experimental Equilibrium Rotational Constants (B_e^x)

The B_e^x constants are obtained for each isotopologue using Eq. 2.S1. The ground-state rotational constants (B_0^x), in this case the averaged determinable constants take from Amberger *et*

al., 2015, are combined with the vibration-rotation interaction corrections ($\frac{1}{2}\sum \alpha_i^x$) and the electron-mass distribution corrections ($-\eta g^{bb} B^x_{\mathrm{CCSD(T)}}$). This evaluation is handled automatically by the *xrefit* module of CFOUR, once provided the requisite information. The moments of inertia and inertial defects are similarly calculated using *xrefit*.

$$B_e^x = B_0^x + \frac{1}{2}\sum \alpha_i^x - \eta g^{bb} B^x_{\mathrm{CCSD(T)}} \tag{2.S1}$$

Complete Basis Set (CBS) Extrapolation

All basis set extrapolations were conducted using Eq. 2.S2, which is the three-point solution to the exponential equation given by Eq. 2.S3, assuming that $x_1 + 2 = x_2 + 1 = x_3$ for the zetas of the basis sets of the calculated parameters.

$$R(\infty) = -\frac{R(x_2)^2 - R(x_1)R(x_3)}{R(x_1) + R(x_3) - 2R(x_2)} \tag{2.S2}$$

$$R(x) = R(\infty) + Ae^{-Bx} \tag{2.S3}$$

Table 2.6. Semi-experimental equilibrium rotational constants (B_e^x) of isotopologues of hydrazoic acid and the CCSD(T) corrections used to obtain them, including CBS extrapolation of the triple-, quadruple-, and quintuple-zeta corrections using Eq. 2.S2. The ground state rotational constants (B_0^x) are the average determinable rotational constants taken from Amberger *et al.* 2015.

		normal					[^{2}H]				
		cc-pCVDZ	cc-pCVTZ	cc-pCVQZ	cc-pCV5Z	CBS	cc-pCVDZ	cc-pCVTZ	cc-pCVQZ	cc-pCV5Z	CBS
B_0^x	*A*			611034.143					344746.621		
	B			12034.984					11350.717		
	C			11782.287					10965.958		
$\frac{1}{2}\sum\alpha_i^x$	*A*	−503.701	−1208.588	−1950.624	−1986.772	−1988.623	340.712	−238.437	−527.732	−534.159	−534.305
	B	57.182	58.478	57.649	57.744	57.734	49.426	51.399	50.764	50.809	50.806
	C	73.384	75.014	74.130	74.253	74.238	67.992	70.059	69.368	69.449	69.440
$\eta g^{bb} B^x_{\mathrm{CCSD(T)}}$	*A*	43.207	54.132	60.262	63.178	65.822	8.334	11.581	13.381	14.230	14.989
	B	−0.405	−0.448	−0.470	−0.486	−0.523	−0.358	−0.396	−0.415	−0.429	−0.463
	C	−0.370	−0.399	−0.414	−0.423	−0.437	−0.324	−0.349	−0.362	−0.370	−0.381
$B_0^x + \frac{1}{2}\sum\alpha_i^x$	*A*	610530.442	609825.555	609083.520	609047.371	609045.520	345087.333	344508.184	344218.889	344212.462	344212.316
	B	12092.165	12093.462	12092.633	12092.727	12092.718	11400.143	11402.117	11401.481	11401.526	11401.523
	C	11855.671	11857.301	11856.417	11856.541	11856.525	11033.951	11036.017	11035.326	11035.407	11035.399
B_e^x	*A*	610573.649	609879.687	609143.782	609110.549	609111.342	345095.667	344519.765	344232.270	344226.693	344227.306
	B	12091.760	12093.014	12092.163	12092.241	12092.194	11399.785	11401.721	11401.065	11401.097	11401.061
	C	11855.301	11856.902	11856.002	11856.117	11856.089	11033.626	11035.668	11034.964	11035.037	11035.018

Table 2.6 (continued)

		[1-^{15}N]					[2-^{15}N]				
		cc-pCVDZ	cc-pCVTZ	cc-pCVQZ	cc-pCV5Z	CBS	cc-pCVDZ	cc-pCVTZ	cc-pCVQZ	cc-pCV5Z	CBS
B_0^x	*A*			605576.900					610033.003		
	B			11668.321					12034.149		
	C			11428.634					11781.100		
$\frac{1}{2}\sum\alpha_i^x$	*A*	−613.863	−1276.628	−2013.172	−2050.642	−2052.650	−676.998	−1337.761	−2083.467	−2121.896	−2123.984
	B	55.010	56.192	55.373	55.466	55.457	56.554	57.796	56.986	57.079	57.070
	C	70.279	71.787	70.915	71.036	71.021	72.736	74.323	73.455	73.577	73.562
$\eta g^{bb} B^x_{\mathrm{CCSD(T)}}$	*A*	43.821	54.590	60.644	63.523	66.137	42.859	53.763	59.868	62.771	65.404
	B	−0.382	−0.423	−0.444	−0.459	−0.493	−0.405	−0.448	−0.470	−0.486	−0.523
	C	−0.349	−0.377	−0.391	−0.399	−0.412	−0.370	−0.399	−0.414	−0.423	−0.436
$B_0^x + \frac{1}{2}\sum\alpha_i^x$	*A*	604963.036	604300.272	603563.727	603526.258	603524.249	609356.005	608695.242	607949.536	607911.106	607909.018
	B	11723.331	11724.513	11723.694	11723.788	11723.778	12090.704	12091.946	12091.136	12091.229	12091.219
	C	11498.914	11500.421	11499.549	11499.670	11499.656	11853.836	11855.423	11854.555	11854.677	11854.662
B_e^x	*A*	605006.857	604354.862	603624.371	603589.781	603590.386	609398.864	608749.005	608009.404	607973.878	607974.422
	B	11722.949	11724.091	11723.250	11723.329	11723.285	12090.299	12091.498	12090.665	12090.743	12090.696
	C	11498.565	11500.045	11499.159	11499.271	11499.244	11853.467	11855.024	11854.141	11854.254	11854.226

Table 2.6 (continued)

		[3-^{15}N]					[^{2}H, 1-^{15}N]				
		cc-pCVDZ	cc-pCVTZ	cc-pCVQZ	cc-pCV5Z	CBS	cc-pCVDZ	cc-pCVTZ	cc-pCVQZ	cc-pCV5Z	CBS
B_0^x	*A*			610977.577					340247.312		
	B			11642.536					11045.521		
	C			11405.842					10676.372		
$\frac{1}{2}\sum\alpha_i^x$	*A*	−522.516	−1220.178	−1962.609	−1998.957	−2000.828	341.460	−212.127	−496.570	−503.009	−503.158
	B	54.951	56.205	55.415	55.507	55.497	47.727	49.573	48.936	48.983	48.980
	C	70.169	71.738	70.895	71.015	71.000	65.408	67.357	66.670	66.751	66.742
$\eta g^{bb} B^x_{\mathrm{CCSD(T)}}$	*A*	43.151	54.072	60.197	63.111	65.755	8.831	12.019	13.794	14.634	15.387
	B	−0.377	−0.418	−0.439	−0.453	−0.489	−0.341	−0.377	−0.395	−0.408	−0.439
	C	−0.345	−0.373	−0.387	−0.395	−0.408	−0.308	−0.332	−0.344	−0.352	−0.362
$B_0^x + \frac{1}{2}\sum\alpha_i^x$	*A*	610455.061	609757.399	609014.968	608978.620	608976.749	340588.773	340035.186	339750.742	339744.304	339744.155
	B	11697.488	11698.742	11697.951	11698.043	11698.034	11093.248	11095.093	11094.457	11094.504	11094.500
	C	11476.011	11477.580	11476.737	11476.856	11476.841	10741.779	10743.729	10743.042	10743.123	10743.114
B_e^x	*A*	610498.211	609811.470	609075.166	609041.731	609042.504	340597.604	340047.205	339764.537	339758.937	339759.541
	B	11697.110	11698.324	11697.513	11697.590	11697.545	11092.907	11094.717	11094.062	11094.095	11094.061
	C	11475.665	11477.207	11476.350	11476.461	11476.433	10741.471	10743.397	10742.697	10742.771	10742.752

Table 2.6 (continued)

		[^{2}H, 2-^{15}N]					[^{2}H, 3-^{15}N]				
		cc-pCVDZ	cc-pCVTZ	cc-pCVQZ	cc-pCV5Z	CBS	cc-pCVDZ	cc-pCVTZ	cc-pCVQZ	cc-pCV5Z	CBS
B_0^x	*A*			344618.818					344727.744		
	B			11348.346					10979.893		
	C			10963.631					10619.408		
$\frac{1}{2}\sum\alpha_i^x$	*A*	328.923	−243.781	−533.488	−539.951	−540.098	341.055	−237.728	−526.734	−533.174	−533.321
	B	48.870	50.795	50.178	50.222	50.219	47.530	49.434	48.826	48.871	48.868
	C	67.428	69.455	68.780	68.860	68.852	64.995	66.988	66.329	66.407	66.399
$\eta g^{bb} B^x_{\mathrm{CCSD(T)}}$	*A*	8.295	11.543	13.341	14.190	14.948	8.351	11.601	13.402	14.253	15.013
	B	−0.358	−0.396	−0.415	−0.429	−0.462	−0.334	−0.369	−0.387	−0.400	−0.432
	C	−0.324	−0.349	−0.362	−0.370	−0.381	−0.303	−0.326	−0.339	−0.346	−0.357
$B_0^x + \frac{1}{2}\sum\alpha_i^x$	*A*	344947.742	344375.038	344085.331	344078.868	344078.720	345068.799	344490.016	344201.010	344194.570	344194.423
	B	11397.216	11399.141	11398.523	11398.568	11398.565	11027.423	11029.327	11028.719	11028.764	11028.761
	C	11031.059	11033.086	11032.411	11032.491	11032.483	10684.403	10686.396	10685.737	10685.815	10685.807
B_e^x	*A*	344956.037	344386.581	344098.672	344093.058	344093.669	345077.149	344501.617	344214.413	344208.823	344209.436
	B	11396.858	11398.745	11398.108	11398.139	11398.103	11027.089	11028.958	11028.331	11028.364	11028.329
	C	11030.735	11032.737	11032.049	11032.121	11032.102	10684.100	10686.070	10685.398	10685.470	10685.451

Table 2.6 (continued)

		[1,2-^{15}N]					[1,3-^{15}N]				
		cc-pCVDZ	cc-pCVTZ	cc-pCVQZ	cc-pCV5Z	CBS	cc-pCVDZ	cc-pCVTZ	cc-pCVQZ	cc-pCV5Z	CBS
B_0^x	*A*			604507.443					605510.191		
	B			11666.355					11283.093		
	C			11426.344					11058.772		
$\frac{1}{2}\sum\alpha_i^x$	*A*	−796.361	−1413.775	−2153.962	−2193.824	−2196.094	−635.009	−1290.280	−2027.282	−2064.976	−2067.007
	B	54.393	55.522	54.721	54.813	54.803	52.845	53.990	53.208	53.299	53.290
	C	69.639	71.104	70.248	70.367	70.352	67.174	68.625	67.794	67.911	67.897
$\eta g^{bb} B^x_{\mathrm{CCSD(T)}}$	*A*	43.465	54.211	60.238	63.105	65.706	43.763	54.527	60.575	63.452	66.063
	B	−0.382	−0.422	−0.443	−0.458	−0.493	−0.356	−0.394	−0.414	−0.427	−0.460
	C	−0.349	−0.376	−0.391	−0.399	−0.411	−0.325	−0.351	−0.365	−0.373	−0.384
$B_0^x + \frac{1}{2}\sum\alpha_i^x$	*A*	603711.082	603093.668	602353.481	602313.618	602311.349	604875.182	604219.911	603482.909	603445.215	603443.184
	B	11720.748	11721.877	11721.075	11721.168	11721.158	11335.938	11337.082	11336.301	11336.392	11336.382
	C	11495.983	11497.448	11496.592	11496.711	11496.697	11125.946	11127.397	11126.566	11126.683	11126.668
B_e^x	*A*	603754.547	603147.879	602413.719	602376.723	602377.055	604918.945	604274.438	603543.484	603508.668	603509.247
	B	11720.366	11721.455	11720.632	11720.709	11720.665	11335.582	11336.689	11335.887	11335.965	11335.922
	C	11495.635	11497.072	11496.201	11496.312	11496.285	11125.621	11127.045	11126.201	11126.310	11126.284

Table 2.6 (continued)

		[2,3-^{15}N]					[^{2}H, 1,2-^{15}N]				
		cc-pCVDZ	cc-pCVTZ	cc-pCVQZ	cc-pCV5Z	CBS	cc-pCVDZ	cc-pCVTZ	cc-pCVQZ	cc-pCV5Z	CBS
B_0^x	*A*			609961.095					340093.984		
	B			11642.642					11041.857		
	C			11405.580					10672.817		
$\frac{1}{2}\sum\alpha_i^x$	*A*	−697.557	−1349.883	−2095.925	−2134.585	−2136.698	328.016	−218.559	−503.447	−509.952	−510.104
	B	54.339	55.541	54.768	54.859	54.849	47.176	48.974	48.355	48.401	48.398
	C	69.540	71.068	70.240	70.358	70.344	64.843	66.754	66.082	66.162	66.153
$\eta g^{bb} B^x_{\mathrm{CCSD(T)}}$	*A*	42.795	53.695	59.794	62.696	65.327	8.790	11.979	13.752	14.590	15.342
	B	−0.377	−0.418	−0.439	−0.453	−0.488	−0.340	−0.376	−0.395	−0.408	−0.439
	C	−0.345	−0.373	−0.387	−0.395	−0.408	−0.308	−0.332	−0.344	−0.351	−0.362
$B_0^x + \frac{1}{2}\sum\alpha_i^x$	*A*	609263.538	608611.212	607865.169	607826.509	607824.396	340422.000	339875.425	339590.537	339584.032	339583.880
	B	11696.980	11698.182	11697.410	11697.500	11697.491	11089.034	11090.831	11090.212	11090.258	11090.255
	C	11475.120	11476.648	11475.820	11475.938	11475.924	10737.660	10739.570	10738.899	10738.978	10738.970
B_e^x	*A*	609306.333	608664.906	607924.964	607889.205	607889.723	340430.790	339887.404	339604.289	339598.622	339599.221
	B	11696.603	11697.765	11696.971	11697.047	11697.002	11088.693	11090.455	11089.818	11089.850	11089.816
	C	11474.775	11476.275	11475.434	11475.543	11475.516	10737.352	10739.239	10738.555	10738.627	10738.608

Table 2.6 (continued)

		[^{2}H, 1,3-^{15}N]					[^{2}H, 2,3-^{15}N]				
		cc-pCVDZ	cc-pCVTZ	cc-pCVQZ	cc-pCV5Z	CBS	cc-pCVDZ	cc-pCVTZ	cc-pCVQZ	cc-pCV5Z	CBS
B_0^x	*A*			340233.197					344602.438		
	B			10680.118					10978.923		
	C			10334.556					10618.402		
$\frac{1}{2}\sum\alpha_i^x$	*A*	341.818	−211.297	−495.478	−501.928	−502.078	329.360	−242.931	−532.355	−538.825	−538.973
	B	45.880	47.660	47.051	47.098	47.095	46.986	48.843	48.253	48.297	48.294
	C	62.496	64.376	63.721	63.799	63.791	64.447	66.403	65.759	65.837	65.828
$\eta g^{bb} B^x_{\mathrm{CCSD(T)}}$	*A*	8.845	12.036	13.812	14.651	15.405	8.312	11.563	13.362	14.211	14.970
	B	−0.317	−0.351	−0.368	−0.380	−0.410	−0.334	−0.369	−0.387	−0.400	−0.431
	C	−0.287	−0.310	−0.321	−0.328	−0.338	−0.303	−0.326	−0.338	−0.346	−0.356
$B_0^x + \frac{1}{2}\sum\alpha_i^x$	*A*	340575.015	340021.900	339737.719	339731.269	339731.120	344931.798	344359.506	344070.083	344063.613	344063.465
	B	10725.998	10727.778	10727.169	10727.216	10727.213	11025.909	11027.766	11027.176	11027.220	11027.217
	C	10397.053	10398.933	10398.277	10398.356	10398.347	10682.850	10684.805	10684.161	10684.239	10684.230
B_e^x	*A*	340583.860	340033.936	339751.531	339745.921	339746.524	344940.109	344371.069	344083.445	344077.824	344078.435
	B	10725.681	10727.427	10726.801	10726.836	10726.803	11025.576	11027.397	11026.788	11026.820	11026.785
	C	10396.765	10398.623	10397.956	10398.027	10398.009	10682.547	10684.479	10683.823	10683.893	10683.874

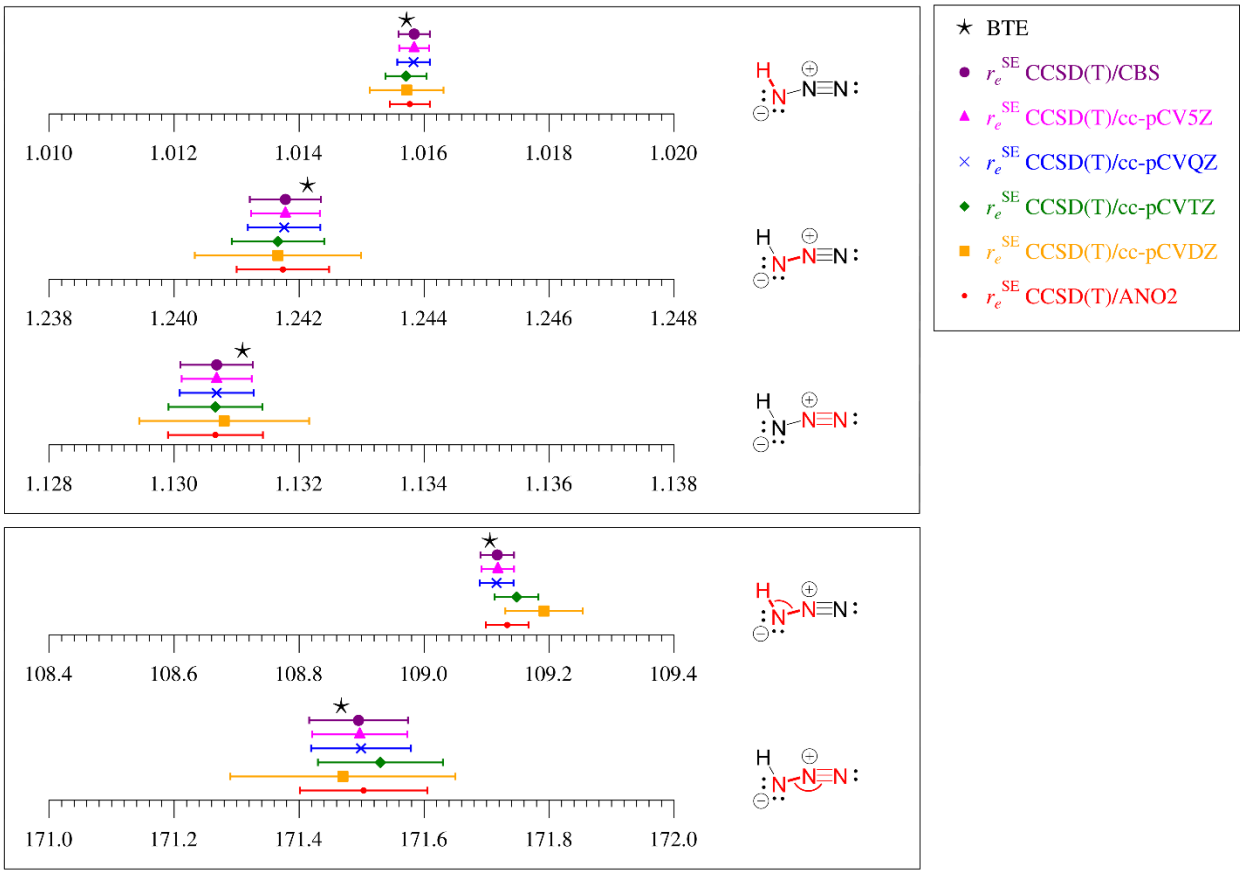

Figure 2.6. Graphical comparison of hydrazoic acid r_e^{SE} structural parameters obtained using CCSD(T) corrections with various levels of theory, with consistent scales for each bond distance (0.01 Å) and each angle (1°).

Table 2.7. Values of δr_e^{SE} of hydrazoic acid during iterative analysis of the r_e^{SE} CCSD(T)/cc-pCV5Z (*xrefiteration*).

	Isotopologue	δr_e^{SE}		
N_{iso} [a]	Added	Total	Bonds	Angles
5	minimal set [b]	0.001756	0.001519	0.000880
6	[^{2}H, 3-^{15}N]	0.001486	0.001289	0.000740
7	[^{2}H, 1,2-^{15}N]	0.001212	0.000985	0.000706
8	[1,2-^{15}N]	0.001113	0.000910	0.000641
9	[2,3-^{15}N]	0.001030	0.000834	0.000604
10	[^{2}H, 2,3-^{15}N]	0.000968	0.000781	0.000571
11	[^{2}H, 1-^{15}N]	0.000912	0.000724	0.000554
12	[^{2}H, 2-^{15}N]	0.000894	0.000712	0.000540
13	[1,3-^{15}N]	0.000878	0.000713	0.000511
14	[^{2}H, 1,3-^{15}N]	0.000865	0.000704	0.000501

[a] Number of isotopologues in the iteration

[b] The initial iteration consists of the normal isotopologue and [^{2}H]-, [1-^{15}N]-, [2-^{15}N]-, and [3-^{15}N]-hydrazoic acid

Table 2.8. Summary of geometry optimizations of hydrazoic acid.

	CCSD(T)						
Parameter	cc-pVTZ	cc-pCVDZ	cc-pCVTZ	cc-pCVQZ	cc-pCV5Z	cc-pCV6Z	CBS [a]
$R_{H\text{-}N1}$ (Å)	1.01808	1.02900	1.01664	1.01567	1.01543	1.01548	1.01547
$R_{N1\text{-}N2}$ (Å)	1.24764	1.25636	1.24416	1.24149	1.24098	1.24078	1.24067
$R_{N2\text{-}N3}$ (Å)	1.13618	1.14961	1.13300	1.13040	1.12948	1.12925	1.12917
$\theta_{H\text{-}N1\text{-}N2}$ (°)	108.308	107.478	108.546	108.918	109.064	109.103	109.118
$\theta_{N1\text{-}N2\text{-}N3}$ (°)	171.655	171.131	171.773	171.741	171.726	171.697	171.760

	CCSDT(Q)			DBOC	SCF
Parameter	cc-pVTZ	cc-pCVDZ	cc-pCVTZ	cc-pCVTZ	cc-pCVTZ
$R_{H\text{-}N1}$ (Å)	1.01820	1.02921	1.01678	1.00317	1.00310
$R_{N1\text{-}N2}$ (Å)	1.24899	1.25787	1.24550	1.23300	1.23306
$R_{N2\text{-}N3}$ (Å)	1.13823	1.15186	1.13513	1.08681	1.08682
$\theta_{H\text{-}N1\text{-}N2}$ (°)	108.364	107.547	108.608	108.196	108.184
$\theta_{N1\text{-}N2\text{-}N3}$ (°)	171.448	170.881	171.565	174.146	174.142

	X2C-1e			
Parameter	cc-pCVDZ	cc-pCVTZ	cc-pCVQZ	cc-pCV5Z
$R_{H\text{-}N1}$ (Å)	1.02907	1.01668	1.01570	1.01545
$R_{N1\text{-}N2}$ (Å)	1.25661	1.24437	1.24168	1.24117
$R_{N2\text{-}N3}$ (Å)	1.14947	1.13282	1.13021	1.12929
$\theta_{H\text{-}N1\text{-}N2}$ (°)	107.388	108.458	108.830	108.976
$\theta_{N1\text{-}N2\text{-}N3}$ (°)	171.105	171.747	171.716	171.700

[a] Extrapolated using Eq. (2.S2) and cc-pCVQZ, cc-pCV5Z, and cc-pCV6Z structures optimized with CCSD(T).

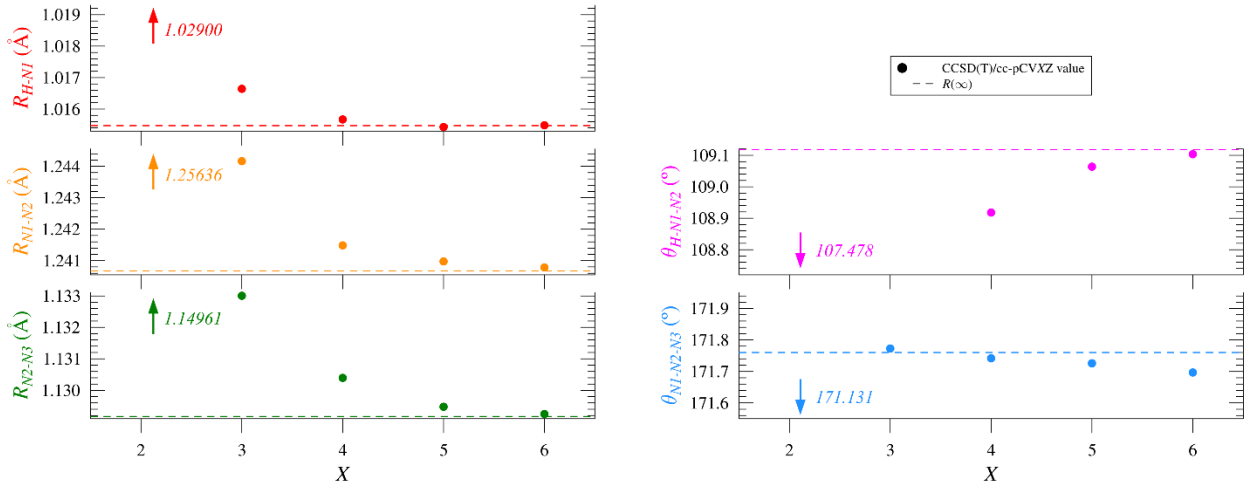

Figure 2.7. Plots of the CCSD(T) optimized parameters of hydrazoic acid using increasingly larger basis sets compared to values [$R(\infty)$] extrapolated using Eq. (2.S2) and cc-pCVQZ, cc-pCV5Z, and cc-pCV6Z basis sets. Values for the cc-pCVDZ calculations not displayed are beyond the scale of the current plots, as indicated by the arrows and accompanying values.

Table 2.9. Cumulative effect of applying corrections to obtain the BTE for hydrazoic acid.

Parameter	r_e [a]	r_e+ΔR(basis)	r_e+ΔR(basis) +ΔR(corr)	r_e+ΔR(basis) +ΔR(corr)+ΔR(rel)	BTE
$R_{\text{H-N1}}$ (Å)	1.01548	1.01547	1.01561	1.01564	1.01572
$R_{\text{N1-N2}}$ (Å)	1.24078	1.24067	1.24200	1.24220	1.24213
$R_{\text{N2-N3}}$ (Å)	1.12925	1.12917	1.13130	1.13111	1.13109
$\theta_{\text{H-N1-N2}}$ (°)	109.103	109.118	109.180	109.093	109.105
$\theta_{\text{N1-N2-N3}}$ (°)	171.697	171.697[b]	171.789	171.463	171.467

[a] CCSD(T)/cc-pCV6Z

[b] This angle does not converge at an exponential rate with respect to the size of the basis set, leading to a spurious $R(\infty)$ value upon extrapolation. As such, the $R(\infty)$ value for this angle has been set to that of the CCSD(T)/cc-pCV6Z structure, which results in a ΔR(basis) of this angle of zero per Eq. (2.2).

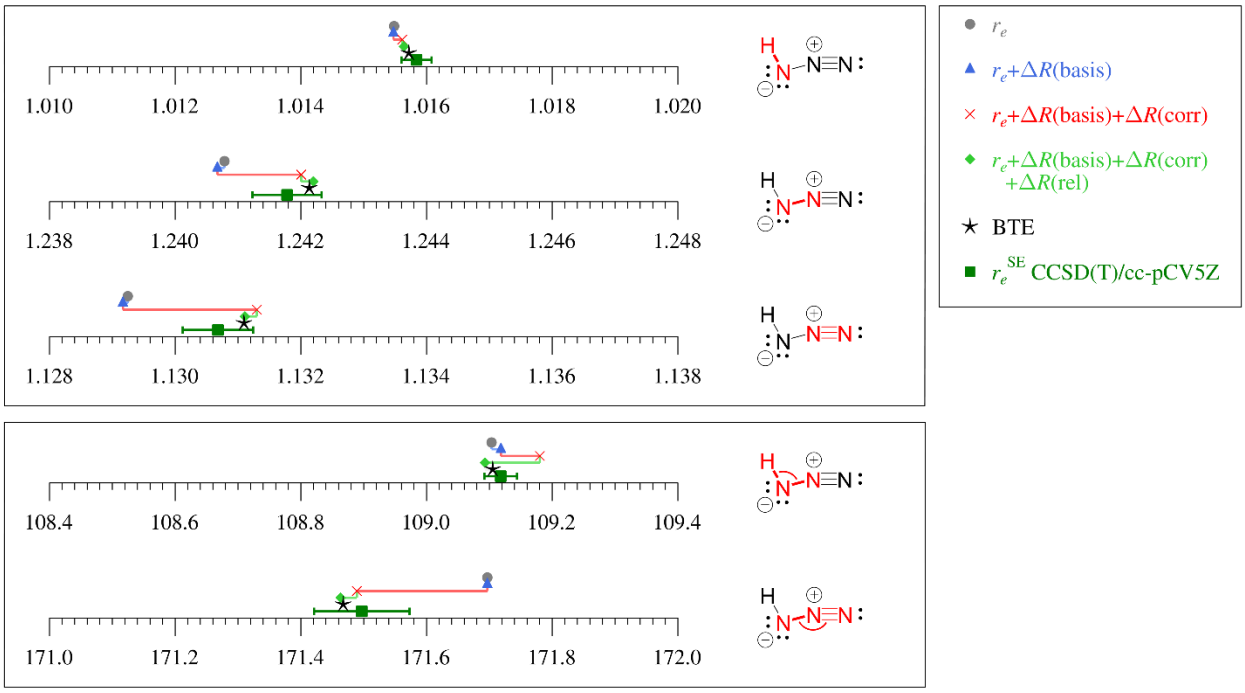

Figure 2.8. Graphical representation of the cumulative effects of corrections used to arrive at the BTE structure of hydrazoic acid, with consistent scales for each bond distance (0.01 Å) and each angle (1°). Parameters from the r_e^{SE} structure with 2σ uncertainties are included for comparison. The r_e in the legend refers to the CCSD(T)/cc-pCV6Z optimized structure. Per Table 2.5, ΔR(basis) for $\theta_{N1–N2–N3}$ has effectively been set to zero.

Chapter 3: The Semi-Experimental and Theoretical Structures of Pyridazine

Previously published in:

Owen, A. N.; Zdanovskaia, M. A.; Esselman, B. J.; Stanton, J. F.; Woods, R. C.; McMahon, R. J., Semi-Experimental Equilibrium (r_e^{SE}) and Theoretical Structures of Pyridazine (o-$C_4H_4N_2$). *Journal of Physical Chemistry A* **2021**, *125* (36), 7976-7987.

https://doi.org/10.1021/acs.jpca.1c06187

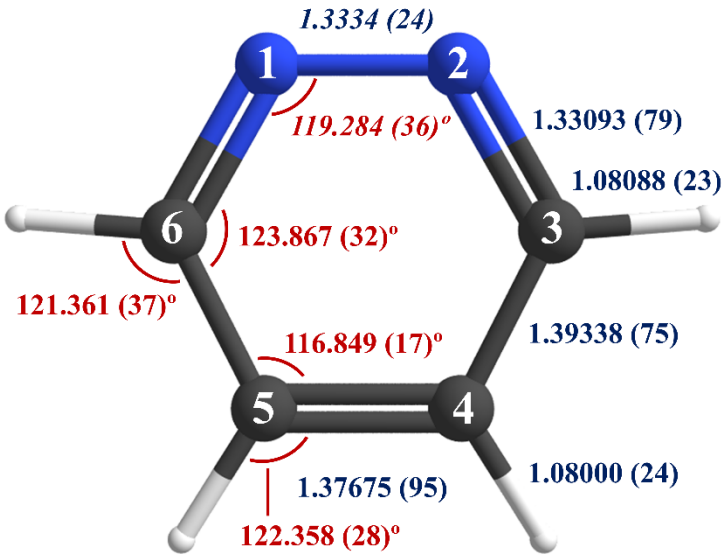

ABSTRACT

A semi-experimental equilibrium structure (r_e^{SE}) of pyridazine (*o*-$C_4H_4N_2$) has been determined using the rotational spectra of 18 isotopologues. Spectroscopic constants of four isotopologues are reported for the first time (measured from 235 to 360 GHz), while spectroscopic constants for previously reported isotopologues are improved by extending the frequency coverage (measured from 130 to 375 GHz). The experimental values of the ground-state rotational constants (A_0, B_0, and C_0) from each isotopologue were converted to determinable constants (A_0'', B_0'', and C_0''), which were then corrected for the effects of vibration-rotation interactions and electron-mass distributions using CCSD(T)/cc-pCVTZ calculations. The resultant r_e^{SE} for pyridazine determines bond distances to within 0.001 Å and bond angles within 0.04°, a reduction in the statistical uncertainties by at least a factor of two relative to the previously reported r_e^{SE}. The improvement in precision appears to be largely due to the use of higher-level theoretical calculations of the vibration-rotation and electron-mass effects, though the incorporation of the newly measured isotopologues ([4-^{2}H, 4-^{13}C]-, [4-^{2}H, 5-^{13}C]-, [4-^{2}H, 6-^{13}C]-, and [4,5-^{2}H, 4-^{13}C]-pyridazine) is partially responsible for the improved determination of the hydrogen-containing bond angles. The computed equilibrium structure (r_e) (CCSD(T)/cc-pCV5Z) and a "best theoretical estimate" of the equilibrium structure (r_e) both agree with the updated r_e^{SE} structure within the statistical experimental uncertainty (2σ) of each structural parameter.

INTRODUCTION

Pyridazine (*o*-$C_4H_4N_2$, C_{2v}, μ = 4.22 D, Figure 3.1) is an aromatic heterocycle in which adjacent C–H units of benzene are replaced by nitrogen atoms (Figure 3.2). As a prototypical aromatic heterocycle,[1-2] it is a species of astrochemical relevance.[3-5] Benzene has been detected

in the interstellar medium by infrared spectroscopy,[6] but it cannot be observed by radioastronomy because it lacks a permanent dipole moment. Aromatic compounds that are polar by virtue of inherent structural factors,[7-9] heteroatom substitution,[3-5] or polar substituents[10-12] have been important targets for astronomical detection (Figure 3.2). The recent detections of polar aromatic compounds by radioastronomy (benzonitrile[13] and cyanonaphthalenes[14]) represent dramatic breakthroughs in astrochemistry and will undoubtedly inspire new searches for aromatic heterocycles.

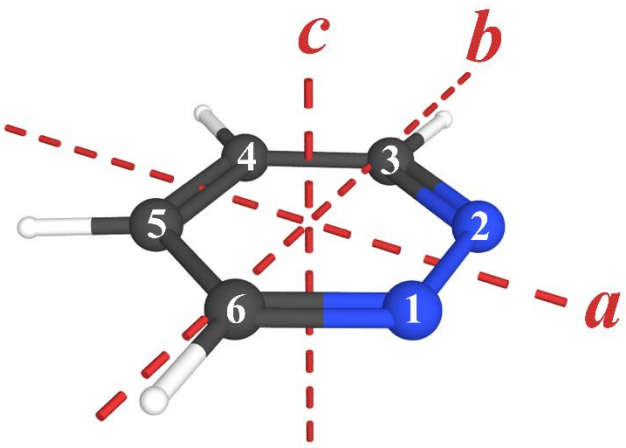

Figure 3.1. Pyridazine (*o*-$C_4H_4N_2$, C_{2v}, μ = 4.22 D, κ = 0.824) with principal axes and atom numbering.

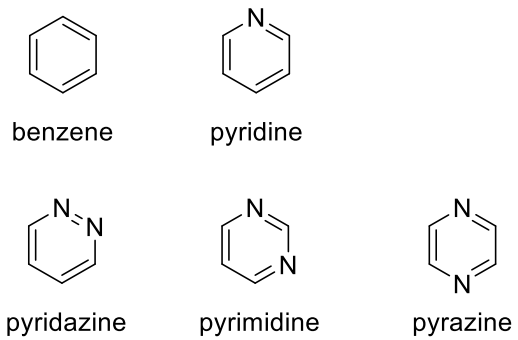

Figure 3.2. Benzene and nitrogen containing analogues.

Some time ago, Werner *et al.*[15] measured the rotational spectrum of pyridazine and its singly heavy-atom-substituted isotopologues from 9 to 33 GHz and obtained a partial substitution structure (r_s). In that first structure determination, parameters involving hydrogen atoms were held constant because rotational constants from deuterium-containing isotopologues were not available. López *et al.*[16] reported improved values for the rotational constants with precise Fourier-transform microwave (FT-MW) measurements of hyperfine-resolved transitions. Several years later, our group measured the spectrum of pyridazine at a higher frequency (235–360 GHz), reporting spectroscopic constants for the ground state and six lowest-energy vibrationally excited states of the normal isotopologue.[3] These measurements enabled the first direct comparison of the experimental and predicted [CCSD(T)] vibration-rotation interaction constants for an organic molecule of this size, demonstrating good agreement between the two. Building on the synergy of experiment and theory, the investigation was expanded to include a semi-experimental structure (r_e^{SE}) determination for pyridazine. Spectroscopic constants for a total of 14 isotopologues were measured, including the normal isotopologue, three singly substituted heavy-atom isotopologues detectable at natural abundance, and ten deuterium-substituted isotopologues from enriched samples. Using CCSD(T) corrections to the rotational constants to account for the vibration-rotation interaction and electron-mass distribution, a complete r_e^{SE} structure of pyridazine including the hydrogen-containing structural parameters was determined for the first time. That study determined a highly precise r_e^{SE} of pyridazine with statistical uncertainties (2σ) on the order of 0.003 Å for bond distances and 0.1° for bond angles.

The semi-experimental equilibrium structure of pyridazine[3] represented a significant advance in the gas-phase structure determination of organic molecules. Since then, however, a new standard for precision and accuracy has been achieved for r_e^{SE} structure determinations, in

general, and for aromatic heterocycles, in particular.[17-19] In a striking result, each of the structural parameters of pyrimidine (the *meta*-dinitrogen analogue of pyridazine; Figure 3.2) predicted by the best available theoretical methods agree with those determined in the semi-experimental equilibrium (r_e^{SE}) structure to within the 2σ statistical uncertainties of the latter.[19] The current work aims to incorporate new spectroscopic data, improve the computational treatment, and raise the precision of the r_e^{SE} structure of pyridazine to that same standard. The previous observation, measurement, and least-squares fitting of the [4-^{2}H, 3-^{13}C]-isotopologue of pyridazine implied that the spectra of the [4-^{2}H, 4-^{13}C]-, [4-^{2}H, 5-^{13}C]-, and [4-^{2}H, 6-^{13}C]-isotopologues* should also be observable in the existing spectrum due to sharing the same natural ^{13}C abundance, without the need for additional syntheses or spectroscopy. Indeed, we identified transitions for these new species and included their spectroscopic constants in the current structure determination. Rotational constants for the normal and singly heavy-atom substituted isotopologues were improved by extending frequency coverage down to 130 GHz and up to 375 GHz. The use of a larger, all-electron basis set (cc-pCVTZ) improved the quality of the vibration-rotation corrections used to determine the equilibrium rotational constants and consequent moments of inertia. Finally, the electron-mass correction was improved by incorporating corrections specific to each isotopologue. Such an improved r_e^{SE} structure for pyridazine provides an opportunity to test the generality of the close agreement between the experiment and theory observed in pyrimidine.[19] Furthermore, the effect on the r_e^{SE} structure determination of including isotopologues beyond those minimally required for a r_s structure determination will be assessed using the novel *xrefiteration* analysis detailed in Chapter 1 of this thesis.

* The systematic IUPAC name for the isotopologue that we designate as [4-^{2}H, 6-^{13}C] is actually [5-^{2}H, 3-^{13}C]. The latter numbering scheme, however, obscures the relationship with the other 4-^{2}H substituted isotopologues.

COMPUTATIONAL METHODS

A developmental version of CFOUR[20] was employed to conduct all *ab initio* calculations, which consisted of geometry optimizations, anharmonic second-order vibrational perturbation theory (VPT2), and magnetic property calculations at the CCSD(T) level of theory using the all-electron cc-pCVTZ basis. Isotopologue-dependent corrections to the rotational constants included vibration-rotation interaction constants from the VPT2 calculations and electron-mass corrections from the magnetic property calculations. Output files of these calculations are provided in the supporting information of Ref. 21.

We calculated a "best theoretical estimate" (BTE) equilibrium structure for pyridazine using the methodology employed in previous studies of pyrimidine,[19] thiophene,[17] and thiazole.[18] The structure computed using a CCSD(T)/cc-pCV5Z optimization is corrected to account for the following limitations associated with the quantum mechanical treatment employed:

1. Residual basis set effects, Eq. 3.1, by means of a complete basis set extrapolation[22-23] using the results of CCSD(T)/cc-pCVXZ (X = T, Q, and 5) calculations in comparison to the quintuple zeta optimization.

$$\Delta R(\text{basis}) = R(\infty) - R(\text{CCSD(T)/cc-pCV5Z}) \tag{3.1}$$

2. Residual electron correlation effects, Eq. 3.2, by use of CCSDT(Q)[24] in comparison to a CCSD(T) optimization.

$$\Delta R(\text{corr}) = R(\text{CCSDT(Q)/cc-pVDZ}) - R(\text{CCSD(T)/cc-pVDZ}) \tag{3.2}$$

3. Scalar relativistic effects, Eq. 3.3, by use of the X2C-1e variant of the coupled-cluster theory[25-27] in comparison to a traditional optimization (NR).

$$\Delta R(\text{rel}) = R(\text{CCSD(T)/cc-pCVTZ})_{\text{SFX2C-1e}} - R(\text{CCSD(T)/cc-pCVTZ})_{\text{NR}} \quad (3.3)$$

4. Effect of the Born–Oppenheimer approximation, Eq. 3.4, by use of the diagonal Born–Oppenheimer correction (DBOC)[28-29] in comparison to a traditional optimization (NR).

$$\Delta R(\text{DBOC}) = R(\text{SCF/cc-pCVTZ})_{\text{DBOC}} - R(\text{SCF/cc-pCVTZ})_{\text{NR}} \quad (3.4)$$

The correction to the CCSD(T)/cc-pCV5Z optimization necessary to obtain the BTE is then given by summation of the above corrections for each parameter, as shown in Eq. 3.5.

$$\Delta R(\text{best}) = \Delta R(\text{basis}) + \Delta R(\text{corr}) + \Delta R(\text{rel}) + \Delta R(\text{DBOC}) \quad (3.5)$$

The semi-experimental equilibrium structural parameters (r_e^{SE}) of pyridazine were determined from the equilibrium moments of inertia by least-squares fitting, as described for previous structure determinations.[3, 17-19, 30] In total, 18 isotopologues yield 36 independent moments of inertia, which produce a highly redundant determination of the 9 independent structural parameters of pyridazine (point group symmetry C_{2v}). In this work, all 3 moments of inertia for all 18 isotopologues were used with equal weighting. To generate constants free of centrifugal distortion and the impact of the choice of an A- or S-reduced Hamiltonian, the rotational constants (B_0^x) determined in each least-squares fit were converted to determinable constants (B_0'') using Eq. 3.S1 – Eq. 3.S6 in the Supporting Information.[31] For each of the isotopologues presented in this work, differences in the determinable constants from the A and S reductions were quite small (Table 3.4 in the Supporting Information), demonstrating that both the A- and S-reduced Hamiltonians produce physically meaningful spectroscopic constants. This gives us high confidence that the average determinable rotational constants are largely free of the effects of centrifugal distortion. The computed vibration-rotation interaction and electron-mass corrections were combined with experimental equilibrium constants (B_e^x) using Eq. 3.S7.[17-19, 30]

These equilibrium constants, after conversion to the corresponding moments of inertia, were used by the *xrefit* module of CFOUR to determine the r_e^{SE} structural parameters *via* a nonlinear least-squares fit, using the Levenberg–Marquardt algorithm. The *xrefiteration* analysis of the r_e^{SE} structure determination described in detail in Chapter 1 of this thesis is applied to assess the impact of including additional isotopologues beyond the minimal set, and for assessing the accuracy and precision of the overall structure.

RESULTS AND DISCUSSION

Improvement in the Precision and Accuracy of Rotational Constants and Moments of Inertia

For a planar molecule such as pyridazine, an indication of the quality of the computational corrections that are applied to the experimentally determined rotational constants is how close the resultant inertial defect (Δ_i) is to zero. Uncorrected experimental rotational constants (B_0^x) produce a non-zero inertial defect ($\Delta_{i\,0}$) due to the effects of electron mass. By correcting the rotational constants for these effects, the magnitude of the inertial defect is decreased, ultimately vanishing in the limit that the applied corrections are exact. Previously, CCSD(T)/ANO0 vibration-rotation interaction corrections[3] reduced the magnitude of the inertial defects for all isotopologues by a factor of 3 and by an additional factor of 10 after the inclusion of electron-mass corrections (Table 3.1). Though the magnitude of the electron-mass corrections to the rotational constants is small compared to that of the vibration-rotation corrections, the impact of including the electron-mass corrections is clearly significant. Despite the larger numbers of transitions for some isotopologues in the current study, the uncorrected inertial defect ($\Delta_{i\,0}$) values are quite similar to those obtained previously.

In this work, CCSD(T)/cc-pCVTZ corrections have been applied to the rotational constants, resulting in superior equilibrium inertial defect ($\Delta_{i\,e}$) values. There is a large reduction of the inertial defects from the CCSD(T)/cc-pCVTZ vibration-rotation interaction corrections than from those using an ANO0 basis set. In both cases, however, these are over-corrections that result in negative inertial defect values. The magnitude of the electron-mass corrections is smaller at the CCSD(T)/cc-pCVTZ level than with the ANO0 basis set. Previously, the same value for the electron-mass correction was applied to every isotopologue, rather than the isotopologue-specific electron-mass corrections used in the current work. As a result, not only are the fully corrected $\Delta_{i\,e}$ values obtained using the cc-pCVTZ basis approximately half the magnitude of those obtained using the ANO0 basis (average values −0.00108 vs 0.00207 μÅ^2, respectively), but they also exhibit a considerably smaller standard deviation (0.00014 vs 0.00104, respectively) (Table 3.1).

The small $\Delta_{i\,e}$ values are consistent with the high quality of the spectroscopic constants from the least-squares fits of the rotational spectra and the theoretical corrections employed in this work. These values are quite similar to those determined for pyrimidine[19] using corrections at the same level of theory: $\Delta_{i\,e}$ = 0.01353 ± 0.00013 without electron-mass corrections and $\Delta_{i\,e}$ = 0.00151 ± 0.00013 with electron-mass corrections. Given the systematic similarities in $\Delta_{i\,e}$ between analogous species pyridazine and pyrimidine, or as previously noted between thiophene[17] and thiazole,[18] it is likely the inertial defects could be further corrected, despite the sophisticated treatments already employed. Such an improved correction of these inertial defects may be possible through the use of a higher level of theory or basis set to perform the VPT2 or magnetic property calculations, or through use of higher-order vibrational perturbation theory to obtain additional vibration-rotation interaction corrections.

Table 3.1 Inertial Defects (Δ_i) of Pyridazine Isotopologues from Various Determinations of the Moments of Inertia

	Pyridazine (2013)[3]			Pyridazine (current work)		
Isotopologue	$\Delta_{i\,0}$ (uÅ^2)	$\Delta_{i\,e}$ (uÅ^2) [a]	$\Delta_{i\,e}$ (uÅ^2) [b]	$\Delta_{i\,0}$ (uÅ^2)	$\Delta_{i\,e}$ (uÅ^2) [c]	$\Delta_{i\,e}$ (uÅ^2) [d]
normal	0.03641	−0.01200	0.00081	0.03622	−0.01414	−0.00095
[3-^{13}C]	0.03702	−0.01193	0.00112	0.03681	−0.01410	−0.00090
[4-^{13}C]	0.03706	−0.01198	0.00116	0.03684	−0.01414	−0.00095
[1-^{15}N]	0.03686	−0.01206	0.00106	0.03671	−0.01414	−0.00095
[3-^{2}H]	0.03367	−0.01235	0.00133	0.03356	−0.01427	−0.00108
[4-^{2}H]	0.03406	−0.01228	0.00160	0.03391	−0.01428	−0.00108
[3,4-^{2}H]	0.03138	−0.01278	0.00195	0.03124	−0.01452	−0.00132
[3,5-^{2}H]	0.03143	−0.01287	0.00191	0.03132	−0.01455	−0.00135
[3,6-^{2}H]	0.03072	−0.01250	0.00224	0.03061	−0.01437	−0.00118
[4,5-^{2}H]	0.03185	−0.01206	0.00283	0.03169	−0.01417	−0.00097
[4-^{2}H, 3-^{13}C]	0.03498	−0.01194	0.00218	0.03441	−0.01433	−0.00114
[4-^{2}H, 4-^{13}C]				0.03456	−0.01416	−0.00097
[4-^{2}H, 5-^{13}C]				0.03450	−0.01419	−0.00099
[4-^{2}H, 6-^{13}C]				0.03462	−0.01420	−0.00100
[3,4,5-^{2}H]	0.02916	−0.01224	0.00351	0.02899	−0.01428	−0.00108
[3,4,6-^{2}H]	0.02852	−0.01283	0.00295	0.02836	−0.01454	−0.00134
[3,4,5,6-^{2}H]	0.02625	−0.01234	0.00440	0.02606	−0.01434	−0.00114
[4,5-^{2}H, 4-^{13}C]				0.03209	−0.01427	−0.00107
Average ($\bar{x}$)	0.03281	−0.01230	0.00207	0.03292	−0.01428	−0.00108
Std. Dev. (s)	0.00347	0.00033	0.00104	0.00310	0.00014	0.00014

[a] Vibration-rotation interaction corrections only (CCSD(T)/ANO0).
[b] Vibration-rotation interaction and electron-mass corrections (CCSD(T)/ANO0).
[c] Vibration-rotation interaction corrections only (CCSD(T)/cc-pCVTZ).
[d] Vibration-rotation interaction and electron-mass corrections (CCSD(T)/cc-pCVTZ).

Improvement in the Precision and Accuracy of the Structure

As demonstrated in Table 3.2, and displayed in Figure 3.3, the r_e^{SE} structure of pyridazine determined in this work exhibits structural parameters for which the statistical uncertainties have been reduced by a factor of 2–3 compared to the previous study. Despite the greater precision of the current work, all of the previously determined structural parameters[3] fall within the 2σ statistical uncertainties of the improved parameters in this work. For all explicitly determined parameters, that is, excluding $R_{N1\text{-}N2}$ and $\theta_{N1\text{-}N2\text{-}C3}$, the statistical uncertainty is less than 0.001 Å

for bond lengths and 0.04° for angles. These uncertainties are comparable to those observed in the r_e^{SE} of pyrimidine,[19] whose bond lengths were slightly better determined with all statistical uncertainties (2σ) less than 0.0006 Å. For pyridazine, the r_e^{SE} statistical uncertainties in the C–H distances, ±0.00023 and ±0.00024 Å, are three times smaller than the statistical uncertainties in the C–C and C–N distances, ±(0.00075–0.00095) Å. This was not the case for pyrimidine, in which the statistical uncertainties in C–H distances, ±(0.00030–0.00039) Å, were only slightly smaller than the statistical uncertainties in C–C and C–N distances, ±(0.00038–0.00052) Å. These differences in the uncertainties in C–H distances between pyridazine and pyrimidine may arise from symmetry considerations. Pyridazine (C_{2v}) possesses two independent C–H bonds with H-atom positions determined by virtue of ^{2}H-isotopic substitution in 11 of 14 isotopologues. Figure 3.3 presents the number of isotopologues with substitution(s) at the designated position used in the least-squares fit of the structure from all 18 isotopologues. For example, 2 at the C3 position indicates that its substitution is present in two isotopologues: [3-^{13}C] and [4-^{2}H, 2-^{13}C]. Symmetric atoms are accounted for separately, as some isotopologues break the C_{2v} symmetry of the parent species.

Table 3.2. Structural Parameters of Pyridazine

	Experimental				Computational	
		r_e^{SE} CCSD(T)/cc-pCVTZ				
Parameter	r_e^{SE} (2013) [a] CCSD(T)/ANO0	minimal data set	full data set excluding [3,4-^{2}H]	full data set	CCSD(T) BTE [b]	CCSD(T)/ cc-pCV5Z
$R_{C3\text{-}H}$ (Å)	1.08104 (54)	1.08088 (20)	1.08093 (15)	1.08088 (23)	1.08108	1.08097
$R_{C4\text{-}H}$ (Å)	1.08021 (74)	1.07992 (22)	1.07989 (16)	1.08000 (24)	1.07995	1.07988
$R_{C4\text{-}C5}$ (Å)	1.3761 (33)	1.37673 (88)	1.37676 (63)	1.37675 (95)	1.37638	1.37656
$R_{C3\text{-}C4}$ (Å)	1.3938 (24)	1.39352 (72)	1.39348 (50)	1.39338 (75)	1.39395	1.39353
$R_{N2\text{-}C3}$ (Å)	1.3302 (24)	1.33085 (70)	1.33082 (53)	1.33093 (79)	1.33091	1.33074
$R_{N1\text{-}N2}$ (Å)		1.33328 (82) [c]	1.33341 (77) [c]	1.33336 (116) [c]	1.33377	1.33215
$\theta_{H\text{-}C3\text{-}C4}$ (°)	121.35 (11)	121.367 (90)	121.396 (26)	121.361 (37)	121.353	121.335
$\theta_{H\text{-}C4\text{-}C5}$ (°)	122.368 (89)	122.344 (41)	122.357 (19)	122.358 (28)	122.349	122.346
$\theta_{C3\text{-}C4\text{-}C5}$ (°)	116.849 (60)	116.849 (16)	116.847 (12)	116.849 (17)	116.847	116.838
$\theta_{N2\text{-}C3\text{-}C4}$ (°)	123.863 (78)	123.860 (23)	123.868 (21)	123.867 (32)	123.879	123.857
$\theta_{N1\text{-}N2\text{-}C3}$ (°)		119.290 (16) [c]	119.285 (17) [c]	119.284 (27) [c]	119.275	119.305
N_{iso}	14	6	17	18		

[a] Data is given to one additional digit relative to the presentation in Ref. 3, and the uncertainties here are 2σ rather than 1σ.

[b] Obtained by applying corrections for the best theoretical estimate [ΔR(best)] to the CCSD(T)/cc-pCV5Z computed values.

[c] Value and uncertainty for additional parameters determined from the r_e^{SE} structure using the alternate Z-matrix described in Supporting Information.

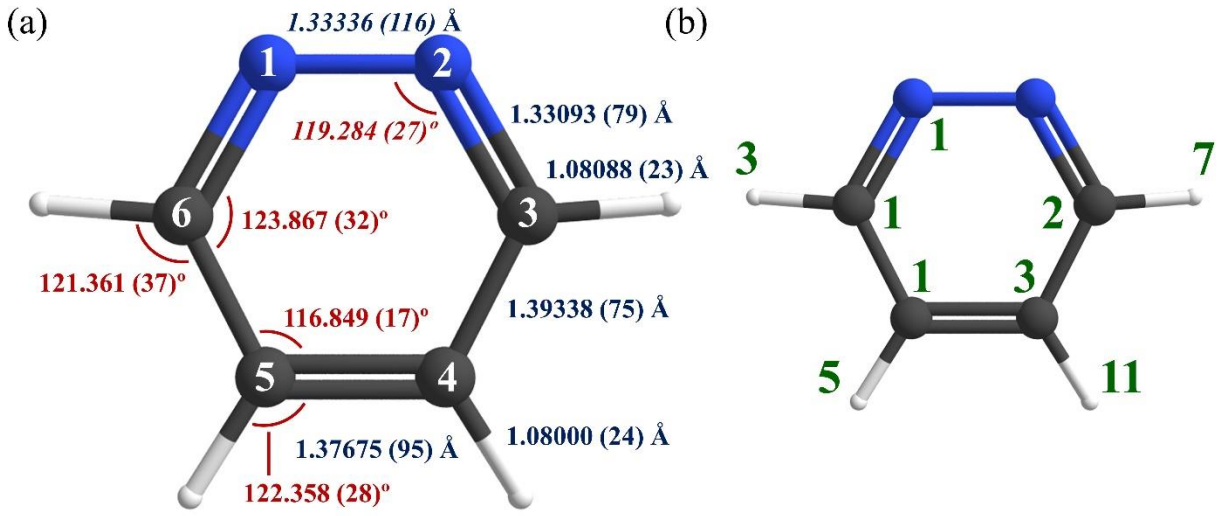

Figure 3.3. (a) Semi-experimental equilibrium structure (r_e^{SE}) of pyridazine with 2σ uncertainties from least-squares fitting of the isotopologue moments of inertia. The values and uncertainties for $R_{N1\text{-}N2}$ and $\theta_{N1\text{-}N2\text{-}C3}$ (in italic) were determined from the r_e^{SE} structure using the alternate Z-matrix described in the Supporting Information. (b) Number of isotopologues with a substitution relative to the main isotopologue (*o*-$C_4H_4N_2$) at the labeled atom.

Quantifying the Importance of Including More Isotopologues in Structure Determinations

To determine the impact on the r_e^{SE} structure of including isotopologues beyond the minimal set necessary to obtain a substitution structure, we obtained an r_e^{SE} structure using only the normal and all single isotopic substitutions, which we refer to as "minimal r_e^{SE}". As shown in Table 3.2, the parameters' values and uncertainties of the minimal r_e^{SE} agree well with those of the full r_e^{SE} structure. In fact, the uncertainties of the minimal r_e^{SE} are slightly smaller for most of the parameters. The exceptions ($\theta_{H\text{-}C3\text{-}C4}$ and $\theta_{H\text{-}C4\text{-}C5}$) are notable, as these are the angles involving a hydrogen atom. The better determination of these angles in the full r_e^{SE} structure is likely due to

the inclusion of many more deuterium-substituted isotopologues, relative to the minimal r_e^{SE} set, which includes only two deuterium-substituted isotopologues. Thus, it appears that bond lengths and angles involving only heavy atoms, as well as bond lengths involving hydrogen, are well determined using a minimal set of isotopologues but angles involving hydrogen are not. This conclusion is supported by the behavior of the parameters in the *xrefiteration* analysis (*vide infra*).

The inclusion of additional isotopologues beyond the "minimal set" does indeed improve the overall relative statistical uncertainty of the results r_e^{SE} structure. To explore the impact of additional isotopologues on the uncertainty and magnitude of each parameter, we conducted the *xrefiteration* analysis described above. The δr_e^{SE} results of *xrefiteration* are plotted in Figure 3.4, showing a dramatic decrease in the relative statistical uncertainty by nearly 50% as the initial isotopologues are added to the r_e^{SE} data set. Such behavior is expected based upon the *xrefiteration* results of pyrimidine, thiophene, thiazole, and hydrazoic acid (*vide infra*). The significant reduction in uncertainty appears to be reversed with the addition of isotopologues in the range N_{iso} = 12–18. There is a slight increase in the uncertainty upon including isotopologues in the range of N_{iso} = 12–17, without any discernable pattern in the isotopic substitution or the number of transitions in the least-squares fits for those isotopologues. Thus, we do not suspect that there is an issue with the experimentally determined spectroscopic constants. The incorporation of [3,4-^{2}H]-pyridazine (N_{iso} = 18), however, results in a dramatic increase in δr_e^{SE} to 0.001204, which is only slightly lower than the value for the minimal r_e^{SE}. From this behavior, we conclude that the structural information provided by [3,4-^{2}H]-pyridazine to the r_e^{SE} determination is in contradiction with the information provided collectively by the other isotopologues. We can infer, based on the *xrefiteration* algorithm, that at every step of the analysis, the addition of the [3,4-^{2}H] isotopologue resulted in a larger δr_e^{SE} than another isotopologue, so the [3,4-^{2}H] isotopologue was not

incorporated into the expanding data set. At the end of the *xrefiteration* analysis, when there were no other isotopologues left, the [3,4-^{2}H] isotopologue was allowed into the structure determination data set.

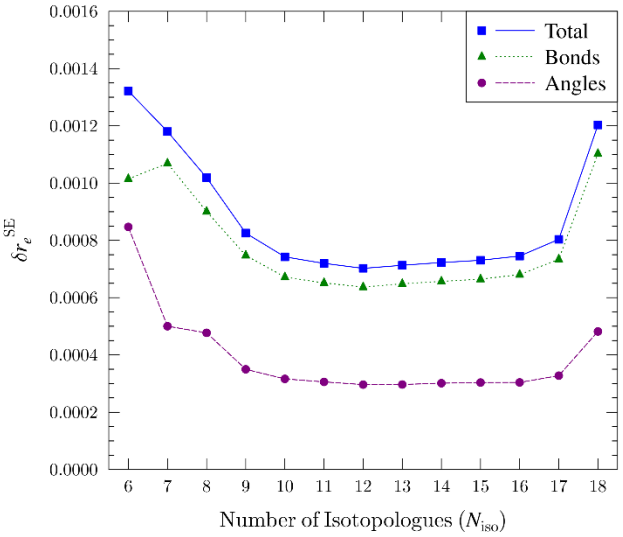

N_{iso}	Isotopologue Added
6	Minimal Set
7	[3,5-^{2}H]
8	[4-^{2}H, 5-^{13}C]
9	[4,5-^{2}H]
10	[4-^{2}H, 3-^{13}C]
11	[4,5-^{2}H, 4-^{13}C]
12	[3,4,5-^{2}H]
13	[4-^{2}H, 4-^{13}C]
14	[3,6-^{2}H]
15	[3,4,5,6-^{2}H]
16	[4-^{2}H, 6-^{13}C]
17	[3,4,6-^{2}H]
18	[3,4-^{2}H]

Figure 3.4. Plot of δr_e^{SE} as a function of the number of isotopologues (N_{iso}) incorporated into the structure determination data set. The total relative statistical uncertainty (δr_e^{SE}, blue squares), the relative statistical uncertainty in the bond distances (green triangles), and the relative statistical uncertainty in the angles (purple circles) are presented.

In the course of this work and other structure determination analyses,[17-18, 32] we observed that similar dramatic increases in the relative statistical uncertainties resulted from a variety of factors, including problems in the fitting of the spectroscopic constants, problems in the rotational constant corrections, or some other problem in the implementation. Such issues appear to be absent in our implementation of the current analysis. For the [3,4-^{2}H] isotopologue in particular, the least-squares fit of the rotational spectrum has low uncertainty (σ_{fit} = 34 kHz) with sufficient line count (N_{lines} = 619), and all spectroscopic constants are in reasonable agreement with

computational predictions. Furthermore, the corrected inertial defect for this isotopologue ($\Delta_{i\ e}$ = −0.0134 μÅ^2) is comparable to those of the other isotopologues, albeit larger than those of all but two isotopologues ([3,5-^{2}H]- and [3,4,6-^{2}H]-pyridazine). Taken collectively, this evidence suggests that the experimental data for the [3,4-^{2}H] isotopologue are accurate and reasonably treated by the vibration-rotation interaction and electron-mass corrections. Thus, we are confident that the behavior of the relative statistical uncertainty of the r_e^{SE} upon addition of the [3,4-^{2}H] isotopologue is not due to an issue in data analysis.

Comparison of the *xrefiteration* analysis of pyridazine to that of other molecules (Figure 1.5 in Chapter 1 of this thesis) clearly demonstrates that the influence of [3,4-^{2}H]-pyridazine on the r_e^{SE} structure is anomalous in relation to the other isotopologues in the limited set of comparison molecules (hydrazoic acid, pyrimidine, thiophene, and thiazole). Even with the increase in the δr_e^{SE} for pyridazine from N_{iso} = 12–18, however, the range of δr_e^{SE} values for pyridazine is similar to that of the other structure determinations. Therefore, the increase in the δr_e^{SE} of pyridazine – particularly due to the inclusion of the [3,4-^{2}H] isotopologue – does not necessarily indicate that the r_e^{SE} is not sufficiently determined.

To further assess the quality of the r_e^{SE} and whether the structural parameters are reliable despite the aforementioned behavior of [3,4-^{2}H]-pyridazine, we examined how the r_e^{SE} parameters change as additional isotopologues are included (Figure 3.5). Interestingly, the value of the $\theta_{H\text{-}C3\text{-}C4}$ angle in the final iteration (N_{iso} = 18) is closer to its value in the minimal set (N_{iso} = 6) than the intermediate iterations, which determine a larger angle. Given our confidence in the data of the [3,4-^{2}H] isotopologue, the trend in the $\theta_{H\text{-}C3\text{-}C4}$ angle suggests that the other isotopologues added to the minimal set are quite consistent with respect to their impact on this angle, while also not providing new or sufficient information for determining this angle. This interpretation is

further supported by comparison to the BTE value, which shows that the intermediate isotopologues cause the angle to deviate away from the BTE value. Examination of the other parameters reveals that $R_{C4\text{-}C5}$, $R_{C3\text{-}C4}$, and $R_{N2\text{-}C3}$ have similar, though less pronounced, behavior. The inclusion of the last few isotopologues, especially the [3,4-^{2}H] isotopologue, brings the parameters into a better agreement with the theoretical prediction because these isotopologues are providing structural information that is not contained in the preceding iterations of the data set.

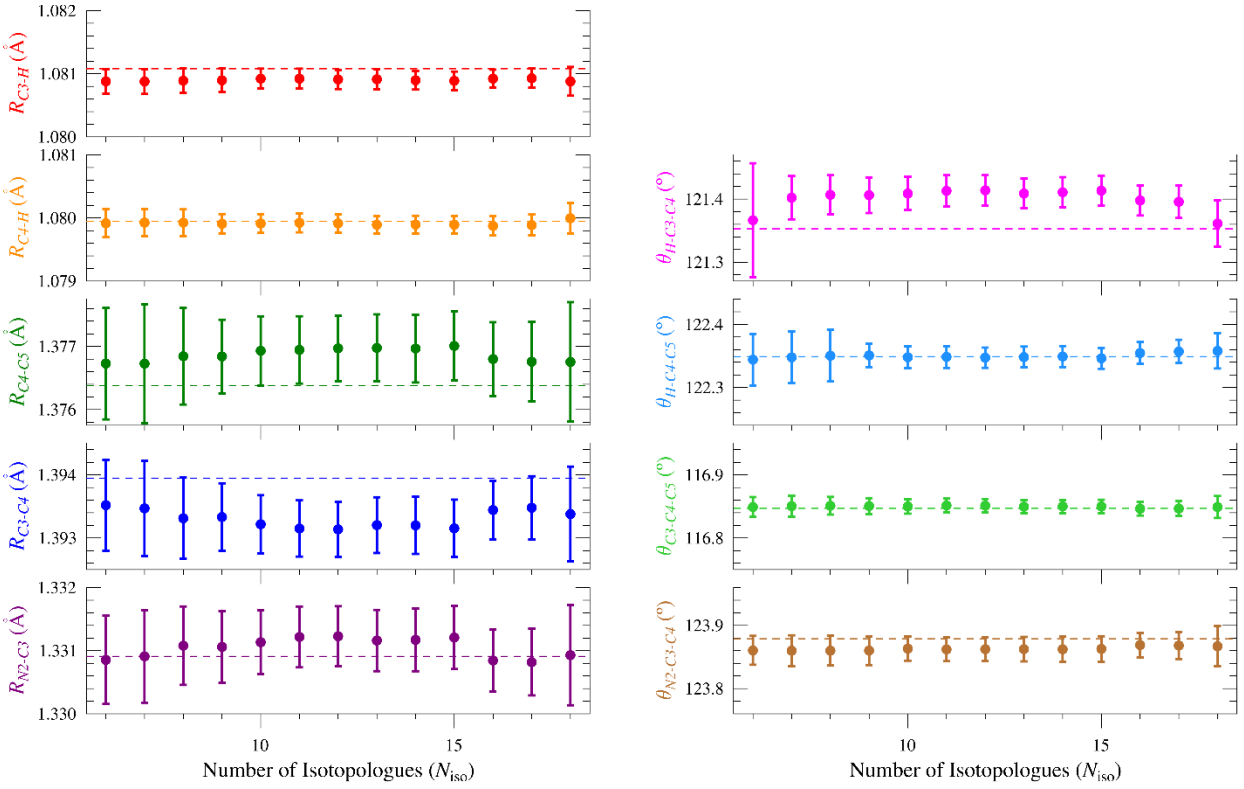

Figure 3.5. Plots of structural parameters as a function of the number of isotopologues (N_{iso}) and their 2σ uncertainties, with consistent scales for each distance (0.002 Å) and each angle (0.2°). The dashed line in each plot is the BTE value calculated for that parameter. The isotopologue ordering along the *x*-axis is the same as that in Figure 3.4.

The C3 atom, which lies very close to the *b*-axis, is present in three of the four parameters whose values deviate away from the BTE. The difficulty in determining the C3 atom position was described in the original r_s structure determination[15] and seemingly addressed in the subsequent r_s and first r_e^{SE} structure determination by greater isotopic substitution.[3] Based upon this analysis, however, it appears that the classical difficulty in determining the position of the atoms that lie close to an inertial axis by Kraitchman analysis[33-34] may not be fully addressed even with the first 17 isotopologues in this work. The inclusion of the [3,4-^{2}H] isotopologue has a profound effect on the $\theta_{H\text{-}C3\text{-}C4}$ angle. The simultaneous isotopic substitution of the hydrogen atoms at C3 and C4 causes a significant rotation of the principal axes (Supporting Information, Table 3.6) such that C3 (and the symmetric C6) are no longer close to the *b*-axis. It should be noted that other isotopologues have rotations of similar magnitude. Finally, the two hydrogen-containing angles have considerable improvement in the uncertainties and the greatest change to their values when isotopologues beyond the minimal set are included. Such behavior suggests that the minimal set of singly substituted isotopologues is not sufficient for a precise determination of these angles and that improvement in the uncertainties in the full r_e^{SE} structure for these angles is partly due to the increased number of isotopologues.

Best Theoretical Estimate

As in the structure determination of pyrimidine,[19] all structural parameters of the BTE of pyridazine fall within the 2σ uncertainties of their corresponding parameters for the r_e^{SE} structure of pyridazine (Figure 3.6 and Table 3.2). Impressively, five of the nine independent BTE structural parameters fall within the 1σ statistical uncertainties of the r_e^{SE} parameters in this work, which is

reasonably close to the statistical expectation for a normal distribution.* As can be seen from Table 3.2, all of the r_e^{SE} bond angles fall within 0.01° of the corresponding BTE values. The agreement is largely due to the quintuple-zeta basis set since all of the CCSD(T)/cc-pCV5Z structural parameters are also within the 2σ uncertainties of the corresponding r_e^{SE} parameters. Indeed, examination of the CCSD(T)/cc-pCVQZ structural parameters (Supporting Information, Table 3.7) reveals that only four of the nine independent parameters resulting from the smaller basis agree with the r_e^{SE} structure. The difference between the quadruple-zeta and quintuple-zeta calculations, however, is only noticeable because of the small uncertainties in the current r_e^{SE} structure of pyridazine. All parameters of the CCSD(T)/cc-pCVQZ r_e fell within 2σ of all the previously determined r_e^{SE} parameters,[3] due to the larger statistical uncertainties in that work.

* A normal distribution of the uncertainties of the parameters suggests that each parameter is being determined equally well by the r_e^{SE} method.

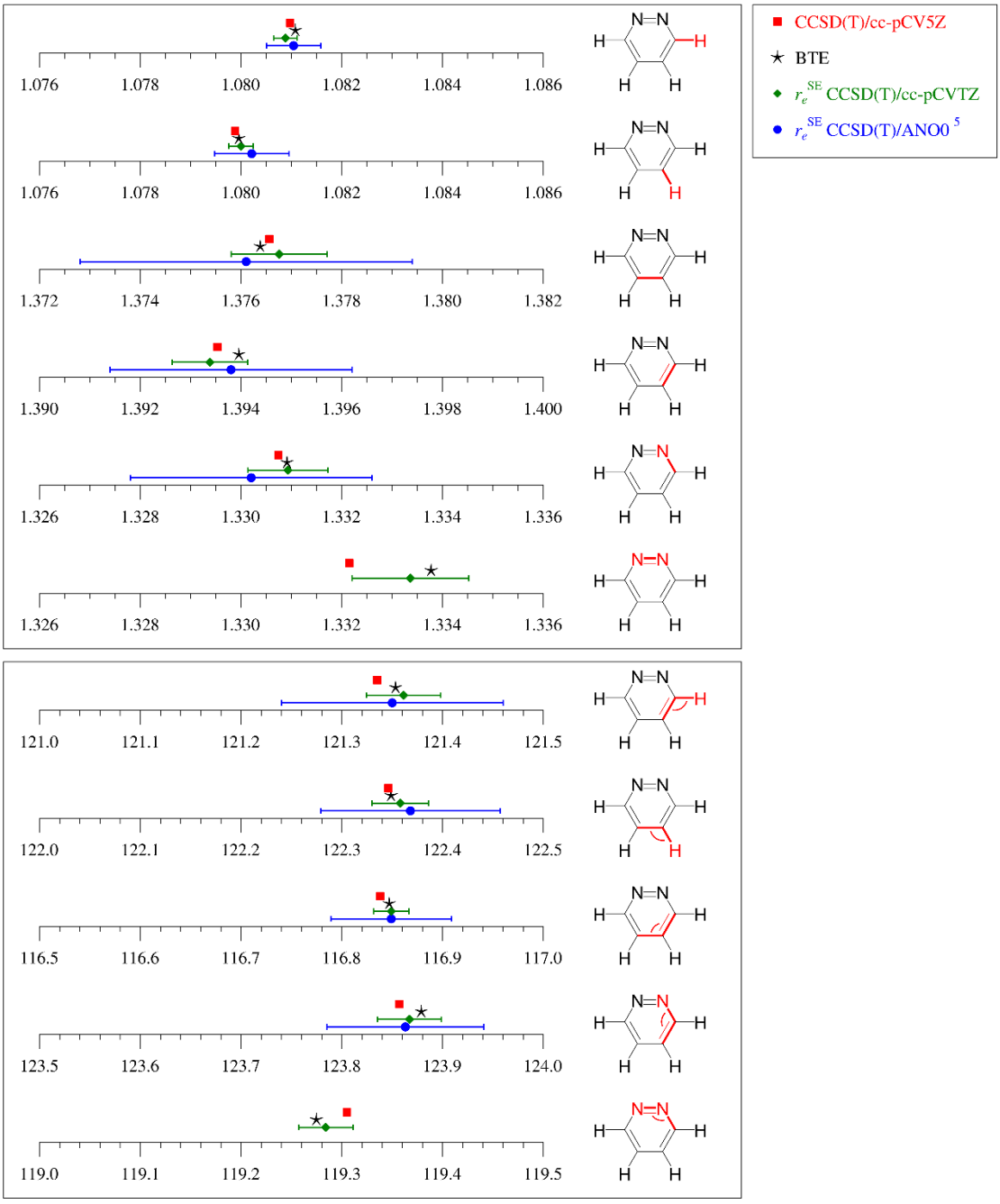

Figure 3.6. Graphical comparison of pyridazine structural parameters with bond distances in angstroms (Å) and angles in degrees (°). Uncertainties shown are 2σ. Data for r_e^{SE} CCSD(T)/ANO0 are taken from Ref. 3. The values and uncertainties for $R_{N1\text{-}N2}$ (top box, last row) and $\theta_{N1\text{-}N2\text{-}C3}$ were determined from the r_e^{SE} structure using the alternate Z-matrix described in the Supporting Information.

Examination of the individual corrections in the BTE in Table 3.3 reveals differences in the effects of the various corrections for bond distances. The ΔR(basis) and ΔR(rel) corrections shorten the bond distances from those predicted at the quintuple-zeta basis set, while the ΔR(corr) correction lengthens them. Overall, the corrections lead to a partial cancellation that brings the BTE r_e structure into better agreement with the r_e^{SE} structure.

Table 3.3. Corrections (ΔR) Used for Obtaining the Best Theoretical Estimate (BTE)

Parameter	ΔR(basis) Eq. (1)	ΔR(corr) Eq. (2)	ΔR(rel) Eq. (3)	ΔR(DBOC) Eq. (4)	ΔR(best) Eq. (5)
$R_{C3\text{-}H}$ (Å)	−0.000040	0.00012	−0.00011	0.00014	0.00011
$R_{C4\text{-}H}$ (Å)	−0.000063	0.00012	−0.00011	0.00014	0.000074
$R_{C4\text{-}C5}$ (Å)	−0.00034	0.00042	−0.00024	−0.000022	−0.00018
$R_{C3\text{-}C4}$ (Å)	−0.00021	0.00080	−0.00023	0.000058	0.00042
$R_{N2\text{-}C3}$ (Å)	−0.00014	0.00042	−0.000089	−0.000022	0.00017
$\theta_{H\text{-}C3\text{-}C4}$ (°)	0.032	−0.019	0.0030	0.0023	0.018
$\theta_{H\text{-}C4\text{-}C5}$ (°)	−0.00085	0.0026	0.0011	0.000045	0.0028
$\theta_{C3\text{-}C4\text{-}C5}$ (°)	0.010	−0.00083	−0.00045	0.00065	0.0090
$\theta_{N2\text{-}C3\text{-}C4}$ (°)	−0.020	0.029	0.014	−0.0012	0.022

CONCLUSION

We determined a highly accurate and precise semi-experimental structure (r_e^{SE}) for pyridazine with statistical uncertainties of <0.001 Å and <0.04° (2σ) for the bond distances and angles, respectively, and in complete agreement with the BTE. The improvement in the r_e^{SE} structure in this work is largely due to improved theoretical corrections. Our iterative analysis of the r_e^{SE} structure determination (*xrefiteration*) as a function of additional isotopologues beyond the minimal set can be utilized to examine not only the improvement in the r_e^{SE} determination as additional isotopologues are added, but also the relationship between an individual isotopologue and the rest of the data set. The *xrefiteration* plots can be especially useful for identifying outliers

that occur due to problems in the spectroscopic analysis or the implementation of the r_e^{SE} structure determination. When the spectroscopic constants are reliable and the structure determination is implemented correctly, the *xrefiteration* plots reveal important trends in how the individual parameters vary as a function of the number of isotopologues. This provides insights into the structural information contributed by individual isotopologues. Finally, the *xrefiteration* plots can reveal which r_e^{SE} parameters are well-converged, and which may benefit from the incorporation of additional isotopologues.

We are confident that the behavior of the [3,4-^{2}H] isotopologue in the *xrefiteration* analysis is a real phenomenon and not a manifestation of a problem in the analysis or implementation. Given the impressive agreement between the BTE and the r_e^{SE} parameters, we can examine how this agreement is affected by the presence or absence of the [3,4-^{2}H] isotopologue. When the [3,4-^{2}H] isotopologue is excluded from the data set, the resulting r_e^{SE} does not display good agreement with the BTE (Table 3.2) for the two hydrogen-containing bond angles, $\theta_{\text{H-C3-C4}}$ and $\theta_{\text{H-C4-C5}}$. The better agreement between the r_e^{SE} structure and the BTE when [3,4-^{2}H] is included indicates that the apparent improvement in the statistical uncertainty as the other isotopologues were added to the minimal set (Figure 3.4) is actually deceptive; the preceding data sets did not include the isotopologue that is important for determining $\theta_{\text{H-C3-C4}}$ and $\theta_{\text{H-C4-C5}}$. If the r_e^{SE} structure remains stable as additional isotopologues are incorporated beyond the 18 utilized in this work, it would confirm the validity of this assertion. New syntheses – beyond the scope of this work – would be required, as all possible isotopologues observable in commercial pyridazine or in the deuteriated samples used in the previous and current works are included in the current r_e^{SE}. While it is not a member of the canonical set of singly substituted isotopologues, the [3,4-^{2}H] isotopologue appears to be vital in the structure determination, as this substitution tends to rotate the principal axes in

such a way that the C3 and C6 atoms are pulled away from the *b*-axis. The standard problem in structure determination that is posed by near-axis atoms is lessened for this isotopomer, and an improved structure determination follows. Regardless of the reason, the impact of the [3,4-^{2}H] on the structure determination is as significant as it is unexpected, serving to reinforce the notion that structure determinations should seek to incorporate a variety of isotopologues to ensure that the atom positions can be satisfactorily determined.

The agreement of the r_e^{SE} and BTE structures is impressive. What was unexpected, to us, is the finding that minimal set of six isotopologues provided r_e^{SE} structural parameters that are equally accurate and precise as those determined using the much larger set of 18 isotopologues. This case stands in sharp contrast to our findings for similar structure determinations of pyrimidine,[19] thiophene,[17] and thiazole.[18] At the current time, it is not understood, *a priori*, whether a particular structure will be accurately determined from the minimal set of isotopologues. The unexpected significance of the [3,4-^{2}H] isotopologue in the structure determination of pyridazine suggests that the best practice remains to include as many isotopologues as is practical.

ACKNOWLEDGEMENTS

We gratefully acknowledge the National Science Foundation for support of this project (CHE-1664912 and CHE-1954270).

REFERENCES

1. Levandowski, B. J.; Abularrage, N. S.; Raines, R. T., Differential Effects of Nitrogen Substitution in 5- and 6-Membered Aromatic Motifs. *Chem. Eur. J.* **2020,** *26* (41), 8862-8866.

2. Dey, S.; Manogaran, D.; Manogaran, S.; Schaefer, H. F., Quantification of Aromaticity of Heterocyclic Systems Using Interaction Coordinates. *J. Phys. Chem. A* **2018,** *122* (34), 6953-6960.

3. Esselman, B. J.; Amberger, B. K.; Shutter, J. D.; Daane, M. A.; Stanton, J. F.; Woods, R. C.; McMahon, R. J., Rotational Spectroscopy of Pyridazine and its Isotopologs from 235-360 GHz: Equilibrium Structure and Vibrational Satellites. *J. Chem. Phys.* **2013,** *139*, 224304.

4. Charnley, S. B.; Kuan, Y.-J.; Huang, H.-C.; Botta, O.; Butner, H. M.; Cox, N.; Despois, D.; Ehrenfreund, P.; Kisiel, Z.; Lee, Y.-Y.; Markwick, A. J.; Peeters, Z.; Rodgers, S. D., Astronomical searches for nitrogen heterocycles. *Adv. Space Res.* **2005,** *36* (2), 137-145.

5. Simon, M. N.; Simon, M., Search for Interstellar Acrylonitrile, Pyrimidine, and Pyridine. *Astrophys. J.* **1973,** *184*, 757.

6. Cernicharo, J.; Heras, A. M.; Tielens, A. G. G. M.; Pardo, J. R.; Herpin, F.; Guélin, M.; Waters, L. B. F. M., Infrared Space Observatory's Discovery of C_4H_2, C_6H_2, and Benzene in CRL 618. *Astrophys. J.* **2001,** *546* (2), L123-L126.

7. Widicus Weaver, S. L.; Remijan, A. J.; McMahon, R. J.; McCall, B. J., A Search for *ortho*-Benzyne (*o*-C_6H_4) in CRL 618. *Astrophys. J.* **2007,** *671* (2), L153-L156.

8. Lovas, F. J.; McMahon, R. J.; Grabow, J.-U.; Schnell, M.; Mack, J.; Scott, L. T.; Kuczkowski, R. L., Interstellar Chemistry: A Strategy for Detecting Polycyclic Aromatic Hydrocarbons in Space. *J. Am. Chem. Soc.* **2005,** *127*, 4345-4349.

9. McMahon, R. J.; McCarthy, M. C.; Gottlieb, C. A.; Dudek, J. B.; Stanton, J. F.; Thaddeus, P., The Radio Spectrum of the Phenyl Radical. *Astrophys. J.* **2003,** *590* (1), L61-L64.

10. Dorman, P. M.; Esselman, B. J.; Woods, R. C.; McMahon, R. J., An analysis of the rotational ground state and lowest-energy vibrationally excited dyad of 3-cyanopyridine: Low symmetry reveals rich complexity of perturbations, couplings, and interstate transitions. *J. Mol. Spectrosc.* **2020,** *373*, 111373.

11. Dorman, P. M.; Esselman, B. J.; Park, J. E.; Woods, R. C.; McMahon, R. J., Millimeter-wave spectrum of 4-cyanopyridine in its ground state and lowest-energy vibrationally excited states, ν_{20} and ν_{30}. *J. Mol. Spectrosc.* **2020,** *369*, 111274.

12. Zdanovskaia, M. A.; Esselman, B. J.; Woods, R. C.; McMahon, R. J., The 130 - 370 GHz Rotational Spectrum of Phenyl Isocyanide (C_6H_5NC). *J. Chem. Phys.* **2019,** *151*, 024301.

13. McGuire, B. A.; Burkhardt, A. M.; Kalenskii, S.; Shingledecker, C. N.; Remijan, A. J.; Herbst, E.; McCarthy, M. C., Detection of the aromatic molecule benzonitrile (c-C6H5CN) in the interstellar medium. *Science* **2018,** *359* (6372), 202-205.

14. McGuire, B. A.; Loomis, R. A.; Burkhardt, A. M.; Lee, K. L. K.; Shingledecker, C. N.; Charnley, S. B.; Cooke, I. R.; Cordiner, M. A.; Herbst, E.; Kalenskii, S.; Siebert, M. A.; Willis, E. R.; Xue, C.; Remijan, A. J.; McCarthy, M. C., Detection of two interstellar polycyclic aromatic hydrocarbons via spectral matched filtering. *Science* **2021,** *371* (6535), 1265-1269.

15. Werner, W.; Dreizler, H.; Rudolph, H. D., Zum Mikrowellenspektrum Des Pyridazins. *Z. Naturforsch., A: Phys. Sci.* **1967,** *22* (4), 531-543.

16. López, J. C.; de Luis, A.; Blanco, S.; Lesarri, A.; Alonso, J. L., Investigation of the quadrupole coupling hyperfine structure due to two nuclei by molecular beam Fourier transform microwave spectroscopy: spectra of dichlorofluoromethane and pyridazine. *J. Mol. Struct.* **2002,** *612* (2-3), 287-303.

17. Orr, V. L.; Ichikawa, Y.; Patel, A. R.; Kougias, S. M.; Kobayashi, K.; Stanton, J. F.; Esselman, B. J.; Woods, R. C.; McMahon, R. J., Precise Equilibrium Structure Determination of Thiophene (C_4H_4S) by Rotational Spectroscopy – Structure of a Five-Membered Heterocycle Containing a Third-Row Atom. *J. Chem. Phys.* **2021,** *154*, 244310.

18. Esselman, B. J.; Zdanovskaia, M. A.; Owen, A. N.; Stanton, J. F.; Woods, R. C.; McMahon, R. J., Precise Equilibrium Structure Determination of Thiazole (C_3H_3NS) from Twenty-Four Isotopologues. *J. Chem. Phys.* **2021,** *155*, 054302.

19. Heim, Z. N.; Amberger, B. K.; Esselman, B. J.; Stanton, J. F.; Woods, R. C.; McMahon, R. J., Molecular structure determination: Equilibrium structure of pyrimidine (*m*-$C_4H_4N_2$) from rotational spectroscopy (r_e^{SE}) and high-level ab initio calculation (r_e) agree within the uncertainty of experimental measurement. *J. Chem. Phys.* **2020,** *152* (10), 104303.

20. . CFOUR, a quantum chemical program package written by J.F. Stanton, J. Gauss, L. Cheng, M.E. Harding, D.A. Matthews, P.G. Szalay with contributions from A.A. Auer, R.J. Bartlett, U. Benedikt, C. Berger, D.E. Bernholdt, Y.J. Bomble, O. Christiansen, F. Engel, R. Faber, M. Heckert, O. Heun, C. Huber, T.-C. Jagau, D. Jonsson, J. Jusélius, K. Klein, W.J. Lauderdale, F. Lipparini, T. Metzroth, L.A. Mück, D.P. O'Neill, D.R. Price, E. Prochnow, C. Puzzarini, K. Ruud, F. Schiffmann, W. Schwalbach, C. Simmons, S. Stopkowicz, A. Tajti, J. Vázquez, F. Wang, J.D. Watts and the integral packages MOLECULE (J. Almlöf and P.R. Taylor), PROPS (P.R. Taylor), ABACUS (T. Helgaker, H.J. Aa. Jensen, P. Jørgensen, and J. Olsen), and ECP routines by A. V. Mitin and C. van Wüllen. For the current version, see http://www.cfour.de.

21. Owen, A. N.; Zdanovskaia, M. A.; Esselman, B. J.; Stanton, J. F.; Woods, R. C.; McMahon, R. J., Semi-Experimental Equilibrium (r_e^{SE}) and Theoretical Structures of Pyridazine (*o*-$C_4H_4N_2$). *J. Phys. Chem. A* **2021,** *125* (36), 7976-7987.

22. Woon, D. E.; Dunning, T. H., Benchmark Calculations with Correlated Molecular Wave-Functions .6. 2nd-Row-a(2) and First-Row 2nd-Row-Ab Diatomic-Molecules. *J. Chem. Phys.* **1994,** *101* (10), 8877-8893.

23. Peterson, K. A.; Kendall, R. A.; Dunning, T. H., Benchmark Calculations with Correlated Molecular Wave-Functions .2. Configuration-Interaction Calculations on 1st-Row Diatomic Hydrides. *J. Chem. Phys.* **1993,** *99* (3), 1930-1944.

24. Bomble, Y. J.; Stanton, J. F.; Kallay, M.; Gauss, J., Coupled-cluster methods including noniterative corrections for quadruple excitations. *J. Chem. Phys.* **2005,** *123* (5), 054101, 054101.

25. Cheng, L.; Gauss, J., Analytic energy gradients for the spin-free exact two-component theory using an exact block diagonalization for the one-electron Dirac Hamiltonian. *J. Chem. Phys.* **2011,** *135* (8), 084114, 084114.

26. Liu, W.; Peng, D., Exact two-component Hamiltonians revisited. *J. Chem. Phys.* **2009,** *131* (3), 031104, 031104.

27. Dyall, K. G., Interfacing relativistic and nonrelativistic methods. IV. One- and two-electron scalar approximations. *J. Chem. Phys.* **2001,** *115* (20), 9136-9143.

28. Handy, N. C.; Yamaguchi, Y.; Schaefer, H. F., The Diagonal Correction to the Born-Oppenheimer Approximation - Its Effect on the Singlet-Triplet Splitting of CH_2 and Other Molecular Effects. *J. Chem. Phys.* **1986,** *84* (8), 4481-4484.

29. Born, M.; Huang, K., *Dynamical Theory of Crystal Lattices*. Oxford University Press: New York, 1956.

30. Amberger, B. K.; Esselman, B. J.; Stanton, J. F.; Woods, R. C.; McMahon, R. J., Precise Equilibrium Structure Determination of Hydrazoic Acid (HN_3) by Millimeter-wave Spectroscopy. *J. Chem. Phys.* **2015,** *143* (10), 104310.

31. Gordy, W.; Cook, R., *Microwave Molecular Spectra*. 3rd. ed.; Wiley Interscience: New York, 1984; Vol. XVIII.

32. Owen, A. N.; Sahool, N. P.; Esselman, B. J.; Stanton, J. F.; Woods, R. C.; McMahon, R. J., Improved Structure Determination of Hydrazoic Acid (HN_3). *Manuscript in Preparation* **2021**.

33. Costain, C. C., Determination of Molecular Structures from Ground State Rotational Constants. *J. Chem. Phys.* **1958,** *29* (4), 864-874.

34. Kraitchman, J., Determination of Molecular Structure from Microwave Spectroscopic Data. *Am. J. Phys.* **1953,** *21* (1), 17-24.

SUPPORTING INFORMATION

Table of Contents

Evaluation of Determinable Rotational Constants

The ground-state rotational constants for both the S- and A-reduced Hamiltonians (I^r representation) were converted to the "determinable constants" (A_0'', B_0'', C_0''), to account for the influence of centrifugal distortion using Eq. 3.S1 – Eq. 3.S6. The constants from each Hamiltonian reduction were then averaged to obtain the final determinable constants. Values of the various forms of the constants (I^r representation) are given in Table 3.4. These averaged determinable constants were used for all structure determinations reported in this work.

A reduction

$$A_0'' = A^{(\mathrm{A})} + 2\Delta_J \tag{3.S1}$$

$$B_0'' = B^{(\mathrm{A})} + 2\Delta_J + \Delta_{JK} - 2\delta_J - 2\delta_K \tag{3.S2}$$

$$C_0'' = C^{(\mathrm{A})} + 2\Delta_J + \Delta_{JK} + 2\delta_J + 2\delta_K \tag{3.S3}$$

S reduction

$$A_0'' = A^{(\mathrm{S})} + 2D_J + 6d_2 \tag{3.S4}$$

$$B_0'' = B^{(\mathrm{S})} + 2D_J + D_{JK} + 2d_1 + 4d_2 \tag{3.S5}$$

$$C_0'' = C^{(\mathrm{S})} + 2D_J + D_{JK} - 2d_1 + 4d_2 \tag{3.S6}$$

Table 3.4. Spectroscopic constants for isotopologues of pyridazine: A- and S-reduced Hamiltonians (I^r representation), determinable constants, their averages and differences (MHz).[a]

	o-$C_4H_4N_2$	[3-^{13}C]	[4-^{13}C]	[^{15}N]	[3-^{2}H]	[4-^{2}H]	[3,4-^{2}H]
Molecular Mass (μ)	80.0374480	81.0408028	81.0408028	81.0344830	81.0437248	81.0437248	82.0500016
A^A	6242.950338	6112.22843	6217.71586	6218.91249	5962.40614	6192.44159	5854.14224
A^S	6242.951681	6112.22970	6217.71724	6218.91389	5962.40719	6192.44249	5854.14296
A″ (A)	6242.951853	6112.22994	6217.71734	6218.91397	5962.40749	6192.44293	5854.14353
A″ (S)	6242.951765	6112.22975	6217.71740	6218.91404	5962.40728	6192.44281	5854.14336
A″ avg	6242.951809	6112.22985	6217.71737	6218.91401	5962.40739	6192.44287	5854.14345
A″ diff	0.000088	0.00018	0.00006	0.00007	0.00022	0.00012	0.00017
B^A	5961.094509	5961.31665	5848.36633	5857.40244	5828.17979	5598.12089	5539.31651
B^S	5961.092358	5961.31423	5848.36415	5857.40070	5828.17845	5598.119084	5539.31509
B″ (A)	5961.093890	5961.31606	5848.36569	5857.40181	5828.17930	5598.12026	5539.31595
B″ (S)	5961.093678	5961.31551	5848.36537	5857.40193	5828.17958	5598.12004	5539.31577
B″ avg	5961.093784	5961.31578	5848.36553	5857.40187	5828.17944	5598.12015	5539.31586
B″ diff	0.000213	0.00055	0.00032	0.00012	0.00027	0.00022	0.00018
C^A	3048.714446	3017.24865	3013.02901	3015.70945	2946.68490	2939.56874	2845.68724
C^S	3048.715012	3017.24860	3013.02980	3015.71022	2946.68588	2939.56921	2845.68726
C″ (A)	3048.717821	3017.25189	3013.03227	3015.71271	2946.68776	2939.57158	2845.68952
C″ (S)	3048.717594	3017.25114	3013.03226	3015.71269	2946.68814	2939.571276	2845.68902
C″ avg	3048.717708	3017.25151	3013.03227	3015.71270	2946.68795	2939.57143	2845.68927
C″ diff	0.000228	0.00075	0.00001	0.00002	0.00038	0.00030	0.00050
D_J	0.000471061	0.00046482	0.00047614	0.00047449	0.00042528	0.000466233	0.000468116
D_{JK}	0.00158089	0.0015538	0.00141934	0.00143106	0.0013460	0.00098613	0.00063917
D_K	−0.00060128	−0.0006085	−0.00044697	−0.00045554	−0.00037785	0.00001682	0.00022290
d_1	−0.000315699	−0.000316053	−0.000308651	−0.000308489	−0.000281463	−0.000277035	−0.000270342
d_2	−0.0001430485	−0.000145153	−0.000132206	−0.000132730	−0.000126602	−0.0001017058	−0.000089180
Δ_J	0.000757397	0.00075569	0.00074068	0.00073994	0.00067815	0.000669857	0.00064671
Δ_{JK}	−0.00013631	−0.00018836	−0.00016800	−0.00016243	−0.00017315	−0.00023475	−0.00043105
Δ_K	0.00082979	0.00084272	0.00087628	0.00087301	0.00088896	0.00103417	0.00111477
δ_J	0.000315729	0.000316069	0.000308725	0.000308458	0.000281432	0.000277056	0.000270311
δ_K	0.000682758	0.00064016	0.000666274	0.00066578	0.00055325	0.000588643	0.000440039

[a] Values in square brackets held constant at the computed value (CCSD(T)/cc-pCVTZ) in least-squares fit.

Table 3.4 (continued)

	[3,5-^{2}H]	[3,6-^{2}H]	[4,5-^{2}H]	[4-^{2}H, 3-^{13}C]	[4-^{2}H, 4-^{13}C]	[4-^{2}H, 5-^{13}C]	[4-^{2}H, 6-^{13}C]
Molecular Mass (μ)	82.0500016	82.0500016	82.0500016	82.0470796	82.0470796	82.0470796	82.0470796
A^A	5889.76350	5959.19547	6002.71658	6079.738	6189.060	6116.705	6081.112
A^S	5889.76437	5959.19634	6002.71765	6079.744	6189.066	6116.715	6081.117
A″ (A)	5889.76477	5959.19663	6002.71773	6079.740	6189.061	6116.706	6081.113
A″ (S)	5889.76475	5959.19654	6002.71774	6079.745	6189.067	6116.715	6081.118
A″ avg	5889.76476	5959.19658	6002.71774	6079.742	6189.064	6116.711	6081.115
A″ diff	0.00002	0.00009	0.00000	0.005	0.006	0.009	0.005
B^A	5498.78476	5460.41884	5388.79929	5587.229	5486.805	5542.241	5580.968
B^S	5498.78347	5460.41744	5388.79769	5587.222	5486.798	5542.231	5580.962
B″ (A)	5498.78420	5460.41837	5388.79879	5587.228	5486.804	5542.240	5580.968
B″ (S)	5498.78418	5460.41843	5388.79889	5587.223	5486.799	5542.232	5580.963
B″ avg	5498.78419	5460.41840	5388.79884	5587.225	5486.801	5542.236	5580.965
B″ diff	0.00002	0.00005	0.00010	0.005	0.005	0.009	0.005
C^A	2843.278197	2848.96318	2839.09924	2910.96433	2907.82551	2907.08010	2909.57499
C^S	2843.278699	2848.96373	2839.10012	2910.96503	2907.82620	2907.08081	2909.57560
C″ (A)	2843.280523	2848.96580	2839.10222	2910.96713	2907.82829	2907.08323	2909.57764
C″ (S)	2843.280465	2848.96567	2839.10226	2910.96700	2907.82818	2907.08297	2909.57755
C″ avg	2843.280494	2848.96574	2839.10224	2910.96707	2907.82823	2907.08310	2909.57760
C″ diff	0.000058	0.00013	0.00003	0.00013	0.00012	0.00026	0.00009
D_J	0.000457079	0.00038762	0.000363674	0.000484	0.000460	0.000438	0.000469
D_{JK}	0.00067631	0.00107532	0.00136927	0.000837	0.000902	0.001183	0.000845
D_K	0.00021466	−0.00007808	−0.00047127	[0.000092387]	[0.000132565]	[−0.000261299]	0.0001725
d_1	−0.000263950	−0.000237830	−0.000235860	−0.0002845	−0.0002676	−0.0002716	−0.0002747
d_2	−0.000088239	−0.000096857	−0.0001069048	−0.00009912	−0.00009440	−0.00010910	[−0.0000965015]
Δ_J	0.000633588	0.00058131	0.000577448	0.0006818	0.0006511	0.000658	0.000665
Δ_{JK}	−0.00038281	−0.00008707	0.00008590	[−0.000285674]	[−0.000232563]	[−0.0000570518]	−0.000308
Δ_K	0.00109746	0.00089097	0.00059882	0.000964	0.001062	0.000691	0.0011143
δ_J	0.000263949	0.000237799	0.000235849	0.0002844	0.0002688	0.0002724	0.0002759
δ_K	0.000456761	0.00053507	0.000633261	0.000575	0.000586	0.000663	[0.000536435]

[a] Values in square brackets held constant at the computed value (CCSD(T)/cc-pCVTZ) in least-squares fit.

Table 3.4 (continued)

	[3,4,5-^{2}H]	[3,4,6-^{2}H]	[3,4,5,6-^{2}H]	[4,5-^{2}H, 4-^{13}C]
Molecular Mass (μ)	83.0562784	83.0562784	84.0625552	83.0533564
A^A	5622.36523	5732.55731	5385.76207	5973.701
A^S	5622.36609	5732.55828	5385.76302	5973.718
A″ (A)	5622.36637	5732.55838	5385.76309	5973.70252
A″ (S)	5622.36617	5732.55844	5385.76307	5973.718
A″ avg	5622.36627	5732.55841	5385.76308	5973.710
A″ diff	0.00021	0.00006	0.00002	0.016
B^A	5385.21994	5299.12035	5275.67739	5307.990
B^S	5385.21826	5299.119120	5275.67618	5307.973
B″ (A)	5385.21949	5299.11993	5275.67704	5307.98933
B″ (S)	5385.21925	5299.12004	5275.67707	5307.974
B″ avg	5385.21937	5299.11998	5275.67706	5307.982
B″ diff	0.00025	0.00010	0.00002	0.015
C^A	2750.18297	2753.23426	2664.70755	2810.09742
C^S	2750.183089	2753.234974	2664.70797	2810.09811
C″ (A)	2750.18548	2753.23667	2664.70973	2810.10054
C″ (S)	2750.18502	2753.23677	2664.70970	2810.10020
C″ avg	2750.18525	2753.23672	2664.70971	2810.10037
C″ diff	0.00045	0.00010	0.00003	0.00034
D_J	0.000359385	0.000354471	0.00031571	0.0003720
D_{JK}	0.00116461	0.00100965	0.00106291	0.001282
D_K	−0.00044108	−0.00013559	−0.00033312	[−0.000448766]
d_1	−0.000237536	−0.000219641	−0.000210119	−0.0002370
d_2	−0.000106279	−0.0000909205	−0.000096842	−0.00010309
Δ_J	0.000572171	0.000536231	0.00050939	0.0005836
Δ_{JK}	−0.00011102	−0.00008172	−0.00009943	[0.000120109]
Δ_K	0.00062213	0.00077436	0.00063576	0.000405
δ_J	0.000237513	0.000219630	0.000210110	0.0002397
δ_K	0.000501466	0.000487271	0.000419902	0.000678

[a] Values in square brackets held constant at the computed value (CCSD(T)/cc-pCVTZ) in least-squares fit.

Evaluation of Semi-Experimental Equilibrium Rotational Constants (B_e^x)

The premise of the r_e^{SE} structure determination method is that the experimentally obtained rotational constants (B_0^x) can be combined with computational corrections to obtain constants that are effectively the (semi-experimental) equilibrium rotational constants (B_e^x). This approach has several key requirements. First, the experimental rotational constants should be well determined and, ideally, free of significant perturbation *i.e.*, due to Coriolis coupling. Second, the computational corrections for vibration-rotation interaction and, to a lesser extent, the electron-mass distribution should be determined at a sufficiently high level of theory. Finally, these corrections should be determined independently for each isotopologue.

To generate constants free of centrifugal distortion and the impact of the choice of an A- or S-reduced Hamiltonian, the rotational constants (B_0^x) determined in each least-squares fit were converted to determinable constants (B_0'') using Eq. 3.S1 – Eq. 3.S6. The computed vibration-rotation interaction and electron-mass corrections were combined with the averaged determinable constants to obtain the semi-experimental equilibrium constants (B_e^x) using Eq. 3.S7. This is the approach taken in this work, and the results of the evaluation using CCSD(T)/cc-pCVTZ corrections are summarized in Table 3.5.

The evaluation of B_e^x is handled automatically by the *xrefit* module of CFOUR, after providing the requisite data. The module also converts these constants into moments of inertia, which are then used to calculate the inertial defects given in Table 3.1.

$$B_e^x = B_0^x + \frac{1}{2}\sum \alpha_i^x - \eta g^{bb} B_{\mathrm{CCSD(T)}}^x \tag{3.S7}$$

Table 3.5. Semi-experimental rotational constants of isotopologues of pyridazine and the corrections (CCSD(T)/cc-pCVTZ) used to obtain them (MHz).

	normal			[3-^{13}C]			[4-^{13}C]			[^{15}N]		
	A	*B*	*C*	*A*	*B*	*C*	*A*	*B*	*C*	*A*	*B*	*C*
B_0^x	6242.952	5961.094	3048.718	6112.230	5961.316	3017.252	6217.717	5848.366	3013.032	6218.914	5857.402	3015.713
$\frac{1}{2}\sum\alpha_i^x$	51.239	41.840	24.103	49.936	41.581	23.751	50.623	40.957	23.687	50.586	41.043	23.703
$\eta g^{bb} B^x_{\mathrm{CCSD(T)}}$	−0.321	−0.416	0.061	−0.308	−0.416	0.060	−0.322	−0.399	0.059	−0.322	−0.399	0.060
$B_0^x + \frac{1}{2}\sum\alpha_i^x$	6294.191	6002.934	3072.821	6162.166	6002.897	3041.002	6268.340	5889.323	3036.720	6269.500	5898.445	3039.416
B_e^x	6294.512	6003.351	3072.760	6162.474	6003.313	3040.943	6268.662	5889.722	3036.661	6269.822	5898.844	3039.356

	[3-^{2}H]			[4-^{2}H]			[3,4-^{2}H]			[3,5-^{2}H]		
	A	*B*	*C*	*A*	*B*	*C*	*A*	*B*	*C*	*A*	*B*	*C*
B_0^x	5962.407	5828.179	2946.688	6192.443	5598.120	2939.571	5854.143	5539.316	2845.689	5889.765	5498.784	2843.280
$\frac{1}{2}\sum\alpha_i^x$	42.142	46.416	22.992	50.226	38.694	22.823	45.165	39.446	21.827	45.226	39.333	21.801
$\eta g^{bb} B^x_{\mathrm{CCSD(T)}}$	−0.414	−0.282	0.057	−0.330	−0.358	0.056	−0.324	−0.325	0.053	−0.334	−0.314	0.053
$B_0^x + \frac{1}{2}\sum\alpha_i^x$	6004.550	5874.595	2969.680	6242.669	5636.815	2962.394	5899.309	5578.762	2867.516	5934.991	5538.118	2865.081
B_e^x	6004.963	5874.878	2969.623	6242.999	5637.172	2962.338	5899.632	5579.086	2867.463	5935.325	5538.432	2865.029

	[3,6-^{2}H]			[4,5-^{2}H]			[4-^{2}H, 3-^{13}C]			[4-^{2}H, 4-^{13}C]		
	A	*B*	*C*	*A*	*B*	*C*	*A*	*B*	*C*	*A*	*B*	*C*
B_0^x	5959.197	5460.418	2848.966	6002.718	5388.799	2839.102	6079.742	5587.225	2910.967	6189.064	5486.801	2907.828
$\frac{1}{2}\sum\alpha_i^x$	42.160	42.496	21.937	48.294	36.514	21.680	48.906	38.552	22.505	49.874	37.736	22.435
$\eta g^{bb} B^x_{\mathrm{CCSD(T)}}$	−0.416	−0.246	0.053	−0.297	−0.343	0.052	−0.322	−0.353	0.055	−0.332	−0.343	0.055
$B_0^x + \frac{1}{2}\sum\alpha_i^x$	6001.357	5502.914	2870.903	6051.012	5425.313	2860.782	6128.649	5625.778	2933.472	6238.938	5524.537	2930.263
B_e^x	6001.773	5503.160	2870.850	6051.309	5425.656	2860.730	6128.971	5626.130	2933.417	6239.270	5524.879	2930.208

Table 3.5 (continued)

	[4-^{2}H, 5-^{13}C]			[4-^{2}H, 6-^{13}C]			[3,4,5-^{2}H]			[3,4,6-^{2}H]		
	A	*B*	*C*	*A*	*B*	*C*	*A*	*B*	*C*	*A*	*B*	*C*
B_0^x	6116.711	5542.236	2907.083	6081.115	5580.965	2909.578	5622.366	5385.219	2750.185	5732.558	5299.120	2753.237
$\frac{1}{2}\sum\alpha_i^x$	49.573	37.906	22.452	48.794	38.620	22.496	44.088	36.631	20.759	41.204	39.620	20.853
$\eta g^{bb} B^x_{\mathrm{CCSD(T)}}$	−0.314	−0.357	0.055	−0.325	−0.350	0.055	−0.261	−0.342	0.049	−0.365	−0.250	0.049
$B_0^x + \frac{1}{2}\sum\alpha_i^x$	6166.283	5580.142	2929.535	6129.909	5619.585	2932.074	5666.455	5421.850	2770.944	5773.763	5338.740	2774.090
B_e^x	6166.598	5580.500	2929.481	6130.234	5619.935	2932.019	5666.716	5422.192	2770.895	5774.128	5338.990	2774.040

	[3,4,5,6-^{2}H]			[4,5-^{2}H, 4-^{13}C]		
	A	*B*	*C*	*A*	*B*	*C*
B_0^x	5385.763	5275.677	2664.710	5973.710	5307.982	2810.100
$\frac{1}{2}\sum\alpha_i^x$	36.707	40.446	19.880	47.768	35.774	21.331
$\eta g^{bb} B^x_{\mathrm{CCSD(T)}}$	−0.343	−0.229	0.046	−0.295	−0.333	0.051
$B_0^x + \frac{1}{2}\sum\alpha_i^x$	5422.470	5316.123	2684.589	6021.478	5343.756	2831.431
B_e^x	5422.813	5316.352	2684.544	6021.773	5344.089	2831.381

Table 3.6. Atomic coordinates of the isotopologues of pyridazine in their respective principal axes systems, using the r_e^{SE} structure determination.

	normal		[3-^{13}C]		[4-^{13}C]		[^{15}N]		[3-^{2}H]		[4-^{2}H]	
Parameter	a	b	a	b	a	b	a	b	a	b	a	b
N1	-1.17903	-0.66645	-1.17085	-0.69631	-1.28854	-0.47046	-1.25249	-0.46976	-0.53374	-1.25972	-1.36248	-0.24978
N2	-1.17903	0.66645	-1.18621	0.63651	-1.07043	0.84448	-1.04586	0.84703	0.78738	-1.08283	-0.92600	1.00963
C3	-0.01906	1.31745	-0.03382	1.30084	0.18043	1.29689	0.20101	1.31033	1.27868	0.15328	0.38319	1.24489
C4	1.22416	0.68812	1.21657	0.68588	1.30391	0.47260	1.33164	0.49588	0.48993	1.30198	1.35178	0.24315
C5	1.22416	-0.68812	1.23243	-0.69027	1.07871	-0.88509	1.11828	-0.86372	-0.87414	1.11934	0.90111	-1.05721
C6	-0.01906	-1.31745	-0.00345	-1.33389	-0.25073	-1.30250	-0.20747	-1.29272	-1.33292	-0.19640	-0.47964	-1.24473
H(C3)	-0.10383	2.39527	-0.13101	2.37761	0.27318	2.37405	0.28435	2.38826	2.35822	0.21230	0.65604	2.29105
H(C4)	2.13683	1.26569	2.12253	1.27393	2.29880	0.89304	2.32282	0.92498	0.94127	2.28324	2.40327	0.49001
H(C5)	2.13683	-1.26569	2.15171	-1.25729	1.88457	-1.60422	1.93039	-1.57580	-1.56773	1.94729	1.57434	-1.90180
H(C6)	-0.10383	-2.39527	-0.07579	-2.41262	-0.51073	-2.35192	-0.45830	-2.34437	-2.38995	-0.42346	-0.91268	-2.23537

	[3,4-^{2}H]		[3,5-^{2}H]		[3,6-^{2}H]		[4,5-^{2}H]		[4-^{2}H, 3-^{13}C]		[4-^{2}H, 4-^{13}C]	
Parameter	a	b	a	b	a	b	a	b	a	b	a	b
N1	-1.38715	-0.17709	-0.48553	-1.29484	-0.66645	-1.17648	-1.23144	-0.66645	-1.38139	-0.17642	-1.38621	0.20966
N2	-0.56926	-1.22956	-1.34188	-0.27343	0.66645	-1.17648	-1.23144	0.66645	-0.86472	1.05228	-0.91071	-1.03554
C3	0.74612	-1.03181	-0.87124	0.97069	1.31745	-0.01651	-0.07147	1.31745	0.45690	1.20274	0.40518	-1.22989
C4	1.34160	0.22798	0.48577	1.28717	0.68812	1.22670	1.17174	0.68812	1.35898	0.14071	1.34208	-0.19846
C5	0.49712	1.31466	1.36997	0.23254	-0.68812	1.22670	1.17174	-0.68812	0.82551	-1.12793	0.85112	1.08723
C6	-0.87070	1.04872	0.82162	-1.04845	-1.31745	-0.01651	-0.07147	-1.31745	-0.56445	-1.22615	-0.53481	1.23164
H(C3)	1.34056	-1.93487	-1.62867	1.74217	2.39527	-0.10128	-0.15624	2.39527	0.79655	2.22916	0.71050	-2.26703
H(C4)	2.41667	0.33196	0.81409	2.31614	1.26569	2.13938	2.08442	1.26569	2.42418	0.31935	2.40076	-0.41243
H(C5)	0.86336	2.33075	2.44044	0.37632	-1.26569	2.13938	2.08442	-1.26569	1.44295	-2.01412	1.49770	1.95239
H(C6)	-1.59901	1.84775	1.44913	-1.92886	-2.39527	-0.10128	-0.15624	-2.39527	-1.06039	-2.18685	-0.99851	2.20830

Table 3.6 (continued)

	[4-^{2}H, 5-^{13}C]		[4-^{2}H, 6-^{13}C]		[3,4,5-^{2}H]		[3,4,6-^{2}H]		[3,4,5,6-^{2}H]		[4,5-^{2}H, 4-^{13}C]	
Parameter	a	b	a	b	a	b	a	b	a	b	a	b
N1	-1.33890	-0.38723	-1.37096	-0.12607	-1.15937	-0.80706	-1.11859	-0.81201	-0.66645	-1.22770	-1.29293	-0.57893
N2	-1.04431	0.91272	-0.83583	1.09470	-1.28361	0.52005	0.09459	-1.36410	0.66645	-1.22770	-1.19243	0.75018
C3	0.23085	1.29125	0.48791	1.22523	-0.18938	1.27633	1.16759	-0.57797	1.31745	-0.06773	0.01332	1.31187
C4	1.30424	0.40272	1.37388	0.14973	1.10709	0.76563	1.10973	0.81426	0.68812	1.17548	1.20555	0.59059
C5	1.00008	-0.93948	0.82135	-1.11073	1.23537	-0.60462	-0.14290	1.38431	-0.68812	1.17548	1.10178	-0.78173
C6	-0.35149	-1.27849	-0.56993	-1.18799	0.05623	-1.34709	-1.23065	0.51342	-1.31745	-0.06773	-0.18535	-1.31553
H(C3)	0.38638	2.36116	0.84299	2.24641	-0.37425	2.34156	2.11349	-1.10156	2.39527	-0.15250	0.01005	2.39301
H(C4)	2.32199	0.76431	2.44165	0.31230	1.96196	1.42576	2.01346	1.40573	1.26569	2.08816	2.15918	1.09771
H(C5)	1.76254	-1.70448	1.42537	-2.00613	2.19792	-1.09460	-0.29056	2.45425	-1.26569	2.08816	1.96832	-1.42647
H(C6)	-0.67237	-2.31093	-1.08029	-2.14111	0.07230	-2.42812	-2.24678	0.88271	-2.39527	-0.15250	-0.35114	-2.38390

Table 3.7. Optimized structural parameters of pyridazine at various levels of theory.

	SCF	SCF DBOC	CCSD(T)					CCSD(T) SFX2C-1e	CCSDT(Q)
Parameter	cc-pCVTZ	cc-pCVTZ	cc-pVDZ	cc-pCVDZ	cc-pCVTZ	cc-pCVQZ	cc-pCV5Z	cc-pCVTZ	cc-pVDZ
$R_{C3\text{-}H}$ (Å)	1.07287	1.07301	1.09804	1.09653	1.08210	1.08115	1.08108	1.08199	1.09816
$R_{C4\text{-}H}$ (Å)	1.07216	1.07229	1.09679	1.09519	1.08106	1.08010	1.07998	1.08094	1.09691
$R_{C4\text{-}C5}$ (Å)	1.36270	1.36268	1.39669	1.39405	1.37994	1.37735	1.37625	1.37970	1.39711
$R_{C3\text{-}C4}$ (Å)	1.39044	1.39050	1.41361	1.41116	1.39699	1.39420	1.39362	1.39676	1.41441
$R_{N2\text{-}C3}$ (Å)	1.30586	1.30584	1.34819	1.34614	1.33404	1.33129	1.33046	1.33395	1.34861
$\theta_{H\text{-}C3\text{-}C4}$ (°)	121.206	121.208	121.089	121.081	121.181	121.290	121.346	121.184	121.069
$\theta_{H\text{-}C4\text{-}C5}$ (°)	122.483	122.483	122.456	122.448	122.397	122.352	122.337	122.398	122.459
$\theta_{C3\text{-}C4\text{-}C5}$ (°)	116.717	116.718	116.560	116.582	116.765	116.819	116.849	116.765	116.560
$\theta_{N2\text{-}C3\text{-}C4}$ (°)	123.223	123.222	124.329	124.324	124.062	123.904	123.861	124.076	124.358

Alternate Z-Matrix

An alternate Z-matrix was constructed to enable the determination of values and uncertainties for structural parameters that were not explicitly part of the original set of internal coordinates. The uncertainties of these parameters are not able to be estimated with typical error propagation methods, which have an underlying assumption that the errors are statistically independent, which they certainly are not in this case.

The alternate Z-matrix defines the structure in terms of an alternate set of bonds and angles in the internal coordinates. The r_e^{SE} structure was re-determined with *xrefit*, using the alternate coordinates, to obtain values and statistical uncertainties of the alternate parameters.

The bond distance and angle parameter values from each set of internal coordinates *i.e.*, each Z-matrix, are identical. The statistical uncertainties are very similar for all parameters from each set of internal coordinates.

Z-Matrix:

```
X
X 1 R1
N 2 RNN* 1 A90
N 2 RNN* 1 A90 3 D180
C 3 RCN* 2 ACNN* 1 Dn90
C 4 RCN* 2 ACNN* 1 D90
C 5 RCC* 3 ACCN* 2 D0
C 6 RCC* 4 ACCN* 2 D0
H 5 RCH1* 3 AHCN* 2 D180
H 6 RCH1* 4 AHCN* 2 D180
H 7 RCH2* 5 AHCC* 3 D180
H 8 RCH2* 6 AHCC* 4 D180

     R1=1.00                  ACCN=123.87
     RNN=0.6665               AHCN=114.77
     RCN=1.3309               AHCC=120.79
     RCC=1.3934               D180=180.0
     RCH1=1.0809              Dn90=-90.0
     RCH2=1.0800              D90=90.0
     A90=90.0                 D0=0.0
     ACNN=119.28
```

Chapter 4: Understanding the Diastereotopic Outcomes of Cyanobutadiene Syntheses *via* Conformational Analysis of Reactions' Potential Energy Surfaces

Previously published within:

Samuel K. Kougias, Stephanie N. Knezz, Andrew N. Owen, Rodrigo A. Sanchez, Grace E. Hyland, Daniel J. Lee, Aatmik R. Patel, Brian J. Esselman, R. Claude Woods, and Robert J. McMahon. Synthesis and Characterization of Cyanobutadiene Isomers – Molecules of Astrochemical Significance. *Journal of Organic Chemistry.* **2020**, *85* (9), 5787-5798.

https://pubs.acs.org/doi/10.1021/acs.joc.9b03388

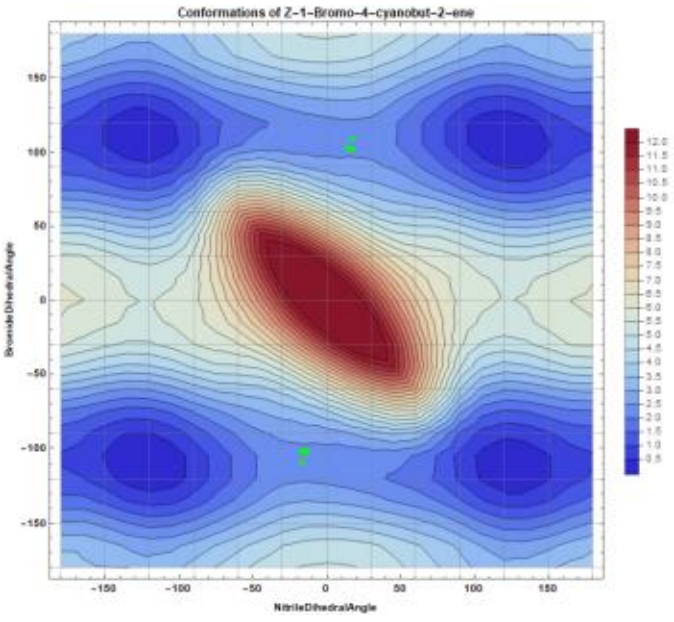

ABSTRACT

In the syntheses of 1-cyano-1,3-butadiene from 1,4-dibromo-2-butene and cyanide, specific diastereoselectivities were observed: reaction of the *E*-diastereomer yielded the desired product in a 10:1 *E*:*Z* ratio, while reaction of the *Z*- diastereomer yielded the desired product in a 2:3 *E*:*Z* ratio. The hypothesized rate-determining step of the reaction – the 1,4-elimination of HBr from the 1-bromo-4-cyano-2-butene intermediate – was investigated using B3LYP/cc-pVTZ, with a polarized continuum model for the solvent (H_2O), at the experimental reaction temperatures. For the rate-determining step of each reaction of the diastereomers, four distinct transition states were identified and determined to be higher in energy by at least 7 kcal/mol than the conformational changes of the preceding intermediate. As such, the Curtin-Hammett principle was applied and using the difference in energy of the product-forming transition states, the observed synthetic diastereoselectivities were reproduced. For the reaction of *E*-1,4-dibromo-2-butene at 273 K (0 °C), the competing product-forming transition states differ by 2.4 kcal/mol in favor of forming (*E*)-1-cyano-1,3-butadiene. This energy difference corresponds to a predicted *E*:*Z* ratio of ca. 60:1. For the reaction of (*Z*)-1,4-dibromo-2-butene at 323 K (50 °C), the competing product-forming transition states differ by only 0.1 kcal/mol, corresponding to a predicted *E*:*Z* ratio of 1:1. The slight overestimation of the production of the *E* diastereomer by the theoretical predictions suggests the relative energies of the product-forming transition states are accurate to within 1 kcal/mol.

INTRODUCTION

Over 200 different molecules have been detected in the interstellar medium (ISM) or circumstellar shells[1-2] and are theorized to be involved in complex reaction networks.[3-7] The vast

majority of these detections have been made *via* radioastronomy, through observation and assignment of rotational spectra. Because of their large dipole moments,[8-10] which confer intense rotational transitions, and composition of relatively abundant elements, nitriles (R–CN) represent attractive targets for detection by radioastronomy. Approximately 10% of the known interstellar molecules are nitriles, including recently detected benzonitrile,[11] hydroxyacetonitrile,[12] and silyl cyanide.[13] Interstellar nitriles are observed in varying degrees of hydrogenation, from highly unsaturated cyanopolyynes, $RC_{2n+1}N$ (R = H, n = 1–4; R = CH_3, n = 1, 2),[14-20] to vinyl and phenyl derivatives [vinyl cyanide (acrylonitrile),[21] cyanoallene,[22] and benzonitrile[11]], to compounds with fully saturated backbones (acetonitrile,[23] hydroxyacetonitrile,[12] propyl cyanide,[24] and isopropyl cyanide[25]). Spectroscopic data for the organic nitriles described herein – (*E*)-1-cyano-1,3-butadiene (***E*-1**), (*Z*)-1-cyano-1,3-butadiene (***Z*-1**) (Figure 4.1) – would enable radioastronomical searches for these compounds. Each of these nitriles has been proposed as a likely component of the ISM.[26-30] Additionally, these nitriles are acyclic isomers of the aromatic heterocycle, pyridine, which has yet to be identified in the ISM.[31] Detection of any of these nitriles would provide additional motivation to detect pyridine and other aromatic heterocycles. The existence of organic nitriles in the ISM is relevant not only to our understanding of the chemical processes in the ISM but also to our understanding of the origin of amino acids, nucleotides, and other prebiotic compounds that are critical for life on Earth.

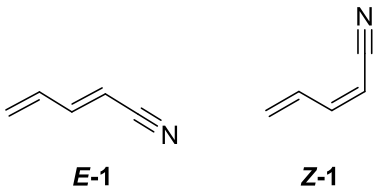

Figure 4.1. Cyanobutadiene isomers: (*E*)-1-cyano-1,3-butadiene (***E*-1**), (*Z*)-1-cyano-1,3-butadiene (***Z*-1**).

Organic nitriles have also been detected in the nitrogen-rich atmosphere of Saturn's largest moon, Titan. Titan has been of interest as a possible analogue to prebiotic Earth[29] and has been visited by the Cassini–Huygens probe.[32] Small organic nitriles (up to four carbon atoms) and their corresponding anions were detected in Titan's atmosphere.[33] Electric discharge experiments performed on various gaseous mixtures *e.g.*, N_2, CH_4, C_2H_6, NH_3, H_2O, and H_2S, simulating the atmosphere of Titan produce a myriad of nitrile-containing small molecules.[7, 34-35] It is plausible that the nitriles in Figure 4.1 are components of Titan's atmosphere.

Despite the sophistication of modern synthetic chemistry, the synthesis, purification, and isolation of simple organic compounds shown in Figure 4.1 remain a challenge. The recently described procedures[36] enable detailed studies of the high-resolution rotational spectroscopy of the cyanobutadiene isomers (Figure 4.1).[37] The rotational spectrum of each of these compounds is very complex; having a pure sample, for which spectral features are not obscured by impurities, is critical to achieve a sophisticated analysis of the complex spectrum. Therefore, procedures were developed to synthesize ***E*-1** and ***Z*-1** separately and in high yield. As shown in Scheme 4.1, the synthesis of ***E*-1** from (*E*)-1,4-dibromo-2-butene (***E*-2**) using cyanide was highly selective for the ***E*-1** over ***Z*-1**. Use of the other diastereomer for the starting material, (*Z*)-1,4-dibromo-2-butene (***Z*-2**), however, resulted in only a slightly selectivity for ***Z*-1** over ***E*-1**, as shown in Scheme 4.2.

Scheme 4.1. Reaction Conditions for Synthesis and Purification of (E)-1-Cyano-1,3-butadiene (E-1)

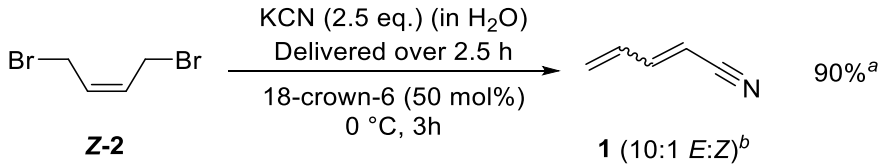

[a]Isolated (gravimetric) yield. [b]Diastereomeric ratio determined *via* ^{1}H NMR.

Scheme 4.2. Reaction Conditions for Synthesis and Purification of (*Z*)-1-Cyano-1,3-butadiene (*Z*-1)

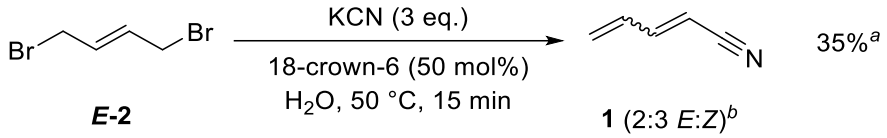

[a]Isolated (gravimetric) yield. [b]Diastereomeric ratio determined *via* ^{1}H NMR.

The reaction to form 1-cyano-1,3-butadiene from (*E*)-1,4-dibromo-2-butene (***E*-2**) is hypothesized to proceed through (*E*)-1-bromo-4-cyano-2-butene (***E*-3**, Scheme 4.3a), which, once formed, reacts with another equivalent of cyanide to eliminate HBr in a concerted 1,4-elimination mechanism (E2′ mechanism), where the position of the dihedral angle determines whether ***E*-1** or ***Z*-1** is formed. Similarly, the reaction to form 1-cyano-1,3-butadiene from (*Z*)-1,4-dibromo-2-butene (***Z*-2**) is hypothesized to proceed through (*Z*)-1-bromo-4-cyano-2-butene (***Z*-3**, Scheme 4.3b) followed by elimination of HBr by cyanide *via* the 1,4-elimination mechanism. Given that ***E*-1** and ***Z*-1** are predicted to be very similar in energy (within 1 kcal/mol) and the reactions of different precursor diastereomers lead to different product ratios, it is clear that a kinetically

controlled reaction is responsible for the observed diastereoselectivity. Thus, the E2′ transition state barriers leading to each diastereomer of 1,4-dibromo-2-butene must be responsible for the selectivity, or lack thereof, in the formation of ***E*-1** and ***Z*-1**. If this is indeed the mechanism, then computational analysis of the reaction should provide insight as to the origins of the diastereoselectivity observed in Schemes 4.2 and 4.3.

Scheme 4.3. Proposed Mechanism for Reaction of 1,4-Dibromo-2-butene with 2 Equivalents of Cyanide to Yield Diastereomers of 1-Cyano-1,3-butadiene

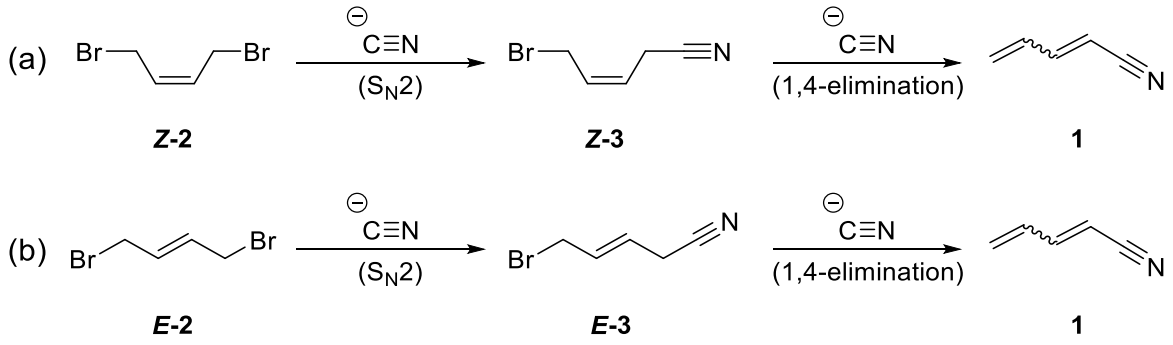

COMPUTATIONAL METHODS

Geometry optimizations, conformational analyses, and harmonic frequency calculations were conducted with density functional theory using the B3LYP functional[38-39] and the cc-pVTZ basis set,[40] correcting for water as a solvent by employing the polarizable continuum model as implemented in Gaussian 16.[41] Thermally corrected Gibbs free energies for all species were obtained from the harmonic frequency calculations at 273, 298, and 323 K. Intrinsic Reaction Coordinate (IRC) calculations were conducted to verify that each transition state smoothly connects on diastereomer of the starting material to one diastereomer of the product. Natural Bond

Orbital (NBO) and Natural Resonance Theory (NRT) calculations[42] were used to analyze the electronic structure, bonding, hyperconjugation, and relative energies of energy minima and transition states on the potential energy surfaces.

RESULTS AND DISCUSSION

The proposed E2′ substrates, ***Z*-3** and ***E*-3**, exhibit multiple conformational isomers due to the bromo-methyl rotor and the cyano-methyl rotor. The conformational isomers were identified using two-dimensional relaxed conformation scans at 15° intervals for the dihedral angle for the bromo- and cyano-methyl rotors of each diastereomer. The stationary points on the 2-D energy surface were then separately optimized to obtain their structures and energies without the 15° interval constraint on the dihedrals. The results of the 2-D scan and the individual optimizations are summarized in Figure 4.2 for ***E*-3** and in Figure 4.3 for ***Z*-3**, with snapshots of the conformational stationary points and their relative energies. In addition, the approximate entrance channels to the E2′ transition states are provided, based on IRC calculations.

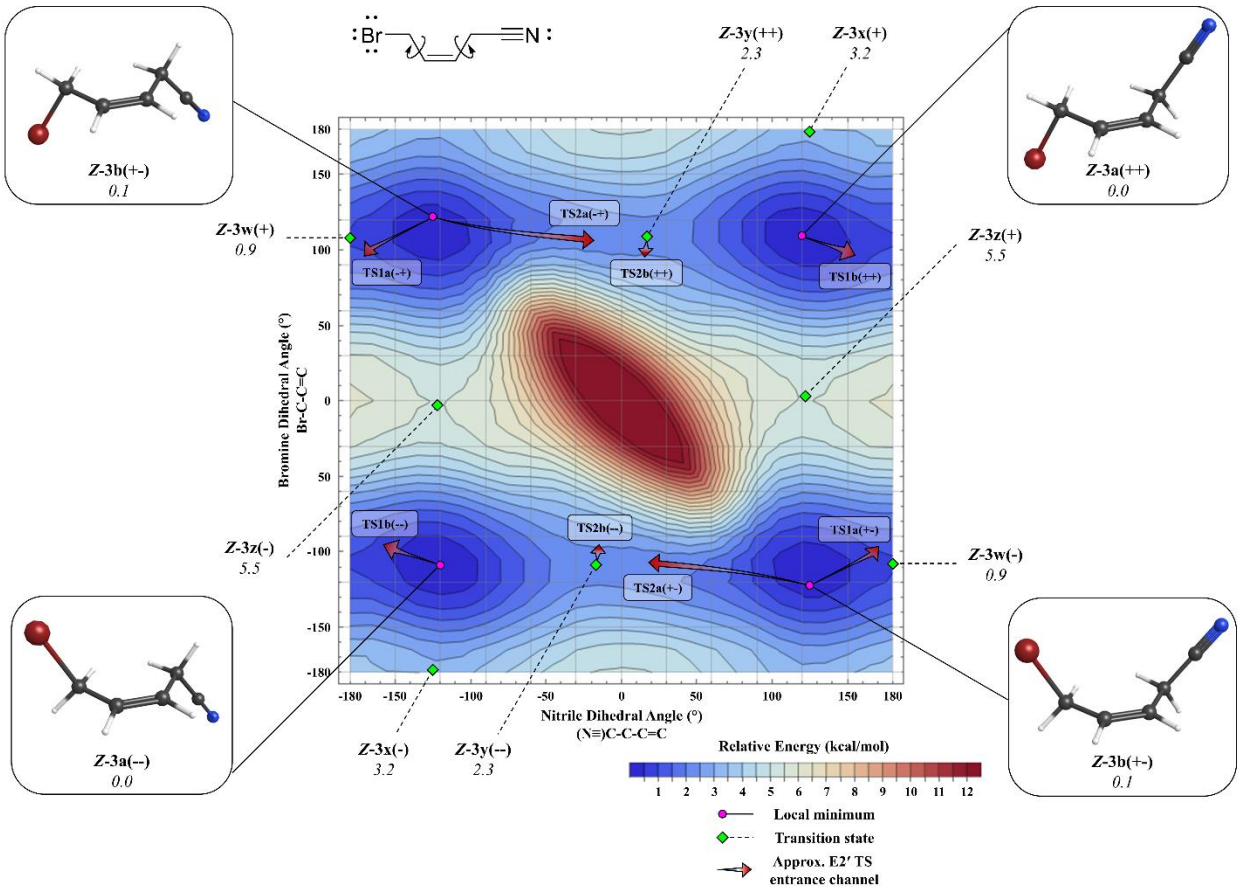

Figure 4.2. Relaxed 2-D conformational scan of (*Z*)-1-bromo-4-cyano-2-butene (**Z-3**) using B3LYP/cc-pVTZ electronic energies with PCM solvent correction for water. Relative energies in kcal/mol. The heat map ranges from 0 kcal/mol (blue) to 12.5 kcal/mol (red).

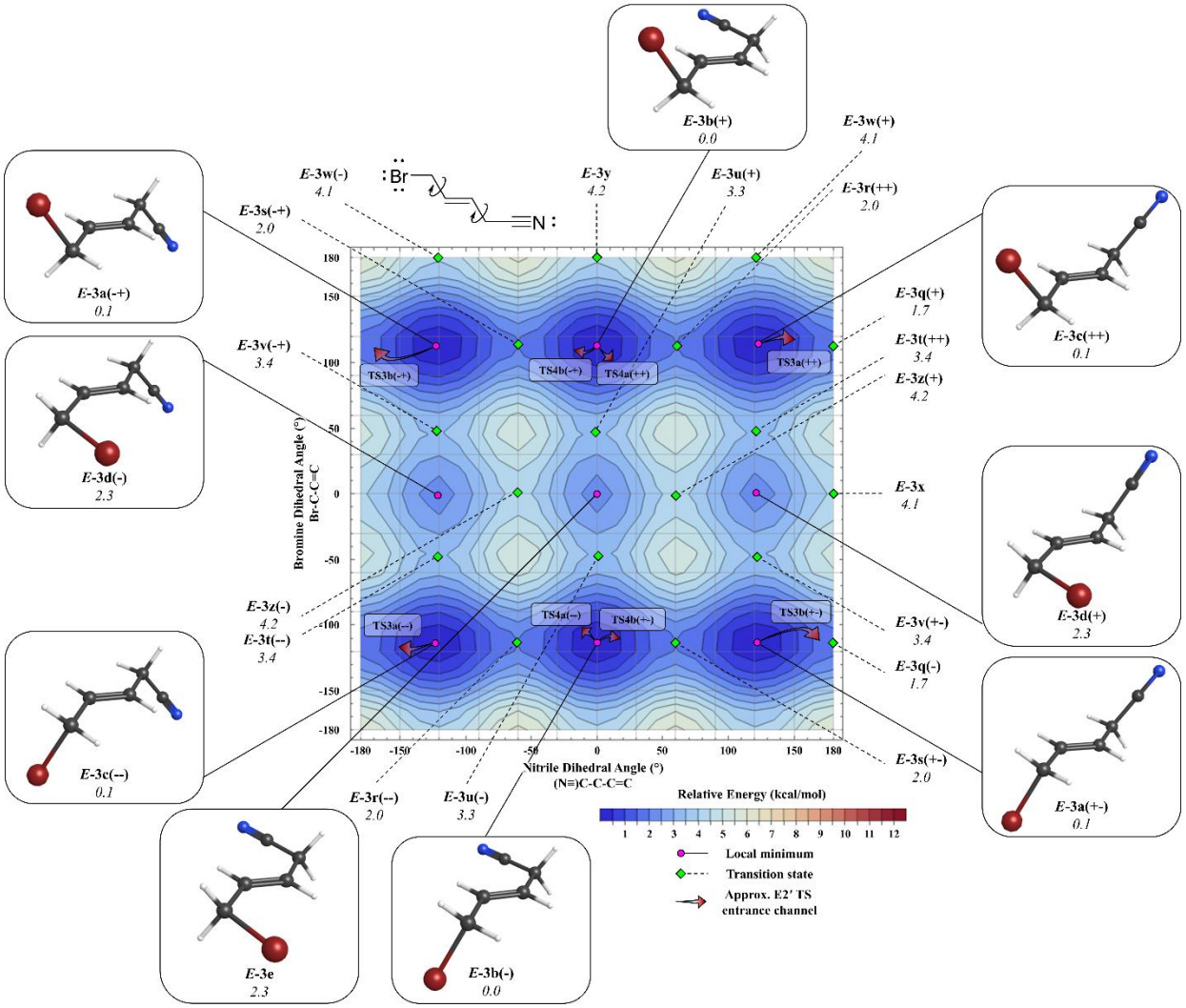

Figure 4.3. Relaxed 2-D conformational scan of (*E*)-1-bromo-4-cyano-2-butene (***E*-3**) using B3LYP/cc-pVTZ electronic energies with PCM solvent correction for water. Relative energies in kcal/mol. The heat map ranges from 0 kcal/mol (blue) to 12.5 kcal/mol (red).

The conformations of the ***Z*-3** species are the possible combinations of the *anti*-clinal bromo-methyl rotor with the *anti*-clinal cyano-methyl group, as the steric interactions of the bromo and cyano groups destabilize the *syn*-periplanar positions. Thus, for ***Z*-3** there are a total of four conformations consisting of two enantiomeric pairs of local minima. Interconnecting these conformations are four pairs of enantiomeric transition states. The stationary points denoted in

Figure 4.2 show that the largest activation barrier for interconversion of any of the conformations is 5.5 kcal/mol (***Z*-3z**), which is at least 10 kcal/mol lower in energy than any of the outgoing E2′ transition state barriers (*vide infra*).

The conformations of the ***E*-3** species are the *anti*-clinal and *syn*-periplanar positions of the bromo-methyl rotor in various combinations with the *anti*-clinal and *syn*-periplanar positions of the cyano-methyl rotor. Thus, for ***E*-3** there are nine conformations consisting of four enantiomeric pairs of local minima and one unique local minimum. Interconnecting these conformations are eight enantiomeric pairs of transition states and two unique transition states. Examination of the stationary points in Figure 4.3 reveals that the largest activation barrier for interconversion of any of the conformations is 4.2 kcal/mol (***E*-3y**), which is at least 10 kcal/mol lower in energy than any of the outgoing E2′ transition state barriers (*vide infra*). This is consistent with the Curtin-Hammett principle, because the energy required to overcome the lowest of the E2′ transition states is more than sufficient to overcome any of the conformational activation barriers.

For the reaction of each diastereomer of (***Z*-3** or ***E*-3**) with cyanide ion, the calculations predict two pairs of E2′ transition states (Figures 4.4 and 4.5) leading to the cyanobutadiene products (***E*-1** and ***Z*-1**). In each of the transition state geometries, an acidic hydrogen atom at C-4 is perpendicular to the plane of the adjacent alkene unit. The bromide leaving group at C-1 can be in an *anti* or *syn* orientation with respect to the acidic hydrogen atom at C-4. The cyano substituent at C-4 may occupy a *syn*-periplanar conformation relative to the alkene moiety, which leads to the formation of (*Z*)-1-cyano-1,3-butadiene (***Z*-1**), or an *anti*-periplanar conformation, which leads to the formation of the (*E*)-1-cyano-1,3-butadiene (***E*-1**). Each transition state was verified to connect one diastereomer of the starting material (**3**) to one diastereomer of the product (**1**), using an IRC calculation. Several attempts to explore a stepwise pathway beginning with

deprotonation of ***Z*-3** or ***E*-3** failed to obtain an anionic intermediate as a stationary point. Therefore, a stepwise mechanism was not considered further.

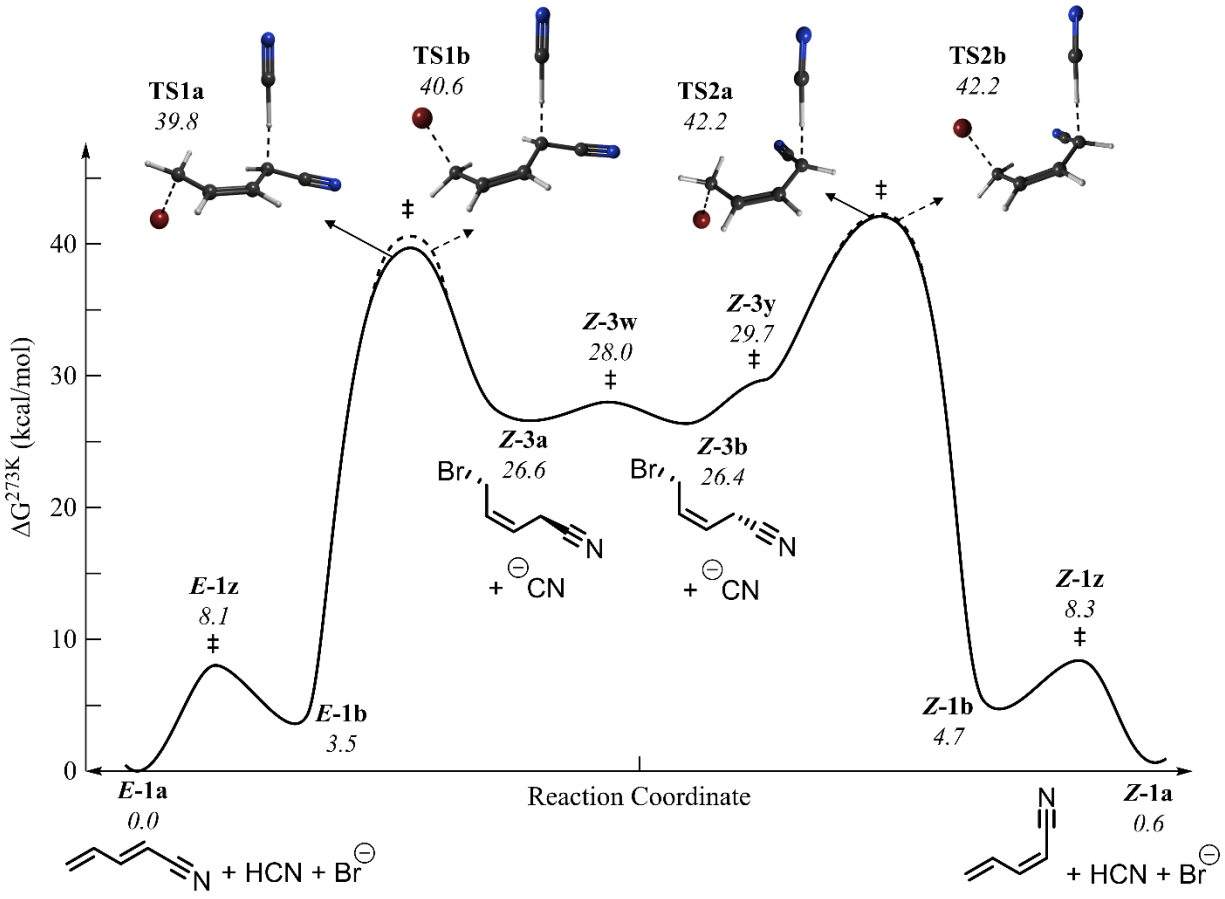

Figure 4.4. Computed reaction coordinate diagram for E2′ reaction of (*Z*)-1-bromo-4-cyano-2-butene (***Z*-3**) with cyanide in water. Gibbs free energies at B3LYP/cc-pVTZ with the polarized continuum model for the solvent (H_2O) at 273 K (0 °C). Solid line: lower energy transition state. Dashed line: higher energy transition state.

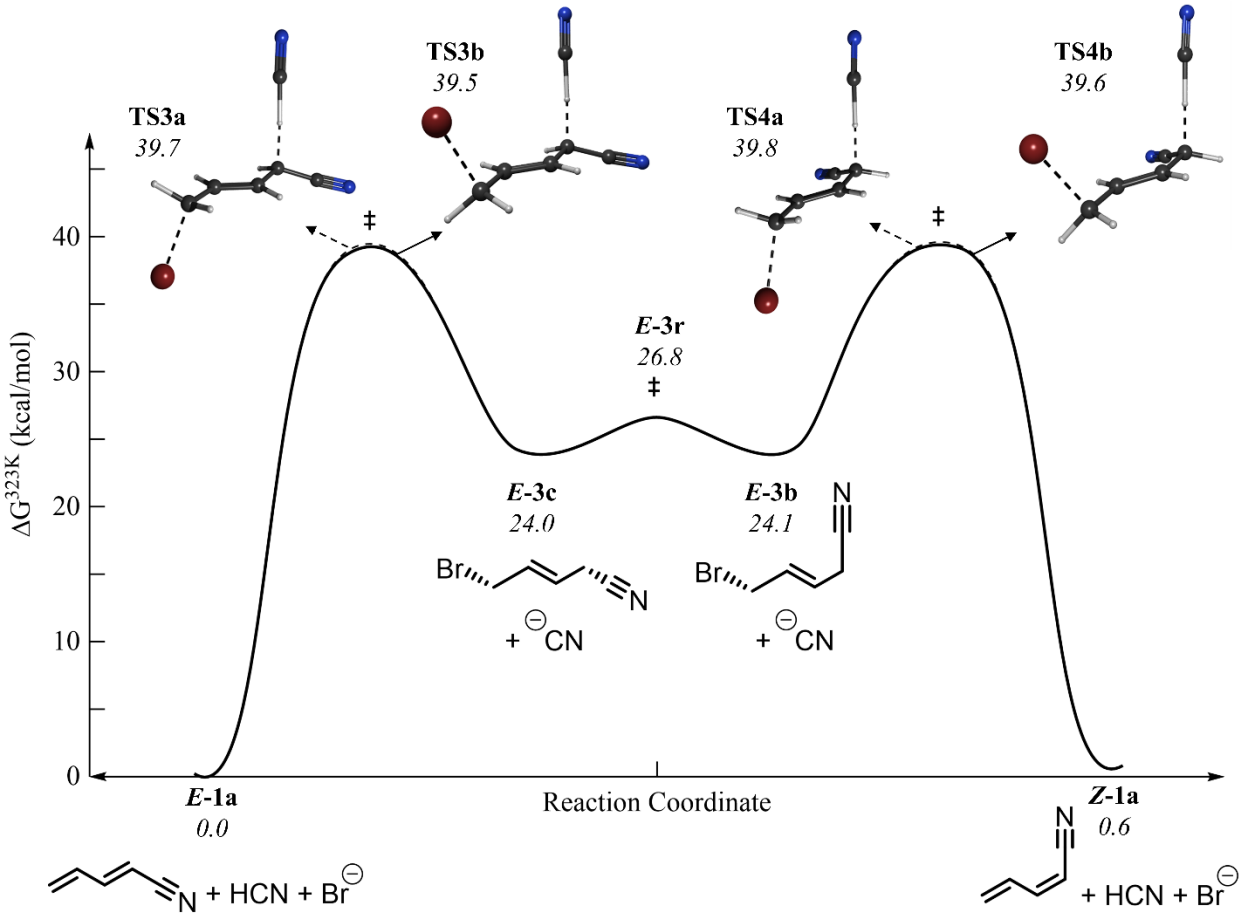

Figure 4.5. Computed reaction coordinate diagram for E2′ reaction of (*E*)-1-bromo-4-cyano-2-butene (***E*-3**) with cyanide in water. Gibbs free energies at B3LYP/cc-pVTZ with the polarized continuum model for the solvent (H_2O) at 323 K (50 °C). Solid line: lower energy transition state. Dashed line: higher energy transition state.

For either diastereomer of 1-bromo-4-cyano-2-butene (***Z*-3** or ***E*-3**), the computed activation barriers of the E2′ transition states are significantly higher (by 7 – 14 kcal/mol) than the activation barriers for conformational interconversion. Thus, the diastereoselectivity in the elimination reaction is interpreted in terms of the Curtin – Hammett principle.[43] Product selectivity is governed by the difference in energy between the competing product-forming transition states

($\Delta\Delta G^{\ddagger}$). The conformational equilibrium in the starting material is rapid and does not govern the composition of products. If the reaction system has enough energy to surmount the lowest-energy E2′ barrier, it has sufficient energy to surmount the conformational barriers. As such, the potential energy surfaces for the E2′ reactions shown in Figures 4.4 and 4.5 contain a simplified surface for the conformational isomerization of each 1-bromo-4-cyano-2-butene (***Z*-3** or ***E*-3**).

In the E2′ reaction of (*Z*)-1-bromo-4-cyano-2-butene (***Z*-3**) with cyanide in water at 273 K (0 °C) (Figure 4.4), the transition states **TS2a** and **TS2b** that lead to (*Z*)-1-cyano-1,3-butadiene (***Z*-1**) are higher in energy than the transition states **TS1a** and **TS1b** that lead to (*E*)-1-cyano-1,3-butadiene (***E*-1**). Thus, the computational analysis is in qualitative accordance with the experimental observation of diastereoselectivity favoring the formation of (*E*)-1-cyano-1,3-butadiene (***E*-1**). The difference in transition state energies ($\Delta\Delta G^{\ddagger}$) appears to arise from a steric interaction in the transition states involving the $-CH_2CN$ group. Both transition states leading to ***Z*-1** (**TS2a** and **TS2b**) have a larger interaction between –CN and $-CH_2Br$, relative to the transition states leading to ***E*-1** (**TS1a** and **TS1b**). The small energy difference between the ***E*-1**-forming transition states **TS1a** and **TS1b** (0.8 kcal/mol) is likely due to a subtle difference in electrostatic interactions (repulsion) between the bromo and cyano substituents in the *anti* versus *syn* E2′ elimination pathways. Natural Bond Orbital (NBO) analysis of each transition state did not reveal any obvious hyperconjugation contribution to the energy differences among **TS1a**, **TS1b**, **TS2a**, and **TS2b**. Assuming that this potential energy surface reasonably models this reaction, the ***E*-1**/***Z*-1** ratio derived from the $\Delta\Delta G^{\ddagger}$ between **TS1a** and **TS2a** (2.4 kcal/mol) is expected to be ca. 60:1. This result is in qualitative agreement with the experimental observation of an ***E*-1**/***Z*-1** ratio of 10:1. This does indicate, however, that the computational prediction of $\Delta\Delta G^{\ddagger}$ is larger than its true value by about 1 kcal/mol.

In a similar fashion, the potential energy surface of the E2′ reaction of (*E*)-1-bromo-4-cyano-2-butene (***E*-3**) with cyanide in water at 323 K (50 °C) is presented in Figure 4.5. Unlike the reaction of the isomeric system (***Z*-3**), the transition states for the E2′ reaction of ***E*-3** leading to (*E*)- and (*Z*)-1-cyano-1,3-butadiene (**1**) are computed to be virtually isoergic ($\Delta\Delta G^{\ddagger}$ = 0.1 kcal/mol favoring the formation of ***E*-1**). With the $–CH_2CN$ and $–CH_2Br$ groups in a *trans* orientation in the ground state of ***E*-3**, there is no significant preference for the –CN substituent to adopt one conformation over the other. This situation is also manifested in the transition states (**TS3a**, **TS3b**, **TS4a**, and **TS4b**); the relative energies of the transition states reveal no preference for the stereochemical course of the reaction. Thus, the rates of product formation would be expected to afford a diastereomeric ratio of nearly 1:1. This prediction is consistent with the experimentally observed product ratio of ***E*-1**/***Z*-1** (*E*/*Z* ratio 2:3). The deviation of the experimental ratio from 1:1 reveals that there is a slight energetic preference (<1 kcal/mol) for the transition states leading to the *Z* diastereomer. Our computational model is not expected to be of sufficient accuracy to account for such a small energetic difference.

SUMMARY

We computationally analyzed the rate-determining step of the proposed mechanism for the synthesis of (*E*)-1-cyano-1,3-butadiene (***E*-1**) and (*Z*)-1-cyano-1,3-butadiene (***Z*-1**) from 1,4-dibromo-2-butene (**2**) and cyanide. The purported intermediate, 1-bromo-4-cyano-2-butene, consists of many conformational isomers arising from the two separate and mostly non-interacting rotors of the bromo-methyl group and the cyano-methyl group. The conformational surface of the intermediate, though complex, does not affect the outcome of the reaction with cyanide because the 1,4-elimination (E2′) transition states are significantly higher in energy than the conformational

transition states, justifying the use of the Curtin–Hammett principle. For the reaction of (*E*)-1-bromo-4-cyano-2-butene (***E*-3**), the transition states leading to the ***Z*-1** product possess increased steric interactions of the cyano-methyl rotor with the bromo-methyl rotor, resulting in higher energies than the transition states leading to the ***E*-1** product, which lack such steric interaction. The difference in energy of the transition states corresponds to a predicted ***E*-1**/***Z*-1** ratio of ca. 60:1, comparable to the 10:1 ratio observed experimentally. For the reaction of (*Z*)-1-bromo-4-cyano-2-butene (***Z*-3**), the transition states leading to either ***E*-1** or ***Z*-1** are effectively the same energies, leading to a predicted ***E*-1**/***Z*-1** ratio of 1:1, comparable to the 2:3 ratio observed experimentally. The agreement between the predicted and experimentally observed diastereoselectivities suggests the computed model free energies are accurate to with 1 kcal/mol, and strongly supports the proposed $S_N2/E2'$ mechanism in the synthesis of ***E*-1** and ***Z*-1** from **2**.

ACKNOWLEDGEMENTS

We gratefully acknowledge the National Science Foundation for support of this project (CHE-1664912, CHE-1362264). We thank Dr. Timothy S. Zwier for stimulating discussions.

REFERENCES

1. Endres, C. P.; Schlemmer, S.; Schilke, P.; Stutzki, J.; Muller, H. S. P., The Cologne Database for Molecular Spectroscopy, CDMS, in the Virtual Atomic and Molecular Data Centre, VAMDC. *J. Mol. Spectrosc.* **2016,** *327,* 95-104.

2. Muller, H. S. P.; Schloder, F.; Stutzki, J.; Winnewisser, G., The Cologne Database for Molecular Spectroscopy, CDMS: a useful tool for astronomers and spectroscopists. *J. Mol. Struct.* **2005,** *742* (1-3), 215-227.

3. Agundez, M.; Wakelam, V., Chemistry of Dark Clouds: Databases, Networks, and Models. *Chem. Rev.* **2013,** *113* (12), 8710-8737.

4. Costes, M.; Naulin, C., Studies of reactions relevant to astrochemistry. In *Annual Reports on the Progress of Chemistry 2013, Vol 109, Section C: Physical Chemistry*, Webb, G. A., Ed. Royal Soc Chemistry: Cambridge, 2013; Vol. 109, pp 189-210.

5. Garrod, R. T.; Weaver, S. L. W.; Herbst, E., Complex chemistry in star-forming regions: An expanded gas-grain warm-up chemical model. *Astrophys. J.* **2008,** *682* (1), 283-302.

6. Herbst, E., Chemistry in the interstellar medium. *Annu. Rev. Phys. Chem.* **1995,** *46*, 27-53.

7. Sagan, C.; Khare, B. N., Tholins - organic chemistry of interstellar grains and gas. *Nature* **1979,** *277* (5692), 102-107.

8. Cumper, C. W. N.; Dev, S. K.; Landor, S. R., Electric dipole-moments of some acrylonitriles, allyl cyanides, and alicyclic nitriles. *J. Chem. Soc.-Perkin Trans. 2* **1973,** (5), 537-540.

9. Hannay, N. B.; Smyth, C. P., The dipole moments and structures of ketene and of several polar molecules containing conjugated systems. *J. Am. Chem. Soc.* **1946,** *68* (7), 1357-1360.

10. Soundararajan, S., Charge distribution, electric dipole moments, and molecular structure of nitriles. *Indian J. Chem.* **1963,** *1* (12), 503-&.

11. McGuire, B. A.; Burkhardt, A. M.; Kalenskii, S.; Shingledecker, C. N.; Remijan, A. J.; Herbst, E.; McCarthy, M. C., Detection of the aromatic molecule benzonitrile (c-C6H5CN) in the interstellar medium. *Science* **2018,** *359* (6372), 202-205.

12. Zeng, S.; Quenard, D.; Jimenez-Serra, I.; Martin-Pintado, J.; Rivilla, V. M.; Testi, L.; Martin-Domenech, R., First detection of the pre-biotic molecule glycolonitrile ($HOCH_2CN$) in the interstellar medium. *Mon. Not. Roy. Astron. Soc.* **2019,** *484* (1), L43-L48.

13. Cernicharo, J.; Agundez, M.; Prieto, L. V.; Guelin, M.; Pardo, J. R.; Kahane, C.; Marka, C.; Kramer, C.; Navarro, S.; Quintana-Lacaci, G.; Fonfria, J. P.; Marcelino, N.; Tercero, B.; Moreno, E.; Massalkhi, S.; Santander-Garcia, M.; McCarthy, M. C.; Gottlieb, C. A.; Alonso, J. L., Discovery of methyl silane and confirmation of silyl cyanide in IRC+10216. *Astron. Astrophys.* **2017,** *606*, L5.

14. Avery, L. W.; Broten, N. W.; Macleod, J. M.; Oka, T.; Kroto, H. W., Detection of heavy interstellar molecule cyanodiacetylene. *Astrophys. J.* **1976,** *205* (3), L173-L175.

15. Broten, N. W.; Macleod, J. M.; Avery, L. W.; Irvine, W. M.; Hoglund, B.; Friberg, P.; Hjalmarson, A., The detection of interstellar methylcyanoacetylene. *Astrophys. J.* **1984,** *276* (1), L25-L29.

16. Broten, N. W.; Oka, T.; Avery, L. W.; Macleod, J. M.; Kroto, H. W., Detection of HC_9N in interstellar space. *Astrophys. J.* **1978,** *223* (2), L105-L107.

17. Kroto, H. W.; Kirby, C.; Walton, D. R. M.; Avery, L. W.; Broten, N. W.; Macleod, J. M.; Oka, T., Detection of cyanohextriyne, $H(C{=}C)_3CN$, in Heiles Cloud 2. *Astrophys. J.* **1978,** *219* (3), L133-L137.

18. Snyder, L. E.; Buhl, D., Observations of radio emission from interstellar hydrogen cyanide. *Astrophys. J.* **1971,** *163* (2), L47-&.

19. Snyder, L. E.; Hollis, J. M.; Jewell, P. R.; Lovas, F. J.; Remijan, A., Confirmation of interstellar methylcyanodiacetylene (CH_3C_5N). *Astrophys. J.* **2006,** *647* (1), 412-417.

20. Walmsley, C. M.; Winnewisser, G.; Toelle, F., Cyanoacetylene and cyanodiacetylene in interstellar clouds. *Astron. Astrophys.* **1980,** *81* (1-2), 245-250.

21. Gardner, F. F.; Winnewisser, G., Detection of interstellar vinyl cyanide (acrylonitrile). *Astrophys. J.* **1975,** *195* (3), L127-L130.

22. Lovas, F. J.; Remijan, A. J.; Hollis, J. M.; Jewell, P. R.; Snyder, L. E., Hyperfine structure identification of interstellar cyanoallene toward TMC-1. *Astrophys. J.* **2006,** *637* (1), L37-L40.

23. Solomon, P. M.; Jefferts, K. B.; Penzias, A. A.; Wilson, R. W., Detection of millimeter emission lines from interstellar methyl cyanide. *Astrophys. J.* **1971,** *168* (3), L107-&.

24. Belloche, A.; Garrod, R. T.; Muller, H. S. P.; Menten, K. M.; Comito, C.; Schilke, P., Increased complexity in interstellar chemistry: detection and chemical modeling of ethyl formate and n-propyl cyanide in Sagittarius B2(N). *Astron. Astrophys.* **2009,** *499* (1), 215-U293.

25. Belloche, A.; Garrod, R. T.; Muller, H. S. P.; Menten, K. M., Detection of a branched alkyl molecule in the interstellar medium: iso-propyl cyanide. *Science* **2014,** *345* (6204), 1584-1587.

26. Jamal, A.; Mebel, A. M., Theoretical Investigation of the Mechanism and Product Branching Ratios of the Reactions of Cyano Radical with 1- and 2-Butyne and 1,2-Butadiene. *J. Phys. Chem. A* **2013,** *117* (4), 741-755.

27. Morales, S. B.; Bennett, C. J.; Le Picard, S. D.; Canosa, A.; Sims, I. R.; Sun, B. J.; Chen, P. H.; Chang, A. H. H.; Kislov, V. V.; Mebel, A. M.; Gu, X.; Zhang, F.; Maksyutenko, P.; Kaiser, R. I., A crossed molecular beam, low-temperature kinetics, and theoretical investigation of the reation of the cyano radical (CN) with 1,3-butadiene (C_4H_6). A route to complex nitrogen-bearing molecules in low-temperature extraterrestrial environments. *Astrophys. J.* **2011,** *742* (1), 26.

28. Moreno, R.; Silla, E.; Tunon, I.; Arnau, A., *Ab initio* rotational constants of the nitriles derived from cyanodiacetylene (HC_4CN). *Astrophys. J.* **1994,** *437* (1), 532-539.

29. Sagan, C.; Thompson, W. R.; Khare, B. N., Titan - A laboratory for prebiological organic chemistry. *Acc. Chem. Res.* **1992,** *25* (7), 286-292.

30. Sun, B. J.; Huang, C. H.; Chen, S. Y.; Chen, S. H.; Kaiser, R. I.; Chang, A. H. H., Theoretical Study on Reaction Mechanism of Ground-State Cyano Radical with 1,3-Butadiene: Prospect of Pyridine Formation. *J. Phys. Chem. A* **2014,** *118* (36), 7715-7724.

31. Charnley, S. B.; Kuan, Y.-J.; Huang, H.-C.; Botta, O.; Butner, H. M.; Cox, N.; Despois, D.; Ehrenfreund, P.; Kisiel, Z.; Lee, Y.-Y.; Markwick, A. J.; Peeters, Z.; Rodgers, S. D., Astronomical searches for nitrogen heterocycles. *Adv. Space Res.* **2005,** *36* (2), 137-145.

32. Cassini Titan Science; NASA Planetary Data System (PDS); National Aeronautics and Space Administration. https://atmos.nmsu.edu/data_and_services/atmospheres_data/Cassini/sci-titan.html#huygens (accessed 2020).

33. Desai, R. T.; Coates, A. J.; Wellbrock, A.; Vuitton, V.; Crary, F. J.; Gonzalez-Caniulef, D.; Shebanits, O.; Jones, G. H.; Lewis, G. R.; Waite, J. H.; Cordiner, M.; Taylor, S. A.; Kataria, D. O.; Wahlund, J. E.; Edberg, N. J. T.; Sittler, E. C., Carbon Chain Anions and the Growth

of Complex Organic Molecules in Titan's Ionosphere. *Astrophys. J. Lett.* **2017,** *844* (2), L18.

34. Cable, M. L.; Horst, S. M.; Hodyss, R.; Beauchamp, P. M.; Smith, M. A.; Willis, P. A., Titan Tholins: Simulating Titan Organic Chemistry in the Cassini-Huygens Era. *Chem. Rev.* **2012,** *112* (3), 1882-1909.

35. Thompson, W. R.; Henry, T. J.; Schwartz, J. M.; Khare, B. N.; Sagan, C., Plasma discharge in N_2 + CH_4 at low pressures - experimental results and applications to Titan. *Icarus* **1991,** *90* (1), 57-73.

36. Kougias, S. M.; Knezz, S. N.; Owen, A. N.; Sanchez, R. A.; Hyland, G. E.; Lee, D. J.; Patel, A. R.; Esselman, B. J.; Woods, R. C.; McMahon, R. J., Synthesis and Characterization of Cyanobutadiene Isomers-Molecules of Astrochemical Significance. *J. Org. Chem.* **2020,** *85* (9), 5787-5798.

37. Zdanovskaia, M. A.; Dorman, P. M.; Orr, V. L.; Owen, A. N.; Kougias, S. M.; Esselman, B. J.; Woods, R. C.; McMahon, R. J., Rotational Spectra of Three Cyanobutadiene Isomers (C_5H_5N) of Relevance to Astrochemistry and Other Harsh Reaction Environments. *J. Am. Chem. Soc.* **2021,** *143* (25), 9551-9564.

38. Becke, A. D., Density-functional thermochemistry .3. The role of exact exchange. *J. Chem. Phys.* **1993,** *98* (7), 5648-5652.

39. Lee, C. T.; Yang, W. T.; Parr, R. G., Development of the Colle-Salvetti correlation energy formula into a functional of the electron density. *Phys. Rev. B* **1988,** *37* (2), 785-789.

40. Dunning, T. H., Gaussian basis sets for use in correlated molecular calculations .1. The atoms boron through neon and hydrogen. *J. Chem. Phys.* **1989,** *90* (2), 1007-1023.

41. Frisch, M. J.; Trucks, G. W.; Schlegel, H. B.; Scuseria, G. E.; Robb, M. A.; Cheeseman, J. R.; Scalmani, G.; Barone, V.; Petersson, G. A.; Nakatsuji, H.; Li, X.; Caricato, M.; Marenich, A. V.; Bloino, J.; Janesko, B. G.; Gomperts, R.; Mennucci, B.; Hratchian, H. P.; Ortiz, J. V.; Izmaylov, A. F.; Sonnenberg, J. L.; Williams-Young, D.; Ding, F.; Lipparini, F.; Egidi, F.; Goings, J.; Peng, B.; Petrone, A.; Henderson, T.; Ranasinghe, D.; Zakrzewski, V. G.; Gao, J.; Rega, N.; Zheng, G.; Liang, W.; Hada, M.; Ehara, M.; Toyota, K.; Fukuda, R.; Hasegawa, J.; Ishida, M.; Nakajima, T.; Honda, Y.; Kitao, O.; Nakai, H.; Vreven, T.; Throssell, K.; Montgomery Jr., J. A.; Peralta, J. E.; Ogliaro, F.; Bearpark, M. J.; Heyd, J. J.; Brothers, E. N.; Kudin, K. N.; Staroverov, V. N.; Keith, T. A.; Kobayashi, R.; Normand, J.; Raghavachari, K.; Rendell, A. P.; Burant, J. C.; Iyengar, S. S.; Tomasi, J.; Cossi, M.; Millam, J. M.; Klene, M.; Adamo, C.; Cammi, R.; Ochterski, J. W.; Martin, R. L.; Morokuma, K.; Farkas, O.; Foresman, J. B.; Fox, D. J. *Gaussian 16, Revision B.01*, Gaussian, Inc.: Wallingford, CT, USA, 2016.

42. Glendening, E. D.; Badenhoop, J. K.; Reed, A. E.; Carpenter, J. E.; Bohmann, J. A.; Morales, C. M.; Landis, C. R.; Weinhold, F. *NBO 6.0*, Theoretical Chemistry Institute, University of Wisconsin: Madison, WI, 2013.

43. Seeman, J. I., Effect of conformational change on reactivity in organic chemistry. Evaluations, applications, and extensions of Curtin-Hammett Winstein-Holness kinetics. *Chem. Rev.* **1983,** *83* (2), 83-134.

SUPPORTING INFORMATION

All computational summaries, including Cartesian coordinates, are available online at https://pubs.acs.org/doi/suppl/10.1021/acs.joc.9b03388/suppl_file/jo9b03388_si_001.pdf

Table of Contents

Table 4.1. Summary of Absolute Electronic and Free Energies Determined by B3LYP/cc-pVTZ with PCM(H_2O).

Molecule	Absolute Energies (Hartrees/Particle)				
	B3LYP/cc-PVTZ + PCM(H_2O)	Zero-Point Energy Correction	$\Delta G_{(273)}$	$\Delta G_{(298)}$	$\Delta G_{(323)}$
Br^-	-2574.418411	0.000000	-2574.418411	-2574.418411	-2574.418411
CN^-	-92.991754	0.004908	-93.004002	-93.005874	-93.007747
HBr	-2574.838558	0.005931	-2574.849968	-2574.851857	-2574.853746
HCN	-93.468406	0.016417	-93.469431	-93.471341	-93.473257
***E*-1a**	-248.340828	0.084356	-248.282958	-248.286009	-248.289100
***E*-1b**	-248.334771	0.084168	-248.277418	-248.280511	-248.283644
***E*-1y**	-248.334559	0.084012	-248.276615	-248.279577	-248.282573
***E*-1z**	-248.327279	0.083381	-248.270103	-248.273087	-248.276106
***Z*-1a**	-248.339893	0.084520	-248.281996	-248.285050	-248.288144
***Z*-1b**	-248.332893	0.084422	-248.275466	-248.278565	-248.281702
***Z*-1y**	-248.332731	0.084419	-248.274222	-248.277149	-248.280110
***Z*-1z**	-248.327168	0.083577	-248.269759	-248.272725	-248.275725
***E*-3a**	-2823.194404	0.098175	-2823.127395	-2823.131032	-2823.134719
***E*-3b**	-2823.194485	0.098159	-2823.127363	-2823.130984	-2823.134655
***E*-3c**	-2823.194389	0.098296	-2823.127250	-2823.130880	-2823.134561
***E*-3d**	-2823.190835	0.097896	-2823.124064	-2823.127694	-2823.131374
***E*-3e**	-2823.190824	0.097840	-2823.123940	-2823.127555	-2823.131221
***E*-3q**	-2823.191723	0.097771	-2823.124021	-2823.127493	-2823.131012
***E*-3r**	-2823.191330	0.097968	-2823.123583	-2823.127067	-2823.130597
***E*-3s**	-2823.191353	0.097961	-2823.123395	-2823.126859	-2823.130370
***E*-3t**	-2823.189099	0.097772	-2823.121718	-2823.125221	-2823.128771
***E*-3u**	-2823.189151	0.097699	-2823.121494	-2823.124965	-2823.128482

Molecule	Absolute Energies (Hartrees/Particle)				
	B3LYP/cc-PVTZ + PCM(H_2O)	Zero-Point Energy Correction	$\Delta G_{(273)}$	$\Delta G_{(298)}$	$\Delta G_{(323)}$
***E*-3v**	-2823.189058	0.097803	-2823.121467	-2823.124954	-2823.128487
***E*-3w**	-2823.187933	0.097626	-2823.120606	-2823.124104	-2823.127648
***E*-3x**	-2823.187932	0.097423	-2823.120623	-2823.124100	-2823.127624
***E*-3y**	-2823.187844	0.097561	-2823.120429	-2823.123910	-2823.127438
***E*-3z**	-2823.187776	0.097621	-2823.120196	-2823.123665	-2823.127180
***Z*-3a**	-2823.191453	0.098526	-2823.124487	-2823.128150	-2823.131863
***Z*-3b**	-2823.191333	0.098385	-2823.124717	-2823.128403	-2823.132138
***Z*-3w**	-2823.189959	0.098048	-2823.122111	-2823.125584	-2823.129102
***Z*-3x**	-2823.186419	0.097900	-2823.119022	-2823.122526	-2823.126077
***Z*-3y**	-2823.187784	0.098354	-2823.119423	-2823.122869	-2823.126361
***Z*-3z**	-2823.182743	0.097987	-2823.115009	-2823.118484	-2823.122004
TS1a	-2916.168979	0.098350	-2916.111809	-2916.107383	-2916.116306
TS1b	-2916.168536	0.098410	-2916.106121	-2916.110469	-2916.114888
TS2a	-2916.166206	0.098627	-2916.103509	-2916.107845	-2916.112252
TS2b	-2916.165918	0.098570	-2916.103504	-2916.107866	-2916.112298
TS3a	-2916.170754	0.098139	-2916.108687	-2916.113050	-2916.117486
TS3b	-2916.170780	0.098076	-2916.108970	-2916.113357	-2916.117816
TS4a	-2916.170427	0.098153	-2916.108532	-2916.112916	-2916.117371
TS4b	-2916.170529	0.098102	-2916.108783	-2916.113178	-2916.117644

Table 4.2. Summary of Relative Electronic and Free Energies Determined by B3LYP/cc-pVTZ with PCM(H_2O).

Molecule	Relative Energies (kcal/mol)[a]				
	B3LYP/cc-PVTZ + PCM(H_2O)	B3LYP/cc-PVTZ + PCM(H_2O) + ZPE	$\Delta G_{(273)}$	$\Delta G_{(298)}$	$\Delta G_{(323)}$
***E*-1a**	0.0	0.0	0.0	0.0	0.0
***E*-1b**	3.8	3.7	3.5	3.5	3.4
***E*-1y**	3.9	3.7	4.0	4.0	4.1
***E*-1z**	8.5	7.9	8.1	8.1	8.2
***Z*-1a**	0.6	0.7	0.6	0.6	0.6
***Z*-1b**	5.0	5.0	4.7	4.7	4.6
***Z*-1y**	5.1	5.1	5.5	5.6	5.6
***Z*-1z**	8.6	8.1	8.3	8.3	8.4
***E*-10a**	26.0	27.5	24.7	24.4	24.0
***E*-10b**	26.0	27.4	24.7	24.4	24.1
***E*-10c**	26.0	27.6	24.8	24.5	24.1
***E*-10d**	28.3	29.5	26.8	26.5	26.1
***E*-10e**	28.3	29.5	26.9	26.6	26.2
***E*-10q**	27.7	28.9	26.8	26.6	26.4
***E*-10r**	28.0	29.3	27.1	26.9	26.6
***E*-10s**	27.9	29.3	27.2	27.0	26.8
***E*-10t**	29.4	30.6	28.3	28.0	27.8
***E*-10u**	29.3	30.5	28.4	28.2	27.9
***E*-10v**	29.4	30.6	28.4	28.2	27.9
***E*-10w**	30.1	31.2	29.0	28.7	28.5
***E*-10x**	30.1	31.1	29.0	28.7	28.5
***E*-10y**	30.1	31.2	29.1	28.9	28.6
***E*-10z**	30.2	31.3	29.2	29.0	28.8
***Z*-10a**	27.9	29.6	26.6	26.2	25.8

Molecule	Relative Energies (kcal/mol)[a]				
	B3LYP/cc-PVTZ + PCM(H_2O)	B3LYP/cc-PVTZ + PCM(H_2O) + ZPE	$\Delta G_{(273)}$	$\Delta G_{(298)}$	$\Delta G_{(323)}$
***Z*-10b**	28.0	29.5	26.4	26.0	25.7
***Z*-10w**	28.8	30.2	28.0	27.8	27.6
***Z*-10x**	31.0	32.3	30.0	29.7	29.5
***Z*-10y**	30.2	31.7	29.7	29.5	29.3
***Z*-10z**	33.4	34.7	32.5	32.3	32.0
TS1a	36.8	35.3	37.0	42.9	40.5
TS1b	37.1	35.6	40.6	41.0	41.3
TS2a	38.6	37.2	42.2	42.6	43.0
TS2b	38.7	37.4	42.2	42.6	43.0
TS3a	35.7	34.0	39.0	39.4	39.7
TS3b	35.7	34.0	38.8	39.2	39.5
TS4a	35.9	34.3	39.1	39.4	39.8
TS4b	35.8	34.2	38.9	39.3	39.6

[a] Mass-balanced energies relative to ***E*-1a** on the $C_6H_6N_2Br^-$ surface.

Chapter 5: Theoretical Investigation of the Conversion of 1-Cyano-1,3-butadiene to Pyridine Under Interstellar Conditions

Unpublished work with contributions from Brian J. Esselman, R. Claude Woods, and Robert J. McMahon.

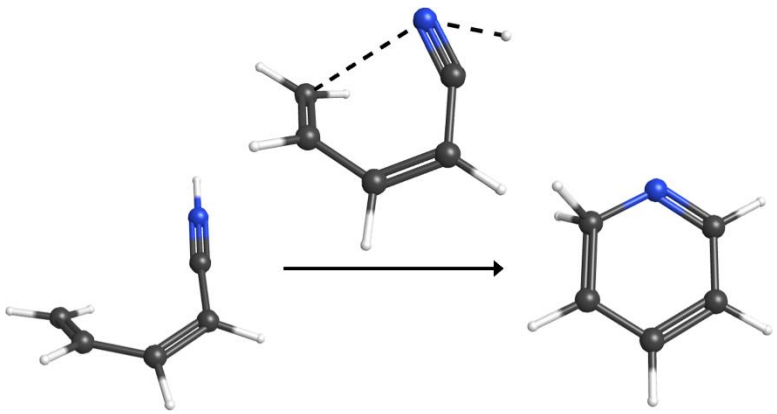

ABSTRACT

Pyridine, the *N*-heterocyclic analog of benzene, has long been a target of astronomical surveys *via* radio astronomy. 1-Cyano-1,3-butadiene, a *N*-heterologue of 1,3-hexadien-5-yne, is known to form predominantly over that of pyridine in the reactions of cyano radicals with butadiene under conditions similar to that of the interstellar medium. Given that 1,3-hexadien-5-yne is known to isomerize to benzene, it may be that the isomerization of 1-cyano-1,3-butadiene to pyridine is a significant pathway to formation of pyridine in the interstellar medium. If so, detection of 1-cyano-1,3-butadienes in the interstellar medium could provide evidence for the likely presence of pyridine in the interstellar medium, as well as to provide insight into the study of the astrochemical processes therein. Our theoretical calculations support the conclusion that 1-cyano-1,3-butadiene is likely to form pyridine under interstellar conditions with the assistance of trihydrogen cation. The potential for astronomical searches of intermediates encountered in the pathways is discussed, and additional avenues of the transformation are considered for future study.

INTRODUCTION

The pervasiveness of aromatic (hetero)cycles in organic and biological chemistry is such that detection and characterization of these species in the interstellar medium is of paramount interest in the fields of astrochemistry and prebiotic chemistry. While the prototypical aromatic molecule – benzene – has been detected in the interstellar medium (ISM) *via* measurements of its infrared spectra,[1] the lack of a permanent dipole (and thus, pure rotational transitions) means that benzene is unable to be detected by radio astronomy, which has become the gold standard for detection of molecules in the ISM. Aromatic heterocycles and aromatic rings with polar

substituents – particularly the cyano substituent – are much more suitable for detection *via* radioastronomy owing to their significant permanent dipole moments. Though such molecules have long been targets for detection *via* radioastronomy,[2-6] the first benzene-derived species (benzonitrile) was only recently detected.[7] While other cyano-substituted molecules have since been detected,[8-11] the nitrogen analog of benzene (pyridine) and other heterocycles have yet to be detected.[5, 12-14]

Kaiser, Chang, and coworkers have considered the formation of pyridine under interstellar conditions both experimentally and computationally.[15-17] They examined the reaction of cyano radical (˙CN) with 1,3-butadiene ($CH_2{-}CH{-}CH{-}CH_2$) using crossed molecular beams under single-collision conditions and estimated that, at most, 6% of the products were attributable to pyridine, while the rest was attributed to the formation 1-cyano-1,3-butadiene.[15] Their experimental results were consistent with that of their electronic structure and kinetics calculations[15] (including the more thorough ensuing computational investigation[17]) which led to the conclusion that while pyridine is significantly more stable than 1-cyano-1,3-butadiene, the radical processes have significantly higher activation barriers for the formation of pyridine than the formation of 1-cyano-1,3-butadiene. The conclusion that the formation of pyridine is not kinetically favored is supported by Jamal and Mebel[18] who examined the reactions of the cyano radical with other open chain isomers of 1,3-butadiene *e.g.*, 1-butyne, 2-butyne, and 1,2-butadiene, using similar computational methods. They also found pyridine formation was negligible compared to a handful of open chain cyano compounds *e.g.*, 2-cyano-1,3-butadiene, 1-cyano-1,2-propadiene, cyanoethyne, and 3-cyano-1-propyne. The formation of pyridine in the ISM, therefore, likely involves isomerization from a less stable constitutional isomer (whose formation is kinetically favorable), or from the decomposition of a larger molecule. An example of the latter

is the reaction of vinyl cyanide (CH_2=CH−CN) with cyanovinyl radical ($^{\bullet}$CH=CH−CN) in a pyrolytic reactor, where it is believed that cyanopyridyl radical [(*cyclic*-$C_5H_5N^{\bullet}$)−CN] is formed before decomposing to yield pyridine and cyano radical.[16]

Since the decomposition of larger molecules to form pyridine represents more complicated formation pathways – and a larger pool of possible reactions – we limit ourselves to examining the constitutional isomers that may rearrange to form pyridine. The constitutional isomers with the simplest intramolecular isomerization to form pyridine are those that have a linear arrangement of the heavy atoms, such as 1-cyanobutadienes, imine-ene-ynes, cyanomethylene-allenes, and substituted ketenimines. We consider such isomerizations to form pyridine to be 'simple' because they require only a single heavy-atom bond formation, whereas the isomerization of species with a branching arrangement of the heavy atoms *e.g.*, 2-cyano-1,3-butadiene, require an additional heavy-atom bond dissociation and bond formation. As noted previously, 1-cyano-1,3-butadiene is the dominant product in the reaction of cyano radical with 1,3-butadiene. Furthermore, the transformation of 1-cyano-1,3-butadiene (**1**) to N-heterocyclic aromatic pyridine (**2**) is isoelectronic with the transformation of 1,3-hexadien-5-yne (**3**) to aromatic benzene (**4**), as is the transformation of protonated 1-cyano-1,3-butadiene (**5)** to protonated pyridine (**6**), as illustrated in Scheme 5.1. Thus, we believe examining the neutral and protonated transformations of 1-cyano-1,3-butadiene (**1**) to pyridine (**2**) represent the most fruitful avenue for investigating the formation of pyridine from a constitutional isomer under interstellar conditions.

Scheme 5.1. Isoelectronic Formation of Six-Membered Aromatic Rings Open Chain Constitutional Isomers.

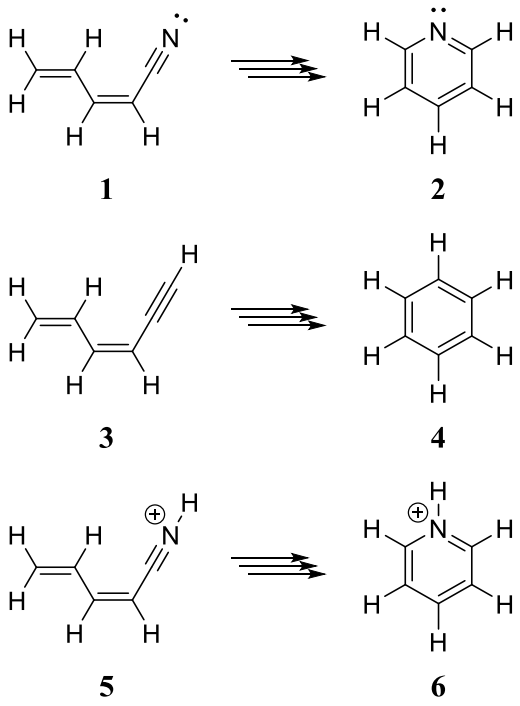

Consideration of the transformation of **1** to **2** in the literature thus far has been incidental[19] and often focuses on the radical formation[15, 17-18] or dissociation[20-22] of pyridine. The most extensive examination of the transformation of **1** to **2** is that of Sun *et al.*,[17] who – in investigating the reaction of cyano radical with 1,3-butadiene – examined over 300 local minima on the doublet $C_5H_6N^{\bullet}$ surface alone, along with over 100 dissociation products and a considerable number of interconnecting transition states. The lowest energy pathway for the reaction **1** + $H^{\bullet}$ → **2** + $H^{\bullet}$ is shown in Figure 5.1. The highest barrier in this pathway is the initial addition of $H^{\bullet}$ to the cyano carbon of **7**, with an activation barrier of 8 kcal/mol. The radical **7** then cyclizes to form **8** and finally ejects $H^{\bullet}$ to yield pyridine. While the computational results are extensive, their focus was not on the transformation of **1** to **2** and so it may be that the pathway in Figure 5.1 is not the lowest

energy pathway for the transformation catalyzed by atomic hydrogen. For example, they report the radical **9** resulting from attachment of H• to the nitrogen of **1** as being 2 kcal/mol lower in energy than **7**, but do not report whether there is an activation energy for the formation of **9** or its cyclization, as highlighted in red in Figure 5.1. Thus, in addition to the neutral and proton catalyzed pathways, we will also examine the transformation of **1** to **2** catalyzed by atomic hydrogen.

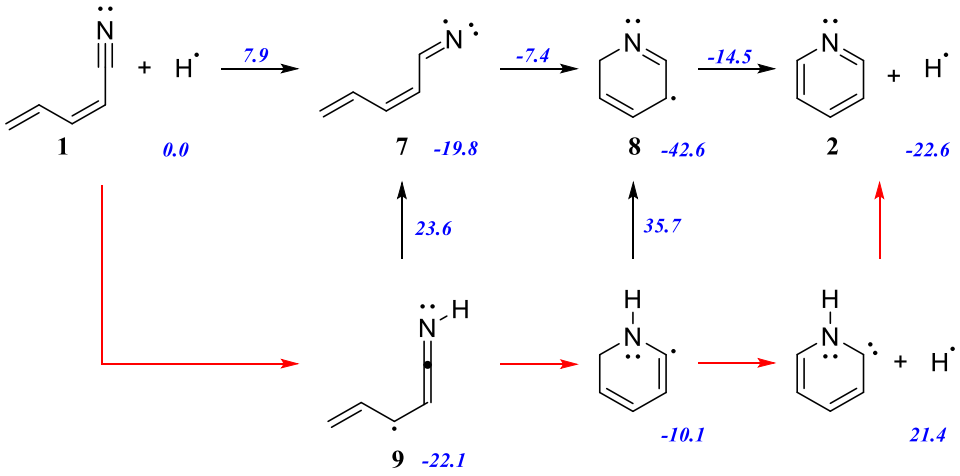

Figure 5.1. Computed energies (kcal/mol) of the H• catalyzed transformation of 1-cyano-1,3-butadiene to pyridine, determined using CCSD(T)/cc-pVTZ//B3LYP/cc-pVTZ + $ZPE_{B3LYP/cc\text{-}pVTZ}$ calculations.[17] Pathways in red were not reported in Ref. 17.

COMPUTATIONAL METHODS

To evaluate reactions of interest, geometry optimizations and frequency calculations were conducted using the B3LYP functional[23-24] and correlation-consistent polarized valence and triple zeta basis set (cc-pVTZ).[25] Transition states were further characterized *via* intrinsic reaction coordinate (IRC) calculations to ensure correspondence to the desired reaction. Following the

methodology of previous works,[15-18] energy calculations utilizing the B3LYP/cc-pVTZ geometries were conducted for each of the stationary points using coupled cluster with single, double, and perturbative triple excitations [CCSD(T)] and the cc-pVTZ basis set. These energies are used in combination with the zero-point energy correction determined at B3LYP/cc-pVTZ to calculate the relative energies of the stationary points, reported herein as CCSD(T)/cc-pVTZ//B3LYP/cc-pVTZ + $ZPE_{B3LYP/cc\text{-}pVTZ}$. All calculations were conducted using Gaussian 16.[26]

RESULTS AND DISCUSSION

The determination of the neutral pathway for the transformation of 1-cyano-1,3-butadiene (**1**) to pyridine (**2**) is based on the isoelectronic isomerization of *Z*-1,3-hexadiene-5-yne to benzene,[27] and on the rather thorough exploration of the C_6H_6 surface.[28] The neutral transformation of **1** to **2** proceeds through intermediates higher in energy than **1**. As shown in Figure 5.2, the lowest energy transformation proceeds through 1-isocyano-1,3-butadiene (**10**). The highest energy point of this pathway is the transformation of **10** to **2** *via* a tandem [3,3]-sigmatropic shift (to form the six-membered ring) and a [1,2]-sigmatropic hydrogen transfer. Alternatively, **1** can cyclize directly *via* a [3,3]-sigmatropic shift to yield intermediate **11**, and two subsequent [1,2]-sigmatropic hydrogen transfers yields **2**. While Balcioglu *et al.*[27] were careful to determine the exact nature of the intermediates, we decline to do so given that the high energies of these pathways precludes the viability of the neutral transformation of **1** to **2** under interstellar conditions. It is also worth noting that the neutral transformation of **1** to **2** is considerably higher in energy than the isoelectronic isomerization of *Z*-1,3-hexadiene-5-yne to benzene,[27] though this may be due to the difference in the choice of theory and basis set.

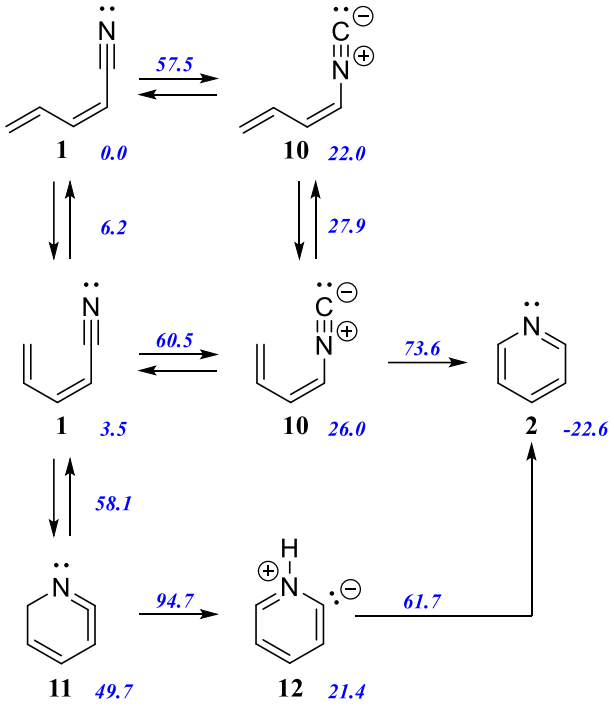

Figure 5.2. The neutral isomerization of 1-cyano-1,3-butadiene (**1**) to pyridine (**2**) with energies as computed using CCSD(T)/cc-pVTZ//B3LYP/cc-pVTZ + $ZPE_{B3LYP/cc\text{-}pVTZ}$.

As shown in Figure 5.3, the radical pathway described indirectly by Sun *et al.*[17] (**1** → **7** → **8** → **2**, green) prevails as the lowest energy pathway for the transformation of **1** to **2** as catalyzed by atomic hydrogen. The transformation begins with H• attacking the cyano carbon of **1** to form **7**, followed by cyclization to form doublet 1H-pyridyl radical **8**, and finally H• is ejected to yield **2**. The highest energy point in this pathway is that of the initial attachment of H• to **1**, with an activation energy of 7.9 kcal/mol. While this has the highest activation barrier for the attachment of H• to **1** – due to the resulting intermediate **7** being the highest in energy of the possible attachment products (**7**, **9**, **13**–**16**) – all other pathways contain higher activation barriers for their respective transformations to **2**. Specifically, attachment of H• to any other atom necessitates at least one subsequent [1,2]-sigmatropic hydrogen transfer (either before or after cyclization to form

the six-membered ring) with an activation barrier of at least 30 kcal/mol. Only by attaching H• to the cyano carbon can this high-energy transition state be avoided. Therefore, provided sufficient collision energy, the attachment of atomic hydrogen to **1** is at least a feasible albeit unlikely pathway for the formation of pyridine in the ISM.

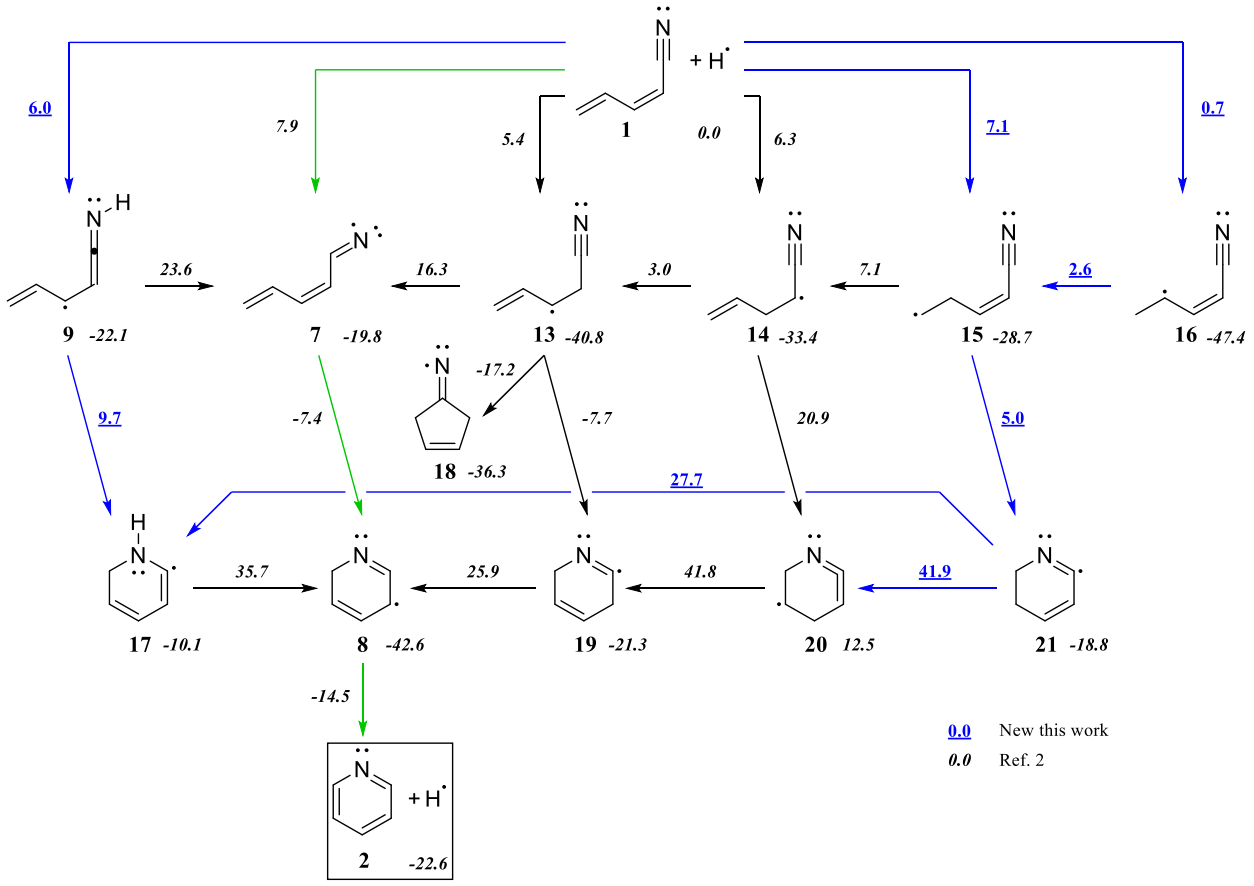

Figure 5.3. The isomerization of 1-cyano-1,3-butadiene (**1**) to pyridine (**2**) catalyzed by atomic hydrogen (H•) with energies as computed by CCSD(T)/cc-pVTZ//B3LYP/cc-pVTZ + $ZPE_{B3LYP/cc\text{-}pVTZ}$ in this work (blue, underlined) or in the previous work of Sun *et al.*[17] (black, italicized). The path highlighted in green represents the minimum energy pathway between **1** and **2**.

We used the trihydrogen cation (H_3^+) as the source of proton for catalyzing the transformation of **1** to **2** under interstellar conditions.[29-32] As shown in Figure 5.4, the transfer of a proton from the trihydrogen cation to **1** is considerably exothermic, a result of the larger $C_5H_6N^+$ molecule distributing the positive charge to a greater degree than H_3^+. This exothermicity provides the resulting $C_5H_6N^+$ intermediate with more than enough internal energy to overcome the large activation barriers that were present in the isoelectronic transformation under neutral conditions (*vide supra*). For simplicity, we have assumed that the transfer of proton from H_3^+ to C_5H_5N (and vice versa) is a barrierless process, as (gas-phase) ion-molecule reactions typically proceed without activation energy.[33]

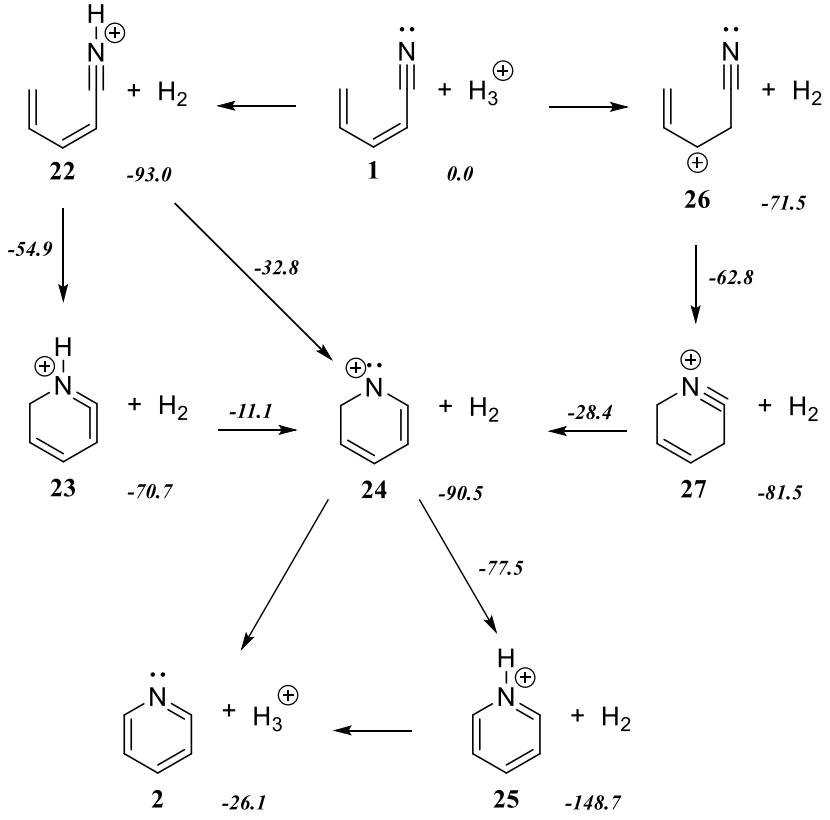

Figure 5.4. The isomerization of 1-cyano-1,3-butadiene (**1**) to pyridine (**2**) catalyzed by trihydrogen cation (H_3^+) with energies computed by CCSD(T)/cc-pVTZ//B3LYP/cc-pVTZ + $ZPE_{B3LYP/cc\text{-}pVTZ}$.

We first considered the attachment of the proton onto the nitrogen atom of **1** to yield **22**, as the nitrogen is the most basic atom of those present in **1**. Cyclization of **22** *via* bond formation between the nitrogen atom and the terminal carbon proceeds akin to that in the neutral pathway to yield **23**, which is the protonated form of **11**. Subsequent transfer of the proton from the nitrogen atom to the former cyano carbon yields 2*H*-pyridinium cation, **24**. The hydrogen transfer can be combined with the cyclization reaction to yield **24** directly from **22** *via* a single transition state, which proceeds by first transferring the proton from the nitrogen to the cyano carbon followed by cyclization. The single-step hydrogen transfer and cyclization has an activation barrier 20 kcal/mol lower than the two-step transformation. Once **24** is formed, a proton can be removed from the sp^3-hybridized carbon by H_2 to yield **2** and trihydrogen cation. Alternatively, the proton can be transferred to the nitrogen atom *via* a [1,2]-sigmatropic shift to yield pyridinium, **25**. Comparison of the relative energies of **2**+H_3^+ and **25**+H_2 reveals pyridine has a vastly greater proton affinity than molecular hydrogen by *ca.* 120 kcal/mol. This is consistent with the experimental proton affinity values of 100 kcal/mol and 222 kcal/mol for molecular hydrogen and pyridine, respectively.[34]

An alternate pathway for the transformation of **1** to **24** begins with the protonation of the C1 position to yield **26**, which is less exothermic than the corresponding formation of **22**. Subsequent cyclization of **26** to yield **27** forms the six-membered ring and is, interestingly, exothermic. At first, the positive charge would appear to be better stabilized by **26** due to the allylic π conjugation, as compared to what is effectively a deprotonated imine in **27**, but as evidenced by the relative energies this argument is insufficient. We propose that additional hyperconjugation with the C–H σ bonds of the newly formed sp^3-hybridized carbon is responsible for the higher stability of **27** compared to **26**. More specifically, we hypothesize that the positive

charge can be delocalized through the entire ring, by the donation of electron density from the C–H σ bonds to the C–N π bond, and in turn donation from the C–C π bond to the C–H σ bonds. While such hyperconjugation is present in **26**, it is not as significant because the group donating electron density to the C–H σ bonds *via* hyperconjugation is the electron-withdrawing cyano π bond. Altogether, the stabilization due to hyperconjugation overcomes the cost of disrupting the allylic π system in **26** to form the six-membered ring of **27**, leading to an exothermic reaction. This hypothesis, however, requires further investigation *via* natural bond orbital (NBO) and natural resonance theory (NRT) calculations, the analysis of which has not been completed at the time of this writing. Regardless, a subsequent [1,2]-sigmatropic hydrogen transfer to the former cyano carbon yields **24**. Overall, the formation of **24** from **1** *via* intermediate **26** has only a slightly higher activation barrier (< 5 kcal/mol) than the path *via* **22**, and so may represent a not insignificant contribution to the formation of **2** from **1**.

CONCLUSION

The high energy calculated for the neutral transformation of 1-cyano-1,3-butadiene **1** to form pyridine **2** makes it clear that a catalyzing event is required to obtain **2** from **1** under astronomical conditions. Catalysis of the transformation by atomic hydrogen is much more feasible, but this radical pathway possesses an activation barrier of 8 kcal/mol. The most likely pathway of those considered thus far is catalysis by the trihydrogen cation H_3^+. The transfer of a proton from H_3^+ to **1** is highly exothermic, owing to the low proton affinity of molecular hydrogen in comparison to the much larger C_5H_5N molecule. This exothermicity in turn ensures the subsequent transition states have activation barriers significantly lower than the energy of the initial reactants, and **1** is easily obtained. The high proton affinity of pyridine, however, is such

that the formation of pyridinium cation **25** is much more exothermic and thus the most likely thermodynamic product of the reaction of **1** with H_3^+.

As can be inferred from the discussion, this study is still a work in progress. In addition to the proposed NBO/NRT supporting calculations, we plan to explore several other avenues for the transformation of **1** to **2**. In particular, the catalyzed pathways studied thus far proceed by attaching and then removing of an external mass ($H^\bullet$ or H^+). In a similar manner, we will consider the transformation of **1** to **2** for the scenario where mass is removed and then reattached, that is, the dissociation of atomic or cationic hydrogen from **1** to form the corresponding $C_5H_4N^\bullet$ radical or $C_4H_5N^-$ anion. Subsequent cyclization to form the six-membered ring and then reattachment of the hydrogen can yield **2** and may involve little to no activation barriers beyond the initial detachment of the hydrogen, which we assume to be the result of a photochemical reaction or impact of cosmic rays. The requisite transfer of a hydrogen atom from the terminal carbon to the cyano carbon – which was the rate-determining step for most transformations considered thus far – is then inherently distinct from the ring formation, and the corresponding activation barrier will be split into (and coupled with) the removal and attachment steps. Further, noting that in both scenarios at least one two-body collision is required, we plan to consider the transformation of **1** to **2** for the case of the removal or attachment of an electron. Such a change in the electronic structure of **1** may facilitate its transformation into **2** and, other than the initial ionization energy, only requires the presence of free electrons to occur. The computational modeling of these reactions is thus an active area of research in pursuit of the completion of this work.

ACKNOWLEDGEMENTS

We gratefully acknowledge the National Science Foundation for support of this project (CHE-1954270).

REFERENCES

1. Cernicharo, J.; Heras, A. M.; Tielens, A. G. G. M.; Pardo, J. R.; Herpin, F.; Guélin, M.; Waters, L. B. F. M., Infrared Space Observatory's Discovery of C_4H_2, C_6H_2, and Benzene in CRL 618. *Astrophys. J.* **2001,** *546* (2), L123-L126.

2. Myers, P. C.; Thaddeus, P.; Linke, R. A., A search for interstellar pyrrole: evidence that rings are less abundant than chains. *Astrophys. J.* **1980,** *241*, 155-157.

3. Irvine, W. M.; Ellder, J.; Hjalmarson, A.; Kollberg, E.; Rydbeck, O. E. H.; Sorensen, G. O.; Bak, B.; Svanholt, H., Searches for interstellar imidazole and cyanoform. *Astron. Astrophys.* **1981,** *97*, 192-194.

4. Simon, M. N.; Simon, M., Search for Interstellar Acrylonitrile, Pyrimidine, and Pyridine. *The Astrophysical Journal* **1973,** *184*, 757-762.

5. Kuan, Y.-J.; Yan, C.-H.; Charnley, S. B.; Kisiel, Z.; Ehrenfreund, P.; Huang, H.-C., A search for interstellar pyrimidine. *Mon. Not. Roy. Astron. Soc.* **2003,** *345* (2), 650-656.

6. Kuan, Y.-J.; Charnley, S. B.; Huang, H.-C.; Kisiel, Z.; Ehrenfreund, P.; Tseng, W.-L.; Yan, C.-H., Searches for interstellar molecules of potential prebiotic importance. *Adv. Space Res.* **2004,** *33* (1), 31-39.

7. McGuire, B. A.; Burkhardt, A. M.; Kalenskii, S.; Shingledecker, C. N.; Remijan, A. J.; Herbst, E.; McCarthy, M. C., Detection of the aromatic molecule benzonitrile (c-C6H5CN) in the interstellar medium. *Science* **2018,** *359* (6372), 202-205.

8. Burkhardt, A. M.; Long Kelvin Lee, K.; Bryan Changala, P.; Shingledecker, C. N.; Cooke, I. R.; Loomis, R. A.; Wei, H.; Charnley, S. B.; Herbst, E.; McCarthy, M. C.; McGuire, B. A., Discovery of the Pure Polycyclic Aromatic Hydrocarbon Indene (*c*-C_9H_8) with GOTHAM Observations of TMC-1. *Astrophys. J. Lett.* **2021,** *913* (2), L18.

9. Kelvin Lee, K. L.; Changala, P. B.; Loomis, R. A.; Burkhardt, A. M.; Xue, C.; Cordiner, M. A.; Charnley, S. B.; McCarthy, M. C.; McGuire, B. A., Interstellar Detection of 2-cyanocyclopentadiene, C_5H_5CN, a Second Five-membered Ring toward TMC-1. *Astrophys. J. Lett.* **2021,** *910* (1), L2.

10. McCarthy, M. C.; Lee, K. L. K.; Loomis, R. A.; Burkhardt, A. M.; Shingledecker, C. N.; Charnley, S. B.; Cordiner, M. A.; Herbst, E.; Kalenskii, S.; Willis, E. R.; Xue, C.; Remijan, A. J.; McGuire, B. A., Interstellar detection of the highly polar five-membered ring cyanocyclopentadiene. *Nature Astronomy* **2021,** *5* (2), 176-180.

11. McGuire, B. A.; Loomis, R. A.; Burkhardt, A. M.; Lee, K. L. K.; Shingledecker, C. N.; Charnley, S. B.; Cooke, I. R.; Cordiner, M. A.; Herbst, E.; Kalenskii, S.; Siebert, M. A.; Willis, E. R.; Xue, C.; Remijan, A. J.; McCarthy, M. C., Detection of two interstellar polycyclic aromatic hydrocarbons via spectral matched filtering. *Science* **2021,** *371* (6535), 1265-1269.

12. Charnley, S. B.; Kuan, Y.-J.; Huang, H.-C.; Botta, O.; Butner, H. M.; Cox, N.; Despois, D.; Ehrenfreund, P.; Kisiel, Z.; Lee, Y.-Y.; Markwick, A. J.; Peeters, Z.; Rodgers, S. D., Astronomical searches for nitrogen heterocycles. *Adv. Space Res.* **2005,** *36* (2), 137-145.

13. Barnum, T. J.; Siebert, M. A.; Lee, K. L. K.; Loomis, R. A.; Changala, P. B.; Charnley, S. B.; Sita, M. L.; Xue, C.; Remijan, A. J.; Burkhardt, A. M.; McGuire, B. A.; Cooke, I. R., A Search for Heterocycles in GOTHAM Observations of TMC-1. *J. Phys. Chem. A* **2022,** *126* (17), 2716-2728.

14. Simon, M. N.; Simon, M., Search for Interstellar Acrylonitrile, Pyrimidine, and Pyridine. *Astrophys. J.* **1973,** *184*, 757.

15. Morales, S. B.; Bennett, C. J.; Le Picard, S. D.; Canosa, A.; Sims, I. R.; Sun, B. J.; Chen, P. H.; Chang, A. H. H.; Kislov, V. V.; Mebel, A. M.; Gu, X.; Zhang, F.; Maksyutenko, P.; Kaiser, R. I., A crossed molecular beam, low-temperature kinetics, and theoretical investigation of the reation of the cyano radical (CN) with 1,3-butadiene (C_4H_6). A route to complex nitrogen-bearing molecules in low-temperature extraterrestrial environments. *Astrophys. J.* **2011,** *742* (1), 26.

16. Parker, D. S. N.; Kaiser, R. I.; Kostko, O.; Troy, T. P.; Ahmed, M.; Sun, B.-J.; Chen, S.-H.; Chang, A. H. H., On the formation of pyridine in the interstellar medium. *PCCP* **2015,** *17* (47), 32000-32008.

17. Sun, B. J.; Huang, C. H.; Chen, S. Y.; Chen, S. H.; Kaiser, R. I.; Chang, A. H. H., Theoretical Study on Reaction Mechanism of Ground-State Cyano Radical with 1,3-Butadiene: Prospect of Pyridine Formation. *J. Phys. Chem. A* **2014,** *118* (36), 7715-7724.

18. Jamal, A.; Mebel, A. M., Theoretical Investigation of the Mechanism and Product Branching Ratios of the Reactions of Cyano Radical with 1- and 2-Butyne and 1,2-Butadiene. *J. Phys. Chem. A* **2013,** *117* (4), 741-755.

19. Lin, M.-F.; Dyakov, Y. A.; Tseng, C.-M.; Mebel, A. M.; Lin, S. H.; Lee, Y. T.; Ni, C.-K., Photodissociation dynamics of pyridine. *J. Chem. Phys.* **2005,** *123* (5), 054309.

20. Mackie, J. C.; Colket, M. B.; Nelson, P. F., Shock tube pyrolysis of pyridine. *J. Phys. Chem.* **1990,** *94* (10), 4099-4106.

21. Liu, R.; Huang, T. T. S.; Tittle, J.; Xia, D., A Theoretical Investigation of the Decomposition Mechanism of Pyridyl Radicals. *J. Phys. Chem. A* **2000,** *104* (36), 8368-8374.

22. Houser, T. J.; McCarville, M. E.; Biftu, T., Kinetics of the thermal decomposition of pyridine in a flow system. *Int. J. Chem. Kinet.* **1980,** *12* (8), 555-568.

23. Lee, C. T.; Yang, W. T.; Parr, R. G., Development of the Colle-Salvetti correlation energy formula into a functional of the electron density. *Phys. Rev. B* **1988,** *37* (2), 785-789.

24. Becke, A. D., Density-functional thermochemistry .3. The role of exact exchange. *J. Chem. Phys.* **1993,** *98* (7), 5648-5652.

25. Dunning, T. H., Gaussian basis sets for use in correlated molecular calculations .1. The atoms boron through neon and hydrogen. *J. Chem. Phys.* **1989,** *90* (2), 1007-1023.

26. Frisch, M. J.; Trucks, G. W.; Schlegel, H. B.; Scuseria, G. E.; Robb, M. A.; Cheeseman, J. R.; Scalmani, G.; Barone, V.; Petersson, G. A.; Nakatsuji, H.; Li, X.; Caricato, M.; Marenich, A. V.; Bloino, J.; Janesko, B. G.; Gomperts, R.; Mennucci, B.; Hratchian, H. P.; Ortiz, J. V.; Izmaylov, A. F.; Sonnenberg, J. L.; Williams-Young, D.; Ding, F.; Lipparini, F.; Egidi, F.; Goings, J.; Peng, B.; Petrone, A.; Henderson, T.; Ranasinghe, D.; Zakrzewski, V. G.; Gao, J.; Rega, N.; Zheng, G.; Liang, W.; Hada, M.; Ehara, M.; Toyota, K.; Fukuda, R.; Hasegawa, J.; Ishida, M.; Nakajima, T.; Honda, Y.; Kitao, O.; Nakai, H.; Vreven, T.; Throssell, K.; Montgomery Jr., J. A.; Peralta, J. E.; Ogliaro, F.; Bearpark, M. J.; Heyd, J. J.; Brothers, E. N.; Kudin, K. N.; Staroverov, V. N.; Keith, T.

A.; Kobayashi, R.; Normand, J.; Raghavachari, K.; Rendell, A. P.; Burant, J. C.; Iyengar, S. S.; Tomasi, J.; Cossi, M.; Millam, J. M.; Klene, M.; Adamo, C.; Cammi, R.; Ochterski, J. W.; Martin, R. L.; Morokuma, K.; Farkas, O.; Foresman, J. B.; Fox, D. J. *Gaussian 16, Revision B.01*, Gaussian, Inc.: Wallingford, CT, USA, 2016.

27. Balcioglu, N.; Özgür Özsar, A., Thermal conversion of 1,3-hexadien-5-yne to benzene: a revisited theoretical study. *J. Mol. Struct. THEOCHEM* **2004,** *677* (1), 125-132.

28. Dinadayalane, T. C.; Priyakumar, U. D.; Sastry, G. N., Exploration of C_6H_6 Potential Energy Surface: A Computational Effort to Unravel the Relative Stabilities and Synthetic Feasibility of New Benzene Isomers. *The Journal of Physical Chemistry A* **2004,** *108* (51), 11433-11448.

29. Watson, W. D., The Rate of Formation of Interstellar Molecules by Ion-Molecule Reactions. *Astrophys. J.* **1973,** *183*, L17.

30. Herbst, E.; Klemperer, W., The Formation and Depletion of Molecules in Dense Interstellar Clouds. *Astrophys. J.* **1973,** *185*, 505-534.

31. Tielens, A. G. G. M., The molecular universe. *Rev. Mod. Phys.* **2013,** *85* (3), 1021-1081.

32. Herbst, E., The astrochemistry of H_3^+. *Philos. Trans. R. Soc. A* **2000,** *358* (1774), 2523-2534.

33. Herbst, E., Chemistry in the interstellar medium. *Annu. Rev. Phys. Chem.* **1995,** *46*, 27-53.

34. Hunter, E. P.; Lias, S. G., Proton Affinity Evaluation. In *NIST Chemistry WebBook, NIST Standard Reference Database Number 69* Linstrom, P. J.; Mallard, W. G., Eds. National Institute of Standards and Technology: Gaithersburg MD. (accessed July 27, 2022).

Chapter 6: Carbon Condensation *via* [4+2] Cycloaddition of Highly Unsaturated Carbon Chains

Unpublished work with contributions from Brian J. Esselman, R. Claude Woods, and Robert J. McMahon

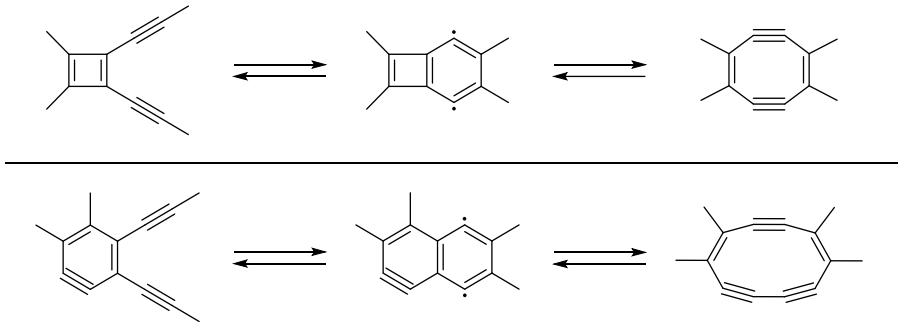

ABSTRACT

We present computational studies of reaction pathways for alkyne / polyyne dimerization that represent plausible early steps in mechanisms for carbon condensation. A previous computational study of the *ring coalescence and annealing* model of C_{60} formation revealed that a 1,4-didehydrobenzocyclobutadiene intermediate (*p*-benzyne derivative) has little to no barrier to undergoing an unproductive *retro*-Bergman cyclization, which brings into question the relevance of that reaction pathway. The current study investigates an alternative model, which proceeds through an initial [4+2] cycloaddition instead of a [2+2] cycloaddition. In this pathway, the problematic intermediate is avoided, with the reaction proceeding *via* a (potentially) more kinetically stable tetradehydronaphthalene derivative. The computational studies herein of the [2+2] and [4+2] model systems, with increasing alkyne substitutions, reveal that the *para*-benzyne diradical of the [4+2] pathway has a significantly greater barrier to ring opening than the analogous intermediates of the [2+2] pathway, and that alkyne substitution has little effect on this important barrier.

INTRODUCTION

Allotropes of carbon continue to be active areas of research in chemistry and materials science. Recent developments include a monolayer fullerene network,[1] graphene nanoribbons of various geometries,[2] and allotropes derived from nonbenzenoid aromatic structures (azulene, biphenylene, *etc*.).[3] Cyclocarbon C_{18},[4-5] a known precursor of C_{60},[6] has been imaged on a surface.[7] A myriad of chemical models for the formation of fullerene have been proposed and can be categorized into two groups: pathways that start from large carbon aggregates that degrade into fullerene (“size-down”) and pathways that start from small carbon aggregates and condense into

fullerene ("size-up"). The "size-down" pathways that have been proposed include the degradations of graphene,[8-9] graphene nanoflakes,[10] carbon nanotubes,[11] and giant fullerenes,[12-13] while "size-up" pathways proposed include the *fullerene road*,[14] *pentagon road*,[15] *closed network growth*,[15-17] and *ring coalescence and annealing*.[6, 18-19] Of the "size-up" pathways, all but the *ring coalescence and annealing* model progress from smaller carbon aggregates to larger fullerenes through the steady incorporation of C_2 fragments. In contrast, the *ring coalescence and annealing* model proposes the addition of medium-sized (C_{12} – C_{20}) cyclic polyynes, and subsequent annealing through a cascading radical mechanism, results in fullerenes.[20] As illustrated in Scheme 6.1, this combination has been proposed to occur through an initial [2+2] cycloaddition to yield a tetraalkynylcylcobuta-1,3-diene intermediate that subsequently undergoes a Bergman cyclization reaction.[19-20]

While formation of a tetraalkynylcyclobutadiene may be a reasonable step in this process, it was previously shown[21] that the model products formed by the subsequent Bergman cyclization reaction may have little or no barrier to undergo an exothermic *retro*-Bergman cyclization to yield an eight-membered ring intermediate. This eight-membered ring intermediate is not currently accounted for in the *ring coalescence and annealing* model, and the structural element of an eight-membered ring is obviously not present in fullerene C_{60}. These findings call into question whether or not the initial [2+2] dimerization represents a productive pathway to fullerene formation. Thus, we turned our attention to the study of an alternative reaction pathway that involves initial [4+2] cycloaddition, or hexadehydro-Diels-Alder reaction (HDDA),[22-23] of two polyynes to give a tetraalkynyl *ortho*-benzyne intermediate (Scheme 6.2). Subsequent Bergman cyclization, followed by a cascading radical mechanism, may afford a viable pathway to C_{60}, as illustrated in Scheme 6.2. This pathway avoids forming a high-energy four-membered ring intermediate and

avoids the problematic *retro*-Bergman cyclization leading to the eight-membered ring species. Thus, we investigate whether a small modification to the *ring coalescence and annealing* model yields a more kinetically realistic reaction pathway.

Scheme 6.1. The [2+2] Ring Coalescence and Annealing Model of Fullerene Formation

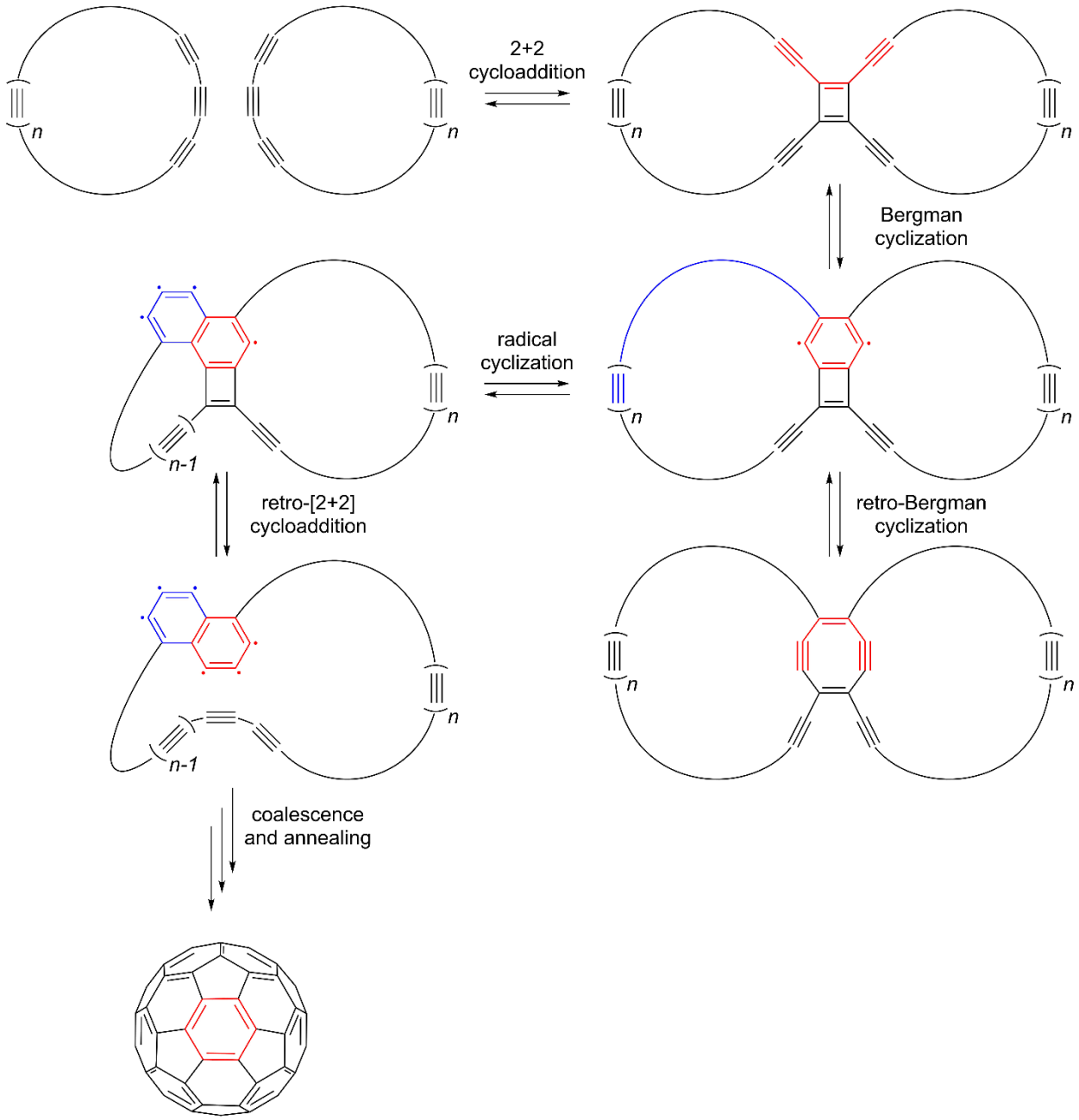

Scheme 6.2. Proposed [4+2] Ring Coalescence and Annealing Model of Fullerene Formation

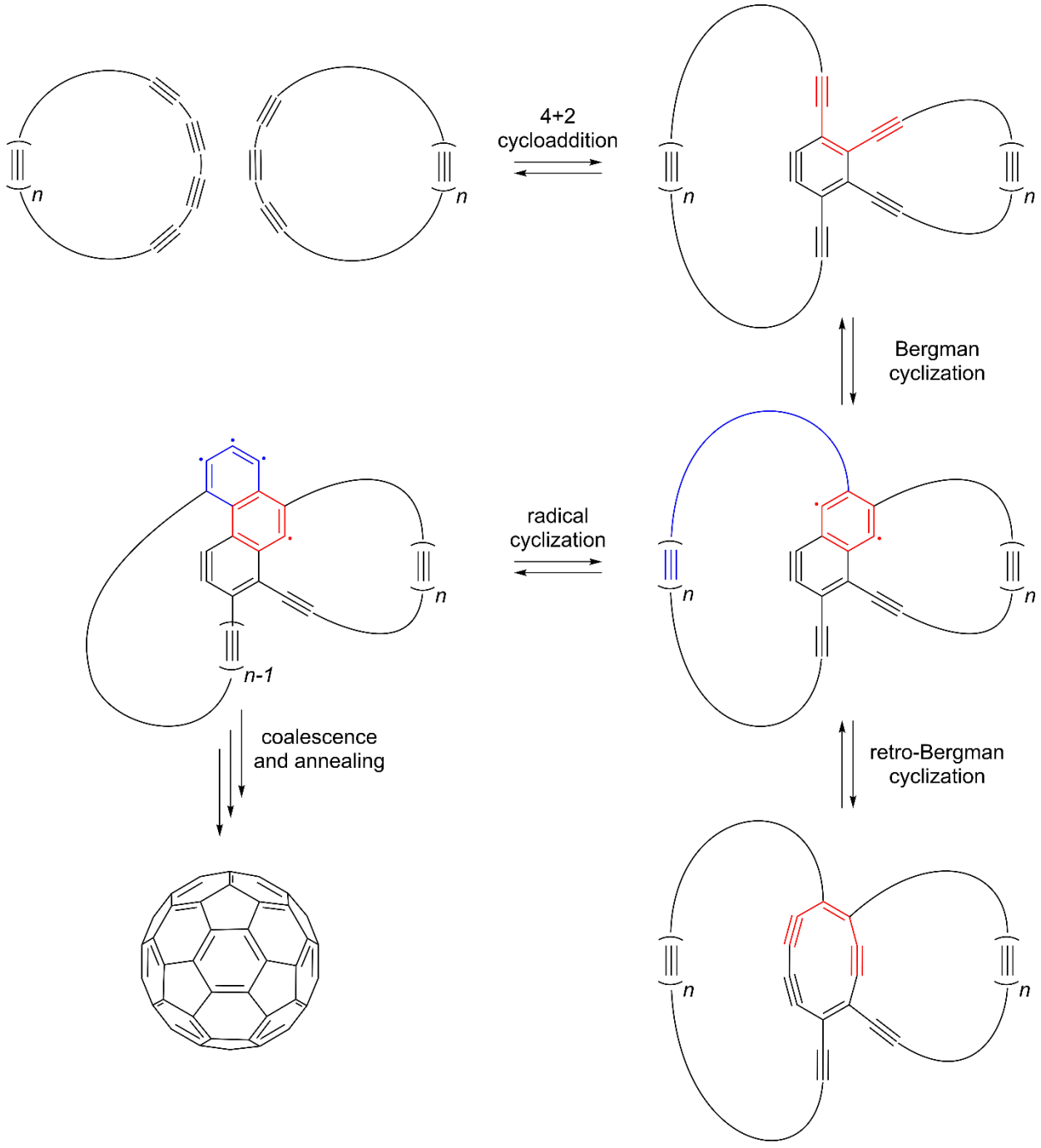

The condensation of highly unsaturated carbon molecules *via* cycloadditions has been evaluated computationally at several levels of theory for a variety of species, as summarized in

Scheme 6.3, but the comparison of polyyne dimerization through [2+2] or [4+2] cycloaddition reactions has not been examined. A thermal, concerted [$2\pi_s$+$2\pi_s$] cycloaddition is symmetry forbidden and thus the [2+2] cycloaddition is expected to proceed through a radical mechanism (top Scheme 6.3).[24-26] The [4+2] cycloaddition can proceed through either a radical mechanism or a concerted [$4\pi_s$+$2\pi_s$] mechanism with the concerted reaction having an activation barrier of 34–36 kcal/mol, compared to the rate-determining step of the radical mechanism having a barrier of 30–37 kcal/mol (middle Scheme 6.3).[26-28] The competition of the [2+2] cycloaddition versus the [4+2] cycloaddition is exemplified by the combination of butadiyne and ethyne (middle Scheme 6.3, gray and underlined) to form either *ortho*-benzyne or ethynylcyclobutadiene.[26] Unsurprisingly, the computed barriers for stepwise and concerted processes are close in energy and the overall prediction of stepwise vs. concerted depends on the level of theory employed. Overall, the formation of the [4+2] product (*ortho*-benzyne) is significantly more exothermic (>40 kcal/mol) than the formation of the [2+2] product (ethynylcyclobutadiene).[26] Interestingly, in considering the stepwise pathway for reaction of *ortho*-benzyne and butadiyne (bottom Scheme 6.3), the [2+2] product is kinetically favored by several kcal/mol, while the formation of the [4+2] product is thermodynamically favored by about 30 kcal/mol.[25]

Scheme 6.3. Mechanisms of Simple Alkyne Cycloadditions

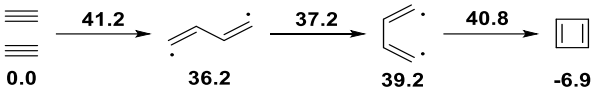

CCSD(T)/cc-pVTZ//B3LYP/6-311++G(3df,3pd)[24]

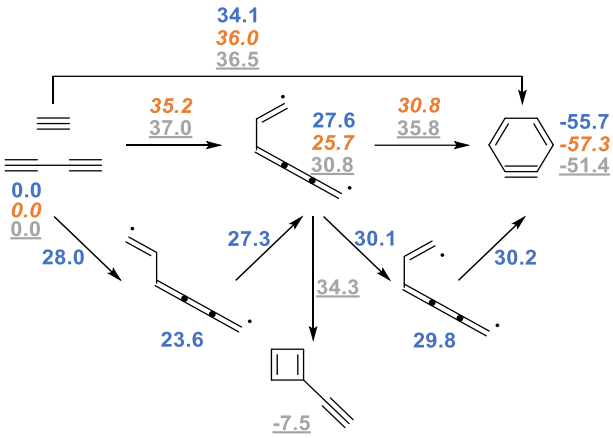

CAS(12,12)-PT2/CBS//CAS(12,12)-PT2/cc-pVTZ + $ZPVE_{CASSCF}$[27]

M06-2X//6-311+G(d,p)[28]

CCSD(T)/6-311+G(d,p)//M05-2X/6-311+G(d,p)[26]

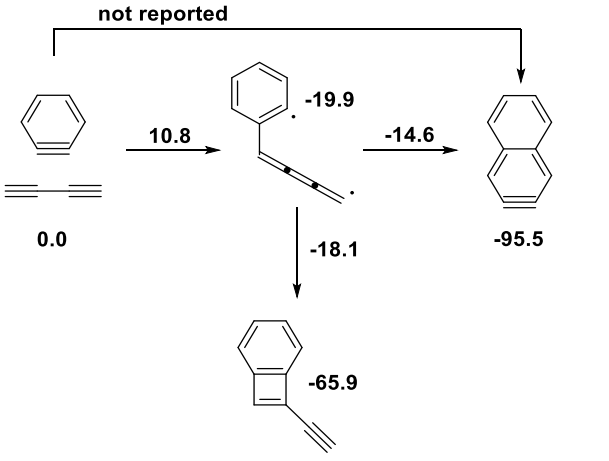

CCSD(T)/6-311+G(d,p)//B3LYP/6-311+G(d,p) + ZPVE[25]

Following initial cycloadditions of the polyynes, the next step toward fullerene formation in the *ring coalescence and annealing* model is a Bergman cyclization.[20, 29] The resulting intermediate for the [2+2] pathway is a substituted tetraalkynyl-didehydrobenzocyclobutadiene, which is a fused *para*-benzyne and cyclobutadiene species (Scheme 6.1), while for the [4+2] pathway the intermediate is a substituted tetraalkynyl-tetradehydronaphthalene, which is a fused *ortho*- and *para*-benzyne species (Scheme 6.2). In principle, the *para*-benzyne intermediate of the [4+2] pathway is expected to be more stable than the corresponding *para*-benzyne intermediate of the [2+2] pathway: the *ortho*-benzyne present in the former is a strained, formally aromatic ring while the cyclobutadiene present in the latter is a highly strained, formally antiaromatic ring. This argument is based upon the computational result that the [4+2] product of *ortho*-benzyne and butadiyne is 30 kcal/mol lower in energy than the [2+2] product (bottom Scheme 6.3). With the [4+2] intermediate considerably lower in energy than the [2+2] intermediate, the subsequent *retro*-Bergman cyclization will have a greater barrier within the [4+2] pathway than within the [2+2] pathway. Thus the [4+2] pathway would be more likely to undergo the subsequent cascading radical mechanism that leads to fullerene.

The [2+2] and [4+2] carbon condensation pathways (**I** and **II**, respectively) studied in this work are illustrated in Scheme 6.4. Because a computational study of a large carbon ring system as described in Schemes 6.1 and 6.2 is not computationally feasible with reasonable *ab initio* methods, we used a simplified substitution pattern described in Scheme 6.4 (**a**–**d**). Substitution **a** is the parent system (R = R' = H). Substitution **b** places additional alkynyl units at the end of the alkyne chains of the cycloaddition products **2b** or **6b**, while substitution **c** places additional alkynyl units on the ring of the cycloaddition products **2c** or **6c**. The **d** substitution places alkynyl units on both the ring and the alkyne chains of the cycloaddition products **2d** or **6d**. Scheme 6.4 (top)

illustrates a [2+2] cycloaddition pathway involving two polyynes (**1a**–**d**) to yield substituted cyclobutadiene **2a**–**d**. A Bergman cyclization of the enediyne unit of **2a**–**d** results in the diradical didehydrobenzocyclobutadiene **3a**–**d**. Diradical species **3a**–**d** can then undergo a *retro*-Bergman cyclization, breaking the shared carbon-carbon bond between the fused rings, to generate cycloocta-1,5-dien-3,7-diyne **4a**–**d**.

Scheme 6.4. [2+2] and [4+2] Reaction Pathways.

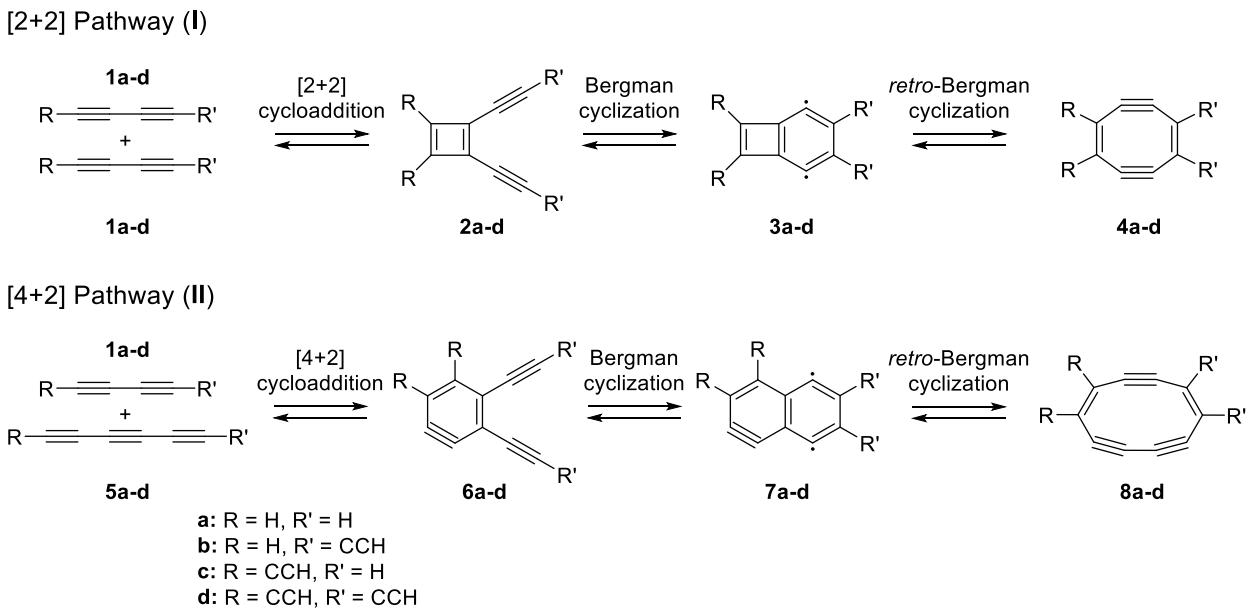

Scheme 6.4 (bottom) illustrates an alternative pathway that proceeds through an initial [4+2] cycloaddition of two polyynes **1**/**5a**–**d**. Necessarily, the pathway involves an extra alkynyl unit in one of the initial polyynes for system **II** compared to system **I**. The [4+2] cycloaddition yields the substituted *ortho*-benzyne **6a**–**d**, which can undergo the Bergman cyclization to generate the diradical tetradehydronaphthalene species **7a**–**d**. The *retro*-Bergman cyclization of **7a**–**d** generates cyclodeca-1,7-dien-3,5,9-triyne **8a**–**d**.

Regardless of whether the initial [2+2] or [4+2] adducts are formed by a stepwise or concerted process, we are keenly interested in elucidating the chemistry of these enediynes (**2a-d** and **6a-d**) with respect to Bergman cyclization and subsequent ring opening. An earlier study of reaction pathway **Ia** at the B3LYP level of theory but was unsuccessful at identifying **3a** as a stationary point for the reactions under investigation.[21] In this work, we revisited pathway **Ia** by utilizing a smaller IRC step size to increase the sampling and produce a finer-detailed potential energy surface for the purpose of comparison to the SF-TDDFT model system. Given the previous poor behavior using B3LYP,[21] and with consideration to the system size, MP2/cc-pVTZ calculations were utilized to find the stationary points in these reaction pathways. As noted previously[21] and discussed further in this work, however, the MP2 description of diradicals **3a**–**d** and **7a**–**d** in these schemes is questionable as it employs a single-reference model for a species that is best treated with a multi-reference model. The multi-reference equation-of-motion and spin-flip coupled cluster method, EOM-SF-CCSD employed previously on MP2 single point calculations,[21] is computationally too intensive and not suitable for studying the larger systems in this work. Analogous spin-flip approaches, however, have been applied to density functional theory[30] and recent advances in the implementation[31] give comparable results. Thus, spin-flip, time-dependent DFT calculations were chosen to evaluate the energetics of the reaction pathways in this investigation.

COMPUTATIONAL METHODS

To evaluate the reactions of interest, restricted Møller-Plesset second-order perturbation theory[32] was employed with the correlation consistent polarized valence and triple zeta basis set[33] (MP2/cc-pVTZ) using Gaussian 09.[34] Geometry optimizations with harmonic frequency

calculations were employed to determine the nature of the stationary points. Intrinsic reaction coordinate (IRC) calculations were used to confirm the location of transition state structures for all model schemes. For **Ia** and **IIa**, single point calculations on the MP2 structures were carried out with coupled-cluster calculations (CCSD(T)/cc-pVTZ) and equation-of-motion spin-flip coupled cluster with single and double excitations (EOM-SF-CCSD/cc-pVDZ) as implemented in Q-Chem 4.4.1.[35] For all reaction schemes (**Ia**–**d** and **IIa**–**d**), single point calculations on the MP2 structures were carried out using spin-flip time-dependent density functional theory within the Tamm-Dancoff approximation (SF-TDDFT)[30] as implemented in Q-Chem 4.4.1[35] with the cc-pVTZ basis set and utilizing the "collinear 50-50" functional[30] (exchange = 50% HF + 8% Slater + 42% Becke; correlation = 19% VWN + 81% LYP). Additional properties of the MP2/cc-pVTZ local minima were analyzed by nuclear-independent chemical shifts (NICS),[36] using the gauge-independent atomic orbital (GIAO) method, and natural bond orbital/natural resonance theory (NBO/NRT)[37] calculations with the B3LYP functional[38-39] and the 6-31G(d) basis set,[40] as implemented in Gaussian 09.[34]

While conducting the EOM-SF-CCSD and SF-TDDFT single point calculations on the MP2 IRC structures, multiple solutions to the reference SCF calculations were observed for closely related structures, particularly those around **3a**–**d** and **7a**–**d**, resulting in a variety of spin-flip excited states regardless of which reaction pathway or substitution pattern was considered. This is partially explained by considering that, for the high-spin triplet reference, there is a change in the energetic ordering of two non-interacting triplet states that occurs near **TS2–3** and **TS6–7** in almost all substitution patterns (**a**–**d**). Unfortunately, the reordering of the triplet states does not account for the varied results in the region around **3a**–**d** and **7a**–**d**, observed in the high-spin triplet reference calculations. Rather, we hypothesize that the documented[41] orbital instability of *ab initio*

calculations of *para*-benzyne (arising from the near-degeneracy of electronic states of different symmetry) is extended to the similar structures that occur in the region around **3a**–**d** and **7a**–**d**, for both CCSD and DFT high-spin reference calculations. The difference between these solutions to the high-spin reference calculations appears to be related to the ordering of two radical-type orbitals associated with the *para*-benzyne structure and two π-type orbitals of the fused ring π system. This variation was corrected by adjusting the orbital guess for the reference calculation to obtain a continuous reference energy surface from the enediyne species (**2a**–**d** and **6a**–**d**) to the ring-opened species (**4a**–**d** and **8a**–**d**). The adjustment provided a continuous surface from the reactant to the product along the IRC, but the resultant energy values were not necessarily the lowest energy result for every electronic state for each structure in the reaction pathway.

RESULTS AND DISCUSSION

The computational results of the [2+2] and [4+2] carbon condensation reaction pathways investigated in this work are displayed in Figures 6.1 and 6.2, respectively and summarized in Tables 6.1 and 6.2. Given the multiple ways in which the condensation of polyynes can proceed through the [2+2] and [4+2] cycloadditions, as discussed above, we did not pursue a comprehensive examination of the transformation from **1a**–**d** to **2a**–**d** and **1**/**5a**–**d** to **6a**–**d**; rather, we directed our attention on the nature of the diradical species **3a**–**d** and **7a**–**d**. As such, we focused on the transformations from **2a**–**d** to **3a**–**d** to **4a**–**d** and from **6a**–**d** to **7a**–**d** to **8a**–**d**. To that end, the reaction coordinate for Figure 6.1 is the combination of the IRC results for the transition states connecting **2a**–**d** and **3a**–**d** with the IRC results for the transition states connecting **3a**–**d** and **4a**–**d**. For several cases, the IRC calculations were unable to be extended all the way to the connected local minima within a reasonable amount of processor time. Thus, the local minima

structures are spaced between the IRC results in an energetically reasonable but ultimately arbitrary fashion. Similarly, Figure 6.2 is the combination of the IRC results for the transition states connecting **6a**–**d** and **7a**–**d** with the IRC results for the transition states connecting **7a**–**d** and **8a**–**d**, with the local minima structures spaced between. For both figures, the reaction coordinate starts at the IRC calculated structure closest to the initial rings **2a**–**d** and **6a**–**d**. To connect the initial ring structures to the transition states *via* the IRC would require an exceedingly long calculation due to the shallowness of the energy surface in this region, at the step size utilized.

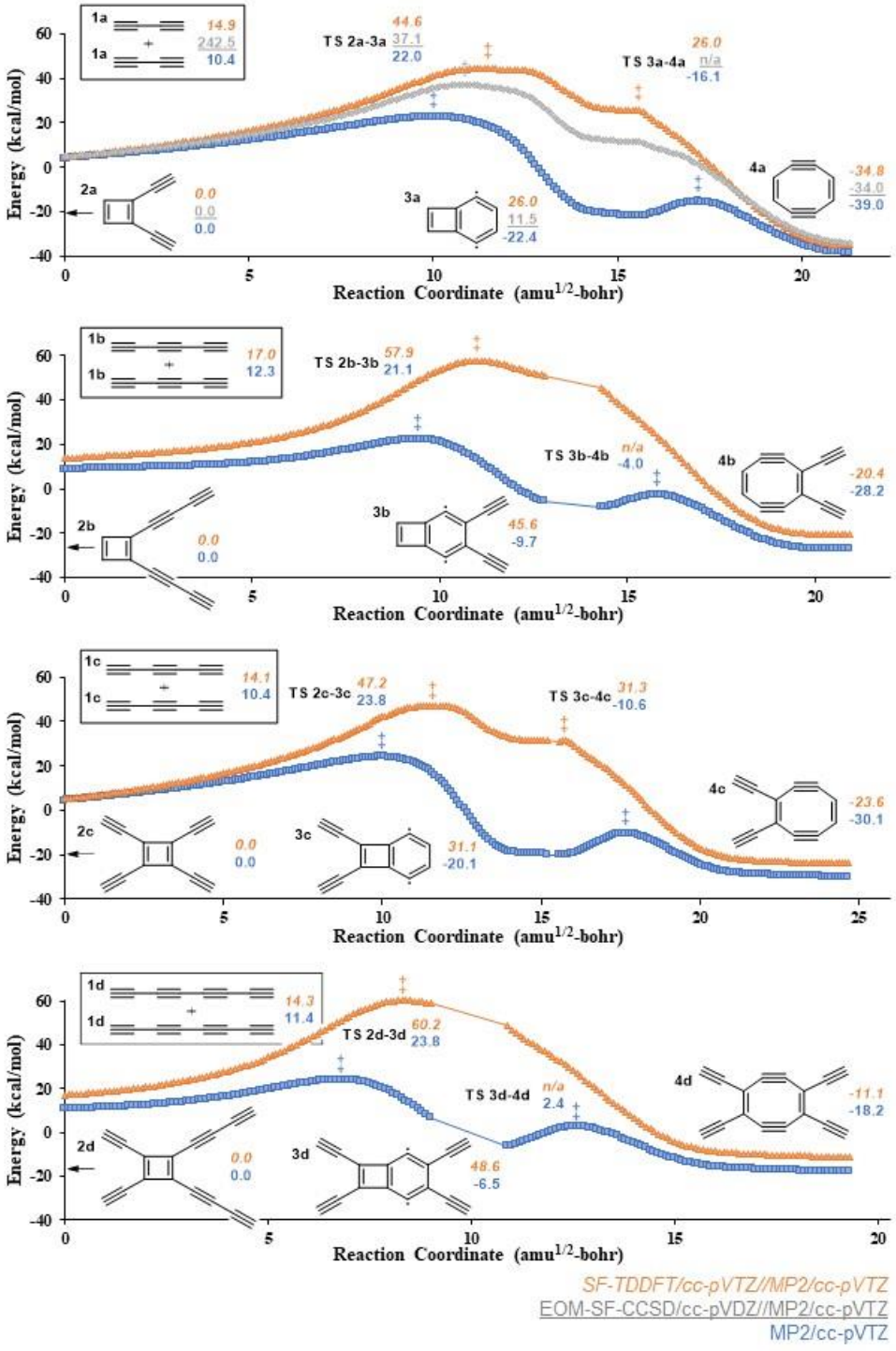

Figure 6.1. Potential energy surfaces for the Bergman cyclization and subsequent *retro*-Bergman cyclization of alkynyl-substituted cyclobutadienes (system **I**).

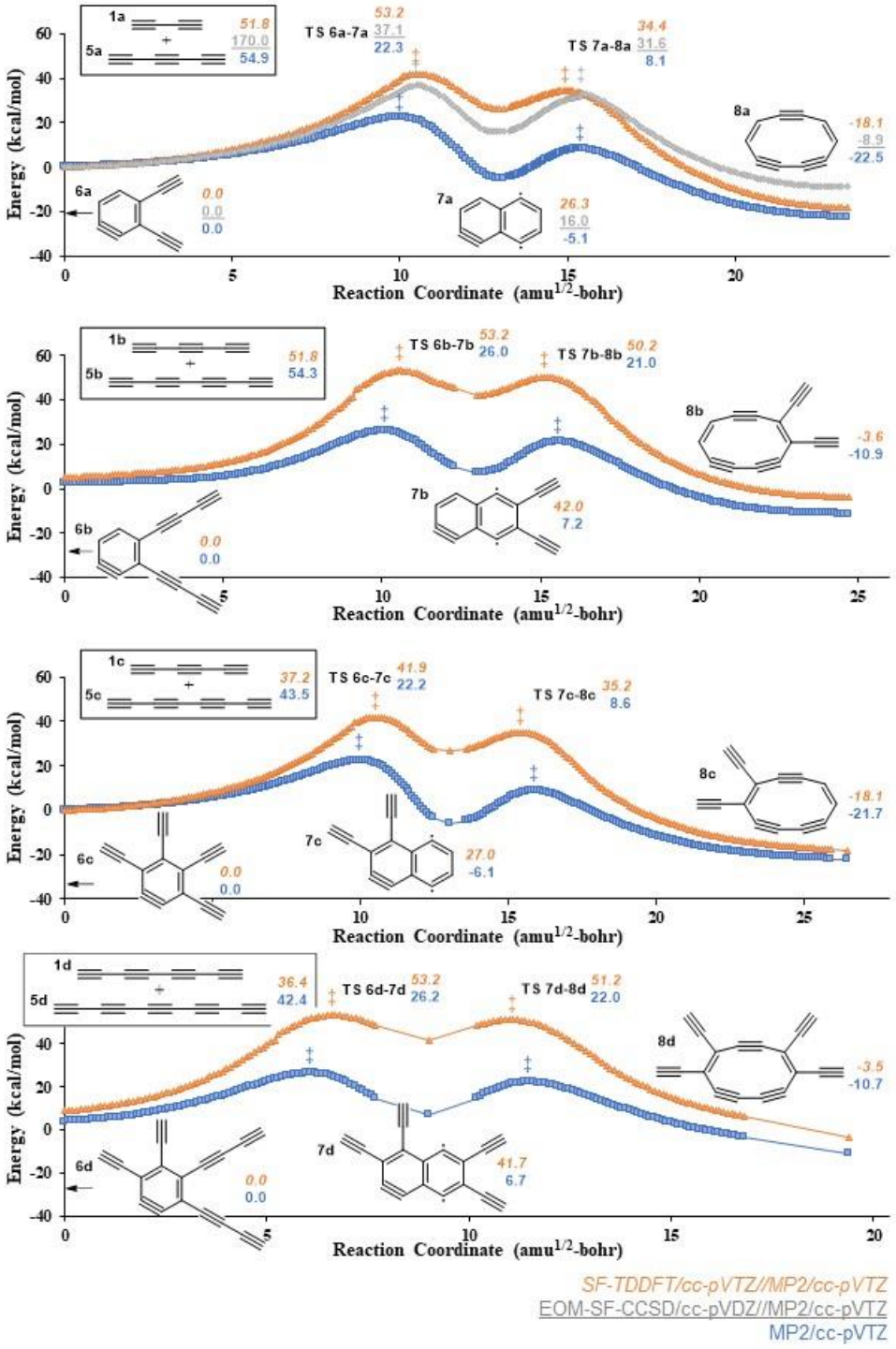

Figure 6.2. Potential energy surfaces for the Bergman cyclization and subsequent *retro*-Bergman cyclization of alkynyl-substituted *ortho*-benzynes (system **II**).

Table 6.1. Relative Energies (kcal/mol) of Stationary Points

	SF-TDDFT [a]							MP2 [d]						
I	**1** [b]	**TS1-2**	**2** [b]	**TS2-3** [c]	**3** [c]	**TS3-4** [c]	**4** [c]	**1**	**TS1-2**	**2**	**TS2-3**	**3**	**TS3-4**	**4**
a	14.9	-	0.0	44.6	26.0	26.0	-34.8	10.4	-	0.0	22.0	-22.4	-16.1	-39.0
	[242]		[0.0]	[37.1]	[11.5]	[-]	[-34.0]							
b	17.0	-	0.0	57.9	45.6	-	-20.4	12.3	-	0.0	21.1	-9.7	-4.0	-28.2
c	14.1	-	0.0	47.2	31.1	31.3	-23.6	10.4	-	0.0	23.8	-20.1	-10.6	-30.1
d	14.3	-	0.0	60.2	48.6	-	-11.1	11.4	-	0.0	23.8	-6.5	2.4	-18.2
II	**1/5** [b]	**TS1/5-6** [b]	**6** [b]	**TS6-7** [c]	**7** [c]	**TS7-8** [c]	**8** [c]	**1/5**	**TS1/5-6**	**6**	**TS6-7**	**7**	**TS7-8**	**8**
a	51.8	104.7	0.0	42.1	26.3	34.4	-18.1	54.9	83.8	0.0	22.3	-5.1	8.1	-22.5
	[170]	[119]	[0.0]	[37.1]	[16.0]	[31.6]	[-8.9]							
b	51.8	-	0.0	53.2	42.0	50.2	-3.6	54.3	-	0.0	26.0	7.2	21.0	-10.9
c	37.2	89.4	0.0	41.9	27.0	35.2	-18.1	43.5	73.8	0.0	22.2	-6.1	8.6	-21.7
d	36.4	-	0.0	53.2	41.7	51.2	-3.5	42.4	-	0.0	26.2	6.7	22.0	-10.7

[a] Energies calculated at SF-TDDFT/cc-pVTZ//MP2/cc-pVTZ; energies in brackets calculated at EOM-SF-CCSD/cc-pVDZ//MP2/cc-pVTZ.
[b] Determined using structures that were stationary points at MP2/cc-pVTZ.
[c] Determined by using the SF energies to identify stationary points based on PES curvature.
[d] Energies calculated at MP2/cc-pVTZ.

Table 6.2. Energetics (kcal/mol) of Reactions in Systems **I** and **II**

	SF-TDDFT [a]						**MP2** [d]					
	Initial Cycloaddition (**1-2** and **1**/**5-6**)		Bergman Cyclization (**2-3** and **6-7**)		*retro*-Bergman Cyclization (**3-4** and **7-8**)		Initial Cycloaddition (**1-2** and **1**/**5-6**)		Bergman Cyclization (**2-3** and **6-7**)		*retro*-Bergman Cyclization (**3-4** and **7-8**)	
	$\Delta G^{\ddagger}$ [b]	ΔG_{rxn} [b]	$\Delta G^{\ddagger}$ [c]	ΔG_{rxn} [c]	$\Delta G^{\ddagger}$ [c]	ΔG_{rxn} [c]	$\Delta G^{\ddagger}$	ΔG_{rxn}	$\Delta G^{\ddagger}$	ΔG_{rxn}	$\Delta G^{\ddagger}$	ΔG_{rxn}
Ia	-	-14.9 [-242]	44.6 [37.1]	26.0 [11.5]	0.0 [N/A]	-60.8 [-45.4]	-	-10.4	22.0	-22.4	6.3	-16.6
Ib	-	-17.0	57.9	45.6	N/A	-66.0	-	-12.3	21.1	-9.7	5.7	-18.6
Ic	-	-14.1	47.2	31.1	0.1	-54.8	-	-10.4	23.8	-20.1	9.5	-10.0
Id	-	-14.3	60.2	48.6	N/A	-59.8	-	-11.4	23.8	-6.5	8.9	-11.7
IIa	52.9 [-51]	-51.8 [-170]	42.1 [37.1]	26.3 [16.0]	8.1 [15.6]	-44.4 [-24.9]	28.9	-54.9	22.3	-5.1	13.2	-17.4
IIb	-	-51.8	53.2	42.0	8.2	-45.6	-	-54.3	26.0	7.2	13.8	-18.7
IIc	52.2	-37.2	41.9	27.0	8.2	-45.1	30.3	-43.5	22.2	-6.1	14.6	-16.2
IId	-	-36.4	53.2	41.7	9.5	-45.1	-	-42.4	26.2	6.7	15.3	-17.5

[a] Energies calculated at SF-TDDFT/cc-pVTZ//MP2/cc-pVTZ; energies in brackets calculated at EOM-SF-CCSD/cc-pVDZ//MP2/cc-pVTZ.

[b] Determined using structures that were stationary points at MP2/cc-pVTZ.

[c] Determined by using the SF energies to identify stationary points based on PES curvature.

[d] Energies calculated at MP2/cc-pVTZ.

The data depicted in Figures 6.1 and 6.2, and summarized in Tables 6.1 and 6.2, are reminiscent of those reported, previously, for the parent system **2a** → **3a** → **4a**.[21] The MP2 energies of the diradicals **3a-d** and **7a-d** are anomalously low, relative to the spin-flip calculations, presumably because of the spin contamination problems that plague the application of MP2 in open shell systems. Not only are the MP2 energies of diradicals **3** and **7** too low, the energies of the transition states leading to the diradicals are also too low. These problems affect the overall reaction thermochemistry and, in the case of diradicals **3a-d**, the interpretation concerning whether these species even exist as intermediates on the potential energy surface.

The reaction pathways detailed herein involve novel, highly unsaturated molecules, particularly that of the 1,2,5,8-tetradehydronaphthalene species **7a**–**d** that result from the Bergman cyclization of **6a**–**d** in the [4+2] pathway. While similar unsaturated naphthalene species have been previously studied computationally,[42] the current work is, to the best of our knowledge, the first to examine the 1,2,5,8 isomer **7a**–**d**. In Figures 6.1 and 6.2, zero-point vibrational energy (ZPVE) corrections were not included in the reported energies due to the unrealistically large vibrational frequencies calculated for the diradical species **3a**–**d** and **7a**–**d**. These frequencies vary from 7,000 cm^{-1} to 42,000 cm^{-1} and are displayed in Figure 6.3 and significantly distort the ZPVE correction. A similar issue was previously observed in Hartree-Fock calculations of *para*-benzyne and was attributed to orbital instability effects in *para*-benzyne caused by the near-degeneracy of electronic configurations of different symmetry among the solutions to the HF equations.[41] This instability manifests in properties of the second-order and higher, such as vibrational frequencies, but in principle has no effect on the structure or its energy.[41] Considering that a *para*-benzyne moiety is present in each of the offending species, the observed orbital instability effects are likely the root cause of the abnormal frequencies. Therefore, the computed energies in Tables 6.1 and

6.2 – describing the energetics of the stationary points of systems **I** and **II** – do not include ZPVE corrections.

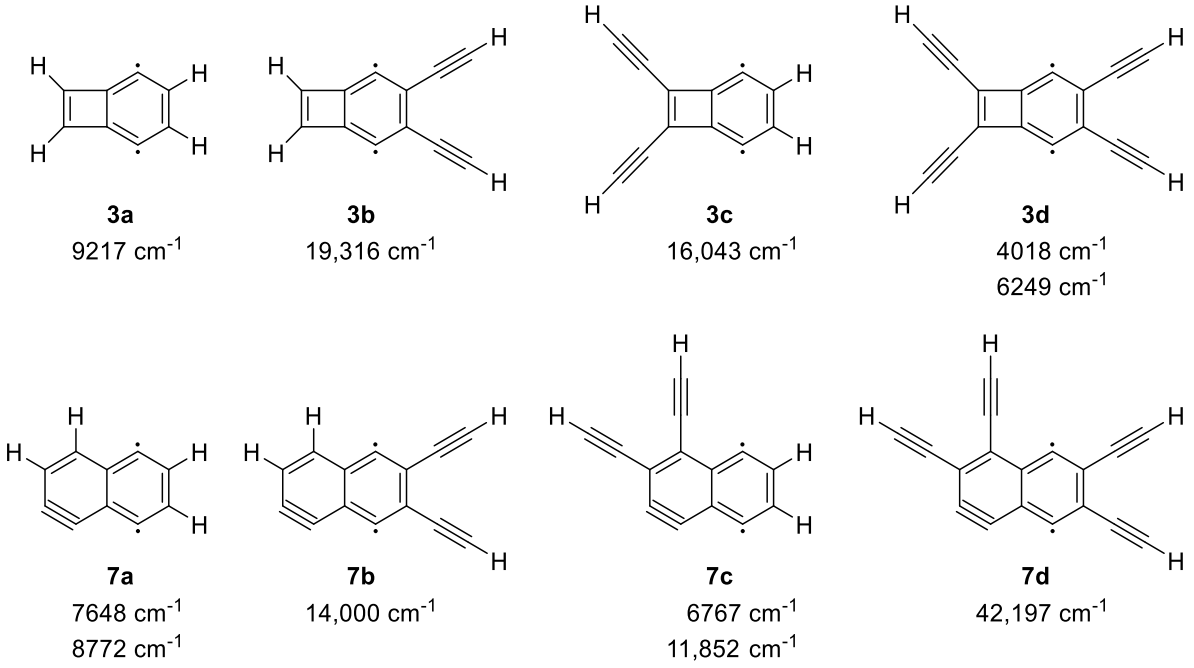

Figure 6.3. Species with unrealistically large harmonic vibrational frequencies as determined using MP2/cc-pVTZ calculations.

Initial Cycloaddition

The initial cycloadditions for the model systems studied are considerably more exothermic for the [4+2] pathways **II** than the [2+2] pathways **I** (by 30 kcal/mol), which agrees with previous studies.[25-26] Such a result is not unexpected as the [4+2] cycloaddition of **II** results in a strained, aromatic ring, whereas the [2+2] cycloaddition of **I** results in a strained, formally antiaromatic ring. The concerted transition states **TS1**/**5**–**6a** and **TS1**/**5**–**6c** that were located for the initial cycloadditions in **II** have a slightly lower activation barrier than those reported previously,[26-27, 43]

attributable to a difference in theory and basis set. There is a small variation in ΔG_{rxn} for the initial cycloaddition to form **2a**–**d**, while it appears that the inclusion of an alkynyl unit on the ring of **6** makes the initial cycloaddition producing **6c**,**d** less exothermic than **6a**,**b** (Table 6.2). The *o*-benzyne derivatives **6b** and **6c** are isomeric, and comparison of their computed energy difference (ΔG = 10.1 kcal/mol, Supporting Information) establishes that the energy difference favoring the bis(diyne) **6b** over the tetrakis(mono-yne) **6c** is thermodynamic in origin. Examination of the NBO results for **6a**, **6b**, and **6c** did not reveal any obvious explanations, so to explore the origin of this energy difference, we computed the free energy of cyclization for a variety of alkynyl substituted *ortho*-benzynes, as shown in Figure 6.4. A standard reference is required to eliminate a dependence of the energy of cyclization on different lengths of the initial polyynes. Thus, the cyclization energies have been calculated relative to acetylene (C_2H_2) and the polyyne (C_mH_2) necessary to obtain the molecular formula of the corresponding *ortho*-benzyne ($C_{m+2}H_4$). Given that the regioisomers of **6a** are all within 1 kcal/mol in energy of one another, and that the linearity of the trend in Figure 6.4 demonstrates group additivity, we conclude that the difference in cyclization energy between **6a** and **6c** is a thermodynamic consequence of the difference in bonding arrangement. The substitution pattern, or steric factors associated with the substitution pattern, do not contribute to the difference in cyclization energy.

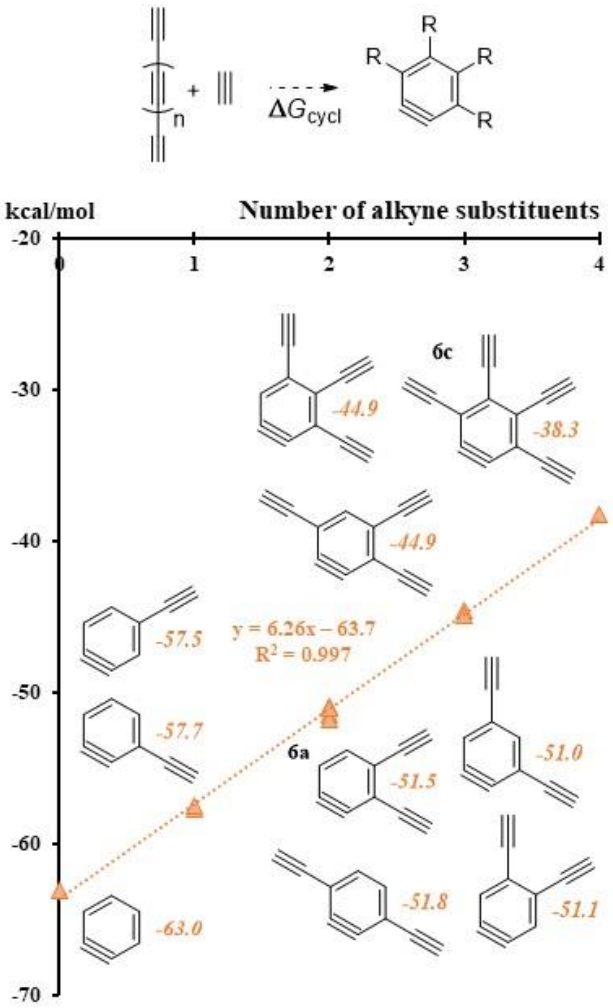

Figure 6.4. Reaction energies for formation of alkynyl-substituted *ortho*-benzynes, relative to acetylene and the appropriately mass-balanced polyyne (MP2/cc-pVTZ).

Bergman Cyclization

Following the initial cyclization event – whether it be a [2+2] (**I**) or a [4+2] (**II**) reaction – the next step in the condensation pathway is proposed to be a Bergman cycloaromatization reaction. The computed activation barriers for the cyclization step (**2** → **3** or **6** → **7**) vary significantly, depending on the computational method used (Table 6.2). This difference is directly attributable to the discrepancy in computed energy of the 1,4-didehydroarene (*p*-benzyne)

intermediates **3** and **7** using SF-TDDFT or MP2 methodology. As described earlier, we do not consider the MP2 values to be reliable for a diradical intermediate of this type, so we focus on the SF-TDDFT values in our discussion. Consideration of the SF-TDDFT values reported in Table 6.2 reveals the Bergman cyclization reaction in the [2+2] pathway (**2** → **3**) exhibits a higher barrier than that of the [4+2] pathway (**6** → **7**). This relationship is consistent with the fact that activation barriers for Bergman cyclizations have been strongly correlated to the distance separating the alkyne units,[44] with decreasing distance corresponding to decreasing activation barrier. As shown in Table 6.3, the average distances are 5.2 and 4.1 angstroms for **2** and **6**, respectively, and the average eneyne angle is 136 and 120 degrees for **2** and **6**, respectively.

Table 6.3. Geometric Parameters of Enediyne Moieties (MP2/cc-pVTZ).

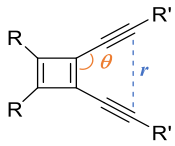

2

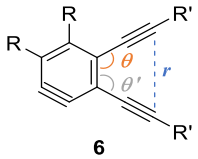

6

		r (Å)	***θ*** (degrees)	***θ′*** (degrees)
2	**a**	5.15	135.5	-
	b	5.14	135.2	-
	c	5.22	136.4	-
	d	5.23	136.3	-
	average	5.18	135.9	-
6	**a**	4.11	118.8	122.4
	b	4.03	118.2	121.8
	c	4.09	118.6	122.4
	d	4.02	118.3	121.7
	average	4.06	118.5	122.1

In the case of both pathways, **I** and **II**, substitution patterns **a** and **c** are less endothermic and, consequently, have lower activation barriers to Bergman cyclization. These cases afford cyclization products that do not bear alkyne substituents directly on the *para*-benzyne ring (**3a**, **3c**,

7a, **7c**). In contrast, the substitution patterns that place alkyne substituents directly on the *para*-benzyne ring (**3b**, **3d**, **7b**, **7d**) ring are more endothermic and have higher activation energies for Bergman cyclization. Analysis of the NBO/NRT results for **3a**, **3b**, **7a**, and **7b** (Supporting Information) suggests that the alkynyl units destabilize the *para*-benzyne portion of the ring due to a decrease in the stabilization of the radical orbitals through hyperconjugation. Specifically, the overlap of the σ_{CH} and σ_{CH}* orbitals with the radical orbitals of the *para*-benzyne moiety in **3a** and **7a** provides stabilization *via* hyperconjugation (8.6 and 9.2 kcal/mol, respectively) that is nearly twice the stabilization from the overlap of the σ_{CC} and σ_{CC}* orbitals with the radical orbitals in **3b** and **7b** (5.0 and 4.9 kcal/mol, respectively). While it is possible that steric repulsions between the *ortho*-substituted alkyne units could be responsible for the destabilization of the *para*-benzyne moiety, this is contradicted by the reaction energy trends shown in Figure 6.5, which illustrates a linear change in the reaction energy of the Bergman cyclizations of **2** and **6** as alkyne units are substituted to the ring. Thus, we conclude that any steric interactions due to adjacent alkynyl units have very little impact on the energy of the molecule, which is consistent with the narrow steric profile of alkynyl substituents.

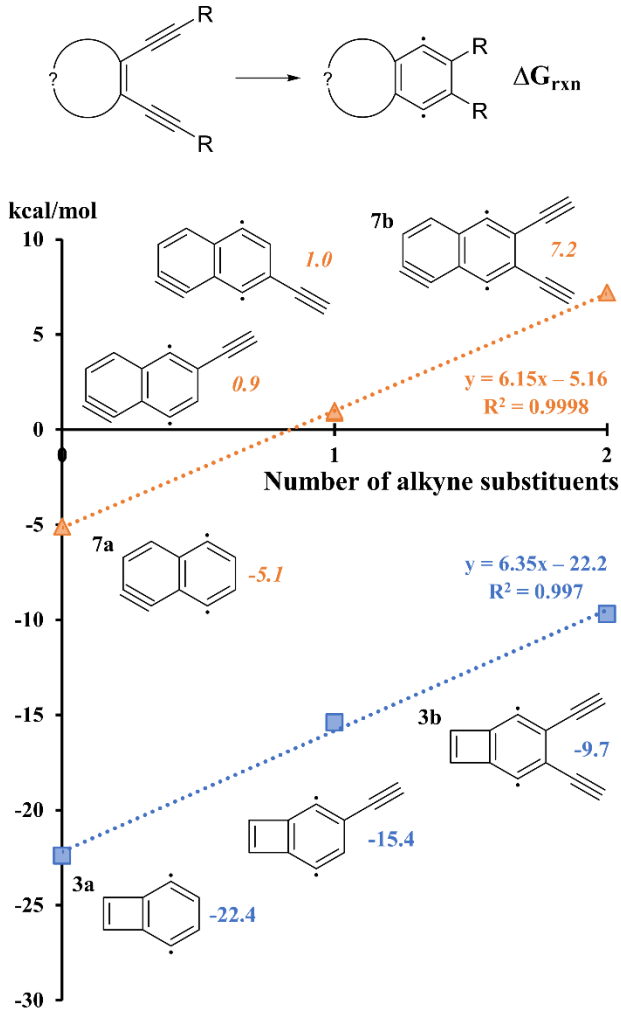

Figure 6.5. Reaction energies for the Bergman cyclizations of alkynyl substituted cyclobutadienes and *ortho*-benzynes that form *para*-benzyne moieties (MP2/cc-pVTZ).

Ring Expansion (*retro*-Bergman Cyclization)

As clearly evident from the SF-TDDFT data in Figure 6.1, the ring expansion (*retro*-Bergman cyclization) of **3a**–**d** to **4a**–**d** occurs virtually without barrier. As described previously for the overall conversion of enediyne **2a** to cyclooctadienediyne **4a**,[21] the very substantial energy change of 70-90 kcal/mol, from the top of the highest barrier (**TS2-3**) to the product (**4**), makes it difficult, topologically, for diradical **3** to exist as a minimum on the potential energy surface and

thus have a barrier to ring opening to cyclooctadienediyne **4**. This contrasts with the *retro*-Bergman cyclizations of **7a**–**d** to **8a**–**d**, which have activation barriers of 8-9 kcal/mol and corresponding energy changes (**TS6-7** to **8**) that are not as dramatically large (*ca.* 60 kcal/mol).

To gain insight into the free energy changes associated with substitution of the ring opened products **4a-d** and **8a-d**, we computed the energies of the ring-opened products relative to acetylene (C_2H_2) and the polyyne (C_mH_2) necessary to obtain the molecular formula of the corresponding product (**4** or **8**) (Figure 6.6). The linearity of the trend for cyclooctadienediyne derivatives (**4)** in Figure 6.6 demonstrates group additivity, which excludes the involvement of steric interactions among the substituents. In the case of cyclodecadienetriyne derivatives (**8**), the regioisomeric monosubstituted compounds are within 0.3 kcal/mol in energy of one another, and the linearity of the trend in Figure 6.6 demonstrates group additivity. We therefore conclude that the difference in cyclization energy **8a-d** is a thermodynamic consequence of the differences in bonding arrangement. The substitution pattern, or steric factors associated with the substitution pattern, do not contribute to the difference in cyclization energy.

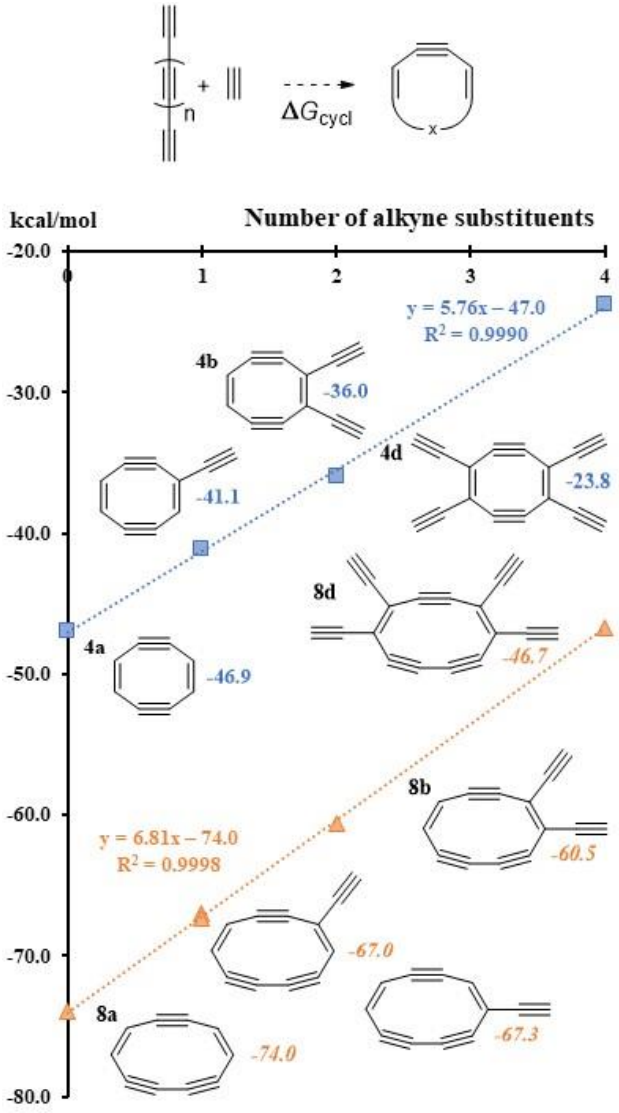

Figure 6.6. Reaction energies for the formation of the ring expansion products (*retro*-Bergman cyclization), relative to acetylene and the appropriately mass-balanced polyyne (MP2/cc-pVTZ).

Reaction Pathways I and II

Consistent with the analyses associated with Figures 6.4 and 6.6, particularly that the alkyne substituents have little interaction with other alkyne substituents, is the fact that the reaction energetics for substitution pattern **d** can be predicted empirically using the reaction energetics of cases **a**–**c**. The **d** substitution pattern has alkyne units substituted on the *para*-benzyne ring and

on the initially formed ring (cyclobutadiene in **I**, *ortho*-benzyne in **II**), while the **a** substitution pattern is the parent, unsubstituted system (R = R' = H). To understand the difference in energy between the structures in **d** compared to those in **a**, we must account for three effects: the energetic impact of replacing hydrogens with alkyne units on the *para*-benzyne ring, the energetic impact of replacing hydrogens with alkyne units on the initially formed ring, and the interaction between the substituents when both rings are substituted with alkyne units. The first effect is accounted for by the difference between **b** and **a**, while the second effect is accounted for by the difference between **c** and **a**. We could attempt to account for the third effect by considering additional substitution patterns, but it is apparent from Table 6.4 that this effect is small in magnitude since the difference between **d** and **a** can be predicted to ± 1 kcal/mol (MP2/cc-pVTZ) and ± 2 kcal/mol (SF-TDDFT/cc-pVTZ//MP2/cc-pVTZ) using only the first two effects.

Table 6.4. Empirical Demonstration of Independent Substituent Effect (kcal/mol)

			Initial Cycloaddition (**1-2** and **1**/**5-6**)		Bergman Cyclization (**2-3** and **6-7**)		*retro*-Bergman Cyclization (**3-4** and **7-8**)	
			$\Delta G^{\ddagger}$	ΔG_{rxn}	$\Delta G^{\ddagger}$	ΔG_{rxn}	$\Delta G^{\ddagger}$	ΔG_{rxn}
MP2	**I**	**d - a**	-	-11.4	23.8	-6.5	8.9	-11.7
		(b - a) + (c - a)		-12.3	22.9	-7.4	8.9	-12
		difference		*-0.9*	*-0.9*	*-0.9*	*0*	*-0.3*
	II	**d - a**	-	-42.4	26.2	6.7	15.3	-17.5
		(b - a) + (c - a)		-42.9	25.9	6.2	15.2	-17.5
		difference		*-0.5*	*-0.3*	*-0.5*	*-0.1*	*0*
SF-TDDFT	**I**	**d - a**	-	-14.3	60.2	48.6	N/A	-59.8
		(b - a) + (c - a)		-16.2	60.5	50.7	N/A	-60
		difference		*-1.9*	*0.3*	*2.1*	*N/A*	*-0.2*
	II	**d - a**	-	-36.4	53.2	41.7	9.5	-45.1
		(b - a) + (c - a)		-37.2	53	42.7	8.3	-46.3
		difference		*-0.8*	*-0.2*	*1*	*-1.2*	*-1.2*

An interesting feature of these reactions is that after the initial cycloaddition of the polyynes, the reactions being investigated involve no formal change in aromaticity: **2** is a 4-electron cyclic π system and both **3** and **4** are 8-electron cyclic π systems, thus **2**, **3**, and **4** are formally antiaromatic; **6** is a 6-electron cyclic π system and both **7** and **8** are 10-electron cyclic π systems, thus **6**, **7**, and **8** are formally aromatic. To assess the degree of aromaticity (or antiaromaticity) in the species studied, NICS values[36] have been calculated at B3LYP/6-31G(d) using the MP2/cc-pVTZ optimized structures. We report the $NICS_{zz}(1)$ in Table 6.5 using the NMR convention where positive values correspond to antiaromatic character and negative values correspond to aromatic character. The $NICS_{zz}(1)$ values, which have been shown to be effective measures of aromaticity,[45] were obtained by taking the *zz* component (the direction perpendicular to the ring) of the magnetic shielding tensor of a ghost atom placed one angstrom above and perpendicular to the center of the ring. In the case of bicyclic structures **3** and **7**, we report the $NICS_{zz}(1)$ values for the center of each of the fused rings. The results given in Table 6.5 confirm that **6**, **7**, and **8** have significant aromatic character and that **2** and **4** have significant antiaromatic character. The $NICS_{zz}(1)$ values for **3** taken at the center of the cyclobutadiene ring and the center of the *para*-benzyne ring indicate antiaromatic and aromatic character, respectively. All species show that substitution of alkyne units decreases the magnitude of the $NICS_{zz}(1)$ values *i.e.*, the values move closer to zero. The results in Table 6.5 show a qualitative agreement with previous studies involving molecules from this work (**2a** and **2c**;[46] **3a**;[36, 47] **4a**[47]) as well as in comparison to similar species (cyclobutadiene;[46, 48] *ortho*-benzyne and *para*-benzyne;[49] naphthalene[36]). We attribute the quantitative differences to the choice of computational methodology and basis sets for the structure optimizations and subsequent NICS calculations.

Table 6.5. Nucleus-Independent Chemical Shift [$NICS_{zz}(1)$] Values of Molecules in Pathways **I** and **II**.

	Center of Ring	Center of Original Ring	Center of *para*-Benzyne Ring	Center of Ring
I	**2**	**3**		**4**
a	14.8	18.8	-9.5	22.1
b	13.8	17.1	-8.9	19.9
c	11.5	15.8	-10.6	19.9
d	11.0	14.3	-9.9	18.1
II	**6**	**7**		**8**
a	-13.5	-12.4	-21.7	-13.9
b	-12.2	-11.6	-21.4	-12.6
c	-11.6	-11.0	-21.1	-12.6
d	-11.3	-10.1	-21.4	-11.4

We can now provide a general explanation of the relative stabilities and reaction energies of the [2+2] (**I**) and [4+2] (**II**) pathways for the condensation of polyynes. The initial cycloaddition to form cyclobutadiene **2** or *ortho*-benzyne **6** is governed by ring strain and degree of (anti)aromatic character. Therefore, formation of **2** (a highly strained and antiaromatic ring) is less exothermic than the formation of **6** (a partially strained and aromatic ring). Bergman cyclization of the alkyne substituents to form a *para*-benzyne ring is endothermic. The activation barriers for the Bergman cyclization of **2** and **6** are in accord with qualitative expectations based upon the distance between terminal carbons of the alkyne substituents. The subsequent ring opening reaction (*retro*-Bergman cyclization) removes the diradical character and relieves the ring strain, and thus is exothermic. The opening of the fused rings has a greater impact on the stability of the structure in **I** compared to that in **II**: the transformation from **3** to **4** has effectively no activation barrier and is more exothermic than the transformation from **6** to **7**, which does have an activation barrier. Substitution of alkyne units to the ring structures in **I** and **II** is destabilizing – most likely

due to the replacement of hydrogen atoms with more electronegative *sp*-hybridized carbon atoms of the alkyne units – but has little effect on the energetics of the *retro*-Bergman cyclization.

The Medium Rings

The current investigation draws attention to highly unsaturated cyclooctane and cyclodecane derivatives – medium ring compounds that are not commonly invoked in carbon condensation processes. Whether derivatives of cyclooctadienediyne **4** or cyclodecadienetriyne **8** might be directly involved in reaction pathways for carbon condensation, or whether they are simply reservoirs of carbon generated under harsh reaction conditions, is a topic for further investigation. It is not inconceivable that medium ring intermediates could lead toward carbon condensation (Scheme 6.5). One mode of cyclization of a cyclooctane derivative may generate a bicyclo[3.3.0]octane structure, which consists of fused 5-membered rings. Although fullerenes do not contain fused 5-membered rings (the 'isolated pentagon rule'),[20, 50-51] the Stone-Wales rearrangement or other rearrangement reactions allow 5-membered rings to migrate in a sheet of carbon.[51-52] In the current study, the cyclodecane skeleton was derived from a dehydronaphthalene precursor (Scheme 6.4). Depending on the nature of substituents and substitution pattern, a cyclodecane derivative may afford the possibility for structural rearrangement and to permute the substituents on a dehydronaphthalene skeleton. The structures depicted in Scheme 6.5 are representative of carbon connectivity and not representative of degree of hydrogenation, nature of substituents, or details of reaction mechanisms (thermal, radical catalyzed, *etc*.). Experimental and computational investigations are ongoing.

Scheme 6.5. Reaction Pathways Involving Collapse of Medium Rings.

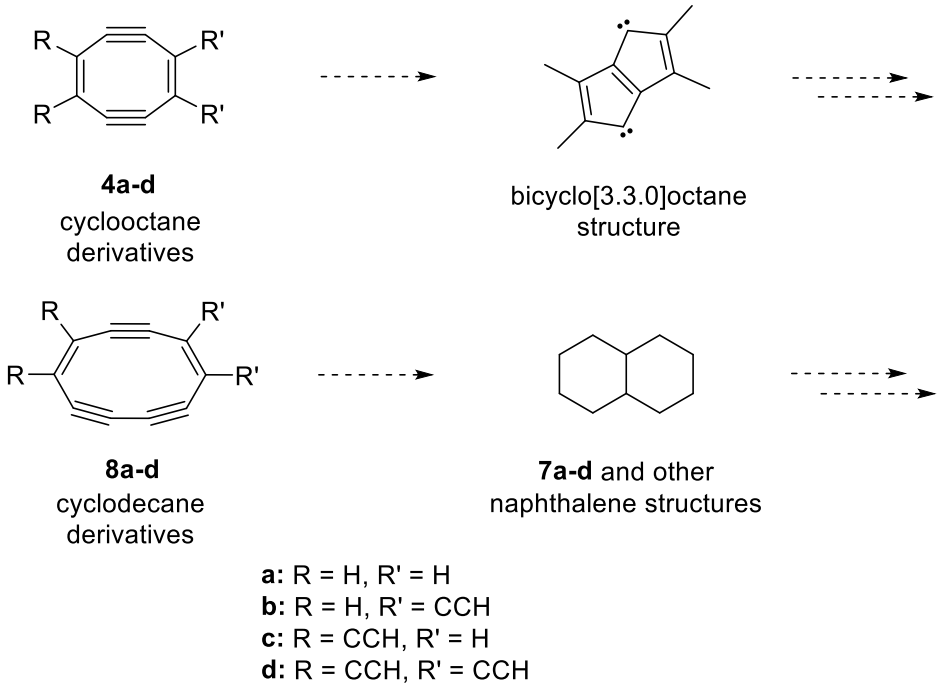

CONCLUSIONS

On consideration of the energies calculated by SF-TDDFT, the *para*-benzyne intermediate in **I** – being fused with a cyclobutadiene ring – has effectively no barrier to undergoing a ring expansion, representing an unproductive pathway within the *ring coalescence and annealing* model. On the other hand, the SF-TDDFT calculations on the *para*-benzyne intermediate in **II** – being fused with an *ortho*-benzyne ring – predict an activation barrier of 8–10 kcal/mol for undergoing a similar ring expansion. The qualitative agreement of this activation barrier as calculated by EOM-SF-CCSD and SF-TDDFT for the parent system of the two pathways lends credence to the qualitative accuracy of the SF-TDDFT activation barriers for the alkynyl substituted species. Further, given the little variation in the activation barriers across the substitution patterns, we may tentatively extend the conclusion to include the *para*-benzyne

intermediates formed by increasingly larger polyynes, as would be found in the *ring coalescence and annealing* model.

As to the origins of the activation barriers (or lack thereof) for the ring expansion of the *para*-benzyne species, we previously proposed[21] that the activation barrier for the *retro*-Bergman cyclization of **3a** to **4a** is small due to the large exothermicity of the reaction of **2a** to **4a**. This argument is undermined, however, by the corresponding SF-TDDFT energies for the substituted versions of these reactions. As more alkyne units are substituted into the system, the exothermicity of the transformation from **2** to **4** clearly decreases; yet there is no significant effect on the activation barrier for the ring expansion of **3** to **4**. Furthermore, the reactions for several of the substitution patterns in **II** have similar exothermicities for the transformation of **6** to **8** yet have significant activation barriers. The activation barriers for the ring expansion do not seem to be strongly correlated to the overall exothermicity of the transformation from **2** to **4** and **6** to **8**. An alternative or concurrent explanation may be the exothermicity of the ring expansion itself: the ring expansion in **I** is exothermic by about 60 kcal/mol and has effectively no activation barrier, while the ring expansion in **II** is exothermic by about 45 kcal/mol and has an activation barrier of around 10 kcal/mol. The larger exothermicity for the *retro*-Bergman cyclization in **I** is likely due to the relief of ring strain from expansion of the cyclobutadiene ring, as compared to that which occurs for the opening of *ortho*-benzyne ring in **II**.

The multi-radical nature of the *para*-benzyne intermediate species complicates the characterization of the reactions of both pathways and may require more advanced treatments to be accurately modeled. The orbital instabilities known to plague calculations of *para*-benzyne may be exacerbated by the incorporation of the cyclobutadiene ring or the *ortho*-benzyne ring, both of which can be considered to have some radical character. The numerous variations in the

triplet reference calculations required by the spin-flip methodologies could indicate that a higher spin reference is necessary for the treatment of these species, though it could also indicate that the underlying single-reference MP2 optimized structures are an insufficient foundation upon which to properly treat the multi-reference problem.

ACKNOWLEDGEMENTS

We thank the late Professor Hans J. Reich for providing the initial inspiration to examine the implications of the [4+2] cycloaddition. We also thank Andrew J. Wiederhold and Desiree M. Bates for conducting preliminary calculations. We gratefully acknowledge the National Science Foundation for support of this project (CHE-1664912 and CHE-1954270).

REFERENCES

1. Hou, L.; Cui, X.; Guan, B.; Wang, S.; Li, R.; Liu, Y.; Zhu, D.; Zheng, J., Synthesis of a monolayer fullerene network. *Nature* **2022,** *606,* 507.

2. Chen, Z.; Narita, A.; Müllen, K., Graphene Nanoribbons: On-Surface Synthesis and Integration into Electronic Devices *Adv. Mater.* **2020,** *32*, 2001893.

3. Fan, Q.; Yan, L.; Tripp, M. W.; Krejčí, O.; Dimosthenous, S.; Kachel, S. R.; Chen, M.; Foster, A. S.; Koert, U.; Liljeroth, P.; Gottfried, J. M., Biphenylene network: A nonbenzenoid carbon allotrope. *Science* **2021,** *372*, 852–856.

4. Diederich, F.; Rubin, Y.; Knobler, C. B.; Whetten, R. L.; Schriver, K. E.; Houk, K. N.; Li, Y., All-Carbon Molecules: Evidence for the Generation of Cyclo[18]carbon from a Stable Organic Precursor. *Science* **1989,** *245*, 1088-1090.

5. Anderson, H. L.; Patrick, C. W.; Scriven, L. M.; Woltering, S. L., A Short History of Cyclocarbons *Bull. Chem. Soc. Jpn.* **2021,** *94*, 798–811.

6. McElvany, S. W.; Ross, M. M.; Goroff, N. S.; Diederich, F., Cyclocarbon Coalescence: Mechanisms for Tailor-Made Fullerene Formation. *Science* **1993,** *259* (5101), 1594-1596.

7. Kaiser, K.; Scriven, L. M.; Schulz, F.; Gawel, P.; Gross, L.; Anderson, H. L., An sp-hybridized molecular carbon allotrope, cyclo[18]carbon. *Science* **2019,** *365*, 1299–1301; see Erratum 1213 March 2020.

8. Chuvilin, A.; Kaiser, U.; Bichoutskaia, E.; Besley, N. A.; Khlobystov, A. N., Direct transformation of graphene to fullerene. *Nature Chemistry* **2010,** *2* (6), 450-453.

9. Thakur, A. K.; Muralidharan, K.; Zega, T. J.; Ziurys, L. M., A nanometric window on fullerene formation in the interstellar medium: Insights from molecular dynamics studies. *J. Chem. Phys.* **2022,** *156*, 154704.

10. Pietrucci, F.; Andreoni, W., Fate of a Graphene Flake: A New Route toward Fullerenes Disclosed with Ab Initio Simulations. *J. Chem. Theory Comput.* **2014,** *10* (3), 913.

11. Neng, W.; Shuang-ying, L.; Jun, X.; Matteo, M.; Yi-long, Z.; Shu, W.; Li-tao, S.; Qing-an, H., Fullerene growth from encapsulated graphene flakes. *Nanoscale* **2014,** *6* (19), 11213-11218.

12. Irle, S.; Zheng, G.; Wang, Z.; Morokuma, K., The C_{60} Formation Puzzle "Solved": QM/MD Simulations Reveal the Shrinking Hot Giant Road of the Dynamic Fullerene Self-Assembly Mechanism. *J. Phys. Chem. B* **2006,** *110* (30), 14531-14545.

13. Huang, J. Y.; Ding, F.; Jiao, K.; Yakobson, B. I., Real Time Microscopy, Kinetics, and Mechanism of Giant Fullerene Evaporation. *Phys. Rev. Lett.* **2007,** *99* (17), 175503.

14. Heath, J. R., Synthesis of C_{60} from Small Carbon Clusters: A Model Based on Experiment and Theory. In *Fullerenes: Synthesis, Properties, and Chemistry of Large Carbon Clusters*, Hammond, G. S.; Kuck, V. J., Eds. American Chemical Society: Washington, DC, 1992; Vol. 481, pp 1-23.

15. Smalley, R. E., Self-assembly of the fullerenes. *Acc. Chem. Res.* **1992,** *25* (3), 98-105.

16. Dunk, P. W.; Kaiser, N. K.; Hendrickson, C. L.; Quinn, J. P.; Ewels, C. P.; Nakanishi, Y.; Sasaki, Y.; Shinohara, H.; Marshall, A. G.; Kroto, H. W., Closed network growth of fullerenes. *Nat Commun* **2012,** *3* (1), 855.

17. Dunk, P. W.; Mulet-Gas, M.; Rodriguez-Fortea, A.; Poblet, J. M.; Marshall, A. G.; Kroto, H. W., Recent advances in fullerene science (Invited). *AIP Conference Proceedings* **2014,** *1628* (1), 862-869.

18. Rubin, Y.; Kahr, M.; Knobler, C. B.; Diederich, F.; Wilkins, C. L., The higher oxides of carbon $C_{8n}O_{2n}$ (n = 3-5): synthesis, characterization, and x-ray crystal structure. Formation of cyclo[n]carbon ions C_n^+ (n = 18, 24), C_n^- (n = 18, 24, 30), and higher carbon ions including C_{60}^+ in laser desorption Fourier transform mass spectrometric experiments. *J. Am. Chem. Soc.* **1991,** *113* (2), 495-500.

19. Hunter, J. M.; Fye, J. L.; Roskamp, E. J.; Jarrold, M. F., Annealing Carbon Cluster Ions: A Mechanism for Fullerene Synthesis. *J. Phys. Chem.* **1994,** *98* (7), 1810-1818.

20. Goroff, N. S., Mechanism of fullerene formation. *Acc. Chem. Res.* **1996,** *29* (2), 77-83.

21. Esselman, B. J.; Emmert, F. L.; Wiederhold, A. J.; Thompson, S. J.; Slipchenko, L. V.; McMahon, R. J., Thermal Isomerizations of Diethynyl Cyclobutadienes and Implications for Fullerene Formation. *J. Org. Chem.* **2015,** *80* (23), 11863-11868.

22. Hoye, T. R.; Baire, B.; Niu, D.; Willoughby, P. H.; Woods, B. P., The hexadehydro-Diels–Alder reaction. *Nature* **2012,** *490* (7419), 208-212.

23. Holden, C.; Greaney, M. F., The Hexadehydro-Diels–Alder Reaction: A New Chapter in Aryne Chemistry. *Angew. Chem. Int. Ed.* **2014,** *53* (23), 5746-5749.

24. Cremer, D.; Kraka, E.; Joo, H.; Stearns, J. A.; Zwier, T. S., Exploration of the potential energy surface of C_4H_4 for rearrangement and decomposition reactions of vinylacetylene: A computational study. Part I. *PCCP* **2006,** *8* (45), 5304-5316.

25. Cahill, K. J.; Ajaz, A.; Johnson, R. P., New Thermal Routes to *ortho*-Benzyne. *Aust. J. Chem.* **2010,** *63* (7), 1007-1012.

26. Ajaz, A.; Bradley, A. Z.; Burrell, R. C.; Li, W. H. H.; Daoust, K. J.; Bovee, L. B.; DiRico, K. J.; Johnson, R. P., Concerted vs Stepwise Mechanisms in Dehydro-Diels–Alder Reactions. *J. Org. Chem.* **2011,** *76* (22), 9320-9328.

27. Ghigo, G.; Maranzana, A.; Tonachini, G., *o*-Benzyne fragmentation and isomerization pathways: a CASPT2 study. *PCCP* **2014,** *16* (43), 23944-23951.

28. Liang, Y.; Hong, X.; Yu, P.; Houk, K. N., Why Alkynyl Substituents Dramatically Accelerate Hexadehydro-Diels–Alder (HDDA) Reactions: Stepwise Mechanisms of HDDA Cycloadditions. *Org. Lett.* **2014,** *16* (21), 5702-5705.

29. Jones, R. R.; Bergman, R. G., *p*-Benzyne. Generation as an intermediate in a thermal isomerization reaction and trapping evidence for the 1,4-benzenediyl structure. *J. Am. Chem. Soc.* **1972,** *94* (2), 660-661.

30. Shao, Y.; Head-Gordon, M.; Krylov, A. I., The spin–flip approach within time-dependent density functional theory: Theory and applications to diradicals. *J. Chem. Phys.* **2003,** *118* (11), 4807-4818.

31. Bernard, Y. A.; Shao, Y.; Krylov, A. I., General formulation of spin-flip time-dependent density functional theory using non-collinear kernels: Theory, implementation, and benchmarks. *J. Chem. Phys.* **2012,** *136* (20), 204103.

32. Møller, C.; Plesset, M. S., Note on an Approximation Treatment for Many-Electron Systems. *Physical Review* **1934,** *46* (7), 618-622.

33. Dunning, T. H., Gaussian basis sets for use in correlated molecular calculations .1. The atoms boron through neon and hydrogen. *J. Chem. Phys.* **1989,** *90* (2), 1007-1023.

34. Frisch, M. J.; Trucks, G. W.; Schlegel, H. B.; Scuseria, G. E.; Robb, M. A.; Cheeseman, J. R.; Scalmani, G.; Barone, V.; Mennucci, B.; Petersson, G. A.; Nakatsuji, H.; Caricato, M.; Li, X.; Hratchian, H. P.; Izmaylov, A. F.; Bloino, J.; Zheng, G.; Sonnenberg, J. L.; Hada, M.; Ehara, M.; Toyota, K.; Fukuda, R.; Hasegawa, J.; Ishida, M.; Nakajima, T.; Honda, Y.; Kitao, O.; Nakai, H.; Vreven, T.; Montgomery Jr., J. A.; Peralta, J. E.; Ogliaro, F.; Bearpark, M. J.; Heyd, J.; Brothers, E. N.; Kudin, K. N.; Staroverov, V. N.; Kobayashi, R.; Normand, J.; Raghavachari, K.; Rendell, A. P.; Burant, J. C.; Iyengar, S. S.; Tomasi, J.; Cossi, M.; Rega, N.; Millam, N. J.; Klene, M.; Knox, J. E.; Cross, J. B.; Bakken, V.; Adamo, C.; Jaramillo, J.; Gomperts, R.; Stratmann, R. E.; Yazyev, O.; Austin, A. J.; Cammi, R.; Pomelli, C.; Ochterski, J. W.; Martin, R. L.; Morokuma, K.; Zakrzewski, V. G.; Voth, G. A.; Salvador, P.; Dannenberg, J. J.; Dapprich, S.; Daniels, A. D.; Farkas, Ö.; Foresman, J. B.; Ortiz, J. V.; Cioslowski, J.; Fox, D. J. *Gaussian 09, Revision D.01*, Gaussian, Inc.: Wallingford, CT, USA, 2009.

35. Shao, Y.; Gan, Z.; Epifanovsky, E.; Gilbert, A. T. B.; Wormit, M.; Kussmann, J.; Lange, A. W.; Behn, A.; Deng, J.; Feng, X.; Ghosh, D.; Goldey, M.; Horn, P. R.; Jacobson, L. D.; Kaliman, I.; Khaliullin, R. Z.; Kuś, T.; Landau, A.; Liu, J.; Proynov, E. I.; Rhee, Y. M.; Richard, R. M.; Rohrdanz, M. A.; Steele, R. P.; Sundstrom, E. J.; Woodcock, H. L.; Zimmerman, P. M.; Zuev, D.; Albrecht, B.; Alguire, E.; Austin, B.; Beran, G. J. O.; Bernard, Y. A.; Berquist, E.; Brandhorst, K.; Bravaya, K. B.; Brown, S. T.; Casanova, D.; Chang, C.-M.; Chen, Y.; Chien, S. H.; Closser, K. D.; Crittenden, D. L.; Diedenhofen, M.; DiStasio, R. A.; Do, H.; Dutoi, A. D.; Edgar, R. G.; Fatehi, S.; Fusti-Molnar, L.; Ghysels, A.; Golubeva-Zadorozhnaya, A.; Gomes, J.; Hanson-Heine, M. W. D.; Harbach, P. H. P.; Hauser, A. W.; Hohenstein, E. G.; Holden, Z. C.; Jagau, T.-C.; Ji, H.; Kaduk, B.; Khistyaev, K.; Kim, J.; Kim, J.; King, R. A.; Klunzinger, P.; Kosenkov, D.; Kowalczyk, T.; Krauter, C. M.; Lao, K. U.; Laurent, A. D.; Lawler, K. V.; Levchenko, S. V.; Lin, C. Y.; Liu, F.; Livshits, E.; Lochan, R. C.; Luenser, A.; Manohar, P.; Manzer, S. F.; Mao, S.-P.; Mardirossian, N.; Marenich, A. V.; Maurer, S. A.; Mayhall, N. J.; Neuscamman, E.; Oana, C. M.; Olivares-Amaya, R.; O'Neill, D. P.; Parkhill, J. A.; Perrine, T. M.; Peverati, R.; Prociuk, A.; Rehn, D. R.; Rosta, E.; Russ, N. J.; Sharada, S. M.; Sharma, S.; Small, D. W.; Sodt, A.; Stein, T.; Stück, D.; Su, Y.-C.; Thom, A. J. W.; Tsuchimochi, T.; Vanovschi, V.; Vogt, L.; Vydrov, O.; Wang, T.; Watson, M. A.; Wenzel, J.; White, A.; Williams, C. F.; Yang, J.; Yeganeh, S.; Yost, S. R.; You, Z.-Q.; Zhang, I. Y.; Zhang, X.; Zhao, Y.; Brooks, B. R.; Chan, G. K. L.; Chipman, D. M.; Cramer, C. J.; Goddard, W. A.; Gordon, M. S.; Hehre, W. J.; Klamt, A.; Schaefer, H. F.; Schmidt, M. W.; Sherrill, C. D.; Truhlar, D. G.; Warshel, A.; Xu, X.; Aspuru-Guzik, A.; Baer, R.; Bell, A. T.; Besley, N. A.; Chai, J.-D.; Dreuw, A.; Dunietz, B. D.; Furlani, T. R.; Gwaltney, S. R.; Hsu, C.-P.; Jung, Y.;

Kong, J.; Lambrecht, D. S.; Liang, W.; Ochsenfeld, C.; Rassolov, V. A.; Slipchenko, L. V.; Subotnik, J. E.; Van Voorhis, T.; Herbert, J. M.; Krylov, A. I.; Gill, P. M. W.; Head-Gordon, M., Advances in molecular quantum chemistry contained in the Q-Chem 4 program package. *Mol. Phys.* **2015,** *113* (2), 184-215.

36. Chen, Z.; Wannere, C. S.; Corminboeuf, C.; Puchta, R.; Schleyer, P. v. R., Nucleus-Independent Chemical Shifts (NICS) as an Aromaticity Criterion. *Chem. Rev.* **2005,** *105* (10), 3842-3888.

37. Glendening, E. D.; Badenhoop, J. K.; Reed, A. E.; Carpenter, J. E.; Bohmann, J. A.; Morales, C. M.; Landis, C. R.; Weinhold, F. *NBO 6.0*, Theoretical Chemistry Institute, University of Wisconsin: Madison, WI, 2013.

38. Lee, C. T.; Yang, W. T.; Parr, R. G., Development of the Colle-Salvetti correlation energy formula into a functional of the electron density. *Phys. Rev. B* **1988,** *37* (2), 785-789.

39. Becke, A. D., Density-functional thermochemistry .3. The role of exact exchange. *J. Chem. Phys.* **1993,** *98* (7), 5648-5652.

40. Hehre, W. J.; Ditchfield, R.; Pople, J. A., Self-Consistent Molecular Orbital Methods. XII. Further Extensions of Gaussian-Type Basis Sets for Use in Molecular Orbital Studies of Organic Molecules. *J. Chem. Phys.* **1972,** *56* (5), 2257-2261.

41. Crawford, T. D.; Kraka, E.; Stanton, J. F.; Cremer, D., Problematic *p*-benzyne: Orbital instabilities, biradical character, and broken symmetry. *J. Chem. Phys.* **2001,** *114* (24), 10638-10650.

42. Pauzat, F.; Talbi, D.; Ellinger, Y., UIR bands: Computational experiments on the IR spectra of naphthalene derivatives as models for PAHs. *Astron. Astrophys.* **1995,** *293* (1), 263-277.

43. Zhang, X.; Maccarone, A. T.; Nimlos, M. R.; Kato, S.; Bierbaum, V. M.; Ellison, G. B.; Ruscic, B.; Simmonett, A. C.; Allen, W. D.; Schaefer, H. F., Unimolecular thermal fragmentation of ortho-benzyne. *J. Chem. Phys.* **2007,** *126* (4), 044312, 044312.

44. Mohamed, R. K.; Peterson, P. W.; Alabugin, I. V., Concerted Reactions That Produce Diradicals and Zwitterions: Electronic, Steric, Conformational, and Kinetic Control of Cycloaromatization Processes. *Chem. Rev.* **2013,** *113* (9), 7089-7129.

45. Fallah-Bagher-Shaidaei, H.; Wannere, C. S.; Corminboeuf, C.; Puchta, R.; Schleyer, P. v. R., Which NICS Aromaticity Index for Planar π Rings Is Best? *Org. Lett.* **2006,** *8* (5), 863-866.

46. Esselman, B. J.; McMahon, R. J., Effects of ethynyl substitution on cyclobutadiene. *J. Phys. Chem. A* **2012,** *116* (1), 483.

47. Tsipis, A. C., Efficiency of the $NICS_{zz}$-scan curves to probe the antiaromaticity of organic and inorganic rings/cages. *PCCP* **2009,** *11* (37), 8244-8261.

48. Schleyer, P. v. R.; Manoharan, M.; Wang, Z.-X.; Kiran, B.; Jiao, H.; Puchta, R.; van Eikema Hommes, N. J. R., Dissected Nucleus-Independent Chemical Shift Analysis of π-Aromaticity and Antiaromaticity. *Org. Lett.* **2001,** *3* (16), 2465-2468.

49. De Proft, F.; von Ragué Schleyer, P.; van Lenthe, J. H.; Stahl, F.; Geerlings, P., Magnetic Properties and Aromaticity of *o*-, *m*-, and *p*-Benzyne. *Chem. Eur. J.* **2002,** *8* (15), 3402-3410.

50. Mintmire, J. W., Fullerene Formation and Annealing. *Science* **1996,** *272*, 45-46.

51. Mitchell, I.; Qiu, L.; Lamb, L. D.; Ding, F., High Temperature Accelerated Stone−Wales Transformation and the Threshold Temperature of IPR-C_{60} Formation. *J. Phys. Chem. A* **2021,** *125*, 4548−4557.

52. Irace, E. E.; Brayfindley, E.; Vinnacombe, G. A.; Castro, C.; Karney, W. L., Stone−Wales Rearrangements in Hydrocarbons: From Planar to Bowl-Shaped Substrates. *J. Org. Chem.* **2015,** *80*, 11718-11725.

SUPPORTING INFORMATION

Table of Contents

Select NBO Orbitals and Hyperconjugation Analysis

B3LYP/6-31G(d) Natural Bond Orbital (NBO) calculations were conducted on the MP2/cc-pVTZ optimized structures using the NBO6 program as implemented in Gaussian 09. Selective analyses consisted of identifying orbital interactions between the *para*-benzyne radical orbitals and *para*-benzyne substituent orbitals (C−H or C−C≡C). The orbitals involved in these interactions are described by an image, the electron occupation, and the coefficients and hybridizations of their component Natural Hybrid Orbitals (NHO). The interactions are reported in the “Second Order Perturbation Analysis” table along with the energy of stabilization.

Format:

Molecule identifier

Orbitals

[orbital image]	*[orbital image]*
(Occupancy) Bond orbital	*(Occupancy) Bond orbital*
Coefficients NHO1 / Hybridization	*Coefficients NHO1 / Hybridization*
Coefficients NHO2 / Hybridization	*Coefficients NHO2 / Hybridization*

Second Order Perturbation Analysis

Donor Orbital	Acceptor Orbital	E(2) (kcal/mol)
Bond orbital	*Bond orbital*	*energy value*

3a

Orbitals

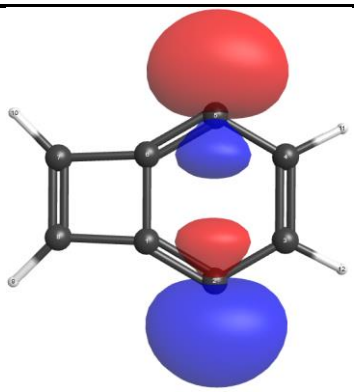	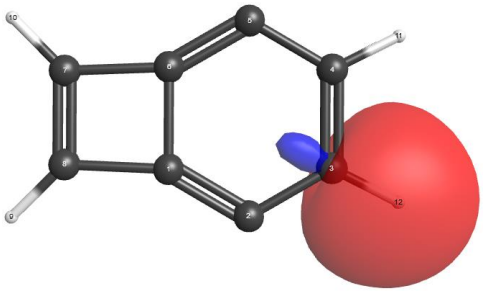
6. (1.81863) BD*(1) C 2 - C 5	9. (1.96666) BD (1) C 3 - H 12
(50.00%) 0.7071* C 2 s(9.43%)p 9.60(90.53%)d 0.00(0.04%)	(63.10%) 0.7944* C 3 s(29.06%)p 2.44(70.88%)d 0.00(0.05%)
(50.00%) -0.7071* C 5 s(9.43%)p 9.60(90.53%)d 0.00(0.04%)	(36.90%) 0.6074* H 12 s(100.00%)
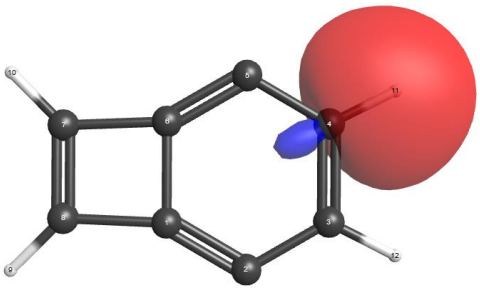	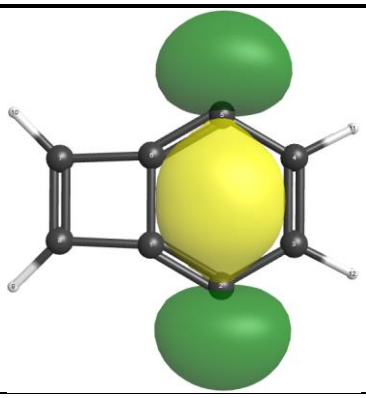
11. (1.96666) BD (1) C 4 - H 11	116. (0.36688) BD (1) C 2 - C 5
(63.10%) 0.7944* C 4 s(29.06%)p 2.44(70.88%)d 0.00(0.05%)	(50.00%) 0.7071* C 2 s(9.43%)p 9.60(90.53%)d 0.00(0.04%)
(36.90%) 0.6074* H 11 s(100.00%)	(50.00%) 0.7071* C 5 s(9.43%)p 9.60(90.53%)d 0.00(0.04%)
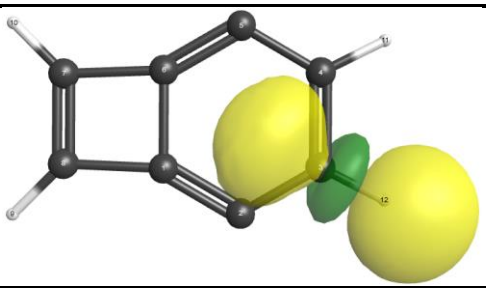	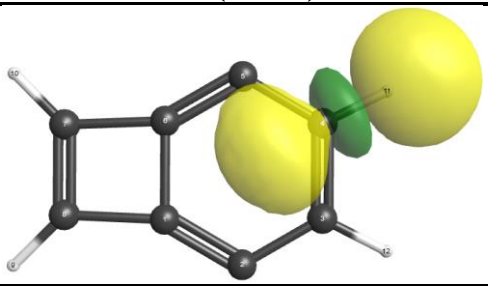
119. (0.01247) BD*(1) C 3 - H 12	121. (0.01247) BD*(1) C 4 - H 11
(36.90%) 0.6074* C 3 s(29.06%)p 2.44(70.88%)d 0.00(0.05%)	(36.90%) 0.6074* C 4 s(29.06%)p 2.44(70.88%)d 0.00(0.05%)
(63.10%) -0.7944* H 12 s(100.00%)	(63.10%) -0.7944* H 11 s(100.00%)

Second Order Perturbation Analysis

Donor Orbital	Acceptor Orbital	E(2) (kcal/mol)
6. BD*(1) C 2 - C 5	119. BD*(1) C 3 - H 12	2.21
6. BD*(1) C 2 - C 5	121. BD*(1) C 4 - H 11	2.21
9. BD (1) C 3 - H 12	116. BD (1) C 2 - C 5	1.16
11. BD (1) C 4 - H 11	116. BD (1) C 2 - C 5	1.16
116. BD (1) C 2 - C 5	119. BD*(1) C 3 - H 12	0.94
116. BD (1) C 2 - C 5	121. BD*(1) C 4 - H 11	0.94

3b

Orbitals

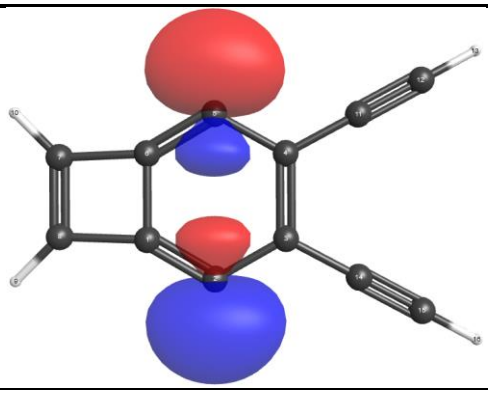	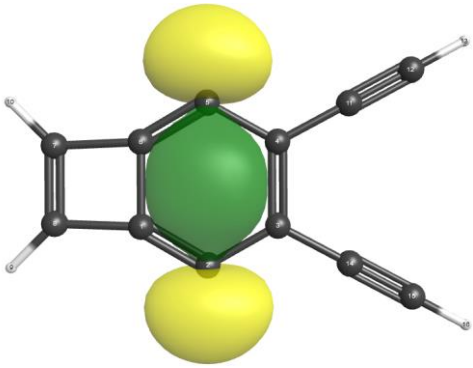
6. (1.80249) BD*(1) C 2 - C 5	168. (0.35483) BD (1) C 2 - C 5
(50.00%) 0.7071* C 2 s(9.69%)p 9.31(90.27%)d 0.00(0.04%)	(50.00%) 0.7071* C 2 s(9.69%)p 9.31(90.27%)d 0.00(0.04%)
(50.00%) -0.7071* C 5 s(9.69%)p 9.31(90.27%)d 0.00(0.04%)	(50.00%) 0.7071* C 5 s(9.69%)p 9.31(90.27%)d 0.00(0.04%)
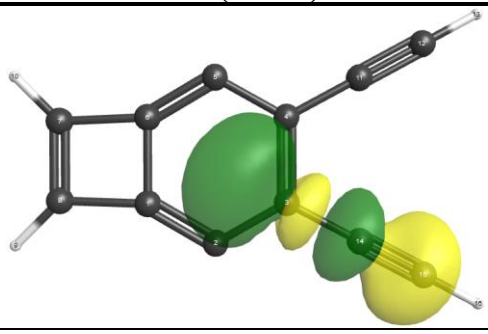	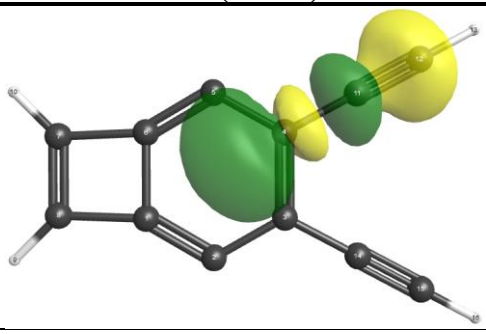
171. (0.02557) BD*(1) C 3 - C 14	173. (0.02557) BD*(1) C 4 - C 11
(48.56%) 0.6968* C 3 s(32.04%)p 2.12(67.92%)d 0.00(0.04%)	(48.56%) 0.6968* C 4 s(32.04%)p 2.12(67.92%)d 0.00(0.04%)
(51.44%) -0.7172* C 14 s(47.16%)p 1.12(52.80%)d 0.00(0.04%)	(51.44%) -0.7172* C 11 s(47.16%)p 1.12(52.80%)d 0.00(0.04%)

Second Order Perturbation Analysis

Donor Orbital	Acceptor Orbital	E(2) (kcal/mol)
6. BD*(1) C 2 - C 5	171. BD*(1) C 3 - C 14	1.71
6. BD*(1) C 2 - C 5	173. BD*(1) C 4 - C 11	1.71
168. BD (1) C 2 - C 5	171. BD*(1) C 3 - C 14	0.78
168. BD (1) C 2 - C 5	173. BD*(1) C 4 - C 11	0.78

7a

Orbitals

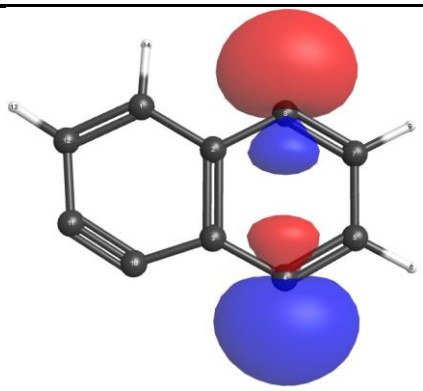	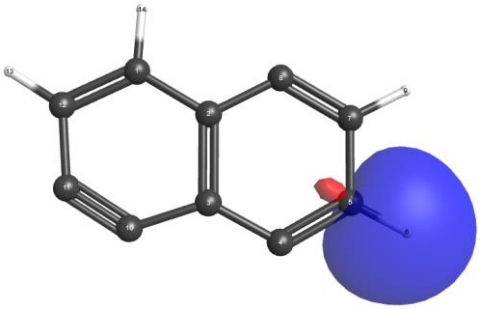
12. (1.83192) BD*(1) C 4 - C 8	13. (1.96015) BD (1) C 5 - H 6
(50.01%) 0.7072* C 4 s(10.82%)p 8.24(89.14%)d 0.00(0.03%)	(63.55%) 0.7972* C 5 s(28.95%)p 2.45(71.01%)d 0.00(0.05%)
(49.99%) -0.7070* C 8 s(10.86%)p 8.21(89.11%)d 0.00(0.03%)	(36.45%) 0.6037* H 6 s(100.00%)
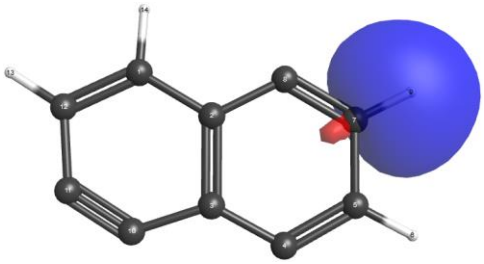	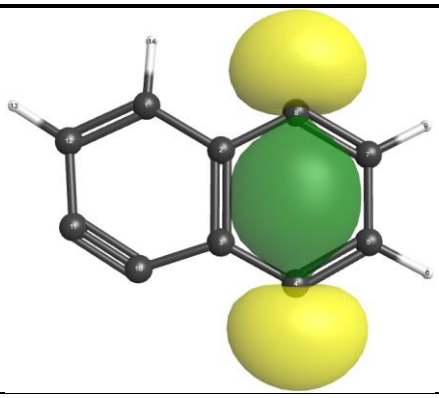
17. (1.96232) BD (1) C 7 - H 9	148. (0.32613) BD (1) C 4 - C 8
(63.47%) 0.7967* C 7 s(28.84%)p 2.47(71.11%)d 0.00(0.05%)	(49.99%) 0.7070* C 4 s(10.82%)p 8.24(89.14%)d 0.00(0.03%)
(36.53%) 0.6044* H 9 s(100.00%)	(50.01%) 0.7072* C 8 s(10.86%)p 8.21(89.11%)d 0.00(0.03%)
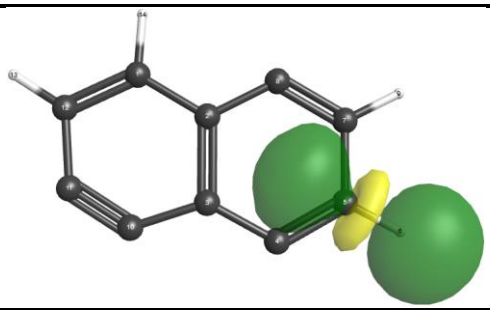	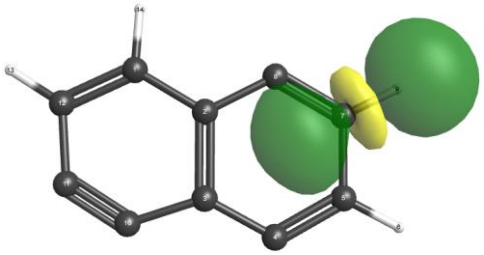
149. (0.01297) BD*(1) C 5 - H 6	153. (0.01348) BD*(1) C 7 - H 9
(36.45%) 0.6037* C 5 s(28.95%)p 2.45(71.01%)d 0.00(0.05%)	(36.53%) 0.6044* C 7 s(28.84%)p 2.47(71.11%)d 0.00(0.05%)
(63.55%) -0.7972* H 6 s(100.00%)	(63.47%) -0.7967* H 9 s(100.00%)

Second Order Perturbation Analysis

Donor Orbital	Acceptor Orbital	E(2) (kcal/mol)
12. BD*(1) C 4 - C 8	149. BD*(1) C 5 - H 6	2.26
12. BD*(1) C 4 - C 8	153. BD*(1) C 7 - H 9	2.22
13. BD (1) C 5 - H 6	148. BD (1) C 4 - C 8	1.51
17. BD (1) C 7 - H 9	148. BD (1) C 4 - C 8	1.41
148. BD (1) C 4 - C 8	149. BD*(1) C 5 - H 6	0.9
148. BD (1) C 4 - C 8	153. BD*(1) C 7 - H 9	0.9

7b

Orbitals

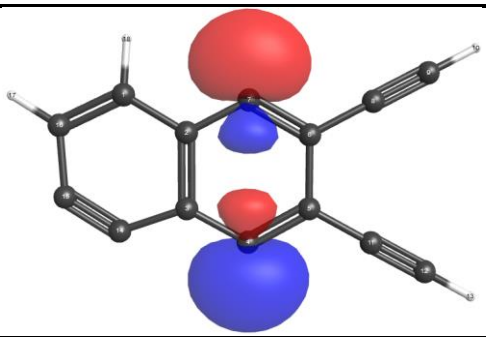	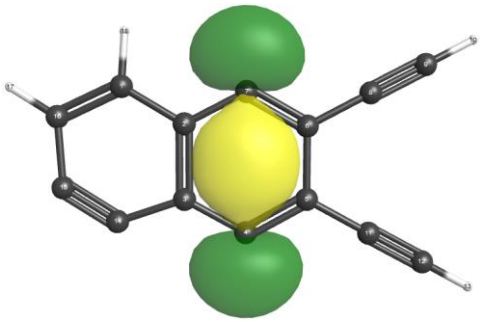
12. (1.81870) BD*(1) C 4 - C 7	200. (0.30753) BD (1) C 4 - C 7
(49.98%) 0.7070* C 4 s(11.10%)p 8.01(88.87%)d 0.00(0.03%)	(50.02%) 0.7072* C 4 s(11.10%)p 8.01(88.87%)d 0.00(0.03%)
(50.02%) -0.7072* C 7 s(11.14%)p 7.98(88.83%)d 0.00(0.03%)	(49.98%) 0.7070* C 7 s(11.14%)p 7.98(88.83%)d 0.00(0.03%)
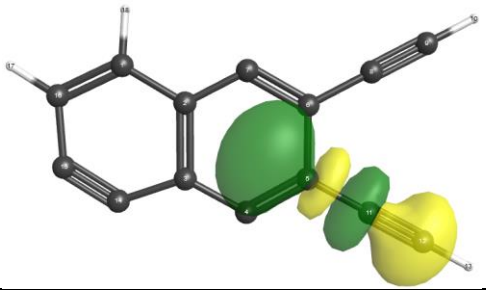	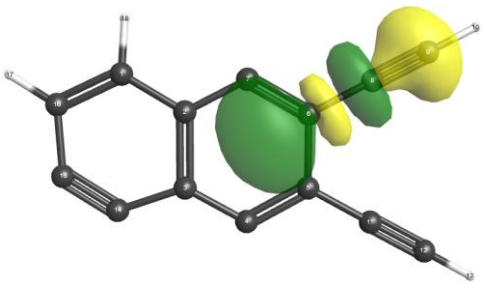
202. (0.02605) BD*(1) C 5 - C 11	205. (0.02657) BD*(1) C 6 - C 8
(48.23%) 0.6945* C 5 s(32.04%)p 2.12(67.92%)d 0.00(0.04%)	(48.24%) 0.6946* C 6 s(31.86%)p 2.14(68.10%)d 0.00(0.04%)
(51.77%) -0.7195* C 11 s(46.91%)p 1.13(53.05%)d 0.00(0.04%)	(51.76%) -0.7194* C 8 s(46.95%)p 1.13(53.00%)d 0.00(0.04%)

Second Order Perturbation Analysis

Donor Orbital	Acceptor Orbital	E(2) (kcal/mol)
12. BD*(1) C 4 - C 7	202. BD*(1) C 5 - C 11	1.72
12. BD*(1) C 4 - C 7	205. BD*(1) C 6 - C 8	1.73
200. BD (1) C 4 - C 7	202. BD*(1) C 5 - C 11	0.74
200. BD (1) C 4 - C 7	205. BD*(1) C 6 - C 8	0.75

Table 6.6. Total Nucleus-Independent Chemical Shift [NICS(1)] Values of Molecules in Pathways **I** and **II**.

	Center of Ring	Center of Original Ring	Center of *para*-Benzyne Ring	Center of Ring
I	**2**	**3**		**4**
a	14.8	18.8	-9.5	22.1
b	13.8	17.1	-8.9	19.9
c	11.5	15.8	-10.6	19.9
d	11.0	14.3	-9.9	18.1
II	**6**	**7**		**8**
a	-13.5	-12.4	-21.7	-13.9
b	-12.2	-11.6	--21.4	-12.6
c	-11.6	-11.0	-21.1	-12.6
d	-11.3	-10.1	-21.4	-11.4

MP2/cc-pVTZ Geometric Parameters of Stationary Points in Pathways I and II

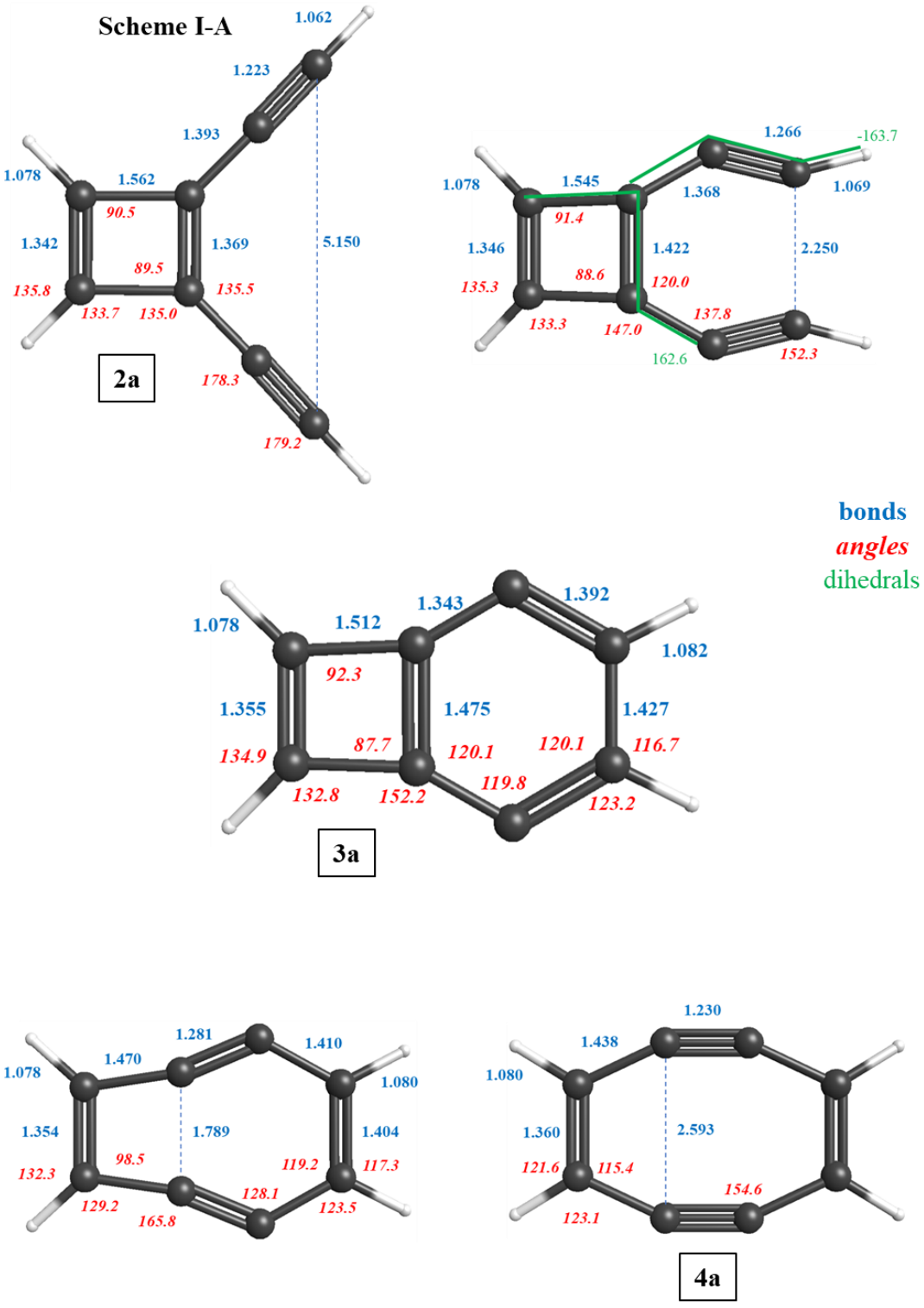

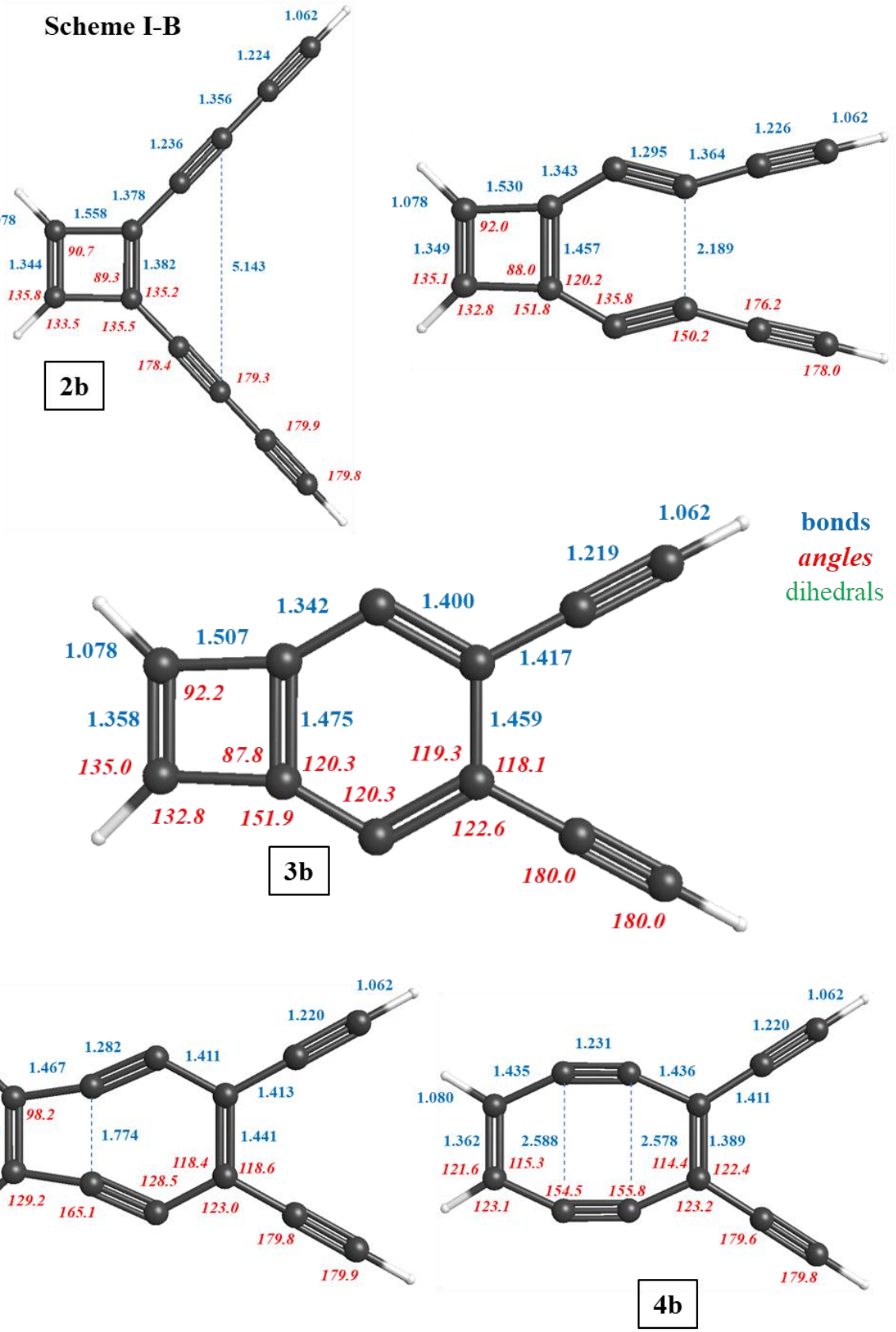
Scheme I-B
1.062
1.224
1.356
1.236
1.378
1.078
1.558
90.7
1.344
1.382
89.3
5.143
135.8
135.2
133.5
135.5
178.4
179.3
179.9
179.8
2b
1.226
1.062
1.295
1.364
1.343
1.530
1.078
92.0
1.349
1.457
2.189
88.0
135.1
120.2
135.8
176.2
132.8
151.8
150.2
178.0
bonds
angles
dihedrals
1.062
1.219
1.342
1.400
1.507
1.078
1.417
92.2
1.358
1.475
1.459
87.8
119.3
135.0
120.3
118.1
120.3
132.8
151.9
122.6
180.0
180.0
3b
1.062
1.220
1.282
1.411
1.467
1.078
1.413
98.2
1.355
1.774
1.441
118.4
118.6
132.6
128.5
129.2
165.1
123.0
179.8
179.9
1.062
1.220
1.231
1.435
1.436
1.080
1.411
1.362
2.588
2.578
1.389
121.6
115.3
114.4
122.4
154.5
155.8
123.1
123.2
179.6
179.8
4b

Scheme I-C

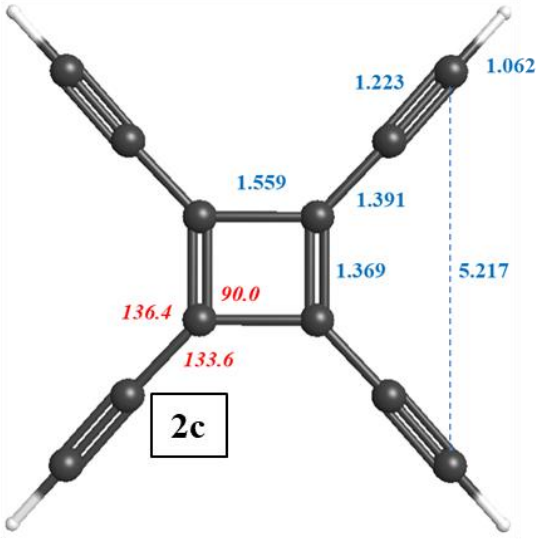

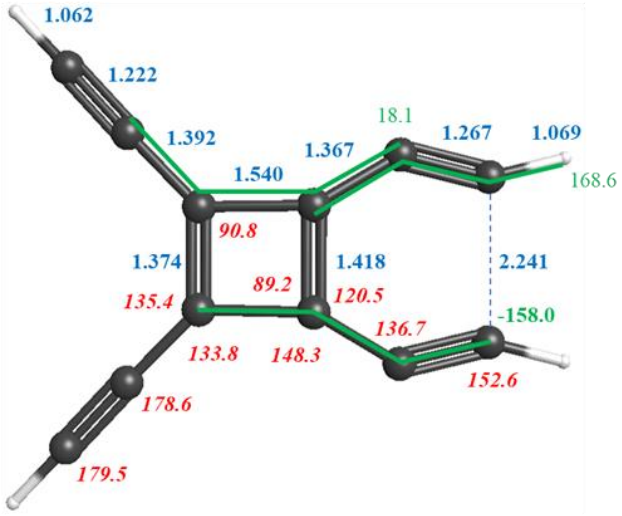

bonds
angles
dihedrals

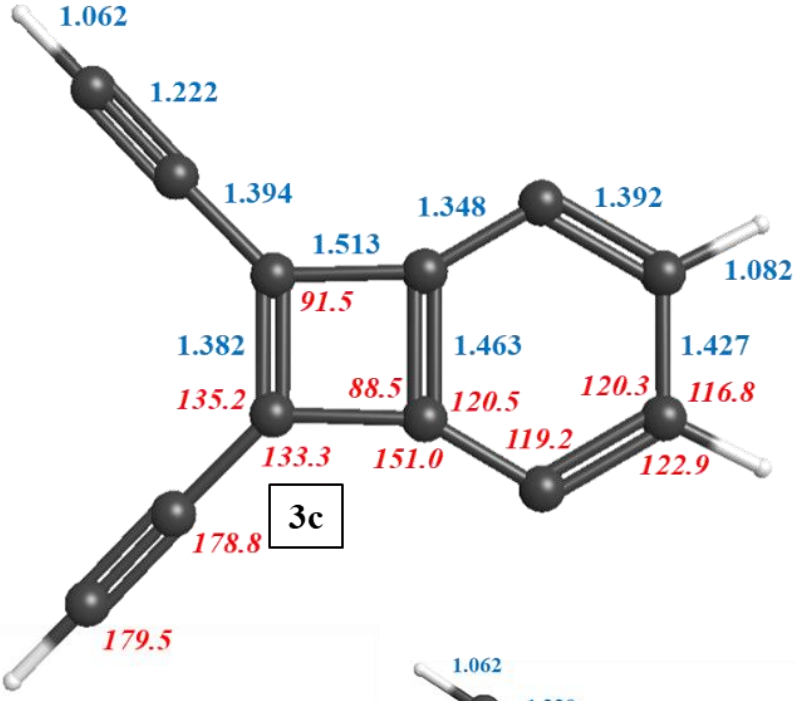

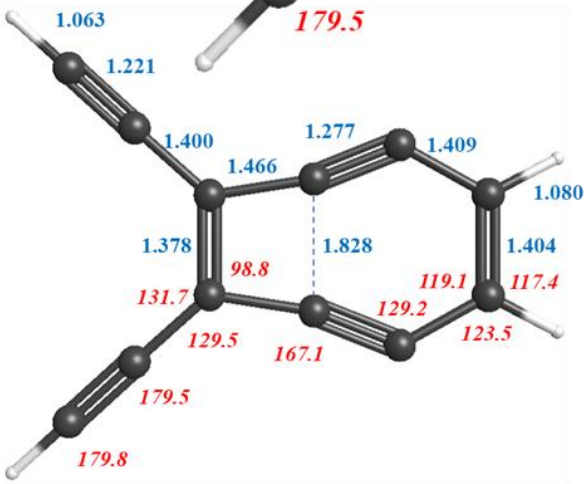

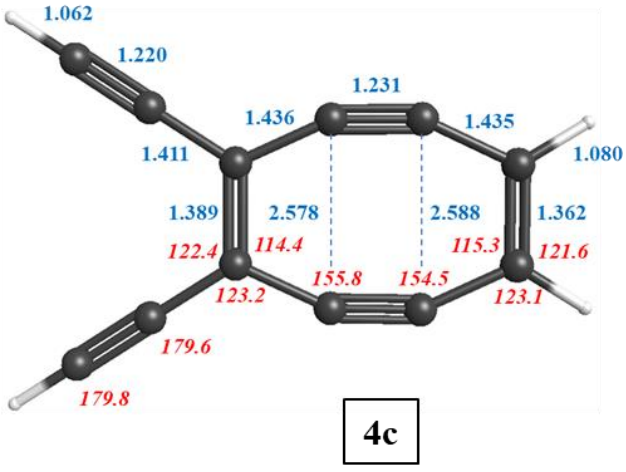

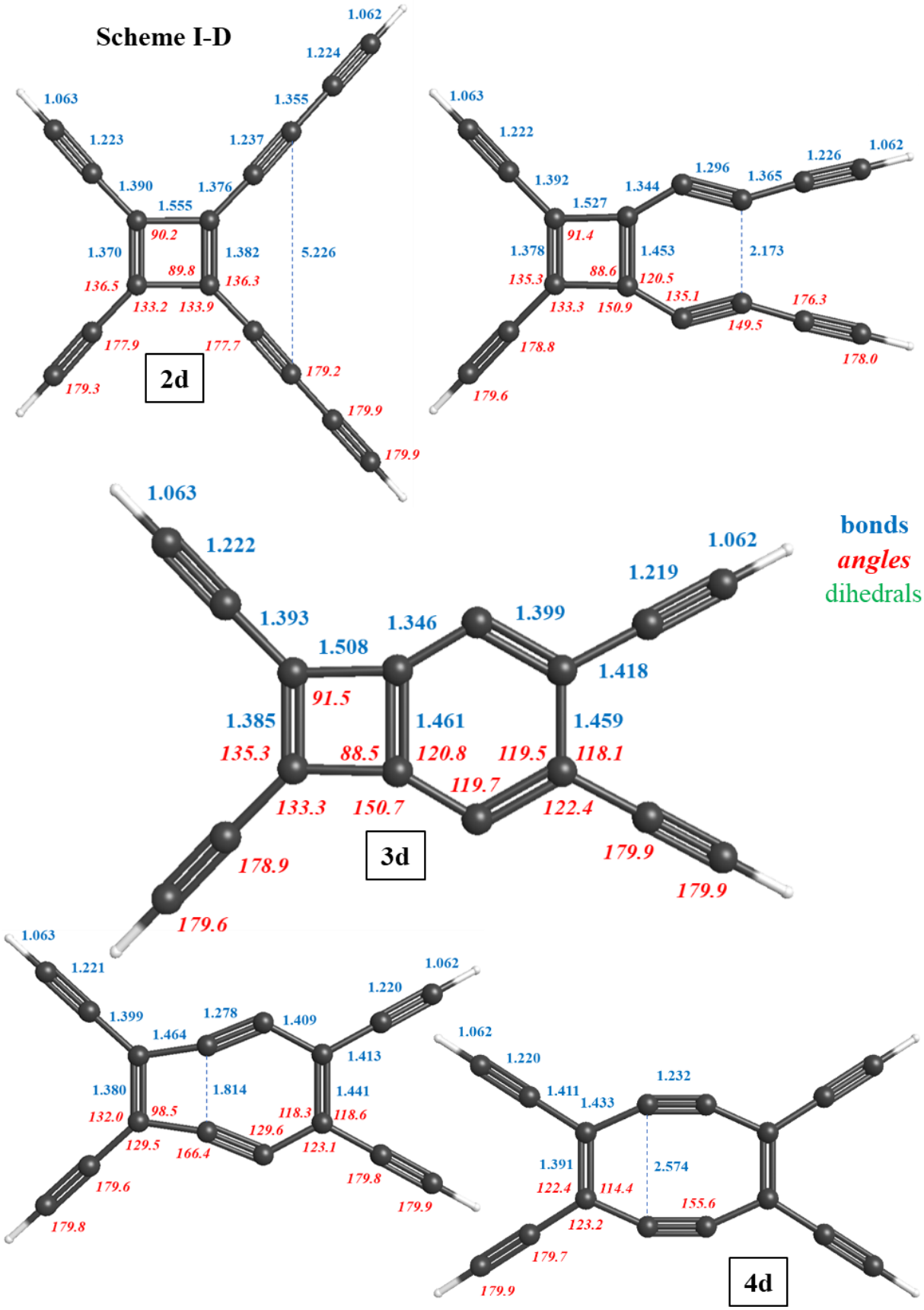
Scheme I-D
1.062
1.224
1.063
1.355
1.223
1.237
1.390
1.376
1.555
90.2
1.370
1.382
5.226
89.8
136.5
136.3
133.2
133.9
177.9
177.7
179.2
179.3
2d
179.9
179.9
1.063
1.222
1.392
1.344
1.296
1.365
1.226
1.062
1.527
91.4
1.378
1.453
2.173
135.3
88.6
120.5
135.1
176.3
133.3
150.9
149.5
178.8
178.0
179.6
bonds
angles
dihedrals
1.063
1.222
1.062
1.219
1.393
1.346
1.399
1.508
1.418
91.5
1.385
1.461
1.459
135.3
88.5
120.8
119.5
118.1
119.7
133.3
150.7
122.4
178.9
3d
179.9
179.9
179.6
1.063
1.221
1.062
1.220
1.399
1.278
1.409
1.464
1.413
1.380
1.814
1.441
132.0
98.5
118.3
118.6
129.6
129.5
166.4
123.1
179.8
179.6
179.9
179.8
1.062
1.220
1.411
1.232
1.433
1.391
2.574
122.4
114.4
155.6
123.2
179.7
179.9
4d

Scheme II-A

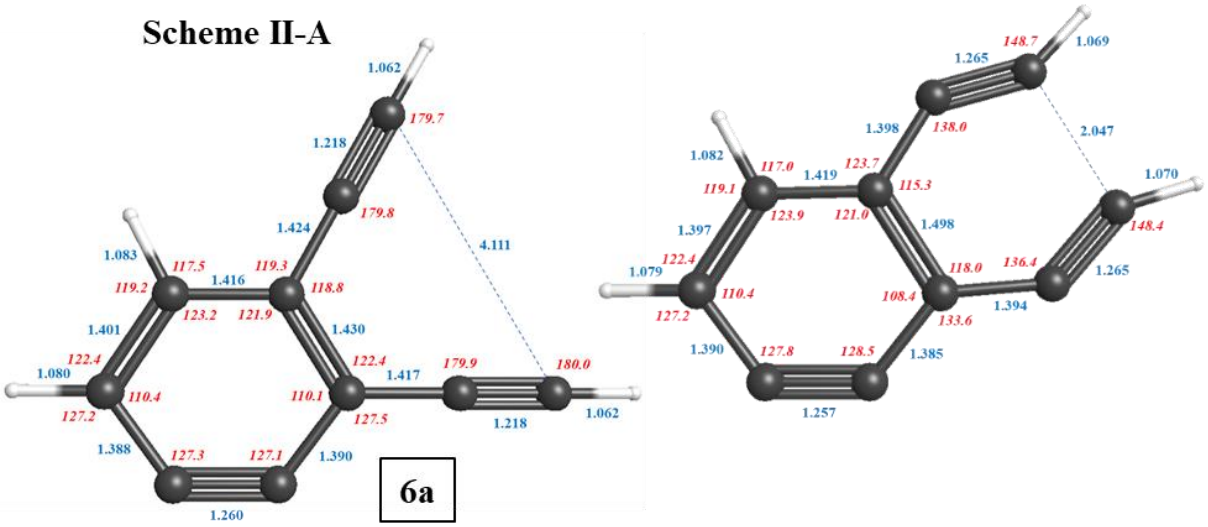

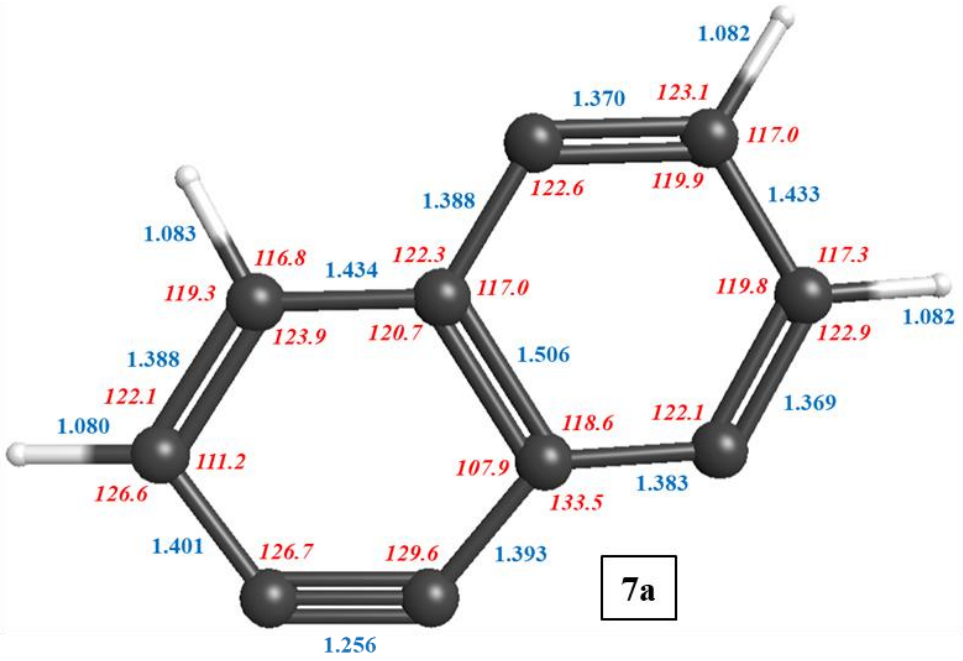

bonds
angles
dihedrals

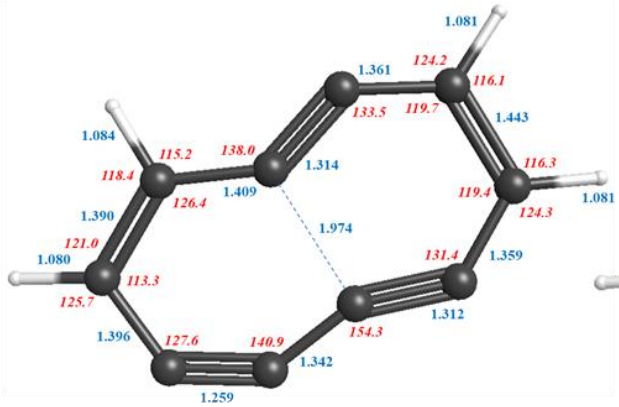

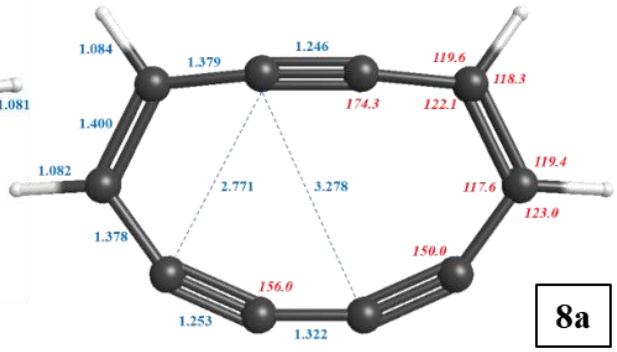

Scheme II-B

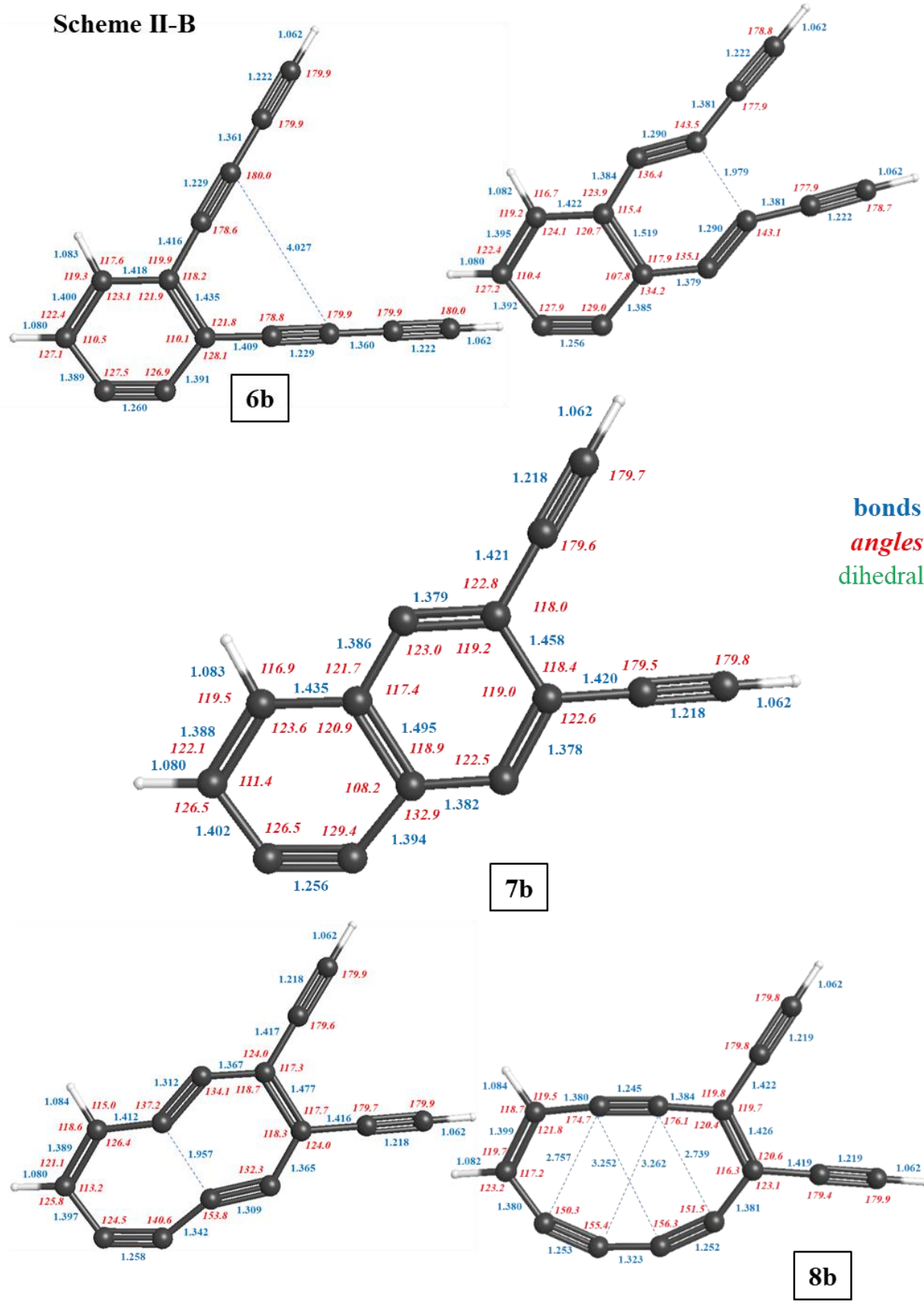

Scheme II-C

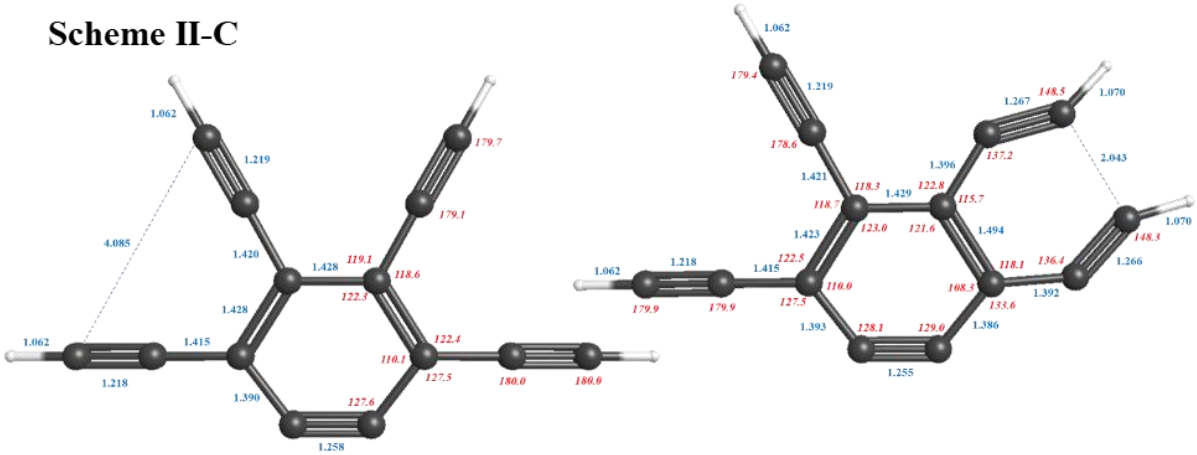

6c

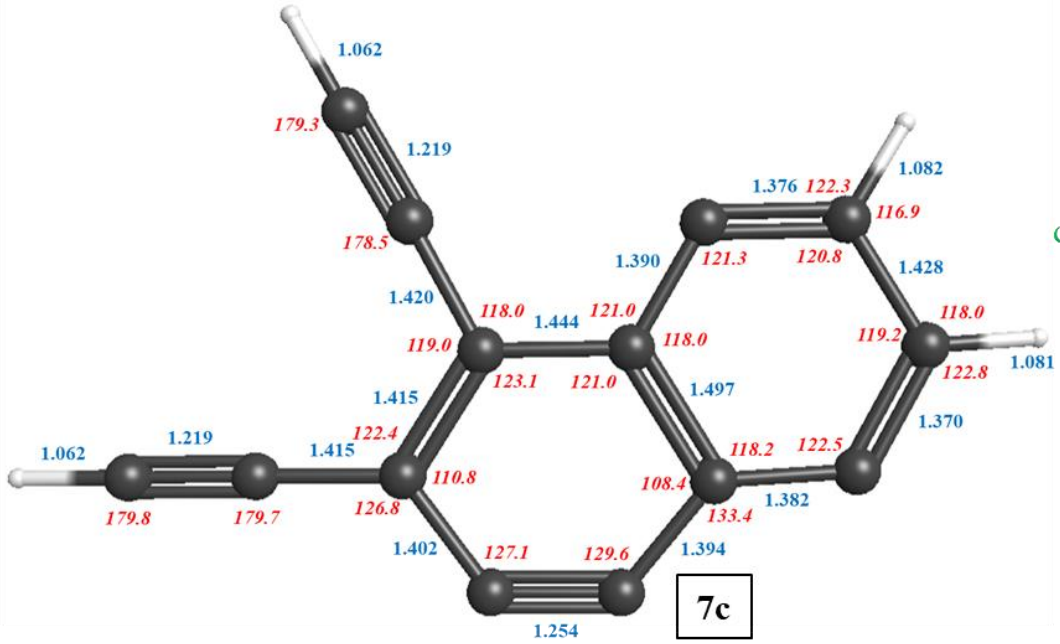

7c

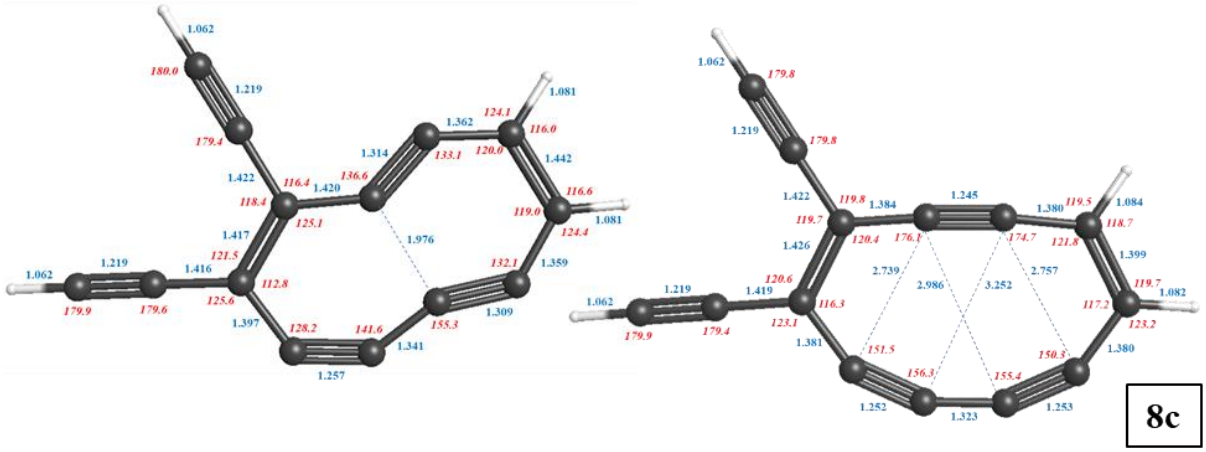

8c

Scheme II-D

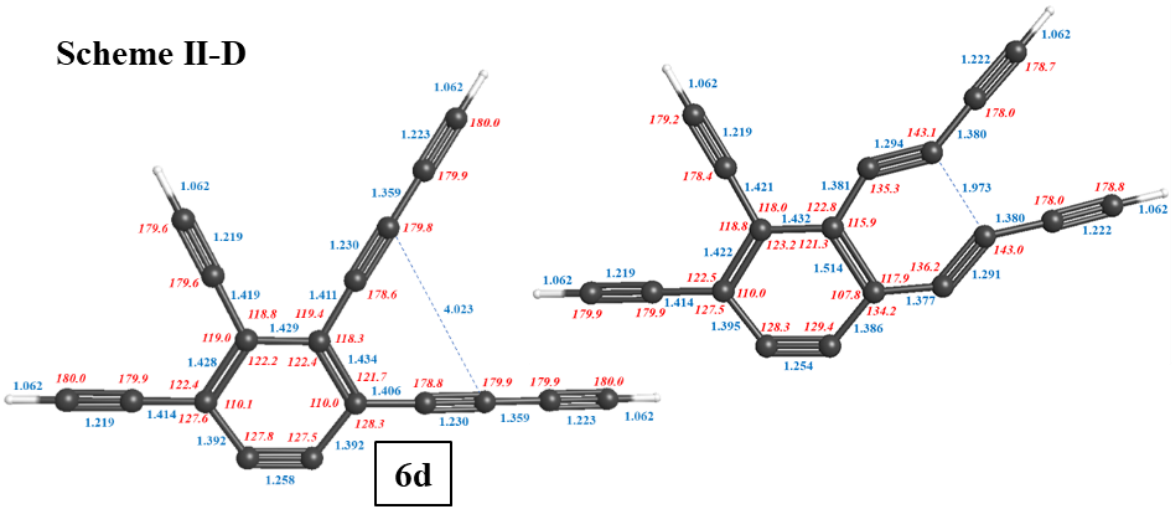

6d

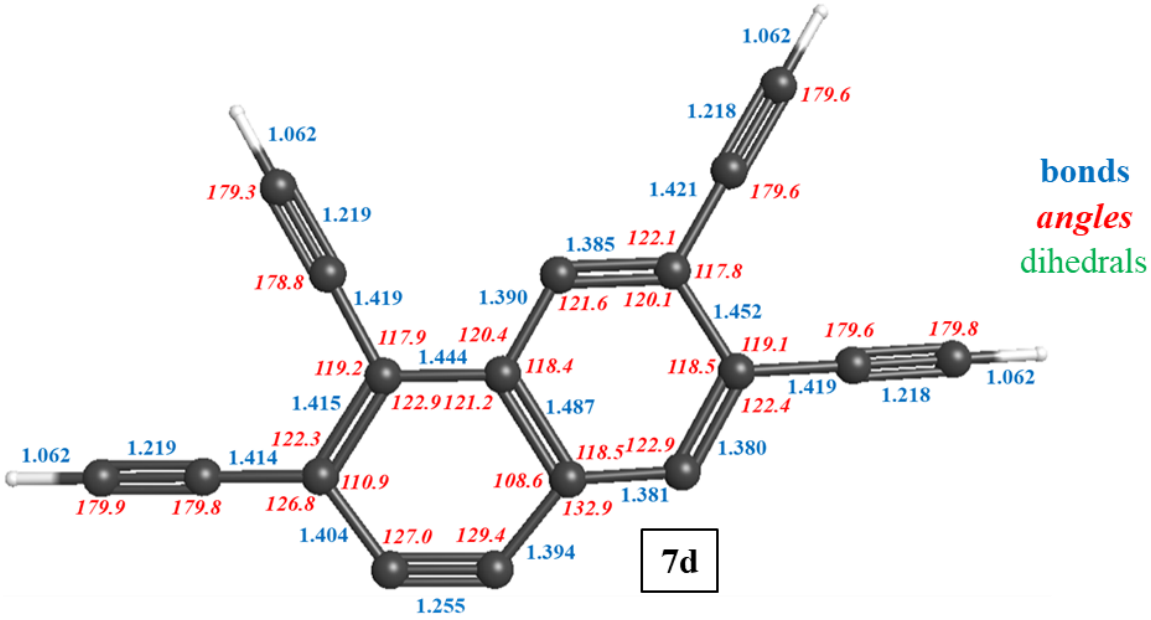

7d

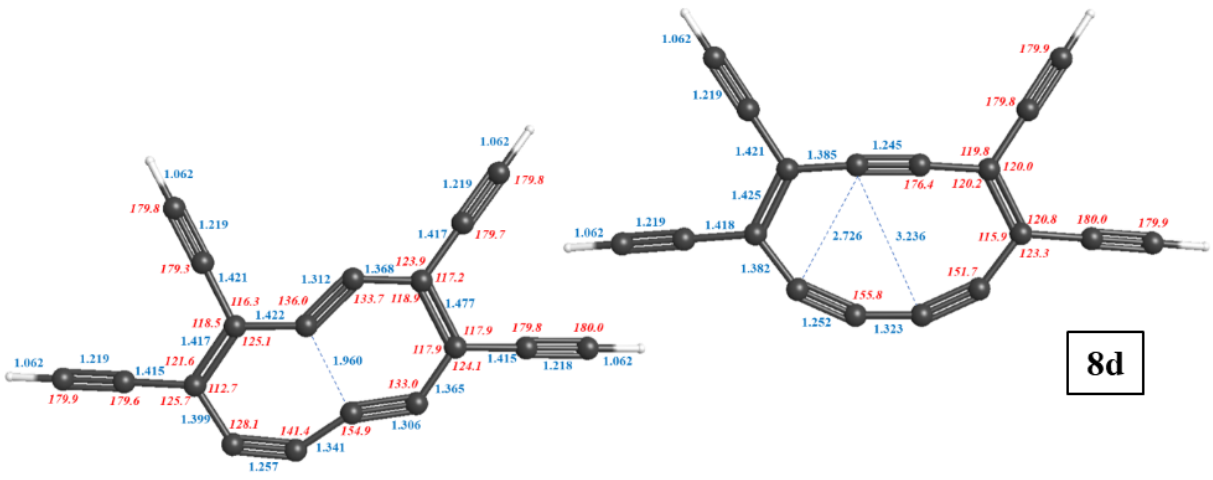

8d

MP2/cc-pVTZ Stationary Point Data Summaries

The following pages summarize the output files for the geometry optimizations and frequency calculations of the stationary point structures (local minima and transition states) obtained using Gaussian 09. Data is ordered by molecule identifier, with duplicate structures noted and referred to the correct summary. The data is tabulated in the format below and includes the structure, Cartesian coordinates, energies, and imaginary frequencies (if a transition state). Note that "Electronic and Zero-Point Energy" values for molecules containing the *para*-benzyne moiety are significantly different than the corresponding "Electronic Energy" values due to the presence of unrealistically large vibrational frequencies, as discussed in the main text.

Format:

Molecule identifier(s)

Molecule name (local minima only)

[molecule Lewis structure]

Charge	**Multiplicity**	**Theory/Basis Set**	**Full Point Group**
[value]	[value]	[value]	[value]
Zero-point Energy	**Electronic Energy**	**Electronic and Zero-Point Energy**	**Dipole Moment (D)**
[value]	[value]	[value]	[value]
$\Delta H_{(298)}$	**$\Delta G_{(298)}$**	(Energies in Hartrees/particle)	**Imaginary Frequency (cm^{-1})**
[value]	[value]		[value (if TS)]

Atom	**Coordinates (Angstroms)**		
	X	**Y**	**Z**
Atom1	[value]	[value]	[value]

Directory of Data Summaries

1a

Buta-1,3-diyne

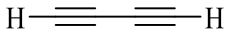

Charge	Multiplicity	Theory/Basis Set	Full Point Group
0	1	MP2/cc-pVTZ	$D_{\infty h}$

Zero-point Energy	Electronic Energy	Electronic and Zero-Point Energy	Dipole Moment (D)
0.036444	-153.152277	-153.115833	0.0000

$\Delta H_{(298)}$	$\Delta G_{(298)}$
-153.110386	-153.138713

(Energies in Hartrees/particle)

Atom	Coordinates (Angstroms)		
	X	Y	Z
C	0.000000	0.000000	0.684361
C	0.000000	0.000000	1.903809
H	0.000000	0.000000	2.965806
C	0.000000	0.000000	-0.684361
C	0.000000	0.000000	-1.903809
H	0.000000	0.000000	-2.965806

1b, 1c, 5a

Hexa-1,3,5-triyne

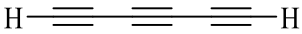

Charge	Multiplicity	Theory/Basis Set	Full Point Group
0	1	MP2/cc-pVTZ	$D_{\infty h}$
Zero-point Energy	**Electronic Energy**	**Electronic and Zero-Point Energy**	**Dipole Moment (D)**
0.046126	-229.149449	-229.103324	0.0000
$\Delta H_{(298)}$	**$\Delta G_{(298)}$**	(Energies in Hartrees/particle)	
-229.095941	-229.129684		

Atom	Coordinates (Angstroms)		
	X	Y	Z
C	0.000000	0.000000	3.197403
C	0.000000	0.000000	1.975050
C	0.000000	0.000000	0.615309
C	0.000000	0.000000	-0.615309
C	0.000000	0.000000	-1.975050
C	0.000000	0.000000	-3.197403
H	0.000000	0.000000	-4.259587
H	0.000000	0.000000	4.259587

1c

*Same as **1b***

1d, 5b, 5c

Octa-1,3,5,7-tetrayne

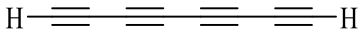

Charge	Multiplicity	Theory/Basis Set	Full Point Group
0	1	MP2/cc-pVTZ	$D_{\infty h}$

Zero-point Energy	Electronic Energy	Electronic and Zero-Point Energy	Dipole Moment (D)
0.055551	-305.147892	-305.092341	0.0000

$\Delta H_{(298)}$	$\Delta G_{(298)}$
-305.082918	-305.122119

(Energies in Hartrees/particle)

Atom	Coordinates (Angstroms)		
	X	Y	Z
C	0.000000	0.000000	4.488254
C	0.000000	0.000000	3.264737
C	0.000000	0.000000	1.908502
C	0.000000	0.000000	0.673601
C	0.000000	0.000000	-0.673601
C	0.000000	0.000000	-1.908502
C	0.000000	0.000000	-3.264737
C	0.000000	0.000000	-4.488254
H	0.000000	0.000000	-5.550741
H	0.000000	0.000000	5.550741

2a

1,2-Diethynylcyclobuta-1,3-diene

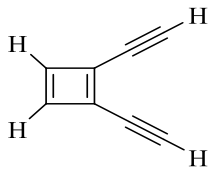

Charge	Multiplicity	Theory/Basis Set	Full Point Group
0	1	MP2/cc-pVTZ	C_{2v}
Zero-point Energy	**Electronic Energy**	**Electronic and Zero-Point Energy**	**Dipole Moment (D)**
0.078705	-306.321131	-306.243186	0.3822
$\Delta H_{(298)}$	**$\Delta G_{(298)}$**	(Energies in Hartrees/particle)	
-306.234308	-306.274637		

Atom	Coordinates (Angstroms)		
	X	Y	Z
C	0.000000	0.684367	0.290682
C	0.000000	-0.684367	0.290682
C	0.000000	-0.671202	1.852710
C	0.000000	0.671202	1.852710
H	0.000000	1.443974	2.604281
H	0.000000	-1.443974	2.604281
C	0.000000	-1.677954	-0.685872
C	0.000000	-2.574934	-1.516685
H	0.000000	-3.343977	-2.249291
C	0.000000	1.677954	-0.685872
C	0.000000	2.574934	-1.516685
H	0.000000	3.343977	-2.249291

2b

1,2-Di(buta-1,3,-diynyl)cyclobuta-1,3-diene

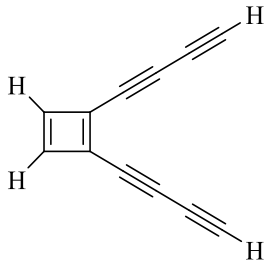

Charge	Multiplicity	Theory/Basis Set	Full Point Group
0	1	MP2/cc-pVTZ	C_{2v}
Zero-point Energy	**Electronic Energy**	**Electronic and Zero-Point Energy**	**Dipole Moment (D)**
0.097969	-458.318462	-458.222249	0.5567
$\Delta H_{(298)}$	**$\Delta G_{(298)}$**	(Energies in Hartrees/particle)	
-458.2094	-458.260502		

Atom	Coordinates (Angstroms)		
	X	Y	Z
C	0.000000	0.691237	1.251041
C	0.000000	-0.691237	1.251041
C	0.000000	-0.671797	2.808774
C	0.000000	0.671797	2.808774
H	0.000000	1.444493	3.560636
H	0.000000	-1.444493	3.560636
C	0.000000	-1.669461	0.280419
C	0.000000	-2.571318	-0.565089
C	0.000000	-3.549664	-1.504115
C	0.000000	-4.434488	-2.350074
H	0.000000	-5.200146	-3.086371
C	0.000000	1.669461	0.280419
C	0.000000	2.571318	-0.565089
C	0.000000	3.549664	-1.504115
C	0.000000	4.434488	-2.350074
H	0.000000	5.200146	-3.086371

2c

1,2,3,4-Tetraethynylbuta-1,3-diene

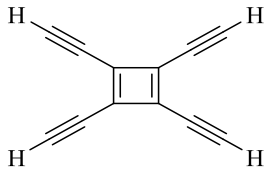

Charge	Multiplicity	Theory/Basis Set	Full Point Group
0	1	MP2/cc-pVTZ	D_{2h}

Zero-point Energy	Electronic Energy	Electronic and Zero-Point Energy	Dipole Moment (D)
0.095842	-458.315530	-458.219689	0.0000

$\Delta H_{(298)}$	$\Delta G_{(298)}$
-458.20631	-458.257528

(Energies in Hartrees/particle)

Atom	Coordinates (Angstroms)		
	X	Y	Z
C	0.000000	0.779379	0.684405
C	0.000000	-0.779379	0.684405
C	0.000000	0.779386	-0.684427
C	0.000000	-0.779386	-0.684427
C	0.000000	1.737731	-1.692163
C	0.000000	2.547279	-2.608564
H	0.000000	3.261001	-3.395549
C	0.000000	-1.737731	-1.692163
C	0.000000	-2.547279	-2.608564
H	0.000000	-3.261001	-3.395549
C	0.000000	-1.737745	1.692173
C	0.000000	-2.547295	2.608574
H	0.000000	-3.261016	3.395559
C	0.000000	1.737745	1.692173
C	0.000000	2.547295	2.608574
H	0.000000	3.261016	3.395559

2d

1,2-Di(buta-1,3-diynyl)-3,4-diethynylcyclobuta-1,3-diene

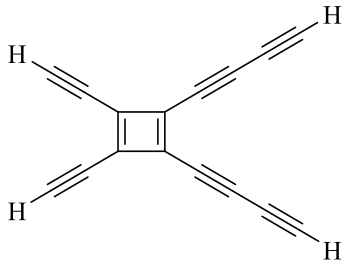

Charge	Multiplicity	Theory/Basis Set	Full Point Group
0	1	MP2/cc-pVTZ	C_{2v}
Zero-point Energy	**Electronic Energy**	**Electronic and Zero-Point Energy**	**Dipole Moment (D)**
0.114980	-610.314202	-610.199222	0.1457
$\Delta H_{(298)}$	**$\Delta G_{(298)}$**	(Energies in Hartrees/particle)	
-610.181812	-610.243793		

Atom	Coordinates (Angstroms)		
	X	Y	Z
C	0.000000	0.691158	0.185167
C	0.000000	-0.691158	0.185167
C	0.000000	-0.685166	1.740266
C	0.000000	0.685166	1.740266
C	0.000000	1.694166	2.696711
C	0.000000	2.612506	3.504195
H	0.000000	3.401989	4.215321
C	0.000000	-1.694166	2.696711
C	0.000000	-2.612506	3.504195
H	0.000000	-3.401989	4.215321
C	0.000000	-1.685438	-0.765613
C	0.000000	-2.612947	-1.583594
C	0.000000	-3.616978	-2.493775
C	0.000000	-4.525493	-3.314532
H	0.000000	-5.312445	-4.028266
C	0.000000	1.685438	-0.765613
C	0.000000	2.612947	-1.583594
C	0.000000	3.616978	-2.493775
C	0.000000	4.525493	-3.314532
H	0.000000	5.312445	-4.028266

TS2–3a

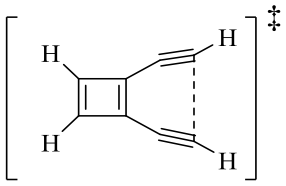

Charge	Multiplicity	Theory/Basis Set	Full Point Group
0	1	MP2/cc-pVTZ	C_S
Zero-point Energy	**Electronic Energy**	**Electronic and Zero-Point Energy**	**Dipole Moment (D)**
0.079357	-306.286070	-306.206713	0.2343
$\Delta H_{(298)}$	**$\Delta G_{(298)}$**	(Energies in Hartrees/particle)	**Imaginary Frequency (cm^{-1})**
-306.199233	-306.236996		364.9256

Atom	Coordinates (Angstroms)		
	X	Y	Z
C	0.088320	2.040737	0.672851
C	-0.187730	0.521206	0.710795
C	-0.187730	0.521206	-0.710795
C	0.088320	2.040737	-0.672851
H	0.249594	2.781385	-1.438796
C	-0.041957	-0.654532	-1.393958
C	0.088320	-1.884500	-1.125005
C	0.088320	-1.884500	1.125005
C	-0.041957	-0.654532	1.393958
H	0.068690	-2.918852	1.392383
H	0.068690	-2.918852	-1.392383
H	0.249594	2.781385	1.438796

TS2–3b

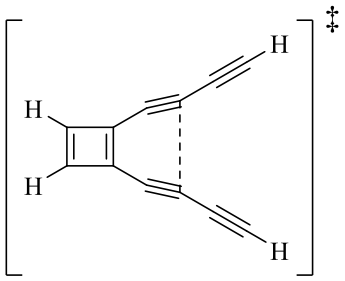

Charge	Multiplicity	Theory/Basis Set	Full Point Group
0	1	MP2/cc-pVTZ	C_{2v}
Zero-point Energy	**Electronic Energy**	**Electronic and Zero-Point Energy**	**Dipole Moment (D)**
0.097699	-458.284832	-458.187133	0.6448
$\Delta H_{(298)}$	**$\Delta G_{(298)}$**	(Energies in Hartrees/particle)	**Imaginary Frequency (cm^{-1})**
-458.175451	-458.223042		476.9346

Atom	Coordinates (Angstroms)		
	X	Y	Z
C	0.061539	1.923362	0.676518
C	0.045580	0.394271	0.729582
C	0.062663	0.394999	-0.727726
C	0.077462	1.924060	-0.672724
H	0.093671	2.684885	-1.436077
C	0.060306	-0.765096	-1.405136
C	0.044960	-2.021865	-1.094613
C	0.019429	-2.022879	1.093824
C	0.027212	-0.766392	1.405738
H	0.060002	2.683433	1.440791
C	0.036746	-3.333719	-1.468392
C	0.028455	-4.532684	-1.725338
H	0.021528	-5.562649	-1.984348
C	0.002466	-3.335060	1.466197
C	-0.011816	-4.534232	1.721903
H	-0.024797	-5.564418	1.979800

TS2–3c

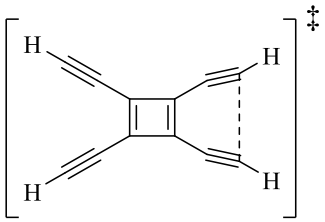

Charge	Multiplicity	Theory/Basis Set	Full Point Group
0	1	MP2/cc-pVTZ	C_s
Zero-point Energy	**Electronic Energy**	**Electronic and Zero-Point Energy**	**Dipole Moment (D)**
0.096359	-458.277524	-458.181165	0.2632
$\Delta H_{(298)}$	**$\Delta G_{(298)}$**	(Energies in Hartrees/particle)	**Imaginary Frequency (cm^{-1})**
-458.169175	-458.218179		404.6684

Atom	Coordinates (Angstroms)		
	X	Y	Z
C	-0.915162	0.687150	-0.079831
C	-0.915162	-0.687150	-0.079831
C	0.621386	-0.708765	-0.187665
C	0.621386	0.708766	-0.187665
C	1.788563	1.401687	-0.027750
C	3.014039	1.120340	0.125516
H	4.049603	1.380874	0.164100
C	1.788562	-1.401687	-0.027750
C	3.014039	-1.120340	0.125517
H	4.049603	-1.380873	0.164100
C	-1.887947	-1.678064	0.014696
C	-2.720586	-2.568886	0.099269
H	-3.451351	-3.336767	0.170485
C	-1.887948	1.678063	0.014696
C	-2.720587	2.568885	0.099269
H	-3.451352	3.336766	0.170485

TS2–3d

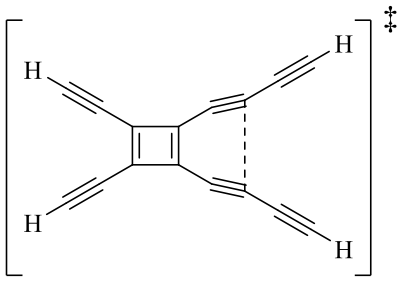

Charge	Multiplicity	Theory/Basis Set	Full Point Group
0	1	MP2/cc-pVTZ	C_{2v}
Zero-point Energy	**Electronic Energy**	**Electronic and Zero-Point Energy**	**Dipole Moment (D)**
0.114905	-610.276225	-610.161320	0.2399
$\Delta H_{(298)}$	**$\Delta G_{(298)}$**	(Energies in Hartrees/particle)	**Imaginary Frequency (cm^{-1})**
-610.145192	-610.20337		486.4716

Atom	Coordinates (Angstroms)		
	X	Y	Z
C	-2.144002	-0.688863	0.000079
C	-0.617967	-0.726713	-0.000321
C	-0.617902	0.726637	-0.000149
C	-2.143941	0.688873	0.000210
C	0.540070	1.408513	-0.000093
C	1.795187	1.086610	-0.000217
C	1.795109	-1.086694	-0.000481
C	0.540007	-1.408611	-0.000532
C	3.106332	1.464912	0.000226
C	4.303936	1.727931	0.000581
H	5.332722	1.992135	0.000873
C	3.106248	-1.465025	-0.000110
C	4.303878	-1.727920	0.000027
H	5.332687	-1.992050	0.000313
C	-3.123401	-1.677811	0.000250
C	-3.965389	-2.563848	0.000522
H	-4.702351	-3.329453	0.000476
C	-3.123265	1.677877	0.000010
C	-3.965089	2.564063	-0.000231
H	-4.701934	3.329782	-0.000289

3a

3,6-Didehydrobicyclo[4.2.0]octa-1,3,5,7-tetraene

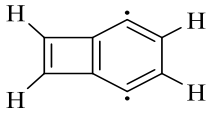

Charge	Multiplicity	Theory/Basis Set	Full Point Group
0	1	MP2/cc-pVTZ	C_{2v}
Zero-point Energy	**Electronic Energy**	**Electronic and Zero-Point Energy**	**Dipole Moment (D)**
0.111118	-306.356867	-306.245749	1.2023
$\Delta H_{(298)}$	**$\Delta G_{(298)}$**	(Energies in Hartrees/particle)	
-306.239651	-306.274741		

Atom	Coordinates (Angstroms)		
	X	Y	Z
C	-0.505417	0.737658	0.004028
C	0.656675	1.411537	0.006717
C	1.861103	0.713345	0.009493
C	1.861102	-0.713351	0.009491
C	0.656674	-1.411541	0.006713
C	-0.505417	-0.737662	0.004025
C	-2.016467	-0.677592	0.000628
C	-2.016466	0.677590	0.000630
H	2.827239	1.199507	0.011793
H	2.827238	-1.199513	0.011791
H	-2.779917	-1.438752	-0.001129
H	-2.779916	1.438751	-0.001125

3b

4,5-Diethynyl-3,6-didehydrobicyclo[4.2.0]octa-1,3,5,7-tetraene

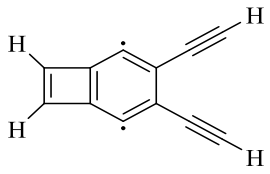

Charge	Multiplicity	Theory/Basis Set	Full Point Group
0	1	MP2/cc-pVTZ	C_{2v}

Zero-point Energy	Electronic Energy	Electronic and Zero-Point Energy	Dipole Moment (D)
0.152357	-458.333903	-458.181546	2.0330

$\Delta H_{(298)}$	$\Delta G_{(298)}$	(Energies in Hartrees/particle)
-458.171133	-458.21631	

Atom	Coordinates (Angstroms)		
	X	Y	Z
C	-0.401767	0.737283	0.004299
C	0.755938	1.415063	0.006984
C	1.976038	0.729260	0.009808
C	1.976038	-0.729265	0.009807
C	0.755937	-1.415067	0.006983
C	-0.401768	-0.737287	0.004298
C	-1.907704	-0.678797	0.000853
C	-1.907704	0.678794	0.000854
H	-2.670085	-1.441058	-0.000886
H	-2.670084	1.441056	-0.000884
C	3.226940	1.395770	0.012761
C	3.226939	-1.395775	0.012759
C	4.302565	-1.969370	0.015286
H	5.239122	-2.469521	0.017485
C	4.302567	1.969364	0.015289
H	5.239123	2.469514	0.017490

3c

1,8-Diethynyl-3,6-didehydrobicyclo[4.2.0]octa-1,3,5,7-tetraene

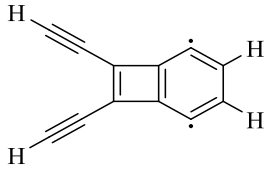

Charge	Multiplicity	Theory/Basis Set	Full Point Group
0	1	MP2/cc-pVTZ	C_{2v}
Zero-point Energy	**Electronic Energy**	**Electronic and Zero-Point Energy**	**Dipole Moment (D)**
0.145689	-458.347600	-458.201911	1.0592
$\Delta H_{(298)}$	**$\Delta G_{(298)}$**	(Energies in Hartrees/particle)	
-458.19135	-458.237144		

Atom	Coordinates (Angstroms)		
	X	Y	Z
C	-0.548087	0.731402	0.003978
C	0.612802	1.415638	0.006646
C	1.814275	0.713537	0.009405
C	1.814275	-0.713542	0.009403
C	0.612801	-1.415642	0.006642
C	-0.548087	-0.731405	0.003976
C	-2.060418	-0.690786	0.000511
C	-2.060417	0.690783	0.000513
H	2.779973	1.201178	0.011630
H	2.779972	-1.201184	0.011626
C	-3.043417	1.679064	-0.001743
C	-3.043419	-1.679065	-0.001747
C	-3.886297	2.563566	-0.003677
H	-4.625865	3.326388	-0.005375
C	-3.886299	-2.563567	-0.003684
H	-4.625868	-3.326388	-0.005384

3d

1,4,5,8-Tetraethynyl-3,6-didehydrobicyclo[4.2.0]octa-1,3,5,7-tetraene

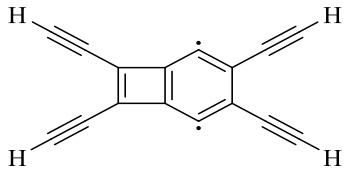

Charge	Multiplicity	Theory/Basis Set	Full Point Group
0	1	MP2/cc-pVTZ	C_{2v}

Zero-point Energy	Electronic Energy	Electronic and Zero-Point Energy	Dipole Moment (D)
0.142098	-610.324577	-610.182479	1.9757

$\Delta H_{(298)}$	$\Delta G_{(298)}$
-610.167532	-610.223354

(Energies in Hartrees/particle)

Atom	Coordinates (Angstroms)		
	X	Y	Z
C	-0.574863	0.730636	0.000042
C	0.581710	1.419188	0.000108
C	1.799135	0.729259	0.000075
C	1.799138	-0.729257	-0.000091
C	0.581712	-1.419180	-0.000109
C	-0.574864	-0.730636	-0.000052
C	-2.082329	-0.692411	-0.000014
C	-2.082328	0.692408	-0.000064
C	-3.062774	1.682350	-0.000038
C	-3.062774	-1.682353	0.000044
C	-3.905339	2.567262	-0.000038
H	-4.643785	3.331514	-0.000246
C	-3.905339	-2.567264	0.000112
H	-4.643823	-3.331481	0.000364
C	3.049963	1.396314	0.000172
C	4.124977	1.971080	0.000165
H	5.060916	2.472601	0.000132
C	3.049965	-1.396313	-0.000116
C	4.124977	-1.971082	-0.000201
H	5.060901	-2.472632	-0.000217

TS3–4a

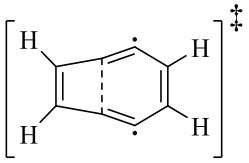

Charge	Multiplicity	Theory/Basis Set	Full Point Group
0	1	MP2/cc-pVTZ	C_{2v}
Zero-point Energy	**Electronic Energy**	**Electronic and Zero-Point Energy**	**Dipole Moment (D)**
0.083487	-306.346856	-306.263369	1.5537
$\Delta H_{(298)}$	**$\Delta G_{(298)}$**	(Energies in Hartrees/particle)	**Imaginary Frequency (cm^{-1})**
-306.25678	-306.292733		673.9821

Atom	Coordinates (Angstroms)		
	X	Y	Z
C	-0.536964	0.894386	0.000000
C	0.644318	1.389017	0.000000
C	1.875381	0.701896	0.000000
C	1.875381	-0.701896	0.000000
C	0.644318	-1.389017	0.000000
C	-0.536964	-0.894386	0.000000
C	-1.990564	-0.676831	0.000000
C	-1.990564	0.676831	0.000000
H	2.835259	1.197055	0.000000
H	2.835259	-1.197055	0.000000
H	-2.788285	-1.402526	0.000000
H	-2.788285	1.402526	0.000000

TS3–4b

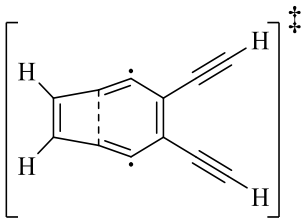

Charge	Multiplicity	Theory/Basis Set	Full Point Group
0	1	MP2/cc-pVTZ	C_{2v}
Zero-point Energy	**Electronic Energy**	**Electronic and Zero-Point Energy**	**Dipole Moment (D)**
0.100188	-458.324859	-458.224671	2.1524
$\Delta H_{(298)}$	**$\Delta G_{(298)}$**	(Energies in Hartrees/particle)	**Imaginary Frequency (cm^{-1})**
-458.213648	-458.259891		675.7682

Atom	Coordinates (Angstroms)		
	X	Y	Z
C	-0.430184	0.887004	0.000000
C	0.748536	1.390817	0.000000
C	1.990092	0.720644	0.000000
C	1.990092	-0.720644	0.000000
C	0.748535	-1.390817	0.000000
C	-0.430184	-0.887004	0.000000
C	-1.882086	-0.677732	0.000000
C	-1.882086	0.677732	0.000000
H	-2.676511	-1.407026	0.000000
H	-2.676511	1.407026	0.000000
C	3.230985	1.397161	0.000000
C	4.299977	1.984308	0.000000
H	5.231578	2.493706	0.000000
C	3.230985	-1.397161	0.000000
C	4.299977	-1.984308	0.000000
H	5.231578	-2.493706	0.000000

TS3–4c

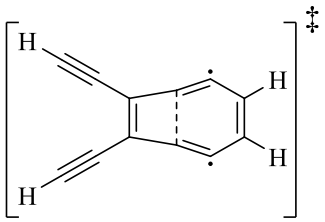

Charge	Multiplicity	Theory/Basis Set	Full Point Group
0	1	MP2/cc-pVTZ	C_{2v}
Zero-point Energy	**Electronic Energy**	**Electronic and Zero-Point Energy**	**Dipole Moment (D)**
0.100457	-458.332498	-458.232041	1.5050
$\Delta H_{(298)}$	**$\Delta G_{(298)}$**	(Energies in Hartrees/particle)	**Imaginary Frequency (cm^{-1})**
-458.22097	-458.26704		671.8994

Atom	Coordinates (Angstroms)		
	X	Y	Z
C	0.000000	0.914137	0.611608
C	0.000000	1.386651	1.797477
C	0.000000	0.701779	3.028448
C	0.000000	-0.701779	3.028448
C	0.000000	-1.386651	1.797477
C	0.000000	-0.914137	0.611608
C	0.000000	-0.689151	-0.837313
C	0.000000	0.689151	-0.837313
H	0.000000	1.198391	3.987611
H	0.000000	-1.198391	3.987611
C	0.000000	1.620684	-1.882517
C	0.000000	-1.620684	-1.882517
C	0.000000	2.440949	-2.786304
H	0.000000	3.151852	-3.576005
C	0.000000	-2.440949	-2.786304
H	0.000000	-3.151852	-3.576005

TS3–4d

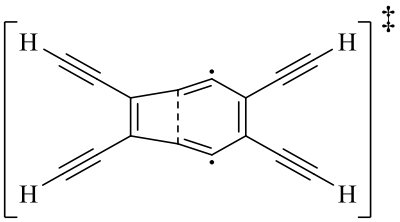

Charge	Multiplicity	Theory/Basis Set	Full Point Group
0	1	MP2/cc-pVTZ	C_{2v}
Zero-point Energy	**Electronic Energy**	**Electronic and Zero-Point Energy**	**Dipole Moment (D)**
0.116959	-610.310447	-610.193489	2.1375
$\Delta H_{(298)}$	**$\Delta G_{(298)}$**	(Energies in Hartrees/particle)	**Imaginary Frequency (cm^{-1})**
-610.177859	-610.234255		677.0181

Atom	Coordinates (Angstroms)		
	X	Y	Z
C	0.000000	0.907231	-0.591851
C	0.000000	1.388076	0.591957
C	0.000000	0.720739	1.833304
C	0.000000	-0.720739	1.833304
C	0.000000	-1.388076	0.591957
C	0.000000	-0.907231	-0.591851
C	0.000000	-0.690146	-2.039199
C	0.000000	0.690146	-2.039199
C	0.000000	1.626183	-3.079383
C	0.000000	-1.626183	-3.079383
C	0.000000	2.449646	-3.980286
H	0.000000	3.164336	-4.766842
C	0.000000	-2.449646	-3.980286
H	0.000000	-3.164336	-4.766842
C	0.000000	1.398105	3.073223
C	0.000000	1.987042	4.141298
H	0.000000	2.497470	5.072465
C	0.000000	-1.398105	3.073223
C	0.000000	-1.987042	4.141298
H	0.000000	-2.497470	5.072465

4a

Cycloocta-1,5-dien-3,7-diyne

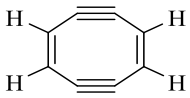

Charge	Multiplicity	Theory/Basis Set	Full Point Group
0	1	MP2/cc-pVTZ	D_{2h}
Zero-point Energy	**Electronic Energy**	**Electronic and Zero-Point Energy**	**Dipole Moment (D)**
0.084590	-306.383357	-306.298767	0.0005
$\Delta H_{(298)}$	**$\Delta G_{(298)}$**	(Energies in Hartrees/particle)	
-306.291416	-306.328763		

Atom	Coordinates (Angstroms)		
	X	Y	Z
C	-0.607758	1.296549	0.001690
C	0.622419	1.296307	0.004406
C	1.921698	0.679874	0.008323
C	1.921592	-0.680349	0.010668
C	0.622207	-1.296616	0.008977
C	-0.607976	-1.296322	0.006337
C	-1.907337	-0.679876	0.002169
C	-1.907206	0.680356	-0.000168
H	2.841827	1.245190	0.009328
H	2.841642	-1.245784	0.013581
H	-2.827457	-1.245200	0.001018
H	-2.827219	1.245848	-0.003275

4b, 4c

1,2-Diethynylcycloocta-1,5-dien-3,7-diyne

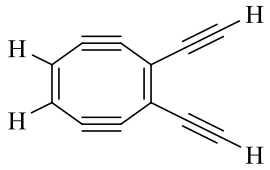

Charge	Multiplicity	Theory/Basis Set	Full Point Group
0	1	MP2/cc-pVTZ	C_{2v}

Zero-point Energy	Electronic Energy	Electronic and Zero-Point Energy	Dipole Moment (D)
0.101343	-458.363501	-458.262166	0.2331

$\Delta H_{(298)}$	$\Delta G_{(298)}$
-458.25042	-458.298199

(Energies in Hartrees/particle)

Atom	Coordinates (Angstroms)		
	X	Y	Z
C	-0.650255	1.288915	0.001508
C	0.580711	1.293800	0.004272
C	1.877761	0.680861	0.008256
C	1.877614	-0.681256	0.010616
C	0.580431	-1.293923	0.008757
C	-0.650534	-1.288781	0.005976
C	-1.958079	-0.694199	0.002000
C	-1.957928	0.694607	-0.000407
H	2.797547	1.246583	0.009346
H	2.797277	-1.247170	0.013668
C	-3.149454	1.451036	-0.004401
C	-3.149767	-1.450379	0.000627
C	-4.174427	2.112251	-0.007856
H	-5.068551	2.685410	-0.010863
C	-4.174883	-2.111379	-0.000536
H	-5.069132	-2.684351	-0.001557

4c

*Same as **4b***

4d

1,2,5,6-Tetraethynylcycloocta-1,5-dien-3,7-diyne

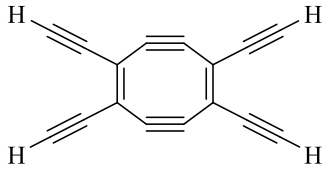

Charge	Multiplicity	Theory/Basis Set	Full Point Group
0	1	MP2/cc-pVTZ	D_{2h}

Zero-point Energy	Electronic Energy	Electronic and Zero-Point Energy	Dipole Moment (D)
0.117873	-610.343230	-610.225357	0.0006

$\Delta H_{(298)}$	$\Delta G_{(298)}$
-610.209071	-610.267376

(Energies in Hartrees/particle)

Atom	Coordinates (Angstroms)		
	X	Y	Z
C	-0.615957	1.286855	0.000009
C	0.615955	1.286856	0.000001
C	1.921352	0.695593	-0.000012
C	1.921353	-0.695596	-0.000026
C	0.615956	-1.286860	-0.000024
C	-0.615956	-1.286860	-0.000016
C	-1.921355	-0.695596	-0.000001
C	-1.921355	0.695590	0.000012
C	-3.112491	1.451684	0.000026
C	-3.112490	-1.451690	-0.000002
C	-4.138544	2.111218	0.000046
H	-5.033103	2.683990	0.000156
C	-4.138547	-2.111218	0.000000
H	-5.033167	-2.683894	0.000034
C	3.112489	1.451682	-0.000014
C	4.138547	2.111210	-0.000010
H	5.033121	2.683957	0.000050
C	3.112490	-1.451685	-0.000045
C	4.138551	-2.111207	-0.000031
H	5.033165	-2.683893	0.000283

5a

*Same as **1b***

5b

*Same as **1d***

5c

*Same as **1d***

5d

Deca-1,3,5,7,9-pentayne

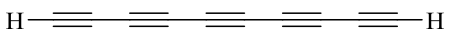

Charge	Multiplicity	Theory/Basis Set	Full Point Group
0	1	MP2/cc-pVTZ	$D_{\infty h}$
Zero-point Energy	**Electronic Energy**	**Electronic and Zero-Point Energy**	**Dipole Moment (D)**
0.064895	-381.147001	-381.082114	0.0000
$\Delta H_{(298)}$	**$\Delta G_{(298)}$**	(Energies in Hartrees/particle)	
-381.07062	-381.115332		

Atom	Coordinates (Angstroms)		
	X	Y	Z
C	0.000000	0.000000	5.778218
C	0.000000	0.000000	4.554099
C	0.000000	0.000000	3.199554
C	0.000000	0.000000	1.962561
C	0.000000	0.000000	0.620134
C	0.000000	0.000000	-0.620134
C	0.000000	0.000000	-1.962561
C	0.000000	0.000000	-3.199554
C	0.000000	0.000000	-4.554099
C	0.000000	0.000000	-5.778218
H	0.000000	0.000000	-6.840807
H	0.000000	0.000000	6.840807

TS1/5–6a

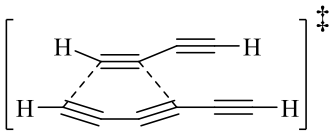

Charge	Multiplicity	Theory/Basis Set	Full Point Group
0	1	MP2/cc-pVTZ	C_s
Zero-point Energy	**Electronic Energy**	**Electronic and Zero-Point Energy**	**Dipole Moment (D)**
0.084385	-382.255699	-382.171314	1.3060
$\Delta H_{(298)}$	**$\Delta G_{(298)}$**	(Energies in Hartrees/particle)	**Imaginary Frequency (cm^{-1})**
-382.160013	-382.206382		367.4296

Atom	Coordinates (Angstroms)		
	X	Y	Z
C	-0.958695	-2.839324	0.000000
C	-0.958695	0.488148	0.000000
C	0.963432	-1.807089	0.000000
C	0.963432	-0.544086	0.000000
H	-0.755793	-3.888610	0.000000
C	-1.725505	-1.836579	0.000000
C	-1.725505	-0.514596	0.000000
C	-0.778028	1.848625	0.000000
C	-0.585642	3.055540	0.000000
H	-0.439343	4.107478	0.000000
H	1.523032	-2.717192	0.000000
C	1.768614	0.578745	0.000000
C	2.465742	1.581242	0.000000
H	3.097198	2.434568	0.000000

TS1/5–6c

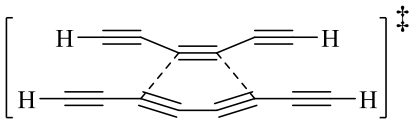

Charge	Multiplicity	Theory/Basis Set	Full Point Group
0	1	MP2/cc-pVTZ	C_{2v}
Zero-point Energy	**Electronic Energy**	**Electronic and Zero-Point Energy**	**Dipole Moment (D)**
0.101967	-534.249058	-534.147091	1.2338
$\Delta H_{(298)}$	**$\Delta G_{(298)}$**	(Energies in Hartrees/particle)	**Imaginary Frequency (cm^{-1})**
-534.132102	-534.186743		412.4567

Atom	Coordinates (Angstroms)		
	X	Y	Z
C	0.000000	1.666236	-1.203133
C	0.000000	0.654969	-1.976117
C	0.000000	-0.654969	-1.976117
C	0.000000	-1.666236	-1.203133
C	0.000000	-3.018515	-0.993783
C	0.000000	-4.215824	-0.741977
H	0.000000	-5.261575	-0.554592
C	0.000000	3.018515	-0.993783
C	0.000000	4.215824	-0.741977
H	0.000000	5.261575	-0.554592
C	0.000000	-0.641230	0.680141
C	0.000000	0.641230	0.680141
C	0.000000	1.710391	1.544491
C	0.000000	2.682448	2.287980
H	0.000000	3.497418	2.968985
C	0.000000	-1.710391	1.544491
C	0.000000	-2.682448	2.287980
H	0.000000	-3.497418	2.968985

6a

3,4-Diethynyl-1,2-didehydrobenzene

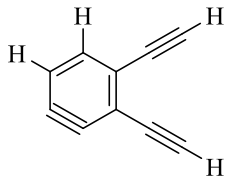

Charge	Multiplicity	Theory/Basis Set	Full Point Group
0	1	MP2/cc-pVTZ	C_s

Zero-point Energy	Electronic Energy	Electronic and Zero-Point Energy	Dipole Moment (D)
0.092756	-382.389139	-382.296383	1.5641

$\Delta H_{(298)}$	$\Delta G_{(298)}$	(Energies in Hartrees/particle)
-382.286827	-382.329681	

Atom	Coordinates (Angstroms)		
	X	Y	Z
C	0.000000	1.508585	-0.117244
C	0.000000	0.667791	-1.223788
C	0.000000	-0.592261	-1.220825
C	0.000000	-1.430761	-0.114686
C	0.000000	-0.678997	1.067539
C	0.000000	0.736953	1.086273
H	0.000000	-1.192333	2.020727
H	0.000000	-2.510394	-0.114468
C	0.000000	2.925793	-0.110831
C	0.000000	4.143665	-0.103147
H	0.000000	5.205444	-0.095703
C	0.000000	1.416881	2.337800
C	0.000000	2.002290	3.405859
H	0.000000	2.517038	4.334520

6b

3,4-di(buta-1,3-diynyl)-1,2-didehydrobenzene

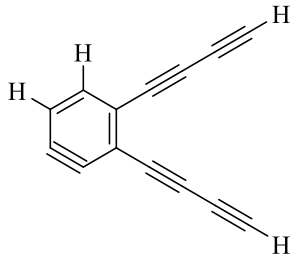

Charge	Multiplicity	Theory/Basis Set	Full Point Group
0	1	MP2/cc-pVTZ	C_s
Zero-point Energy	**Electronic Energy**	**Electronic and Zero-Point Energy**	**Dipole Moment (D)**
0.111879	-534.383930	-534.272051	1.4785
$\Delta H_{(298)}$	**$\Delta G_{(298)}$**	(Energies in Hartrees/particle)	
-534.258380	-534.312209		

Atom	Coordinates (Angstroms)		
	X	Y	Z
C	-1.017559	-0.927015	0.000000
C	-2.231495	-1.606108	0.000000
C	-3.383985	-1.096945	0.000000
C	-3.712050	0.252870	0.000000
C	-2.552668	1.038405	0.000000
C	-1.245659	0.489713	0.000000
H	-2.643410	2.117374	0.000000
H	-4.702397	0.682838	0.000000
C	0.282772	-1.468965	0.000000
C	1.426574	-1.917952	0.000000
C	-0.120319	1.348919	0.000000
C	0.873686	2.070860	0.000000
C	2.693233	-2.413683	0.000000
C	3.832039	-2.857607	0.000000
H	4.821631	-3.243229	-0.000001
C	1.974522	2.871148	0.000000
C	2.964159	3.588392	0.000000
H	3.824677	4.210825	-0.000004

6c

3,4,5,6-Tetraethynyl-1,2-didehydrobenzene

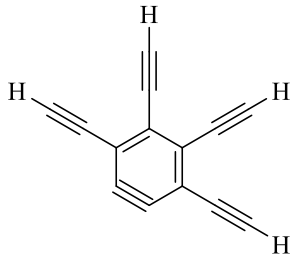

Charge	Multiplicity	Theory/Basis Set	Full Point Group
0	1	MP2/cc-pVTZ	C_{2v}

Zero-point Energy	Electronic Energy	Electronic and Zero-Point Energy	Dipole Moment (D)
0.109079	-534.366717	-534.257638	1.6943

$\Delta H_{(298)}$	$\Delta G_{(298)}$
-534.243517	-534.296092

(Energies in Hartrees/particle)

Atom	Coordinates (Angstroms)		
	X	Y	Z
C	0.000000	1.477324	-0.925307
C	0.000000	0.629053	-2.026850
C	0.000000	-0.629053	-2.026850
C	0.000000	-1.477324	-0.925307
C	0.000000	-0.714050	0.281843
C	0.000000	0.714050	0.281843
C	0.000000	1.405329	1.522117
C	0.000000	2.014724	2.577389
H	0.000000	2.540990	3.499865
C	0.000000	-1.405329	1.522117
C	0.000000	-2.014724	2.577389
H	0.000000	-2.540990	3.499865
C	0.000000	-2.892120	-0.927826
C	0.000000	-4.110441	-0.929590
H	0.000000	-5.172448	-0.930520
C	0.000000	2.892120	-0.927826
C	0.000000	4.110441	-0.929590
H	0.000000	5.172448	-0.930520

6d

3,4-di(buta-1,3-diynyl)-5,6-diethynyl-1,2-didehydrobenzene

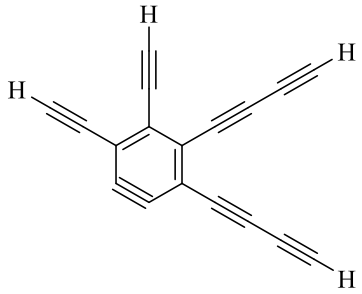

Charge	Multiplicity	Theory/Basis Set	Full Point Group
0	1	MP2/cc-pVTZ	C_s

Zero-point Energy	Electronic Energy	Electronic and Zero-Point Energy	Dipole Moment (D)
0.128176	-686.362493	-686.234317	1.6970

$\Delta H_{(298)}$	$\Delta G_{(298)}$
-686.216041	-686.280277

(Energies in Hartrees/particle)

Atom	Coordinates (Angstroms)		
	X	Y	Z
C	-1.402953	0.027434	0.000000
C	-2.137518	1.209417	0.000000
C	-1.693781	2.386717	0.000000
C	-0.364193	2.797610	0.000000
C	0.500325	1.661282	0.000000
C	0.000000	0.322742	0.000000
C	0.909654	-0.756025	0.000000
C	1.679290	-1.714927	0.000000
C	1.904595	1.865836	0.000000
C	3.109342	2.050825	0.000000
H	4.160370	2.204751	0.000000
C	0.128283	4.122927	0.000000
C	0.555118	5.264228	0.000000
H	0.927043	6.259083	0.000000
C	-1.880338	-1.294768	0.000000
C	-2.274366	-2.459454	0.000000
C	-2.708239	-3.747698	0.000000
C	-3.097299	-4.906668	0.000000
H	-3.435080	-5.913726	0.000000
C	2.534099	-2.771967	0.000000
C	3.301304	-3.724015	0.000000
H	3.967736	-4.551077	0.000000

TS6–7a

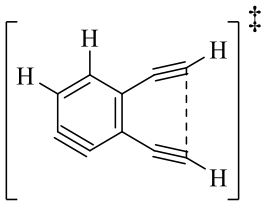

Charge	Multiplicity	Theory/Basis Set	Full Point Group
0	1	MP2/cc-pVTZ	C_S
Zero-point Energy	**Electronic Energy**	**Electronic and Zero-Point Energy**	**Dipole Moment (D)**
0.093144	-382.353579	-382.260435	2.0373
$\Delta H_{(298)}$	**$\Delta G_{(298)}$**	(Energies in Hartrees/particle)	**Imaginary Frequency (cm^{-1})**
-382.252372	-382.291779		569.5936

Atom	Coordinates (Angstroms)		
	X	Y	Z
C	-1.165650	1.447277	0.000000
C	0.000000	0.638286	0.000000
C	-2.467034	0.939702	0.000000
C	-0.098937	-0.856752	0.000000
H	-3.337185	1.578559	0.000000
C	-2.444784	-0.450321	0.000000
C	1.085755	-1.591740	0.000000
C	-1.439273	-1.205189	0.000000
C	2.324202	-1.332229	0.000000
H	3.330681	-1.694609	0.000000
H	-1.019857	2.519487	0.000000
C	1.301152	1.150785	0.000000
C	2.486170	0.708221	0.000000
H	3.536756	0.908320	0.000000

TS6–7b

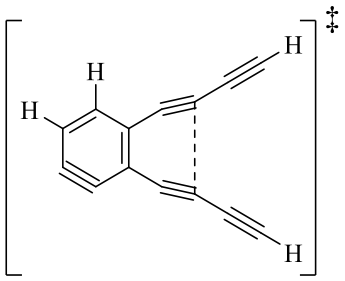

Charge	Multiplicity	Theory/Basis Set	Full Point Group
0	1	MP2/cc-pVTZ	C_s
Zero-point Energy	**Electronic Energy**	**Electronic and Zero-Point Energy**	**Dipole Moment (D)**
0.111545	-534.342555	-534.231010	1.8661
$\Delta H_{(298)}$	**$\Delta G_{(298)}$**	(Energies in Hartrees/particle)	**Imaginary Frequency (cm^{-1})**
-534.21871	-534.267927		615.1327

Atom	Coordinates (Angstroms)		
	X	Y	Z
C	-2.588534	1.239821	0.000116
C	-1.316867	0.602451	0.000111
C	-3.805182	0.558092	-0.000045
C	-1.208966	-0.912552	-0.000105
H	-4.754942	1.071225	-0.000042
C	-3.591616	-0.817667	-0.000102
C	0.052621	-1.470575	-0.000022
C	-2.494094	-1.428980	-0.000104
C	1.256756	-1.006837	0.000015
H	-2.590235	2.322003	0.000204
C	-0.112123	1.282896	0.000108
C	1.138966	0.968201	0.000114
C	2.416024	1.495103	0.000097
C	3.561416	1.920238	-0.000325
H	4.549152	2.310275	-0.000285
C	2.585496	-1.383046	0.000041
C	3.772395	-1.673112	0.000099
H	4.798274	-1.947714	0.000129

TS6–7c

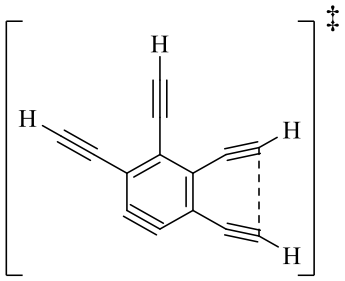

Charge	Multiplicity	Theory/Basis Set	Full Point Group
0	1	MP2/cc-pVTZ	C_s
Zero-point Energy	**Electronic Energy**	**Electronic and Zero-Point Energy**	**Dipole Moment (D)**
0.109611	-534.331267	-534.221656	2.2667
$\Delta H_{(298)}$	**$\Delta G_{(298)}$**	(Energies in Hartrees/particle)	**Imaginary Frequency (cm^{-1})**
-534.209053	-534.258812		572.2312

Atom	Coordinates (Angstroms)		
	X	Y	Z
C	-0.718904	0.331992	-0.000234
C	0.705034	0.211308	-0.000192
C	-1.591932	-0.791879	0.000179
C	1.376579	-1.123063	-0.000786
C	-0.851354	-1.971740	-0.000115
C	2.767954	-1.157132	-0.000385
C	0.397002	-2.103316	-0.000322
C	3.705047	-0.306366	0.000429
H	4.757032	-0.110902	0.000692
C	1.556753	1.317104	0.000195
C	2.806186	1.527742	0.000906
H	3.612499	2.230712	0.000830
C	-1.285278	1.635652	-0.000427
C	-1.797178	2.741596	-0.000659
H	-2.233366	3.709822	-0.000849
C	-3.000414	-0.659809	0.000439
C	-4.213682	-0.548714	0.000704
H	-5.271046	-0.449892	0.000935

TS6–7d

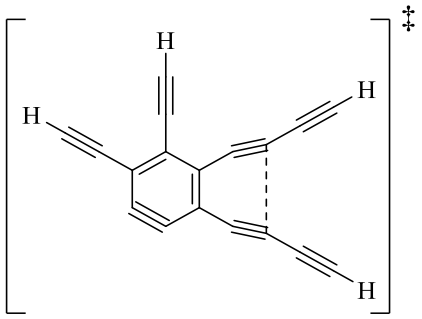

Charge	Multiplicity	Theory/Basis Set	Full Point Group
0	1	MP2/cc-pVTZ	C_s
Zero-point Energy	**Electronic Energy**	**Electronic and Zero-Point Energy**	**Dipole Moment (D)**
0.127971	-686.320807	-686.192836	2.2073
$\Delta H_{(298)}$	**$\Delta G_{(298)}$**	(Energies in Hartrees/particle)	**Imaginary Frequency (cm^{-1})**
-686.175945	-686.235507		622.053

Atom	Coordinates (Angstroms)		
	X	**Y**	**Z**
C	1.798976	0.307225	0.000026
C	0.409167	-0.039133	-0.000011
C	2.841573	-0.659059	-0.000142
C	-0.040948	-1.484709	-0.000239
C	2.301766	-1.945537	-0.000342
C	-1.393787	-1.739189	-0.000261
C	1.093103	-2.281078	-0.000381
C	-2.462695	-1.014933	-0.000129
C	-0.597888	0.906292	0.000153
C	-1.891007	0.873238	0.000165
C	-3.015950	1.673221	0.000308
C	-4.036368	2.345929	0.000426
H	-4.910007	2.949885	0.000536
C	-3.841069	-1.085176	-0.000120
C	-5.062948	-1.103782	-0.000105
H	-6.124368	-1.142954	-0.000096
C	4.208789	-0.300079	-0.000095
C	5.388123	0.006749	-0.000055
H	6.415474	0.276090	-0.000019
C	2.143047	1.685542	0.000233
C	2.471002	2.859544	0.000407
H	2.741590	3.886597	0.000559

7a

1,2,5,8-Tetradehydronaphthalene

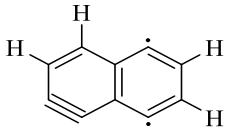

Charge	Multiplicity	Theory/Basis Set	Full Point Group
0	1	MP2/cc-pVTZ	C_s
Zero-point Energy	**Electronic Energy**	**Electronic and Zero-Point Energy**	**Dipole Moment (D)**
0.133465	-382.397318	-382.263853	1.8638
$\Delta H_{(298)}$	**$\Delta G_{(298)}$**	(Energies in Hartrees/particle)	
-382.256699	-382.294597		

Atom	Coordinates (Angstroms)		
	X	Y	Z
C	-1.208993	1.405694	0.000000
C	0.000000	0.634794	0.000000
C	-2.480637	0.850205	0.000000
C	-0.047533	-0.870241	0.000000
H	-3.372929	1.458308	0.000000
C	-2.423320	-0.549516	0.000000
C	1.146021	-1.569534	0.000000
C	-1.386215	-1.257228	0.000000
C	2.359109	-0.936108	0.000000
H	3.300193	-1.469336	0.000000
H	-1.101132	2.482938	0.000000
C	1.255662	1.225433	0.000000
C	2.415299	0.496270	0.000000
H	3.397506	0.949474	0.000000

7b

6,7-Diethynyl-1,2,5,8-tetradehydronaphthalene

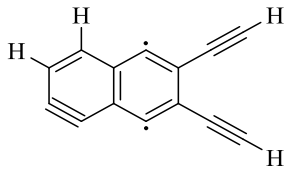

Charge	Multiplicity	Theory/Basis Set	Full Point Group
0	1	MP2/cc-pVTZ	C_s

Zero-point Energy	Electronic Energy	Electronic and Zero-Point Energy	Dipole Moment (D)
0.153654	-534.372380	-534.218725	1.7612

$\Delta H_{(298)}$	$\Delta G_{(298)}$	(Energies in Hartrees/particle)
-534.207254	-534.255084	

Atom	Coordinates (Angstroms)		
	X	Y	Z
C	-2.462795	1.387021	0.000000
C	-1.225110	0.661655	0.000000
C	-3.709838	0.778585	0.000000
C	-1.210348	-0.833319	0.000000
H	-4.626483	1.349448	0.000000
C	-3.596907	-0.619284	0.000000
C	0.006549	-1.488725	0.000000
C	-2.530471	-1.282008	0.000000
C	1.209629	-0.816150	0.000000
H	-2.397733	2.467784	0.000000
C	0.000000	1.310812	0.000000
C	1.205702	0.641738	0.000000
C	2.460918	-1.487676	0.000000
C	3.538706	-2.055110	0.000000
H	4.476249	-2.553714	0.000000
C	2.457967	1.313284	0.000000
C	3.535303	1.881667	0.000000
H	4.472130	2.381534	0.000000

7c

3,4-Diethynyl-1,2,5,8-tetradehydronaphthalene

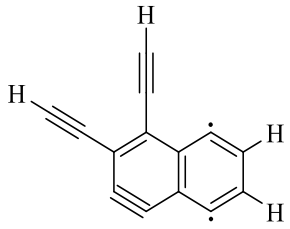

Charge	Multiplicity	Theory/Basis Set	Full Point Group
0	1	MP2/cc-pVTZ	C_s
Zero-point Energy	**Electronic Energy**	**Electronic and Zero-Point Energy**	**Dipole Moment (D)**
0.155138	-534.376362	-534.221224	2.0202
$\Delta H_{(298)}$	**$\Delta G_{(298)}$**	(Energies in Hartrees/particle)	
-534.209537	-534.257777		

Atom	Coordinates (Angstroms)		
	X	Y	Z
C	0.300610	1.737859	0.000000
C	-0.524098	0.587951	0.000000
C	0.000000	-0.757682	0.000000
C	1.475493	-1.010636	0.000000
C	2.132484	0.218570	0.000000
C	1.656237	1.379009	0.000000
C	1.912823	-2.321228	0.000000
C	1.050373	-3.385238	0.000000
C	-0.356920	-3.141979	0.000000
C	-0.850452	-1.857573	0.000000
H	-1.003439	-4.009828	0.000000
H	1.388078	-4.412641	0.000000
C	-0.228446	3.050452	0.000000
C	-0.678650	4.182772	0.000000
H	-1.073685	5.168488	0.000000
C	-1.934426	0.754116	0.000000
C	-3.141189	0.928064	0.000000
H	-4.193991	1.067236	0.000000

7d

3,4,6,7-tetraethynyl-1,2,5,8-tetradehydronaphthalene

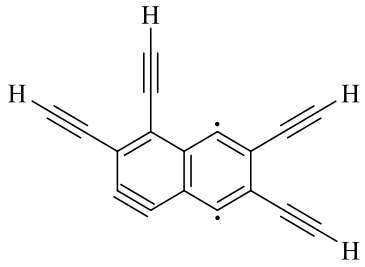

Charge	Multiplicity	Theory/Basis Set	Full Point Group
0	1	MP2/cc-pVTZ	C_s
Zero-point Energy	**Electronic Energy**	**Electronic and Zero-Point Energy**	**Dipole Moment (D)**
0.233121	-686.351769	-686.118648	1.7902
$\Delta H_{(298)}$	**$\Delta G_{(298)}$**	(Energies in Hartrees/particle)	
-686.102453	-686.161260		

Atom	Coordinates (Angstroms)		
	X	Y	Z
C	2.794722	0.673762	-0.000015
C	1.764335	-0.296622	-0.000021
C	0.362262	0.049514	-0.000012
C	-0.081465	1.468292	-0.000003
C	1.046253	2.288492	0.000001
C	2.260209	1.971857	-0.000001
C	-1.436471	1.734046	0.000006
C	-2.394803	0.741103	0.000009
C	-1.959126	-0.643739	0.000013
C	-0.607131	-0.945993	-0.000009
C	4.164567	0.321611	-0.000005
C	5.345714	0.021489	0.000020
H	6.374674	-0.241567	0.000031
C	2.109377	-1.673423	-0.000014
C	2.430461	-2.849717	-0.000016
H	2.696757	-3.877970	0.000006
C	-2.959009	-1.653847	0.000020
C	-3.822147	-2.513661	0.000023
H	-4.569376	-3.268187	0.000030
C	-3.785043	1.027204	-0.000003
C	-4.979610	1.265046	-0.000005
H	-6.020630	1.475248	-0.000008

TS7–8a

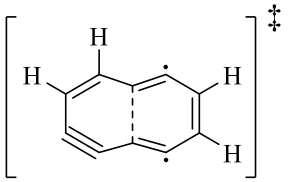

Charge	Multiplicity	Theory/Basis Set	Full Point Group
0	1	MP2/cc-pVTZ	C_s
Zero-point Energy	**Electronic Energy**	**Electronic and Zero-Point Energy**	**Dipole Moment (D)**
0.096577	-382.376294	-382.279717	2.0070
$\Delta H_{(298)}$	**$\Delta G_{(298)}$**	(Energies in Hartrees/particle)	**Imaginary Frequency (cm^{-1})**
-382.272148	-382.310751		607.1488

Atom	Coordinates (Angstroms)		
	X	Y	Z
C	-0.014280	0.012989	-0.000005
C	1.229012	0.635001	-0.000002
C	2.484322	-0.005104	0.000004
C	2.441858	-1.978685	0.000009
C	1.104984	-2.090502	0.000012
C	0.065611	-1.380295	0.000007
C	3.667522	-2.447353	0.000002
C	4.870844	-1.816236	0.000001
C	4.914383	-0.373987	-0.000001
C	3.753449	0.335532	0.000008
H	5.899176	0.071260	-0.000006
H	5.825051	-2.323856	-0.000009
H	1.264357	1.718171	-0.000006
H	-0.925766	0.592279	-0.000015

TS7–8b

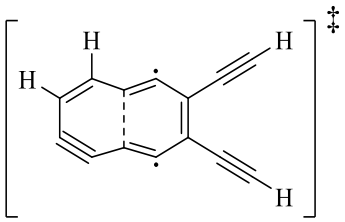

Charge	Multiplicity	Theory/Basis Set	Full Point Group
0	1	MP2/cc-pVTZ	C_s
Zero-point Energy	**Electronic Energy**	**Electronic and Zero-Point Energy**	**Dipole Moment (D)**
0.113158	-534.350463	-534.237305	1.9896
$\Delta H_{(298)}$	**$\Delta G_{(298)}$**	(Energies in Hartrees/particle)	**Imaginary Frequency (cm^{-1})**
-534.225199	-534.274105		627.5896

Atom	Coordinates (Angstroms)		
	X	Y	Z
C	-3.788378	0.528854	0.000060
C	-2.621212	1.281993	0.000013
C	-1.301658	0.780515	0.000120
C	-1.125910	-1.168874	0.000032
C	-2.441372	-1.436811	-0.000241
C	-3.553707	-0.848459	-0.000015
C	0.141023	-1.499834	-0.000134
C	1.285092	-0.755648	-0.000147
C	1.163975	0.716037	-0.000048
C	-0.084968	1.271257	0.000201
H	-2.700292	2.362904	0.000195
H	-4.758328	1.003754	0.000298
C	2.365355	1.468052	-0.000027
C	3.402349	2.107600	-0.000164
H	4.304929	2.666971	-0.000310
C	2.589344	-1.308150	0.000010
C	3.713559	-1.777399	0.000229
H	4.692749	-2.188414	0.000494

TS7–8c

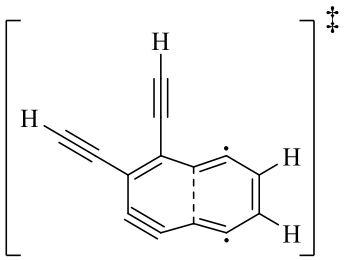

Charge	Multiplicity	Theory/Basis Set	Full Point Group
0	1	MP2/cc-pVTZ	C_s
Zero-point Energy	**Electronic Energy**	**Electronic and Zero-Point Energy**	**Dipole Moment (D)**
0.113082	-534.353074	-534.239992	2.0827
$\Delta H_{(298)}$	**$\Delta G_{(298)}$**	(Energies in Hartrees/particle)	**Imaginary Frequency (cm^{-1})**
-534.227890	-534.276830		595.3388

Atom	Coordinates (Angstroms)		
	X	Y	Z
C	1.564804	-0.787347	-0.000027
C	0.773712	0.388645	-0.000254
C	-0.645790	0.418573	-0.000379
C	-1.572148	-1.326284	-0.000457
C	-0.453333	-2.064766	-0.000465
C	0.798913	-1.956157	-0.000145
C	-2.865617	-1.127482	0.000028
C	-3.612346	0.007802	0.000487
C	-2.943291	1.285189	0.000456
C	-1.582194	1.340734	-0.000116
H	-3.585073	2.155153	0.000862
H	-4.692920	0.028444	0.001115
C	1.433507	1.647904	-0.000283
C	2.011323	2.720994	-0.000305
H	2.514140	3.656300	-0.000345
C	2.979387	-0.727791	0.000354
C	4.197292	-0.685518	0.000679
H	5.258540	-0.646873	0.000940

TS7–8d

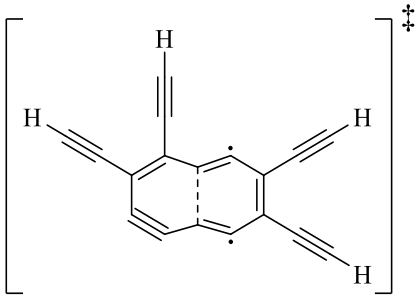

Charge	Multiplicity	Theory/Basis Set	Full Point Group
0	1	MP2/cc-pVTZ	C_s
Zero-point Energy	**Electronic Energy**	**Electronic and Zero-Point Energy**	**Dipole Moment (D)**
0.129583	-686.327474	-686.197892	1.9809
$\Delta H_{(298)}$	**$\Delta G_{(298)}$**	(Energies in Hartrees/particle)	**Imaginary Frequency (cm^{-1})**
-686.18119	-686.240457		616.2097

Atom	Coordinates (Angstroms)		
	X	Y	Z
C	2.799490	-0.677884	0.000164
C	1.824587	0.350546	-0.000001
C	0.417434	0.143804	-0.000173
C	-0.205812	-1.714035	-0.000193
C	1.016070	-2.267032	-0.000328
C	2.233903	-1.957271	0.000125
C	-1.511697	-1.731365	0.000067
C	-2.456120	-0.746116	-0.000082
C	-1.993115	0.656358	-0.000119
C	-0.648385	0.909284	-0.000187
C	2.263181	1.701707	-0.000038
C	2.652717	2.856695	-0.000115
H	2.988529	3.864298	-0.000219
C	4.183743	-0.386275	0.000165
C	5.378048	-0.143112	0.000200
H	6.418418	0.070579	0.000174
C	-3.851200	-0.983057	0.000086
C	-5.053024	-1.182961	0.000186
H	-6.100727	-1.357365	0.000140
C	-2.987421	1.665418	0.000035
C	-3.847611	2.528537	0.000140
H	-4.594943	3.283045	0.000292

8a

Cyclodeca-1,7-diene-3,5,9-triyne

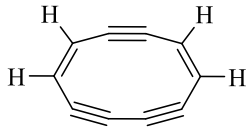

Charge	Multiplicity	Theory/Basis Set	Full Point Group
0	1	MP2/cc-pVTZ	C_{2v}

Zero-point Energy	Electronic Energy	Electronic and Zero-Point Energy	Dipole Moment (D)
0.096006	-382.424980	-382.328974	1.8484

$\Delta H_{(298)}$	$\Delta G_{(298)}$
-382.320169	-382.361117

(Energies in Hartrees/particle)

Atom	Coordinates (Angstroms)		
	X	Y	Z
C	-0.098296	0.033726	0.000358
C	0.960203	0.950023	0.015468
C	2.278483	0.545408	0.014216
C	3.427410	0.063394	0.011682
C	4.639871	-0.593498	0.008144
C	4.727889	-1.990708	-0.009113
H	5.702426	-2.460995	-0.011669
C	3.549127	-2.704959	-0.022249
C	2.296096	-2.732170	-0.026925
C	1.076724	-2.220698	-0.024487
C	0.218107	-1.307710	-0.015738
H	5.559802	-0.019573	0.018432
H	0.725030	2.008469	0.028042
H	-1.116708	0.399408	0.001653

8b, 8c

1,2-Diethynylcyclodeca-1,7-diene-3,5,9-triyne

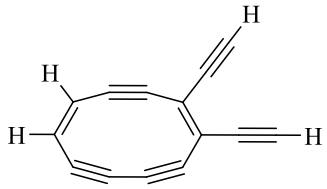

Charge	Multiplicity	Theory/Basis Set	Full Point Group
0	1	MP2/cc-pVTZ	C_s
Zero-point Energy	**Electronic Energy**	**Electronic and Zero-Point Energy**	**Dipole Moment (D)**
0.112972	-534.402199	-534.288338	1.8356
$\Delta H_{(298)}$	**$\Delta G_{(298)}$**	(Energies in Hartrees/particle)	
-534.275023	-534.326392		

Atom	Coordinates (Angstroms)		
	X	**Y**	**Z**
C	-1.379789	-0.744394	0.000068
C	-1.033918	0.612302	0.000119
C	0.279405	1.032729	-0.000350
C	1.497878	1.292919	-0.000567
C	2.868355	1.445805	0.000213
C	3.738350	0.348832	0.000326
H	4.806952	0.519090	0.000512
C	3.178387	-0.910631	0.000091
C	2.165186	-1.648380	-0.000124
C	0.872059	-1.924605	-0.000144
C	-0.354133	-1.665181	-0.000113
H	3.295937	2.442270	0.000224
C	-2.078089	1.574513	0.000079
C	-2.974214	2.400299	0.000044
H	-3.755208	3.119991	0.000014
C	-2.750917	-1.113379	0.000094
C	-3.927642	-1.430049	0.000116
H	-4.953186	-1.706034	0.000135

8c

*Same as **8b***

8d

1,2,7,8-Tetraethynylcyclodeca-1,7-diene-3,5,9-triyne

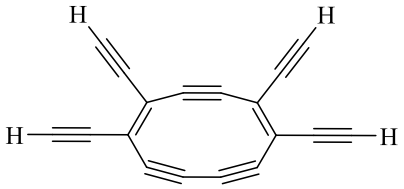

Charge	Multiplicity	Theory/Basis Set	Full Point Group
0	1	MP2/cc-pVTZ	C_{2v}
Zero-point Energy	**Electronic Energy**	**Electronic and Zero-Point Energy**	**Dipole Moment (D)**
0.129321	-686.379594	-686.250273	1.8704

$\Delta H_{(298)}$	$\Delta G_{(298)}$
-686.23234	-686.294244

(Energies in Hartrees/particle)

Atom	Coordinates (Angstroms)		
	X	Y	Z
C	2.644009	-0.670417	0.000072
C	2.004593	0.603575	0.000052
C	0.622406	0.689493	0.000012
C	-0.622409	0.689504	-0.000024
C	-2.004595	0.603578	-0.000060
C	-2.644006	-0.670419	-0.000074
C	-1.803153	-1.767382	-0.000049
C	-0.661460	-2.280758	-0.000017
C	0.661467	-2.280756	0.000019
C	1.803161	-1.767382	0.000050
C	-4.058016	-0.772922	-0.000114
C	-5.273634	-0.860625	-0.000137
H	-6.333052	-0.938108	-0.000047
C	-2.786564	1.789596	-0.000085
C	-3.454095	2.809501	-0.000104
H	-4.036746	3.697642	-0.000098
C	2.786555	1.789599	0.000069
C	3.454077	2.809509	0.000089
H	4.036786	3.697613	0.000152
C	4.058020	-0.772917	0.000111
C	5.273638	-0.860621	0.000149
H	6.333058	-0.938073	0.000235

Chapter 7: *Ab initio* Predictions of Higher Order Vibration-Rotation Coupling Constants for Rotational Spectroscopy

Unpublished work with contributions from Brian J. Esselman, R. Claude Woods, and Robert J. McMahon

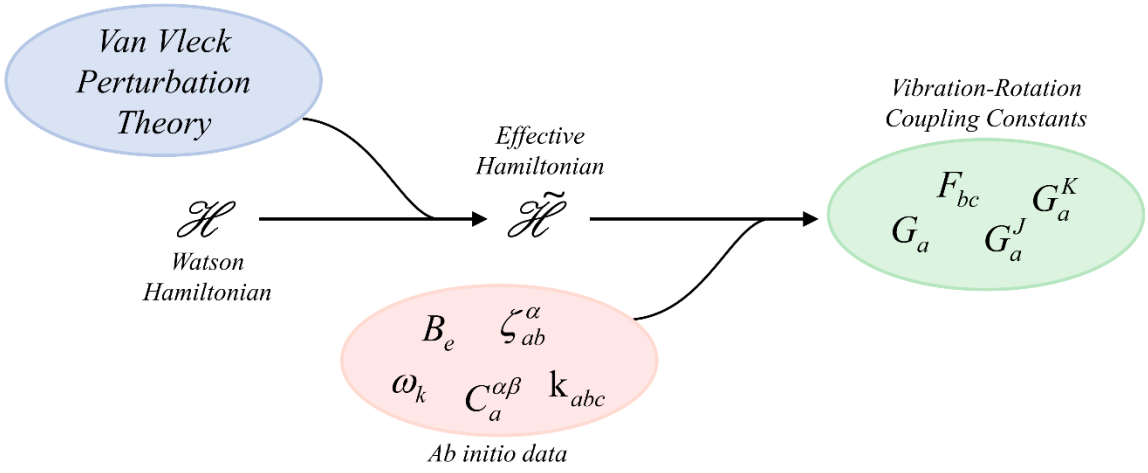

ABSTRACT

The theoretical framework for the prediction of higher order vibration-rotation coupling constants has been known for some time – including derivations of formulas for several low order constants – but to date there has been no implementation of the theory for routine application to vibration-rotation coupling in rotational spectroscopy. We have thus used established theory to derive analytic expressions for the second order Coriolis coupling constants F_{bc}, F_{ac}, and F_{ab} through the use of contact transformations *i.e.*, Van Vleck perturbation theory, including defining rotational reductions to obtain results directly comparable to experiment. In doing so, we have endeavored to make the theoretical framework more accessible for the broader rotational spectroscopy community. We then used the results of a CCSD(T)/ANO0 anharmonic frequency calculation on benzonitrile to obtain theoretical predictions of the coupling constants for comparison to the recent coupled-state fits of the lowest dyad and triad of benzonitrile. We found the predictions to be within 15% of the experimentally determined values and determined the origin of the multiplicative relationship between the coupling constants of the dyad and those of the triad. We also present preliminary results of a computer-aided derivation program we are developing with the goal of more easily extending the theoretical framework to higher order coupling constants and to facilitate numeric predictions. Lastly, we discuss implications of the results on experimental efforts of fitting rotational spectra of coupled vibrational states, and on the derivation of higher order coupling constants.

INTRODUCTION

Our group has taken advantage of VPT2 calculations to obtain theoretical predictions of various constants relevant to the fitting of rotational spectra: vibrational α corrections to the ground

state rotational constants, rotational constants of vibrationally excited states and the ground states of isotopologues, and quartic and sextic centrifugal distortion constants. These *ab initio* constants can be used to predict the rotational spectra to aid in the search for transitions, and agreement of the final experimentally determined constants with the theoretical predictions provides confidence that the fit can be used for accurate prediction of transitions outside of the original frequency range. While these *ab initio* predictions of the rotational constants are useful, they are only comparable to experiment if vibration-rotation coupling is absent or, alternatively, if the coupling has been suitably accounted for. The vibrational ground state of a molecule, barring the presence of a large-amplitude motion such as an internal rotor, typically lacks vibration-rotation coupling to other vibrational states. As we consider the excited vibrational states, however, the likelihood of vibrational states being coupled to one another increases with increasing energy.

Successful coupled state fits have generally been limited to dyads of fundamental states for which the coupling is typically well described by a first-order Coriolis coupling constant, which is proportional to the Coriolis zeta (ζ) coupling constant. The *ab initio* predictions of the two vibrational states in question will generally be in good agreement with the experimentally determined constants obtained from a coupled state fit in which the first order Coriolis coupling constants G_α are adequately determined. Other vibrational states, however, may be coupled to one or more other vibrational states *via* higher-order coupling constants. The fitting of such spectra can be a monumental task due to the complex interplay of the coupling constants and their effect on the rotational transitions. Furthermore, the lack of theoretical predictions for the higher-order coupling constants means there is no point of reference for assessing the quality of the fit.

Our goal in analyzing rotational spectra is to obtain fits that are predictive and physically meaningful. We consider a fit to be predictive if we can accurately predict spectra outside of the

original frequency window of the spectra being fitted. For example, if a fit was determined from the measurement of the rotational spectra from 100–300 GHz, it is predictive if the fitted constants can accurately determine the frequency of transitions <100 GHz and >300 GHz. The broad applicability of a fit to spectra outside of the original frequency range gives us confidence that we are at least sufficiently modeling the vibrational and rotational quantum mechanics of the molecule. This in turn makes it likely that the fit is also physically meaningful, but not necessarily so. We consider a predictive fit to also be physically meaningful if the determined constants are in good agreement with theoretical calculations and if the fit is stable *i.e.*, changes very little, upon the addition of more data. In such a case, we believe the constants are not just empirical values devoid of meaning, but are accurate representations of the quantum structure of the molecule. We can then have confidence that constants resulting from the fit can be used in broader contexts for the study of that particular molecule. In summation, a predictive fit is not necessarily physically meaningful, but a physically meaningful fit can be expected to be highly predictive.

This discussion on the nature of the fits of rotational spectra is particularly important in the context of astrochemistry. Rotational spectra obtained from astronomical observations are often outside of the frequency range of laboratory spectra, and a highly predictive fit can be used for identifying transitions of a molecule in such spectra. Furthermore, the astronomical application of fits of laboratory spectra is not limited to ground vibrational states, as molecules in astronomical sources can be vibrationally excited. Thus, accurate fits of the rotational spectra of vibrationally excited states are important for determining the abundance and local conditions of a molecule in an astronomical source, especially if the observed spectra are outside of the frequency range of the laboratory data. Since a molecule's vibrational states are more than likely coupled to one another,

having accurate *ab initio* predictions of vibration-rotation coupling is essential for obtaining high quality and physically meaningful coupled-state fits.

The theoretical framework for predicting vibration-rotation coupling constants has been known since the 1980s, as it is closely related to the theory for the prediction of centrifugal distortion constants and other molecular parameters.[1-4] There are even several works that contain derived formulas that in principle can be used to calculate some of these coupling constants.[3-5] Yet, there are very few examples of the application of these formulas, and to our knowledge no methodology for routine application to such predictions has been developed. We suspect there are several reasons why this is the case, owing to the state of the field several decades ago. First, high-quality rotational spectra of vibrationally coupled states and corresponding coupled-state fits were largely limited to di- and triatomic molecules. The quality and quantity of the spectra was limited by the frequency range and resolution obtainable by laboratory instruments at the time. Furthermore, the processing and analysis of enough data to obtain the higher order coupling constants requires considerable computational resources, as well as software that can process the voluminous amounts of data. Second, the process of deriving the requisite formulas is even more complex than that for deriving the centrifugal distortion constants. Of the formulas that have been derived, some involve assumptions specific to a particular problem,[3] and none contain the full derivation.[3-5] The complexity of the theory is further increased by the necessity of rotational reductions of higher order constants in order to compare the predictions to experiments. The nature of this reduction differs significantly from the corresponding reduction used to transform the centrifugal distortion constants[2] and while a methodology for conducting such rotational reductions was developed,[6-7] it appears to have mostly been applied to variational fits of high-resolution infrared spectra of triatomic molecules, and ozone in particular (see Ref. 8 and citations

therein). Furthermore, the limited experimental data prevented the assessment of the accuracy of predictions obtained from the theory. Finally, application of the theoretical formulas requires sufficiently accurate *ab initio* data, particularly for the cubic force constants, which in turn would have required considerable computational resources, and so was limited, again, to small molecules. In total, development of the theory for routine prediction of higher order coupling constants was precluded by the instrumental and computational resources of the time, as well as the limited number of experimentally studied cases for which the theory was applicable.

Since the theoretical framework was developed several decades ago, advances in instrumentation have increased the quantity and quality of rotational spectra that can be measured for a molecule, and corresponding advances in computational resources allows for the processing, analysis, and fitting of such data. These advances in turn have led to the fitting of the rotational spectra of numerous coupled vibrational states across molecules of increasing size. The amount of data means that not only can we experimentally determine higher order coupling constants, for many cases we are *required* to include the higher order coupling constants to obtain predictive fits of the spectra. Having reasonable predictions of the coupling constants not only allows us to assess the physical meaningfulness of the fit, but can also constrain the range of possible values over which the constants are allowed to vary. Thus, our goal in this work is to develop a methodology for routinely predicting higher-order vibration-rotation coupling constants for application to coupled-state fits of rotational spectra.

Before we begin, we wish to highlight several important points. First, many of the derivations conducted herein (particularly involving the sequential contact transformations) have been previously done, albeit tersely explained. We report these derivations nonetheless, with the goal of producing a coherent, seamless, and more digestible framework for the broader community

that is not intimately familiar with Van Vleck perturbation theory. Second, in composing this work we uncovered the theoretical origin for the proportional relationship of coupling constants that we had previously observed for the lowest dyad and triad of benzonitrile.[9] In extending the analysis, we found that a similar relationship exists across coupled vibrational states that share the same vibrational modes and selection rules, which has significant implications for the fitting of even higher energy coupled vibrational states. Finally, the rotational reduction of vibration-rotation coupling constants has significant implications in the experimental fitting of the rotational spectra of coupled vibrational states. Foremost of these is that for the higher order coupling constants (on the order of $\mathbf{J}^3$ and higher), there is more than one way in which the reduction can be conducted, leading to the possibility of a choice of which form of the reduction should be used for fitting spectra. This choice of the reduction of the coupling constants is analogous to the situation encountered for the centrifugal distortion constants, in which the choice of terms that are to be eliminated leads to the Asymmetric and Symmetric reductions of the distorted rotor Hamiltonian. The presence of a choice in reduction of the coupling constants in turn begs the question of if and how the choice of reduction for the coupling constants is related to the choice of reduction for the centrifugal distortion constants. To our knowledge, there has been no such consideration in the published fittings of rotational spectra of coupled vibrational states, until now.

COMPUTATIONAL METHODS

All *ab initio* data was taken from anharmonic vibrational calculations conducted using CFOUR[10] and the method of coupled cluster with single, double, and perturbative triple excitations [CCSD(T)] using the ANO0 basis set. The open-source computer algebra package SymPy[11] was used in conjunction with Python 3.6 in our developmental computer-aided derivation program,

vib-rot-Van-Vleck. Additional Python packages utilized by the program are listed in the Supporting Information, along with a brief description of the program and its structure.

METHODOLOGY AND DERIVATIONS

The vibration-rotation coupling constants are derived from application of Van Vleck perturbation theory to the Watson Hamiltonian, in a similar manner to that used to derive the centrifugal distortion constants.[1-4] The full reasoning behind the derivation methodology and how the initial stage is reached is provided elsewhere,[3-4] therefore we provide an overview of the mechanics necessary to obtain theoretical predictions of the coupling constants. The methodology and derivations that follow are for application to asymmetric top rotors.

Ordering the Hamiltonian

To begin, Taylor expansions of the potential energy and the term containing the inverse inertial tensor are applied with respect to the normal coordinate position vibrational operators. The resulting Hamiltonian contains terms with various orders of vibrational and rotational operator products. Terms with *m* vibrational operators and *n* rotational operators are grouped under the label $\mathbf{H}_{mn}$, which is said to have *m* degrees of vibration and *n* degrees of rotation. The Hamiltonian is separated into different orders with regards to the magnitudes of their expectation values for application of perturbation theory. There are several different ways of ordering the Hamiltonian, but we will follow the approach taken by Aliev and Watson[4]: the order of a term $\mathbf{H}_{mn}$ of the Hamiltonian is given by $m+n-2$, with the exception of the rigid rotor $\mathbf{H}_{02}$, which is arbitrarily assigned an order of one. The zeroth order part of the Hamiltonian is then given by $\mathbf{H}_{20}$, which is

simply the harmonic oscillator Hamiltonian in normal coordinates. The Watson Hamiltonian is now given by Eq. (7.1), where λ is the perturbation parameter.

$$\begin{aligned}\mathbf{H} &= \mathbf{H}_0 + \lambda\mathbf{H}_1 + \lambda^2\mathbf{H}_2 + \cdots \\ &= \mathbf{H}_{20} + \lambda(\mathbf{H}_{30} + \mathbf{H}_{21} + \mathbf{H}_{12} + \mathbf{H}_{02}) + \lambda^2(\mathbf{H}_{40} + \mathbf{H}_{31} + \mathbf{H}_{22}) \\ &\quad + \cdots + \lambda^n(\mathbf{H}_{n+2,0} + \mathbf{H}_{n+1,1} + \mathbf{H}_{n2}) + \cdots\end{aligned} \tag{7.1}$$

Contact Transformation

With the vibration-rotation Hamiltonian so ordered, Van Vleck perturbation theory is applied. The Hamiltonian is transformed using an arbitrary Hermitian function $\mathbf{S}$, as given by Eq. (7.2). This transformation can be rewritten in terms of a linear combination of (nested) commutators, as in Eq. (7.3)–(7.5), and the general form of an arbitrary order of the transformed Hamiltonian is given by Eq. (7.6). The transform function is chosen such that the transformed Hamiltonian $\tilde{\mathbf{H}}$ has the desired form, which in the present case is one that leads to a Hamiltonian matrix that is block diagonal with respect to the vibrational states. Use of a transform function that satisfies Eq. (7.7) will accomplish this goal for the term of the transformed Hamiltonian with *m* vibrational degrees and *n* rotational degrees.

$$\tilde{\mathbf{H}} = e^{i\mathbf{S}}\mathbf{H}e^{-i\mathbf{S}} \tag{7.2}$$

$$\tilde{\mathbf{H}}_0 = \mathbf{H}_0 \tag{7.3}$$

$$\tilde{\mathbf{H}}_1 = \mathbf{H}_1 + i\left[\mathbf{S}, \mathbf{H}_0\right] \tag{7.4}$$

$$\tilde{\mathbf{H}}_2 = \mathbf{H}_2 + i\left[\mathbf{S}, \mathbf{H}_1\right] - \frac{1}{2}\left[\mathbf{S}, \left[\mathbf{S}, \mathbf{H}_0\right]\right] \tag{7.5}$$

$$\tilde{\mathbf{H}}_{a\geq 1} = \mathbf{H}_a + \sum_{b=0}^{a-1} \frac{i^{a-b}}{(a-b)!} \underbrace{\left[\mathbf{S}, \left[\mathbf{S}, \ldots, \left[\mathbf{S}, \mathbf{H}_0\right]\ldots\right]\right]}_{a-b \text{ nested commutators}} \tag{7.6}$$

$$\tilde{\mathbf{H}}_{mn}\left(\text{block diagonal}\right) = \mathbf{H}_{mn} + i\left[\mathbf{S}, \mathbf{H}_0\right] \tag{7.7}$$

Sequential Contact Transformation

To obtain the block-diagonal term $\tilde{\mathbf{H}}_{mn}$, all lower order terms must similarly be made block diagonal. While there are many possible ways to transform the Hamiltonian, it has been shown that the resulting formulas are equivalent[12]; the differences lie in the complexity of the derivation to obtain said results.[4, 12] Again, we follow the approach used by Aliev and Watson:[4] the transform functions with the lowest degree in vibration are applied first, in order of increasing degree of rotation, with each subsequent transform function defined by and applied to the result of the previous transformation. This approach minimizes the complexity in the derivations of the desired formulas and the definitions of the requisite transform functions. Once the final transformation has been applied, the Hamiltonian is block diagonal with respect to terms of *m* vibrational and *n* rotational degrees and lower, and the desired vibrational matrix element can be calculated. To distinguish the transformations, we use the notation $\mathbf{H}^{(j)}$ to represent the Hamiltonian after *j* transformations have been applied, and $\mathbf{S}^{(j)}$ is the transform function used to obtain $\mathbf{H}^{(j)}$ *via* Eq. (7.8). Thus, $\mathbf{H}^{(0)}$ is the expanded and ordered Watson Hamiltonian, $\mathbf{H}^{(1)}$ is the Hamiltonian after the first transform function ($\mathbf{S}^{(1)}$) has been applied to $\mathbf{H}^{(0)}$, $\mathbf{H}^{(2)}$ is the Hamiltonian after the second transform function ($\mathbf{S}^{(2)}$) has been applied to $\mathbf{H}^{(1)}$, and so on.

$$\mathbf{H}^{(j)} = e^{i\mathbf{S}^{(j)}}\mathbf{H}^{(j-1)}e^{-i\mathbf{S}^{(j)}} \tag{7.8}$$

The transform function is defined using the previously transformed Hamiltonian as in Eq. (7.9), in accordance with Eq. (7.7), where "b.d." is short for "block diagonal" and the property $\mathbf{H}_0^{(j)} = \mathbf{H}_0$ has been applied. We refer to Eq. (7.9) as the "defining equation" for the transform

function $\mathbf{S}_{mn}^{(j)}$, and we refer to the term $\mathbf{H}_{mn}^{(j-1)}$ within Eq. (7.9) as the "defining part" of the defining equation. We use $\tilde{\mathbf{H}}$ to refer to the final transformed function, that is, for a sequential contact transformation with *k* total transformations, $\tilde{\mathbf{H}} \equiv \mathbf{H}^{(k)}$. When deriving a particular sequential contact transformation, $\mathbf{S}_{mn}$ is used instead of $\mathbf{S}_{mn}^{(j)}$ because the transformation number *j* is implicitly given by the sequence being applied.

$$\mathbf{H}_{mn}^{(j)}\left(\text{b.d.}\right) = \mathbf{H}_{mn}^{(j-1)} + i\left[\mathbf{S}_{mn}^{(j)}, \mathbf{H}_0\right] \tag{7.9}$$

Vibrational and Rotational Commutators

The commutators evaluated during the contact transformation may involve either vibrational operators, rotational operators, or both. Consider a pair of terms $\mathbf{A}_1$ and $\mathbf{A}_2$ each consisting of a coefficient *c*, a vibrational part **V** containing vibrational operators, and a rotational part **R** containing rotational operators. The commutator of these two terms can be expanded and then consolidated into the expression in Eq. (7.10), using the property that the vibrational parts **V** commute with the rotational parts **R**. The commutator, thus, can be written in terms of a vibrational commutator and a rotational commutator in Eq. (7.11), using the definitions in Eq. (7.12). This is the notation used in the works of Papousek and Aliev, and of Aliev and Watson.[3-4]

$$\begin{aligned}\left[\mathbf{A}_1, \mathbf{A}_2\right] &= \left[\mathrm{c}_1\,\mathbf{V}_1\mathbf{R}_1, \mathrm{c}_2\,\mathbf{V}_2\mathbf{R}_2\right] \\ &= \frac{1}{2}\mathrm{c}_1\,\mathrm{c}_2\left[\mathbf{V}_1, \mathbf{V}_2\right]\left(\mathbf{R}_1\mathbf{R}_2 + \mathbf{R}_2\mathbf{R}_1\right) + \frac{1}{2}\mathrm{c}_1\,\mathrm{c}_2\left(\mathbf{V}_1\mathbf{V}_2 + \mathbf{V}_2\mathbf{V}_1\right)\left[\mathbf{R}_1, \mathbf{R}_2\right]\end{aligned} \tag{7.10}$$

$$\left[\mathbf{A}_1, \mathbf{A}_2\right] = \left[\mathbf{A}_1, \mathbf{A}_2\right]_{\mathrm{V}} + \left[\mathbf{A}_1, \mathbf{A}_2\right]_{\mathrm{R}} \tag{7.11}$$

$$\begin{aligned}\left[\mathbf{A}_1,\mathbf{A}_2\right]_{\mathrm{V}} &\equiv \frac{1}{2}c_1c_2\left[\mathbf{V}_1,\mathbf{V}_2\right]\left(\mathbf{R}_1\mathbf{R}_2+\mathbf{R}_2\mathbf{R}_1\right)\\ \left[\mathbf{A}_1,\mathbf{A}_2\right]_{\mathrm{R}} &\equiv \frac{1}{2}c_1c_2\left(\mathbf{V}_1\mathbf{V}_2+\mathbf{V}_2\mathbf{V}_1\right)\left[\mathbf{R}_1,\mathbf{R}_2\right]\end{aligned} \tag{7.12}$$

Selecting Desired Degrees of Vibration and Rotation

In principle, the full Hamiltonian in Eq. (7.1) is subjected to the sequential contact transformations, but in practice this is unnecessary. If the system in question is well described by the perturbation ordering in Eq. (7.1) *i.e.*, the magnitude of terms λ^j is much larger than that of terms λ^{j+1}, then the original and transformed Hamiltonians can be truncated at the order of the desired term. For the sequential contact transformation to obtain the formula for $\tilde{\mathbf{H}}_{mn}$, the full Hamiltonian can be approximated by Eq. (7.13). Furthermore, only terms with *m* vibrational degrees and *n* rotational degrees in the final transformed Hamiltonian contribute to $\tilde{\mathbf{H}}_{mn}$, therefore the formula for $\tilde{\mathbf{H}}_{mn}$ is obtained by selecting the terms with degrees *m* and *n*. We can represent this "selection" using a set of braces, demonstrated by Eq. (7.14). This notation is particularly powerful when applied to commutators generated by the transformation. It can be shown that the "selection braces" can "pass through" a commutator using the formulas in Eq. (7.15) and Eq. (7.16) for vibrational and rotational commutators (respectively) of the transform function $\mathbf{S}_{ab}$ with an unspecified expression $\mathbf{A}$. This process can be applied recursively until the selection braces have reached the original Hamiltonian, at which point they are trivially evaluated by Eq. (7.17). This process eliminates commutators that do not ultimately contribute to the desired degrees in vibration and rotation. Eq. (7.15) and Eq. (7.16) can also be used to simplify the evaluation of defining equations.

$$\mathbf{H}^{(j)} \approx \sum_{p=0}^{m+n-2} \lambda^p \mathbf{H}_p^{(j)} \tag{7.13}$$

$$\begin{aligned} \tilde{\mathbf{H}}_{mn} \equiv \left\{\tilde{\mathbf{H}}\right\}_{mn} &= \left\{\sum_{jk} \tilde{\mathbf{H}}_{jk}\right\}_{mn} \\ &= \sum_{jk} \left\{\tilde{\mathbf{H}}_{jk}\right\}_{mn} \end{aligned} \tag{7.14}$$

$$\left\{\left[\mathbf{S}_{ab}, \mathbf{A}\right]_{\mathrm{V}}\right\}_{mn} = \left[\mathbf{S}_{ab}, \left\{\mathbf{A}\right\}_{m-a+2,n-b}\right]_{\mathrm{V}} \tag{7.15}$$

$$\left\{\left[\mathbf{S}_{ab}, \mathbf{A}\right]_{\mathrm{R}}\right\}_{mn} = \left[\mathbf{S}_{ab}, \left\{\mathbf{A}\right\}_{m-a,n-b+1}\right]_{\mathrm{R}} \tag{7.16}$$

$$\left\{\mathbf{H}_{cd}\right\}_{mn} = \delta_{mc}\delta_{nd}\mathbf{H}_{cd} \tag{7.17}$$

General Definition of Hamiltonian Terms

To obtain analytic formulas, more explicit definitions of the original Hamiltonian are required. We use definitions adapted from those provided by Aliev and Watson.[4] Specifically, we have ensured that every term in the definitions is in the form of – or a combination of terms in the form of – Eq. (7.18), where $3N-6$ is the number of vibrational modes of the asymmetric rotor, $\boldsymbol{\rho}$ is either a position vibrational quantum operator $\mathbf{q}$ or a momentum vibrational quantum operator $\mathbf{p}$ in the normal coordinate system, $\mathbf{J}$ is the angular momentum quantum operator, and H_{mn} is the coefficient containing the constants and functions that commute with $\mathbf{q}$, $\mathbf{p}$, and $\mathbf{J}$. The vibrational and rotational operator parts are restricted to a single product; if a summation contains an addition or subtraction of operators, then the summation is subdivided into additional summations until this requirement is met for each of the resulting terms. Such a form ensures that the coefficients will always commute. A complete list of the definitions used in this work is provided in the Supporting Information.

$$\mathbf{H}_{mn} = \sum_{v_0,v_1,\ldots}^{3N-6} \sum_{r_0,r_1,\ldots}^{3} \mathrm{H}_{mn}\left(v_0,v_1,\ldots;r_0,r_1,\ldots\right) \prod_{j}^{v_0,v_1,\ldots} \boldsymbol{\rho}_j \prod_{k}^{r_0,r_1,\ldots} \mathbf{J}_k \tag{7.18}$$

Obtaining Definitions of Transform Functions

The exact definition of a transform function $\mathbf{S}_{mn}^{(j)}$ is arbitrary, so long as the definition satisfies Eq. (7.9). We employed one of two different approaches for solving Eq. (7.9) to obtain the definitions of all the transform functions within a given sequential contact transformation. The first, which we'll refer to as the "ladder" solution, follows the method described by Aliev and Watson.[4] The second, which we'll refer to as the "trial" solution, evaluates the commutator in Eq. (7.9) using a trial transform function and uses the results to identify a valid solution. The ladder solution is easier for manually deriving the definitions of the transform functions but is limited to the case where $\mathbf{H}_0 = \mathbf{H}_{20}$.

Using vibrational ladder operators

The ladder solution uses the approach described by Aliev and Watson,[4] in which the defining equation is rewritten in terms of one-dimensional ladder operators $\mathcal{L}^{+} \equiv \mathbf{q} - i\mathbf{p}$ and $\mathcal{L}^{-} \equiv \mathbf{q} + i\mathbf{p}$. Using σ as the sign of the ladder operator and the general definition given by Eq. (7.19), the vibrational quantum operators $\mathbf{q}$ and $\mathbf{p}$ can be defined with respect to these ladder operators as in Eq. (7.20) and Eq. (7.21), where $\sigma_k = \pm 1$ and the summation over σ_k is implied to be over the set of $\{-1,1\}$. Substituting these definitions into Eq. (7.18) leads directly to the "ladder form" of an expression, as shown in Eq. (7.22). For the particular case of Eq. (7.9) where the defining part $\tilde{\mathbf{H}}_{mn}^{(j-1)}$ is written in the form of Eq. (7.22) and the zeroth order Hamiltonian is the harmonic oscillator *i.e.*, $\mathbf{H}_0 = \mathbf{H}_{20}$, Aliev and Watson[4] showed the definition of the transform

function in Eq. (7.23) will satisfy the condition of Eq. (7.9). Terms involving resonant vibrational modes may have very small denominators and so the summations are restricted to avoid such terms.

$$\mathcal{L}_k^{\sigma_k} = \mathbf{q}_k - i\sigma_k \mathbf{p}_k \tag{7.19}$$

$$\mathbf{q}_k = \frac{1}{2}\sum_{\sigma_k} \mathcal{L}_k^{\sigma_k} \tag{7.20}$$

$$\mathbf{p}_k = \frac{1}{2} i \sum_{\sigma_k} \sigma_k \mathcal{L}_k^{\sigma_k} \tag{7.21}$$

$$\mathbf{H}_{mn} = \sum_{\nu_0,\nu_1,\ldots}^{3N-6} \sum_{\sigma_{\nu_0},\sigma_{\nu_1},\ldots}^{\{-1,1\}} \sum_{r_0,r_1,\ldots}^{3} \mathrm{H}_{mn}\left(\nu_0,\nu_1,\ldots;\sigma_{\nu_0},\sigma_{\nu_1},\ldots;r_0,r_1,\ldots\right) \prod_j^{\nu_0,\nu_1,\ldots} \mathcal{L}_j^{\sigma_j} \prod_k^{r_0,r_1,\ldots} \mathbf{J}_k \tag{7.22}$$

$$\mathbf{S}_{mn} = -i \sum_{\nu_0,\nu_1,\ldots}^{3N-6*} \sum_{\sigma_{\nu_0},\sigma_{\nu_1},\ldots}^{\{-1,1\}*} \sum_{r_0,r_1,\ldots}^{3} \frac{\mathrm{H}_{mn}\left(\nu_0,\nu_1,\ldots;\sigma_{\nu_0},\sigma_{\nu_1},\ldots;r_0,r_1,\ldots\right)}{\sigma_{\nu_0}\omega_{\nu_0} + \sigma_{\nu_1}\omega_{\nu_1} + \cdots} \prod_j^{\nu_0,\nu_1,\ldots} \mathcal{L}_j^{\sigma_j} \prod_k^{r_0,r_1,\ldots} \mathbf{J}_k \tag{7.23}$$

We expand on the definition of the transform function in Eq. (7.23) in two ways. First, we introduce a piece-wise "denominator" function D defined in Eq. (7.24) (where "r.t." is short for resonance threshold) and which can be shown to have the properties given in Eq. (7.25). Use of this function allows us to lift the restrictions from the summation indices; if the combination of indices results in a denominator that approaches zero, the removal of that combination is handled by the piece-wise function. Second, although not strictly necessary, we ensure the transform function is Hermitian by rewriting the coefficient to contain both the forward and reverse ordering of the vibrational indices. The formula for the definition of the transform function is now given by Eq. (7.26), but only if $\mathbf{H}_0$ is the harmonic oscillator.

$$\mathrm{D}\left(\sigma_{v_0}, v_0; \sigma_{v_1}, v_1; \ldots\right) \equiv \begin{cases} 0 & \left|\sigma_{v_0}\omega_{v_0} + \sigma_{v_1}\omega_{v_1} + \cdots\right| \leq \text{r.t.} \\ \dfrac{1}{\sigma_{v_0}\omega_{v_0} + \sigma_{v_1}\omega_{v_1} + \cdots} & \left|\sigma_{v_0}\omega_{v_0} + \sigma_{v_1}\omega_{v_1} + \cdots\right| > \text{r.t.} \end{cases} \tag{7.24}$$

(i)

$$\mathrm{D}\left(\sigma_{v_0}, v_0; \sigma_{v_1}, v_1; \ldots\right) = -\mathrm{D}\left(-\sigma_{v_0}, v_0; -\sigma_{v_1}, v_1; \ldots\right)$$

(ii)

$$\begin{aligned} \mathrm{D}\left(\sigma_{v_0}, v_0; \sigma_{v_1}, v_1; \ldots\right) &= \mathrm{D}\left(\sigma_{v_1}, v_1; \sigma_{v_0}, v_0; \ldots\right) \\ &\vdots \\ &= \mathrm{D}\left(\ldots; \sigma_{v_0}, v_0; \sigma_{v_1}, v_1\right) \\ &= \mathrm{D}\left(\ldots; \sigma_{v_1}, v_1; \sigma_{v_0}, v_0\right) \end{aligned} \tag{7.25}$$

$$\begin{aligned} \mathbf{S}_{mn} = \sum_{v_0, v_1, \ldots}^{N} \sum_{\sigma_{v_0}, \sigma_{v_1}, \ldots}^{\{-1,1\}} \sum_{r_0, r_1, \ldots}^{3} \frac{-i}{2} \mathrm{D}\left(\sigma_{v_0}, v_0; \sigma_{v_1}, v_1; \ldots\right) \times \\ \times \left(\mathrm{H}_{mn}\left(v_0, v_1, \ldots; \sigma_{v_0}, \sigma_{v_1}, \ldots; r_0, r_1, \ldots\right) + \mathrm{H}_{mn}\left(\ldots, v_1, v_0; \ldots, \sigma_{v_1}, \sigma_{v_0}; r_0, r_1, \ldots\right)\right) \times \\ \times \prod_{j}^{v_0, v_1, \ldots} \mathcal{L}_j^{\sigma_j} \prod_{k}^{r_0, r_1, \ldots} \mathbf{J}_k \end{aligned} \tag{7.26}$$

Using a trial transform function

The trial solution of Eq. (7.9) for the transform function consists of evaluating the commutator therein for all possible operator combinations with the necessary degrees of vibration and rotation. The trial transform function is defined as in Eq. (7.27), where $\mathcal{V}_i$ is a member of the set of permutations of possible vibrational operators (Eq. (7.28)) and the coefficients $\mathrm{S}_{mn,i}$ are undefined. For example, the trial transforms for $\mathbf{S}_{12}$ and $\mathbf{S}_{22}$ would be given by Eq. (7.29) and Eq. (7.30). Then, the commutator $i\left[\mathbf{S}_{mn}, \mathbf{H}_0\right]$ of Eq. (7.9) is evaluated and the results combined with $\mathbf{H}_{mn}$. Each resulting term that corresponds with a term of $\mathbf{H}_{mn}$ that is to be eliminated is then set to zero, which yields a system of equations that can be used to solve for the coefficients $\mathrm{S}_{mn,i}$.

Any coefficient $S_{mn,i}$ not required to block-diagonalize $\mathbf{H}_{mn}$ is set to zero. Substitution of these definitions into (7.27) yields a solution of the transform function that satisfies (7.9).

$$\mathbf{S}_{mn} = \sum_{i}^{N_{\text{perm}}} \sum_{v_0,v_1,\ldots,v_m}^{3N-6} \sum_{r_0,r_1,\ldots,r_n}^{3} S_{mn,i}\left(v_0,v_1,\ldots,v_m;r_0,r_1,\ldots,r_n\right)\mathcal{V}_i\left(v_0,v_1,\ldots,v_m\right)\prod_{k}^{r_0,r_1,\ldots,r_n}\mathbf{J}_k \qquad (7.27)$$

$$\mathcal{V}_i\left(v_0,v_1,\ldots,v_m\right) = \boldsymbol{\rho}_{v_0}\cdot\boldsymbol{\rho}_{v_1}\cdots\boldsymbol{\rho}_{v_m} \in \left\{\left(x_0,x_1,\ldots,x_m\right)\middle| x_j \in \{\mathbf{q},\mathbf{p}\} \text{ for every } j \in \{0,1,\ldots,m\}\right\} \qquad (7.28)$$

$$\mathbf{S}_{12} = \sum_{v_0}^{3N-6}\sum_{r_0,r_1}^{3} S_{12,0}\left(v_0,r_0,r_1\right)\mathbf{q}_{v_0}\mathbf{J}_{r_0}\mathbf{J}_{r_1} + \sum_{v_0}^{3N-6}\sum_{r_0,r_1}^{3} S_{12,1}\left(v_0,r_0,r_1\right)\mathbf{p}_{v_0}\mathbf{J}_{r_0}\mathbf{J}_{r_1} \qquad (7.29)$$

$$\begin{aligned}\mathbf{S}_{22} = &\sum_{v_0,v_1}^{3N-6}\sum_{r_0,r_1}^{3} S_{22,0}\left(v_0,v_1,r_0,r_1\right)\mathbf{q}_{v_0}\mathbf{q}_{v_1}\mathbf{J}_{r_0}\mathbf{J}_{r_1} + \sum_{v_0,v_1}^{3N-6}\sum_{r_0,r_1}^{3} S_{22,1}\left(v_0,v_1,r_0,r_1\right)\mathbf{q}_{v_0}\mathbf{p}_{v_1}\mathbf{J}_{r_0}\mathbf{J}_{r_1} \\ &+ \sum_{v_0,v_1}^{3N-6}\sum_{r_0,r_1}^{3} S_{22,3}\left(v_0,v_1,r_0,r_1\right)\mathbf{p}_{v_0}\mathbf{q}_{v_1}\mathbf{J}_{r_0}\mathbf{J}_{r_1} + \sum_{v_0,v_1}^{3N-6}\sum_{r_0,r_1}^{3} S_{22,4}\left(v_0,v_1,r_0,r_1\right)\mathbf{p}_{v_0}\mathbf{p}_{v_1}\mathbf{J}_{r_0}\mathbf{J}_{r_1}\end{aligned} \qquad (7.30)$$

Rotational Reductions

For terms of the transformed Hamiltonian with rotational degrees of greater than two, it is necessary to apply additional transformations to obtain results that can be compared to directly experimentally determined constants. For terms that are vibrationally diagonal, the same methodology used to reduce the quartic and sextic distortion constants can be applied.[1-4] This methodology, however, cannot be applied to the terms that are not vibrationally diagonal[6-7] (which are those necessary for predicting the vibration-rotation coupling constants). This is because the methodology to reduce the centrifugal distortion constants eliminates only the terms that are not

totally symmetric in the rotational operators and keeps those that are totally symmetric, but the coupling constants used for fitting coupled states are all not totally symmetric. In fact, the nature of the methodology is such that it is impossible to remove the totally symmetric terms regardless of the definition of the transform functions.

To reduce the rotational operators for the vibrationally off-diagonal terms, it is necessary to modify the known procedure used for the centrifugal distortion constants. The solution – first described by Perevalov and Tyuterev[6-7] – is to modify the zeroth order Hamiltonian to include the both the harmonic oscillator $\mathbf{H}_{20}$ and the rigid rotor $\mathbf{H}_{02}$. Doing so introduces vibrational commutators into the reduction that, with proper definition of the transform functions, can eliminate the rotationally totally symmetric terms while keeping the rotationally non-totally symmetric terms. Then, after evaluating the expectation value of the vibrational operators, these rotationally reduced coupling constants can be compared to those of experimental coupled-state fits. To maintain a consistent form of the Hamiltonian throughout the derivation, however, our implementation of the rotational reduction for the off-diagonal terms differs from that described by Perevalov and Tyuterev.[6-7]

We can write the rotational reduction as in Eq. (7.31), where the transform function $\mathbf{S}$ is chosen such that the reduced Hamiltonian has the desired form. In order for the transform function to affect the terms contained within $\tilde{\mathbf{H}}_{mn}$, the commutator expression must yield terms with *m* and *n* degrees of vibration and rotation, respectively. That is, we can apply the selection brackets as in Eq. (7.14)–(7.17) to determine the transform function degrees that can perform the reduction. As illustrated by Eq. (7.32), we can use a transform function $\mathbf{S}^{\mathrm{r}} = \mathbf{S}^{\mathrm{r}}_{mn} + \mathbf{S}^{\mathrm{r}}_{m,n-1}$ to apply the rotational reduction, where the ‘r’ superscript is used to distinguish the transform functions for applying the reduction from the transform functions used to vibrationally block diagonalize the

Hamiltonian. The definitions of the transform functions can be obtained *via* the trial method (*vide infra*) once the desired form of the reduced rotational Hamiltonian $\tilde{\mathbf{H}}_{mn}^{\mathrm{red}}$ is determined.

$$\tilde{\mathbf{H}}_{mn}^{\mathrm{red}} = \tilde{\mathbf{H}}_{mn} + i\left[\mathbf{S}^{\mathrm{r}}, \mathbf{H}_{20} + \mathbf{H}_{02}\right] \tag{7.31}$$

$$\begin{aligned}
\left\{\left[\mathbf{S}^{\mathrm{r}}, \mathbf{H}_{20} + \mathbf{H}_{02}\right]\right\}_{mn} &= \left\{\left[\mathbf{S}^{\mathrm{r}}, \mathbf{H}_{20}\right]_{\mathrm{V}}\right\}_{mn} + \left\{\left[\mathbf{S}^{\mathrm{r}}, \mathbf{H}_{02}\right]_{\mathrm{V}}\right\}_{mn} \\
&\quad + \left\{\left[\mathbf{S}^{\mathrm{r}}, \mathbf{H}_{20}\right]_{\mathrm{R}}\right\}_{mn} + \left\{\left[\mathbf{S}^{\mathrm{r}}, \mathbf{H}_{02}\right]_{\mathrm{R}}\right\}_{mn} \\
&= \left\{\left[\mathbf{S}^{\mathrm{r}}, \mathbf{H}_{20}\right]_{\mathrm{V}}\right\}_{mn} + \left\{\left[\mathbf{S}^{\mathrm{r}}, \mathbf{H}_{02}\right]_{\mathrm{R}}\right\}_{mn} \\
&= \left[\left\{\mathbf{S}^{\mathrm{r}}\right\}_{mn}, \mathbf{H}_{20}\right]_{\mathrm{V}} + \left[\left\{\mathbf{S}^{\mathrm{r}}\right\}_{m,n-1}, \mathbf{H}_{02}\right]_{\mathrm{R}}
\end{aligned} \tag{7.32}$$

To identify which terms are to be eliminated, the rotational Hamiltonian is often written in terms of the cylindrical tensor coordinate system ($\mathbf{J}^2, \mathbf{J}_z, \mathbf{J}_{\pm} \equiv \mathbf{J}_x \mp i\mathbf{J}_y$) and so a transformation from the Cartesian coordinates outputted by an anharmonic frequency calculation is necessary. Such a transformation can be accomplished by using the substitutions $\mathbf{J}_x = \left(\mathbf{J}_- + \mathbf{J}_+\right)/2$ and $\mathbf{J}_y = \left(\mathbf{J}_- - \mathbf{J}_+\right)/2i$, and is straightforward (though tedious) for higher orders. For the on-diagonal vibration-rotation coupling terms ($\tilde{\mathbf{H}}_{m2}^{\mathrm{d}}, \tilde{\mathbf{H}}_{m4}^{\mathrm{d}}, \tilde{\mathbf{H}}_{m6}^{\mathrm{d}}, \ldots$), the method prescribed by Watson[2] is sufficient to achieve the desired result. For the even-ordered off-diagonal vibration-rotation coupling terms ($\tilde{\mathbf{H}}_{m2}^{\mathrm{od}}, \tilde{\mathbf{H}}_{m4}^{\mathrm{od}}, \tilde{\mathbf{H}}_{m6}^{\mathrm{od}}, \ldots$), it is necessary to follow the guidance of Perevalov and Tyuterev.[6-7] At this time, we are still developing the treatment of the odd-ordered vibration-rotation coupling terms ($\tilde{\mathbf{H}}_{m1}, \tilde{\mathbf{H}}_{m3}, \tilde{\mathbf{H}}_{m5} \ldots$), which are inherently off-diagonal in rotation. Our initial efforts used an adapted version of the procedure prescribed by Watson,[2] but we are not certain the result will be the same as that following the prescription of Perevalov and Tyuterev.[6-7] Further discussion on this point occurs in the preliminary rotational reduction of $\tilde{\mathbf{H}}_{23}$ (*vide infra*).

Connection to Experimental Vibration-Rotation Coupling Constants

Predicting the vibration-rotation coupling between two vibrational states requires determination of the vibrationally off-diagonal transformed Hamiltonian. Specifically, we need to evaluate the vibrational matrix element $\langle i|\tilde{\mathbf{H}}|j\rangle$ of the transformed Hamiltonian. The first order Coriolis coupling constant is the coefficient of a single rotational operator, thus the largest contribution to the first order Coriolis coupling constants (G_a, G_b, G_c) comes from $\tilde{\mathbf{H}}_{21}$. Similarly, the largest contribution to the second order Coriolis coupling constants (F_{bc}, F_{ac}, F_{ab}) comes from $\tilde{\mathbf{H}}_{22}$, while $\tilde{\mathbf{H}}_{23}$ is the largest contributor to the third order Coriolis coupling constants (G_a^J, G_b^J, G_c^J, G_a^K, G_b^K, G_c^K), and so forth. The sequential contact transformations to obtain $\tilde{\mathbf{H}}_{21}$, $\tilde{\mathbf{H}}_{22}$, and $\tilde{\mathbf{H}}_{23}$ are provided in Table 7.1. We first derive the formula for $\tilde{\mathbf{H}}_{21}$ as an introduction to the methodology. We then derive the formula for $\tilde{\mathbf{H}}_{22}$, the derivation of which is more representative of the methodology required to obtain predictions of other coupling constants. Finally, we describe our current efforts for obtaining $\tilde{\mathbf{H}}_{23}$, and provide a preliminary rotational reduction for terms with three rotational degrees. Application of these derivations to experimental coupled-state fits is discussed in the subsequent *Results and Discussion* section.

Table 7.1. Sequence of Contact Transformations and the Corresponding Defining Equations to Obtain $\tilde{\mathbf{H}}_{21}$, $\tilde{\mathbf{H}}_{22}$, and $\tilde{\mathbf{H}}_{23}$.

	$\tilde{\mathbf{H}}_{21}$		$\tilde{\mathbf{H}}_{22}$		$\tilde{\mathbf{H}}_{23}$	
Transform number j	$\mathbf{S}^{(j)}$	Defining Equation	$\mathbf{S}^{(j)}$	Defining Equation	$\mathbf{S}^{(j)}$	Defining Equation
1	$\mathbf{S}_{21}$	$\mathbf{H}_{21}^{(1)}(\text{b.d.}) = \mathbf{H}_{21}^{(0)} + i[\mathbf{S}_{21}, \mathbf{H}_0]$	$\mathbf{S}_{12}$	$\mathbf{H}_{12}^{(1)}(\text{b.d.}) = \mathbf{H}_{12}^{(0)} + i[\mathbf{S}_{12}, \mathbf{H}_0]$	$\mathbf{S}_{12}$	$\mathbf{H}_{12}^{(1)}(\text{b.d.}) = \mathbf{H}_{12}^{(0)} + i[\mathbf{S}_{12}, \mathbf{H}_0]$
2			$\mathbf{S}_{21}$	$\mathbf{H}_{21}^{(2)}(\text{b.d.}) = \mathbf{H}_{21}^{(1)} + i[\mathbf{S}_{21}, \mathbf{H}_0]$	$\mathbf{S}_{13}$	$\mathbf{H}_{13}^{(2)}(\text{b.d.}) = \mathbf{H}_{13}^{(1)} + i[\mathbf{S}_{13}, \mathbf{H}_0]$
3			$\mathbf{S}_{22}$	$\mathbf{H}_{22}^{(3)}(\text{b.d.}) = \mathbf{H}_{22}^{(2)} + i[\mathbf{S}_{22}, \mathbf{H}_0]$	$\mathbf{S}_{21}$	$\mathbf{H}_{21}^{(3)}(\text{b.d.}) = \mathbf{H}_{21}^{(2)} + i[\mathbf{S}_{21}, \mathbf{H}_0]$
4					$\mathbf{S}_{22}$	$\mathbf{H}_{22}^{(4)}(\text{b.d.}) = \mathbf{H}_{22}^{(3)} + i[\mathbf{S}_{22}, \mathbf{H}_0]$
5					$\mathbf{S}_{23}$	$\mathbf{H}_{23}^{(5)}(\text{b.d.}) = \mathbf{H}_{23}^{(4)} + i[\mathbf{S}_{22}, \mathbf{H}_0]$

Derivation of $\tilde{\mathbf{H}}_{21}$

Identifying the sequential contact transformation

As shown in Table 7.1, only a single contact transformation using $\mathbf{S}_{21}$ is required to obtain $\tilde{\mathbf{H}}_{21}$. The transform function will be defined using the terms of the original Hamiltonian with two (2) degrees in vibration and one (1) degree in rotation. The sequence can be obtained as described previously, but effectively is the result of alphabetically sorting the transform functions with vibrational degrees up to two and rotational degrees up to one, excluding the trivially zero transform functions. That is, we can write the sequence as $\mathbf{S}_{00}$, $\mathbf{S}_{01}$, $\mathbf{S}_{10}$, $\mathbf{S}_{11}$, $\mathbf{S}_{20}$, and $\mathbf{S}_{21}$, where the only nonzero transform function is given by $\mathbf{S}_{21}$: $\mathbf{S}_{00}$, $\mathbf{S}_{01}$, $\mathbf{S}_{10}$, and $\mathbf{S}_{11}$ are zero since there are no corresponding terms in the ordered Hamiltonian by which they could be defined, while $\mathbf{S}_{20}$ is zero because the harmonic oscillator is diagonal in the basis set of normal modes.

Finding the general equation

Next, we obtain the general equation for calculating $\tilde{\mathbf{H}}_{21}$. To do so, the original Hamiltonian is approximated as in Eq. (7.33) by keeping only terms of up to and including λ^1 of the ordered Hamiltonian in Eq. (7.1), per Eq. (7.13). We then apply the sequential contact transformation using the commutator expressions given in Eq. (7.2)–(7.6), resulting in the transformed Hamiltonian given by Eq. (7.34). Of the terms present in the transformed Hamiltonian in Eq. (7.34), only those with two degrees of vibration and one degree of rotation will contribute to $\tilde{\mathbf{H}}_{21}$. Using Eq. (7.14)–(7.17), we can exclude the unnecessary terms to yield the "general equation" for calculating $\tilde{\mathbf{H}}_{21}$, given by Eq. (7.35).

$$\begin{aligned}\mathbf{H} &\approx \lambda^0\mathbf{H}_0 + \lambda^1\mathbf{H}_1 \\ &= \lambda^0\mathbf{H}_{20} + \lambda^1\left(\mathbf{H}_{30} + \mathbf{H}_{21} + \mathbf{H}_{12} + \mathbf{H}_{02}\right)\end{aligned} \tag{7.33}$$

$$\begin{aligned}\mathbf{H}^{(1)} &= \lambda^0\mathbf{H}_0^{(1)} + \lambda^1\mathbf{H}_1^{(1)} \\ &= \lambda^0\mathbf{H}_0 + \lambda^1\left(\mathbf{H}_1 + i\left[\mathbf{S}_1, \mathbf{H}_0\right]\right) \\ &= \lambda^0\mathbf{H}_{20} + \lambda^1\left(\mathbf{H}_{30} + \mathbf{H}_{21} + \mathbf{H}_{12} + \mathbf{H}_{02} + i\left[\mathbf{S}_{21}, \mathbf{H}_{20}\right]\right)\end{aligned} \tag{7.34}$$

$$\begin{aligned}\tilde{\mathbf{H}}_{21} \equiv \left\{\mathbf{H}^{(1)}\right\}_{21} &= \left\{\mathbf{H}_{20} + \mathbf{H}_{30} + \mathbf{H}_{21} + \mathbf{H}_{12} + \mathbf{H}_{02} + i\left[\mathbf{S}_{21}, \mathbf{H}_{20}\right]\right\}_{21} \\ &= \left\{\mathbf{H}_{20}\right\}_{21} + \left\{\mathbf{H}_{30}\right\}_{21} + \left\{\mathbf{H}_{21}\right\}_{21} + \left\{\mathbf{H}_{12}\right\}_{21} + \left\{\mathbf{H}_{02}\right\}_{21} + i\left\{\left[\mathbf{S}_{21}, \mathbf{H}_{20}\right]\right\}_{21} \\ &= \mathbf{H}_{21} + i\left[\mathbf{S}_{21}, \left\{\mathbf{H}_{20}\right\}_{20}\right]_{\mathrm{V}} \\ &= \mathbf{H}_{21} + i\left[\mathbf{S}_{21}, \mathbf{H}_{20}\right]_{\mathrm{V}}\end{aligned} \tag{7.35}$$

General equation for defining $\boldsymbol{S}_{21}$

A similar process used to obtain the general equation of $\tilde{\mathbf{H}}_{21}$ is applied in Eq. (7.36) to obtain the general form of the "defining part" of the defining equation in Table 7.1. The resulting Eq. (7.37) is equivalent to the general equation found in Eq. (7.35). As we will see, the correspondence of the defining equation of the transform function and the general equation for a particular problem only occurs for the last transformation in the sequence.

$$\begin{aligned}\mathbf{H}_{21}^{(0)} \equiv \left\{\mathbf{H}^{(0)}\right\}_{21} &= \left\{\mathbf{H}_0^{(0)} + \mathbf{H}_1^{(0)}\right\}_{21} \\ &= \left\{\mathbf{H}_0\right\}_{21} + \left\{\mathbf{H}_1\right\}_{21} \\ &= \left\{\mathbf{H}_{20}\right\}_{21} + \left\{\mathbf{H}_{30} + \mathbf{H}_{21} + \mathbf{H}_{12} + \mathbf{H}_{02}\right\}_{21} \\ &= \mathbf{H}_{21}\end{aligned} \tag{7.36}$$

$$\mathbf{H}_{21}^{(1)}\left(\text{b.d.}\right) = \mathbf{H}_{21} + i\left[\mathbf{S}_{21}, \mathbf{H}_{20}\right]_{\mathrm{V}} \tag{7.37}$$

Required definitions of the original Hamiltonian

Examination of the general equations for the final transformed Hamiltonian $\tilde{\mathbf{H}}_{21}$ and the for definition of $\mathbf{S}_{21}$ reveals that the only terms of the original Hamiltonian that are required are $\mathbf{H}_{20}$ and $\mathbf{H}_{21}$, which are defined in Eq. (7.38) and Eq. (7.39), respectively. Now, the definition of $\mathbf{S}_{21}$ is all that is needed to evaluate the commutator in Eq. (7.35) and obtain an analytic expression of $\tilde{\mathbf{H}}_{21}$.

$$\mathbf{H}_{20} = \sum_{j}^{N} \frac{1}{2} \omega_j \mathbf{q}_j^2 + \sum_{j}^{N} \frac{1}{2} \omega_j \mathbf{p}_j^2 \tag{7.38}$$

$$\mathbf{H}_{21} = \sum_{jk}^{N} \sum_{\alpha}^{3} \left(-2 \sqrt{\frac{\omega_k}{\omega_j}} B_\alpha \zeta_{jk}^{\alpha} \right) \mathbf{q}_j \mathbf{p}_k \mathbf{J}_\alpha \tag{7.39}$$

Finding the definition of $\mathbf{S}_{21}$

The exact definition of $\mathbf{S}_{21}$ is inherently arbitrary, so long as the result of Eq. (7.37) is block diagonal with respect to vibration. We'll apply the ladder solution to define the transform function. Using the definitions provided in Eq. (7.20) and Eq. (7.21), we can express $\mathbf{H}_{21}$ in terms of the vibrational ladder operators, as given by Eq. (7.40). This expression is in the form described by Eq. (7.22), and so we can apply the formula Eq. (7.26) to obtain the definition of $\mathbf{S}_{21}$, as given in Eq. (7.41). By applying the definition of the vibrational ladder operator from Eq. (7.19), we can rewrite the definition of $\mathbf{S}_{21}$ in terms of **q** and **p**. The substitution of the vibrational operators is shown in Eq. (7.42) along with a condensed form, which uses the definitions of the coefficients provided in Eq. (7.43).

$$\begin{aligned}\mathbf{H}_{21} &= \sum_{jk}^{N}\sum_{\alpha}^{3}\left(-2\sqrt{\frac{\omega_k}{\omega_j}}B_\alpha\zeta_{jk}^{\alpha}\right)\left(\frac{1}{2}\sum_{\sigma_j}\mathcal{L}_j^{\sigma_j}\right)\left(\frac{1}{2}i\sum_{\sigma_k}\sigma_k\mathcal{L}_k^{\sigma_k}\right)\mathbf{J}_\alpha \\ &= \sum_{jk}^{N}\sum_{\sigma_j\sigma_k}^{\{-1,1\}}\sum_{\alpha}^{3}\left(-\frac{1}{2}i\sigma_k\sqrt{\frac{\omega_k}{\omega_j}}B_\alpha\zeta_{jk}^{\alpha}\right)\mathcal{L}_j^{\sigma_j}\mathcal{L}_k^{\sigma_k}\mathbf{J}_\alpha\end{aligned} \tag{7.40}$$

$$\begin{aligned}\mathbf{S}_{21} &= \sum_{jk}^{N}\sum_{\sigma_j\sigma_k}^{\{-1,1\}}\sum_{\alpha}^{3}\frac{-i}{2}\mathrm{D}\left(\sigma_j, j, \sigma_k, k\right)\left(\left(-\frac{1}{2}i\sigma_k\sqrt{\frac{\omega_k}{\omega_j}}B_\alpha\zeta_{jk}^{\alpha}\right)+\left(-\frac{1}{2}i\sigma_j\sqrt{\frac{\omega_j}{\omega_k}}B_\alpha\zeta_{kj}^{\alpha}\right)\right)\times \\ &\quad\times\mathcal{L}_j^{\sigma_j}\mathcal{L}_k^{\sigma_k}\mathbf{J}_\alpha \\ &= \sum_{jk}^{N}\sum_{\sigma_j\sigma_k}^{\{-1,1\}}\sum_{\alpha}^{3}\frac{-1}{4}\mathrm{D}\left(\sigma_j, j, \sigma_k, k\right)\left(\sigma_k\sqrt{\frac{\omega_k}{\omega_j}}-\sigma_j\sqrt{\frac{\omega_j}{\omega_k}}\right)B_\alpha\zeta_{jk}^{\alpha}\mathcal{L}_j^{\sigma_j}\mathcal{L}_k^{\sigma_k}\mathbf{J}_\alpha\end{aligned} \tag{7.41}$$

$$\begin{aligned}\mathbf{S}_{21} &= \sum_{jk}^{N}\sum_{\sigma_j\sigma_k}^{\{-1,1\}}\sum_{\alpha}^{3}\frac{-1}{4}\mathrm{D}\left(\sigma_j, j, \sigma_k, k\right)\left(\sigma_k\sqrt{\frac{\omega_k}{\omega_j}}-\sigma_j\sqrt{\frac{\omega_j}{\omega_k}}\right)B_\alpha\zeta_{jk}^{\alpha}\times \\ &\quad\times\left(\mathbf{q}_j-i\sigma_j\mathbf{p}_j\right)\left(\mathbf{q}_k-i\sigma_k\mathbf{p}_k\right)\mathbf{J}_\alpha \\ &= \sum_{jk}^{N}\sum_{\alpha}^{3}\mathrm{S}_{21,0}\left(j,k,\alpha\right)\mathbf{q}_j\mathbf{q}_k\mathbf{J}_\alpha+\sum_{jk}^{N}\sum_{\alpha}^{3}\mathrm{S}_{21,1}\left(j,k,\alpha\right)\mathbf{p}_j\mathbf{p}_k\mathbf{J}_\alpha\end{aligned} \tag{7.42}$$

$$\begin{aligned}\mathrm{S}_{21,0}\left(j,k,\alpha\right) &= \frac{1}{2}\left(\mathrm{D}\left(1, j, 1, k\right)\left(-\sqrt{\frac{\omega_k}{\omega_j}}+\sqrt{\frac{\omega_j}{\omega_k}}\right)+\mathrm{D}\left(1, j, -1, k\right)\left(\sqrt{\frac{\omega_k}{\omega_j}}+\sqrt{\frac{\omega_j}{\omega_k}}\right)\right)B_\alpha\zeta_{jk}^{\alpha} \\ \mathrm{S}_{21,1}\left(j,k,\alpha\right) &= \frac{1}{2}\left(\mathrm{D}\left(1, j, 1, k\right)\left(\sqrt{\frac{\omega_k}{\omega_j}}-\sqrt{\frac{\omega_j}{\omega_k}}\right)+\mathrm{D}\left(1, j, -1, k\right)\left(\sqrt{\frac{\omega_k}{\omega_j}}+\sqrt{\frac{\omega_j}{\omega_k}}\right)\right)B_\alpha\zeta_{jk}^{\alpha}\end{aligned} \tag{7.43}$$

Evaluating the commutator

With the transform function $\mathbf{S}_{21}$ defined, the commutator $i\left[\mathbf{S}_{21},\mathbf{H}_{20}\right]_{\mathrm{V}}$ can be evaluated. Using the definitions of Eq. (7.38) and Eq. (7.42), the commutator can be written as in Eq. (7.44). This expression is expanded using the commutator rules, and by keeping only the nonzero commutators we can write the expression as given in Eq. (7.45). The vibrational commutators are evaluated using the identities provided in the Supporting Information to yield Eq. (7.46). The expression is then expanded into individual summations following the form given in Eq. (7.18). Doing so allows us to evaluate the Kronecker delta functions for each summation, resulting in Eq. (7.47). With judicious relabeling of the summation indices, these summations can be consolidated to just two, as in Eq. (7.48).

$$\begin{aligned} i\left[\mathbf{S}_{21},\mathbf{H}_{20}\right]_{\mathrm{V}} = i\Bigg[& \sum_{jk}^{N}\sum_{\alpha}^{3}\mathrm{S}_{21,0}\left(j,k,\alpha\right)\mathbf{q}_j\mathbf{q}_k\mathbf{J}_\alpha + \sum_{jk}^{N}\sum_{\alpha}^{3}\mathrm{S}_{21,1}\left(j,k,\alpha\right)\mathbf{p}_j\mathbf{p}_k\mathbf{J}_\alpha \\ & ,\sum_{j}^{N}\frac{1}{2}\omega_j\mathbf{q}_j^2 + \sum_{j}^{N}\frac{1}{2}\omega_j\mathbf{p}_j^2\Bigg]_{\mathrm{V}} \end{aligned} \tag{7.44}$$

$$\begin{aligned} i\left[\mathbf{S}_{21},\mathbf{H}_{20}\right]_{\mathrm{V}} = & \sum_{jkl}^{N}\sum_{\alpha}^{3}\frac{i}{2}\omega_l\,\mathrm{S}_{21,1}\left(j,k,\alpha\right)\left[\mathbf{p}_j\mathbf{p}_k,\mathbf{q}_l^2\right]\mathbf{J}_\alpha \\ & +\sum_{jkl}^{N}\sum_{\alpha}^{3}\frac{i}{2}\omega_l\,\mathrm{S}_{21,0}\left(j,k,\alpha\right)\left[\mathbf{q}_j\mathbf{q}_k,\mathbf{p}_l^2\right]\mathbf{J}_\alpha \end{aligned} \tag{7.45}$$

$$\begin{aligned} i\left[\mathbf{S}_{21},\mathbf{H}_{20}\right]_{\mathrm{V}} = & \sum_{jkl}^{N}\sum_{\alpha}^{3}\frac{i}{2}\omega_l\,\mathrm{S}_{21,1}\left(j,k,\alpha\right)(-1)\left(i\delta_{lk}\mathbf{q}_l\mathbf{p}_j + i\delta_{lj}\mathbf{q}_l\mathbf{p}_k + i\delta_{lk}\mathbf{p}_j\mathbf{q}_l + i\delta_{lj}\mathbf{p}_k\mathbf{q}_l\right)\mathbf{J}_\alpha \\ & +\sum_{jkl}^{N}\sum_{\alpha}^{3}\frac{i}{2}\omega_l\,\mathrm{S}_{21,0}\left(j,k,\alpha\right)\left(i\delta_{kl}\mathbf{q}_j\mathbf{p}_l + i\delta_{kl}\mathbf{q}_j\mathbf{p}_l + i\delta_{jl}\mathbf{p}_l\mathbf{q}_k + i\delta_{jl}\mathbf{p}_l\mathbf{q}_k\right)\mathbf{J}_\alpha \end{aligned} \tag{7.46}$$

$$
\begin{aligned}
i\left[\mathbf{S}_{21},\mathbf{H}_{20}\right]_{\mathrm{V}} = &\sum_{jk}^{N}\sum_{\alpha}^{3}\frac{1}{2}\omega_k \mathrm{S}_{21,1}\left(j,k,\alpha\right)\mathbf{q}_k\mathbf{p}_j\mathbf{J}_\alpha + \sum_{jk}^{N}\sum_{\alpha}^{3}\frac{1}{2}\omega_j \mathrm{S}_{21,1}\left(j,k,\alpha\right)\mathbf{q}_j\mathbf{p}_k\mathbf{J}_\alpha \\
&+\sum_{jk}^{N}\sum_{\alpha}^{3}\frac{1}{2}\omega_k \mathrm{S}_{21,1}\left(j,k,\alpha\right)\mathbf{p}_j\mathbf{q}_k\mathbf{J}_\alpha + \sum_{jk}^{N}\sum_{\alpha}^{3}\frac{1}{2}\omega_j \mathrm{S}_{21,1}\left(j,k,\alpha\right)\mathbf{p}_k\mathbf{q}_j\mathbf{J}_\alpha \\
&+\sum_{jk}^{N}\sum_{\alpha}^{3}\frac{-1}{2}\omega_k \mathrm{S}_{21,0}\left(j,k,\alpha\right)\mathbf{q}_j\mathbf{p}_k\mathbf{J}_\alpha + \sum_{jk}^{N}\sum_{\alpha}^{3}\frac{-1}{2}\omega_k \mathrm{S}_{21,0}\left(j,k,\alpha\right)\mathbf{q}_j\mathbf{p}_k\mathbf{J}_\alpha \\
&+\sum_{jk}^{N}\sum_{\alpha}^{3}\frac{-1}{2}\omega_j \mathrm{S}_{21,0}\left(j,k,\alpha\right)\mathbf{p}_j\mathbf{q}_k\mathbf{J}_\alpha + \sum_{jk}^{N}\sum_{\alpha}^{3}\frac{-1}{2}\omega_j \mathrm{S}_{21,0}\left(j,k,\alpha\right)\mathbf{p}_j\mathbf{q}_k\mathbf{J}_\alpha
\end{aligned}
\tag{7.47}
$$

$$
\begin{aligned}
i\left[\mathbf{S}_{21},\mathbf{H}_{20}\right]_{\mathrm{V}} = &\sum_{jk}^{N}\sum_{\alpha}^{3}\left(\frac{1}{2}\omega_j\left(\mathrm{S}_{21,1}\left(k,j,\alpha\right)+\mathrm{S}_{21,1}\left(j,k,\alpha\right)\right)-\omega_k \mathrm{S}_{21,0}\left(j,k,\alpha\right)\right)\mathbf{q}_j\mathbf{p}_k\mathbf{J}_\alpha \\
&+\sum_{jk}^{N}\sum_{\alpha}^{3}\left(\frac{1}{2}\omega_k\left(\mathrm{S}_{21,1}\left(j,k,\alpha\right)+\mathrm{S}_{21,1}\left(k,j,\alpha\right)\right)-\omega_j \mathrm{S}_{21,0}\left(j,k,\alpha\right)\right)\mathbf{p}_j\mathbf{q}_k\mathbf{J}_\alpha
\end{aligned}
\tag{7.48}
$$

Obtaining the analytic expression

The transformed Hamiltonian $\tilde{\mathbf{H}}_{21}$ can be obtained by combining the definition of $\mathbf{H}_{21}$ in Eq. (7.39) with the evaluated commutator obtained in Eq. (7.48). This initially yields Eq. (7.49), which is dependent on the definitions of the coefficients of the transform function. Substitution of the transform coefficient definitions from Eq. (7.43) and use of the properties of the denominator function from Eq. (7.25) allows us to write Eq. (7.50). For convenience, we define a pair of coefficients (Eq. (7.51)) to shorten the expression, yielding Eq. (7.52).

$$\begin{aligned}\tilde{\mathbf{H}}_{21} &= \mathbf{H}_{21} + i\left[\mathbf{S}_{21}, \mathbf{H}_{20}\right]_{\mathrm{V}} \\ &= \sum_{jk}^{N}\sum_{\alpha}^{3}\left(-2\sqrt{\frac{\omega_k}{\omega_j}}B_\alpha \zeta_{jk}^{\alpha} + \frac{1}{2}\omega_j\left(\mathrm{S}_{21,1}(k,j,\alpha) + \mathrm{S}_{21,1}(j,k,\alpha)\right) - \omega_k \mathrm{S}_{21,0}(j,k,\alpha)\right)\times \\ &\qquad \times \mathbf{q}_j \mathbf{p}_k \mathbf{J}_\alpha \\ &\quad + \sum_{jk}^{N}\sum_{\alpha}^{3}\left(\frac{1}{2}\omega_k\left(\mathrm{S}_{21,1}(j,k,\alpha) + \mathrm{S}_{21,1}(k,j,\alpha)\right) - \omega_j \mathrm{S}_{21,0}(j,k,\alpha)\right)\times \\ &\qquad \times \mathbf{p}_j \mathbf{q}_k \mathbf{J}_\alpha\end{aligned} \tag{7.49}$$

$$\begin{aligned}\tilde{\mathbf{H}}_{21} &= \mathbf{H}_{21} + i\left[\mathbf{S}_{21}, \mathbf{H}_{20}\right]_{\mathrm{V}} \\ &= \sum_{jk}^{N}\sum_{\alpha}^{3}\left(-2\sqrt{\frac{\omega_k}{\omega_j}} - \frac{1}{2}\frac{\left(\omega_j+\omega_k\right)\left(\omega_j-\omega_k\right)}{\sqrt{\omega_j\omega_k}}\left(\mathrm{D}(1,j,1,k) - \mathrm{D}(1,j,-1,k)\right)\right)B_\alpha \zeta_{jk}^{\alpha}\mathbf{q}_j\mathbf{p}_k\mathbf{J}_\alpha \\ &\quad + \sum_{jk}^{N}\sum_{\alpha}^{3}\left(-\frac{1}{2}\frac{\left(\omega_j+\omega_k\right)\left(\omega_j-\omega_k\right)}{\sqrt{\omega_j\omega_k}}\left(\mathrm{D}(1,j,1,k) + \mathrm{D}(1,j,-1,k)\right)\right)B_\alpha \zeta_{jk}^{\alpha}\mathbf{p}_j\mathbf{q}_k\mathbf{J}_\alpha\end{aligned} \tag{7.50}$$

$$\begin{aligned}\tilde{\mathrm{H}}_{21,0}(j,k,\alpha) &= \left(-2\sqrt{\frac{\omega_k}{\omega_j}} - \frac{1}{2}\frac{\left(\omega_j+\omega_k\right)\left(\omega_j-\omega_k\right)}{\sqrt{\omega_j\omega_k}}\left(\mathrm{D}(1,j,1,k) - \mathrm{D}(1,j,-1,k)\right)\right)B_\alpha \zeta_{jk}^{\alpha} \\ \tilde{\mathrm{H}}_{21,1}(j,k,\alpha) &= \left(-\frac{1}{2}\frac{\left(\omega_j+\omega_k\right)\left(\omega_j-\omega_k\right)}{\sqrt{\omega_j\omega_k}}\left(\mathrm{D}(1,j,1,k) + \mathrm{D}(1,j,-1,k)\right)\right)B_\alpha \zeta_{jk}^{\alpha}\end{aligned} \tag{7.51}$$

$$\tilde{\mathbf{H}}_{21} = \sum_{jk}^{N}\sum_{\alpha}^{3}\tilde{\mathrm{H}}_{21,0}(j,k,\alpha)\mathbf{q}_j\mathbf{p}_k\mathbf{J}_\alpha + \sum_{jk}^{N}\sum_{\alpha}^{3}\tilde{\mathrm{H}}_{21,1}(j,k,\alpha)\mathbf{p}_j\mathbf{q}_k\mathbf{J}_\alpha \tag{7.52}$$

Vibrational matrix element of two fundamentals

Let us now consider the vibrational matrix elements for the case of a pair of fundamentals ν_{A} and ν_{B}. We can find the expression for the matrix element by evaluating Eq. (7.52) by

applying a sum over states. The nonzero contributions to the matrix element are then given by Eq. (7.54). Evaluation of the vibrational expectation values yields Eq. (7.55), and substitution of the definitions of the $\tilde{\mathrm{H}}_{21}$ coefficients from Eq. (7.51) gives the expression in Eq. (7.56). There are two possible outcomes depending on whether the pair of fundamentals are resonant or not. If they are not resonant, then the denominator function in Eq. (7.56) will cancel its multiplier to yield one, which in turn leads to zero within the parentheses and a zero value overall. For the case of a resonant pair, the denominator function in Eq. (7.56) yields zero, leading to a value of one within the parentheses, and an overall nonzero value (assuming the ζ constant is nonzero as well). The outcomes, summarized in Eq. (7.57), are effectively block diagonal with respect to vibration and thus we have successfully transformed the Hamiltonian to obtain $\tilde{\mathbf{H}}_{21}$.

$$\begin{aligned}\left\langle \nu_{\mathrm{A}} \left| \tilde{\mathbf{H}}_{21} \right| \nu_{\mathrm{B}} \right\rangle &= \sum_{jk}^{N} \sum_{\alpha}^{3} \tilde{\mathrm{H}}_{21,0}(j,k,\alpha) \left\langle \nu_{\mathrm{A}} \left| \mathbf{q}_j \mathbf{p}_k \right| \nu_{\mathrm{B}} \right\rangle \mathbf{J}_\alpha \\ &\quad + \sum_{jk}^{N} \sum_{\alpha}^{3} \tilde{\mathrm{H}}_{21,1}(j,k,\alpha) \left\langle \nu_{\mathrm{A}} \left| \mathbf{p}_j \mathbf{q}_k \right| \nu_{\mathrm{B}} \right\rangle \mathbf{J}_\alpha \\ &= \sum_{jk}^{N} \sum_{\alpha}^{3} \tilde{\mathrm{H}}_{21,0}(j,k,\alpha) \left\langle \nu_{\mathrm{A}} \left| \mathbf{q}_j \left(\sum_i |i\rangle\langle i| \right) \mathbf{p}_k \right| \nu_{\mathrm{B}} \right\rangle \mathbf{J}_\alpha \\ &\quad + \sum_{jk}^{N} \sum_{\alpha}^{3} \tilde{\mathrm{H}}_{21,1}(j,k,\alpha) \left\langle \nu_{\mathrm{A}} \left| \mathbf{p}_j \left(\sum_i |i\rangle\langle i| \right) \mathbf{q}_k \right| \nu_{\mathrm{B}} \right\rangle \mathbf{J}_\alpha \end{aligned} \tag{7.53}$$

$$\begin{aligned}\left\langle \nu_{\mathrm{A}} \left| \tilde{\mathbf{H}}_{21} \right| \nu_{\mathrm{B}} \right\rangle &= \sum_{jk}^{N} \sum_{\alpha}^{3} \tilde{\mathrm{H}}_{21,0}(j,k,\alpha) \left\langle \nu_{\mathrm{A}} \left| \mathbf{q}_j \left(|0\rangle\langle 0| + |\nu_{\mathrm{A}}, \nu_{\mathrm{B}}\rangle\langle \nu_{\mathrm{A}}, \nu_{\mathrm{B}}| \right) \mathbf{p}_k \right| \nu_{\mathrm{B}} \right\rangle \mathbf{J}_\alpha \\ &\quad + \sum_{jk}^{N} \sum_{\alpha}^{3} \tilde{\mathrm{H}}_{21,1}(j,k,\alpha) \left\langle \nu_{\mathrm{A}} \left| \mathbf{p}_j \left(|0\rangle\langle 0| + |\nu_{\mathrm{A}}, \nu_{\mathrm{B}}\rangle\langle \nu_{\mathrm{A}}, \nu_{\mathrm{B}}| \right) \mathbf{q}_k \right| \nu_{\mathrm{B}} \right\rangle \mathbf{J}_\alpha \end{aligned} \tag{7.54}$$

$$\begin{aligned}\left\langle \nu_{\mathrm{A}} \left| \tilde{\mathbf{H}}_{21} \right| \nu_{\mathrm{B}} \right\rangle = \frac{1}{2} i \sum_{\alpha}^{3} \Big(& -\tilde{\mathrm{H}}_{21,0}\left(\mathrm{A},\mathrm{B},\alpha\right) + \tilde{\mathrm{H}}_{21,0}\left(\mathrm{B},\mathrm{A},\alpha\right) \\ & + \tilde{\mathrm{H}}_{21,1}\left(\mathrm{A},\mathrm{B},\alpha\right) - \tilde{\mathrm{H}}_{21,1}\left(\mathrm{B},\mathrm{A},\alpha\right) \Big) \mathbf{J}_{\alpha}\end{aligned} \tag{7.55}$$

$$\left\langle \nu_{\mathrm{A}} \left| \tilde{\mathbf{H}}_{21} \right| \nu_{\mathrm{B}} \right\rangle = i \frac{\left(\omega_{\mathrm{A}} + \omega_{\mathrm{B}}\right)}{\sqrt{\omega_{\mathrm{A}} \omega_{\mathrm{B}}}} \left(1 - \left(\omega_{\mathrm{A}} - \omega_{\mathrm{B}}\right) \mathrm{D}\left(1,\mathrm{A},-1,\mathrm{B}\right)\right) \sum_{\alpha}^{3} B_{\alpha} \zeta_{\mathrm{AB}}^{\alpha} \mathbf{J}_{\alpha} \tag{7.56}$$

$$\left\langle \nu_{\mathrm{A}} \left| \tilde{\mathbf{H}}_{21} \right| \nu_{\mathrm{B}} \right\rangle = \begin{cases} 0 & \omega_{\mathrm{A}} - \omega_{\mathrm{B}} \gg 0 \\ i \dfrac{\left(\omega_{\mathrm{A}} + \omega_{\mathrm{B}}\right)}{\sqrt{\omega_{\mathrm{A}} \omega_{\mathrm{B}}}} \displaystyle\sum_{\alpha}^{3} B_{\alpha} \zeta_{\mathrm{AB}}^{\alpha} \mathbf{J}_{\alpha} & \omega_{\mathrm{A}} - \omega_{\mathrm{B}} \sim 0 \end{cases} \tag{7.57}$$

Definition of G_a

The Hamiltonian used to treat the first-order Coriolis coupling in experimental fitting of rotational spectra is given by Eq. (7.58). By comparison to Eq. (7.57), we can then define the first-order Coriolis coupling constant G_a as Eq. (7.59), with the definitions of G_b and G_c obtained *via* permutation of the axes. This formula agrees with that previously obtained and frequently utilized.

$$\left\langle \nu_{\mathrm{A}} \left| \mathbf{H}_{\text{coupling}} \right| \nu_{\mathrm{B}} \right\rangle = iG_a \mathbf{J}_a + iG_b \mathbf{J}_b + iG_c \mathbf{J}_c \tag{7.58}$$

$$G_a = \frac{\left(\omega_{\mathrm{A}} + \omega_{\mathrm{B}}\right)}{\sqrt{\omega_{\mathrm{A}} \omega_{\mathrm{B}}}} B_a \zeta_{\mathrm{AB}}^{a} \tag{7.59}$$

Connection of G_a to higher quanta states

Formulas for the first order Coriolis coupling for different combinations of vibrational states can also be obtained by the evaluation of Eq. (7.52) for the appropriate vibrational matrix element *e.g.*, the overtone $2\nu_{\mathrm{A}}$ with the combination $\nu_{\mathrm{A}} + \nu_{\mathrm{B}}$, as allowed by the vibrational

operators. The Hamiltonian will still be block diagonal with respect to vibration for these other matrix elements. Furthermore, the exact formula for G_a, *etc*. will be some multiple of Eq. (7.59). This can be inferred from the evaluation of Eq. (7.54) to yield Eq. (7.55), where the whole expression is multiplied by the evaluation of the vibrational expectation values. A clearer proof is obtained by determining the general expression of the vibrational matrix element for a Hamiltonian with two degrees of vibration (*vide infra*).

Derivation of $\tilde{\mathbf{H}}_{22}$

Sequential contact transformation and the general equation

As shown in Table 7.1, three contact transformations are required to obtain $\tilde{\mathbf{H}}_{22}$: (1) $\mathbf{S}_{12}$, (2) $\mathbf{S}_{21}$, and (3) $\mathbf{S}_{22}$. With the sequential contact transformation identified, we can begin the process of writing the general equation of $\tilde{\mathbf{H}}_{22}$. The original Hamiltonian is approximated in Eq. (7.60) by keeping only terms of up to and including λ^2, as per Eq. (7.1) and Eq. (7.13). The Hamiltonian at each level of transformation is given by Eq. (7.61), with each order of the transformed Hamiltonian defined as in Eq. (7.62).

$$\begin{aligned}\mathbf{H} &\approx \lambda^0\mathbf{H}_0 + \lambda^1\mathbf{H}_1 + \lambda^2\mathbf{H}_2 \\ &= \lambda^0\left(\mathbf{H}_{20}\right) + \lambda^1\left(\mathbf{H}_{30} + \mathbf{H}_{21} + \mathbf{H}_{12} + \mathbf{H}_{02}\right) + \lambda^2\left(\mathbf{H}_{40} + \mathbf{H}_{31} + \mathbf{H}_{22}\right)\end{aligned} \tag{7.60}$$

$$\mathbf{H}^{(j)} = \mathbf{H}_0^{(j)} + \mathbf{H}_1^{(j)} + \mathbf{H}_2^{(j)} \tag{7.61}$$

$$
\begin{aligned}
\mathbf{H}_0^{(j)} &= \mathbf{H}_{20}^{(j-1)} \\
\mathbf{H}_1^{(j)} &= \mathbf{H}_{30}^{(j-1)} + \mathbf{H}_{21}^{(j-1)} + \mathbf{H}_{12}^{(j-1)} + \mathbf{H}_{02}^{(j-1)} + i\left[\mathbf{S}^{(j)}, \mathbf{H}_{20}\right] \\
\mathbf{H}_2^{(j)} &= \mathbf{H}_{40}^{(j-1)} + \mathbf{H}_{31}^{(j-1)} + \mathbf{H}_{22}^{(j-1)} + i\left[\mathbf{S}^{(j)}, \mathbf{H}_{30}^{(j-1)} + \mathbf{H}_{21}^{(j-1)} + \mathbf{H}_{12}^{(j-1)} + \mathbf{H}_{02}^{(j-1)}\right] \\
&\quad -\frac{1}{2}\left[\mathbf{S}^{(j)}, \left[\mathbf{S}^{(j)}, \mathbf{H}_{20}\right]\right]
\end{aligned}
\tag{7.62}
$$

The final transformed Hamiltonian is given by the terms of $\mathbf{H}^{(3)}$ with two degrees of vibration and two degrees of rotation. Iterative application of our selection brace definitions from Eq. (7.14)–(7.17) to Eq. (7.60)–(7.62) yields the expressions in Eq. (7.63). Using these results allows us to write the expression for the final transformed Hamiltonian $\tilde{\mathbf{H}}_{22}$ in Eq. (7.64), first in terms of the twice-transformed Hamiltonian $\mathbf{H}^{(2)}$, then in terms of the once-transformed Hamiltonian $\mathbf{H}^{(1)}$, and finally the original Hamiltonian $\mathbf{H}$.

$$
\begin{aligned}
\tilde{\mathbf{H}}_{22} &\equiv \left\{\mathbf{H}^{(3)}\right\}_{22} = \mathbf{H}_{22}^{(2)} + i\left[\mathbf{S}_{22}, \mathbf{H}_{20}\right]_{\mathrm{V}} \\
\mathbf{H}_{22}^{(2)} &= \left\{\mathbf{H}^{(2)}\right\}_{22} = \mathbf{H}_{22}^{(1)} + i\left[\mathbf{S}_{21}, \mathbf{H}_{21}^{(1)}\right]_{\mathrm{V}} + i\left[\mathbf{S}_{21}, \mathbf{H}_{02}^{(1)}\right]_{\mathrm{R}} - \frac{1}{2}\left[\mathbf{S}_{21}, \left[\mathbf{S}_{21}, \mathbf{H}_{20}\right]_{\mathrm{V}}\right]_{\mathrm{V}} \\
\mathbf{H}_{22}^{(1)} &= \left\{\mathbf{H}^{(1)}\right\}_{22} = \mathbf{H}_{22} + i\left[\mathbf{S}_{12}, \mathbf{H}_{30}\right]_{\mathrm{V}} \\
\mathbf{H}_{21}^{(1)} &= \left\{\mathbf{H}^{(1)}\right\}_{21} = \mathbf{H}_{21} \\
\mathbf{H}_{02}^{(1)} &= \left\{\mathbf{H}^{(1)}\right\}_{02} = \mathbf{H}_{02}
\end{aligned}
\tag{7.63}
$$

$$
\begin{aligned}
\tilde{\mathbf{H}}_{22} \equiv \left\{\mathbf{H}^{(3)}\right\}_{22} &= \mathbf{H}_{22}^{(2)} + i\left[\mathbf{S}_{22}, \mathbf{H}_{20}\right]_{\mathrm{V}} \\
&= \mathbf{H}_{22}^{(1)} + i\left[\mathbf{S}_{21}, \mathbf{H}_{21}^{(1)}\right]_{\mathrm{V}} + i\left[\mathbf{S}_{21}, \mathbf{H}_{02}^{(1)}\right]_{\mathrm{R}} - \frac{1}{2}\left[\mathbf{S}_{21}, \left[\mathbf{S}_{21}, \mathbf{H}_{20}\right]_{\mathrm{V}}\right]_{\mathrm{V}} \\
&\quad + i\left[\mathbf{S}_{22}, \mathbf{H}_{20}\right]_{\mathrm{V}} \\
&= \mathbf{H}_{22} + i\left[\mathbf{S}_{12}, \mathbf{H}_{30}\right]_{\mathrm{V}} + i\left[\mathbf{S}_{21}, \mathbf{H}_{21}\right]_{\mathrm{V}} + i\left[\mathbf{S}_{21}, \mathbf{H}_{02}\right]_{\mathrm{R}} \\
&\quad - \frac{1}{2}\left[\mathbf{S}_{21}, \left[\mathbf{S}_{21}, \mathbf{H}_{20}\right]_{\mathrm{V}}\right]_{\mathrm{V}} + i\left[\mathbf{S}_{22}, \mathbf{H}_{20}\right]_{\mathrm{V}}
\end{aligned}
\tag{7.64}
$$

General equations for defining the transform functions

The defining parts of the transform definitions in Table 7.1 can be similarly derived. The resulting defining equations for $\mathbf{S}_{12}$, $\mathbf{S}_{21}$, and $\mathbf{S}_{22}$ are then given by Eq. (7.65)–(7.67), respectively. Again, the defining equation for the last transform ($\mathbf{S}_{22}$, Eq. (7.67)) is the same as the general equation for the final transformed Hamiltonian term ($\tilde{\mathbf{H}}_{22}$, Eq. (7.64)).

$$\mathbf{H}_{12}^{(1)}\left(\text{b.d.}\right) = \mathbf{H}_{12} + i\left[\mathbf{S}_{12}, \mathbf{H}_{20}\right]_{\text{V}} \tag{7.65}$$

$$\mathbf{H}_{21}^{(2)}\left(\text{b.d.}\right) = \mathbf{H}_{21} + i\left[\mathbf{S}_{21}, \mathbf{H}_{20}\right]_{\text{V}} \tag{7.66}$$

$$\begin{aligned}\mathbf{H}_{22}^{(3)}\left(\text{b.d.}\right) = \mathbf{H}_{22} &+ i\left[\mathbf{S}_{12}, \mathbf{H}_{30}\right]_{\text{V}} + i\left[\mathbf{S}_{21}, \mathbf{H}_{21}\right]_{\text{V}} + i\left[\mathbf{S}_{21}, \mathbf{H}_{02}\right]_{\text{R}} - \frac{1}{2}\left[\mathbf{S}_{21}, \left[\mathbf{S}_{21}, \mathbf{H}_{20}\right]_{\text{V}}\right]_{\text{V}} \\ &+ i\left[\mathbf{S}_{22}, \mathbf{H}_{20}\right]_{\text{V}}\end{aligned} \tag{7.67}$$

Required definitions of the original Hamiltonian

Examination of the general equations for $\tilde{\mathbf{H}}_{22}$ and the defining parts of the transform functions reveals that definitions of the following terms of the original Hamiltonian are required to obtain an analytic expression: $\mathbf{H}_{20}$, $\mathbf{H}_{30}$, $\mathbf{H}_{21}$, $\mathbf{H}_{12}$, $\mathbf{H}_{02}$, $\mathbf{H}_{22}$. We will use abbreviated definitions of these functions as provided in Eq. (7.68)–(7.73); definitions of the coefficients are provided in the Supporting Information and will be used to obtain the final analytic expression.

$$\mathbf{H}_{20} = \sum_{v_0} \mathrm{H}_{20}\left(v_0\right)\mathbf{q}_{v_0}^2 + \sum_{v_0} \mathrm{H}_{20}\left(v_0\right)\mathbf{p}_{v_0}^2 \tag{7.68}$$

$$\mathbf{H}_{30} = \sum_{v_0 v_1 v_2} \mathrm{H}_{30}\left(v_0, v_1, v_2\right)\mathbf{q}_{v_0}\mathbf{q}_{v_1}\mathbf{q}_{v_2} \tag{7.69}$$

$$\mathbf{H}_{21} = \sum_{v_0 v_1}\sum_{r_0} \mathrm{H}_{21}\left(v_0, v_1, r_0\right)\mathbf{q}_{v_0}\mathbf{p}_{v_1}\mathbf{J}_{r_0} \tag{7.70}$$

$$\mathbf{H}_{12} = \sum_{v_0} \sum_{r_0 r_1} \mathrm{H}_{12}\left(v_0, r_0, r_1\right) \mathbf{q}_{v_0} \mathbf{J}_{r_0} \mathbf{J}_{r_1} \tag{7.71}$$

$$\mathbf{H}_{02} = \sum_{r_0} \mathrm{H}_{02}\left(r_0\right) \mathbf{J}_{r_0}^2 \tag{7.72}$$

$$\mathbf{H}_{22} = \sum_{v_0 v_1} \sum_{r_0 r_1} \mathrm{H}_{22}\left(v_0, v_1, r_0, r_1\right) \mathbf{q}_{v_0} \mathbf{q}_{v_1} \mathbf{J}_{r_0} \mathbf{J}_{r_1} \tag{7.73}$$

Finding the definitions of $\boldsymbol{S}_{12}$ and $\boldsymbol{S}_{21}$

The derivation of the first two transform functions $\mathbf{S}_{12}$ and $\mathbf{S}_{21}$ using Eq. (7.65) and Eq. (7.66), respectively, is straightforward, as their definitions are dependent only their counterparts from the original Hamiltonian. A more detailed derivation is provided in the Supporting Information, and yields the results given in Eq. (7.74) and Eq. (7.75) using the coefficients defined in Eq. (7.76) and Eq. (7.77), respectively.

$$\mathbf{S}_{12} = \sum_{v_0} \sum_{r_0 r_1} \mathrm{S}_{12}\left(v_0, r_0, r_1\right) \mathbf{p}_{v_0} \mathbf{J}_{r_0} \mathbf{J}_{r_1} \tag{7.74}$$

$$\mathbf{S}_{21} = \sum_{v_0 v_1} \sum_{r_0} \mathrm{S}_{21,0}\left(v_0, v_1, r_0\right) \mathbf{q}_{v_0} \mathbf{q}_{v_1} \mathbf{J}_{r_0} + \sum_{v_0 v_1} \sum_{r_0} \mathrm{S}_{21,1}\left(v_0, v_1, r_0\right) \mathbf{p}_{v_0} \mathbf{p}_{v_1} \mathbf{J}_{r_0} \tag{7.75}$$

$$\mathrm{S}_{12}\left(v_0, r_0, r_1\right) = -\mathrm{D}\left(1, v_0\right) \mathrm{H}_{12}\left(v_0, r_0, r_1\right) \tag{7.76}$$

$$\begin{aligned} \mathrm{S}_{21,0}\left(v_0, v_1, r_0\right) &= \frac{1}{4}\Big(\mathrm{D}\left(1, v_0; 1, v_1\right)\left(\mathrm{H}_{21}\left(v_0, v_1, r_0\right) + \mathrm{H}_{21}\left(v_1, v_0, r_0\right)\right) \\ &\qquad - \mathrm{D}\left(1, v_0; -1, v_1\right)\left(\mathrm{H}_{21}\left(v_0, v_1, r_0\right) - \mathrm{H}_{21}\left(v_1, v_0, r_0\right)\right)\Big) \\ \mathrm{S}_{21,1}\left(v_0, v_1, r_0\right) &= \frac{-1}{4}\Big(\mathrm{D}\left(1, v_0; 1, v_1\right)\left(\mathrm{H}_{21}\left(v_0, v_1, r_0\right) + \mathrm{H}_{21}\left(v_1, v_0, r_0\right)\right) \\ &\qquad + \mathrm{D}\left(1, v_0; -1, v_1\right)\left(\mathrm{H}_{21}\left(v_0, v_1, r_0\right) - \mathrm{H}_{21}\left(v_1, v_0, r_0\right)\right)\Big) \end{aligned} \tag{7.77}$$

Evaluating the commutators from the first two transformations

The derivation of the third transform function $\mathbf{S}_{22}$ requires evaluation of two vibrational commutators and one rotational commutator, as well as a nested vibrational commutator, using the transform functions that we just defined. These same commutators will need to be evaluated to obtain an expression for $\tilde{\mathbf{H}}_{22}$. These commutators can be written as in Eq. (7.78)–(7.81), where the coefficients are defined in Eq. (7.82)–(7.85), respectively. More detailed derivations of these expressions are provided in the Supporting Information.

$$i\left[\mathbf{S}_{12},\mathbf{H}_{30}\right]_{\mathrm{V}} = \sum_{v_0 v_1 v_2}\sum_{r_0 r_1} \mathrm{A}_{22}\left(v_0,v_1,v_2,r_0,r_1\right)\mathbf{q}_{v_0}\mathbf{q}_{v_1}\mathbf{J}_{r_0}\mathbf{J}_{r_1} \tag{7.78}$$

$$\begin{aligned} i\left[\mathbf{S}_{21},\mathbf{H}_{21}\right]_{\mathrm{V}} = &\sum_{v_0 v_1 v_2}\sum_{r_0 r_1} \mathrm{B}_{22,0}\left(v_0,v_1,v_2,r_0,r_1\right)\mathbf{q}_{v_0}\mathbf{q}_{v_1}\mathbf{J}_{r_0}\mathbf{J}_{r_1} \\ &+\sum_{v_0 v_1 v_2}\sum_{r_0 r_1} \mathrm{B}_{22,1}\left(v_0,v_1,v_2,r_0,r_1\right)\mathbf{p}_{v_0}\mathbf{p}_{v_1}\mathbf{J}_{r_0}\mathbf{J}_{r_1} \end{aligned} \tag{7.79}$$

$$\begin{aligned} i\left[\mathbf{S}_{21},\mathbf{H}_{02}\right]_{\mathrm{R}} = &\sum_{v_0 v_1}\sum_{r_0 r_1 r_2} \mathrm{C}_{22,0}\left(v_0,v_1,r_0,r_1,r_2\right)\mathbf{q}_{v_0}\mathbf{q}_{v_1}\mathbf{J}_{r_0}\mathbf{J}_{r_1} \\ &+\sum_{v_0 v_1}\sum_{r_0 r_1 r_2} \mathrm{C}_{22,1}\left(v_0,v_1,r_0,r_1,r_2\right)\mathbf{p}_{v_0}\mathbf{p}_{v_1}\mathbf{J}_{r_0}\mathbf{J}_{r_1} \end{aligned} \tag{7.80}$$

$$\begin{aligned} -\frac{1}{2}\Big[\mathbf{S}_{21},\left[\mathbf{S}_{21},\mathbf{H}_{20}\right]_{\mathrm{V}}\Big]_{\mathrm{V}} = &\sum_{v_0 v_1 v_2}\sum_{r_0 r_1} \mathrm{D}_{22,0}\left(v_0,v_1,v_2,r_0,r_1\right)\mathbf{q}_{v_0}\mathbf{q}_{v_1}\mathbf{J}_{r_0}\mathbf{J}_{r_1} \\ &+\sum_{v_0 v_1 v_2}\sum_{r_0 r_1} \mathrm{D}_{22,1}\left(v_0,v_1,v_2,r_0,r_1\right)\mathbf{p}_{v_0}\mathbf{p}_{v_1}\mathbf{J}_{r_0}\mathbf{J}_{r_1} \end{aligned} \tag{7.81}$$

$$\mathrm{A}_{22}\left(v_0,v_1,v_2,r_0,r_1\right) = \mathrm{S}_{12}\left(v_2,r_0,r_1\right)\Big(\mathrm{H}_{30}\left(v_0,v_1,v_2\right)+\mathrm{H}_{30}\left(v_0,v_2,v_1\right)+\mathrm{H}_{30}\left(v_2,v_0,v_1\right)\Big) \tag{7.82}$$

$$\begin{aligned}
\mathrm{B}_{22,0}\left(v_0,v_1,v_2,r_0,r_1\right) = \frac{-1}{2}\Big(&\mathrm{S}_{21,0}\left(v_0,v_2,r_0\right)\mathrm{H}_{21}\left(v_1,v_2,r_1\right)\\
&+\mathrm{S}_{21,0}\left(v_2,v_1,r_0\right)\mathrm{H}_{21}\left(v_0,v_2,r_1\right)\\
&+\mathrm{S}_{21,0}\left(v_0,v_2,r_1\right)\mathrm{H}_{21}\left(v_1,v_2,r_0\right)\\
&+\mathrm{S}_{21,0}\left(v_2,v_1,r_1\right)\mathrm{H}_{21}\left(v_0,v_2,r_0\right)\Big)\\
\mathrm{B}_{22,1}\left(v_0,v_1,v_2,r_0,r_1\right) = \frac{1}{2}\Big(&\left(\mathrm{S}_{21,1}\left(v_0,v_2,r_0\right)+\mathrm{S}_{21,1}\left(v_2,v_0,r_0\right)\right)\mathrm{H}_{21}\left(v_2,v_1,r_1\right)\\
&+\left(\mathrm{S}_{21,1}\left(v_0,v_2,r_1\right)+\mathrm{S}_{21,1}\left(v_2,v_0,r_1\right)\right)\mathrm{H}_{21}\left(v_2,v_1,r_0\right)\Big)
\end{aligned} \tag{7.83}$$

$$\begin{aligned}
\mathrm{C}_{22,0}\left(v_0,v_1,r_0,r_1,r_2\right) &= \epsilon_{r_0r_1r_2}\,\mathrm{S}_{21,0}\left(v_0,v_1,r_2\right)\left(\mathrm{H}_{02}\left(r_0\right)-\mathrm{H}_{02}\left(r_1\right)\right)\\
\mathrm{C}_{22,1}\left(v_0,v_1,r_0,r_1,r_2\right) &= \epsilon_{r_0r_1r_2}\,\mathrm{S}_{21,1}\left(v_0,v_1,r_2\right)\left(\mathrm{H}_{02}\left(r_0\right)-\mathrm{H}_{02}\left(r_1\right)\right)
\end{aligned} \tag{7.84}$$

(7.85)

Finding the definition of $\boldsymbol{S}_{22}$

Now that the commutators contained within the defining part of $\mathbf{S}_{22}$ have been evaluated, the transform function can be defined. The process of applying the ladder solution (rewriting the defining part of $\mathbf{S}_{22}$ in terms of vibrational ladder operators, applying the formula in Eq. (7.26), and rewriting the result in terms of vibrational operators **q** and **p**) is the same as described before, albeit more extensive. The transform function can then be written as Eq. (7.86), using the coefficients defined in Eq. (7.87) and Eq. (7.88). The derivation of these expressions is provided in the Supporting Information.

$$\mathbf{S}_{22} = \sum_{v_0v_1}\sum_{r_0r_1}\mathrm{S}_{22,0}\left(v_0,v_1,r_0,r_1\right)\mathbf{q}_{v_0}\mathbf{p}_{v_1}\mathbf{J}_{r_0}\mathbf{J}_{r_1} + \sum_{v_0v_1}\sum_{r_0r_1}\mathrm{S}_{22,1}\left(v_0,v_1,r_0,r_1\right)\mathbf{p}_{v_0}\mathbf{q}_{v_1}\mathbf{J}_{r_0}\mathbf{J}_{r_1} \tag{7.86}$$

$$
\begin{aligned}
&\mathrm{S}_{22,0}\left(v_0,v_1,r_0,r_1\right)\\
&\quad=\frac{1}{4}\Big(\Big(-\mathrm{D}\left(1,v_0;1,v_1\right)+\mathrm{D}\left(1,v_0;-1,v_1\right)\Big)\Big(\mathrm{E}_{22,0}\left(v_0,v_1,r_0,r_1\right)+\mathrm{E}_{22,0}\left(v_1,v_0,r_0,r_1\right)\Big)\\
&\qquad+\Big(\mathrm{D}\left(1,v_0;1,v_1\right)+\mathrm{D}\left(1,v_0;-1,v_1\right)\Big)\Big(\mathrm{E}_{22,1}\left(v_0,v_1,r_0,r_1\right)+\mathrm{E}_{22,1}\left(v_1,v_0,r_0,r_1\right)\Big)\Big)\\
&\mathrm{S}_{22,1}\left(v_0,v_1,r_0,r_1\right)\\
&\quad=\frac{-1}{4}\Big(\Big(\mathrm{D}\left(1,v_0;1,v_1\right)+\mathrm{D}\left(1,v_0;-1,v_1\right)\Big)\Big(\mathrm{E}_{22,0}\left(v_0,v_1,r_0,r_1\right)+\mathrm{E}_{22,0}\left(v_1,v_0,r_0,r_1\right)\Big)\\
&\qquad+\Big(-\mathrm{D}\left(1,v_0;1,v_1\right)+\mathrm{D}\left(1,v_0;-1,v_1\right)\Big)\Big(\mathrm{E}_{22,1}\left(v_0,v_1,r_0,r_1\right)+\mathrm{E}_{22,1}\left(v_1,v_0,r_0,r_1\right)\Big)\Big)
\end{aligned}
\tag{7.87}
$$

$$
\begin{aligned}
\mathrm{E}_{22,0}\left(v_0,v_1,r_0,r_1\right)=\sum_{v_2}\sum_{r_2}\Bigg(&\frac{1}{3N}\mathrm{H}_{22}\left(v_0,v_1,r_0,r_1\right)+\frac{1}{3}\mathrm{A}_{22}\left(v_0,v_1,v_2,r_0,r_1\right)\\
&+\frac{1}{3}\mathrm{B}_{22,0}\left(v_0,v_1,v_2,r_0,r_1\right)+\frac{1}{N}\mathrm{C}_{22,0}\left(v_0,v_1,r_0,r_1,r_2\right)\\
&+\frac{1}{3}\mathrm{D}_{22,0}\left(v_0,v_1,v_2,r_0,r_1\right)\Bigg)
\end{aligned}
\tag{7.88}
$$

$$
\begin{aligned}
\mathrm{E}_{22,1}\left(v_0,v_1,r_0,r_1\right)=\sum_{v_2}\sum_{r_2}\Bigg(&\frac{1}{3}\mathrm{B}_{22,1}\left(v_0,v_1,v_2,r_0,r_1\right)+\frac{1}{N}\mathrm{C}_{22,1}\left(v_0,v_1,r_0,r_1,r_2\right)\\
&+\frac{1}{3}\mathrm{D}_{22,1}\left(v_0,v_1,v_2,r_0,r_1\right)\Bigg)
\end{aligned}
$$

Evaluating the final commutator

All that remains to obtain the analytic expression for $\tilde{\mathbf{H}}_{22}$ is to evaluate the commutator between the transform function $\mathbf{S}_{22}$ and the zeroth order term of the original Hamiltonian, $\mathbf{H}_{20}$. Applying the definitions from Eq. (7.68) and Eq. (7.86) yields Eq. (7.89), using the coefficients defined in Eq. (7.90).

$$
\begin{aligned}
i\left[\mathbf{S}_{22},\mathbf{H}_{20}\right]_{\mathrm{V}}=&\sum_{v_0v_1}\sum_{r_0r_1}\mathrm{F}_{22,0}\left(v_0,v_1,r_0,r_1\right)\mathbf{q}_{v_0}\mathbf{q}_{v_1}\mathbf{J}_{r_0}\mathbf{J}_{r_1}\\
&+\sum_{v_0v_1}\sum_{r_0r_1}\mathrm{F}_{22,1}\left(v_0,v_1,r_0,r_1\right)\mathbf{p}_{v_0}\mathbf{p}_{v_1}\mathbf{J}_{r_0}\mathbf{J}_{r_1}
\end{aligned}
\tag{7.89}
$$

$$\begin{aligned}\mathrm{F}_{22,0}\left(v_0,v_1,r_0,r_1\right)&=2\left(\mathrm{S}_{22,0}\left(v_0,v_1,r_0,r_1\right)\mathrm{H}_{20}\left(v_1\right)+\mathrm{S}_{22,1}\left(v_0,v_1,r_0,r_1\right)\mathrm{H}_{20}\left(v_0\right)\right)\\ \mathrm{F}_{22,1}\left(v_0,v_1,r_0,r_1\right)&=\left(-2\right)\left(\mathrm{S}_{22,0}\left(v_0,v_1,r_0,r_1\right)\mathrm{H}_{20}\left(v_0\right)+\mathrm{S}_{22,1}\left(v_0,v_1,r_0,r_1\right)\mathrm{H}_{20}\left(v_1\right)\right)\end{aligned} \tag{7.90}$$

The analytic expression

Combining this commutator with the rest of the general equation (which were evaluated in order to obtain $\mathbf{S}_{22}$) yields Eq. (7.91) using the coefficients in Eq. (7.92). A definition expressed in terms of the molecular properties can be obtained through iterative substitution of the coefficients that we've defined thus far. Such a definition is provided in the Supporting Information.

$$\tilde{\mathbf{H}}_{22}=\sum_{v_0v_1}\sum_{r_0r_1}\tilde{\mathrm{H}}_{22,0}\left(v_0,v_1,r_0,r_1\right)\mathbf{q}_{v_0}\mathbf{q}_{v_1}\mathbf{J}_{r_0}\mathbf{J}_{r_1}+\sum_{v_0v_1}\sum_{r_0r_1}\tilde{\mathrm{H}}_{22,1}\left(v_0,v_1,r_0,r_1\right)\mathbf{p}_{v_0}\mathbf{p}_{v_1}\mathbf{J}_{r_0}\mathbf{J}_{r_1} \tag{7.91}$$

$$\begin{aligned}\tilde{\mathrm{H}}_{22,0}\left(v_0,v_1,r_0,r_1\right)&=\mathrm{E}_{22,0}\left(v_0,v_1,r_0,r_1\right)+\mathrm{F}_{22,0}\left(v_0,v_1,r_0,r_1\right)\\ \tilde{\mathrm{H}}_{22,1}\left(v_0,v_1,r_0,r_1\right)&=\mathrm{E}_{22,1}\left(v_0,v_1,r_0,r_1\right)+\mathrm{F}_{22,1}\left(v_0,v_1,r_0,r_1\right)\end{aligned} \tag{7.92}$$

Rotational Reduction of $\tilde{\mathbf{H}}_{22}$

The rotational contact transformation

Using Eq. (7.31), the transform function that will affect $\tilde{\mathbf{H}}_{22}$ is given by $\mathbf{S}^{\mathrm{r}}=\mathbf{S}^{\mathrm{r}}_{22}+\mathbf{S}^{\mathrm{r}}_{21}$, which results in the reduction equation Eq. (7.93). The 'r' superscript for the transform functions is to denote that these transform functions are distinct from the ones used to block diagonalize the Hamiltonian in the previous section. The definitions of the reducing transform functions are unknown at this point, and what follows is the process of defining them such that the Hamiltonian will be reduced as per Eq. (7.93).

$$\tilde{\mathbf{H}}^{\mathrm{red}}_{22}=\tilde{\mathbf{H}}_{22}+i\left[\mathbf{S}^{\mathrm{r}}_{22},\mathbf{H}_{20}\right]_{\mathrm{V}}+i\left[\mathbf{S}^{\mathrm{r}}_{21},\mathbf{H}_{02}\right]_{\mathrm{R}} \tag{7.93}$$

Trial transform functions

Effectively, we are applying an abbreviated form of the trial solution approach to obtain definitions of the rotational reduction transform functions. Consider that $\tilde{\mathbf{H}}_{22}$ contains only the products of vibrational operators $\mathbf{qq}$ and $\mathbf{pp}$. The terms of the commutators containing those same products are all that are required to affect the transformation, and similarly only the terms of the transform functions that will yield said terms of the commutator are required. Since the rotational commutator does not affect the vibrational operators, the transform function $\mathbf{S}^{\mathrm{r}}_{21}$ is readily written as in Eq. (7.94). Then, a quick consideration of the possible combinations of vibrational commutators leaves us with the definition of the transform function $\mathbf{S}^{\mathrm{r}}_{22}$ as in Eq. (7.95) . The coefficients used in these expressions are yet to be defined, and the process of defining them constitutes the bulk of the effort for reducing the Hamiltonian.

$$\mathbf{S}^{\mathrm{r}}_{21} = \sum_{v_0 v_1}\sum_{r_0} \mathrm{S}^{\mathrm{r}}_{21,0}\left(v_0, v_1, r_0\right)\mathbf{q}_{v_0}\mathbf{q}_{v_1}\mathbf{J}_{r_0} + \sum_{v_0 v_1}\sum_{r_0} \mathrm{S}^{\mathrm{r}}_{21,1}\left(v_0, v_1, r_0\right)\mathbf{p}_{v_0}\mathbf{p}_{v_1}\mathbf{J}_{r_0} \tag{7.94}$$

$$\mathbf{S}^{\mathrm{r}}_{22} = \sum_{v_0 v_1}\sum_{r_0 r_1} \mathrm{S}^{\mathrm{r}}_{22,0}\left(v_0, v_1, r_0, r_1\right)\mathbf{q}_{v_0}\mathbf{p}_{v_1}\mathbf{J}_{r_0}\mathbf{J}_{r_1} + \sum_{v_0 v_1}\sum_{r_0 r_1} \mathrm{S}^{\mathrm{r}}_{22,1}\left(v_0, v_1, r_0, r_1\right)\mathbf{p}_{v_0}\mathbf{q}_{v_1}\mathbf{J}_{r_0}\mathbf{J}_{r_1} \tag{7.95}$$

The reduced Hamiltonian

Evaluation of the two commutators in Eq. (7.93) results in Eq. (7.96) and Eq. (7.97). Substituting these expressions back into Eq. (7.93) yields the reduced Hamiltonian shown in Eq. (7.98), using the coefficient defined in Eq. (7.99). With the reduced Hamiltonian thus defined, we can begin the process of defining the coefficients of the transform functions that are contained within Eq. (7.99) so as to obtain the rotational reduction.

$$
\begin{aligned}
&i\Big[\mathbf{S}^{\mathrm{r}}_{22},\mathbf{H}_{20}\Big]_{\mathrm{V}} \\
&\quad= i\Bigg[\sum_{v_0v_1}\sum_{r_0r_1}\mathrm{S}^{\mathrm{r}}_{22,0}\left(v_0,v_1,r_0,r_1\right)\mathbf{q}_{v_0}\mathbf{p}_{v_1}\mathbf{J}_{r_0}\mathbf{J}_{r_1}+\sum_{v_0v_1}\sum_{r_0r_1}\mathrm{S}^{\mathrm{r}}_{22,1}\left(v_0,v_1,r_0,r_1\right)\mathbf{p}_{v_0}\mathbf{q}_{v_1}\mathbf{J}_{r_0}\mathbf{J}_{r_1} \\
&\qquad\qquad ,\sum_{v_2}\frac{1}{2}\omega_{v_2}\mathbf{q}_{v_2}\mathbf{q}_{v_2}+\sum_{v_2}\frac{1}{2}\omega_{v_2}\mathbf{p}_{v_2}\mathbf{p}_{v_2}\Bigg]_{\mathrm{V}} \\
&\quad=\sum_{v_0v_1}\sum_{r_0r_1}\Big(\omega_{v_1}\,\mathrm{S}^{\mathrm{r}}_{22,0}\left(v_0,v_1,r_0,r_1\right)+\omega_{v_0}\,\mathrm{S}^{\mathrm{r}}_{22,1}\left(v_0,v_1,r_0,r_1\right)\Big)\mathbf{q}_{v_0}\mathbf{q}_{v_1}\mathbf{J}_{r_0}\mathbf{J}_{r_1} \\
&\qquad+\sum_{v_0v_1}\sum_{r_0r_1}(-1)\Big(\omega_{v_0}\,\mathrm{S}^{\mathrm{r}}_{22,0}\left(v_0,v_1,r_0,r_1\right)+\omega_{v_1}\,\mathrm{S}^{\mathrm{r}}_{22,1}\left(v_0,v_1,r_0,r_1\right)\Big)\mathbf{p}_{v_0}\mathbf{p}_{v_1}\mathbf{J}_{r_0}\mathbf{J}_{r_1}
\end{aligned}
\tag{7.96}
$$

$$
\begin{aligned}
i\Big[\mathbf{S}^{\mathrm{r}}_{21},\mathbf{H}_{02}\Big]_{\mathrm{R}} &= i\Bigg[\sum_{v_0v_1}\sum_{r_0}\mathrm{S}^{\mathrm{r}}_{21,0}\left(v_0,v_1,r_0\right)\mathbf{q}_{v_0}\mathbf{q}_{v_1}\mathbf{J}_{r_0}+\sum_{v_0v_1}\sum_{r_0}\mathrm{S}^{\mathrm{r}}_{21,1}\left(v_0,v_1,r_0\right)\mathbf{p}_{v_0}\mathbf{p}_{v_1}\mathbf{J}_{r_0} \\
&\qquad\qquad ,\sum_{r_1}B_{r_1}\mathbf{J}_{r_1}\mathbf{J}_{r_1}\Bigg]_{\mathrm{R}} \\
&=\sum_{v_0v_1}\sum_{r_0r_1r_2}\epsilon_{r_0r_1r_2}\left(B_{r_0}-B_{r_1}\right)\mathrm{S}^{\mathrm{r}}_{21,0}\left(v_0,v_1,r_2\right)\mathbf{q}_{v_0}\mathbf{q}_{v_1}\mathbf{J}_{r_0}\mathbf{J}_{r_1} \\
&\qquad+\sum_{v_0v_1}\sum_{r_0r_1r_2}\epsilon_{r_0r_1r_2}\left(B_{r_0}-B_{r_1}\right)\mathrm{S}^{\mathrm{r}}_{21,1}\left(v_0,v_1,r_2\right)\mathbf{p}_{v_0}\mathbf{p}_{v_1}\mathbf{J}_{r_0}\mathbf{J}_{r_1}
\end{aligned}
\tag{7.97}
$$

$$
\tilde{\mathbf{H}}^{\mathrm{red}}_{22}=\sum_{r_0r_1}\tilde{\mathrm{H}}^{\mathrm{red}}_{22}\left(r_0,r_1\right)\mathbf{J}_{r_0}\mathbf{J}_{r_1}
\tag{7.98}
$$

$$
\begin{aligned}
\tilde{\mathrm{H}}^{\mathrm{red}}_{22}\left(r_0,r_1\right)=\sum_{v_0v_1}\Big(&\tilde{\mathrm{H}}_{22,0}\left(v_0,v_1,r_0,r_1\right)+\omega_{v_1}\,\mathrm{S}^{\mathrm{r}}_{22,0}\left(v_0,v_1,r_0,r_1\right)+\omega_{v_0}\,\mathrm{S}^{\mathrm{r}}_{22,1}\left(v_0,v_1,r_0,r_1\right) \\
&+\sum_{r_2}\epsilon_{r_0r_1r_2}\left(B_{r_0}-B_{r_1}\right)\mathrm{S}^{\mathrm{r}}_{21,0}\left(v_0,v_1,r_2\right)\Big)\mathbf{q}_{v_0}\mathbf{q}_{v_1} \\
+\sum_{v_0v_1}\Big(&\tilde{\mathrm{H}}_{22,1}\left(v_0,v_1,r_0,r_1\right)-\omega_{v_0}\,\mathrm{S}^{\mathrm{r}}_{22,0}\left(v_0,v_1,r_0,r_1\right)-\omega_{v_1}\,\mathrm{S}^{\mathrm{r}}_{22,1}\left(v_0,v_1,r_0,r_1\right) \\
&+\sum_{r_2}\epsilon_{r_0r_1r_2}\left(B_{r_0}-B_{r_1}\right)\mathrm{S}^{\mathrm{r}}_{21,1}\left(v_0,v_1,r_2\right)\Big)\mathbf{p}_{v_0}\mathbf{p}_{v_1}
\end{aligned}
\tag{7.99}
$$

The reduced Hamiltonian in cylindrical tensor form

The reduced Hamiltonian in Cartesian coordinates is shown in Eq. (7.100). The Hamiltonian can be written in the cylindrical tensor form by substitution of the definitions of $\mathbf{J}_x$ and $\mathbf{J}_y$ in terms of $\mathbf{J}_\pm$ and judicious application of commutator relations, as well as the identity $\mathbf{J}_-\mathbf{J}_+ + \mathbf{J}_+\mathbf{J}_- = 2\mathbf{J}^2 - 2\mathbf{J}_z{}^2$ (derived from $\mathbf{J}^2 = \mathbf{J}_x{}^2 + \mathbf{J}_y{}^2 + \mathbf{J}_z{}^2$). The result is given by Eq. (7.101) , in which we have made no assumptions regarding the nature of the coefficient and we use the anticommutator notation ($\left[A,B\right]_+ \equiv A\cdot B + B\cdot A$) to abbreviate the expression. (Note that in principle, the process currently being discussed should include all terms $\tilde{\mathbf{H}}^{\text{red}}_{m2}$, but for convenience we are assuming that the rotational reductions can be applied separately for each $\tilde{\mathbf{H}}_{mn}$.) Within the expression are terms of order ~**J**, detailed in Eq. (7.102), but if the coefficient $\tilde{\mathrm{H}}^{\text{red}}_{22}$ is invariant to reversal of indices *i.e.*, if $\tilde{\mathrm{H}}^{\text{red}}_{22}(i,j) = \tilde{\mathrm{H}}^{\text{red}}_{22}(j,i)$, they will be eliminated ($\mathcal{O}(\sim\mathbf{J}) \to 0$). Otherwise, these terms can be removed from $\tilde{\mathbf{H}}^{\text{red}}_{22}$ and placed in the expression for $\tilde{\mathbf{H}}_{m1}$. We now have an expression for $\tilde{\mathbf{H}}^{\text{red}}_{22}$, but it contains a total of six rotational operator terms, while only three such terms are required for the fitting of second-order Coriolis coupling constants. Elimination of terms from this expression is required and can be achieved through proper definition of the transform function coefficients.

$$\begin{aligned}\tilde{\mathbf{H}}^{\text{red}}_{22} = {} & \tilde{\mathrm{H}}^{\text{red}}_{22}(x,x)\mathbf{J}_x\mathbf{J}_x + \tilde{\mathrm{H}}^{\text{red}}_{22}(x,y)\mathbf{J}_x\mathbf{J}_y + \tilde{\mathrm{H}}^{\text{red}}_{22}(x,z)\mathbf{J}_x\mathbf{J}_z \\ & + \tilde{\mathrm{H}}^{\text{red}}_{22}(y,x)\mathbf{J}_y\mathbf{J}_x + \tilde{\mathrm{H}}^{\text{red}}_{22}(y,y)\mathbf{J}_y\mathbf{J}_y + \tilde{\mathrm{H}}^{\text{red}}_{22}(y,z)\mathbf{J}_y\mathbf{J}_z \\ & + \tilde{\mathrm{H}}^{\text{red}}_{22}(z,x)\mathbf{J}_z\mathbf{J}_x + \tilde{\mathrm{H}}^{\text{red}}_{22}(z,y)\mathbf{J}_z\mathbf{J}_y + \tilde{\mathrm{H}}^{\text{red}}_{22}(z,z)\mathbf{J}_z\mathbf{J}_z\end{aligned} \qquad (7.100)$$

$$\begin{aligned}\tilde{\mathbf{H}}_{22}^{\mathrm{red}} &= \frac{1}{2}\left(\tilde{\mathrm{H}}_{22}^{\mathrm{red}}(x,x)+\tilde{\mathrm{H}}_{22}^{\mathrm{red}}(y,y)\right)\mathbf{J}^2-\frac{1}{2}\left(\tilde{\mathrm{H}}_{22}^{\mathrm{red}}(x,x)+\tilde{\mathrm{H}}_{22}^{\mathrm{red}}(y,y)-2\tilde{\mathrm{H}}_{22}^{\mathrm{red}}(z,z)\right)\mathbf{J}_z^2 \\ &+\frac{1}{4}\left(\tilde{\mathrm{H}}_{22}^{\mathrm{red}}(x,x)-\tilde{\mathrm{H}}_{22}^{\mathrm{red}}(y,y)\right)\left(\mathbf{J}_-^2+\mathbf{J}_+^2\right) \\ &-\frac{i}{4}\left(\tilde{\mathrm{H}}_{22}^{\mathrm{red}}(x,y)+\tilde{\mathrm{H}}_{22}^{\mathrm{red}}(y,x)\right)\left(\mathbf{J}_-^2-\mathbf{J}_+^2\right) \\ &+\frac{1}{4}\left(\tilde{\mathrm{H}}_{22}^{\mathrm{red}}(x,z)+\tilde{\mathrm{H}}_{22}^{\mathrm{red}}(z,x)\right)\left[\mathbf{J}_z,\mathbf{J}_-+\mathbf{J}_+\right]_+ \\ &-\frac{i}{4}\left(\tilde{\mathrm{H}}_{22}^{\mathrm{red}}(y,z)+\tilde{\mathrm{H}}_{22}^{\mathrm{red}}(z,y)\right)\left[\mathbf{J}_z,\mathbf{J}_--\mathbf{J}_+\right]_+ +\mathcal{O}(\sim\mathbf{J})\end{aligned} \tag{7.101}$$

$$\begin{aligned}\mathcal{O}(\sim\mathbf{J}) = -\frac{i}{2}\left(\tilde{\mathrm{H}}_{22}^{\mathrm{red}}(x,y)-\tilde{\mathrm{H}}_{22}^{\mathrm{red}}(y,x)\right)\mathbf{J}_z-\frac{i}{4}\left(\tilde{\mathrm{H}}_{22}^{\mathrm{red}}(y,z)-\tilde{\mathrm{H}}_{22}^{\mathrm{red}}(z,y)\right)\left(\mathbf{J}_-+\mathbf{J}_+\right) \\ +\frac{1}{4}\left(\tilde{\mathrm{H}}_{22}^{\mathrm{red}}(x,z)-\tilde{\mathrm{H}}_{22}^{\mathrm{red}}(z,x)\right)\left(\mathbf{J}_--\mathbf{J}_+\right)\end{aligned} \tag{7.102}$$

Connection to experimental coupling constants

First, however, we must determine what terms are to be eliminated from Eq. (7.101). For second order in rotation, there are two instances for which $\tilde{\mathbf{H}}_{22}^{\mathrm{red}}$ can be used: (a) vibrationally on-diagonal matrix elements $\langle i|\tilde{\mathbf{H}}_{22}^{\mathrm{red}}|i\rangle$ and (b) vibrationally off-diagonal matrix elements $\langle i|\tilde{\mathbf{H}}_{22}^{\mathrm{red}}|j\rangle$. The former matrix element corresponds to a correction to the rotational constants $\langle i|\mathbf{H}_{02}|i\rangle$ due to vibration-rotation coupling *i.e.*, the α constants, while the latter corresponds to the second-order Coriolis coupling constants F_{ab}, F_{ac}, and F_{bc} connecting the vibrational states $|i\rangle$ and $|j\rangle$. Note that such differentiation is absent for terms of odd order with respect to rotation, as only vibrationally off-diagonal matrix elements are allowed in that case.

(a) Vibrationally on-diagonal (α constants)

TERMS TO BE ELIMINATED.

The rotational Hamiltonian in the I^r reduction for the vibrationally on-diagonal matrix element requires that the non-totally symmetric terms $\mathbf{J}_-^2 - \mathbf{J}_+^2$, $\left[\mathbf{J}_z, \mathbf{J}_- + \mathbf{J}_+\right]_+$, and $\left[\mathbf{J}_z, \mathbf{J}_- - \mathbf{J}_+\right]_+$ are eliminated. This can be achieved by defining the transform function coefficients such that the corresponding three coefficients will be zero. We can therefore write Eq. (7.103)–(7.105).

$$0 = \left\langle i \middle| \tilde{\mathrm{H}}_{22}^{\mathrm{red}}(x,y) + \tilde{\mathrm{H}}_{22}^{\mathrm{red}}(y,x) \middle| i \right\rangle \tag{7.103}$$

$$0 = \left\langle i \middle| \tilde{\mathrm{H}}_{22}^{\mathrm{red}}(x,z) + \tilde{\mathrm{H}}_{22}^{\mathrm{red}}(z,x) \middle| i \right\rangle \tag{7.104}$$

$$0 = \left\langle i \middle| \tilde{\mathrm{H}}_{22}^{\mathrm{red}}(y,z) + \tilde{\mathrm{H}}_{22}^{\mathrm{red}}(z,y) \middle| i \right\rangle \tag{7.105}$$

SOLVING FOR THE TRANSFORM COEFFICIENTS

Considering the first condition, Eq. (7.103), we can substitute in the definition of $\tilde{\mathrm{H}}_{22}^{\mathrm{red}}$ and write the condition as Eq. (7.106). Ideally, to avoid a dependence of the solution on the particulars of the vibrational matrix elements $\left\langle i \middle| \mathbf{q}_{v_0} \mathbf{q}_{v_1} \middle| i \right\rangle$ and $\left\langle i \middle| \mathbf{p}_{v_0} \mathbf{p}_{v_1} \middle| i \right\rangle$, we solve for the coefficients to yield zero. There are then effectively two equations, and so only two of the transform function coefficients can be solved for. The simplest is to set the $\mathrm{S}_{22}^{\mathrm{r}}$ transform coefficients to zero and solve for the $\mathrm{S}_{21}^{\mathrm{r}}$ transform coefficients. We then have the trivial definition in Eq. (7.107) and the nonzero definitions in Eq. (7.108) and Eq. (7.109), where the other required definitions can be obtained through cyclic permutation of the axes *x*, *y*, and *z*. The superscript ‘r’ for the transform functions is now replaced by the superscript ‘d’ to indicate that these terms are for applying the (on) diagonal reduction.

$$
\begin{aligned}
0 = \sum_{v_0 v_1} \Big(& \tilde{\mathrm{H}}_{22,0}(v_0, v_1, x, y) + \tilde{\mathrm{H}}_{22,0}(v_0, v_1, y, x) \\
& + \omega_{v_1} \left(\mathrm{S}^{\mathrm{r}}_{22,0}(v_0, v_1, x, y) + \mathrm{S}^{\mathrm{r}}_{22,0}(v_0, v_1, y, x) \right) \\
& + \omega_{v_0} \left(\mathrm{S}^{\mathrm{r}}_{22,1}(v_0, v_1, x, y) + \mathrm{S}^{\mathrm{r}}_{22,1}(v_0, v_1, y, x) \right) + 2\left(B_x - B_y\right) \mathrm{S}^{\mathrm{r}}_{21,0}(v_0, v_1, z) \Big) \times \\
& \times \langle i | \mathbf{q}_{v_0} \mathbf{q}_{v_1} | i \rangle \\
+ \sum_{v_0 v_1} \Big(& \tilde{\mathrm{H}}_{22,1}(v_0, v_1, x, y) + \tilde{\mathrm{H}}_{22,1}(v_0, v_1, y, x) \\
& - \omega_{v_0} \left(\mathrm{S}^{\mathrm{r}}_{22,0}(v_0, v_1, x, y) + \mathrm{S}^{\mathrm{r}}_{22,0}(v_0, v_1, y, x) \right) \\
& - \omega_{v_1} \left(\mathrm{S}^{\mathrm{r}}_{22,1}(v_0, v_1, x, y) + \mathrm{S}^{\mathrm{r}}_{22,1}(v_0, v_1, y, x) \right) + 2\left(B_x - B_y\right) \mathrm{S}^{\mathrm{r}}_{21,1}(v_0, v_1, z) \Big) \times \\
& \times \langle i | \mathbf{p}_{v_0} \mathbf{p}_{v_1} | i \rangle
\end{aligned}
\tag{7.106}
$$

$$
\mathrm{S}^{\mathrm{d}}_{22,0}(v_0, v_1, r_0, r_1) = \mathrm{S}^{\mathrm{d}}_{22,1}(v_0, v_1, r_0, r_1) = 0 \tag{7.107}
$$

$$
\mathrm{S}^{\mathrm{d}}_{21,0}(v_0, v_1, z) = \frac{\tilde{\mathrm{H}}_{22,0}(v_0, v_1, x, y) + \tilde{\mathrm{H}}_{22,0}(v_0, v_1, y, x)}{-2\left(B_x - B_y\right)} \text{ and cyclic permutations} \tag{7.108}
$$

$$
\mathrm{S}^{\mathrm{d}}_{21,1}(v_0, v_1, z) = \frac{\tilde{\mathrm{H}}_{22,1}(v_0, v_1, x, y) + \tilde{\mathrm{H}}_{22,1}(v_0, v_1, y, x)}{-2\left(B_x - B_y\right)} \text{ and cyclic permutations} \tag{7.109}
$$

DEFINITION OF THE REDUCED COEFFICIENTS

Substitution of the definitions of coefficients of the transform functions into Eq. (7.106) confirms they satisfy the conditions Eq. (7.103)–(7.105). After applying these definitions to the possible combinations of $\tilde{\mathrm{H}}^{\mathrm{red}}_{22}$, the generalized definitions in Eq. (7.110) and Eq. (7.111) become apparent.

$$
\tilde{\mathrm{H}}^{\mathrm{d,red}}_{22}(a, a) = \sum_{v_0 v_1} \tilde{\mathrm{H}}_{22,0}(v_0, v_1, a, a) \mathbf{q}_{v_0} \mathbf{q}_{v_1} + \sum_{v_0 v_1} \tilde{\mathrm{H}}_{22,1}(v_0, v_1, a, a) \mathbf{p}_{v_0} \mathbf{p}_{v_1} \tag{7.110}
$$

$$\begin{aligned}\tilde{\mathrm{H}}_{22}^{\mathrm{d,red}}(a,b) &= -\tilde{\mathrm{H}}_{22}^{\mathrm{d,red}}(b,a) \\ &= \sum_{v_0 v_1}\frac{1}{2}\left(\tilde{\mathrm{H}}_{22,0}(v_0,v_1,a,b)-\tilde{\mathrm{H}}_{22,0}(v_0,v_1,b,a)\right)\mathbf{q}_{v_0}\mathbf{q}_{v_1} \\ &\quad +\sum_{v_0 v_1}\frac{1}{2}\left(\tilde{\mathrm{H}}_{22,1}(v_0,v_1,a,b)-\tilde{\mathrm{H}}_{22,1}(v_0,v_1,b,a)\right)\mathbf{p}_{v_0}\mathbf{p}_{v_1}\end{aligned} \tag{7.111}$$

The rotational Hamiltonian from Eq. (7.101) can now be written as in Eq. (7.112). The lower order terms $\mathcal{O}(\sim \mathbf{J})$ can be written as Eq. (7.113), which per Eq. (7.111) will go to zero if $\tilde{\mathrm{H}}_{22,0}(v_0,v_1,a,b)=\tilde{\mathrm{H}}_{22,0}(v_0,v_1,b,a)$ and $\tilde{\mathrm{H}}_{22,1}(v_0,v_1,a,b)=\tilde{\mathrm{H}}_{22,1}(v_0,v_1,b,a)$. Returning to the Cartesian form, the reduced Hamiltonian can be written as in Eq. (7.114).

$$\begin{aligned}\tilde{\mathbf{H}}_{22}^{\mathrm{d,red}} &= \frac{1}{2}\left(\tilde{\mathrm{H}}_{22}^{\mathrm{d,red}}(x,x)+\tilde{\mathrm{H}}_{22}^{\mathrm{d,red}}(y,y)\right)\mathbf{J}^2 \\ &\quad -\frac{1}{2}\left(\tilde{\mathrm{H}}_{22}^{\mathrm{d,red}}(x,x)+\tilde{\mathrm{H}}_{22}^{\mathrm{d,red}}(y,y)-2\tilde{\mathrm{H}}_{22}^{\mathrm{d,red}}(z,z)\right)\mathbf{J}_z^2 \\ &\quad +\frac{1}{4}\left(\tilde{\mathrm{H}}_{22}^{\mathrm{d,red}}(x,x)-\tilde{\mathrm{H}}_{22}^{\mathrm{d,red}}(y,y)\right)\left(\mathbf{J}_-^2+\mathbf{J}_+^2\right)+\mathcal{O}(\sim \mathbf{J})\end{aligned} \tag{7.112}$$

$$\mathcal{O}(\sim \mathbf{J}) = -i\tilde{\mathrm{H}}_{22}^{\mathrm{d,red}}(x,y)\mathbf{J}_z-\frac{i}{2}\tilde{\mathrm{H}}_{22}^{\mathrm{d,red}}(y,z)\left(\mathbf{J}_-+\mathbf{J}_+\right)+\frac{1}{2}\tilde{\mathrm{H}}_{22}^{\mathrm{d,red}}(x,z)\left(\mathbf{J}_--\mathbf{J}_+\right) \tag{7.113}$$

$$\begin{aligned}\tilde{\mathbf{H}}_{22}^{\mathrm{d,red}} &= \tilde{\mathrm{H}}_{22}^{\mathrm{d,red}}(x,x)\mathbf{J}_x^2+\tilde{\mathrm{H}}_{22}^{\mathrm{d,red}}(y,y)\mathbf{J}_y^2+\tilde{\mathrm{H}}_{22}^{\mathrm{d,red}}(z,z)\mathbf{J}_z^2 \\ &= \sum_{r_0}\tilde{\mathrm{H}}_{22}^{\mathrm{d,red}}(r_0,r_0)\mathbf{J}_{r_0}^2\end{aligned} \tag{7.114}$$

THE α CORRECTIONS

For the ground state, we can write the vibrational matrix element as in Eq. (7.115). By comparison to Eq. (7.116), the α corrections are given by Eq. (7.117). The general formula for application to other vibrational states can be obtained in a similar manner. Applying successive

substitutions of the previously obtained coefficient definitions yields Eq. (7.118), which in turn leads to the analytic expression for the α corrections in Eq. (7.119). For these equations, we apply a strict resonance condition; that is, the resonance threshold is zero. This expression is identical to the one previously obtained by Aliev and Watson (Eq. (100) in Ref. 4) once the on-diagonal condition has been applied. The "deperturbed" expression for the α correction is similarly obtained, but where the resonance threshold is greater than zero. The formula is effectively the same, except that $\left(\omega_{v_0}-\omega_{v_1}\right)^{-1}$ in the last summation of Eq. (7.119) is replaced with the denominator function $\mathrm{D}\left(1,\omega_{v_0},-1,\omega_{v_1}\right)$.

$$\begin{aligned}
\left\langle 0\middle|\mathbf{H}_{02}+\tilde{\mathbf{H}}_{22}^{\mathrm{d,red}}\middle|0\right\rangle &= \left\langle 0\middle|\mathbf{H}_{02}\middle|0\right\rangle + \left\langle 0\middle|\tilde{\mathbf{H}}_{22}^{\mathrm{d,red}}\middle|0\right\rangle \\
&= \left\langle 0\middle|\sum_{r_0}\mathrm{H}_{02}\left(r_0\right)\mathbf{J}_{r_0}^2\middle|0\right\rangle + \left\langle 0\middle|\sum_{v_0v_1}\sum_{r_0}\tilde{\mathrm{H}}_{22,0}\left(v_0,v_1,r_0,r_0\right)\mathbf{q}_{v_0}\mathbf{q}_{v_1}\mathbf{J}_{r_0}^2\middle|0\right\rangle \\
&\quad + \left\langle 0\middle|\sum_{v_0v_1}\sum_{r_0}\tilde{\mathrm{H}}_{22,1}\left(v_0,v_1,r_0,r_0\right)\mathbf{p}_{v_0}\mathbf{p}_{v_1}\mathbf{J}_{r_0}^2\middle|0\right\rangle \\
&= \sum_{r_0}B_{r_0}\mathbf{J}_{r_0}^2 + \sum_{v_0}\sum_{r_0}\tilde{\mathrm{H}}_{22,0}\left(v_0,v_0,r_0,r_0\right)\left\langle 0\middle|\mathbf{q}_{v_0}\middle|v_0\right\rangle\left\langle v_0\middle|\mathbf{q}_{v_0}\middle|0\right\rangle\mathbf{J}_{r_0}^2 \\
&\quad + \sum_{v_0}\sum_{r_0}\tilde{\mathrm{H}}_{22,1}\left(v_0,v_0,r_0,r_0\right)\left\langle 0\middle|\mathbf{p}_{v_0}\middle|v_0\right\rangle\left\langle v_0\middle|\mathbf{p}_{v_0}\middle|0\right\rangle\mathbf{J}_{r_0}^2 \\
&= \sum_{r_0}\left(B_{r_0}+\frac{1}{2}\sum_{v_0}\left(\tilde{\mathrm{H}}_{22,0}\left(v_0,v_0,r_0,r_0\right)+\tilde{\mathrm{H}}_{22,1}\left(v_0,v_0,r_0,r_0\right)\right)\right)\mathbf{J}_{r_0}^2
\end{aligned} \tag{7.115}$$

$$B_{r_0}^0 = B_{r_0}^{\mathrm{e}} - \frac{1}{2}\sum_{v_0}\alpha\left(v_0,r_0\right) \tag{7.116}$$

$$\alpha\left(v_0,r_0\right) = -\left(\tilde{\mathrm{H}}_{22,0}\left(v_0,v_0,r_0,r_0\right)+\tilde{\mathrm{H}}_{22,1}\left(v_0,v_0,r_0,r_0\right)\right) \tag{7.117}$$

$$\begin{aligned}\tilde{\mathrm{H}}_{22,0}\left(v_0,v_0,r_0,r_0\right) &= \tilde{\mathrm{H}}_{22,1}\left(v_0,v_0,r_0,r_0\right)\\ &= \frac{3}{8}\sum_{r_1}\frac{1}{B_{r_1}}{\omega_{v_0}}^2 C_{v_0}^{r_0 r_1 2} + \frac{1}{4}\sum_{v_1} C_{v_1}^{r_0 r_0}\,\mathrm{k}_{v_0 v_0 v_1} + \frac{1}{2}\sum_{v_1}\frac{\left(\omega_{v_0}-\omega_{v_1}\right)^2}{\omega_{v_0}\omega_{v_1}\left(\omega_{v_0}+\omega_{v_1}\right)}{B_{r_0}}^2{\zeta_{v_0 v_1}^{r_0}}^2\\ &\quad + \frac{1}{2}\sum_{v_1^*}\frac{\left(\omega_{v_0}+\omega_{v_1}\right)^2}{\omega_{v_0}\omega_{v_1}\left(\omega_{v_0}-\omega_{v_1}\right)}{B_{r_0}}^2{\zeta_{v_0 v_1}^{r_0}}^2\end{aligned} \tag{7.118}$$

$$\begin{aligned}\alpha\left(v_0,r_0\right) &= -\frac{3}{4}\sum_{r_1}\frac{1}{B_{r_1}}{\omega_{v_0}}^2 C_{v_0}^{r_0 r_1 2} - \frac{1}{2}\sum_{v_1} C_{v_1}^{r_0 r_0}\,\mathrm{k}_{v_0 v_0 v_1} - \sum_{v_1}\frac{\left(\omega_{v_0}-\omega_{v_1}\right)^2}{\omega_{v_0}\omega_{v_1}\left(\omega_{v_0}+\omega_{v_1}\right)}{B_{r_0}}^2{\zeta_{v_0 v_1}^{r_0}}^2\\ &\quad - \sum_{v_1^*}\frac{\left(\omega_{v_0}+\omega_{v_1}\right)^2}{\omega_{v_0}\omega_{v_1}\left(\omega_{v_0}-\omega_{v_1}\right)}{B_{r_0}}^2{\zeta_{v_0 v_1}^{r_0}}^2\end{aligned} \tag{7.119}$$

(b) Vibrationally off-diagonal (F_{bc})

TERMS TO ELIMINATE

The rotational Hamiltonian in the I^{r} reduction for the vibrationally off-diagonal matrix element requires that the totally symmetric terms $\mathbf{J}^2$, $\mathbf{J}_z^2$, and $\mathbf{J}_-^2+\mathbf{J}_+^2$ are eliminated. This can be achieved by defining the transform function coefficients such that the corresponding three coefficients will be zero, as in Eq. (7.120)–(7.122), which immediately leads to the requirement that $\left\langle i\left|\tilde{\mathrm{H}}_{22}^{\mathrm{red}}\left(a,a\right)\right|j\right\rangle = 0$.

$$0 = \left\langle i\left|\tilde{\mathrm{H}}_{22}^{\mathrm{red}}\left(x,x\right)+\tilde{\mathrm{H}}_{22}^{\mathrm{red}}\left(y,y\right)\right|j\right\rangle \tag{7.120}$$

$$0 = \left\langle i\left|\tilde{\mathrm{H}}_{22}^{\mathrm{red}}\left(x,x\right)+\tilde{\mathrm{H}}_{22}^{\mathrm{red}}\left(y,y\right)-2\tilde{\mathrm{H}}_{22}^{\mathrm{red}}\left(z,z\right)\right|j\right\rangle \tag{7.121}$$

$$0 = \left\langle i\left|\tilde{\mathrm{H}}_{22}^{\mathrm{red}}\left(x,x\right)-\tilde{\mathrm{H}}_{22}^{\mathrm{red}}\left(y,y\right)\right|j\right\rangle \tag{7.122}$$

SOLVING FOR THE TRANSFORM COEFFICIENTS

We can now write Eq. (7.123), and again set the coefficients of the vibrational expectation values to zero and solve for $S^{r}_{22,0}$ and $S^{r}_{22,1}$. Doing this leads to the solutions Eq. (7.124) and Eq. (7.125), but since the summations in Eq. (7.123) are not restricted, there are terms unaffected by the transformation. Thus, at this point, the Hamiltonian is not fully reduced. Note that the superscript 'r' of the transform functions is replaced with the superscript 'od' to indicate that these solutions of the transform functions are for obtaining the off-diagonal reduction of the Hamiltonian.

$$\begin{aligned}
&\left\langle i\left|\tilde{H}^{\mathrm{red}}_{22}\left(a,a\right)\right|j\right\rangle \\
&\quad=\sum_{v_0 v_1}\left(\tilde{H}_{22,0}\left(v_0,v_1,a,a\right)+\omega_{v_1}S^{r}_{22,0}\left(v_0,v_1,a,a\right)+\omega_{v_0}S^{r}_{22,1}\left(v_0,v_1,a,a\right)\right)\times \\
&\qquad\times\left\langle i\left|\mathbf{q}_{v_0}\mathbf{q}_{v_1}\right|j\right\rangle \\
&\quad+\sum_{v_0 v_1}\left(\tilde{H}_{22,1}\left(v_0,v_1,a,a\right)-\omega_{v_0}S^{r}_{22,0}\left(v_0,v_1,a,a\right)-\omega_{v_1}S^{r}_{22,1}\left(v_0,v_1,a,a\right)\right)\times \\
&\qquad\times\left\langle i\left|\mathbf{p}_{v_0}\mathbf{p}_{v_1}\right|j\right\rangle
\end{aligned} \tag{7.123}$$

$$S^{\mathrm{od}}_{22,0}\left(v_0,v_{1\neq 0},a,a\right)=\frac{1}{\left(\omega_{v_0}{}^2-\omega_{v_1}{}^2\right)}\left(\omega_{v_1}\tilde{H}_{22,0}\left(v_0,v_1,a,a\right)+\omega_{v_0}\tilde{H}_{22,1}\left(v_0,v_1,a,a\right)\right) \tag{7.124}$$

$$S^{\mathrm{od}}_{22,1}\left(v_0,v_{1\neq 0},a,a\right)=-\frac{1}{\left(\omega_{v_0}{}^2-\omega_{v_1}{}^2\right)}\left(\omega_{v_0}\tilde{H}_{22,0}\left(v_0,v_1,a,a\right)+\omega_{v_1}\tilde{H}_{22,1}\left(v_0,v_1,a,a\right)\right) \tag{7.125}$$

DEPENDENCE ON VIBRATIONAL EXPECTATION VALUES

To ensure that the Hamiltonian is fully reduced, we have to distinguish the solutions for when the vibrational indices match and for when they do not match. Thus, we separate each of the summations in Eq. (7.123) into two parts, as in Eq. (7.126). The solutions Eq. (7.124) and Eq. (7.125) apply to the restricted summation, but solutions for the single-index summation are still

required. Furthermore, we must consider the vibrational expectation values in order to affect a result that differs from the restricted solutions.

$$\begin{aligned}
&\left\langle i\left|\tilde{\mathrm{H}}_{22}^{\mathrm{red}}\left(a,a\right)\right|j\right\rangle \\
&\quad=\sum_{v_0 v_{1\neq 0}}\left(\tilde{\mathrm{H}}_{22,0}\left(v_0,v_1,a,a\right)+\omega_{v_1}\,\mathrm{S}_{22,0}^{\mathrm{r}}\left(v_0,v_{1\neq 0},a,a\right)+\omega_{v_0}\,\mathrm{S}_{22,1}^{\mathrm{r}}\left(v_0,v_{1\neq 0},a,a\right)\right)\times \\
&\qquad\times\left\langle i\left|\mathbf{q}_{v_0}\mathbf{q}_{v_1}\right|j\right\rangle \\
&\quad+\sum_{v_0 v_{1\neq 0}}\left(\tilde{\mathrm{H}}_{22,1}\left(v_0,v_1,a,a\right)-\omega_{v_0}\,\mathrm{S}_{22,0}^{\mathrm{r}}\left(v_0,v_{1\neq 0},a,a\right)-\omega_{v_1}\,\mathrm{S}_{22,1}^{\mathrm{r}}\left(v_0,v_{1\neq 0},a,a\right)\right)\times \\
&\qquad\times\left\langle i\left|\mathbf{p}_{v_0}\mathbf{p}_{v_1}\right|j\right\rangle \\
&\quad+\sum_{v_0}\left(\tilde{\mathrm{H}}_{22,0}\left(v_0,v_0,a,a\right)+\omega_{v_0}\,\mathrm{S}_{22,0}^{\mathrm{r}}\left(v_0,v_0,a,a\right)+\omega_{v_0}\,\mathrm{S}_{22,1}^{\mathrm{r}}\left(v_0,v_0,a,a\right)\right)\times \\
&\qquad\times\left\langle i\left|\mathbf{q}_{v_0}\mathbf{q}_{v_0}\right|j\right\rangle \\
&\quad+\sum_{v_0}\left(\tilde{\mathrm{H}}_{22,1}\left(v_0,v_0,a,a\right)-\omega_{v_0}\,\mathrm{S}_{22,0}^{\mathrm{r}}\left(v_0,v_0,a,a\right)-\omega_{v_0}\,\mathrm{S}_{22,1}^{\mathrm{r}}\left(v_0,v_0,a,a\right)\right)\times \\
&\qquad\times\left\langle i\left|\mathbf{p}_{v_0}\mathbf{p}_{v_0}\right|j\right\rangle
\end{aligned} \tag{7.126}$$

The terms in the single-index summations will only be nonzero if the change in the quantum number of the *k*th mode is $\Delta n_k = 0,\pm 2$ and all other quantum numbers are unchanged between $\left|i\right\rangle$ and $\left|j\right\rangle$. The case where $\Delta n_k = 0$ occurs only when $\left|i\right\rangle = \left|j\right\rangle$, which is clearly not an off-diagonal vibrational matrix element and thus can be ignored. For the case where $\Delta n_k = \pm 2$, the single-index summations reduce to Eq. (7.127). This expression is set to zero and the transform coefficients are solved for. Only one transform coefficient can be defined, so the other is arbitrarily set to zero leading to Eq. (7.128) and $\mathrm{S}_{22,1}^{\mathrm{od}}\left(v_0,v_0,a,a\right)=0$. Any remaining transform coefficient not explicitly defined is set to zero. That is, the remaining definitions are given by Eq. (7.129).

$$\begin{aligned}
&\left(\tilde{\mathrm{H}}_{22,0}\left(k,k,a,a\right)+\omega_k\,\mathrm{S}_{22,0}^{\mathrm{r}}\left(k,k,a,a\right)+\omega_k\,\mathrm{S}_{22,1}^{\mathrm{r}}\left(k,k,a,a\right)\right)\left\langle n_k\left|\mathbf{q}^2\right|n_k\pm 2\right\rangle \\
&\quad+\left(\tilde{\mathrm{H}}_{22,1}\left(k,k,a,a\right)-\omega_k\,\mathrm{S}_{22,0}^{\mathrm{r}}\left(k,k,a,a\right)-\omega_k\,\mathrm{S}_{22,1}^{\mathrm{r}}\left(k,k,a,a\right)\right)\left\langle n_k\left|\mathbf{p}^2\right|n_k\pm 2\right\rangle
\end{aligned} \tag{7.127}$$

$$\mathrm{S}^{\mathrm{od}}_{22,0}\left(v_0,v_0,a,a\right)=-\frac{1}{2}\frac{1}{\omega_{v_0}}\left(\tilde{\mathrm{H}}_{22,0}\left(v_0,v_0,a,a\right)-\tilde{\mathrm{H}}_{22,1}\left(v_0,v_0,a,a\right)\right) \tag{7.128}$$

$$\begin{aligned}0&=\mathrm{S}^{\mathrm{od}}_{21,0}\left(v_0,v_1,r_0\right)=\mathrm{S}^{\mathrm{od}}_{21,1}\left(v_0,v_1,r_0\right)\\&=\mathrm{S}^{\mathrm{od}}_{22,0}\left(v_0,v_1,r_0,r_{1\neq0}\right)=\mathrm{S}^{\mathrm{od}}_{22,1}\left(v_0,v_1,r_0,r_{1\neq0}\right)\end{aligned} \tag{7.129}$$

DEFINITION OF F_{bc} BETWEEN FUNDAMENTALS

We now consider the case of the vibrationally off-diagonal matrix element between two fundamental vibrations, $\left|\nu_{\mathrm{A}}\right\rangle$ and $\left|\nu_{\mathrm{B}}\right\rangle$. Using the above definitions, the nonzero contributions to the matrix element are given by Eq. (7.130), and the full expression in terms of molecular properties is given by Eq. (7.131).

$$\begin{aligned}\left\langle\nu_{\mathrm{A}}\left|\tilde{\mathrm{H}}^{\mathrm{od,red}}_{22}\left(r_0,r_{1\neq0}\right)\right|\nu_{\mathrm{B}}\right\rangle&=\left\langle\nu_{\mathrm{A}}\left|\tilde{\mathrm{H}}^{\mathrm{od,red}}_{22}\left(r_{1\neq0},r_0\right)\right|\nu_{\mathrm{B}}\right\rangle\\&=\sum_{v_0v_1}\tilde{\mathrm{H}}_{22,0}\left(v_0,v_1,r_0,r_1\right)\left\langle\nu_{\mathrm{A}}\left|\mathbf{q}_{v_0}\mathbf{q}_{v_1}\right|\nu_{\mathrm{B}}\right\rangle+\sum_{v_0v_1}\tilde{\mathrm{H}}_{22,1}\left(v_0,v_1,r_0,r_1\right)\left\langle\nu_{\mathrm{A}}\left|\mathbf{p}_{v_0}\mathbf{p}_{v_1}\right|\nu_{\mathrm{B}}\right\rangle\\&=\frac{1}{2}\tilde{\mathrm{H}}_{22,0}\left(\nu_{\mathrm{A}},\nu_{\mathrm{B}},r_0,r_1\right)+\frac{1}{2}\tilde{\mathrm{H}}_{22,0}\left(\nu_{\mathrm{B}},\nu_{\mathrm{A}},r_0,r_1\right)\\&\qquad+\frac{1}{2}\tilde{\mathrm{H}}_{22,1}\left(\nu_{\mathrm{A}},\nu_{\mathrm{B}},r_0,r_1\right)+\frac{1}{2}\tilde{\mathrm{H}}_{22,1}\left(\nu_{\mathrm{B}},\nu_{\mathrm{A}},r_0,r_1\right)\end{aligned} \tag{7.130}$$

$$
\begin{aligned}
\left\langle \nu_{\mathrm{A}} \left| \tilde{\mathrm{H}}_{22}^{\mathrm{od,red}}\left(r_0, r_{1\neq 0}\right) \right| \nu_{\mathrm{B}} \right\rangle &= \left\langle \nu_{\mathrm{A}} \left| \tilde{\mathrm{H}}_{22}^{\mathrm{od,red}}\left(r_{1\neq 0}, r_0\right) \right| \nu_{\mathrm{B}} \right\rangle \\
&= \frac{3}{8}\sum_{r_2}\frac{1}{B_{r_2}}\omega_{\nu_{\mathrm{A}}}\omega_{\nu_{\mathrm{B}}}\left(C_{\nu_{\mathrm{A}}}^{r_0 r_2}C_{\nu_{\mathrm{B}}}^{r_2 r_1}+C_{\nu_{\mathrm{B}}}^{r_0 r_2}C_{\nu_{\mathrm{A}}}^{r_2 r_1}\right)+\frac{1}{2}\sum_{\nu_2}\mathrm{k}_{\nu_{\mathrm{A}}\nu_{\mathrm{B}}\nu_2}\,C_{\nu_2}^{r_0 r_1} \\
&-\frac{1}{4}\sum_{\nu_2}\frac{\left(\omega_{\nu_{\mathrm{A}}}-\omega_{\nu_2}\right)\left(\omega_{\nu_{\mathrm{B}}}-\omega_{\nu_2}\right)\left(\omega_{\nu_{\mathrm{A}}}+\omega_{\nu_{\mathrm{B}}}+2\omega_{\nu_2}\right)}{\sqrt{\omega_{\nu_{\mathrm{A}}}\omega_{\nu_{\mathrm{B}}}}\,\omega_{\nu_2}\left(\omega_{\nu_{\mathrm{A}}}+\omega_{\nu_2}\right)\left(\omega_{\nu_{\mathrm{B}}}+\omega_{\nu_2}\right)}B_{r_0}B_{r_1}\left(\zeta_{\nu_{\mathrm{A}}\nu_2}^{r_0}\zeta_{\nu_{\mathrm{B}}\nu_2}^{r_1}+\zeta_{\nu_{\mathrm{A}}\nu_2}^{r_1}\zeta_{\nu_{\mathrm{B}}\nu_2}^{r_0}\right) \\
&+\frac{1}{4}\sum_{\nu_2}\mathrm{D}\left(1,\nu_{\mathrm{A}};-1,\nu_2\right)\mathrm{D}\left(1,\nu_{\mathrm{B}};-1,\nu_2\right)\times \\
&\quad\times\frac{\left(\omega_{\nu_{\mathrm{A}}}+\omega_{\nu_2}\right)\left(\omega_{\nu_{\mathrm{B}}}+\omega_{\nu_2}\right)\left(\omega_{\nu_{\mathrm{A}}}+\omega_{\nu_{\mathrm{B}}}-2\omega_{\nu_2}\right)}{\sqrt{\omega_{\nu_{\mathrm{A}}}\omega_{\nu_{\mathrm{B}}}}\,\omega_{\nu_2}}B_{r_0}B_{r_1}\left(\zeta_{\nu_{\mathrm{A}}\nu_2}^{r_0}\zeta_{\nu_{\mathrm{B}}\nu_2}^{r_1}+\zeta_{\nu_{\mathrm{A}}\nu_2}^{r_1}\zeta_{\nu_{\mathrm{B}}\nu_2}^{r_0}\right) \\
&+\sum_{r_2}\epsilon_{r_0 r_1 r_2}\,\mathrm{D}\left(1,\nu_{\mathrm{A}};-1,\nu_{\mathrm{B}}\right)\frac{\left(\omega_{\nu_{\mathrm{A}}}+\omega_{\nu_{\mathrm{B}}}\right)}{\sqrt{\omega_{\nu_{\mathrm{A}}}\omega_{\nu_{\mathrm{B}}}}}\zeta_{\nu_{\mathrm{A}}\nu_{\mathrm{B}}}^{r_2}B_{r_2}\left(B_{r_0}-B_{r_1}\right)
\end{aligned}
\tag{7.131}
$$

The rotational Hamiltonian is then given by Eq. (7.132), where the $\mathcal{O}(\sim \mathbf{J})$ terms previously discussed go to zero using the definition of Eq. (7.130). Returning to Cartesian form, the rotational Hamiltonian is given by Eq. (7.133) from which we can define the *F* Coriolis coupling constant between two fundamentals as Eq. (7.134). The *F* Coriolis coupling constant between other vibrational states is readily obtained from evaluating the vibrational matrix element of Eq. (7.130), so long as the total change in quanta between the two vibrational states is $\sum_i \left|\Delta n_i\right| = 2$.

$$
\begin{aligned}
\left\langle \nu_{\mathrm{A}} \left| \tilde{\mathbf{H}}_{22}^{\mathrm{od,red}} \right| \nu_{\mathrm{B}} \right\rangle = &-\frac{i}{2}\left\langle \nu_{\mathrm{A}} \left| \tilde{\mathrm{H}}_{22}^{\mathrm{od,red}}\left(x,y\right) \right| \nu_{\mathrm{B}} \right\rangle\left(\mathbf{J}_{-}^2-\mathbf{J}_{+}^2\right) \\
&+\frac{1}{2}\left\langle \nu_{\mathrm{A}} \left| \tilde{\mathrm{H}}_{22}^{\mathrm{od,red}}\left(x,z\right) \right| \nu_{\mathrm{B}} \right\rangle\left[\mathbf{J}_z,\mathbf{J}_{-}+\mathbf{J}_{+}\right]_{+} \\
&-\frac{i}{2}\left\langle \nu_{\mathrm{A}} \left| \tilde{\mathrm{H}}_{22}^{\mathrm{od,red}}\left(y,z\right) \right| \nu_{\mathrm{B}} \right\rangle\left[\mathbf{J}_z,\mathbf{J}_{-}-\mathbf{J}_{+}\right]_{+}
\end{aligned}
\tag{7.132}
$$

$$
\begin{aligned}
\left\langle \nu_{\mathrm{A}} \left| \tilde{\mathbf{H}}_{22}^{\mathrm{od,red}} \right| \nu_{\mathrm{B}} \right\rangle = &\left\langle \nu_{\mathrm{A}} \left| \tilde{\mathrm{H}}_{22}^{\mathrm{od,red}}\left(x,y\right) \right| \nu_{\mathrm{B}} \right\rangle\left(\mathbf{J}_x\mathbf{J}_y+\mathbf{J}_y\mathbf{J}_x\right) \\
&+\left\langle \nu_{\mathrm{A}} \left| \tilde{\mathrm{H}}_{22}^{\mathrm{od,red}}\left(x,z\right) \right| \nu_{\mathrm{B}} \right\rangle\left(\mathbf{J}_x\mathbf{J}_z+\mathbf{J}_z\mathbf{J}_x\right) \\
&+\left\langle \nu_{\mathrm{A}} \left| \tilde{\mathrm{H}}_{22}^{\mathrm{od,red}}\left(y,z\right) \right| \nu_{\mathrm{B}} \right\rangle\left(\mathbf{J}_y\mathbf{J}_z+\mathbf{J}_z\mathbf{J}_y\right)
\end{aligned}
\tag{7.133}
$$

$$F_{\alpha\beta} = \langle \nu_A | \tilde{H}_{22}^{od,red}(\alpha,\beta) | \nu_B \rangle \tag{7.134}$$

The expression obtained in Eq. (7.130) is nearly identical to that previously derived by Aliev and Watson,[4] except their formula (Eq. (101) of Ref. 4) appears to be lacking the last summation of Eq. (7.130), which is the contribution arising from the only rotational commutator within the transformation to obtain $\tilde{\mathbf{H}}_{22}$, $i[\mathbf{S}_{21},\mathbf{H}_{02}]_R$. The denominator function in this term, however, must always yield zero for the off-diagonal matrix element of a pair of resonant states and thus the two expressions are equivalent.

Preliminary Rotational Reduction of $\tilde{\mathbf{H}}_{23}$

We are still in the process of deriving the analytic expression for $\tilde{\mathbf{H}}_{23}$, but we can discuss our efforts in obtaining its rotational reduction. Prior to encountering the work of Perevalov and Tyuterev,[6-7] we derived a rotational reduction for $\tilde{\mathbf{H}}_{23}$ using an approach adapted from the procedure used for the rotational reduction of the centrifugal distortion constants, as presented in the review by Watson.[2] This is the derivation provided in this section. While we are optimistic that a rotation reduction obtained in a manner similar to that for $\tilde{\mathbf{H}}_{22}$ in the previous section will yield the same result, we are still in the process of confirming that such is the case. Thus, we consider the rotational reduction that follows to be preliminary.

The rotational contact transformation

The approach used for the centrifugal distortion constants uses the transform function $\mathbf{S}_{0,n-1}^{r}$ to reduce the Hamiltonian $\tilde{\mathbf{H}}_{0n}$. Similarly, we will use the transform function $\mathbf{S}_{02}^{r}$ to reduce the Hamiltonian $\tilde{\mathbf{H}}_{23}$, specifically its vibrational matrix element. We begin by defining $\mathcal{H}_{03}$ as an

arbitrary off-diagonal vibrational matrix element of $\tilde{\mathbf{H}}_{23}$, as in Eq. (7.135), which can be written as a linear combination of rotational operator. The coefficients H_{03} in this linear combination are the vibrational expectation values of $\tilde{\mathbf{H}}_{23}$ with the rotational operators removed and is simply some complex number as a function of the rotational indices. With the Hamiltonian written as such, we can write the rotational contact transformation as Eq. (7.136), where the definition of the transform function is chosen to obtain the desired, reduced form of the Hamiltonian.

$$\mathcal{H}_{03} \equiv \left\langle i \middle| \tilde{\mathbf{H}}_{23} \middle| j \neq i \right\rangle = \sum_{r_0 r_1 r_2} \mathrm{H}_{03}\left(r_0, r_1, r_2\right) \mathbf{J}_{r_0} \mathbf{J}_{r_1} \mathbf{J}_{r_2} \tag{7.135}$$

$$\mathcal{H}_{03}^{\mathrm{red}} = \mathcal{H}_{03} + i\left[\mathbf{S}_{02}, \mathbf{H}_{02}\right] \tag{7.136}$$

The trial transform function

Since the vibrational dependence of the current rotational reduction is ignored, the form of the transform function is simplified: it is simply a linear combination of rotational operators of order $\sim \mathbf{J}^2$. At the moment, the coefficients in the definition of the transform function (Eq. (7.137)) are undefined; finding/choosing their definitions is the primary work in deriving the rotation reduction.

$$\mathbf{S}_{02}^{r} = \sum_{r_0 r_1} \mathrm{S}_{02}^{r}\left(r_0, r_1\right) \mathbf{J}_{r_0} \mathbf{J}_{r_1} \tag{7.137}$$

The rotational commutator

We can evaluate the rotational commutator of the transform function with the rigid rotor, as the evaluation is independent of the definition of the transform function's coefficients. The commutator evaluates to Eq. (7.138).

$$i\left[\mathbf{S}_{02}^{r},\mathbf{H}_{02}\right]=\sum_{r_0r_1r_2r_3}\left(\left(B_{r_1}-B_{r_2}\right)\mathrm{S}_{02}^{r}\left(r_0,r_3\right)\epsilon_{r_1r_2r_3}+\left(B_{r_0}-B_{r_1}\right)\mathrm{S}_{02}^{r}\left(r_3,r_2\right)\epsilon_{r_0r_1r_3}\right)\mathbf{J}_{r_0}\mathbf{J}_{r_1}\mathbf{J}_{r_2} \quad (7.138)$$

The reduced Hamiltonian

With the commutator evaluated, we can now write the reduced Hamiltonian as in Eq. (7.139), where we have defined the coefficients as in Eq. (7.140). The full Cartesian form of the reduced Hamiltonian is simply given by the permutations of the rotational indices over the *x*, *y*, and *z* axes.

$$\mathcal{H}_{03}^{\mathrm{red}}=\sum_{r_0r_1r_2}\mathrm{H}_{03}^{\mathrm{red}}\left(r_0,r_1,r_2\right)\mathbf{J}_{r_0}\mathbf{J}_{r_1}\mathbf{J}_{r_2} \quad (7.139)$$

$$\begin{aligned}&\mathrm{H}_{03}^{\mathrm{red}}\left(r_0,r_1,r_2\right)\\&\quad=\mathrm{H}_{03}\left(r_0,r_1,r_2\right)+\sum_{r_3}\left(\left(B_{r_1}-B_{r_2}\right)\mathrm{S}_{02}^{r}\left(r_0,r_3\right)\epsilon_{r_1r_2r_3}+\left(B_{r_0}-B_{r_1}\right)\mathrm{S}_{02}^{r}\left(r_3,r_2\right)\epsilon_{r_0r_1r_3}\right)\end{aligned} \quad (7.140)$$

The reduced Hamiltonian in cylindrical tensor form

As was done in the reduction of $\tilde{\mathbf{H}}_{22}$, we will rewrite the reduced Hamiltonian in terms of products of $\mathbf{J}^2$, $\mathbf{J}_z$, $\mathbf{J}_-+\mathbf{J}_+$, and $\mathbf{J}_--\mathbf{J}_+$. The process is extensive and requires judicial use of commutator relations, but eventually we obtain the expression given in Eq. (7.141), using the coefficients defined in Eq. (7.142).

$$\begin{aligned}\mathcal{H}_{03}^{\mathrm{red}}&=c_{2100}\mathbf{J}^2\mathbf{J}_z+c_{2010}\mathbf{J}^2\left(\mathbf{J}_-+\mathbf{J}_+\right)+c_{2001}\mathbf{J}^2\left(\mathbf{J}_--\mathbf{J}_+\right)+c_{0300}\mathbf{J}_z^3\\&\quad+c_{0210}\left[\mathbf{J}_z^2,\mathbf{J}_-+\mathbf{J}_+\right]_++c_{0201}\left[\mathbf{J}_z^2,\mathbf{J}_--\mathbf{J}_+\right]_++c_{0120}\left[\mathbf{J}_z,\mathbf{J}_-^2+\mathbf{J}_+^2\right]_+\\&\quad+c_{0102}\left[\mathbf{J}_z,\mathbf{J}_-^2-\mathbf{J}_+^2\right]_++c_{0030}\left(\mathbf{J}_-^3+\mathbf{J}_+^3\right)+c_{0003}\left(\mathbf{J}_-^3-\mathbf{J}_+^3\right)+\mathcal{O}\left(\sim\mathbf{J}^2\right)+\mathcal{O}\left(\sim\mathbf{J}\right)\end{aligned} \quad (7.141)$$

$$
\begin{aligned}
c_{2100} &= \frac{1}{2}\left(\mathrm{H}_{03}^{\mathrm{red}}\left(x,x,z\right)+\mathrm{H}_{03}^{\mathrm{red}}\left(x,z,x\right)+\mathrm{H}_{03}^{\mathrm{red}}\left(z,x,x\right)\right) \\
&\quad +\frac{1}{2}\left(\mathrm{H}_{03}^{\mathrm{red}}\left(y,y,z\right)+\mathrm{H}_{03}^{\mathrm{red}}\left(y,z,y\right)+\mathrm{H}_{03}^{\mathrm{red}}\left(z,y,y\right)\right) \\
c_{2010} &= \frac{3}{8}\mathrm{H}_{03}^{\mathrm{red}}\left(x,x,x\right)+\frac{1}{8}\left(\mathrm{H}_{03}^{\mathrm{red}}\left(x,y,y\right)+\mathrm{H}_{03}^{\mathrm{red}}\left(y,x,y\right)+\mathrm{H}_{03}^{\mathrm{red}}\left(y,y,x\right)\right) \\
c_{2001} &= -\frac{3i}{8}\mathrm{H}_{03}^{\mathrm{red}}\left(y,y,y\right)-\frac{i}{8}\left(\mathrm{H}_{03}^{\mathrm{red}}\left(x,x,y\right)+\mathrm{H}_{03}^{\mathrm{red}}\left(x,y,x\right)+\mathrm{H}_{03}^{\mathrm{red}}\left(y,x,x\right)\right) \\
c_{0300} &= -c_{2100}+\mathrm{H}_{03}^{\mathrm{red}}\left(z,z,z\right) \\
c_{0210} &= -\frac{1}{2}c_{2010}+\frac{1}{4}\left(\mathrm{H}_{03}^{\mathrm{red}}\left(x,z,z\right)+\mathrm{H}_{03}^{\mathrm{red}}\left(z,x,z\right)+\mathrm{H}_{03}^{\mathrm{red}}\left(z,z,x\right)\right) \\
c_{0201} &= -\frac{1}{2}c_{2001}-\frac{i}{4}\left(\mathrm{H}_{03}^{\mathrm{red}}\left(y,z,z\right)+\mathrm{H}_{03}^{\mathrm{red}}\left(z,y,z\right)+\mathrm{H}_{03}^{\mathrm{red}}\left(z,z,y\right)\right) \\
c_{0120} &= \frac{1}{8}\left(\mathrm{H}_{03}^{\mathrm{red}}\left(x,x,z\right)+\mathrm{H}_{03}^{\mathrm{red}}\left(x,z,x\right)+\mathrm{H}_{03}^{\mathrm{red}}\left(z,x,x\right)\right) \\
&\quad -\frac{1}{8}\left(\mathrm{H}_{03}^{\mathrm{red}}\left(y,y,z\right)+\mathrm{H}_{03}^{\mathrm{red}}\left(y,z,y\right)+\mathrm{H}_{03}^{\mathrm{red}}\left(z,y,y\right)\right) \\
c_{0102} &= -\frac{i}{8}\left(\mathrm{H}_{03}^{\mathrm{red}}\left(x,y,z\right)+\mathrm{H}_{03}^{\mathrm{red}}\left(x,z,y\right)+\mathrm{H}_{03}^{\mathrm{red}}\left(y,x,z\right)\right. \\
&\qquad \left.+\mathrm{H}_{03}^{\mathrm{red}}\left(y,z,x\right)+\mathrm{H}_{03}^{\mathrm{red}}\left(z,x,y\right)+\mathrm{H}_{03}^{\mathrm{red}}\left(z,y,x\right)\right) \\
c_{0030} &= \frac{1}{8}\mathrm{H}_{03}^{\mathrm{red}}\left(x,x,x\right)-\frac{1}{8}\left(\mathrm{H}_{03}^{\mathrm{red}}\left(x,y,y\right)+\mathrm{H}_{03}^{\mathrm{red}}\left(y,x,y\right)+\mathrm{H}_{03}^{\mathrm{red}}\left(y,y,x\right)\right) \\
c_{0003} &= \frac{i}{8}\mathrm{H}_{03}^{\mathrm{red}}\left(y,y,y\right)-\frac{i}{8}\left(\mathrm{H}_{03}^{\mathrm{red}}\left(x,x,y\right)+\mathrm{H}_{03}^{\mathrm{red}}\left(x,y,x\right)+\mathrm{H}_{03}^{\mathrm{red}}\left(y,x,x\right)\right)
\end{aligned}
\tag{7.142}
$$

The terms lower in order with respect to the rotational operator are given by Eq. (7.143) and Eq. (7.144), using the coefficients defined in Eq. (7.145) and Eq. (7.146), respectively. Given the preliminary nature of this reduction, we will ignore these lower order terms for the present work.

$$
\begin{aligned}
\mathcal{O}\left(\sim \mathbf{J}^2\right) &= c_{2000}\mathbf{J}^2+c_{0200}\mathbf{J}_z^2+c_{0110}\left[\mathbf{J}_z,\mathbf{J}_-+\mathbf{J}_+\right]_+ +c_{0101}\left[\mathbf{J}_z,\mathbf{J}_--\mathbf{J}_+\right]_+ \\
&\quad +c_{0020}\left(\mathbf{J}_-^2+\mathbf{J}_+^2\right)+c_{0002}\left(\mathbf{J}_-^2-\mathbf{J}_+^2\right)
\end{aligned}
\tag{7.143}
$$

$$
\mathcal{O}\left(\sim \mathbf{J}\right) = c_{0100}\mathbf{J}_z+c_{0010}\left(\mathbf{J}_-+\mathbf{J}_+\right)+c_{0001}\left(\mathbf{J}_--\mathbf{J}_+\right) \tag{7.144}
$$

$$
\begin{aligned}
c_{2000} &= \frac{i}{2}\left(\mathrm{H}_{03}^{\mathrm{red}}\left(x,z,y\right)-\mathrm{H}_{03}^{\mathrm{red}}\left(y,z,x\right)\right)\\
c_{0200} &= -\frac{i}{2}\left(\mathrm{H}_{03}^{\mathrm{red}}\left(x,y,z\right)-\mathrm{H}_{03}^{\mathrm{red}}\left(z,y,x\right)\right)+\frac{i}{2}\left(\mathrm{H}_{03}^{\mathrm{red}}\left(y,x,z\right)-\mathrm{H}_{03}^{\mathrm{red}}\left(z,x,y\right)\right)\\
&\quad -i\left(\mathrm{H}_{03}^{\mathrm{red}}\left(x,z,y\right)-\mathrm{H}_{03}^{\mathrm{red}}\left(y,z,x\right)\right)\\
c_{0110} &= -\frac{i}{4}\left(\mathrm{H}_{03}^{\mathrm{red}}\left(x,x,y\right)-\mathrm{H}_{03}^{\mathrm{red}}\left(y,x,x\right)\right)-\frac{i}{4}\left(\mathrm{H}_{03}^{\mathrm{red}}\left(y,z,z\right)-\mathrm{H}_{03}^{\mathrm{red}}\left(z,z,y\right)\right)\\
c_{0101} &= -\frac{1}{4}\left(\mathrm{H}_{03}^{\mathrm{red}}\left(x,y,y\right)-\mathrm{H}_{03}^{\mathrm{red}}\left(y,y,x\right)\right)+\frac{1}{4}\left(\mathrm{H}_{03}^{\mathrm{red}}\left(x,z,z\right)-\mathrm{H}_{03}^{\mathrm{red}}\left(z,z,x\right)\right)\\
c_{0020} &= -\frac{i}{4}\left(\mathrm{H}_{03}^{\mathrm{red}}\left(x,y,z\right)-\mathrm{H}_{03}^{\mathrm{red}}\left(z,y,x\right)\right)-\frac{i}{4}\left(\mathrm{H}_{03}^{\mathrm{red}}\left(y,x,z\right)-\mathrm{H}_{03}^{\mathrm{red}}\left(z,x,y\right)\right)\\
c_{0002} &= \frac{1}{4}\left(\mathrm{H}_{03}^{\mathrm{red}}\left(x,x,z\right)-\mathrm{H}_{03}^{\mathrm{red}}\left(z,x,x\right)\right)-\frac{1}{4}\left(\mathrm{H}_{03}^{\mathrm{red}}\left(y,y,z\right)-\mathrm{H}_{03}^{\mathrm{red}}\left(z,y,y\right)\right)
\end{aligned}
\tag{7.145}
$$

$$
\begin{aligned}
c_{0100} &= -\frac{1}{2}\left(\mathrm{H}_{03}^{\mathrm{red}}\left(x,z,x\right)+\mathrm{H}_{03}^{\mathrm{red}}\left(y,z,y\right)\right)\\
c_{0010} &= -\frac{1}{16}\left(\mathrm{H}_{03}^{\mathrm{red}}\left(x,x,x\right)+3\mathrm{H}_{03}^{\mathrm{red}}\left(y,x,y\right)+4\,\mathrm{H}_{03}^{\mathrm{red}}\left(z,x,z\right)\right)\\
&\quad +\frac{1}{16}\left(\mathrm{H}_{03}^{\mathrm{red}}\left(x,y,y\right)+\mathrm{H}_{03}^{\mathrm{red}}\left(y,y,x\right)\right)\\
c_{0001} &= \frac{i}{16}\left(3\mathrm{H}_{03}^{\mathrm{red}}\left(x,y,x\right)+\mathrm{H}_{03}^{\mathrm{red}}\left(y,y,y\right)+4\,\mathrm{H}_{03}^{\mathrm{red}}\left(z,y,z\right)\right)\\
&\quad -\frac{i}{16}\left(\mathrm{H}_{03}^{\mathrm{red}}\left(x,x,y\right)+\mathrm{H}_{03}^{\mathrm{red}}\left(y,x,x\right)\right)
\end{aligned}
\tag{7.146}
$$

Terms to be eliminated

Before we proceed further, we will first consider the conditions by which the Asymmetric and Symmetric reductions were chosen for the centrifugal distortion constants. As described in Watson's review,[2] the Asymmetric reduction was obtained by defining the transform function coefficients such that terms with the rotational selection rules of $\left|\Delta k\right|>2$ were eliminated. On the other hand, the Symmetric reduction was obtained by defining the transform function's

coefficients such that terms containing the $\mathbf{J}_z$ operator with rotational selection rules of $|\Delta k| > 0$ were eliminated. We will keep these constraints in mind as we consider how to reduce the third order Coriolis coupling Hamiltonian.

"Asymmetric" reduction

Now, we consider the third order Coriolis coupling Hamiltonian that is used for the fitting of experimental spectra. This Hamiltonian is limited to a maximum of six terms, and is given by Eq. (7.147) for the I^r representation. Examination of this Hamiltonian in comparison to the full Hamiltonian written in Eq. (7.141) shows that the expression used experimentally has removed the $\mathbf{J}_-^n \pm \mathbf{J}_+^n$ terms from Eq. (7.141) for $n > 1$. Written another way, the Hamiltonian used experimentally can be obtained by eliminating the terms with rotational selection rules of $|\Delta k| > 1$ (or equivalently, $|\Delta k| \geq 2$). To us, this appears analogous to the condition applied to the centrifugal distortion constants to obtain the Asymmetric reduction. Thus, we refer to the expression in Eq. (7.148) as the "asymmetric" reduction of $\tilde{\mathbf{H}}_{23}$, which is what the 'a' in the scripts of the equation is denoting (and is distinct from the '*a*' used to represent the rotational axis in the rotational constants in Eq. (7.147)). We will refer to this reduction with explicit use of the quotation marks because we are unsure of how or if this Hamiltonian interacts with the Asymmetric centrifugal distortion constants.

$$\begin{aligned}\mathbf{H}_3^{\text{coupling}} = {} & G_a^J \mathbf{J}^2 \mathbf{J}_z + G_b^J \mathbf{J}^2 \left(\mathbf{J}_- + \mathbf{J}_+\right) + G_c^J \mathbf{J}^2 \left(\mathbf{J}_- - \mathbf{J}_+\right) \\ & + G_a^K \mathbf{J}_z^3 + G_b^K \left[\mathbf{J}_z^2, \left(\mathbf{J}_- + \mathbf{J}_+\right)\right]_+ + G_c^K \left[\mathbf{J}_z^2, \left(\mathbf{J}_- - \mathbf{J}_+\right)\right]_+\end{aligned} \tag{7.147}$$

$$\begin{aligned}\mathcal{H}_{03}^{\text{a}} = {} & c_{2100\text{a}} \mathbf{J}^2 \mathbf{J}_z + c_{2010\text{a}} \mathbf{J}^2 \left(\mathbf{J}_- + \mathbf{J}_+\right) + c_{2001\text{a}} \mathbf{J}^2 \left(\mathbf{J}_- - \mathbf{J}_+\right) \\ & + c_{0300\text{a}} \mathbf{J}_z^3 + c_{0210\text{a}} \left[\mathbf{J}_z^2, \mathbf{J}_- + \mathbf{J}_+\right]_+ + c_{0201\text{a}} \left[\mathbf{J}_z^2, \mathbf{J}_- - \mathbf{J}_+\right]_+\end{aligned} \tag{7.148}$$

By comparison of the two expressions in Eq. (7.147) and Eq. (7.148), we can write the definitions of the third order Coriolis coupling constants as in Eq. (7.149), which are in turn dependent on the definitions of the transform function coefficients, defined below. Note that these definitions are assuming the I^{r} representation.

$$\begin{aligned} G_a^J &= c_{2100\mathrm{a}}, G_b^J = c_{2010\mathrm{a}}, G_c^J = c_{2001\mathrm{a}} \\ G_a^K &= c_{0300\mathrm{a}}, G_b^K = c_{0210\mathrm{a}}, G_c^K = c_{0201\mathrm{a}} \end{aligned} \tag{7.149}$$

The constraint that the reduced form of $\tilde{\mathbf{H}}_{23}$ should not have terms with rotational selection rules of $|\Delta k| \geq 2$ is equivalent to enforcing the condition in Eq. (7.150). By substituting the definitions of the coefficients from above, we can – with sufficient algebraic manipulation – show that the transform function coefficients provided in Eq. (7.151)–(7.155) will satisfy the constraint given by Eq. (7.150). Here the superscript 'a' is used to represent that these transform coefficients are for obtaining the "asymmetric" reduction of the Hamiltonian.

$$0 = c_{0120} = c_{0102} = c_{0030} = c_{0003} \tag{7.150}$$

$$\begin{aligned} \mathrm{S}_{02}^{\mathrm{a}}(x,x) = -\frac{1}{4\left(B_y - B_z\right)} \Big(& \mathrm{H}_{03}(x,y,z) + \mathrm{H}_{03}(x,z,y) + \mathrm{H}_{03}(y,x,z) \\ & + \mathrm{H}_{03}(y,z,x) + \mathrm{H}_{03}(z,x,y) + \mathrm{H}_{03}(z,y,x) \Big) \end{aligned} \tag{7.151}$$

$$\begin{aligned} \mathrm{S}_{02}^{\mathrm{a}}(x,y) = \frac{1}{2\left(2B_z - B_x - B_y\right)} \Big(& -\mathrm{H}_{03}(x,x,z) - \mathrm{H}_{03}(x,z,x) - \mathrm{H}_{03}(z,x,x) \\ & + \mathrm{H}_{03}(y,y,z) + \mathrm{H}_{03}(y,z,y) + \mathrm{H}_{03}(z,y,y) \Big) \end{aligned} \tag{7.152}$$

$$\mathrm{S}_{02}^{\mathrm{a}}(x,z) = \frac{1}{2\left(B_x - B_y\right)} \Big(\mathrm{H}_{03}(y,y,y) - \mathrm{H}_{03}(x,x,y) - \mathrm{H}_{03}(x,y,x) - \mathrm{H}_{03}(y,x,x) \Big) \tag{7.153}$$

$$\mathrm{S}_{02}^{\mathrm{a}}(y,z) = \frac{1}{2\left(B_x - B_y\right)} \Big(\mathrm{H}_{03}(x,x,x) - \mathrm{H}_{03}(x,y,y) - \mathrm{H}_{03}(y,x,y) - \mathrm{H}_{03}(y,y,x) \Big) \tag{7.154}$$

$$0 = \mathrm{S}^{\mathrm{a}}_{02}(y,y) = \mathrm{S}^{\mathrm{a}}_{02}(z,z) = \mathrm{S}^{\mathrm{a}}_{02}(y,x) = \mathrm{S}^{\mathrm{a}}_{02}(z,x) = \mathrm{S}^{\mathrm{a}}_{02}(z,y) \tag{7.155}$$

DEFINITION OF THE REDUCED COEFFICIENTS

We can now write the full expression for the coefficients of the reduced Hamiltonian. Substituting the "asymmetric" reduction transform function coefficients into the reduced coefficients allows us to write the definitions for the reduced Hamiltonian in the cylindrical tensor form, as shown in Eq. (7.156)–(7.158).

$$\begin{aligned}
c_{2100\mathrm{a}} &= \frac{\left(B_z - B_y\right)}{\left(2B_z - B_x - B_y\right)}\left(\mathrm{H}_{03}(x,x,z) + \mathrm{H}_{03}(x,z,x) + \mathrm{H}_{03}(z,x,x)\right) \\
&\quad + \frac{\left(B_z - B_x\right)}{\left(2B_z - B_x - B_y\right)}\left(\mathrm{H}_{03}(y,y,z) + \mathrm{H}_{03}(y,z,y) + \mathrm{H}_{03}(z,y,y)\right) \\
c_{2010\mathrm{a}} &= \frac{1}{2}\mathrm{H}_{03}(x,x,x) \\
c_{2001\mathrm{a}} &= -\frac{i}{2}\mathrm{H}_{03}(y,y,y)
\end{aligned} \tag{7.156}$$

$$\begin{aligned}
c_{0300\mathrm{a}} &= -c_{2100\mathrm{a}} + \mathrm{H}_{03}(z,z,z) \\
c_{0210\mathrm{a}} &= \frac{1}{4}\frac{\left(-2B_x + B_y + B_z\right)}{\left(B_x - B_y\right)}\mathrm{H}_{03}(x,x,x) \\
&\quad + \frac{1}{4}\left(\mathrm{H}_{03}(x,z,z) + \mathrm{H}_{03}(z,x,z) + \mathrm{H}_{03}(z,z,x)\right) \\
&\quad - \frac{\left(B_z - B_x\right)}{4\left(B_x - B_y\right)}\left(\mathrm{H}_{03}(x,y,y) + \mathrm{H}_{03}(y,x,y) + \mathrm{H}_{03}(y,y,x)\right) \\
c_{0201\mathrm{a}} &= \frac{i}{4}\frac{\left(B_x - 2B_y + B_z\right)}{\left(B_x - B_y\right)}\mathrm{H}_{03}(y,y,y) \\
&\quad - \frac{i}{4}\left(\mathrm{H}_{03}(y,z,z) + \mathrm{H}_{03}(z,y,z) + \mathrm{H}_{03}(z,z,y)\right) \\
&\quad + \frac{i}{4}\frac{\left(B_y - B_z\right)}{\left(B_x - B_y\right)}\left(\mathrm{H}_{03}(x,x,y) + \mathrm{H}_{03}(x,y,x) + \mathrm{H}_{03}(y,x,x)\right)
\end{aligned} \tag{7.157}$$

$$0 = c_{0120\mathrm{a}} = c_{0102\mathrm{a}} = c_{0030\mathrm{a}} = c_{0003\mathrm{a}} \tag{7.158}$$

"Symmetric" reduction

If the experimental Hamiltonian in Eq. (7.147) is indeed analogous to the Asymmetric reduction of the centrifugal distortion constants, then we can attempt to extend the analogy to include the Symmetric reduction. Let us write the Hamiltonian that would result from eliminating terms from the full Hamiltonian in Eq. (7.141) that contain the $\mathbf{J}_z$ operator and have rotational selection rules of $|\Delta k| > 0$. The result, shown in Eq. (7.159), has removed four terms as required, and consideration of the symmetries of the remaining terms suggests this Hamiltonian can be used to fit coupled state rotational spectra. We consider this to be the "symmetric" reduction of $\tilde{\mathbf{H}}_{23}$, but again we are unclear as to the relationship between this form of the coupling Hamiltonian and the Symmetric reduction of the centrifugal distortion constants. The 's' in the scripts again denotes that these definitions are explicitly for this "symmetric" reduction.

$$\begin{aligned}\mathcal{H}_{03}^{\mathrm{s}} = {} & c_{2100\mathrm{s}}\mathbf{J}^2\mathbf{J}_z + c_{2010\mathrm{s}}\mathbf{J}^2\left(\mathbf{J}_- + \mathbf{J}_+\right) + c_{2001\mathrm{s}}\mathbf{J}^2\left(\mathbf{J}_- - \mathbf{J}_+\right) \\ & + c_{0300\mathrm{s}}\mathbf{J}_z^3 + c_{0030\mathrm{s}}\left(\mathbf{J}_-^3 + \mathbf{J}_+^3\right) + c_{0003\mathrm{s}}\left(\mathbf{J}_-^3 - \mathbf{J}_+^3\right)\end{aligned} \tag{7.159}$$

The definition of the third order Coriolis coupling constants in this reduction is somewhat complicated by the different choice in terms that were kept. By comparison of Eq. (7.147) and Eq. (7.159), the definitions of some of the constants is still clear, as shown in Eq. (7.160), but there does not appear to be an obvious definition for G_b^K and G_c^K. Following the analogy to the centrifugal distortion constants, we propose the use of the constants G_+ and G_- as defined in Eq. (7.161) to denote the coefficients of $\left(\mathbf{J}_-^3 + \mathbf{J}_+^3\right)$ and $\left(\mathbf{J}_-^3 - \mathbf{J}_+^3\right)$, respectively, for the "symmetric" reduction of the third order Coriolis coupling constants.

$$\begin{aligned} G_a^J &= c_{2100\mathrm{s}}, G_b^J = c_{2010\mathrm{s}}, G_c^J = c_{2001\mathrm{s}} \\ G_a^K &= c_{0300\mathrm{s}} \end{aligned} \tag{7.160}$$

$$\begin{aligned} G_+ &= c_{0030\mathrm{s}} \\ G_- &= c_{0003\mathrm{s}} \end{aligned} \tag{7.161}$$

The constraint that the reduced form of $\tilde{\mathbf{H}}_{23}$ should not have terms with a $\mathbf{J}_z$ operator and rotational selection rules of $|\Delta k| > 0$ is equivalent to enforcing the condition in Eq (7.162). Using the definitions provided earlier, we can show that the definitions provided in Eq. (7.163)–(7.167) will satisfy this condition. Here the superscript 's' represents that these coefficients for the transform functions are for obtaining the "symmetric" reduction of the Hamiltonian.

$$0 = c_{0210} = c_{0201} = c_{0120} = c_{0102} \tag{7.162}$$

$$\begin{aligned} \mathrm{S}_{02}^{\mathrm{s}}(x,y) = \frac{1}{2}\frac{1}{\left(B_x + B_y - 2B_z\right)}\Big(&\left(\mathrm{H}_{03}(x,x,z) + \mathrm{H}_{03}(x,z,x) + \mathrm{H}_{03}(z,x,x)\right) \\ &-\left(\mathrm{H}_{03}(y,y,z) + \mathrm{H}_{03}(y,z,y) + \mathrm{H}_{03}(z,y,y)\right)\Big) \end{aligned} \tag{7.163}$$

$$\begin{aligned} \mathrm{S}_{02}^{\mathrm{s}}(x,z) = &\frac{1}{\left(B_x - 5B_y + 4B_z\right)} \times \\ &\times\Bigg(-\frac{3}{2}\mathrm{H}_{03}(y,y,y) - \frac{1}{2}\left(\mathrm{H}_{03}(x,x,y) + \mathrm{H}_{03}(x,y,x) + \mathrm{H}_{03}(y,x,x)\right) \\ &+2\left(\mathrm{H}_{03}(y,z,z) + \mathrm{H}_{03}(z,z,y) + \mathrm{H}_{03}(z,y,z)\right)\Bigg) \end{aligned} \tag{7.164}$$

$$\begin{aligned} \mathrm{S}_{02}^{\mathrm{s}}(y,z) = &\frac{1}{\left(-5B_x + B_y + 4B_z\right)} \times \\ &\times\Bigg(\frac{3}{2}\mathrm{H}_{03}(x,x,x) + \frac{1}{2}\left(\mathrm{H}_{03}(x,y,y) + \mathrm{H}_{03}(y,x,y) + \mathrm{H}_{03}(y,y,x)\right) \\ &-2\left(\mathrm{H}_{03}(x,z,z) + \mathrm{H}_{03}(z,x,z) + \mathrm{H}_{03}(z,z,x)\right)\Bigg) \end{aligned} \tag{7.165}$$

$$\mathrm{S}_{02}\left(x,x\right)=-\frac{1}{4}\frac{1}{\left(B_y-B_z\right)}\left(\mathrm{H}_{03}\left(x,y,z\right)+\mathrm{H}_{03}\left(x,z,y\right)+\mathrm{H}_{03}\left(y,x,z\right)\right.$$
$$\left.+\mathrm{H}_{03}\left(y,z,x\right)+\mathrm{H}_{03}\left(z,x,y\right)+\mathrm{H}_{03}\left(z,y,x\right)\right) \tag{7.166}$$

$$0=\mathrm{S}^{\mathrm{s}}_{02}\left(y,y\right)=\mathrm{S}^{\mathrm{s}}_{02}\left(z,z\right)=\mathrm{S}^{\mathrm{s}}_{02}\left(y,x\right)=\mathrm{S}^{\mathrm{s}}_{02}\left(z,x\right)=\mathrm{S}^{\mathrm{s}}_{02}\left(z,y\right) \tag{7.167}$$

DEFINITION OF THE REDUCED COEFFICIENTS

We can now write the full expression for the coefficients of the reduced Hamiltonian. Substituting the "symmetric" reduction transform function coefficients into the reduced coefficients allows us to write the definitions for the reduced Hamiltonian in the cylindrical tensor form, as shown in Eq. (7.168)–(7.170).

$$\begin{aligned}
c_{2100\mathrm{s}} &= \frac{\left(B_y-B_z\right)}{\left(B_x+B_y-2B_z\right)}\left(\mathrm{H}_{03}\left(x,x,z\right)+\mathrm{H}_{03}\left(x,z,x\right)+\mathrm{H}_{03}\left(z,x,x\right)\right)\\
&\quad+\frac{\left(B_x-B_z\right)}{\left(B_x+B_y-2B_z\right)}\left(\mathrm{H}_{03}\left(y,y,z\right)+\mathrm{H}_{03}\left(y,z,y\right)+\mathrm{H}_{03}\left(z,y,y\right)\right)\\
c_{2010\mathrm{s}} &= \frac{1}{2}\frac{\left(-B_x+B_z\right)}{\left(-5B_x+B_y+4B_z\right)}\times\\
&\quad\times\left(3\mathrm{H}_{03}\left(x,x,x\right)+\mathrm{H}_{03}\left(x,y,y\right)+\mathrm{H}_{03}\left(y,x,y\right)+\mathrm{H}_{03}\left(y,y,x\right)\right)\\
&\quad-\frac{1}{2}\frac{\left(B_x-B_y\right)}{\left(-5B_x+B_y+4B_z\right)}\left(\mathrm{H}_{03}\left(x,z,z\right)+\mathrm{H}_{03}\left(z,x,z\right)+\mathrm{H}_{03}\left(z,z,x\right)\right)\\
c_{2001\mathrm{s}} &= \frac{i}{2}\frac{\left(B_y-B_z\right)}{\left(B_x-5B_y+4B_z\right)}\times\\
&\quad\times\left(3\mathrm{H}_{03}\left(y,y,y\right)+\mathrm{H}_{03}\left(x,x,y\right)+\mathrm{H}_{03}\left(x,y,x\right)+\mathrm{H}_{03}\left(y,x,x\right)\right)\\
&\quad-\frac{i}{2}\frac{\left(B_x-B_y\right)}{\left(B_x-5B_y+4B_z\right)}\left(\mathrm{H}_{03}\left(y,z,z\right)+\mathrm{H}_{03}\left(z,z,y\right)+\mathrm{H}_{03}\left(z,y,z\right)\right)
\end{aligned} \tag{7.168}$$

$$
\begin{aligned}
c_{0300\mathrm{s}} &= -c_{2100} + \mathrm{H}_{03}(z,z,z) \\
c_{0030\mathrm{s}} &= \frac{1}{2}\frac{\left(-2B_x + B_y + B_z\right)}{\left(-5B_x + B_y + 4B_z\right)}\mathrm{H}_{03}(x,x,x) \\
&\quad + \frac{1}{2}\frac{\left(B_x - B_z\right)}{\left(-5B_x + B_y + 4B_z\right)}\left(\mathrm{H}_{03}(x,y,y) + \mathrm{H}_{03}(y,x,y) + \mathrm{H}_{03}(y,y,x)\right) \\
&\quad + \frac{1}{2}\frac{\left(B_x - B_y\right)}{\left(-5B_x + B_y + 4B_z\right)}\left(\mathrm{H}_{03}(x,z,z) + \mathrm{H}_{03}(z,x,z) + \mathrm{H}_{03}(z,z,x)\right) \\
c_{0003\mathrm{s}} &= \frac{i}{2}\frac{\left(B_x - 2B_y + B_z\right)}{\left(B_x - 5B_y + 4B_z\right)}\mathrm{H}_{03}(y,y,y) \\
&\quad + \frac{i}{2}\frac{\left(B_y - B_z\right)}{\left(B_x - 5B_y + 4B_z\right)}\left(\mathrm{H}_{03}(x,x,y) + \mathrm{H}_{03}(x,y,x) + \mathrm{H}_{03}(y,x,x)\right) \\
&\quad - \frac{i}{2}\frac{\left(B_x - B_y\right)}{\left(B_x - 5B_y + 4B_z\right)}\left(\mathrm{H}_{03}(y,z,z) + \mathrm{H}_{03}(z,z,y) + \mathrm{H}_{03}(z,y,z)\right)
\end{aligned}
\tag{7.169}
$$

$$
0 = c_{0210\mathrm{s}} = c_{0201\mathrm{s}} = c_{0120\mathrm{s}} = c_{0102\mathrm{s}} \tag{7.170}
$$

Ratio of Coupling Constants of Combinations and Overtones with Common Vibrational Modes

We again consider the vibrational matrix element of $\tilde{\mathbf{H}}_{21}$ (Eq. (7.52)), but now for a pair of undefined states $|n_a, n_b\rangle$ and $|n_a + 1, n_b - 1\rangle$ involving the normal modes ν_a and ν_b. When the vibrational expectation values are evaluated, as in Eq. (7.171), we see that the only dependence on the quantum numbers n_a and n_b occurs in the constant that multiplies the rest of the expression. Using this expression, we can define a relationship between the coupling constants of different sets of coupled states. That is, using Eq. (7.172), we can write a ratio of the vibrational matrix

elements as in Eq. (7.173). As will be discussed, this ratio has been observed experimentally in the fitting of the lowest dyad and triad of benzonitrile (*vide infra*).[9]

$$\begin{aligned}
&\left\langle n_a, n_b \left| \tilde{\mathbf{H}}_{21} \right| n_a + 1, n_b - 1 \right\rangle \\
&\quad = \sum_{jk} \sum_{\alpha} \tilde{\mathrm{H}}_{21,0}\left(j,k,\alpha\right) \left\langle n_a, n_b \left| \mathbf{q}_j \mathbf{p}_k \right| n_a + 1, n_b - 1 \right\rangle \mathbf{J}_\alpha \\
&\qquad + \sum_{jk} \sum_{\alpha} \tilde{\mathrm{H}}_{21,1}\left(j,k,\alpha\right) \left\langle n_a, n_b \left| \mathbf{p}_j \mathbf{q}_k \right| n_a + 1, n_b - 1 \right\rangle \mathbf{J}_\alpha \\
&\quad = \frac{i}{2} \sqrt{\left(n_a + 1\right) n_b} \sum_{\alpha} \Big(\tilde{\mathrm{H}}_{21,0}\left(a,b,\alpha\right) - \tilde{\mathrm{H}}_{21,0}\left(b,a,\alpha\right) \\
&\qquad\qquad - \tilde{\mathrm{H}}_{21,1}\left(a,b,\alpha\right) + \tilde{\mathrm{H}}_{21,1}\left(b,a,\alpha\right) \Big) \mathbf{J}_\alpha
\end{aligned} \tag{7.171}$$

$$\begin{aligned}
&\left\langle n_a + \Delta_a, n_b + \Delta_b \left| \tilde{\mathbf{H}}_{21} \right| n_a + \Delta_a + 1, n_b + \Delta_b - 1 \right\rangle \\
&\quad = \frac{i}{2} \sqrt{\left(n_a + \Delta_a + 1\right)\left(n_b + \Delta_b\right)} \sum_{\alpha} \Big(\tilde{\mathrm{H}}_{21,0}\left(a,b,\alpha\right) - \tilde{\mathrm{H}}_{21,0}\left(b,a,\alpha\right) \\
&\qquad\qquad - \tilde{\mathrm{H}}_{21,1}\left(a,b,\alpha\right) + \tilde{\mathrm{H}}_{21,1}\left(b,a,\alpha\right) \Big) \mathbf{J}_\alpha
\end{aligned} \tag{7.172}$$

$$\frac{\left\langle n_a + \Delta_a, n_b + \Delta_b \left| \tilde{\mathbf{H}}_{21} \right| n_a + \Delta_a + 1, n_b + \Delta_b - 1 \nu_b \right\rangle}{\left\langle n_a, n_b \left| \tilde{\mathbf{H}}_{21} \right| n_a + 1, n_b - 1 \right\rangle} = \frac{\sqrt{\left(n_a + \Delta_a + 1\right)\left(n_b + \Delta_b\right)}}{\sqrt{\left(n_a + 1\right) n_b}} \tag{7.173}$$

In fact, the derivation of the ratio of coupling constants can be generalized to describe the relationship of any off-diagonal vibrational matrix elements that involve the same set of vibrational modes. We can define an arbitrary vibration-rotation Hamiltonian with vibrational degree of two as in Eq. (7.174). Evaluation of this Hamiltonian for an arbitrary pair of vibrational states leads to an extensive expression (see Supporting Information) that can be used to obtain the relationship provided in Eq. (7.175). The ratio for matrix elements of $\tilde{\mathbf{H}}_{21}$ derived previously (*vide supra*) can be obtained from Eq. (7.175) using the values $n_a' = n_a + 1$, $n_b' = n_b - 1$, and $\tilde{\mathbf{H}}_{2n} = \tilde{\mathbf{H}}_{21}$. More

importantly, however, the formula shows that every off-diagonal matrix element is directly proportional to other off-diagonal matrix elements involving the same set of vibrational modes and selection rules. To illustrate, per Eq. (7.175) the coupling constants of $\langle \nu_a | \tilde{\mathbf{H}}_{2n} | \nu_b \rangle$ are directly proportional to the coupling constants of $\langle 2\nu_a | \tilde{\mathbf{H}}_{2n} | \nu_a, \nu_b \rangle$, $\langle 2\nu_a, 2\nu_b | \tilde{\mathbf{H}}_{2n} | \nu_a, 3\nu_b \rangle$, $\langle \nu_a, \nu_b | \tilde{\mathbf{H}}_{2n} | 2\nu_b \rangle$, $\langle 2\nu_a, \nu_b | \tilde{\mathbf{H}}_{2n} | \nu_a, 2\nu_b \rangle$, $\langle \nu_a, 3\nu_b | \tilde{\mathbf{H}}_{2n} | 4\nu_b \rangle$, and more. Note that while this derivation ignores contributions from terms with higher degrees of vibration *i.e.*, $\tilde{\mathbf{H}}_{4n}$, such terms are at least two orders smaller, and excluding them should have little to no effect on the outcome. Furthermore, our discussions regarding the reduction of rotational operators have no impact on the relationships of these coupling constants, as the ratios are independent of the nature of the rotational operators.

$$\begin{aligned}\tilde{\mathbf{H}}_{2n} \equiv & \sum_{r_0,r_1,\ldots,r_n} \sum_{kl} \tilde{\mathrm{H}}_{2n,0}(k,l;r_0,r_1,\ldots,r_n)\mathbf{q}_k\mathbf{q}_l\mathbf{J}_{r_0}\mathbf{J}_{r_1}\times\cdots\times\mathbf{J}_{r_n} \\ & + \sum_{r_0,r_1,\ldots,r_n} \sum_{kl} \tilde{\mathrm{H}}_{2n,1}(k,l;r_0,r_1,\ldots,r_n)\mathbf{q}_k\mathbf{p}_l\mathbf{J}_{r_0}\mathbf{J}_{r_1}\times\cdots\times\mathbf{J}_{r_n} \\ & + \sum_{r_0,r_1,\ldots,r_n} \sum_{kl} \tilde{\mathrm{H}}_{2n,2}(k,l;r_0,r_1,\ldots,r_n)\mathbf{p}_k\mathbf{q}_l\mathbf{J}_{r_0}\mathbf{J}_{r_1}\times\cdots\times\mathbf{J}_{r_n} \\ & + \sum_{r_0,r_1,\ldots,r_n} \sum_{kl} \tilde{\mathrm{H}}_{2n,3}(k,l;r_0,r_1,\ldots,r_n)\mathbf{p}_k\mathbf{p}_l\mathbf{J}_{r_0}\mathbf{J}_{r_1}\times\cdots\times\mathbf{J}_{r_n}\end{aligned} \tag{7.174}$$

$$\frac{\left\langle n_a+\Delta_a, n_b+\Delta_b \left| \tilde{\mathbf{H}}_{2n} \right| n_a'+\Delta_a, n_b'+\Delta_b \nu_b \right\rangle}{\left\langle n_a, n_b \left| \tilde{\mathbf{H}}_{2n} \right| n_a', n_b' \right\rangle}$$

$$= \delta_{n_a', n_a+2}\delta_{n_b n_b'} \frac{\sqrt{(n_a+\Delta_a+1)(n_a+\Delta_a+2)}}{\sqrt{(n_a+1)(n_a+2)}} + \delta_{n_a', n_a-2}\delta_{n_b n_b'} \frac{\sqrt{(n_a+\Delta_a)(n_a+\Delta_a-1)}}{\sqrt{n_a(n_a-1)}}$$

$$+\delta_{n_a', n_a+1}\delta_{n_b', n_b+1} \frac{\sqrt{(n_a+\Delta_a+1)(n_b+\Delta_b+1)}}{\sqrt{(n_a+1)(n_b+1)}} + \delta_{n_a', n_a+1}\delta_{n_b', n_b-1} \frac{\sqrt{(n_a+\Delta_a+1)(n_b+\Delta_b)}}{\sqrt{(n_a+1)n_b}}$$

$$+\delta_{n_a', n_a-1}\delta_{n_b', n_b+1} \frac{\sqrt{(n_a+\Delta_a)(n_b+\Delta_b+1)}}{\sqrt{n_a(n_b+1)}} + \delta_{n_a', n_a-1}\delta_{n_b', n_b-1} \frac{\sqrt{(n_a+\Delta_a)(n_b+\Delta_b)}}{\sqrt{n_a n_b}}$$

$$+\delta_{n_a n_a'}\delta_{n_b', n_b+2} \frac{\sqrt{(n_b+\Delta_b+1)(n_b+\Delta_b+2)}}{\sqrt{(n_b+1)(n_b+2)}} + \delta_{n_a n_a'}\delta_{n_b', n_b-2} \frac{\sqrt{(n_b+\Delta_b)(n_b+\Delta_b-1)}}{\sqrt{n_b(n_b-1)}}$$

(7.175)

RESULTS AND DISCUSSION

In principle, the vibration-rotation coupling constants can be predicted using the results of anharmonic frequency calculations and the formulas we have derived. To assess the quality of these predictions, we compare the computational predictions to the experimental coupled-state fits of benzonitrile.[9]

First, we consider the lowest energy dyad consisting of vibration-rotation coupling between the fundamentals ν_{22} (141 cm^{-1}) and ν_{33} (160 cm^{-1}). Using the I^r representation and the formulas in Eq. (7.59) and Eq. (7.130), we can predict the values of the first and second order Coriolis coupling constants using the results of a CCSD(T)/ANO0 VPT2 calculation. As shown in Table 7.2, the F_{bc} coupling constants predicted by Eq. (7.130) are indeed quite close to those determined from the coupled-state fit of the experimental data, with the predicted constants being 14% smaller. Whether or not a higher level of theory results in improved theoretical values remains to be seen.

Table 7.2. Comparison of Theoretical Predictions of Coriolis Coupling Constants using CCSD(T)/ANO0 to Experimental Results for the Lowest Energy Dyad and Triad of Benzonitrile.

		G_a (MHz)		F_{bc} (MHz)	
State 1	State 2	Exp.[9]	Eq. (7.52)	Exp.[9]	Eq. (7.134)
ν_{22}	ν_{33}	9531. (46)	9351.	0.412 (30)	0.355
$2\nu_{22}$	$\nu_{22}+\nu_{33}$	13476.329 (25) [a]	13223.615	0.58568 (16)	0.503
$\nu_{22}+\nu_{33}$	$2\nu_{33}$	13476.329 (25) [a]	13223.615	0.58657 (14)	0.503
$2\nu_{22}+\nu_{33}$	$\nu_{22}+2\nu_{33}$		18701.015		0.711

[a] These G_a values were set equal to each other in the fit

As mentioned earlier, a rather particular relationship was observed in the coupled state fits of the lowest energy dyad and triad of benzonitrile.[9] Specifically, the first order Coriolis coupling between an overtone and combination band, $\langle 2\nu_{33}|G_a|1\nu_{22},1\nu_{33}\rangle$, was found to be larger than the corresponding coupling of the fundamentals of the two modes in question, $\langle \nu_{22}|G_a|\nu_{33}\rangle$, by approximately a factor of $\sqrt{2}$. Using the ratio provided in Eq. (7.173) and the values $n_{33}=0$, $n_{22}=1$, $\Delta_{33}=1$, and $\Delta_{22}=0$, we find that such indeed is the factor by which these two coupling constants should differ. If instead we use the values $\Delta_{33}=0$ and $\Delta_{22}=1$, the same ratio is obtained for the coupling of the same combination band with the other overtone, $\langle 2\nu_{22}|G_a|1\nu_{22},1\nu_{33}\rangle$. And, using the expression derived in Eq. (7.175), we can extend this statement to include the rest of the coupling constants involved. That is, the ratio in Eq. (7.176) is independent of the rotational operators, and so applies to G_a, G_b, G_c, F_{bc}, F_{ac}, F_{ab}, G_a^J, G_a^K, G_b^J, *etc*.

$$\frac{\langle 1\nu_{33},1\nu_{22}|G_a|2\nu_{33},0\nu_{22}\rangle}{\langle 0\nu_{33},1\nu_{22}|G_a|1\nu_{33},0\nu_{22}\rangle}=\frac{\langle 0\nu_{33},2\nu_{22}|G_a|1\nu_{33},1\nu_{22}\rangle}{\langle 0\nu_{33},1\nu_{22}|G_a|1\nu_{33},0\nu_{22}\rangle}=\frac{\sqrt{2}}{1} \tag{7.176}$$

This can be further illustrated by considering the formulas for the second order Coriolis coupling constants obtained from the vibrational matrix element of $\tilde{\mathbf{H}}_{22}$. The generalized matrix element of Eq. (7.177) can be applied to the coupled states in question to yield Eq. (7.178)–(7.180) . Comparison of these matrix elements reveals that the ratio of Eq. (7.176) does indeed hold for the second order Coriolis coupling. Thus, the theoretical predictions of the coupling values of these states are multiples of the coupling constants of the two fundamental states. The theoretical values provided in Table 7.2 reflect this fact, and the complete expression for calculating ratios of $\tilde{\mathbf{H}}_{2n}$ coupling terms is provided in Eq. (7.175).

$$\begin{aligned}\left\langle n_a, n_b \left| \tilde{\mathbf{H}}_{22} \right| n_a+1, n_b-1 \right\rangle \\ = \frac{1}{2}\sqrt{(n_a+1)n_b}\sum_{r_0,r_1}\Big(\tilde{\mathrm{H}}_{22,0}(a,b,r_0,r_1)+\tilde{\mathrm{H}}_{22,0}(b,a,r_0,r_1) \\ +\tilde{\mathrm{H}}_{22,1}(a,b,r_0,r_1)+\tilde{\mathrm{H}}_{22,1}(b,a,r_0,r_1)\Big)\mathbf{J}_{r_0}\mathbf{J}_{r_1}\end{aligned} \tag{7.177}$$

$$\begin{aligned}\left\langle \nu_{22} \left| \tilde{\mathbf{H}}_{22} \right| \nu_{33} \right\rangle = \frac{1}{2}\sum_{r_0,r_1}\Big(\tilde{\mathrm{H}}_{22,0}(22,33,r_0,r_1)+\tilde{\mathrm{H}}_{22,0}(33,22,r_0,r_1) \\ +\tilde{\mathrm{H}}_{22,1}(22,33,r_0,r_1)+\tilde{\mathrm{H}}_{22,1}(33,22,r_0,r_1)\Big)\mathbf{J}_{r_0}\mathbf{J}_{r_1}\end{aligned} \tag{7.178}$$

$$\begin{aligned}\left\langle 2\nu_{33} \left| \tilde{\mathbf{H}}_{22} \right| \nu_{22}, \nu_{33} \right\rangle = \frac{\sqrt{2}}{2}\sum_{r_0,r_1}\Big(\tilde{\mathrm{H}}_{22,0}(22,33,r_0,r_1)+\tilde{\mathrm{H}}_{22,0}(33,22,r_0,r_1) \\ +\tilde{\mathrm{H}}_{22,1}(22,33,r_0,r_1)+\tilde{\mathrm{H}}_{22,1}(33,22,r_0,r_1)\Big)\mathbf{J}_{r_0}\mathbf{J}_{r_1}\end{aligned} \tag{7.179}$$

$$\begin{aligned}\left\langle 2\nu_{22} \left| \tilde{\mathbf{H}}_{22} \right| \nu_{22}, \nu_{33} \right\rangle = \frac{\sqrt{2}}{2}\sum_{r_0,r_1}\Big(\tilde{\mathrm{H}}_{22,0}(22,33,r_0,r_1)+\tilde{\mathrm{H}}_{22,0}(33,22,r_0,r_1) \\ +\tilde{\mathrm{H}}_{22,1}(22,33,r_0,r_1)+\tilde{\mathrm{H}}_{22,1}(33,22,r_0,r_1)\Big)\mathbf{J}_{r_0}\mathbf{J}_{r_1}\end{aligned} \tag{7.180}$$

Preliminary Results of the *vib-rot-Van-Vleck* Program

As discussed in the Introduction and Methods sections, we are developing a computer-aided derivation program for the derivation and numeric calculation of effective Hamiltonians using Van Vleck perturbation theory. From our efforts in deriving various transformed Hamiltonians, and as illustrated in the Derivations section, the complexity and length of the derivation of the transformed Hamiltonians greatly increases as the order of the terms get larger. As such, though the derivation process is unchanged, the derivation of higher order terms requires a considerable amount of time and effort. Therefore, the primary goal of program is to reproduce the methodology described in this work, so that we can more easily extend the methodology to higher order transformations. A secondary goal of the program is to facilitate the calculation of numeric predictions of the coupling constants of any given molecule by combining the results of the computer-aided derivation with the results of *ab initio* calculations. We assess the efficacy of the program by considering the results for the derivation of $\tilde{\mathbf{H}}_{22}$. We limit this evaluation to numeric results at this time, as the current symbolic results are rather unwieldy and require the implementation of a simplification procedure to obtain expressions like those derived above.

First, the numeric results obtained using the *vib-rot-Van-Vleck* program and a CCSD(T)/ANO0 VPT2 calculation of benzonitrile agree exactly with the numeric results in Table 7.2 obtained from evaluating the vibrational matrix elements of Eq. (7.52) and (7.134). Next, we considered the α corrections to the rotational constants for the ground state as well as the ν_{22} and ν_{33} fundamentals. As demonstrated in Table 7.3, the α corrections of the ground state calculated using the *vib-rot-Van-Vleck* program (*vrVV*, r.t. = 30 cm^{-1}) agree well with those reported by the VPT2 calculation. The α corrections for the two fundamentals examined are considerably different, but we believe this is due to the known absence of "deperturbation" in the VPT2 results.

More specifically, for the *A* rotational axis the VPT2 α corrections for the two fundamentals are unexpectedly large, roughly equal in magnitude, and opposite in sign. This arises due to the presence of Coriolis coupling between the two states and is manifest in the α corrections because the resonant denominators have not been removed from the expression used to calculate them. Since the *vib-rot-Van-Vleck* program uses the methodology we describe in this work, however, the resonant denominators are inherently excluded from the evaluation of the α corrections, which yields results more similar to the ground state corrections.

Table 7.3. Comparison of Theoretical Calculations of the α Corrections to the Rotational Constants of Benzonitrile using CCSD(T)/ANO0

State		$B_a^e - B_a^0$	$B_b^e - B_b^0$	$B_c^e - B_c^0$
Ground	VPT2	45.658	6.779	6.544
	vrVV (r.t. = 30 cm^{-1})	45.663	6.779	6.544
	vrVV (r.t. = 0 cm^{-1})	45.663	6.779	6.544
ν_{22}	VPT2	-167.892	1.656	1.751
	vrVV (r.t. = 30 cm^{-1})	50.773	5.123	4.794
	vrVV (r.t. = 0 cm^{-1})	213.554	5.123	4.794
ν_{33}	VPT2	166.698	2.747	0.795
	vrVV (r.t. = 30 cm^{-1})	41.747	4.032	5.750
	vrVV (r.t. = 0 cm^{-1})	-121.035	4.032	5.750

We can test this assertion by enforcing a strict resonance threshold of zero, thereby removing the deperturbation effect of the denominator function. That is, by setting the resonance threshold to zero we can calculate the perturbed α corrections. As we can see by the results in Table 7.3, the α corrections calculated with the strict resonance threshold ('r.t. = 0 cm^{-1}') for the fundamental states manifests a large and opposite magnitude α correction for the *A* rotational axis, similar to the result of the VPT2 calculation. Interestingly, it appears that even though these are

the perturbed α corrections, the values for the *B* and *C* rotational axes are identical to those of the deperturbed calculation. We are thus fairly confident that the *vib-rot-Van-Vleck* results are accurate for predictions of second order Coriolis coupling constants derived from $\tilde{\mathbf{H}}_{22}$, and are optimistic about the results of higher order terms.

Next, we demonstrate the character of coupling for benzonitrile by reporting the nonzero *vib-rot-Van-Vleck* predictions of the first and second order Coriolis coupling constants in Table 7.4 for unique combinations of the fundamental states of benzonitrile with energy *ca.* 1000 cm^{-1} or less. An interesting feature of Table 7.4 is the coupling between ν_{21} and ν_{15} and the coupling between ν_{13} and ν_{16}: despite the absence of first order Coriolis coupling, each set of states has significant second order Coriolis coupling. Attempts to fit experimental spectra of these coupled states with a first order term would likely be unsuccessful.

Table 7.4. The Nonzero *vib-rot-Van-Vleck* Predictions of 1st and 2nd Order Coriolis Coupling Constants for Fundamental States (<1000 cm^{-1}) of Benzonitrile using CCSD(T)/ANO0.

State 1[a]	State 2[a]	Axis *x*	G_x (MHz)	F_{yz} (MHz)
ν_{22} (B_1)	ν_{33} (B_2)	A	-9350.508	0.355
ν_{21} (B_1)	ν_{15} (A_2)	C	0.	-1.080
ν_{32} (B_2)	ν_{20} (B_1)	A	7409.005	0.065
ν_{11} (A_1)	ν_{18} (B_1)	B	-760.620	0.034
ν_{13} (A_2)	ν_{16} (B_1)	C	0.	0.217
ν_{13} (A_2)	ν_{10} (A_1)	A	1683.940	0.007
ν_{16} (B_1)	ν_{10} (A_1)	B	193.834	-0.051

[a] The state is followed by its symmetry in parentheses.

As stated above, our goal for the *vib-rot-Van-Vleck* program is to be able to obtain predictions of even higher order coupling constants. The next order of consideration is the third order Coriolis coupling constants *i.e.*, G_a^J, G_a^K, *etc*., derived from the transformed Hamiltonian

$\tilde{\mathbf{H}}_{23}$. The *vib-rot-Van-Vleck* is able to derive the symbolic form of $\tilde{\mathbf{H}}_{23}$, but the expression is extensive (several thousand lines), due to the present lack of a routine for the simplification of the computer algebra representation of the Hamiltonian, and so it is impractical to report the symbolic form at this time. Despite the size of the expression, the *vib-rot-Van-Vleck* program is still able to use the symbolic result it derived to conduct numeric calculations, provided sufficient computational data from a VPT2 calculation is provided to the program. The numeric results obtained are effectively the H_{03} coefficients described in Eq. (7.135). The nonzero results for the vibrational matrix element between the ν_{22} and ν_{33} fundamentals are presented in Table 7.5. Similar numeric results can be obtained for the coupling between $2\nu_{22}$ and $\nu_{22}+\nu_{33}$ as well as the coupling between $\nu_{22}+\nu_{33}$ and $2\nu_{33}$, and they are simply larger by a factor of $\sqrt{2}$, consistent with our previous analysis (*vide supra*).

Table 7.5. Nonzero Coefficients of Third Order Rotational Operators Describing the Coupling Between ν_{22} and ν_{33} Fundamentals of Benzonitrile. [a]

Operator Term (I^{r} representation)	Value of the coefficient from *vrVV* (MHz)
$\mathrm{H}_{03}(x,x,z)\mathbf{J}_x\mathbf{J}_x\mathbf{J}_z$	0.001831
$\mathrm{H}_{03}(x,z,x)\mathbf{J}_x\mathbf{J}_z\mathbf{J}_x$	0.003867
$\mathrm{H}_{03}(y,y,z)\mathbf{J}_y\mathbf{J}_y\mathbf{J}_z$	0.000108
$\mathrm{H}_{03}(y,z,y)\mathbf{J}_y\mathbf{J}_z\mathbf{J}_y$	0.000021
$\mathrm{H}_{03}(z,x,x)\mathbf{J}_z\mathbf{J}_x\mathbf{J}_x$	0.001831
$\mathrm{H}_{03}(z,y,y)\mathbf{J}_z\mathbf{J}_y\mathbf{J}_y$	0.000108
$\mathrm{H}_{03}(z,z,z)\mathbf{J}_z\mathbf{J}_z\mathbf{J}_z$	0.005073

[a] Using computed data from CCSD(T)/ANO0 VPT2 calculation

With the coefficients of the third order coupling Hamiltonian so defined, and using the computed rotational constants of B_x = 1527.107883, B_y = 1200.894594, and B_z = 5621.768537 MHz, we can numerically evaluate the reduced coefficients we obtained in the preliminary rotational reduction of $\tilde{\mathbf{H}}_{23}$, given by Eq. (7.156)–(7.158) and Eq. (7.168)–(7.170). The nonzero coefficients that result are $c_{2100a} = c_{2100s}$ = 0.004023 MHz and $c_{0300a} = c_{0300s}$ = 0.001050 MHz, which should correspond to $G_a{}^J$ and $G_a{}^K$, respectively, for the coupling between the ν_{22} and ν_{33} fundamentals of benzonitrile. Experimentally, $G_a{}^J$ was determined with a value of −0.004594 (20) MHz, while $G_a{}^K$ was not reported.[9] Ignoring the difference in sign (which is due to the *vrVV* prediction of G_a being negative instead of positive), we see that the value of $G_a{}^J$ is predicted to within 15% of the experimentally determined value. Since the H_{03} coefficients calculated for the coupling in the higher quanta triad are proportional to the coefficients calculated for the dyad, so too are the resulting predictions of $G_a{}^J$ and $G_a{}^K$. We are thus optimistic that the *vib-rot-Van-Vleck* program is correctly calculating the numeric (and by inference, the symbolic) expressions of $\tilde{\mathbf{H}}_{23}$ and that the preliminary reduction we determined for $\tilde{\mathbf{H}}_{23}$ is likely close to the outcome that will be achieved after application of the reduction formalism that was applied to $\tilde{\mathbf{H}}_{22}$.

CONCLUSION

While the formula $\tilde{\mathbf{H}}_{22}$ derived in this work has been in the literature for nearly a half-century, and so too the method for the rotational reduction of its vibrational matrix elements, the application of Van Vleck perturbation theory to obtain theoretical predictions of Coriolis coupling constants has largely been absent. At the time the theoretical framework was being developed, rotational spectroscopy was limited to low values of J and K and the effects of Coriolis coupling

were well treated by a first order term. In addition, the high computational cost for obtaining the requisite cubic force constants limited the application of the theory to small molecules. Thus, for the most part, the application of the theory to obtain predictions of higher order coupling constants remained a potential.

Now, the advances in hardware and analysis allow for the measurement and fitting of rotational spectra to values of J and K in the hundreds. The fitting of such spectra, particularly for coupled vibrational states, requires higher order terms to properly describe the Coriolis coupling. Combined with the advances in computing power, we are now in a position where the theoretical framework previously developed can be applied and adequately assessed for larger molecules. Such is the primary focus of the present work, and in works to come.

In addition to obtaining formulas for the theoretical prediction of second order Coriolis coupling constants, the implementation of the theory has revealed a potentially powerful insight into the relationships of coupled vibrational states. The multiplicative relationship of coupling constants that share common vibrational modes and selection rules expands the set of spectroscopic data that can be used to determine the coupling constants. For example, the coupled state fitting of the lowest energy dyad in benzonitrile was conducted separately from the coupled state fitting of the corresponding triad, but by applying the results of the ratio expression in Eq. (7.175) these treatments could have been combined. Furthermore, the coupling constants determined for a relatively isolated set of coupled vibrational states could be used to assist in the fitting of a more complex polyad that shares some of the same vibrational modes, and this potential is further extended by the observation that the ratio expression in Eq. (7.175) is not limited to describing the relationship of coupled states to their corresponding pair of fundamentals. Regardless of how this insight is applied, the proportional relationship of the coupling constants

can be used to reduce the number of parameters that require optimization in the fitting of coupled vibrational states.

At present, the prediction of the first and second order Coriolis coupling constants is limited to the case where the change in vibrational quanta between the resonant states is $\sum_i |\Delta n_i| = 2$, which largely limits the predictions to pairs of fundamental states and their higher quanta combinations. The prediction of the coupling between other resonant vibrational states requires different terms of the transformed Hamiltonian. For example, the first order Coriolis coupling constant between a fundamental and an unrelated combination – $\langle \nu_A | G_x | \nu_B, \nu_C \rangle$ – involves a change in vibrational quanta of three separate vibrational modes, and as such requires a product of three different vibrational operators to obtain a nonzero expectation value; that is, the prediction of such a value requires the determination of $\tilde{\mathbf{H}}_{31}$. Similarly, the corresponding second order Coriolis coupling constant requires determination of $\tilde{\mathbf{H}}_{32}$. If instead the resonant states are an overtone and an unrelated combination *i.e.*, $\langle 2\nu_A | G_x | \nu_B, \nu_C \rangle$, then a product of four vibrational operators is required, and so on and so forth. The determination and application of such expressions to obtain predictions of vibration-rotation coupling constants is of considerable interest to us in our works involving the fitting of rotational spectra of coupled vibrational states, and as we continue to develop the *vib-rot-Van-Vleck* program. Before we reach too far, however, we will need to explore the accuracy of the predictions that we can calculate now for a variety of experimentally measured and fit coupled-state rotational spectra and consider the dependence of the predictions on the level of theory employed for the underlying vibrational calculation.

ACKNOWLEDGEMENTS

We gratefully acknowledge the National Science Foundation for support of this project (CHE-1664912 and CHE-1954270).

REFERENCES

1. Watson, J. K. G., Determination of Centrifugal Distortion Coefficients of Asymmetric-Top Molecules. *J. Chem. Phys.* **1967,** *46* (5), 1935-1949.

2. Watson, J. K. G., Aspects of quartic and sextic centrifugal effects on rotational energy levels. *Vib. Spectra Struct.* **1977,** *6*, 1-89.

3. Papousek, D.; Aliev, M. R., *Molecular Vibrational-Rotational Spectra: Theory and Applications of High Resolution Infrared, Microwave, and Raman Spectroscopy of Polyatomic Molecules*. Elsevier Scientific Pub. Co.: New York, 1982.

4. Aliev, M. R.; Watson, J. K. G., Chapter 1 - Higher-order effects in the vibration-rotation spectra of semirigid molecules. In *Molecular Spectroscopy: Modern Research*, Rao, K. N., Ed. Academic Press: 1985; pp 1-67.

5. Aliev, M. R.; Watson, J. K. G., The rotational dependence of diagonal Coriolis coupling. *J. Mol. Spectrosc.* **1979,** *75* (1), 150-160.

6. Perevalov, V. I.; Tyuterev, V. G., Effective centrifugal Hamiltonian with empirically reconstructable parameters in the case of Coriolis resonances in asymmetric-top molecules. *Opt. Spectrosc.* **1982,** *52* (4), 384-388.

7. Perevalov, V. I.; Tyuterev, V. G., Effective centrifugal Hamiltonian with empirically restorable parameters in the case of Coriolis resonances in symmetric-top type molecules. *Opt. Spektrosk.* **1982,** *52* (4), 644-650.

8. Barbe, A.; Mikhailenko, S.; Starikova, E.; Tyuterev, V., High Resolution Infrared Spectroscopy in Support of Ozone Atmospheric Monitoring and Validation of the Potential Energy Function. *Molecules* **2022,** *27* (3), 911.

9. Zdanovskaia, M. A.; Martin-Drumel, M.-A.; Kisiel, Z.; Pirali, O.; Esselman, B. J.; Woods, R. C.; McMahon, R. J., The eight lowest-energy vibrational states of benzonitrile: analysis of Coriolis and Darling-Dennison couplings by millimeter-wave and far-infrared spectroscopy. *J. Mol. Spectrosc.* **2022,** *383*, 111568.

10. Stanton, J. F.; Gauss, J.; Harding, M. E.; Szalay, P. G. *CFOUR*, 2.0; 2014.

11. Meurer, A.; Smith, C. P.; Paprocki, M.; Certik, O.; Kirpichev, S. B.; Rocklin, M.; Kumar, A.; Ivanov, S.; Moore, J. K.; Singh, S.; Rathnayake, T.; Vig, S.; Granger, B. E.; Muller, R. P.; Bonazzi, F.; Gupta, H.; Vats, S.; Johansson, F.; Pedregosa, F.; Curry, M. J.; Terrel, A. R.; Roucka, S.; Saboo, A.; Fernando, I.; Kulal, S.; Cimrman, R.; Scopatz, A., SymPy: symbolic computing in Python. *PeerJ Comput. Sci.* **2017**, e103.

12. Niroomand-Rad, A.; Parker, P. M., Sequential contact transformation formulation of asymmetric-rotator vibration-rotation Hamiltonian. *J. Mol. Spectrosc.* **1981,** *85* (1), 40-54.

SUPPORTING INFORMATION

Table of Contents

Vibrational Commutator and Quick Reference

$$\begin{aligned} \left[\mathbf{q}_a, \mathbf{p}_b\right] &= i\delta_{ab} \\ \left[\mathbf{q}_a, \mathbf{q}_b\right] &= 0 \\ \left[\mathbf{p}_a, \mathbf{p}_b\right] &= 0 \end{aligned} \tag{7.S1}$$

$$\begin{aligned}
\left[\mathbf{q}_a, \mathbf{q}_b \mathbf{p}_c\right] &= i\delta_{ac}\mathbf{q}_b \\
\left[\mathbf{q}_a, \mathbf{p}_b \mathbf{q}_c\right] &= i\delta_{ab}\mathbf{q}_c \\
\left[\mathbf{q}_a, \mathbf{p}_b \mathbf{p}_c\right] &= i\delta_{ac}\mathbf{p}_b + i\delta_{ab}\mathbf{p}_c
\end{aligned} \tag{7.S2}$$

$$\begin{aligned}
\left[\mathbf{q}_a \mathbf{q}_b, \mathbf{p}_c\right] &= i\delta_{bc}\mathbf{q}_a + i\delta_{ac}\mathbf{q}_b \\
\left[\mathbf{q}_a \mathbf{p}_b, \mathbf{p}_c\right] &= i\delta_{ac}\mathbf{p}_b \\
\left[\mathbf{p}_a \mathbf{q}_b, \mathbf{p}_c\right] &= i\delta_{bc}\mathbf{p}_a
\end{aligned} \tag{7.S3}$$

Generalized Rotational Commutator

$$\left[\mathbf{J}_\alpha, \mathbf{J}_\beta\right] = -i\sum_\gamma \epsilon_{\alpha\beta\gamma}\mathbf{J}_\gamma \tag{7.S4}$$

Vibrational Matrix Elements

$$\langle v|\mathbf{q}|v\pm 1\rangle = \sqrt{\frac{1}{2}\left(v + \frac{1}{2}(1\pm 1)\right)} \tag{7.S5}$$

$$\langle v|\mathbf{p}|v\pm 1\rangle = \mp i\sqrt{\frac{1}{2}\left(v + \frac{1}{2}(1\pm 1)\right)} \tag{7.S6}$$

Coefficients of the Expanded and Ordered Vibration-Rotation Hamiltonian

The following are the definitions of the coefficients used to abbreviate the terms of the original Hamiltonian, where ω_k is the frequency of the *k*th harmonic vibrational mode, k_{abc} is the cubic force constant (invariant to change in ordering of indices), B_α is the rotational constant for the α axis, ζ_{ab}^{α} is the Coriolis zeta coupling constant between the *a* and *b* harmonic vibrations through the α axis, and $C_a^{\alpha\beta}$ is the unitless rotational derivative. The cubic force constant k_{abc} is invariant to changes in the ordering of its indices, $\zeta_{ab}^{\alpha} = -\zeta_{ba}^{\alpha}$, $\zeta_{aa}^{\alpha} = 0$, and $C_a^{\alpha\beta} = C_a^{\beta\alpha}$.

$$\mathrm{H}_{20}\left(v_0\right)=\frac{1}{2}\omega_{v_0} \tag{7.S7}$$

$$\mathrm{H}_{30}\left(v_0,v_1,v_2\right)=\frac{1}{6}\mathrm{k}_{v_0v_1v_2} \tag{7.S8}$$

$$\mathrm{H}_{21}\left(v_0,v_1,r_0\right)=-2\frac{\sqrt{\omega_{v_1}}}{\sqrt{\omega_{v_0}}}B_{r_0}\zeta_{v_0v_1}^{r_0} \tag{7.S9}$$

$$\mathrm{H}_{12}\left(v_0,r_0,r_1\right)=-\omega_{v_0}C_{v_0}^{r_0r_1} \tag{7.S10}$$

$$\mathrm{H}_{02}\left(r_0\right)=B_{r_0} \tag{7.S11}$$

$$\mathrm{H}_{22}\left(v_0,v_1,r_0,r_1\right)=\frac{3}{8}\sum_{r_2}\frac{1}{B_{r_2}}\omega_{v_0}\omega_{v_1}\left(C_{v_0}^{r_0r_2}C_{v_1}^{r_2r_1}+C_{v_1}^{r_0r_2}C_{v_0}^{r_2r_1}\right) \tag{7.S12}$$

Table 7.6. Transformation of $\sim \mathbf{J}^2$ Rotational Operators from Cartesian to Cylindrical Form

Cartesian Form	Cylindrical Tensor Form
$\mathbf{J}_x\mathbf{J}_x$	$\frac{1}{2}\mathbf{J}^2-\frac{1}{2}\mathbf{J}_z^2+\frac{1}{4}\left(\mathbf{J}_-^2+\mathbf{J}_+^2\right)$
$\mathbf{J}_x\mathbf{J}_y$	$-\frac{i}{4}\left(\mathbf{J}_-^2-\mathbf{J}_+^2\right)-\frac{i}{2}\mathbf{J}_z$
$\mathbf{J}_x\mathbf{J}_z$	$\frac{1}{4}\left(\mathbf{J}_z\left(\mathbf{J}_-+\mathbf{J}_+\right)+\left(\mathbf{J}_-+\mathbf{J}_+\right)\mathbf{J}_z\right)+\frac{1}{4}\left(\mathbf{J}_--\mathbf{J}_+\right)$
$\mathbf{J}_y\mathbf{J}_x$	$-\frac{i}{4}\left(\mathbf{J}_-^2-\mathbf{J}_+^2\right)+\frac{i}{2}\mathbf{J}_z$
$\mathbf{J}_y\mathbf{J}_y$	$\frac{1}{2}\mathbf{J}^2-\frac{1}{2}\mathbf{J}_z^2-\frac{1}{4}\left(\mathbf{J}_-^2+\mathbf{J}_+^2\right)$
$\mathbf{J}_y\mathbf{J}_z$	$-\frac{i}{4}\left(\mathbf{J}_z\left(\mathbf{J}_--\mathbf{J}_+\right)+\left(\mathbf{J}_--\mathbf{J}_+\right)\mathbf{J}_z\right)-\frac{i}{4}\left(\mathbf{J}_-+\mathbf{J}_+\right)$
$\mathbf{J}_z\mathbf{J}_x$	$\frac{1}{4}\left(\mathbf{J}_z\left(\mathbf{J}_-+\mathbf{J}_+\right)+\left(\mathbf{J}_-+\mathbf{J}_+\right)\mathbf{J}_z\right)-\frac{1}{4}\left(\mathbf{J}_--\mathbf{J}_+\right)$
$\mathbf{J}_z\mathbf{J}_y$	$-\frac{i}{4}\left(\mathbf{J}_z\left(\mathbf{J}_--\mathbf{J}_+\right)+\left(\mathbf{J}_--\mathbf{J}_+\right)\mathbf{J}_z\right)+\frac{i}{4}\left(\mathbf{J}_-+\mathbf{J}_+\right)$
$\mathbf{J}_z\mathbf{J}_z$	$\mathbf{J}_z^2$

Overview of the *vib-rot-Van-Vleck* Program

The *vib-rot-Van-Vleck* program is a computer-aided derivation program for obtaining transformed Hamiltonians using contact transformations. The program also has features for routine numeric evaluation of the vibrational matrix elements of such transformed Hamiltonians, using results of *ab initio* calculations. Essentially, the program is an object-oriented implementation of the methodology described in the paper. In addition to the use of the *SymPy* package, the program utilizes open-source packages of *NumPy, tqdm*, *pandas*, and *SciPy*.

The program contains three classes: the DataObject, the EquationObject, and the NumericObject classes. The DataObject contains *ab initio* data of a molecule and is initialized using the output files of an *ab initio* calculation which are formatted in a consist fashion for later use in the NumericObject. The EquationObject is the core of the symbolic derivation of the transformed Hamiltonian and is initialized by providing the degrees of vibration and rotation of the desired Hamiltonian. The NumericObject combines one DataObject and one EquationObject and creates the numeric functions necessary to evaluate definitions contained within the EquationObject.

The DataObject first parses the provided computational output files and organizes the data it reads in. Furthermore, the DataObject defines a function for creation of VibState objects, each one of which consists of a dictionary of the vibrational modes and their corresponding quanta. Effectively, the VibState object is a representation of a particular row (or column) of the vibrational matrix of the molecule in question and can be used to evaluate expectation values within the NumericObject.

The EquationObject applies the transformations discussed in the paper to a Term or Expression class. Specifically, a Term is a representation of a summation in the form of Eq. (7.18)

and an Expression is a combination (addition) of Terms. A Term consists of vibrational operators, rotational operators, a symbolic coefficient, and the vibration and rotation indices of which the operators and coefficient are functions of, along withs methods for the arithmetic manipulation of the summation it represents. Combining two Term objects creates an Expression, which sorts and assesses the component Terms to obtain the smallest Expression object possible. That is, if Term A uses the same operators as Term B and if it has the same number of vibration and rotation indices, the Expression will consolidate the two Terms by judicious relabeling of the summation indices and adding together the relabeled coefficients. The Term and Expression also contain methods for implementing vibration and rotation commutators, as per the formulation in Eq. (7.10) –(7.12).

To obtain the transformed Hamiltonian, the EquationObject determines the necessary sequence of contact transformations required. Using a generic set of term objects (composed of *m* vibrational degrees, *n* rotational degrees, and "H" or "S" designation), the EquationObject iteratively applies the contact transformations to obtain an expression of the *j*th transformed Hamiltonian, and application of the selection braces using the relations in Eq. (7.13)–(7.17) quickly yields the general equation that must be evaluated. The defining equations of the transform functions are similarly obtained as per Eq. (7.9).

To obtain solutions of the transform functions, the EquationObject makes use of the ladder solution. Thus, analogous LadderTerm and LadderExpression objects are utilized, and – provided the defining equation and using a symbolic representation of the denominator – the definition of the transform function is obtained, as per Eq. (7.26). The Term and Expression and the corresponding LadderTerm and LadderExpression objects include methods for interconverting between the two types using the definitions in Eq. (7.19)–(7.21) and properly accounts for the

summation over σ. The definitions of the transform functions are obtained in order as per their sequence, with the previous definitions incorporated as required.

Commutators of Terms are evaluated as per the method demonstrated in Eq. (7.44)–(7.48) and described in the corresponding text. Once the Kronecker deltas are evaluated, the resulting Terms are combined into an Expression, which as noted previously will consolidate the expression to obtain the minimum number of Terms. Once the transform functions are defined, the expression of the desired transformed Hamiltonian can be obtained by evaluation of the proper set of commutators. During the symbolic derivation process, the program defines new coefficients to simplify the representation of expressions, akin to the process in the paper. The implementation of a simplification routine is currently underway to allow for the evaluation and consolidation of expressions into molecular terms, as per the expression provided in Eq. (7.130). Meanwhile, the development of a rotational reduction procedure is still in progress as the implications of the reduction of higher order coupling constants are considered.

The results of the derivation program can be exported and saved, and the exported files can be imported back into the program at a later time. Thus, the program does not have to redo the symbolic derivation to utilize expressions in the NumericObject.

The coefficients of the original Hamiltonian can be defined with respect to the components contained by the DataObject. These definitions are symbolic within the EquationObject. Thus, a core purpose of the NumericObject is to create numeric functions by connecting the symbolic definitions contained within the EquationObject with the numeric definitions of the computational data contained with the DataObject. The NumericObject can also define numeric functions for the coefficients created by the EquationObject and uses these definitions to obtain numeric functions for the final coefficients of the transformed Hamiltonian. The numeric functions defined by the

NumericObject utilize a cache function to accelerate evaluation of frequently used coefficients. Using a pair of VibState objects from the DataObject, the NumericObject can calculate an arbitrary vibrational matrix element for the transformed Hamiltonian contained within the EquationObject.

The program is under active development with the goal of fully reproducing the methodology described within the paper and to make execution of the program user-friendly. More details about the structure, features, and execution of the program will be provided at a later time, and we are planning to make the project freely available through GitHub. Communications regarding this program should be directed to A.N.O.

Off-Diagonal Vibrational Matrix Element of $\tilde{\mathbf{H}}_{2n}$

The general evaluation of the off-diagonal matrix elements of a Hamiltonian with two degrees of vibration is given by Eq. (7.S13) . The definitions $\tilde{\mathrm{H}}_{2n,0}, \tilde{\mathrm{H}}_{2n,1}, \tilde{\mathrm{H}}_{2n,2}$, and $\tilde{\mathrm{H}}_{2n,3}$ are the coefficients of the vibrational operators $\mathbf{qq}$, $\mathbf{qp}$, $\mathbf{pq}$, and $\mathbf{pp}$, respectively. The ratio discussed in the main text is implied to be the ratio of the coefficients of the same product of arbitrary rotational operators *i.e.*, both the numerator and denominator are coefficients of the same product $\mathbf{J}_{r_0}\mathbf{J}_{r_1}\times\cdots\times\mathbf{J}_{r_n}$.

(7.S13)

Supporting Derivations for $\tilde{\mathbf{H}}_{22}$

Derivation of $\boldsymbol{S}_{12}$

First, we rewrite the defining part of Eq. (7.65) as an expression in terms of the ladder operators $\mathcal{L}^{\pm}$.

$$\begin{aligned}\mathbf{H}_{12} &= \sum_{v_0}\sum_{r_0 r_1}\mathrm{H}_{12}\left(v_0, r_0, r_1\right)\left(\frac{1}{2}\sum_{\sigma_{v_0}}\mathcal{L}_{v_0}^{\sigma_{v_0}}\right)\mathbf{J}_{r_0}\mathbf{J}_{r_1} \\ &= \sum_{v_0}\sum_{r_0 r_1}\sum_{\sigma_{v_0}}\left(\frac{1}{2}\mathrm{H}_{12}\left(v_0, r_0, r_1\right)\right)\mathcal{L}_{v_0}^{\sigma_{v_0}}\mathbf{J}_{r_0}\mathbf{J}_{r_1}\end{aligned} \tag{7.S14}$$

The transform function can then be defined as Eq. (7.S15), as per Eq. (7.26).

$$\mathbf{S}_{12} = \sum_{v_0} \sum_{r_0 r_1} \sum_{\sigma_{v_0}} \frac{-i}{2} \mathrm{D}\left(\sigma_{v_0}, v_0\right) \mathrm{H}_{12}\left(v_0, r_0, r_1\right) \mathcal{L}_{v_0}^{\sigma_{v_0}} \mathbf{J}_{r_0} \mathbf{J}_{r_1} \tag{7.S15}$$

Substituting back in the definition for the ladder operator yields Eq. (7.S16) where the coefficient is defined in Eq. (7.S17).

$$\begin{aligned} \mathbf{S}_{12} &= \sum_{v_0} \sum_{r_0 r_1} \sum_{\sigma_{v_0}} \frac{-i}{2} \mathrm{D}\left(\sigma_{v_0}, v_0\right) \mathrm{H}_{12}\left(v_0, r_0, r_1\right) \left(\mathbf{q}_{v_0} - i\sigma_{v_0} \mathbf{p}_{v_0}\right) \mathbf{J}_{r_0} \mathbf{J}_{r_1} \\ &= \sum_{v_0} \sum_{r_0 r_1} \mathrm{S}_{12}\left(v_0, r_0, r_1\right) \mathbf{p}_{v_0} \mathbf{J}_{r_0} \mathbf{J}_{r_1} \end{aligned} \tag{7.S16}$$

$$\mathrm{S}_{12}\left(v_0, r_0, r_1\right) = -\mathrm{D}\left(1, v_0\right) \mathrm{H}_{12}\left(v_0, r_0, r_1\right) \tag{7.S17}$$

Derivation of $\boldsymbol{S}_{21}$

First, we rewrite the defining part of Eq. (7.67) in terms of the ladder operators $\mathcal{L}^{\pm}$.

$$\begin{aligned} \mathbf{H}_{21} &= \sum_{v_0 v_1} \sum_{r_0} \mathrm{H}_{21}\left(v_0, v_1, r_0\right) \left(\frac{1}{2} \sum_{\sigma_{v_0}} \mathcal{L}_{v_0}^{\sigma_{v_0}} \right) \left(\frac{1}{2} i \sum_{\sigma_{v_1}} \sigma_{v_1} \mathcal{L}_{v_1}^{\sigma_{v_1}} \right) \mathbf{J}_{r_0} \\ &= \sum_{v_0 v_1} \sum_{r_0} \sum_{\sigma_{v_0} \sigma_{v_1}} \left(\frac{1}{4} i \sigma_{v_1} \mathrm{H}_{21}\left(v_0, v_1, r_0\right) \right) \mathcal{L}_{v_0}^{\sigma_{v_0}} \mathcal{L}_{v_1}^{\sigma_{v_1}} \mathbf{J}_{r_0} \end{aligned} \tag{7.S18}$$

The transform function can then be defined as Eq. (7.S19), as per Eq. (7.26).

$$\mathbf{S}_{21} = \sum_{v_0 v_1} \sum_{r_0} \sum_{\sigma_{v_0} \sigma_{v_1}} \frac{1}{8} \mathrm{D}\left(\sigma_{v_0}, v_0; \sigma_{v_1}, v_1\right) \left(\sigma_{v_1} \mathrm{H}_{21}\left(v_0, v_1, r_0\right) + \sigma_{v_0} \mathrm{H}_{21}\left(v_1, v_0, r_0\right)\right) \mathcal{L}_{v_0}^{\sigma_{v_0}} \mathcal{L}_{v_1}^{\sigma_{v_1}} \mathbf{J}_{r_0} \tag{7.S19}$$

Substituting back in the definition for the ladder operator yields Eq. (7.S20), where the coefficients are defined in Eq. (7.S21).

$$\begin{aligned}\mathbf{S}_{21} &= \sum_{v_0 v_1}\sum_{r_0}\sum_{\sigma_{v_0}\sigma_{v_1}} \frac{1}{8}\mathrm{D}\left(\sigma_{v_0}, v_0; \sigma_{v_1}, v_1\right)\left(\sigma_{v_1}\mathrm{H}_{21}\left(v_0, v_1, r_0\right) + \sigma_{v_0}\mathrm{H}_{21}\left(v_1, v_0, r_0\right)\right)\left(\mathbf{q}_{v_0} - i\sigma_{v_0}\mathbf{p}_{v_0}\right)\left(\mathbf{q}_{v_1} - i\sigma_{v_1}\mathbf{p}_{v_1}\right)\mathbf{J}_{r_0} \\ &= \sum_{v_0 v_1}\sum_{r_0}\mathrm{S}_{21,0}\left(v_0, v_1, r_0\right)\mathbf{q}_{v_0}\mathbf{q}_{v_1}\mathbf{J}_{r_0} + \sum_{v_0 v_1}\sum_{r_0}\mathrm{S}_{21,1}\left(v_0, v_1, r_0\right)\mathbf{p}_{v_0}\mathbf{p}_{v_1}\mathbf{J}_{r_0}\end{aligned} \tag{7.S20}$$

$$\begin{aligned}\mathrm{S}_{21,0}\left(v_0, v_1, r_0\right) &= \frac{1}{4}\left(\mathrm{D}\left(1, v_0; 1, v_1\right)\left(\mathrm{H}_{21}\left(v_0, v_1, r_0\right) + \mathrm{H}_{21}\left(v_1, v_0, r_0\right)\right) - \mathrm{D}\left(1, v_0; -1, v_1\right)\left(\mathrm{H}_{21}\left(v_0, v_1, r_0\right) - \mathrm{H}_{21}\left(v_1, v_0, r_0\right)\right)\right) \\ \mathrm{S}_{21,1}\left(v_0, v_1, r_0\right) &= \frac{-1}{4}\left(\mathrm{D}\left(1, v_0; 1, v_1\right)\left(\mathrm{H}_{21}\left(v_0, v_1, r_0\right) + \mathrm{H}_{21}\left(v_1, v_0, r_0\right)\right) + \mathrm{D}\left(1, v_0; -1, v_1\right)\left(\mathrm{H}_{21}\left(v_0, v_1, r_0\right) - \mathrm{H}_{21}\left(v_1, v_0, r_0\right)\right)\right)\end{aligned} \tag{7.S21}$$

Derivation of $\boldsymbol{S}_{22}$

Two vibrational, one rotational, and one nested pair of vibrational commutators need to be evaluated prior to defining $\mathbf{S}_{22}$.

EVALUATION OF $i[\mathbf{S}_{12}, \mathbf{H}_{30}]_{\mathrm{V}}$

Substituting in the definitions from Eq. (7.65) and Eq. (7.69) yields Eq. (7.S22), where we have ensured that each summation index is distinct.

$$\begin{aligned}i\left[\mathbf{S}_{12}, \mathbf{H}_{30}\right]_{\mathrm{V}} &= i\left[\sum_{v_0}\sum_{r_0 r_1}\mathrm{S}_{12}\left(v_0, r_0, r_1\right)\mathbf{p}_{v_0}\mathbf{J}_{r_0}\mathbf{J}_{r_1}, \sum_{v_1 v_2 v_3}\mathrm{H}_{30}\left(v_1, v_2, v_3\right)\mathbf{q}_{v_1}\mathbf{q}_{v_2}\mathbf{q}_{v_3}\right]_{\mathrm{V}} \\ &= i\sum_{v_0 v_1 v_2 v_3}\sum_{r_0 r_1}\left[\mathrm{S}_{12}\left(v_0, r_0, r_1\right)\mathbf{p}_{v_0}\mathbf{J}_{r_0}\mathbf{J}_{r_1}, \mathrm{H}_{30}\left(v_1, v_2, v_3\right)\mathbf{q}_{v_1}\mathbf{q}_{v_2}\mathbf{q}_{v_3}\right]_{\mathrm{V}}\end{aligned} \tag{7.S22}$$

We then apply the definition of the vibrational commutator from Eq. (7.12) to obtain the pure vibrational commutator in Eq. (7.S23).

$$\begin{aligned} i\left[\mathbf{S}_{12},\mathbf{H}_{30}\right]_{\mathrm{V}} &= i\sum_{v_0v_1v_2v_3}\sum_{r_0r_1}\frac{1}{2}\mathrm{S}_{12}\left(v_0,r_0,r_1\right)\mathrm{H}_{30}\left(v_1,v_2,v_3\right)\left[\mathbf{p}_{v_0},\mathbf{q}_{v_1}\mathbf{q}_{v_2}\mathbf{q}_{v_3}\right]_{\mathrm{V}}\left(\mathbf{J}_{r_0}\mathbf{J}_{r_1}\cdot 1+1\cdot\mathbf{J}_{r_0}\mathbf{J}_{r_1}\right) \\ &= \sum_{v_0v_1v_2v_3}\sum_{r_0r_1} i\,\mathrm{S}_{12}\left(v_0,r_0,r_1\right)\mathrm{H}_{30}\left(v_1,v_2,v_3\right)\left[\mathbf{p}_{v_0},\mathbf{q}_{v_1}\mathbf{q}_{v_2}\mathbf{q}_{v_3}\right]_{\mathrm{V}}\mathbf{J}_{r_0}\mathbf{J}_{r_1} \end{aligned} \tag{7.S23}$$

Next, the pure vibrational commutator is evaluated to give Eq. (7.S24).

$$i\left[\mathbf{S}_{12},\mathbf{H}_{30}\right]_{\mathrm{V}} = \sum_{v_0v_1v_2v_3}\sum_{r_0r_1}\mathrm{S}_{12}\left(v_0,r_0,r_1\right)\mathrm{H}_{30}\left(v_1,v_2,v_3\right)\left(\delta_{v_3v_0}\mathbf{q}_{v_1}\mathbf{q}_{v_2}+\delta_{v_2v_0}\mathbf{q}_{v_1}\mathbf{q}_{v_3}+\delta_{v_1v_0}\mathbf{q}_{v_2}\mathbf{q}_{v_3}\right)\mathbf{J}_{r_0}\mathbf{J}_{r_1} \tag{7.S24}$$

The summations are expanded (Eq. (7.S25)), the Kronecker deltas are evaluated (Eq. (7.S26)), and the results consolidated (Eq. (7.S27)).

$$\begin{aligned} i\left[\mathbf{S}_{12},\mathbf{H}_{30}\right]_{\mathrm{V}} = &\sum_{v_0v_1v_2v_3}\sum_{r_0r_1}\mathrm{S}_{12}\left(v_0,r_0,r_1\right)\mathrm{H}_{30}\left(v_1,v_2,v_3\right)\delta_{v_3v_0}\mathbf{q}_{v_1}\mathbf{q}_{v_2}\mathbf{J}_{r_0}\mathbf{J}_{r_1} \\ &+\sum_{v_0v_1v_2v_3}\sum_{r_0r_1}\mathrm{S}_{12}\left(v_0,r_0,r_1\right)\mathrm{H}_{30}\left(v_1,v_2,v_3\right)\delta_{v_2v_0}\mathbf{q}_{v_1}\mathbf{q}_{v_3}\mathbf{J}_{r_0}\mathbf{J}_{r_1} \\ &+\sum_{v_0v_1v_2v_3}\sum_{r_0r_1}\mathrm{S}_{12}\left(v_0,r_0,r_1\right)\mathrm{H}_{30}\left(v_1,v_2,v_3\right)\delta_{v_1v_0}\mathbf{q}_{v_2}\mathbf{q}_{v_3}\mathbf{J}_{r_0}\mathbf{J}_{r_1} \end{aligned} \tag{7.S25}$$

$$\begin{aligned} i\left[\mathbf{S}_{12},\mathbf{H}_{30}\right]_{\mathrm{V}} = &\sum_{v_0v_1v_2}\sum_{r_0r_1}\mathrm{S}_{12}\left(v_0,r_0,r_1\right)\mathrm{H}_{30}\left(v_1,v_2,v_0\right)\mathbf{q}_{v_1}\mathbf{q}_{v_2}\mathbf{J}_{r_0}\mathbf{J}_{r_1} \\ &+\sum_{v_0v_1v_3}\sum_{r_0r_1}\mathrm{S}_{12}\left(v_0,r_0,r_1\right)\mathrm{H}_{30}\left(v_1,v_0,v_3\right)\mathbf{q}_{v_1}\mathbf{q}_{v_3}\mathbf{J}_{r_0}\mathbf{J}_{r_1} \\ &+\sum_{v_0v_2v_3}\sum_{r_0r_1}\mathrm{S}_{12}\left(v_0,r_0,r_1\right)\mathrm{H}_{30}\left(v_0,v_2,v_3\right)\mathbf{q}_{v_2}\mathbf{q}_{v_3}\mathbf{J}_{r_0}\mathbf{J}_{r_1} \end{aligned} \tag{7.S26}$$

$$i\left[\mathbf{S}_{12},\mathbf{H}_{30}\right]_{\mathrm{V}}=\sum_{v_0v_1v_2}\sum_{r_0r_1}\mathrm{S}_{12}\left(v_2,r_0,r_1\right)\left(\mathrm{H}_{30}\left(v_0,v_1,v_2\right)+\mathrm{H}_{30}\left(v_0,v_2,v_1\right)+\mathrm{H}_{30}\left(v_2,v_0,v_1\right)\right)\mathbf{q}_{v_0}\mathbf{q}_{v_1}\mathbf{J}_{r_0}\mathbf{J}_{r_1} \quad (7.S27)$$

EVALUATION OF $i[\mathbf{S}_{12},\mathbf{H}_{30}]_{\mathrm{V}}$

Substituting in the definitions from Eq. (7.75) and Eq. (7.70) yields Eq. (7.S28), where we have ensured that each summation index is distinct.

$$\begin{aligned}i\left[\mathbf{S}_{21},\mathbf{H}_{21}\right]_{\mathrm{V}}&=i\left[\sum_{v_0v_1}\sum_{r_0}\mathrm{S}_{21,0}\left(v_0,v_1,r_0\right)\mathbf{q}_{v_0}\mathbf{q}_{v_1}\mathbf{J}_{r_0}+\sum_{v_0v_1}\sum_{r_0}\mathrm{S}_{21,1}\left(v_0,v_1,r_0\right)\mathbf{p}_{v_0}\mathbf{p}_{v_1}\mathbf{J}_{r_0},\sum_{v_0v_1}\sum_{r_0}\mathrm{H}_{21}\left(v_0,v_1,r_0\right)\mathbf{q}_{v_0}\mathbf{p}_{v_1}\mathbf{J}_{r_0}\right]_{\mathrm{V}}\\&=i\sum_{v_0v_1v_2v_3}\sum_{r_0r_1}\left[\mathrm{S}_{21,0}\left(v_0,v_1,r_0\right)\mathbf{q}_{v_0}\mathbf{q}_{v_1}\mathbf{J}_{r_0},\mathrm{H}_{21}\left(v_2,v_3,r_1\right)\mathbf{q}_{v_2}\mathbf{p}_{v_3}\mathbf{J}_{r_1}\right]_{\mathrm{V}}\\&\quad+i\sum_{v_0v_1v_2v_3}\sum_{r_0r_1}\left[\mathrm{S}_{21,1}\left(v_0,v_1,r_0\right)\mathbf{p}_{v_0}\mathbf{p}_{v_1}\mathbf{J}_{r_0},\mathrm{H}_{21}\left(v_2,v_3,r_1\right)\mathbf{q}_{v_2}\mathbf{p}_{v_3}\mathbf{J}_{r_1}\right]_{\mathrm{V}}\end{aligned} \quad (7.S28)$$

We then apply the definition of the vibrational commutator from Eq. (7.12) to obtain the pure vibrational commutators in Eq. (7.S29).

$$\begin{aligned}i\left[\mathbf{S}_{21},\mathbf{H}_{21}\right]_{\mathrm{V}}&=i\sum_{v_0v_1v_2v_3}\sum_{r_0r_1}\frac{1}{2}\mathrm{S}_{21,0}\left(v_0,v_1,r_0\right)\mathrm{H}_{21}\left(v_2,v_3,r_1\right)\left[\mathbf{q}_{v_0}\mathbf{q}_{v_1},\mathbf{q}_{v_2}\mathbf{p}_{v_3}\right]_{\mathrm{V}}\left(\mathbf{J}_{r_0}\mathbf{J}_{r_1}+\mathbf{J}_{r_1}\mathbf{J}_{r_0}\right)\\&\quad+i\sum_{v_0v_1v_2v_3}\sum_{r_0r_1}\frac{1}{2}\mathrm{S}_{21,1}\left(v_0,v_1,r_0\right)\mathrm{H}_{21}\left(v_2,v_3,r_1\right)\left[\mathbf{p}_{v_0}\mathbf{p}_{v_1},\mathbf{q}_{v_2}\mathbf{p}_{v_3}\right]_{\mathrm{V}}\left(\mathbf{J}_{r_0}\mathbf{J}_{r_1}+\mathbf{J}_{r_1}\mathbf{J}_{r_0}\right)\end{aligned} \quad (7.S29)$$

Next, the pure vibrational commutator is evaluated to give Eq. (7.S30).

$$i\left[\mathbf{S}_{21},\mathbf{H}_{21}\right]_{\mathrm{V}} = i\sum_{v_0v_1v_2v_3}\sum_{r_0r_1}\frac{1}{2}\mathrm{S}_{21,0}\left(v_0,v_1,r_0\right)\mathrm{H}_{21}\left(v_2,v_3,r_1\right)\left(i\delta_{v_1v_3}\mathbf{q}_{v_0}\mathbf{q}_{v_2}+i\delta_{v_0v_3}\mathbf{q}_{v_2}\mathbf{q}_{v_1}\right)\left(\mathbf{J}_{r_0}\mathbf{J}_{r_1}+\mathbf{J}_{r_1}\mathbf{J}_{r_0}\right)$$
$$+i\sum_{v_0v_1v_2v_3}\sum_{r_0r_1}\frac{1}{2}\mathrm{S}_{21,1}\left(v_0,v_1,r_0\right)\mathrm{H}_{21}\left(v_2,v_3,r_1\right)\left(-\left(i\delta_{v_2v_1}\mathbf{p}_{v_0}\mathbf{p}_{v_3}+i\delta_{v_2v_0}\mathbf{p}_{v_1}\mathbf{p}_{v_3}\right)\right)\left(\mathbf{J}_{r_0}\mathbf{J}_{r_1}+\mathbf{J}_{r_1}\mathbf{J}_{r_0}\right) \tag{7.S30}$$

The summations are expanded (Eq. (7.S31)), the Kronecker deltas are evaluated (Eq. (7.S32)), and the results consolidated (Eq. (7.S33)).

$$\begin{aligned}i\left[\mathbf{S}_{21},\mathbf{H}_{21}\right]_{\mathrm{V}} = &\sum_{v_0v_1v_2v_3}\sum_{r_0r_1}\frac{-1}{2}\mathrm{S}_{21,0}\left(v_0,v_1,r_0\right)\mathrm{H}_{21}\left(v_2,v_3,r_1\right)\delta_{v_1v_3}\mathbf{q}_{v_0}\mathbf{q}_{v_2}\left(\mathbf{J}_{r_0}\mathbf{J}_{r_1}+\mathbf{J}_{r_1}\mathbf{J}_{r_0}\right)\\ &+\sum_{v_0v_1v_2v_3}\sum_{r_0r_1}\frac{-1}{2}\mathrm{S}_{21,0}\left(v_0,v_1,r_0\right)\mathrm{H}_{21}\left(v_2,v_3,r_1\right)\delta_{v_0v_3}\mathbf{q}_{v_2}\mathbf{q}_{v_1}\left(\mathbf{J}_{r_0}\mathbf{J}_{r_1}+\mathbf{J}_{r_1}\mathbf{J}_{r_0}\right)\\ &+\sum_{v_0v_1v_2v_3}\sum_{r_0r_1}\frac{1}{2}\mathrm{S}_{21,1}\left(v_0,v_1,r_0\right)\mathrm{H}_{21}\left(v_2,v_3,r_1\right)\delta_{v_2v_1}\mathbf{p}_{v_0}\mathbf{p}_{v_3}\left(\mathbf{J}_{r_0}\mathbf{J}_{r_1}+\mathbf{J}_{r_1}\mathbf{J}_{r_0}\right)\\ &+\sum_{v_0v_1v_2v_3}\sum_{r_0r_1}\frac{1}{2}\mathrm{S}_{21,1}\left(v_0,v_1,r_0\right)\mathrm{H}_{21}\left(v_2,v_3,r_1\right)\delta_{v_2v_0}\mathbf{p}_{v_1}\mathbf{p}_{v_3}\left(\mathbf{J}_{r_0}\mathbf{J}_{r_1}+\mathbf{J}_{r_1}\mathbf{J}_{r_0}\right)\end{aligned} \tag{7.S31}$$

$$\begin{aligned}i\left[\mathbf{S}_{21},\mathbf{H}_{21}\right]_{\mathrm{V}} = &\sum_{v_0v_1v_2}\sum_{r_0r_1}\frac{-1}{2}\mathrm{S}_{21,0}\left(v_0,v_1,r_0\right)\mathrm{H}_{21}\left(v_2,v_1,r_1\right)\mathbf{q}_{v_0}\mathbf{q}_{v_2}\left(\mathbf{J}_{r_0}\mathbf{J}_{r_1}+\mathbf{J}_{r_1}\mathbf{J}_{r_0}\right)\\ &+\sum_{v_0v_1v_2}\sum_{r_0r_1}\frac{-1}{2}\mathrm{S}_{21,0}\left(v_0,v_1,r_0\right)\mathrm{H}_{21}\left(v_2,v_0,r_1\right)\mathbf{q}_{v_2}\mathbf{q}_{v_1}\left(\mathbf{J}_{r_0}\mathbf{J}_{r_1}+\mathbf{J}_{r_1}\mathbf{J}_{r_0}\right)\\ &+\sum_{v_0v_1v_3}\sum_{r_0r_1}\frac{1}{2}\mathrm{S}_{21,1}\left(v_0,v_1,r_0\right)\mathrm{H}_{21}\left(v_1,v_3,r_1\right)\mathbf{p}_{v_0}\mathbf{p}_{v_3}\left(\mathbf{J}_{r_0}\mathbf{J}_{r_1}+\mathbf{J}_{r_1}\mathbf{J}_{r_0}\right)\\ &+\sum_{v_0v_1v_3}\sum_{r_0r_1}\frac{1}{2}\mathrm{S}_{21,1}\left(v_0,v_1,r_0\right)\mathrm{H}_{21}\left(v_0,v_3,r_1\right)\mathbf{p}_{v_1}\mathbf{p}_{v_3}\left(\mathbf{J}_{r_0}\mathbf{J}_{r_1}+\mathbf{J}_{r_1}\mathbf{J}_{r_0}\right)\end{aligned} \tag{7.S32}$$

$$i\left[\mathbf{S}_{21},\mathbf{H}_{21}\right]_{\mathrm{V}}=\sum_{v_0v_1v_2}\sum_{r_0r_1}\frac{-1}{2}\left(\mathrm{S}_{21,0}\left(v_0,v_2,r_0\right)\mathrm{H}_{21}\left(v_1,v_2,r_1\right)+\mathrm{S}_{21,0}\left(v_2,v_1,r_0\right)\mathrm{H}_{21}\left(v_0,v_2,r_1\right)\right)\mathbf{q}_{v_0}\mathbf{q}_{v_1}\left(\mathbf{J}_{r_0}\mathbf{J}_{r_1}+\mathbf{J}_{r_1}\mathbf{J}_{r_0}\right)$$
$$+\sum_{v_0v_1v_2}\sum_{r_0r_1}\frac{1}{2}\left(\mathrm{S}_{21,1}\left(v_0,v_2,r_0\right)+\mathrm{S}_{21,1}\left(v_2,v_0,r_0\right)\right)\mathrm{H}_{21}\left(v_2,v_1,r_1\right)\mathbf{p}_{v_0}\mathbf{p}_{v_1}\left(\mathbf{J}_{r_0}\mathbf{J}_{r_1}+\mathbf{J}_{r_1}\mathbf{J}_{r_0}\right) \tag{7.S33}$$

This process is repeated to consolidate the rotational operators as well.

$$\begin{aligned}i\left[\mathbf{S}_{21},\mathbf{H}_{21}\right]_{\mathrm{V}}=&\sum_{v_0v_1v_2}\sum_{r_0r_1}\frac{-1}{2}\left(\mathrm{S}_{21,0}\left(v_0,v_2,r_0\right)\mathrm{H}_{21}\left(v_1,v_2,r_1\right)+\mathrm{S}_{21,0}\left(v_2,v_1,r_0\right)\mathrm{H}_{21}\left(v_0,v_2,r_1\right)\right)\mathbf{q}_{v_0}\mathbf{q}_{v_1}\mathbf{J}_{r_0}\mathbf{J}_{r_1}\\&+\sum_{v_0v_1v_2}\sum_{r_0r_1}\frac{-1}{2}\left(\mathrm{S}_{21,0}\left(v_0,v_2,r_0\right)\mathrm{H}_{21}\left(v_1,v_2,r_1\right)+\mathrm{S}_{21,0}\left(v_2,v_1,r_0\right)\mathrm{H}_{21}\left(v_0,v_2,r_1\right)\right)\mathbf{q}_{v_0}\mathbf{q}_{v_1}\mathbf{J}_{r_1}\mathbf{J}_{r_0}\\&+\sum_{v_0v_1v_2}\sum_{r_0r_1}\frac{1}{2}\left(\mathrm{S}_{21,1}\left(v_0,v_2,r_0\right)+\mathrm{S}_{21,1}\left(v_2,v_0,r_0\right)\right)\mathrm{H}_{21}\left(v_2,v_1,r_1\right)\mathbf{p}_{v_0}\mathbf{p}_{v_1}\mathbf{J}_{r_0}\mathbf{J}_{r_1}\\&+\sum_{v_0v_1v_2}\sum_{r_0r_1}\frac{1}{2}\left(\mathrm{S}_{21,1}\left(v_0,v_2,r_0\right)+\mathrm{S}_{21,1}\left(v_2,v_0,r_0\right)\right)\mathrm{H}_{21}\left(v_2,v_1,r_1\right)\mathbf{p}_{v_0}\mathbf{p}_{v_1}\mathbf{J}_{r_1}\mathbf{J}_{r_0}\end{aligned} \tag{7.S34}$$

$$\begin{aligned}i\left[\mathbf{S}_{21},\mathbf{H}_{21}\right]_{\mathrm{V}}=&\sum_{v_0v_1v_2}\sum_{r_0r_1}\frac{-1}{2}\left(\mathrm{S}_{21,0}\left(v_0,v_2,r_0\right)\mathrm{H}_{21}\left(v_1,v_2,r_1\right)+\mathrm{S}_{21,0}\left(v_2,v_1,r_0\right)\mathrm{H}_{21}\left(v_0,v_2,r_1\right)+\mathrm{S}_{21,0}\left(v_0,v_2,r_1\right)\mathrm{H}_{21}\left(v_1,v_2,r_0\right)\right.\\&\left.+\mathrm{S}_{21,0}\left(v_2,v_1,r_1\right)\mathrm{H}_{21}\left(v_0,v_2,r_0\right)\right)\mathbf{q}_{v_0}\mathbf{q}_{v_1}\mathbf{J}_{r_0}\mathbf{J}_{r_1}\\&+\sum_{v_0v_1v_2}\sum_{r_0r_1}\frac{1}{2}\left(\left(\mathrm{S}_{21,1}\left(v_0,v_2,r_0\right)+\mathrm{S}_{21,1}\left(v_2,v_0,r_0\right)\right)\mathrm{H}_{21}\left(v_2,v_1,r_1\right)\right.\\&\left.+\left(\mathrm{S}_{21,1}\left(v_0,v_2,r_1\right)+\mathrm{S}_{21,1}\left(v_2,v_0,r_1\right)\right)\mathrm{H}_{21}\left(v_2,v_1,r_0\right)\right)\mathbf{p}_{v_0}\mathbf{p}_{v_1}\mathbf{J}_{r_0}\mathbf{J}_{r_1}\end{aligned} \tag{7.S35}$$

EVALUATION OF $i[\mathbf{S}_{21},\mathbf{H}_{02}]_{\mathrm{R}}$

Substituting in the definitions from Eq. (7.75) and Eq. (7.72) yields Eq. (7.S36), where we have ensured that each summation index is distinct.

$$\begin{aligned} i\left[\mathbf{S}_{21},\mathbf{H}_{02}\right]_{\mathrm{R}} &= i\left[\sum_{v_0 v_1}\sum_{r_0}\mathrm{S}_{21,0}\left(v_0,v_1,r_0\right)\mathbf{q}_{v_0}\mathbf{q}_{v_1}\mathbf{J}_{r_0}+\sum_{v_0 v_1}\sum_{r_0}\mathrm{S}_{21,1}\left(v_0,v_1,r_0\right)\mathbf{p}_{v_0}\mathbf{p}_{v_1}\mathbf{J}_{r_0},\sum_{r_0}\mathrm{H}_{02}\left(r_0\right)\mathbf{J}_{r_0}^2\right]_{\mathrm{R}} \\ &= i\sum_{v_0 v_1}\sum_{r_0 r_1}\left[\mathrm{S}_{21,0}\left(v_0,v_1,r_0\right)\mathbf{q}_{v_0}\mathbf{q}_{v_1}\mathbf{J}_{r_0},\mathrm{H}_{02}\left(r_1\right)\mathbf{J}_{r_1}^2\right]_{\mathrm{R}}+i\sum_{v_0 v_1}\sum_{r_0 r_1}\left[\mathrm{S}_{21,1}\left(v_0,v_1,r_0\right)\mathbf{p}_{v_0}\mathbf{p}_{v_1}\mathbf{J}_{r_0},\mathrm{H}_{02}\left(r_1\right)\mathbf{J}_{r_1}^2\right]_{\mathrm{R}} \end{aligned} \tag{7.S36}$$

We then apply the definition of the rotational commutator from Eq. (7.12) to obtain the pure rotational commutators in Eq. (7.S37).

$$i\left[\mathbf{S}_{21},\mathbf{H}_{02}\right]_{\mathrm{R}} = i\sum_{v_0 v_1}\sum_{r_0 r_1}\mathrm{S}_{21,0}\left(v_0,v_1,r_0\right)\mathrm{H}_{02}\left(r_1\right)\mathbf{q}_{v_0}\mathbf{q}_{v_1}\left[\mathbf{J}_{r_0},\mathbf{J}_{r_1}^2\right]_{\mathrm{R}}+i\sum_{v_0 v_1}\sum_{r_0 r_1}\mathrm{S}_{21,1}\left(v_0,v_1,r_0\right)\mathrm{H}_{02}\left(r_1\right)\mathbf{p}_{v_0}\mathbf{p}_{v_1}\left[\mathbf{J}_{r_0},\mathbf{J}_{r_1}^2\right]_{\mathrm{R}} \tag{7.S37}$$

Next, the pure rotational commutators are evaluated to give Eq. (7.S38).

$$\begin{aligned} i\left[\mathbf{S}_{21},\mathbf{H}_{02}\right]_{\mathrm{R}} = {} & i\sum_{v_0 v_1}\sum_{r_0 r_1 r_2}\left(-i\epsilon_{r_0 r_1 r_2}\right)\mathrm{S}_{21,0}\left(v_0,v_1,r_0\right)\mathrm{H}_{02}\left(r_1\right)\mathbf{q}_{v_0}\mathbf{q}_{v_1}\left(\mathbf{J}_{r_1}\mathbf{J}_{r_2}+\mathbf{J}_{r_2}\mathbf{J}_{r_1}\right) \\ & +i\sum_{v_0 v_1}\sum_{r_0 r_1 r_2}\left(-i\epsilon_{r_0 r_1 r_2}\right)\mathrm{S}_{21,1}\left(v_0,v_1,r_0\right)\mathrm{H}_{02}\left(r_1\right)\mathbf{p}_{v_0}\mathbf{p}_{v_1}\left(\mathbf{J}_{r_1}\mathbf{J}_{r_2}+\mathbf{J}_{r_2}\mathbf{J}_{r_1}\right) \end{aligned} \tag{7.S38}$$

The summations are expanded (Eq. (7.S39)) and the results consolidated (Eq. (7.S40)).

$$
\begin{aligned}
i\left[\mathbf{S}_{21},\mathbf{H}_{02}\right]_{\mathrm{R}} = {} & i\sum_{v_0v_1}\sum_{r_0r_1r_2}\left(-i\epsilon_{r_0r_1r_2}\right)\mathrm{S}_{21,0}\left(v_0,v_1,r_0\right)\mathrm{H}_{02}\left(r_1\right)\mathbf{q}_{v_0}\mathbf{q}_{v_1}\mathbf{J}_{r_1}\mathbf{J}_{r_2} + i\sum_{v_0v_1}\sum_{r_0r_1r_2}\left(-i\epsilon_{r_0r_1r_2}\right)\mathrm{S}_{21,0}\left(v_0,v_1,r_0\right)\mathrm{H}_{02}\left(r_1\right)\mathbf{q}_{v_0}\mathbf{q}_{v_1}\mathbf{J}_{r_2}\mathbf{J}_{r_1} \\
& + i\sum_{v_0v_1}\sum_{r_0r_1r_2}\left(-i\epsilon_{r_0r_1r_2}\right)\mathrm{S}_{21,1}\left(v_0,v_1,r_0\right)\mathrm{H}_{02}\left(r_1\right)\mathbf{p}_{v_0}\mathbf{p}_{v_1}\mathbf{J}_{r_1}\mathbf{J}_{r_2} + i\sum_{v_0v_1}\sum_{r_0r_1r_2}\left(-i\epsilon_{r_0r_1r_2}\right)\mathrm{S}_{21,1}\left(v_0,v_1,r_0\right)\mathrm{H}_{02}\left(r_1\right)\mathbf{p}_{v_0}\mathbf{p}_{v_1}\mathbf{J}_{r_2}\mathbf{J}_{r_1}
\end{aligned}
\tag{7.S39}
$$

$$
\begin{aligned}
i\left[\mathbf{S}_{21},\mathbf{H}_{02}\right]_{\mathrm{R}} = {} & \sum_{v_0v_1}\sum_{r_0r_1r_2}\epsilon_{r_0r_1r_2}\,\mathrm{S}_{21,0}\left(v_0,v_1,r_2\right)\left(\mathrm{H}_{02}\left(r_0\right)-\mathrm{H}_{02}\left(r_1\right)\right)\mathbf{q}_{v_0}\mathbf{q}_{v_1}\mathbf{J}_{r_0}\mathbf{J}_{r_1} \\
& + \sum_{v_0v_1}\sum_{r_0r_1r_2}\epsilon_{r_0r_1r_2}\,\mathrm{S}_{21,1}\left(v_0,v_1,r_2\right)\left(\mathrm{H}_{02}\left(r_0\right)-\mathrm{H}_{02}\left(r_1\right)\right)\mathbf{p}_{v_0}\mathbf{p}_{v_1}\mathbf{J}_{r_0}\mathbf{J}_{r_1}
\end{aligned}
\tag{7.S40}
$$

EVALUATION OF $-\frac{1}{2}\left[\mathbf{S}_{21},\left[\mathbf{S}_{21},\mathbf{H}_{20}\right]_{\mathrm{V}}\right]_{\mathrm{V}}$

(i) Inner commutator

Substituting in the definitions from Eq. (7.75) and Eq. (7.68) yields Eq. (7.S41), where we have ensured that each summation index is distinct.

$$
\begin{aligned}
\left[\mathbf{S}_{21},\mathbf{H}_{20}\right]_{\mathrm{V}} &= \left[\sum_{v_0v_1}\sum_{r_0}\mathrm{S}_{21,0}\left(v_0,v_1,r_0\right)\mathbf{q}_{v_0}\mathbf{q}_{v_1}\mathbf{J}_{r_0} + \sum_{v_0v_1}\sum_{r_0}\mathrm{S}_{21,1}\left(v_0,v_1,r_0\right)\mathbf{p}_{v_0}\mathbf{p}_{v_1}\mathbf{J}_{r_0}, \sum_{v_0}\mathrm{H}_{20}\left(v_0\right)\mathbf{q}_{v_0}^2 + \sum_{v_0}\mathrm{H}_{20}\left(v_0\right)\mathbf{p}_{v_0}^2\right]_{\mathrm{V}} \\
&= \sum_{v_0v_1v_2}\sum_{r_0}\left[\mathrm{S}_{21,0}\left(v_0,v_1,r_0\right)\mathbf{q}_{v_0}\mathbf{q}_{v_1}\mathbf{J}_{r_0},\mathrm{H}_{20}\left(v_2\right)\mathbf{q}_{v_2}^2\right]_{\mathrm{V}} + \sum_{v_0v_1v_2}\sum_{r_0}\left[\mathrm{S}_{21,0}\left(v_0,v_1,r_0\right)\mathbf{q}_{v_0}\mathbf{q}_{v_1}\mathbf{J}_{r_0},\mathrm{H}_{20}\left(v_2\right)\mathbf{p}_{v_2}^2\right]_{\mathrm{V}} \\
&\quad + \sum_{v_0v_1v_2}\sum_{r_0}\left[\mathrm{S}_{21,1}\left(v_0,v_1,r_0\right)\mathbf{p}_{v_0}\mathbf{p}_{v_1}\mathbf{J}_{r_0},\mathrm{H}_{20}\left(v_2\right)\mathbf{q}_{v_2}^2\right]_{\mathrm{V}} + \sum_{v_0v_1v_2}\sum_{r_0}\left[\mathrm{S}_{21,1}\left(v_0,v_1,r_0\right)\mathbf{p}_{v_0}\mathbf{p}_{v_1}\mathbf{J}_{r_0},\mathrm{H}_{20}\left(v_2\right)\mathbf{p}_{v_2}^2\right]_{\mathrm{V}}
\end{aligned}
\tag{7.S41}
$$

We then apply the definition of the vibrational commutator from Eq. (7.12) and eliminate the trivially zero commutators to obtain the pure vibrational commutators in Eq. (7.S42).

$$\left[\mathbf{S}_{21},\mathbf{H}_{20}\right]_{\mathrm{V}}=\sum_{v_0v_1v_2}\sum_{r_0}\mathrm{S}_{21,0}\left(v_0,v_1,r_0\right)\mathrm{H}_{20}\left(v_2\right)\left[\mathbf{q}_{v_0}\mathbf{q}_{v_1},\mathbf{p}_{v_2}^2\right]_{\mathrm{V}}\mathbf{J}_{r_0}+\sum_{v_0v_1v_2}\sum_{r_0}\mathrm{S}_{21,1}\left(v_0,v_1,r_0\right)\mathrm{H}_{20}\left(v_2\right)\left[\mathbf{p}_{v_0}\mathbf{p}_{v_1},\mathbf{q}_{v_2}^2\right]_{\mathrm{V}}\mathbf{J}_{r_0} \quad (7.S42)$$

Next, the pure vibrational commutator is evaluated to give Eq. (7.S43).

$$\begin{aligned}\left[\mathbf{S}_{21},\mathbf{H}_{20}\right]_{\mathrm{V}}=&\sum_{v_0v_1v_2}\sum_{r_0}\mathrm{S}_{21,0}\left(v_0,v_1,r_0\right)\mathrm{H}_{20}\left(v_2\right)\left(2i\delta_{v_1v_2}\mathbf{q}_{v_0}\mathbf{p}_{v_2}+2i\delta_{v_0v_2}\mathbf{p}_{v_2}\mathbf{q}_{v_1}\right)\mathbf{J}_{r_0}\\&+\sum_{v_0v_1v_2}\sum_{r_0}\mathrm{S}_{21,1}\left(v_0,v_1,r_0\right)\mathrm{H}_{20}\left(v_2\right)\left(-2i\delta_{v_1v_2}\mathbf{p}_{v_0}\mathbf{q}_{v_2}-2i\delta_{v_0v_2}\mathbf{q}_{v_2}\mathbf{p}_{v_1}\right)\mathbf{J}_{r_0}\end{aligned} \quad (7.S43)$$

The summations are expanded (Eq. (7.S44)), the Kronecker deltas are evaluated (Eq. (7.S45)), and the results consolidated (Eq. (7.S46)).

$$\begin{aligned}\left[\mathbf{S}_{21},\mathbf{H}_{20}\right]_{\mathrm{V}}=&\sum_{v_0v_1v_2}\sum_{r_0}2i\delta_{v_1v_2}\,\mathrm{S}_{21,0}\left(v_0,v_1,r_0\right)\mathrm{H}_{20}\left(v_2\right)\mathbf{q}_{v_0}\mathbf{p}_{v_2}\mathbf{J}_{r_0}\\&+\sum_{v_0v_1v_2}\sum_{r_0}2i\delta_{v_0v_2}\,\mathrm{S}_{21,0}\left(v_0,v_1,r_0\right)\mathrm{H}_{20}\left(v_2\right)\mathbf{p}_{v_2}\mathbf{q}_{v_1}\mathbf{J}_{r_0}\\&+\sum_{v_0v_1v_2}\sum_{r_0}\left(-2\right)i\delta_{v_1v_2}\,\mathrm{S}_{21,1}\left(v_0,v_1,r_0\right)\mathrm{H}_{20}\left(v_2\right)\mathbf{p}_{v_0}\mathbf{q}_{v_2}\mathbf{J}_{r_0}\\&+\sum_{v_0v_1v_2}\sum_{r_0}\left(-2\right)i\delta_{v_0v_2}\,\mathrm{S}_{21,1}\left(v_0,v_1,r_0\right)\mathrm{H}_{20}\left(v_2\right)\mathbf{q}_{v_2}\mathbf{p}_{v_1}\mathbf{J}_{r_0}\end{aligned} \quad (7.S44)$$

$$\begin{aligned}\left[\mathbf{S}_{21},\mathbf{H}_{20}\right]_{\mathrm{V}}=&\sum_{v_0v_1}\sum_{r_0}2i\,\mathrm{S}_{21,0}\left(v_0,v_1,r_0\right)\mathrm{H}_{20}\left(v_1\right)\mathbf{q}_{v_0}\mathbf{p}_{v_1}\mathbf{J}_{r_0}+\sum_{v_0v_1}\sum_{r_0}2i\,\mathrm{S}_{21,0}\left(v_0,v_1,r_0\right)\mathrm{H}_{20}\left(v_0\right)\mathbf{p}_{v_0}\mathbf{q}_{v_1}\mathbf{J}_{r_0}\\&+\sum_{v_0v_1}\sum_{r_0}\left(-2\right)i\,\mathrm{S}_{21,1}\left(v_0,v_1,r_0\right)\mathrm{H}_{20}\left(v_1\right)\mathbf{p}_{v_0}\mathbf{q}_{v_1}\mathbf{J}_{r_0}+\sum_{v_0v_1}\sum_{r_0}\left(-2\right)i\,\mathrm{S}_{21,1}\left(v_0,v_1,r_0\right)\mathrm{H}_{20}\left(v_0\right)\mathbf{q}_{v_0}\mathbf{p}_{v_1}\mathbf{J}_{r_0}\end{aligned} \quad (7.S45)$$

$$\left[\mathbf{S}_{21},\mathbf{H}_{20}\right]_{\mathrm{V}}=\sum_{v_0v_1}\sum_{r_0}2i\left(\mathrm{S}_{21,0}\left(v_0,v_1,r_0\right)\mathrm{H}_{20}\left(v_1\right)-\mathrm{S}_{21,1}\left(v_0,v_1,r_0\right)\mathrm{H}_{20}\left(v_0\right)\right)\mathbf{q}_{v_0}\mathbf{p}_{v_1}\mathbf{J}_{r_0}$$
$$+\sum_{v_0v_1}\sum_{r_0}2i\left(\mathrm{S}_{21,0}\left(v_0,v_1,r_0\right)\mathrm{H}_{20}\left(v_0\right)-\mathrm{S}_{21,1}\left(v_0,v_1,r_0\right)\mathrm{H}_{20}\left(v_1\right)\right)\mathbf{p}_{v_0}\mathbf{q}_{v_1}\mathbf{J}_{r_0} \tag{7.S46}$$

(ii) Outer commutator

Substituting in the definitions from Eq. (7.75) and Eq. (7.S46) yields Eq. (7.S47), where we have ensured that each summation index is distinct.

$$
\begin{aligned}
-\frac{1}{2}\Big[\mathbf{S}_{21},\big[\mathbf{S}_{21},\mathbf{H}_{20}\big]_{\mathrm{V}}\Big]_{\mathrm{V}} = -\frac{1}{2}\Bigg[&\sum_{v_0v_1}\sum_{r_0}\mathrm{S}_{21,0}\left(v_0,v_1,r_0\right)\mathbf{q}_{v_0}\mathbf{q}_{v_1}\mathbf{J}_{r_0}+\sum_{v_0v_1}\sum_{r_0}\mathrm{S}_{21,1}\left(v_0,v_1,r_0\right)\mathbf{p}_{v_0}\mathbf{p}_{v_1}\mathbf{J}_{r_0}\\
&,\sum_{v_0v_1}\sum_{r_0}2i\Big(\mathrm{S}_{21,0}\left(v_0,v_1,r_0\right)\mathrm{H}_{20}\left(v_1\right)-\mathrm{S}_{21,1}\left(v_0,v_1,r_0\right)\mathrm{H}_{20}\left(v_0\right)\Big)\mathbf{q}_{v_0}\mathbf{p}_{v_1}\mathbf{J}_{r_0}\\
&+\sum_{v_0v_1}\sum_{r_0}2i\Big(\mathrm{S}_{21,0}\left(v_0,v_1,r_0\right)\mathrm{H}_{20}\left(v_0\right)-\mathrm{S}_{21,1}\left(v_0,v_1,r_0\right)\mathrm{H}_{20}\left(v_1\right)\Big)\mathbf{p}_{v_0}\mathbf{q}_{v_1}\mathbf{J}_{r_0}\Bigg]_{\mathrm{V}}\\
=-\frac{1}{2}\sum_{v_0v_1v_2v_3}\sum_{r_0r_1}\Big[&\mathrm{S}_{21,0}\left(v_0,v_1,r_0\right)\mathbf{q}_{v_0}\mathbf{q}_{v_1}\mathbf{J}_{r_0}\\
&,2i\Big(\mathrm{S}_{21,0}\left(v_2,v_3,r_1\right)\mathrm{H}_{20}\left(v_3\right)-\mathrm{S}_{21,1}\left(v_2,v_3,r_1\right)\mathrm{H}_{20}\left(v_2\right)\Big)\mathbf{q}_{v_2}\mathbf{p}_{v_3}\mathbf{J}_{r_1}\Big]_{\mathrm{V}}\\
-\frac{1}{2}\sum_{v_0v_1v_2v_3}\sum_{r_0r_1}\Big[&\mathrm{S}_{21,0}\left(v_0,v_1,r_0\right)\mathbf{q}_{v_0}\mathbf{q}_{v_1}\mathbf{J}_{r_0}\\
&,2i\Big(\mathrm{S}_{21,0}\left(v_2,v_3,r_1\right)\mathrm{H}_{20}\left(v_2\right)-\mathrm{S}_{21,1}\left(v_2,v_3,r_1\right)\mathrm{H}_{20}\left(v_3\right)\Big)\mathbf{p}_{v_2}\mathbf{q}_{v_3}\mathbf{J}_{r_1}\Big]_{\mathrm{V}}\\
-\frac{1}{2}\sum_{v_0v_1v_2v_3}\sum_{r_0r_1}\Big[&\mathrm{S}_{21,1}\left(v_0,v_1,r_0\right)\mathbf{p}_{v_0}\mathbf{p}_{v_1}\mathbf{J}_{r_0}\\
&,2i\Big(\mathrm{S}_{21,0}\left(v_2,v_3,r_1\right)\mathrm{H}_{20}\left(v_3\right)-\mathrm{S}_{21,1}\left(v_2,v_3,r_1\right)\mathrm{H}_{20}\left(v_2\right)\Big)\mathbf{q}_{v_2}\mathbf{p}_{v_3}\mathbf{J}_{r_1}\Big]_{\mathrm{V}}\\
-\frac{1}{2}\sum_{v_0v_1v_2v_3}\sum_{r_0r_1}\Big[&\mathrm{S}_{21,1}\left(v_0,v_1,r_0\right)\mathbf{p}_{v_0}\mathbf{p}_{v_1}\mathbf{J}_{r_0}\\
&,2i\Big(\mathrm{S}_{21,0}\left(v_2,v_3,r_1\right)\mathrm{H}_{20}\left(v_2\right)-\mathrm{S}_{21,1}\left(v_2,v_3,r_1\right)\mathrm{H}_{20}\left(v_3\right)\Big)\mathbf{p}_{v_2}\mathbf{q}_{v_3}\mathbf{J}_{r_1}\Big]_{\mathrm{V}}
\end{aligned}
\tag{7.S47}
$$

We then apply the definition of the vibrational commutator from Eq. (7.12) to obtain the pure vibrational commutators in Eq. (7.S48).

$$
\begin{aligned}
-\frac{1}{2}\Big[\mathbf{S}_{21},\big[\mathbf{S}_{21},\mathbf{H}_{20}\big]_{\mathrm{V}}\Big]_{\mathrm{V}} = &\sum_{v_0v_1v_2v_3}\sum_{r_0r_1}\frac{-i}{2}\mathrm{S}_{21,0}\left(v_0,v_1,r_0\right)\Big(\mathrm{S}_{21,0}\left(v_2,v_3,r_1\right)\mathrm{H}_{20}\left(v_3\right)-\mathrm{S}_{21,1}\left(v_2,v_3,r_1\right)\mathrm{H}_{20}\left(v_2\right)\Big)\times\\
&\times\Big[\mathbf{q}_{v_0}\mathbf{q}_{v_1},\mathbf{q}_{v_2}\mathbf{p}_{v_3}\Big]\Big(\mathbf{J}_{r_0}\mathbf{J}_{r_1}+\mathbf{J}_{r_1}\mathbf{J}_{r_0}\Big)\\
+\sum_{v_0v_1v_2v_3}\sum_{r_0r_1}&\frac{-i}{2}\mathrm{S}_{21,0}\left(v_0,v_1,r_0\right)\Big(\mathrm{S}_{21,0}\left(v_2,v_3,r_1\right)\mathrm{H}_{20}\left(v_2\right)-\mathrm{S}_{21,1}\left(v_2,v_3,r_1\right)\mathrm{H}_{20}\left(v_3\right)\Big)\times\\
&\times\Big[\mathbf{q}_{v_0}\mathbf{q}_{v_1},\mathbf{p}_{v_2}\mathbf{q}_{v_3}\Big]\Big(\mathbf{J}_{r_0}\mathbf{J}_{r_1}+\mathbf{J}_{r_1}\mathbf{J}_{r_0}\Big)\\
+\sum_{v_0v_1v_2v_3}\sum_{r_0r_1}&\frac{-i}{2}\mathrm{S}_{21,1}\left(v_0,v_1,r_0\right)\Big(\mathrm{S}_{21,0}\left(v_2,v_3,r_1\right)\mathrm{H}_{20}\left(v_3\right)-\mathrm{S}_{21,1}\left(v_2,v_3,r_1\right)\mathrm{H}_{20}\left(v_2\right)\Big)\times\\
&\times\Big[\mathbf{p}_{v_0}\mathbf{p}_{v_1},\mathbf{q}_{v_2}\mathbf{p}_{v_3}\Big]\Big(\mathbf{J}_{r_0}\mathbf{J}_{r_1}+\mathbf{J}_{r_1}\mathbf{J}_{r_0}\Big)\\
+\sum_{v_0v_1v_2v_3}\sum_{r_0r_1}&\frac{-i}{2}\mathrm{S}_{21,1}\left(v_0,v_1,r_0\right)\Big(\mathrm{S}_{21,0}\left(v_2,v_3,r_1\right)\mathrm{H}_{20}\left(v_2\right)-\mathrm{S}_{21,1}\left(v_2,v_3,r_1\right)\mathrm{H}_{20}\left(v_3\right)\Big)\times\\
&\times\Big[\mathbf{p}_{v_0}\mathbf{p}_{v_1},\mathbf{p}_{v_2}\mathbf{q}_{v_3}\Big]\Big(\mathbf{J}_{r_0}\mathbf{J}_{r_1}+\mathbf{J}_{r_1}\mathbf{J}_{r_0}\Big)
\end{aligned}
\tag{7.S48}
$$

Next, the pure vibrational commutator is evaluated to give Eq. (7.S49).

$$
\begin{aligned}
-\frac{1}{2}\Big[\mathbf{S}_{21},\big[\mathbf{S}_{21},\mathbf{H}_{20}\big]_{\mathrm{V}}\Big]_{\mathrm{V}} = &\sum_{v_0v_1v_2v_3}\sum_{r_0r_1}\frac{-i}{2}\mathrm{S}_{21,0}\left(v_0,v_1,r_0\right)\Big(\mathrm{S}_{21,0}\left(v_2,v_3,r_1\right)\mathrm{H}_{20}\left(v_3\right)-\mathrm{S}_{21,1}\left(v_2,v_3,r_1\right)\mathrm{H}_{20}\left(v_2\right)\Big)\times \\
&\times\Big(i\delta_{v_1v_3}\mathbf{q}_{v_0}\mathbf{q}_{v_2}+i\delta_{v_0v_3}\mathbf{q}_{v_2}\mathbf{q}_{v_1}\Big)\Big(\mathbf{J}_{r_0}\mathbf{J}_{r_1}+\mathbf{J}_{r_1}\mathbf{J}_{r_0}\Big) \\
+\sum_{v_0v_1v_2v_3}\sum_{r_0r_1}&\frac{-i}{2}\mathrm{S}_{21,0}\left(v_0,v_1,r_0\right)\Big(\mathrm{S}_{21,0}\left(v_2,v_3,r_1\right)\mathrm{H}_{20}\left(v_2\right)-\mathrm{S}_{21,1}\left(v_2,v_3,r_1\right)\mathrm{H}_{20}\left(v_3\right)\Big)\times \\
&\times\Big(i\delta_{v_1v_2}\mathbf{q}_{v_0}\mathbf{q}_{v_3}+i\delta_{v_0v_2}\mathbf{q}_{v_3}\mathbf{q}_{v_1}\Big)\Big(\mathbf{J}_{r_0}\mathbf{J}_{r_1}+\mathbf{J}_{r_1}\mathbf{J}_{r_0}\Big) \\
+\sum_{v_0v_1v_2v_3}\sum_{r_0r_1}&\frac{-i}{2}\mathrm{S}_{21,1}\left(v_0,v_1,r_0\right)\Big(\mathrm{S}_{21,0}\left(v_2,v_3,r_1\right)\mathrm{H}_{20}\left(v_3\right)-\mathrm{S}_{21,1}\left(v_2,v_3,r_1\right)\mathrm{H}_{20}\left(v_2\right)\Big)\times \\
&\times\Big(-i\delta_{v_1v_2}\mathbf{p}_{v_0}\mathbf{p}_{v_3}-i\delta_{v_0v_2}\mathbf{p}_{v_3}\mathbf{p}_{v_1}\Big)\Big(\mathbf{J}_{r_0}\mathbf{J}_{r_1}+\mathbf{J}_{r_1}\mathbf{J}_{r_0}\Big) \\
+\sum_{v_0v_1v_2v_3}\sum_{r_0r_1}&\frac{-i}{2}\mathrm{S}_{21,1}\left(v_0,v_1,r_0\right)\Big(\mathrm{S}_{21,0}\left(v_2,v_3,r_1\right)\mathrm{H}_{20}\left(v_2\right)-\mathrm{S}_{21,1}\left(v_2,v_3,r_1\right)\mathrm{H}_{20}\left(v_3\right)\Big)\times \\
&\times\Big(-i\delta_{v_1v_3}\mathbf{p}_{v_0}\mathbf{p}_{v_2}-i\delta_{v_0v_3}\mathbf{p}_{v_2}\mathbf{p}_{v_1}\Big)\Big(\mathbf{J}_{r_0}\mathbf{J}_{r_1}+\mathbf{J}_{r_1}\mathbf{J}_{r_0}\Big)
\end{aligned}
\tag{7.S49}
$$

The summations are expanded (Eq. (7.S50)), the Kronecker deltas are evaluated (Eq. (7.S51)), and the results consolidated (Eq. (7.S53)), after repeating the same process with the rotational operators.

(7.S50)

(7.S51)

$$
\begin{aligned}
-\frac{1}{2}\Big[\mathbf{S}_{21},\big[\mathbf{S}_{21},\mathbf{H}_{20}\big]_{\mathrm{V}}\Big]_{\mathrm{V}} = \sum_{v_0v_1v_2}\sum_{r_0r_1}\frac{1}{2}\Big(&-\mathrm{S}_{21,0}\left(v_2,v_1,r_0\right)\Big(\mathrm{S}_{21,1}\left(v_0,v_2,r_1\right)+\mathrm{S}_{21,1}\left(v_2,v_0,r_1\right)\Big)\mathrm{H}_{20}\left(v_0\right)\\
&-\mathrm{S}_{21,0}\left(v_0,v_2,r_0\right)\Big(\mathrm{S}_{21,1}\left(v_1,v_2,r_1\right)+\mathrm{S}_{21,1}\left(v_2,v_1,r_1\right)\Big)\mathrm{H}_{20}\left(v_1\right)\\
&+\mathrm{S}_{21,0}\left(v_0,v_2,r_0\right)\Big(\mathrm{S}_{21,0}\left(v_1,v_2,r_1\right)+\mathrm{S}_{21,0}\left(v_2,v_1,r_1\right)\Big)\mathrm{H}_{20}\left(v_2\right)\\
&+\mathrm{S}_{21,0}\left(v_2,v_1,r_0\right)\Big(\mathrm{S}_{21,0}\left(v_0,v_2,r_1\right)+\mathrm{S}_{21,0}\left(v_2,v_0,r_1\right)\Big)\mathrm{H}_{20}\left(v_2\right)\Big)\mathbf{q}_{v_0}\mathbf{q}_{v_1}\left(\mathbf{J}_{r_0}\mathbf{J}_{r_1}+\mathbf{J}_{r_1}\mathbf{J}_{r_0}\right)\\
+\sum_{v_0v_1v_2}\sum_{r_0r_1}\frac{1}{2}\Big(&-\mathrm{S}_{21,1}\left(v_2,v_1,r_0\right)\Big(\mathrm{S}_{21,0}\left(v_0,v_2,r_1\right)+\mathrm{S}_{21,0}\left(v_2,v_0,r_1\right)\Big)\mathrm{H}_{20}\left(v_0\right)\\
&-\mathrm{S}_{21,1}\left(v_0,v_2,r_0\right)\Big(\mathrm{S}_{21,0}\left(v_1,v_2,r_1\right)+\mathrm{S}_{21,0}\left(v_2,v_1,r_1\right)\Big)\mathrm{H}_{20}\left(v_1\right)\\
&+\mathrm{S}_{21,1}\left(v_0,v_2,r_0\right)\Big(\mathrm{S}_{21,1}\left(v_1,v_2,r_1\right)+\mathrm{S}_{21,1}\left(v_2,v_1,r_1\right)\Big)\mathrm{H}_{20}\left(v_2\right)\\
&+\mathrm{S}_{21,1}\left(v_2,v_1,r_0\right)\Big(\mathrm{S}_{21,1}\left(v_0,v_2,r_1\right)+\mathrm{S}_{21,1}\left(v_2,v_0,r_1\right)\Big)\mathrm{H}_{20}\left(v_2\right)\Big)\mathbf{p}_{v_0}\mathbf{p}_{v_1}\left(\mathbf{J}_{r_0}\mathbf{J}_{r_1}+\mathbf{J}_{r_1}\mathbf{J}_{r_0}\right)
\end{aligned}
\tag{7.S52}
$$

(7.S53)

DEFINING THE TRANSFORM FUNCTION

Using the abbreviated definitions provided in Eq. (7.73) and Eq. (7.78)–(7.85) we can now write the defining part for the transform function in Eq. (7.S54).

(7.S54)

For application of the formula for defining the transform function, it is helpful to define separate coefficients so that only the vibrational indices connected with vibrational operators, and similarly the rotational indices with the rotational operators, are being summed over

explicitly. That is, we define coefficients in Eq. (7.S55) so as to write Eq. (7.S56), which simplifies the process of finding the definition of the transform function.

$$\begin{aligned}
\mathrm{E}_{22,0}\left(v_0,v_1,r_0,r_1\right) &= \sum_{v_2}\sum_{r_2}\Bigg(\frac{1}{3N}\mathrm{H}_{22}\left(v_0,v_1,r_0,r_1\right)+\frac{1}{3}\mathrm{A}_{22}\left(v_0,v_1,v_2,r_0,r_1\right)+\frac{1}{3}\mathrm{B}_{22,0}\left(v_0,v_1,v_2,r_0,r_1\right) \\
&\qquad +\frac{1}{N}\mathrm{C}_{22,0}\left(v_0,v_1,r_0,r_1,r_2\right)+\frac{1}{3}\mathrm{D}_{22,0}\left(v_0,v_1,v_2,r_0,r_1\right)\Bigg) \qquad (7.S55) \\
\mathrm{E}_{22,1}\left(v_0,v_1,r_0,r_1\right) &= \sum_{v_2}\sum_{r_2}\Bigg(\frac{1}{3}\mathrm{B}_{22,1}\left(v_0,v_1,v_2,r_0,r_1\right)+\frac{1}{N}\mathrm{C}_{22,1}\left(v_0,v_1,r_0,r_1,r_2\right)+\frac{1}{3}\mathrm{D}_{22,1}\left(v_0,v_1,v_2,r_0,r_1\right)\Bigg)
\end{aligned}$$

$$\begin{aligned}
&\mathbf{H}_{22}+i\left[\mathbf{S}_{12},\mathbf{H}_{30}\right]_{\mathrm{V}}+i\left[\mathbf{S}_{21},\mathbf{H}_{21}\right]_{\mathrm{V}}+i\left[\mathbf{S}_{21},\mathbf{H}_{02}\right]_{\mathrm{R}}-\frac{1}{2}\Big[\mathbf{S}_{21},\left[\mathbf{S}_{21},\mathbf{H}_{20}\right]_{\mathrm{V}}\Big]_{\mathrm{V}} \\
&\quad=\sum_{v_0v_1}\sum_{r_0r_1}\mathrm{E}_{22,0}\left(v_0,v_1,r_0,r_1\right)\mathbf{q}_{v_0}\mathbf{q}_{v_1}\mathbf{J}_{r_0}\mathbf{J}_{r_1}+\sum_{v_0v_1}\sum_{r_0r_1}\mathrm{E}_{22,1}\left(v_0,v_1,r_0,r_1\right)\mathbf{p}_{v_0}\mathbf{p}_{v_1}\mathbf{J}_{r_0}\mathbf{J}_{r_1}
\end{aligned} \qquad (7.S56)$$

We now endeavor to write the defining part in terms of the ladder operators $\mathcal{L}^{\pm}$.

$$
\begin{aligned}
&\mathbf{H}_{22}+i\left[\mathbf{S}_{12},\mathbf{H}_{30}\right]_{\mathrm{V}}+i\left[\mathbf{S}_{21},\mathbf{H}_{21}\right]_{\mathrm{V}}+i\left[\mathbf{S}_{21},\mathbf{H}_{02}\right]_{\mathrm{R}}-\frac{1}{2}\left[\mathbf{S}_{21},\left[\mathbf{S}_{21},\mathbf{H}_{20}\right]_{\mathrm{V}}\right]_{\mathrm{V}}\\
&\quad=\sum_{v_0v_1}\sum_{r_0r_1}\mathrm{E}_{22,0}\left(v_0,v_1,r_0,r_1\right)\left(\frac{1}{2}\sum_{\sigma_{v0}}\mathcal{L}_{v_0}^{\sigma_{v0}}\right)\left(\frac{1}{2}\sum_{\sigma_{v1}}\mathcal{L}_{v_1}^{\sigma_{v1}}\right)\mathbf{J}_{r_0}\mathbf{J}_{r_1}\\
&\qquad+\sum_{v_0v_1}\sum_{r_0r_1}\mathrm{E}_{22,1}\left(v_0,v_1,r_0,r_1\right)\left(\frac{1}{2}i\sum_{\sigma_{v0}}\sigma_{v_0}\mathcal{L}_{v_0}^{\sigma_{v0}}\right)\left(\frac{1}{2}i\sum_{\sigma_{v1}}\sigma_{v_1}\mathcal{L}_{v_1}^{\sigma_{v1}}\right)\mathbf{J}_{r_0}\mathbf{J}_{r_1}\\
&\quad=\sum_{v_0v_1}\sum_{r_0r_1}\sum_{\sigma_{v_0}\sigma_{v_1}}\frac{1}{4}\mathrm{E}_{22,0}\left(v_0,v_1,r_0,r_1\right)\mathcal{L}_{v_0}^{\sigma_{v0}}\mathcal{L}_{v_1}^{\sigma_{v1}}\mathbf{J}_{r_0}\mathbf{J}_{r_1}\\
&\qquad+\sum_{v_0v_1}\sum_{r_0r_1}\sum_{\sigma_{v_0}\sigma_{v_1}}\frac{-1}{4}\sigma_{v_0}\sigma_{v_1}\mathrm{E}_{22,1}\left(v_0,v_1,r_0,r_1\right)\mathcal{L}_{v_0}^{\sigma_{v0}}\mathcal{L}_{v_1}^{\sigma_{v1}}\mathbf{J}_{r_0}\mathbf{J}_{r_1}\\
&\quad=\sum_{v_0v_1}\sum_{r_0r_1}\sum_{\sigma_{v_0}\sigma_{v_1}}\left(\frac{1}{4}\left(\mathrm{E}_{22,0}\left(v_0,v_1,r_0,r_1\right)-\sigma_{v_0}\sigma_{v_1}\mathrm{E}_{22,1}\left(v_0,v_1,r_0,r_1\right)\right)\right)\mathcal{L}_{v_0}^{\sigma_{v0}}\mathcal{L}_{v_1}^{\sigma_{v1}}\mathbf{J}_{r_0}\mathbf{J}_{r_1}
\end{aligned}
\tag{7.S57}
$$

We can now define the transform function.

$$
\begin{aligned}
\mathbf{S}_{22}=\sum_{v_0v_1}\sum_{r_0r_1}\sum_{\sigma_{v_0}\sigma_{v_1}}\frac{-i}{2}\mathrm{D}\left(\sigma_{v_0},v_0;\sigma_{v_1},v_1\right)&\left(\left(\frac{1}{4}\left(\mathrm{E}_{22,0}\left(v_0,v_1,r_0,r_1\right)-\sigma_{v_0}\sigma_{v_1}\mathrm{E}_{22,1}\left(v_0,v_1,r_0,r_1\right)\right)\right)\right.\\
&\left.+\left(\frac{1}{4}\left(\mathrm{E}_{22,0}\left(v_1,v_0,r_0,r_1\right)-\sigma_{v_0}\sigma_{v_1}\mathrm{E}_{22,1}\left(v_1,v_0,r_0,r_1\right)\right)\right)\right)\mathcal{L}_{v_0}^{\sigma_{v0}}\mathcal{L}_{v_1}^{\sigma_{v1}}\mathbf{J}_{r_0}\mathbf{J}_{r_1}
\end{aligned}
\tag{7.S58}
$$

$$
\begin{aligned}
\mathbf{S}_{22} = \sum_{v_0 v_1} \sum_{r_0 r_1} \sum_{\sigma_{v_0} \sigma_{v_1}} \frac{-i}{2} \mathrm{D}\left(\sigma_{v_0}, v_0; \sigma_{v_1}, v_1\right) \Bigg(\Bigg(\frac{1}{4} \Big(\mathrm{E}_{22,0}\left(v_0, v_1, r_0, r_1\right) - \sigma_{v_0} \sigma_{v_1} \mathrm{E}_{22,1}\left(v_0, v_1, r_0, r_1\right) \Big) \Bigg) \\
+ \Bigg(\frac{1}{4} \Big(\mathrm{E}_{22,0}\left(v_1, v_0, r_0, r_1\right) - \sigma_{v_0} \sigma_{v_1} \mathrm{E}_{22,1}\left(v_1, v_0, r_0, r_1\right) \Big) \Bigg) \Bigg) \left(\mathbf{q}_{v_0} - i \sigma_{v_0} \mathbf{p}_{v_0}\right) \left(\mathbf{q}_{v_1} - i \sigma_{v_1} \mathbf{p}_{v_1}\right) \mathbf{J}_{r_0} \mathbf{J}_{r_1} \\
= \sum_{v_0 v_1} \sum_{r_0 r_1} \frac{1}{4} \Big(\Big(-\mathrm{D}\left(1, v_0; 1, v_1\right) + \mathrm{D}\left(1, v_0; -1, v_1\right) \Big) \Big(\mathrm{E}_{22,0}\left(v_0, v_1, r_0, r_1\right) + \mathrm{E}_{22,0}\left(v_1, v_0, r_0, r_1\right) \Big) \\
+ \Big(\mathrm{D}\left(1, v_0; 1, v_1\right) + \mathrm{D}\left(1, v_0; -1, v_1\right) \Big) \Big(\mathrm{E}_{22,1}\left(v_0, v_1, r_0, r_1\right) + \mathrm{E}_{22,1}\left(v_1, v_0, r_0, r_1\right) \Big) \Big) \mathbf{q}_{v_0} \mathbf{p}_{v_1} \mathbf{J}_{r_0} \mathbf{J}_{r_1} \\
+ \sum_{v_0 v_1} \sum_{r_0 r_1} \frac{-1}{4} \Big(\Big(\mathrm{D}\left(1, v_0; 1, v_1\right) + \mathrm{D}\left(1, v_0; -1, v_1\right) \Big) \Big(\mathrm{E}_{22,0}\left(v_0, v_1, r_0, r_1\right) + \mathrm{E}_{22,0}\left(v_1, v_0, r_0, r_1\right) \Big) \\
+ \Big(-\mathrm{D}\left(1, v_0; 1, v_1\right) + \mathrm{D}\left(1, v_0; -1, v_1\right) \Big) \Big(\mathrm{E}_{22,1}\left(v_0, v_1, r_0, r_1\right) + \mathrm{E}_{22,1}\left(v_1, v_0, r_0, r_1\right) \Big) \Big) \mathbf{p}_{v_0} \mathbf{q}_{v_1} \mathbf{J}_{r_0} \mathbf{J}_{r_1}
\end{aligned}
\tag{7.S59}
$$

Evaluation of $i[\boldsymbol{S}_{22}, \boldsymbol{H}_{20}]_V$

Substituting in the definitions from Eq. (7.86) and Eq. (7.68) yields Eq. (7.S60), where we have ensured that each summation index is distinct.

$$
\begin{aligned}
i\left[\mathbf{S}_{22},\mathbf{H}_{20}\right]_{\mathrm{V}} &= i\left[\sum_{v_0v_1}\sum_{r_0r_1}\mathrm{S}_{22,0}\left(v_0,v_1,r_0,r_1\right)\mathbf{q}_{v_0}\mathbf{p}_{v_1}\mathbf{J}_{r_0}\mathbf{J}_{r_1}+\sum_{v_0v_1}\sum_{r_0r_1}\mathrm{S}_{22,1}\left(v_0,v_1,r_0,r_1\right)\mathbf{p}_{v_0}\mathbf{q}_{v_1}\mathbf{J}_{r_0}\mathbf{J}_{r_1},\sum_{v_0}\mathrm{H}_{20}\left(v_0\right)\mathbf{q}_{v_0}^2+\sum_{v_0}\mathrm{H}_{20}\left(v_0\right)\mathbf{p}_{v_0}^2\right]_{\mathrm{V}} \\
&= i\sum_{v_0v_1v_2}\sum_{r_0r_1}\left[\mathrm{S}_{22,0}\left(v_0,v_1,r_0,r_1\right)\mathbf{q}_{v_0}\mathbf{p}_{v_1}\mathbf{J}_{r_0}\mathbf{J}_{r_1},\mathrm{H}_{20}\left(v_2\right)\mathbf{q}_{v_2}^2\right]_{\mathrm{V}} \\
&\quad +i\sum_{v_0v_1v_2}\sum_{r_0r_1}\left[\mathrm{S}_{22,0}\left(v_0,v_1,r_0,r_1\right)\mathbf{q}_{v_0}\mathbf{p}_{v_1}\mathbf{J}_{r_0}\mathbf{J}_{r_1},\mathrm{H}_{20}\left(v_2\right)\mathbf{p}_{v_2}^2\right]_{\mathrm{V}} \\
&\quad +i\sum_{v_0v_1v_2}\sum_{r_0r_1}\left[\mathrm{S}_{22,1}\left(v_0,v_1,r_0,r_1\right)\mathbf{p}_{v_0}\mathbf{q}_{v_1}\mathbf{J}_{r_0}\mathbf{J}_{r_1},\mathrm{H}_{20}\left(v_2\right)\mathbf{q}_{v_2}^2\right]_{\mathrm{V}} \\
&\quad +i\sum_{v_0v_1v_2}\sum_{r_0r_1}\left[\mathrm{S}_{22,1}\left(v_0,v_1,r_0,r_1\right)\mathbf{p}_{v_0}\mathbf{q}_{v_1}\mathbf{J}_{r_0}\mathbf{J}_{r_1},\mathrm{H}_{20}\left(v_2\right)\mathbf{p}_{v_2}^2\right]_{\mathrm{V}}
\end{aligned}
\tag{7.S60}
$$

We then apply the definition of the vibrational commutator from Eq. (7.12) to obtain the pure vibrational commutators in Eq. (7.S61).

$$
\begin{aligned}
i\left[\mathbf{S}_{22},\mathbf{H}_{20}\right]_{\mathrm{V}} &= i\sum_{v_0v_1v_2}\sum_{r_0r_1}\mathrm{S}_{22,0}\left(v_0,v_1,r_0,r_1\right)\mathrm{H}_{20}\left(v_2\right)\left[\mathbf{q}_{v_0}\mathbf{p}_{v_1},\mathbf{q}_{v_2}^2\right]\mathbf{J}_{r_0}\mathbf{J}_{r_1} \\
&\quad +i\sum_{v_0v_1v_2}\sum_{r_0r_1}\mathrm{S}_{22,0}\left(v_0,v_1,r_0,r_1\right)\mathrm{H}_{20}\left(v_2\right)\left[\mathbf{q}_{v_0}\mathbf{p}_{v_1},\mathbf{p}_{v_2}^2\right]\mathbf{J}_{r_0}\mathbf{J}_{r_1} \\
&\quad +i\sum_{v_0v_1v_2}\sum_{r_0r_1}\mathrm{S}_{22,1}\left(v_0,v_1,r_0,r_1\right)\mathrm{H}_{20}\left(v_2\right)\left[\mathbf{p}_{v_0}\mathbf{q}_{v_1},\mathbf{q}_{v_2}^2\right]\mathbf{J}_{r_0}\mathbf{J}_{r_1} \\
&\quad +i\sum_{v_0v_1v_2}\sum_{r_0r_1}\mathrm{S}_{22,1}\left(v_0,v_1,r_0,r_1\right)\mathrm{H}_{20}\left(v_2\right)\left[\mathbf{p}_{v_0}\mathbf{q}_{v_1},\mathbf{p}_{v_2}^2\right]\mathbf{J}_{r_0}\mathbf{J}_{r_1}
\end{aligned}
\tag{7.S61}
$$

Next, the pure vibrational commutator is evaluated to give Eq. (7.S62).

$$
\begin{aligned}
i\left[\mathbf{S}_{22},\mathbf{H}_{20}\right]_{\mathrm{V}} = i\sum_{v_0v_1v_2}\sum_{r_0r_1}&\mathrm{S}_{22,0}\left(v_0,v_1,r_0,r_1\right)\mathrm{H}_{20}\left(v_2\right)\left(-2i\delta_{v_1v_2}\mathbf{q}_{v_0}\mathbf{q}_{v_2}\right)\mathbf{J}_{r_0}\mathbf{J}_{r_1}\\
+i\sum_{v_0v_1v_2}\sum_{r_0r_1}&\mathrm{S}_{22,0}\left(v_0,v_1,r_0,r_1\right)\mathrm{H}_{20}\left(v_2\right)\left(2i\delta_{v_0v_2}\mathbf{p}_{v_2}\mathbf{p}_{v_1}\right)\mathbf{J}_{r_0}\mathbf{J}_{r_1}\\
+i\sum_{v_0v_1v_2}\sum_{r_0r_1}&\mathrm{S}_{22,1}\left(v_0,v_1,r_0,r_1\right)\mathrm{H}_{20}\left(v_2\right)\left(-2i\delta_{v_0v_2}\mathbf{q}_{v_2}\mathbf{q}_{v_1}\right)\mathbf{J}_{r_0}\mathbf{J}_{r_1}\\
+i\sum_{v_0v_1v_2}\sum_{r_0r_1}&\mathrm{S}_{22,1}\left(v_0,v_1,r_0,r_1\right)\mathrm{H}_{20}\left(v_2\right)\left(2i\delta_{v_1v_2}\mathbf{p}_{v_0}\mathbf{p}_{v_2}\right)\mathbf{J}_{r_0}\mathbf{J}_{r_1}
\end{aligned}
\tag{7.S62}
$$

The summations are already expanded so now the Kronecker deltas are evaluated (Eq. (7.S63)), and the results consolidated (Eq. (7.S64)).

$$
\begin{aligned}
i\left[\mathbf{S}_{22},\mathbf{H}_{20}\right]_{\mathrm{V}} = \sum_{v_0v_1}\sum_{r_0r_1}&2\mathrm{S}_{22,0}\left(v_0,v_1,r_0,r_1\right)\mathrm{H}_{20}\left(v_1\right)\mathbf{q}_{v_0}\mathbf{q}_{v_1}\mathbf{J}_{r_0}\mathbf{J}_{r_1}\\
+\sum_{v_0v_1}\sum_{r_0r_1}&(-2)\mathrm{S}_{22,0}\left(v_0,v_1,r_0,r_1\right)\mathrm{H}_{20}\left(v_0\right)\mathbf{p}_{v_0}\mathbf{p}_{v_1}\mathbf{J}_{r_0}\mathbf{J}_{r_1}\\
+\sum_{v_0v_1}\sum_{r_0r_1}&2\mathrm{S}_{22,1}\left(v_0,v_1,r_0,r_1\right)\mathrm{H}_{20}\left(v_0\right)\mathbf{q}_{v_0}\mathbf{q}_{v_1}\mathbf{J}_{r_0}\mathbf{J}_{r_1}\\
+\sum_{v_0v_1v_{2,1}}\sum_{r_0r_1}&(-2)\mathrm{S}_{22,1}\left(v_0,v_1,r_0,r_1\right)\mathrm{H}_{20}\left(v_1\right)\mathbf{p}_{v_0}\mathbf{p}_{v_1}\mathbf{J}_{r_0}\mathbf{J}_{r_1}
\end{aligned}
\tag{7.S63}
$$

$$
\begin{aligned}
i\left[\mathbf{S}_{22},\mathbf{H}_{20}\right]_{\mathrm{V}} = \sum_{v_0v_1}\sum_{r_0r_1}&2\left(\mathrm{S}_{22,0}\left(v_0,v_1,r_0,r_1\right)\mathrm{H}_{20}\left(v_1\right)+\mathrm{S}_{22,1}\left(v_0,v_1,r_0,r_1\right)\mathrm{H}_{20}\left(v_0\right)\right)\mathbf{q}_{v_0}\mathbf{q}_{v_1}\mathbf{J}_{r_0}\mathbf{J}_{r_1}\\
+\sum_{v_0v_1}\sum_{r_0r_1}&(-2)\left(\mathrm{S}_{22,0}\left(v_0,v_1,r_0,r_1\right)\mathrm{H}_{20}\left(v_0\right)+\mathrm{S}_{22,1}\left(v_0,v_1,r_0,r_1\right)\mathrm{H}_{20}\left(v_1\right)\right)\mathbf{p}_{v_0}\mathbf{p}_{v_1}\mathbf{J}_{r_0}\mathbf{J}_{r_1}
\end{aligned}
\tag{7.S64}
$$

Obtaining the analytic expression

Applying the previously obtained evaluations of the commutators, we can write

$$\begin{aligned}\tilde{\mathbf{H}}_{22} &= \left(\mathbf{H}_{22} + i\left[\mathbf{S}_{12},\mathbf{H}_{30}\right]_{\mathrm{V}} + i\left[\mathbf{S}_{21},\mathbf{H}_{21}\right]_{\mathrm{V}} + i\left[\mathbf{S}_{21},\mathbf{H}_{02}\right]_{\mathrm{R}} - \frac{1}{2}\left[\mathbf{S}_{21},\left[\mathbf{S}_{21},\mathbf{H}_{20}\right]_{\mathrm{V}}\right]_{\mathrm{V}}\right) + \left(i\left[\mathbf{S}_{22},\mathbf{H}_{20}\right]_{\mathrm{V}}\right) \\ &= \left(\sum_{v_0 v_1}\sum_{r_0 r_1} \mathrm{E}_{22,0}\left(v_0,v_1,r_0,r_1\right)\mathbf{q}_{v_0}\mathbf{q}_{v_1}\mathbf{J}_{r_0}\mathbf{J}_{r_1} + \sum_{v_0 v_1}\sum_{r_0 r_1} \mathrm{E}_{22,1}\left(v_0,v_1,r_0,r_1\right)\mathbf{p}_{v_0}\mathbf{p}_{v_1}\mathbf{J}_{r_0}\mathbf{J}_{r_1}\right) \\ &\qquad + \left(\sum_{v_0 v_1}\sum_{r_0 r_1} \mathrm{F}_{22,0}\left(v_0,v_1,r_0,r_1\right)\mathbf{q}_{v_0}\mathbf{q}_{v_1}\mathbf{J}_{r_0}\mathbf{J}_{r_1} + \sum_{v_0 v_1}\sum_{r_0 r_1} \mathrm{F}_{22,1}\left(v_0,v_1,r_0,r_1\right)\mathbf{p}_{v_0}\mathbf{p}_{v_1}\mathbf{J}_{r_0}\mathbf{J}_{r_1}\right) \\ &= \sum_{v_0 v_1}\sum_{r_0 r_1}\left(\mathrm{E}_{22,0}\left(v_0,v_1,r_0,r_1\right) + \mathrm{F}_{22,0}\left(v_0,v_1,r_0,r_1\right)\right)\mathbf{q}_{v_0}\mathbf{q}_{v_1}\mathbf{J}_{r_0}\mathbf{J}_{r_1} \\ &\qquad + \sum_{v_0 v_1}\sum_{r_0 r_1}\left(\mathrm{E}_{22,1}\left(v_0,v_1,r_0,r_1\right) + \mathrm{F}_{22,1}\left(v_0,v_1,r_0,r_1\right)\right)\mathbf{p}_{v_0}\mathbf{p}_{v_1}\mathbf{J}_{r_0}\mathbf{J}_{r_1}\end{aligned} \tag{7.S65}$$

IN TERMS OF MOLECULAR PROPERTIES

Applying the definitions of the coefficients for the terms of the original Hamiltonian from Eq. (7.S7)–(7.S12), we can rewrite the expression in terms of the molecular properties.

$$\mathrm{S}_{12}\left(v_0,r_0,r_1\right) = \mathrm{D}\left(1,v_0\right)\omega_{v_0}C_{v_0}^{r_0 r_1} \tag{7.S66}$$

$$\mathrm{S}_{21,0}\left(v_0,v_1,r_0\right) = \frac{1}{2}\mathrm{D}\left(1,v_0;1,v_1\right)\frac{\omega_{v_0}-\omega_{v_1}}{\sqrt{\omega_{v_0}\omega_{v_1}}}B_{r_0}\zeta_{v_0 v_1}^{r_0} + \frac{1}{2}\mathrm{D}\left(1,v_0;-1,v_1\right)\frac{\omega_{v_0}+\omega_{v_1}}{\sqrt{\omega_{v_0}\omega_{v_1}}}B_{r_0}\zeta_{v_0 v_1}^{r_0} \tag{7.S67}$$

$$\mathrm{S}_{21,1}\left(v_0,v_1,r_0\right)=-\frac{1}{2}\mathrm{D}\left(1,v_0;1,v_1\right)\frac{\omega_{v_0}-\omega_{v_1}}{\sqrt{\omega_{v_0}\omega_{v_1}}}B_{r_0}\zeta^{r_0}_{v_0v_1}+\frac{1}{2}\mathrm{D}\left(1,v_0;-1,v_1\right)\frac{\omega_{v_0}+\omega_{v_1}}{\sqrt{\omega_{v_0}\omega_{v_1}}}B_{r_0}\zeta^{r_0}_{v_0v_1} \quad (7.S68)$$

$$\mathrm{A}_{22}\left(v_0,v_1,v_2,r_0,r_1\right)=\frac{1}{2}\mathrm{D}\left(1,v_2\right)\omega_{v_2}C^{r_0r_1}_{v_2}\,\mathrm{k}_{v_0v_1v_2} \quad (7.S69)$$

$$\begin{aligned}\mathrm{B}_{22,0}\left(v_0,v_1,v_2,r_0,r_1\right)=&\frac{1}{2}\mathrm{D}\left(1,v_0;1,v_2\right)\frac{\omega_{v_0}-\omega_{v_2}}{\sqrt{\omega_{v_0}\omega_{v_1}}}B_{r_0}B_{r_1}\left(\zeta^{r_0}_{v_0v_2}\zeta^{r_1}_{v_1v_2}+\zeta^{r_1}_{v_0v_2}\zeta^{r_0}_{v_1v_2}\right)\\&+\frac{1}{2}\mathrm{D}\left(1,v_0;-1,v_2\right)\frac{\omega_{v_0}+\omega_{v_2}}{\sqrt{\omega_{v_0}\omega_{v_1}}}B_{r_0}B_{r_1}\left(\zeta^{r_0}_{v_0v_2}\zeta^{r_1}_{v_1v_2}+\zeta^{r_1}_{v_0v_2}\zeta^{r_0}_{v_1v_2}\right)\\&+\frac{1}{2}\mathrm{D}\left(1,v_1;1,v_2\right)\frac{\omega_{v_1}-\omega_{v_2}}{\sqrt{\omega_{v_0}\omega_{v_1}}}B_{r_0}B_{r_1}\left(\zeta^{r_0}_{v_0v_2}\zeta^{r_1}_{v_1v_2}+\zeta^{r_1}_{v_0v_2}\zeta^{r_0}_{v_1v_2}\right)\\&+\frac{1}{2}\mathrm{D}\left(1,v_1;-1,v_2\right)\frac{\omega_{v_1}+\omega_{v_2}}{\sqrt{\omega_{v_0}\omega_{v_1}}}B_{r_0}B_{r_1}\left(\zeta^{r_0}_{v_0v_2}\zeta^{r_1}_{v_1v_2}+\zeta^{r_1}_{v_0v_2}\zeta^{r_0}_{v_1v_2}\right)\end{aligned} \quad (7.S70)$$

$$\begin{aligned}\mathrm{B}_{22,1}\left(v_0,v_1,v_2,r_0,r_1\right)=&-\mathrm{D}\left(1,v_0;1,v_2\right)\frac{\omega_{v_0}-\omega_{v_2}}{\sqrt{\omega_{v_0}\omega_{v_2}}}\frac{\sqrt{\omega_{v_1}}}{\sqrt{\omega_{v_2}}}B_{r_0}B_{r_1}\left(\zeta^{r_0}_{v_0v_2}\zeta^{r_1}_{v_1v_2}+\zeta^{r_1}_{v_0v_2}\zeta^{r_0}_{v_1v_2}\right)\\&+\mathrm{D}\left(1,v_0;-1,v_2\right)\frac{\omega_{v_0}+\omega_{v_2}}{\sqrt{\omega_{v_0}\omega_{v_2}}}\frac{\sqrt{\omega_{v_1}}}{\sqrt{\omega_{v_2}}}B_{r_0}B_{r_1}\left(\zeta^{r_0}_{v_0v_2}\zeta^{r_1}_{v_1v_2}+\zeta^{r_1}_{v_0v_2}\zeta^{r_0}_{v_1v_2}\right)\end{aligned} \quad (7.S71)$$

$$\mathrm{C}_{22,0}\left(v_0,v_1,r_0,r_1,r_2\right)=\frac{1}{2}\mathrm{D}\left(1,v_0;1,v_1\right)\epsilon_{r_0r_1r_2}\frac{\omega_{v_0}-\omega_{v_1}}{\sqrt{\omega_{v_0}\omega_{v_1}}}\left(B_{r_0}-B_{r_1}\right)B_{r_2}\zeta^{r_2}_{v_0v_1}+\frac{1}{2}\mathrm{D}\left(1,v_0;-1,v_1\right)\epsilon_{r_0r_1r_2}\frac{\omega_{v_0}+\omega_{v_1}}{\sqrt{\omega_{v_0}\omega_{v_1}}}\left(B_{r_0}-B_{r_1}\right)B_{r_2}\zeta^{r_2}_{v_0v_1} \quad (7.S72)$$

$$\mathrm{C}_{22,1}\left(v_0,v_1,r_0,r_1,r_2\right)=-\frac{1}{2}\mathrm{D}\left(1,v_0;1,v_1\right)\epsilon_{r_0r_1r_2}\frac{\omega_{v_0}-\omega_{v_1}}{\sqrt{\omega_{v_0}\omega_{v_1}}}\left(B_{r_0}-B_{r_1}\right)B_{r_2}\zeta^{r_2}_{v_0v_1}+\frac{1}{2}\mathrm{D}\left(1,v_0;-1,v_1\right)\epsilon_{r_0r_1r_2}\frac{\omega_{v_0}+\omega_{v_1}}{\sqrt{\omega_{v_0}\omega_{v_1}}}\left(B_{r_0}-B_{r_1}\right)B_{r_2}\zeta^{r_2}_{v_0v_1} \quad (7.S73)$$

$$\begin{aligned}\mathrm{D}_{22,0}\left(v_0,v_1,v_2,r_0,r_1\right)=&\frac{1}{8}\mathrm{D}\left(1,v_0;1,v_2\right)\mathrm{D}\left(1,v_1;1,v_2\right)\frac{\left(\omega_{v_0}+\omega_{v_1}+2\omega_{v_2}\right)\left(\omega_{v_0}-\omega_{v_2}\right)\left(\omega_{v_1}-\omega_{v_2}\right)}{\sqrt{\omega_{v_0}\omega_{v_1}}\omega_{v_2}}\left(\zeta^{r_0}_{v_0v_2}\zeta^{r_1}_{v_1v_2}+\zeta^{r_1}_{v_0v_2}\zeta^{r_0}_{v_1v_2}\right)B_{r_0}B_{r_1}\\&+\frac{1}{8}\mathrm{D}\left(1,v_0;1,v_2\right)\mathrm{D}\left(1,v_1;-1,v_2\right)\frac{\left(\omega_{v_0}-\omega_{v_1}+2\omega_{v_2}\right)\left(\omega_{v_0}-\omega_{v_2}\right)\left(\omega_{v_1}+\omega_{v_2}\right)}{\sqrt{\omega_{v_0}\omega_{v_1}}\omega_{v_2}}\left(\zeta^{r_0}_{v_0v_2}\zeta^{r_1}_{v_1v_2}+\zeta^{r_1}_{v_0v_2}\zeta^{r_0}_{v_1v_2}\right)B_{r_0}B_{r_1}\\&+\frac{1}{8}\mathrm{D}\left(1,v_0;-1,v_2\right)\mathrm{D}\left(1,v_1;1,v_2\right)\frac{\left(-\omega_{v_0}+\omega_{v_1}+2\omega_{v_2}\right)\left(\omega_{v_0}+\omega_{v_2}\right)\left(\omega_{v_1}-\omega_{v_2}\right)}{\sqrt{\omega_{v_0}\omega_{v_1}}\omega_{v_2}}\left(\zeta^{r_0}_{v_0v_2}\zeta^{r_1}_{v_1v_2}+\zeta^{r_1}_{v_0v_2}\zeta^{r_0}_{v_1v_2}\right)B_{r_0}B_{r_1}\\&+\frac{1}{8}\mathrm{D}\left(1,v_0;-1,v_2\right)\mathrm{D}\left(1,v_1;-1,v_2\right)\frac{\left(-\omega_{v_0}-\omega_{v_1}+2\omega_{v_2}\right)\left(\omega_{v_0}+\omega_{v_2}\right)\left(\omega_{v_1}+\omega_{v_2}\right)}{\sqrt{\omega_{v_0}\omega_{v_1}}\omega_{v_2}}\left(\zeta^{r_0}_{v_0v_2}\zeta^{r_1}_{v_1v_2}+\zeta^{r_1}_{v_0v_2}\zeta^{r_0}_{v_1v_2}\right)B_{r_0}B_{r_1}\end{aligned} \quad (7.S74)$$

$$
\begin{aligned}
\mathrm{D}_{22,1}\left(v_0,v_1,v_2,r_0,r_1\right) = {} & \frac{1}{8}\mathrm{D}\left(1,v_0;1,v_2\right)\mathrm{D}\left(1,v_1;1,v_2\right)\frac{\left(\omega_{v_0}+\omega_{v_1}+2\omega_{v_2}\right)\left(\omega_{v_0}-\omega_{v_2}\right)\left(\omega_{v_1}-\omega_{v_2}\right)}{\sqrt{\omega_{v_0}\omega_{v_1}}\,\omega_{v_2}}\left(\zeta^{r_0}_{v_0v_2}\zeta^{r_1}_{v_1v_2}+\zeta^{r_0}_{v_1v_2}\zeta^{r_1}_{v_0v_2}\right)B_{r_0}B_{r_1} \\
& -\frac{1}{8}\mathrm{D}\left(1,v_0;1,v_2\right)\mathrm{D}\left(1,v_1;-1,v_2\right)\frac{\left(\omega_{v_0}-\omega_{v_1}+2\omega_{v_2}\right)\left(\omega_{v_0}-\omega_{v_2}\right)\left(\omega_{v_1}+\omega_{v_2}\right)}{\sqrt{\omega_{v_0}\omega_{v_1}}\,\omega_{v_2}}\left(\zeta^{r_0}_{v_0v_2}\zeta^{r_1}_{v_1v_2}+\zeta^{r_1}_{v_0v_2}\zeta^{r_0}_{v_1v_2}\right)B_{r_0}B_{r_1} \\
& -\frac{1}{8}\mathrm{D}\left(1,v_0;-1,v_2\right)\mathrm{D}\left(1,v_1;1,v_2\right)\frac{\left(-\omega_{v_0}+\omega_{v_1}+2\omega_{v_2}\right)\left(\omega_{v_0}+\omega_{v_2}\right)\left(\omega_{v_1}-\omega_{v_2}\right)}{\sqrt{\omega_{v_0}\omega_{v_1}}\,\omega_{v_2}}\left(\zeta^{r_0}_{v_0v_2}\zeta^{r_1}_{v_1v_2}+\zeta^{r_1}_{v_0v_2}\zeta^{r_0}_{v_1v_2}\right)B_{r_0}B_{r_1} \\
& +\frac{1}{8}\mathrm{D}\left(1,v_0;-1,v_2\right)\mathrm{D}\left(1,v_1;-1,v_2\right)\frac{\left(-\omega_{v_0}-\omega_{v_1}+2\omega_{v_2}\right)\left(\omega_{v_0}+\omega_{v_2}\right)\left(\omega_{v_1}+\omega_{v_2}\right)}{\sqrt{\omega_{v_0}\omega_{v_1}}\,\omega_{v_2}}\left(\zeta^{r_0}_{v_0v_2}\zeta^{r_1}_{v_1v_2}+\zeta^{r_1}_{v_0v_2}\zeta^{r_0}_{v_1v_2}\right)B_{r_0}B_{r_1}
\end{aligned}
\tag{7.S75}
$$

(7.S76)

(7.S77)

(7.S78)

(7.S79)

(7.S80)

(7.S81)

$$\tilde{\mathrm{H}}_{22,0}\left(v_0,v_1,r_0,r_1\right)=+\sum_{v_2}\sum_{r_2}\left(\left(\tilde{\mathrm{H}}_{22,0\mathrm{a}}\left(v_0,v_1,v_2,r_0,r_1,r_2\right)-\frac{1}{24}\tilde{\mathrm{H}}_{22,0\mathrm{b}}\left(v_0,v_1,v_2,r_0,r_1,r_2\right)\frac{\left(\zeta^{r_0}_{v_0v_2}\zeta^{r_1}_{v_1v_2}+\zeta^{r_1}_{v_0v_2}\zeta^{r_0}_{v_1v_2}\right)}{\sqrt{\omega_{v_0}\omega_{v_1}}\omega_{v_2}}B_{r_0}B_{r_1}\right)\right) \quad (7.S82)$$

(7.S83)

(7.S84)

$$\tilde{\mathrm{H}}_{22,1}\left(v_0,v_1,r_0,r_1\right)=\sum_{v_2}\sum_{r_2}\left(\tilde{\mathrm{H}}_{22,1\mathrm{a}}\left(v_0,v_1,v_2,r_0,r_1,r_2\right)+\frac{1}{24}\left(\tilde{\mathrm{H}}_{22,1\mathrm{b}}\left(v_0,v_1,v_2,r_0,r_1,r_2\right)\right)\frac{\left(\zeta^{r_0}_{v_0v_2}\zeta^{r_1}_{v_1v_2}+\zeta^{r_1}_{v_0v_2}\zeta^{r_0}_{v_1v_2}\right)}{\sqrt{\omega_{v_0}\omega_{v_1}}\omega_{v_2}}B_{r_0}B_{r_1}\right) \quad (7.S85)$$

(7.S86)

(7.S87)

Appendix A: Theoretical Investigation of the Reaction Mechanism of the NHC-Catalyzed Transesterification of Benzyl Alcohol and Vinyl Acetate

Portions of this work were included in the laboratory manual for the Introductory Organic Chemistry Laboratory course at the University of Wisconsin – Madison in the Spring 2017 semester and for several subsequent semesters.

Includes contributions from Nicholas J. Hill, Brian J. Esselman, Maria A. Zdanovskaia, Ryan Van Hoveln, and Cheri A. Barta

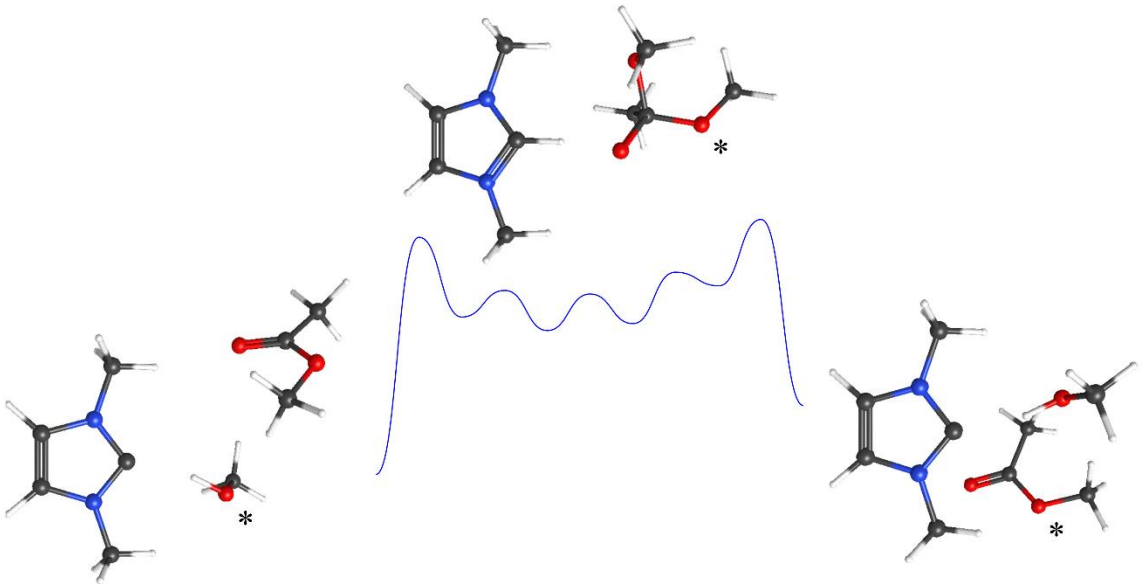

ABSTRACT

In support of the development of an experiment for the introductory organic laboratory course, we used B3LYP calculations with and without solvent corrections to investigate the reaction mechanisms of the transesterification under basic conditions with and without the use of a catalytic *N*-heterocyclic carbene (NHC). Three mechanisms were considered: the base-catalyzed, nucleophilic attachment of the alcohol to the ester and subsequent transesterification; the analogous nucleophilic reaction where the NHC catalyst first replaces the carboxylate substituent to yield a NHC substituted ketone and then is in turn replaced by the alcohol reagent; and a mechanism wherein the carbene of the NHC forms an acid-base complex with the hydrogen of the alcohol, the activated alcohol oxygen attaches to the carbonyl, and the NHC assists the transfer of the proton to the ester substituent, which is eliminated and forms another acid-base complex with the NHC catalyst. These mechanisms were considered on a small, model system as well as the full reaction that is conducted experimentally in the laboratory course. Our calculations showed that the first two mechanisms considered had considerable activation barriers, while the mechanism where the NHC catalyst serves as a proton shuttle had little to no activation barrier. Within the low energy pathway is a considerable number of conformational isomers which do not appear to have a significant impact on the energetics of the reaction. We thus present a simplified catalytic cycle for the NHC catalyzed transesterification that utilizes the NHC as a proton shuttle.

INTRODUCTION

The reaction under present consideration was the focus of a multi-session laboratory experiment in the introductory organic laboratory course at the University of Wisconsin – Madison. A primary goal of the experiment was to introduce students to a catalytic cycle in the

form of a transesterification catalyzed by a *N*-heterocyclic carbene (NHC). Before they could carry out the target reaction, they first had to synthesize the catalyzing compound. As illustrated in Scheme A.1, students first obtained a mesityl substituted diimine (**1**) *via* acid-catalyzed condensation of glyoxal and mesityl amine. Next, the diimine was combined with methanediol (delivered in the form of methylene glycol) and a sterically hindered base to undergo base-catalyzed condensation to yield the five-membered cyclic, aromatic carbene precursor (**2**) as a salt. The precursor **2** is isolated and can then be used to generate the NHC catalyst (**3**) *in situ* under mildly basic conditions. Once generated, **3** can be used to catalyze the transesterification of an alcohol and an ester. By using benzyl alcohol (**4**) and vinyl acetate (**5**) as the reagents, the resulting ester (**6**) can be easily isolated from the resulting vinyl alcohol, which readily tautomerizes to acetaldehyde (**7**) under the reaction conditions.

Scheme A.1. Transesterification of benzyl alcohol (**4**) and vinyl acetate (**5**) catalyzed by *N*-heterocyclic carbene (**3**) to produce benzyl acetate (**6**) and acetaldehyde (**7**).

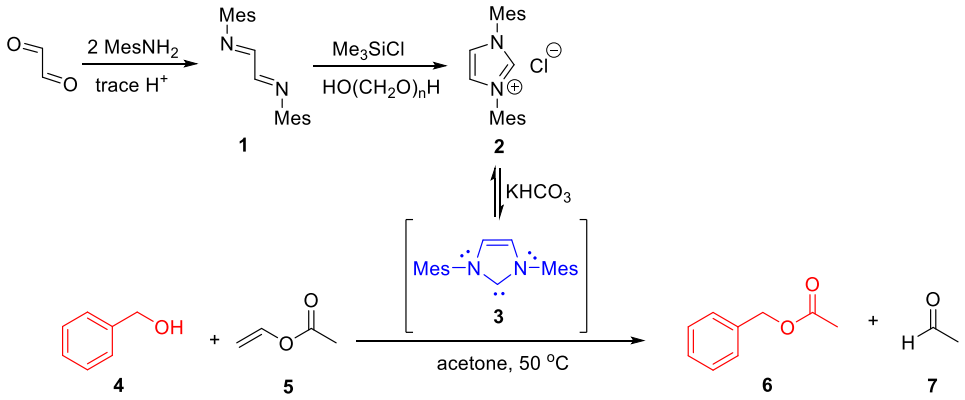

Prior to this work, the laboratory manual presented a mechanism of the NHC catalyzed reaction in which the NHC catalyst **3** acts as an intermediate nucleophile in the acid catalyzed

transesterification. That is, the carbene of **3** forms a covalent bond with the carbonyl carbon of **5** and the ethoxy group leaves to reform the carbonyl, which is now conjugated to the π system of **3**. Subsequently, the carbonyl carbon undergoes nucleophilic attack by the benzyl alkoxide and the NHC carbene is removed, reforming the catalyst, and the product ester **6** is formed. The goal of the present work was to obtain a computational model of the reaction mechanism, to facilitate students' analysis of the reaction and its outcomes.

In addition to the nucleophilic NHC mechanism that has been discussed, we were inspired by the work of Lai *et. al*.[1] to consider a mechanism for the NHC-catalyzed transesterification that proceeds through a concerted transition state, wherein the NHC carbene assisted a 1,3-hydride shift between the alcohol oxygen and the carbonyl oxygen during the nucleophilic attack by the alcohol oxygen. The result of the process is a tetrahedral intermediate where the proton is attached to the carbonyl oxygen, and the carbene of the NHC is associated with that proton. Finally, to further illustrate the effect of the NHC catalysis on the reaction energetics, we considered the mechanism of the base catalyzed transesterification reaction absent of the NHC carbene.

We initially considered a simplified form of the reaction presented in Scheme A.1, where the structures were substituted with methyl groups to reduce the size of the calculations. More specifically, the mesityl groups of **3**, the benzyl group of the alcohol **4**, and the ethylene group of the ester **5** were each replaced with a methyl carbon so that the reaction consists of the NHC catalyst **9**, methanol (**10**), and methyl acetate (**11**), respectively, as illustrated in Scheme A.2. Calculations using the smaller system could be conducted faster than on the larger target reaction and served as starting points for the optimization of the larger species. Altogether, three different reaction mechanisms for two different transesterification reactions were modeled computationally.

Scheme A.2. Transesterification of benzyl alcohol (**4**) and vinyl acetate (**5**) catalyzed by *N*-heterocyclic carbene (**3**) to produce benzyl acetate (**6**) and acetaldehyde (**7**).

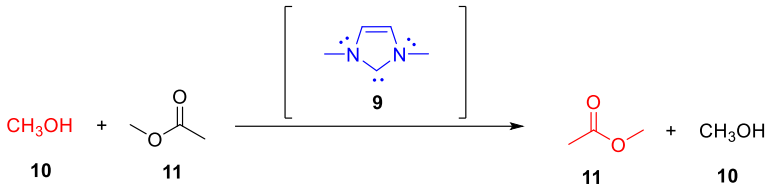

COMPUTATIONAL METHODS

All calculations were carried out using the Gaussian 09 software package[2] as implemented on the Sunbird cluster at the University of Wisconsin – Madison Chemistry Department. Stationary points were determined using geometry optimizations and vibrational frequency calculations to evaluate their nature. Intrinsic reaction coordinate (IRC) calculations were attempted for each local maximum to confirm that the transition state leads to the expected local minima. All structures were optimized using the B3LYP density functional theory and the 6-31G(d) basis set. Additional calculations were carried out on the model systems using the cc-pVDZ basis set in conjunction with the C-PCM solvation model[3] in tetrahydrofuran to reproduce previous work.[1]

RESULTS AND DISCUSSION

A simplified mechanism for the NHC-catalyzed transesterification of benzyl alcohol and vinyl acetate is presented in Scheme A.3. As described in Lai *et. al.*,[1] the *N*-heterocyclic carbene **3** (formed *in situ* by reaction of $KHCO_3$ with precursor **2**) interacts with benzylic alcohol **4** to form the acid-base complex **INT1**. The O-atom of **INT1** binds to the carbonyl C-atom of **5** while

simultaneously transferring the bridging H-atom to the carbonyl O-atom. This produces the neutral tetrahedral intermediate **INT2** from which **3** facilitates the intramolecular transfer of the H-atom to either of the other O-atoms. Thus, in the forward reaction, the H-atom is transferred to the vinyl O-atom and the carbonyl reforms, generating the desired transesterification product **6** and expelling the acid-base complex **INT3**. This intermediate dissociates to **3** and vinyl alcohol **8**, the latter undergoing tautomerization to acetaldehyde **7**. An alternate mechanism involving nucleophilic acyl substitution to form an acylimidazolium species was calculated to be of higher energy than the acid-base pathway, and thus less likely to be operative.

Scheme A.3. Simplified catalytic cycle for the NHC-catalyzed transesterification of benzyl alcohol **4** and vinyl acetate **5**, based on computational results.

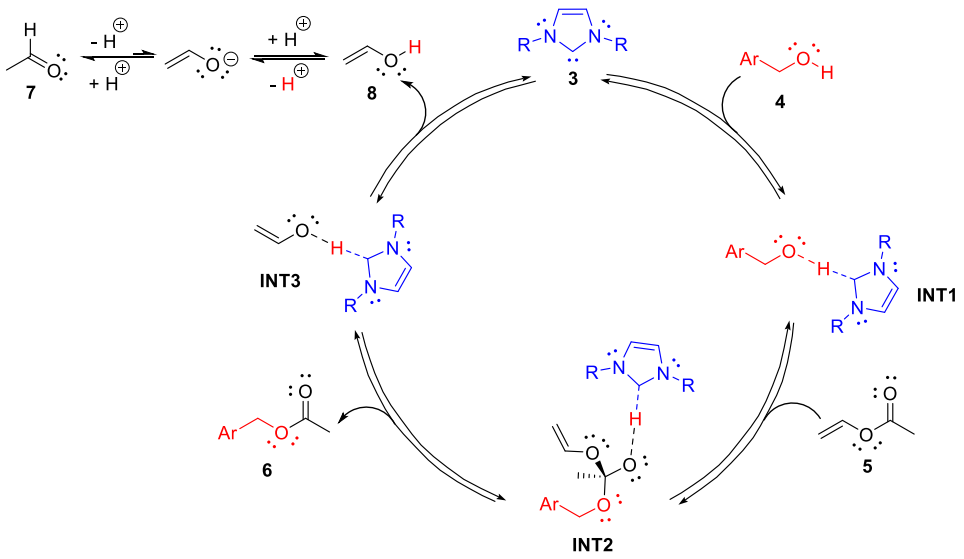

The simplifications to the mechanism presented in Scheme A.3 are related to (i) the synchronicity of the nucleophilic attack at the carbonyl carbon by the alcohol oxygen *i.e.*, reaction of **INT1** with **5**, and (ii) the intramolecular transfer of an H-atom facilitated by **3** to form **INT2**

and **INT3**. As shown in Figure A.1, the reaction of **INT1** with **5** to generate **INT2** proceeds through multiple intermediates rather than a single transition state. Each intermediate represents a discrete step in the NHC-assisted intramolecular transfer of the H-atom. The exact number and relative energies of the intermediates involved in the NHC-catalyzed transesterification are sensitive to the substituents of the alcohol and the NHC, as well as the level of theory used in the calculation. Nevertheless, the motions of the H-atom and the NHC unit during the H-atom transfer processes are consistent with literature data regardless of the number and relative energies of the intermediates. The additional intermediates and transition states are located in a relatively flat region of the potential energy surface and have minimal impact on the activation barriers, thus the simplifications made in the mechanism in Scheme A.3 are reasonable.

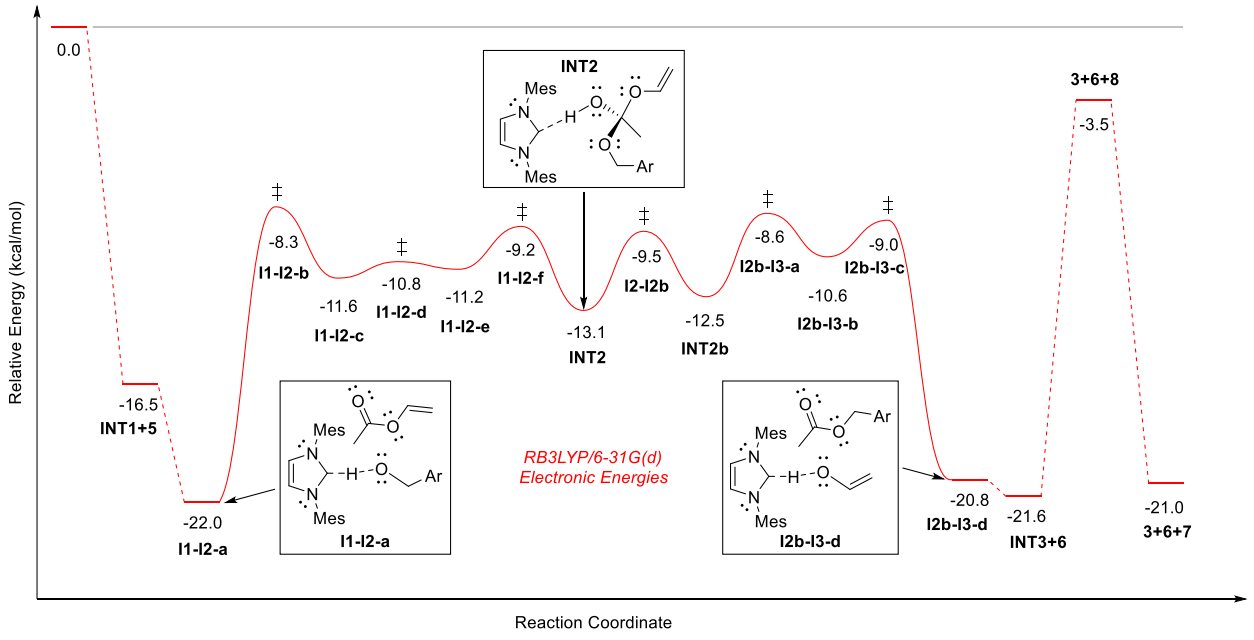

Figure A.1. Potential energy surface for the NHC-catalyzed transesterification of benzyl alcohol **4** and vinyl acetate **5**, with B3LYP/6-31G(d) relative energies.

Comparison of the potential energy surfaces of the three model pathways (Figures A.2 and A.3) suggests the proton shuttle mechanism (a) is a much more favorable process, regardless of theory, with activation barriers of no more than 20 kcal/mol (15 kcal/mol in THF). The nucleophilic NHC mechanism (b) has a very high energy intermediate and, even though the corresponding transition state could not be located, an activation barrier at least as high and thus greater than 140 kcal/mol (50 kcal/mol in THF). Similarly, the uncatalyzed mechanism (c) is estimated to have a barrier greater than 125 kcal/mol (35 kcal/mol in THF) for the deprotonation of methanol by the NHC. Note that the nucleophilic NHC and the uncatalyzed mechanisms are shown as symmetric pathways, while the proton shuttle mechanism is not. This is to illustrate that unlike the other mechanisms, the proton shuttle mechanism (a) has several conformations, and the nature of the structures is such that even though the same process is happening for **I4-I5-b** and **I5b-I4-c**, they are diastereotopic in nature and thus have different energies.

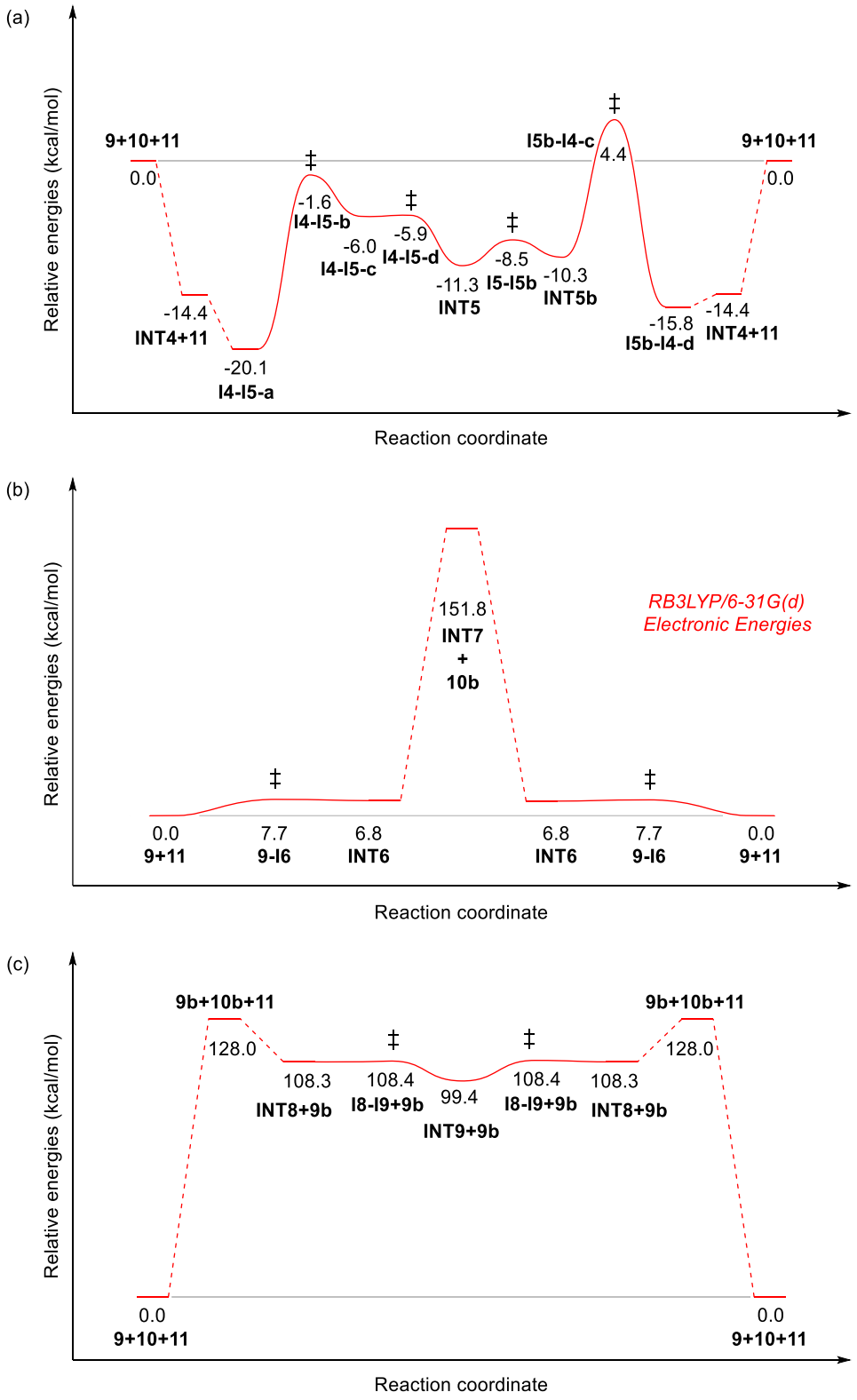

Figure A.2. Comparison of relevant pathways of transesterification mechanisms of methanol **10** and methyl acetate **11**, evaluated at B3LYP/6-31G(d), with relative energies in kcal/mol. (a) Proton shuttle NHC catalysis, (b) nucleophilic NHC catalysis, and (c) uncatalyzed with basic NHC.

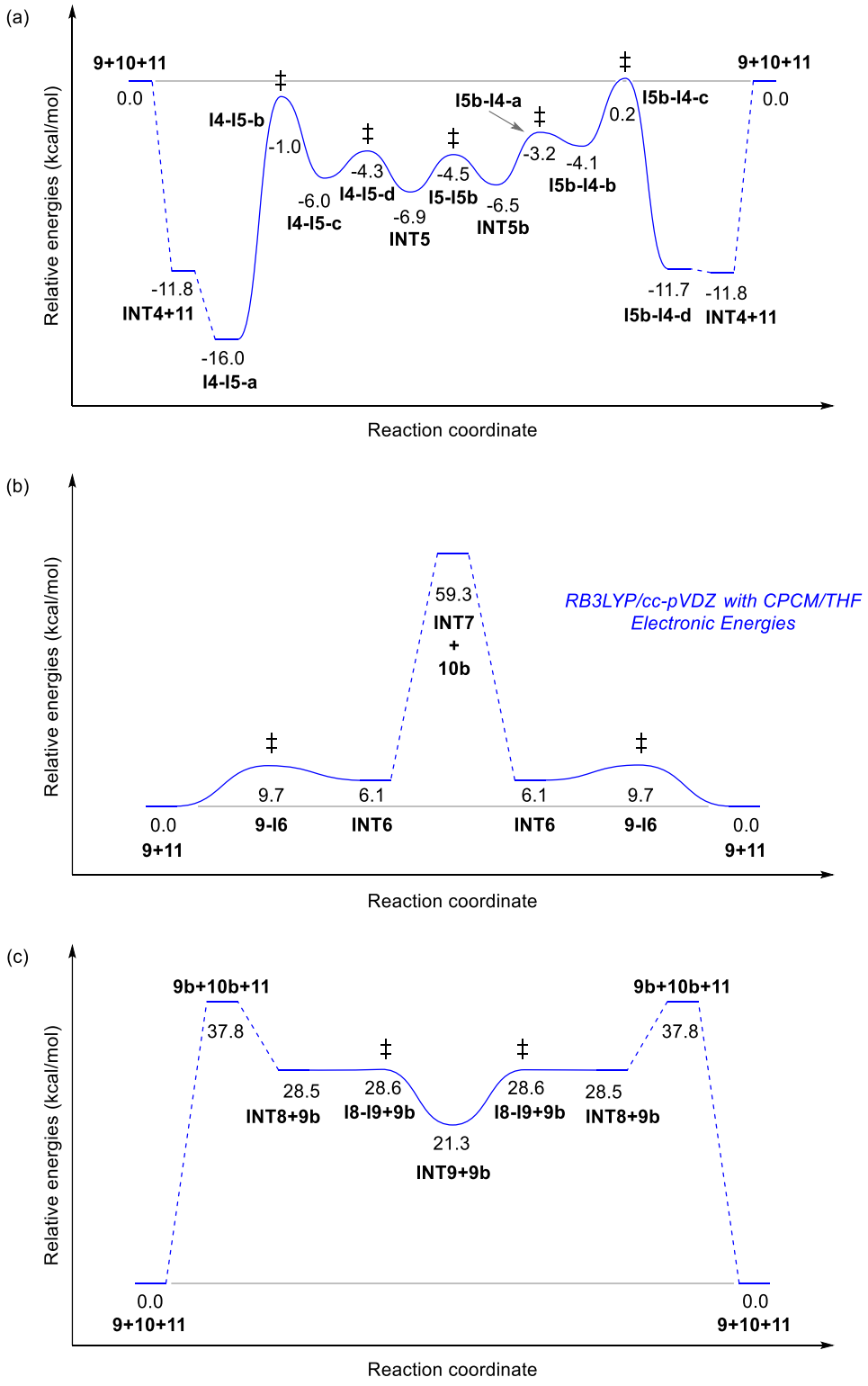

Figure A.3. Comparison of relevant pathways of transesterification mechanisms of methanol **10** and methyl acetate **11**, evaluated at B3LYP/cc-pVDZ in tetrahydrofuran using C-PCM solvation model, with relative energies in kcal/mol. (a) Proton shuttle NHC catalysis, (b) nucleophilic NHC catalysis, and (c) uncatalyzed with basic NHC.

The full reaction pathway (Scheme A.4) for the NHC-catalyzed transesterification of benzyl alcohol **4** and vinyl acetate **5** proceeds surprisingly like that of the model system [Scheme A.5(a)], with the exception that the addition of benzyl alcohol includes another local minimum. As in the model system, the carbene of the NHC catalyst associates with the proton of the alcohol oxygen which makes the oxygen more nucleophilic. The subsequent nucleophilic addition of the alcohol oxygen to the carbonyl carbon (**I1-I2-a** → **I1-I2-b**) has the largest activation barrier in the pathway at 14 kcal/mol. As in the model systems, this addition step is a concerted by asynchronous process as evidenced by the IRC of the corresponding transition state: first is the transfer of the alcohol proton from the oxygen to the carbene carbon, followed by bond formation between the alcohol oxygen and the carbonyl carbon. After the formation of **I1-I2-c**, multiple and various proton transfers assisted by the NHC catalyst occur, with barriers ranging from less than 1 kcal/mol up to 4 kcal/mol. The number of these high-energy intermediates and their activation barriers are sensitive to the substituents involved and the level of theory used, though similar activation barriers were reported for the analogous NHC proton shuttle behavior by Lyu[4] using the M06-2X functional (specifically, the NHC-3 → NHC-4 reaction in the NHC-CO_2/1a/CO_2 pathway reported therein). As expected, elimination of the vinyl alcohol (**I2b-I3-c**) is also a concerted by asynchronous process that first breaks the bond between the vinyl oxygen and the carbonyl carbon, followed by the transfer of the proton from the carbene carbon to the vinyl oxygen, resulting in an NHC/vinyl alcohol dimer **INT3** analogous to that of the NHC/benzyl alcohol dimer **INT1**. The resulting vinyl alcohol **8** tautomerizes to form the acetaldehyde product **7**, and the relative energies confirm that the keto-enol tautomerization is the overall driving force for the full reaction pathway. Finally, we note that in carrying out the calculations on the full reaction pathway, we observed

multiple conformations for each of the high-energy intermediates; these conformational isomers are not reported in this work.

In examining the model systems, we obtained different stationary points than were reported in previous work.[1] The stationary points we located, however, were in qualitative agreement with their structures and the motion of atoms. In addition, we found a local minimum (**I5b-I4-b** in Scheme A.5 and Scheme A.6.) that exists between the concerted transition state and the tetrahedral intermediate. Similar structures were found in the full reaction mechanism.

Scheme A.4. Stationary points modeled for the NHC-catalyzed transesterification of benzyl alcohol **4** and vinyl acetate **5** using mesityl substituted NHC **3** to produce acetaldehyde **7** and benzyl acetate **6**.

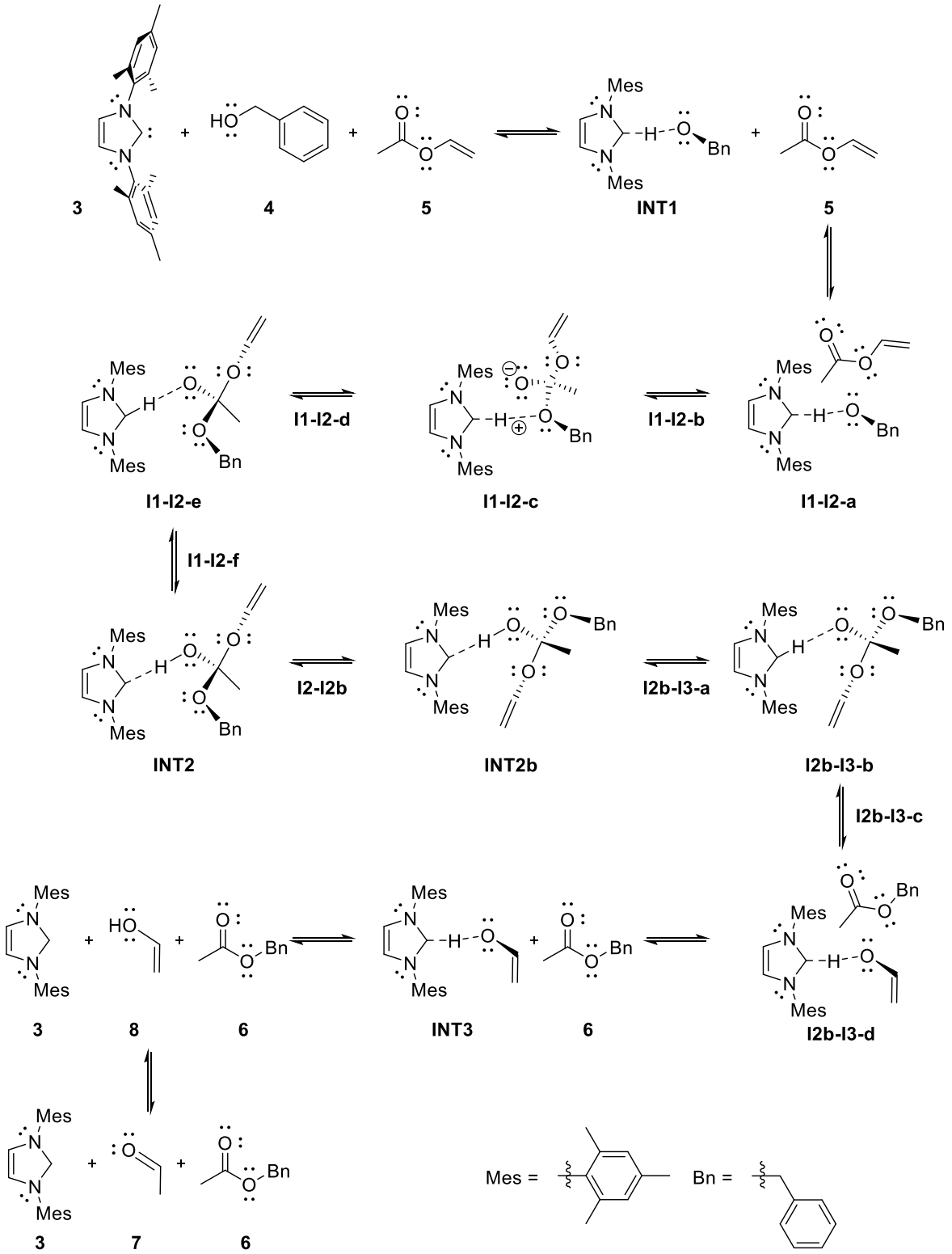

Scheme A.5. Stationary points modeled for the transesterification of methanol **10** and methyl acetate **11** *via* three different pathways: (a) Proton shuttle NHC mechanism catalyzed by methyl substituted NHC **9**, (b) nucleophilic NHC mechanism catalyzed by **9**, and (c) uncatalyzed mechanism with basic **9**.

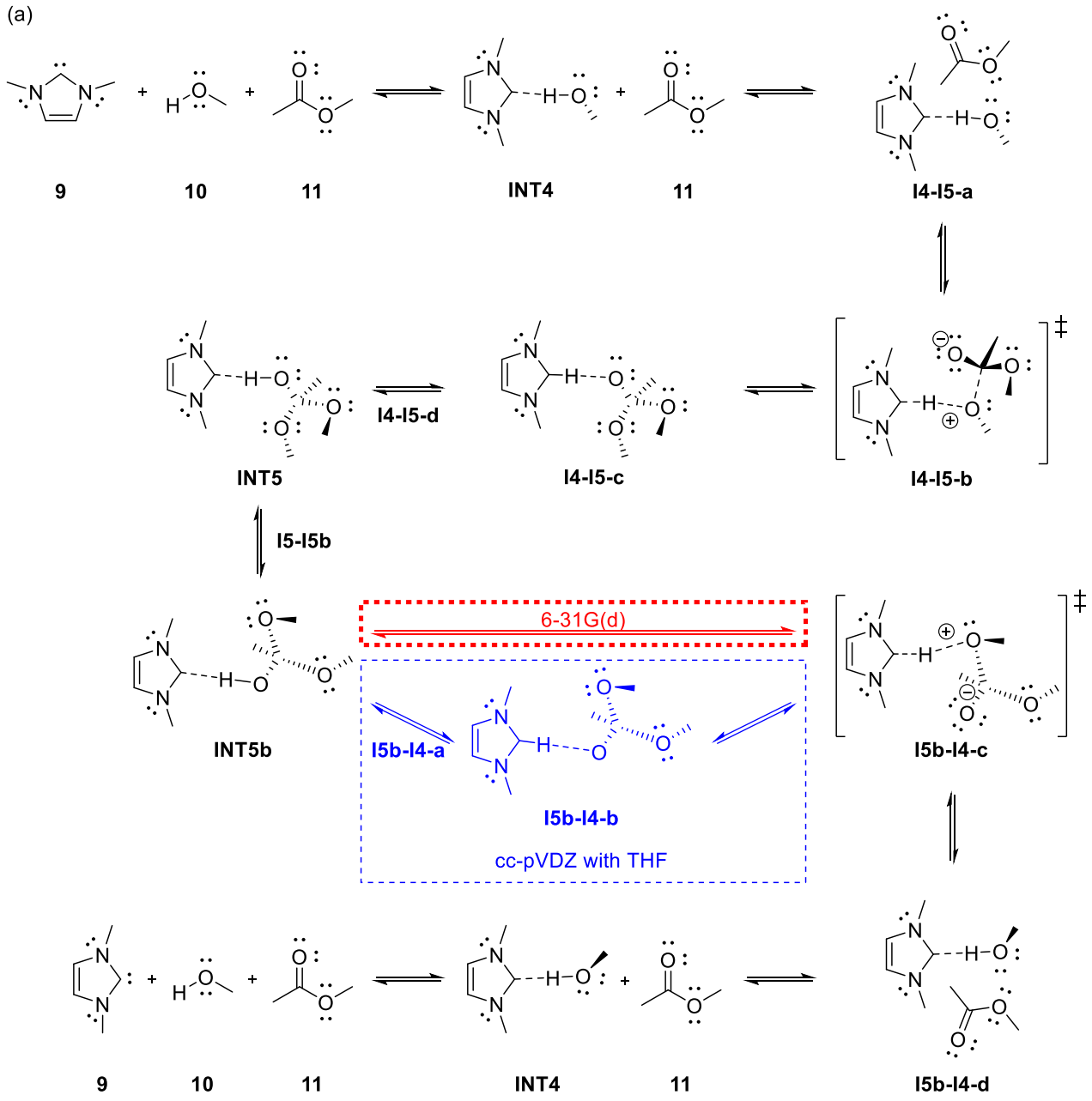

(b)

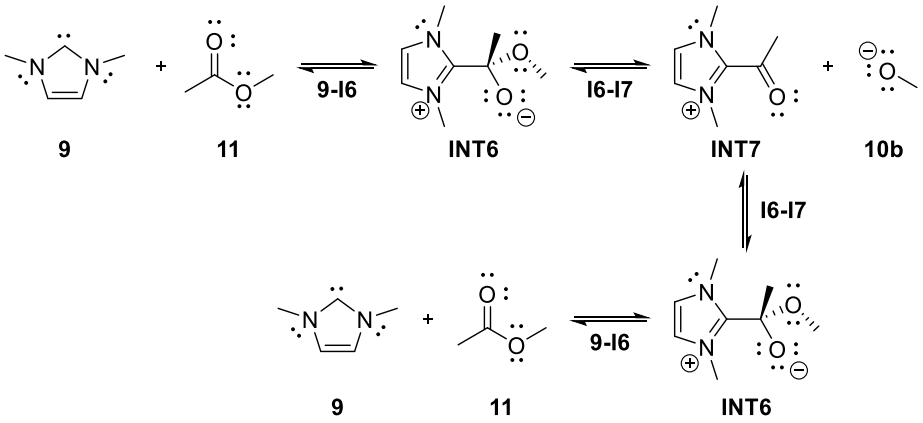
9
11
9-I6
INT6
I6-I7
INT7
10b
I6-I7
9
11
9-I6
INT6

(c)

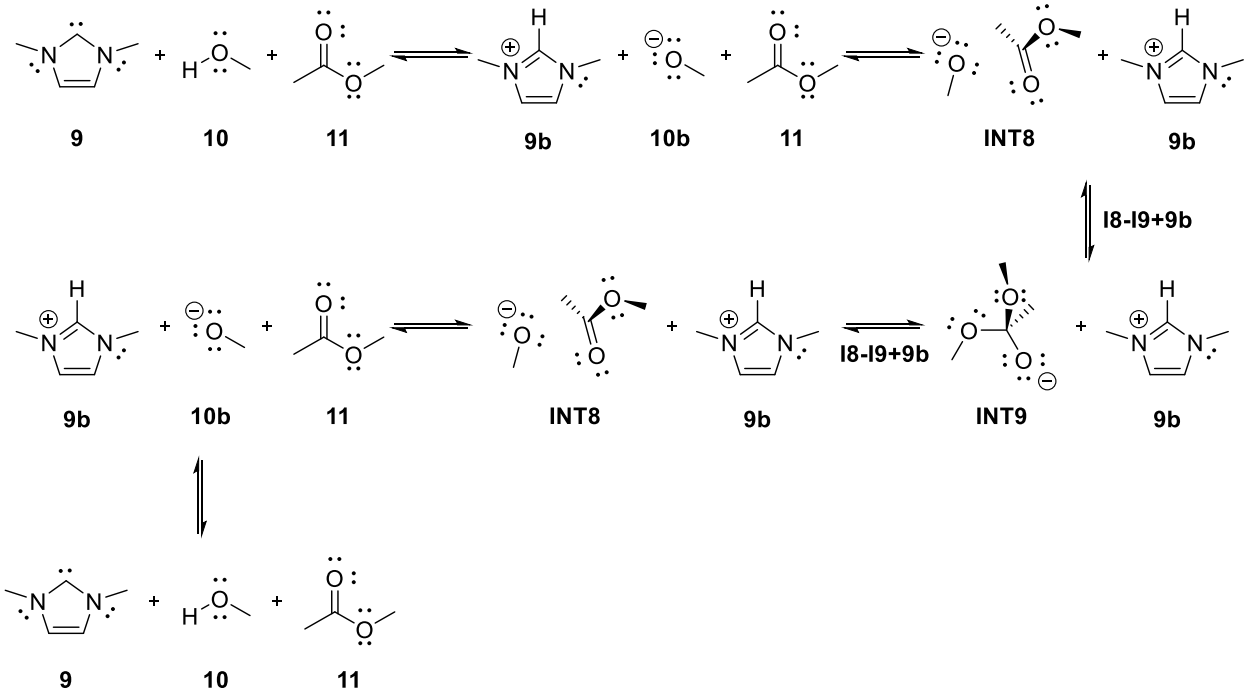
9
10
11
9b
10b
11
INT8
9b
I8-I9+9b
9b
10b
11
INT8
9b
I8-I9+9b
INT9
9b
9
10
11

REFERENCES

1. Lai, C. L.; Lee, H. M.; Hu, C. H., Theoretical study on the mechanism of N-heterocyclic carbene catalyzed transesterification reactions. *Tetrahedron Lett.* **2005,** *46* (37), 6265-6270.

2. Frisch, M. J.; Trucks, G. W.; Schlegel, H. B.; Scuseria, G. E.; Robb, M. A.; Cheeseman, J. R.; Scalmani, G.; Barone, V.; Mennucci, B.; Petersson, G. A.; Nakatsuji, H.; Caricato, M.; Li, X.; Hratchian, H. P.; Izmaylov, A. F.; Bloino, J.; Zheng, G.; Sonnenberg, J. L.; Hada, M.; Ehara, M.; Toyota, K.; Fukuda, R.; Hasegawa, J.; Ishida, M.; Nakajima, T.; Honda, Y.; Kitao, O.; Nakai, H.; Vreven, T.; Montgomery Jr., J. A.; Peralta, J. E.; Ogliaro, F.; Bearpark, M. J.; Heyd, J.; Brothers, E. N.; Kudin, K. N.; Staroverov, V. N.; Kobayashi, R.; Normand, J.; Raghavachari, K.; Rendell, A. P.; Burant, J. C.; Iyengar, S. S.; Tomasi, J.; Cossi, M.; Rega, N.; Millam, N. J.; Klene, M.; Knox, J. E.; Cross, J. B.; Bakken, V.; Adamo, C.; Jaramillo, J.; Gomperts, R.; Stratmann, R. E.; Yazyev, O.; Austin, A. J.; Cammi, R.; Pomelli, C.; Ochterski, J. W.; Martin, R. L.; Morokuma, K.; Zakrzewski, V. G.; Voth, G. A.; Salvador, P.; Dannenberg, J. J.; Dapprich, S.; Daniels, A. D.; Farkas, Ö.; Foresman, J. B.; Ortiz, J. V.; Cioslowski, J.; Fox, D. J. *Gaussian 09, Revision D.01*, Gaussian, Inc.: Wallingford, CT, USA, 2009.

3. Cossi, M.; Rega, N.; Scalmani, G.; Barone, V., Energies, structures, and electronic properties of molecules in solution with the C-PCM solvation model. *J. Comput. Chem.* **2003,** *24* (6), 669-681.

4. Li, W. Y.; Huang, D. F.; Lyu, Y. J., A comparative computational study of N-heterocyclic olefin and N-heterocyclic carbene mediated carboxylative cyclization of propargyl alcohols with CO_2. *Org. Biomol. Chem.* **2016,** *14* (46), 10875-10885.

SUPPORTING INFORMATION

Scheme A.6. Molecular structures of the stationary points modeled for the transesterification of methanol **10** and methyl acetate **11** *via* three different pathways: (a) Proton shuttle NHC mechanism catalyzed by methyl substituted NHC **9**, (b) nucleophilic NHC mechanism catalyzed by **9**, (c) uncatalyzed mechanism with basic **9**.

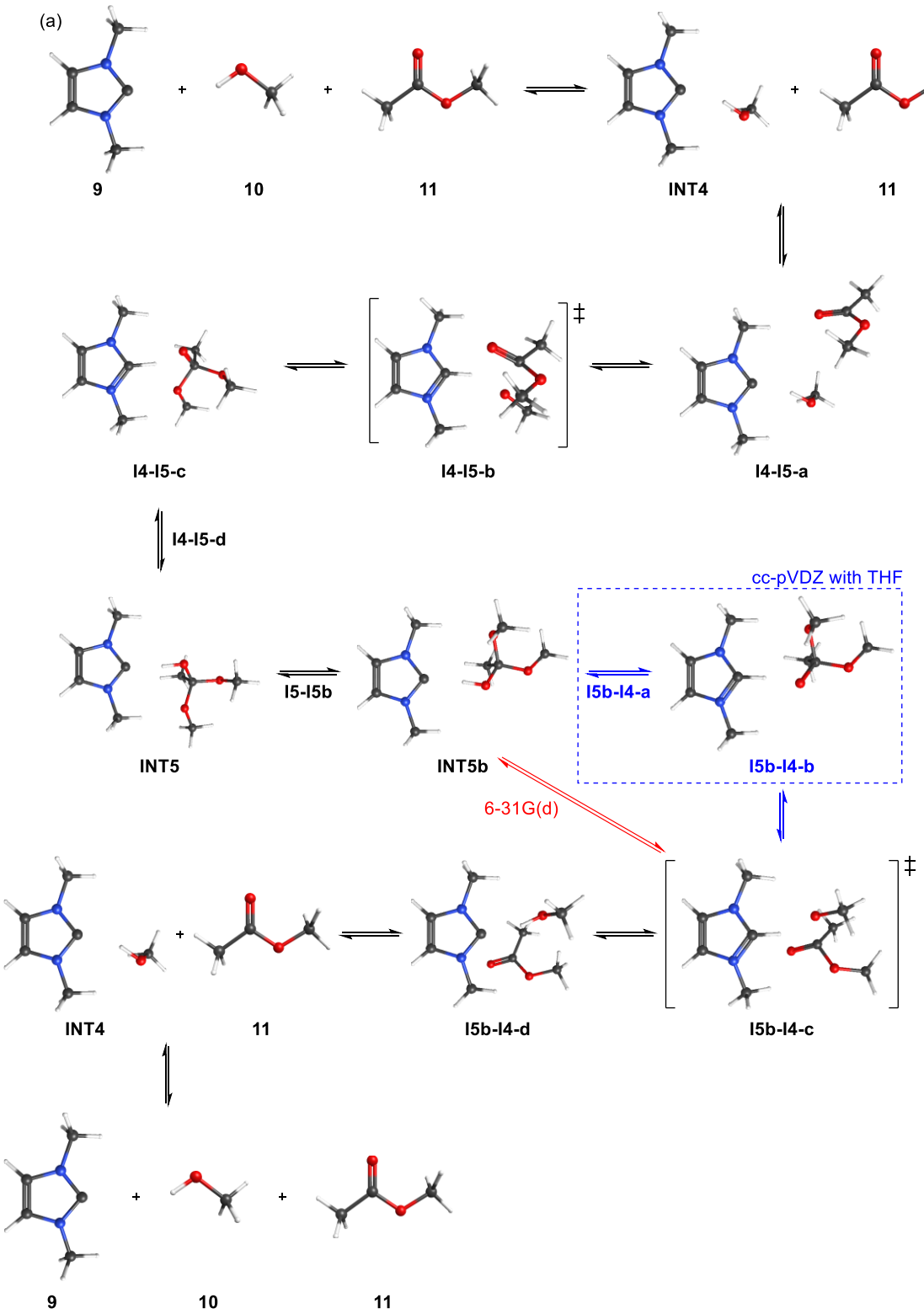
(a)
9
10
11
INT4
11
I4-I5-c
I4-I5-b
I4-I5-a
I4-I5-d
cc-pVDZ with THF
I5-I5b
I5b-I4-a
INT5
INT5b
I5b-I4-b
6-31G(d)
INT4
11
I5b-I4-d
I5b-I4-c
9
10
11

(b)

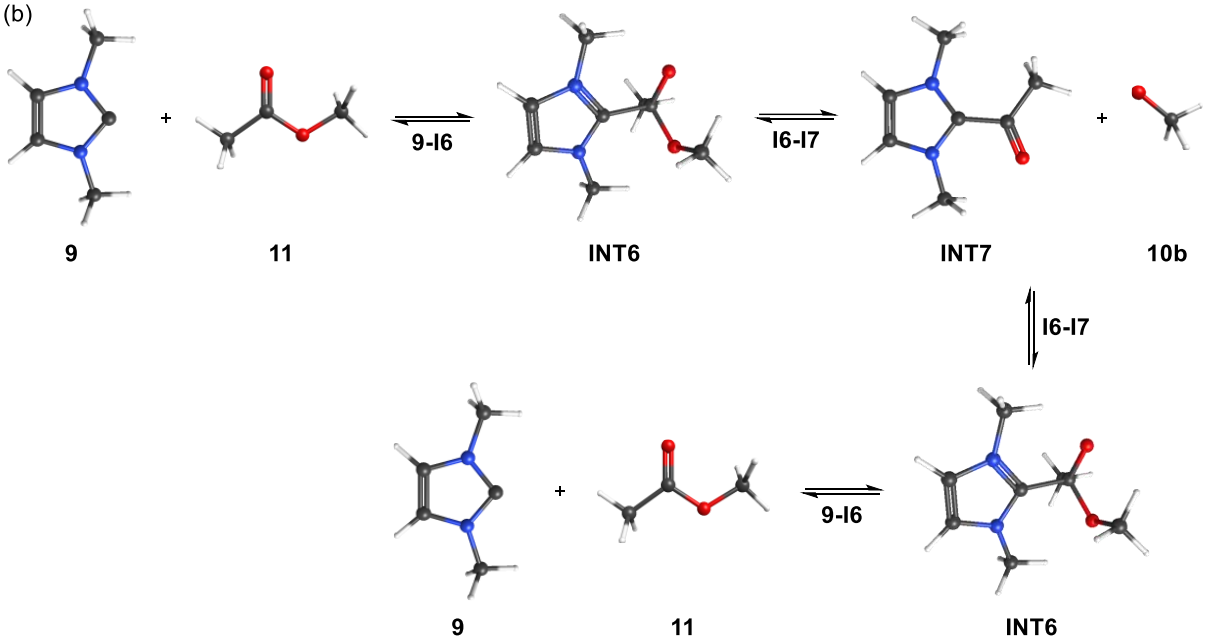

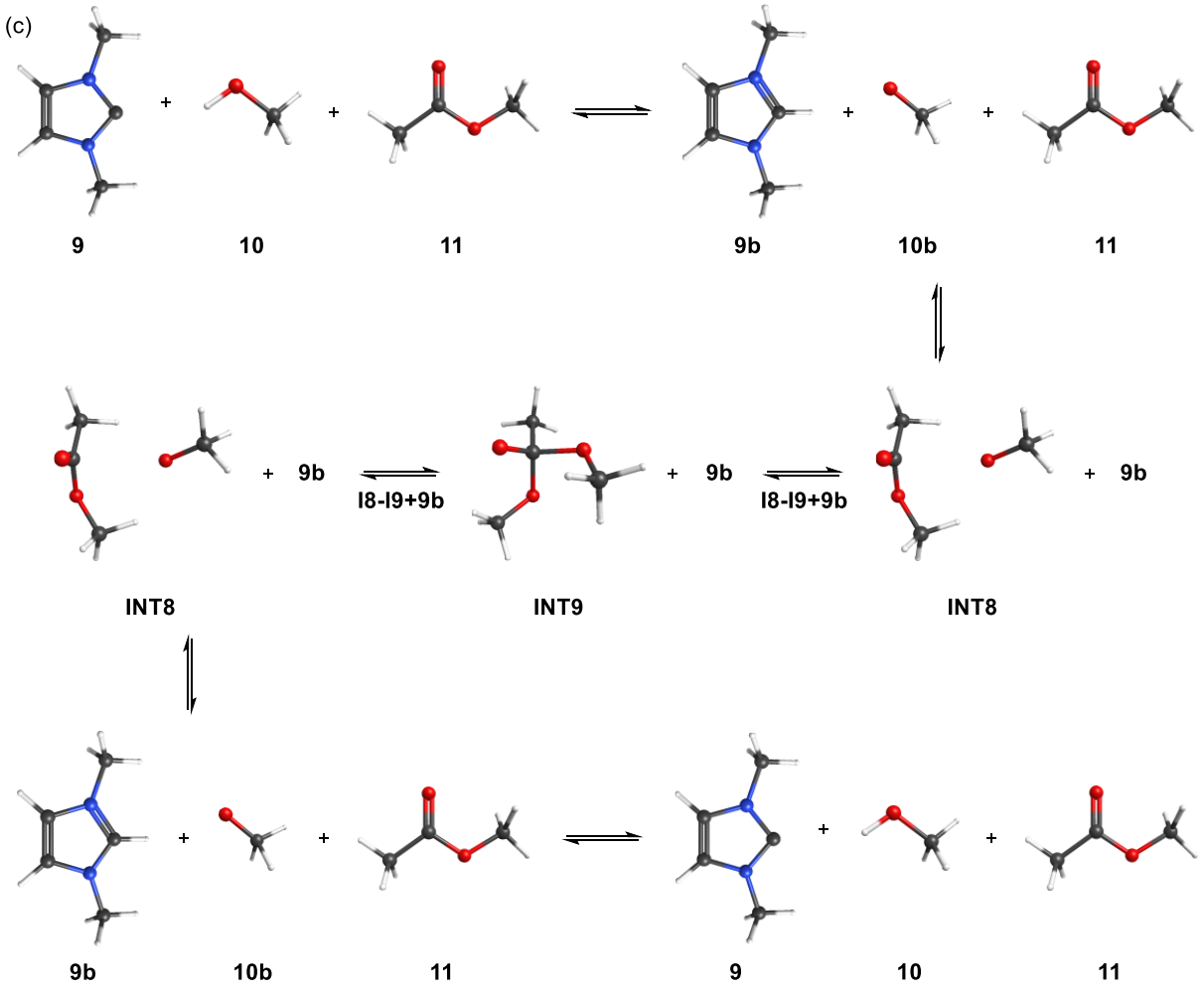
(c)
9
10
11
9b
10b
11
INT8
9b
I8-I9+9b
INT9
9b
I8-I9+9b
INT8
9b
9b
10b
11
9
10
11